RITARS-14-H-UVA

InSAR Remote Sensing for Performance Monitoring of Transportation Infrastructure at the Network Level

Final Report

Principal Investigator:
Prof. Scott Acton
University of Virginia

Program Manager:
Mr. Caesar Singh
Office of the Assistant Secretary for Research and Technology
U.S. Department of Transportation

DISCLAIMER

The views, opinions, findings and conclusions reflected in this presentation are the responsibility of the authors only and do not represent the official policy or position of the US Department of Transportation/Office of the Assistant Secretary for Research and Technology, or any state or other entity.

EXECUTIVE SUMMARY

The goal of the project was the implementation of interferometric synthetic aperture radar (InSAR) monitoring techniques to allow for early detection of geohazard, potentially affecting the transportation infrastructure, as well as the monitoring of current status at the network level.

The InSAR datasets collected by TRE provided rich information with extremely accurate sub-centimeter data about the history of the displacement over two areas. For the first area (AOI1), located near Staunton in central Virginia, the dataset covered a period of almost four years allowing for a very accurate analysis of the temporal behavior of the observed displacements. A second area (AOI2) including Northern Virginia and a section of Washington, DC was included to extend the analysis to a region with high urban density and highways with extreme traffic volume.

The InSAR data was analyzed using several tools that were developed to address specific issues such as: subsidence detection, bridge motion, road smoothness, and pavement motion. These tools were either fully integrated within the ArcGIS environment (as toolboxes) or were developed in the form of standalone app (for the major operating systems). In the latter case, the output of the tool analysis was formatted to seamlessly integrate within ArcGIS using the geo-referenced tagged image file format (geotiff). Independently of the implementation, all the tools produce outputs in either geotiff or shapefiles in order to allow for easy import in all the major GIS analysis software thus removing the restriction on the requirement for ArcGIS and are available for download from the project website:

http://viva-lab.ece.virginia.edu/foswiki/InSAR/RitaSoftware

To provide an alternative interface were existing transportation dataset can be integrated with the analyses results, we developed a web-based decision support system where the output of our tools can be analyzed in conjunction with the pavement quality dataset from VDOT. The DSS is a web-app developed in JavaScript that make use exclusively of open source libraries. GeoJson (an industry standard) was used for data representation. This format is extremely portable and the majority of GIS environments allows for translation to and from this format to all the other major GIS representations allowing for ultimate flexibility.

A parallel effort was conducted by the team to increase the visibility of this project and advertise the potential application of the InSAR technique to the transportation infrastructure. To this end, half a day workshop was held during TRB2016 and the results of the project were showcased in several venues, including meeting with the US Army Corps of Engineers and at a NISAR meeting held at NASA (NISAR is a new US-Indian InSAR mission, expected to launch in 2019 and designed to provide full and constant monitoring of the Earth’s surface. Two webinars were conducted in 2015 and the recordings are posted on the project website together with a complete set of educational documents detailing the fundamental and advance uses of InSAR techniques with a specific focus towards transportation and geohazard:

http://viva-lab.ece.virginia.edu/foswiki/InSAR/RitaOutreach
http://viva-lab.ece.virginia.edu/foswiki/InSAR/RitaEducation

ACKNOWLEDGEMENTS

We wish to acknowledge the participants in this project.

For the University of Virginia (UVA) team, Dr. Scott Acton served as principal investigator and led the research in image analysis. Andrea Vaccari was the lead researcher. Dr. Vaccari, along with Tamal Batabyal, Nazia Tabassum, and Lingfeng Cao, developed algorithms that enabled analysis of geohazards, bridge displacement, and pavement motion analysis. Dr. Vaccari also performed the majority of budgetary, reporting and documentation duties and led the web-based deployment effort.

Dr. Edward Hoppe led the Virginia Transportation Research Council (VTRC). This Virginia Department of Transportation (VDOT) center perform ground studies and validation. In this work, Dr. Bruckno was the lead geologist. Audrey Moruza was the main architect behind the cost-benefit analysis whereas Elizabeth Campbell provided the support required to install and run ArcGIS Online for organizations, a geographical information system. Special thanks go to Rob Minford of VDOT and Dan Widner of the Virginia Information Technologies Agency (VITA) for their help in converting the existing pavement quality dataset into shapefiles.

Dr. Franz Meyer, Dr. Wenyu Gong, Olaniyi Ajadi, and Anna Worden of the Geophysical Institute at the University of Alaska Fairbanks provided their expertise in the remote sensing area of the project and focused on the development of change detection techniques centered on the use of SAR amplitude images.

The TRE Altamira team was led by CEO Adrian Bohane. Dr. Giacomo Falorni provided data analysis and technical assistance on remote sensing. Geographical information system expertise was added by Vicky Hsiao.

The technical advisory board consisted of:

Chad A. Allen - Vermont Agency of Transportation (VTrans)
Scott A. Anderson - Federal Highways Administration (FHWA)
Melba Crawford - Purdue University
Emmet Heltzel - Virginia Department of Transportation (VDOT)
Michael Mathioudakis - New York State Department of Transportation (NYSDOT)
Ty Ortiz - Colorado Department of Transportation (CDOT)

Glossary

AOI	Area Of Interest
ArcGIS	Arc geographic information system
CSK	COSMO-SKyMed
DEM	Digital Elevation Model
DInSAR	Differential InSAR
DOT	Department Of Transportation
DS	Distributed Scatterer
FHWA	Federal HighWay Administration
Geotiff	Geo-referenced tagged image file format
GIS	Geographic Information System
IEEE	Institute of Electrical and Electronics Engineers
InSAR	Interferometric Synthetic Aperture Radar
LiDAR	Light Detection And Ranging
LOS	Line-Of-Sight
NED	National Elevation Dataset
PS	Permanent Scatterer
PSInSAR	Permanent Scatterer InSAR
RADAR	RAdio Detection And Ranging
SAR	Synthetic Aperture RADAR
SSIAI	IEEE Southwest Symposium on Image Analysis and Interpretation
TRE	TRE Altamira
TS	Temporary Scatterer
USGS	U.S. Geological Survey
UVA	University of Virginia
VDOT	Virginia Department of Transportation
VIVA	Virginia Image and Video Analysis
VTRC	Virginia Transportation Research Council

TABLE OF CONTENTS

LIST OF FIGURES

LIST OF TABLES

CHAPTER 1: INTRODUCTION

The Virginia Image and Video Analysis (VIVA) laboratory at the University of Virginia (UVA) is leading a research project with the Virginia Department of Transportation (VDOT) and TRE Altamira entitled "InSAR Remote Sensing for Performance Monitoring of Transportation Infrastructure at the Network Level " (RITARS-14-H-UVA). The work was awarded to the University of Virginia as a research grant funded by the US Department of Transportation Office of Research, Development and Technology.

The main objective of this project is to provide a framework for the consistent and reliable delivery of information about subsidence/sinkhole formation, bridge settlement, slope stability and pavement distortion to state departments of transportation (DOTs) in the form of geographic information system (GIS) layers that can be seamlessly integrated within existing decision support systems. The goal of the project is to help DOTs with the optimization of resource allocation for maintenance and inspection of the transportation infrastructure at the network level.

Building on the success of RITARS-11-H-UVA, brought forth by the UVA team (with collaborators VTRC and TRE-Altamira), the project pushes the use of novel space-borne radar technology (Interferometric Synthetic Aperture Radar – InSAR) from the validation to the network level implementation stage by packaging the analysis tools, developed during RITARS-11-H-UVA, into deployable ArcGIS toolboxes. This allows for the development of a comprehensive remote-sensing-based inspection framework for the early detection of ground deformations which might be precursors of potential hazardous situations within the transportation corridor.

TRE Altamira Inc. (TRE) has been contracted to perform the InSAR component over two main areas, 1,600 kilometers squared in size. The first is centered over the town of Middlebrook, Virginia whereas the second includes most of Washington, DC metropolitan area. InSAR monitoring was carried out using TRE's proprietary SqueeSAR™ algorithm. COSMO-SkyMed (CSK) imagery was used for this monitoring project due to the high spatial resolution and acquisition frequency of the CSK satellites.

The Virginia Transportation Research Council (VTRC) was selected as second subcontractor for this project. VTRC is a collaboration between the Virginia Department of Transportation and the University of Virginia dating back to 1948. VTRC had the responsibility for identifying study areas, performing on-site analysis and baseline verification, cost-benefit analysis as well as evaluating GIS tools for integration of the analysis results obtained by the project into VDOT framework. Along with the parent organization VDOT, VTRC provided the necessary facilities in GIS management, transportation databases access, and expertise in geology.

The Geophysical Institute at the University of Alaska Fairbanks was contracted to provide outreach material about InSAR technology and its application within the transportation framework as well as the study of potential correlations between the remote sensing imagery and the quality of the imaged pavement.

CHAPTER 2: SATELLITE IMAGE ACQUISITION AND PRE-PROCESSING

Areas of interest

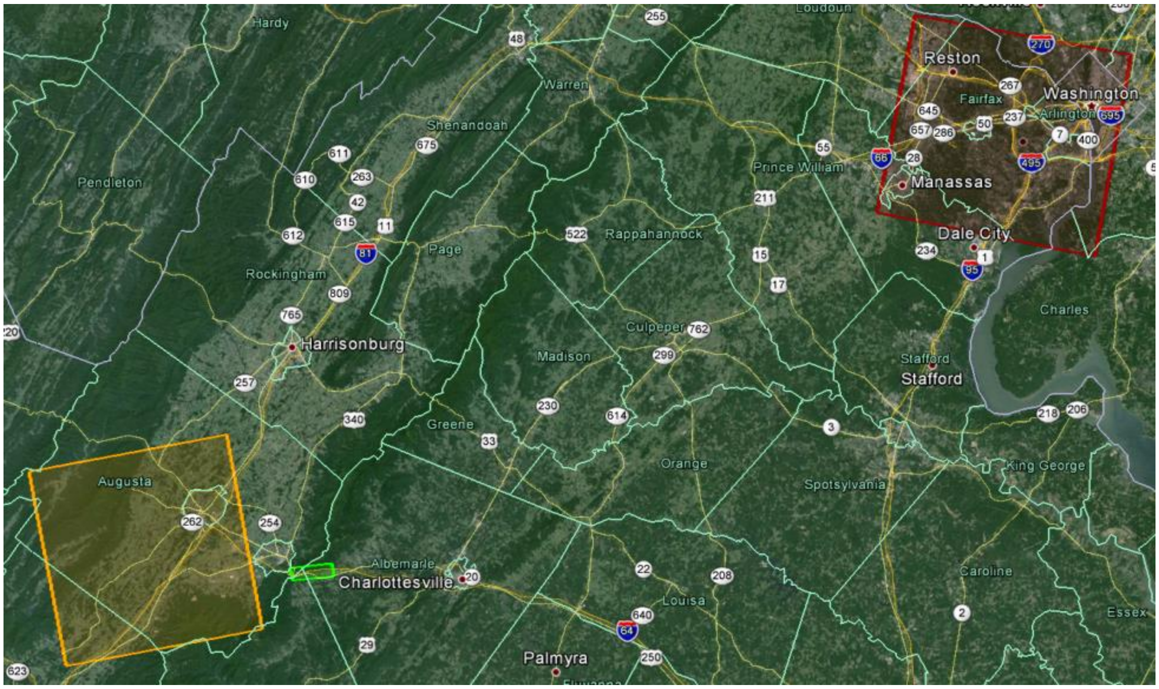

Figure 1 - Areas of interest.

The project continued the acquisition of data over the area identified during RITA RS-11-H-UVA (Figure 1, orange area – AOI1) and acquired data over a new area (Figure 1, red area – AOI2). The extension of data acquisition over the original area provided increased temporal coverage, longer time series of the ground displacement and better characterization of ground subsidence features. Imaging the same site allowed for further refinement of the sinkhole detection model and aided in the development of the robust detection algorithms at the core of the ArcGIS toolboxes designed for the bridge, slopes and road distortion analyses.

AOI1 is a region of about 40x40 km (618 miles^2) chosen because of the diversity of geological conditions. This area, represented in details in Figure 2, is centered roughly on the locality of Middlebrook, Augusta County, Virginia, and is a tectonically complex area spanning the Valley and Ridge and Blue Ridge physiographic provinces (Bingham, 1991).

Geological ages ranging from Holocene sediments to Precambrian granulite gneiss (Bartholomew, 1977), with frequent nonconformities, are represented within the AOI. The predominant tectonic framework consists of eastward-dipping thrust faults and decollements related to repeated orogenic cycles (Rader & Wilkesm, 2001). The AOI contains carbonate, non-carbonate clastic, and metamorphic terrains, resulting in both rock slope stability and karst geohazards. The karst areas range in age from Cambrian to Devonian and formed during the Taconic and Acadian Orogenies and their associated divergent and inter-orogenic periods. Karst lithologies consist mainly of limestone and dolostone, while non-carbonate clastic lithologies consist of occasionally interbedded shales, siltstone, conglomerates and sandstone, and the metamorphic lithologies consist of charnockite, granulite gneiss, quartzite, and greenschist and blueschist-grade metabasalt. Figure 2 illustrates karst terrains in light blue, with areas of known sinkhole locations and previously-repaired sinkholes located in red. Slightly over half of the site is underlain by karst geology. VDOT has remediated over 200 sinkholes within the past twenty years, many of which do not appear in the Virginia Department of Mines, Minerals and Energy (DMME) dataset. Rock slopes have never been inventoried by VDOT; however, several interstate, primary and high-volume secondary lane miles within the site are at risk for rock fall or rock slope instability.

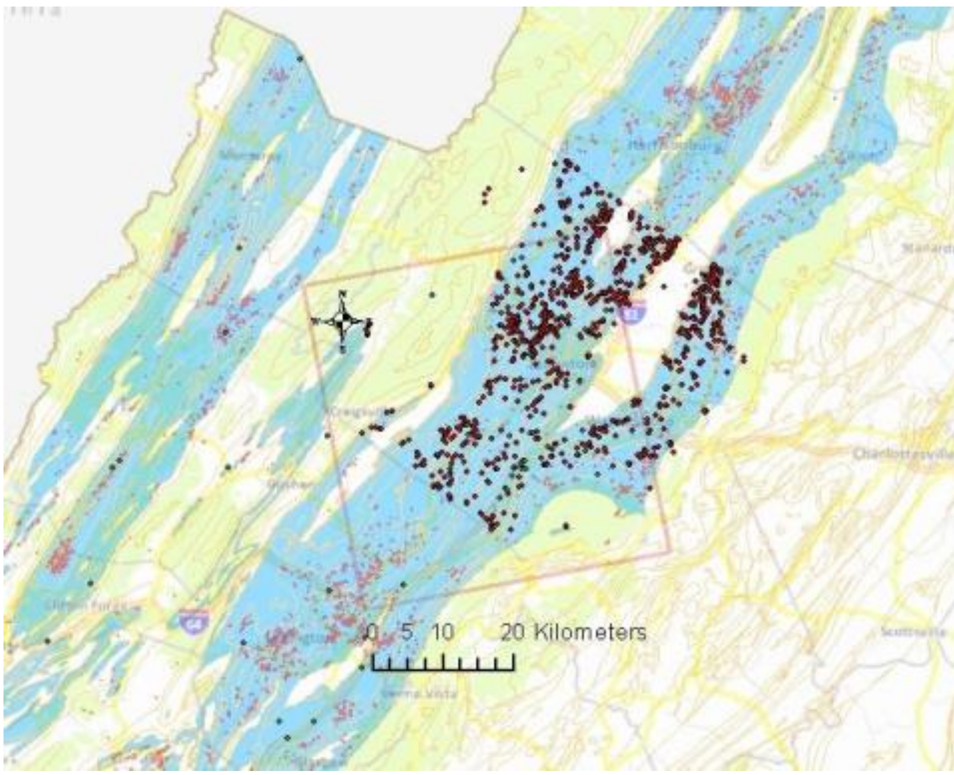

Figure 2 - AOI1 details.

From a radar imaging point of view, the environment of the AOI is mixed between dense vegetation, active agriculture, fallow fields, exposed ground, infrastructure and towns. Mountainous terrain and areas of highly variable topography are present in the northwest and southeast corners of the scene. Human-made structures, bare or sparsely vegetated ground often yield a high number of measurement points. In contrast, areas of dense vegetation, active agriculture and steep slopes often produce a low density of measurement points. This AOI contains approximately 100 lane miles of interstate and over 200 lane miles of primary and high-volume secondary routes, as well as approximately 600 bridges, culvert, and major transportation structures.

The second area of interest (AOI2) is located in northern Virginia and includes most of Washington, DC metropolitan area. The addition of this new study area allowed the project to focus on an area with higher density of urban infrastructure with a large number of transportation features including numerous bridges and area with slope stability issues. Furthermore, this new area includes some of the highest volume traffic routes in Virginia, which facilitates the evaluation of road response to high traffic loading (subsidence and pavement condition). Hundreds of miles of existing and newly built interstate, primary and secondary roads exist in this site

Together, the two sites are representative of different transportation infrastructures and in sum allowed the project to evaluate the extensibility of the technology and the approach to the network and state wide level implementation.

A third area of interest was located just east of the first area over Afton Mountain (Figure 1, green area – AOI3). This area had experienced rockslides and landslides that have closed a major interstate, I-64. The rationale for the third site was to investigate if differential InSAR (DInSAR) techniques could be applied to map and monitor specific features and provide useful information to network and transportation managers.

Satellite data were acquired by TRE-Altamira and processed with the various InSAR techniques as summarized in Table 1.

Table 1 - InSAR techniques used in pre-processing of the three selected test sites.

	AOI1	**AOI2**	**AOI3**
Data Acquisition	Acquire Cosmo-Skymed satellite data at 16 day intervals and process the data stack at 8 and 16 months to create InSAR databases	Acquire Cosmo-Skymed satellite data at 16 day intervals and process the data stack at 8 and 16 months to create InSAR databases	Acquire two Cosmo-Skymed satellite data and process at 2 months
Algorithm used	SqueeSAR	SqueeSAR	DInSAR

The processed data consisted of two main products: pointcloud data sets including the displacement time series of the permanent and distributed scatterers detected within the imaged are, raster images identifying temporary scatterers as well as raster images providing the geo-referenced amplitude measurements as observed by the satellite. These processed were analyzed as described in this report.

Technology

The project was based on the use of a technology known as interferometric synthetic aperture radar (InSAR). This technology allows the derivation of very accurate ground deformation measurement from space borne platforms.

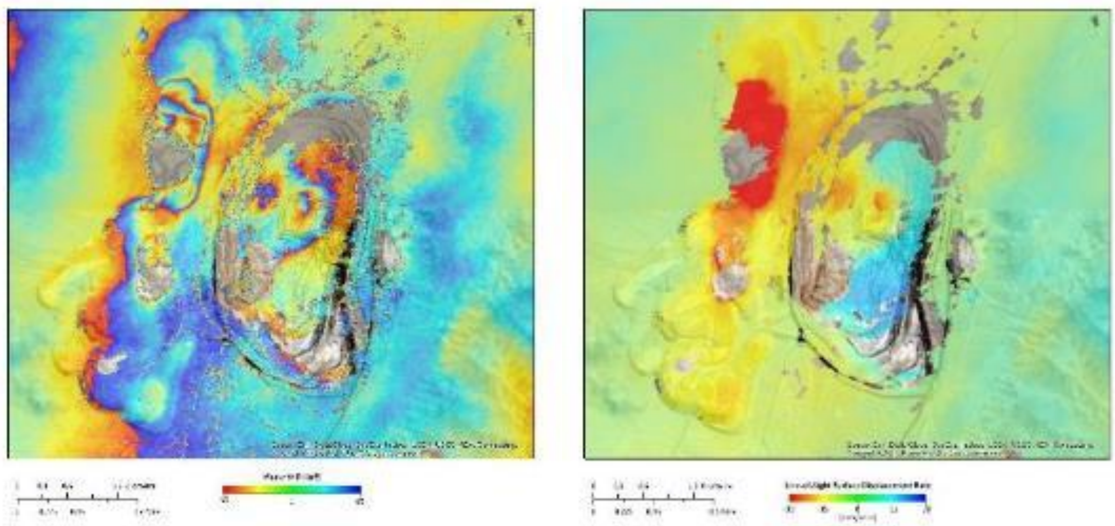

Figure 3 - Example of InSAR interferogram (left) and deformation map derived from it (right).

InSAR

InSAR, also referred to as SAR interferometry, is the measurement of signal phase change (interference) between radar images. When a point on the ground moves, the distance between the sensor and the point changes, thereby producing a corresponding shift in signal phase. This shift is used to quantify the ground movement. An interferogram is a 2D representation of the difference in phase values. Variations of phase in an interferogram are identified by fringes, colored bands that indicate location and extent of movement. The precision with which the movement can be measured is usually in the centimeter range as the phase shift is also impacted by topographic distortions, atmospheric effects, and other sources of noise.

Differential InSAR (DInSAR) and deformation maps

When InSAR is used to identify and quantify ground movement, the process is referred to as Differential InSAR (DInSAR). In DInSAR topographic effects are removed by using a Digital Elevation Model (DEM) of the area of interest to create a differential interferogram that is then converted into a deformation map by transforming the phase values to ground deformation in the satellite Line-Of-Sight (LOS). Only interferograms with good coherence can be converted into a deformation map. Although DInSAR is still impacted by atmospheric effects, as there is no method for removing this signal phase contribution, it is nevertheless a useful tool for identifying footprints of progressing movement and creating deformation maps. The limitation of DInSAR is its relatively low precision (centimeter scale) and that it cannot distinguish between linear and non-linear motion.

Permanent Scatterer InSAR (PSInSAR™)

PSInSAR™ (Ferretti, Prati, & Rocca, Permanent scatterers in SAR interferometry, 2001) is an advanced form of DInSAR. The fundamental difference is that it uses multiple interferograms created from a stack of at least 15 radar images. PSInSAR™ was developed to overcome the errors produced by atmospheric artifacts on signal phase. The

PSInSAR™ algorithm automatically searches the interferograms for pixels that display stable radar reflectivity characteristics throughout every image of the dataset. In PSInSAR™ these pixels are referred to as Permanent Scatterer(s) (PS). The result is the identification of a sparse grid of point-like targets on which an atmospheric correction procedure can be performed. Once these errors are removed, a history of motion can be created for each target, allowing the detection of both linear and non-linear motion.

The result is a sparse grid of PS that are color-coded according to their deformation rate and direction of movement. The information available for each PS includes its deformation rate, acceleration, total deformation, elevation, coherence as well as a time series of movement. PSInSAR™ measures ground movement with millimeter accuracy.

SqueeSAR™

PSs are objects, such as buildings, fences, lampposts, transmission towers, crash barriers, rocky outcrops, *etc*., that are excellent reflectors of radar microwaves. However, TRE has noticed that many other signals are present in the processed data. These do not produce the same high signal-to-noise ratios of PS but are nonetheless distinguishable from the background noise. Upon further investigation it was found that the signals are reflected from extensive homogeneous areas where the back-scattered energy is less strong, but statistically consistent. These areas have been called distributed scatterer(s) (DS) and correspond to rangeland, pastures, bare earth, scree, debris fields, arid environments, *etc*.

The SqueeSAR™ algorithm (Ferretti, et al., 2011) was developed to process the signals reflected from these areas. As SqueeSAR™ incorporates PSInSAR™ no information is lost and movement measurement accuracy is unchanged. SqueeSAR™ also produces improvements in the quality of the displacement time series. The homogeneous areas that produce DS normally comprise several pixels. The single time series attributed to each DS is estimated by averaging the time series of all pixels within the DS, effectively reducing noise in the data.

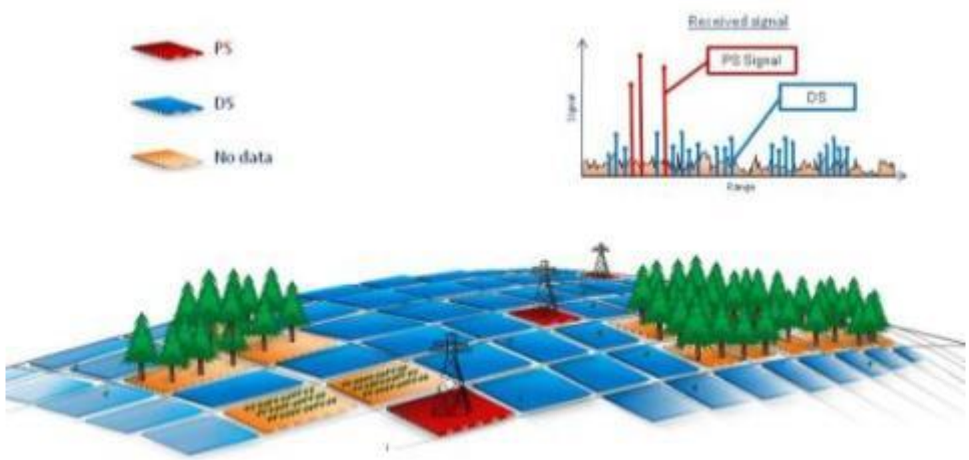

Figure 4 - Illustration of the identification of PS and DS as obtained by application of SqueeSAR.

Temporary Scatterer

To address some of the requirements of this project, an innovative technique known as Temporary Coherence Scatterer(s) (TS) was developed by TRE. This technique examines information on a point-by-point basis (every cell of data within the radar scene). In this advanced approach, each image pair (interferogram) within the entire data tack is examined and any coherent information is extracted. The result is a single image representing information measured from all coherent data contained throughout the entire stack. The technique works by removing the constraint that every point must remain coherent throughout the entire stack of radar scenes (critical in the SqueeSAR algorithm). This relaxation of the coherence paradigm typically leads to a greater spatial coverage of the results, including over areas where PS and DS cannot be identified.

Figure 5 - Comparison between the PS and DS results (left) and the TS results (right). Note the subsidence areas identified on the right by the use of the TS technique.

The output is a non-continuous raster map representing average surface displacement rates. The TS approach represents a more robust solution for increasing the density of ground deformation data compared to a simple relaxation of coherence thresholds. As TS are actually pixels in which several points are averaged, noise is suppressed, while a simple reduction of the coherence threshold for the selection of PS/DS would introduce lower quality points into the analysis. Reliable ground motion would be difficult to extract from these low coherence points as time series would be noisier and difficult to interpret. The use of the TS approach assisted in the detection and delineation of unstable areas.

It is important to note that there are several limitations inherent to this approach. First, it is not known which scenes contribute information to any particular TS. As a result, the time interval over which ground displacement occurs is unknown and may vary across the end result. Furthermore, as numerous interferograms are used, the time of year may also fluctuate among these data cells. Finally, as the product of a TS analysis is static, no time series information can be extracted.

Data acquisition, pre-processing and manual analysis results

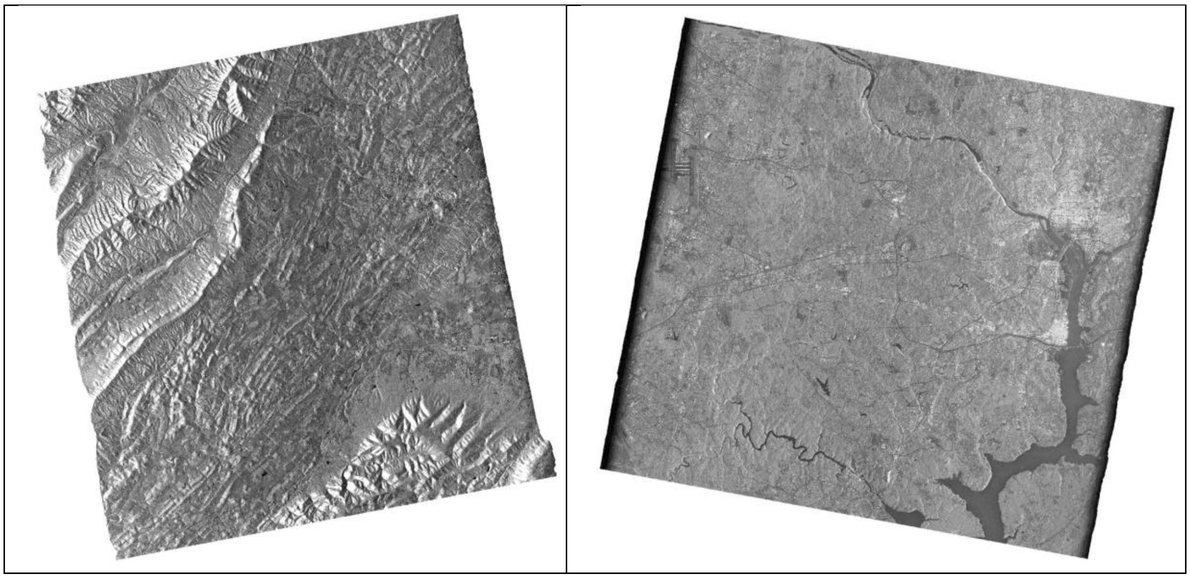

Figure 6 - Multi Image Reflectivity (MIR) maps for AOI1 (left) and AOI2 (right).

The processing pipeline saw the data being acquired by the Cosmo Sky-Med (CSK) satellite constellation over the regions of interest. The complex data, comprising of amplitude and phase data, was then analyzed using the SqueeSAR algorithm to identify high-coherence scatterers and track their displacements over time with high accuracy. We will also refer to the results of this analysis as "phase" data since the main component used to extract displacement information is the phase of the satellite data. The amplitude data were used to study potential correlations between pavement conditions and variation of amplitude values. Figure 6 show an example of how amplitude data looks like. These MIR maps are evaluated by averaging all the acquisition over time. Although this provides a very clean image of the average response at the satellite radar frequency highly reducing the level of the speckle noise associated with this type of observations, the information about how the response changes over time is lost. At VIVA we worked on an approach to remove the noise while maintaining the temporal information. For more information, please refer to the project website:

http://viva-lab.ece.virginia.edu/foswiki/InSAR/WebHome

After the satellite images are sifted through the SqueeSAR algorithm and the collection of high-coherence scatterers is identified, the resulting dataset is a pointcloud where to each scatterer (location) is associated a very high resolution (less than a centimeter) measurement of the temporal displacement occurred since the first pass of the satellite. This extremely reach dataset is then analyzed both "manually" and automatically. A very detailed manual analysis was performed by TRE. This type of analysis focused on specific location of interest (rock slopes, specific highways tracts, *etc*.). The time series of the displacements for scatterer over these locations was studied in detail by TRE geospatial analysis and the presence of trends (or lack thereof) identified. Here we present a brief summary of the results of these analyses. For more information, please consult the detailed reports generated by TRE and attached in appendices (Appendix A, Appendix B, Appendix C, Appendix D, and Appendix E).

AOI1 – Central Virginia

This is the region that was observed for the longest time The first image was acquired on August 29, 2011 and the last on November 24 allowing for a long term analysis of the displacement within the region. The total number of processed images was 62 with a typical revisit frequency of 16 days.

Two different analyses were performed on this region one including the data acquired up to June 2014 and one including the entire dataset (up to November 2014).

The following key findings were reported by TRE for the June 2014 measurements (the section numbers refer to the report attached in Appendix B):

- Up to -30 mm of subsidence was identified along primary roads, such as at Jefferson Highway near Greenview Dr. where sudden movement begins in early 2014 (Section 5.2.2). Displacement was also observed on the State Route 635 bridge overpass of I-81 (Section 5.2.1).
- A rock slope along Route 600 exhibited subsidence rates of up to -9.1 mm/year (Section 5.3.1).
- Movement was identified on riprap placed along several routes within the AOI (Sections 5.3.2, 5.3.3, 5.3.4).
- Observations in the area of two sinkholes active in the past do not show recent movement (Section 5.3.6).
- Measurement point density has more than doubled compared to the previous results (180 points per km^2 vs 83 per km^2).
- Three out of four reflectors installed on the Route 262 Bridge were visible. -4.6 mm of settlement was detected from reflector #2 on top of the parapet mid-span between March to June, 2014 (Section 5.1.2).

The last finding refers to a special experiment where artificial retroreflectors of increasing radar cross-section were installed along a bridge along Route 262 to evaluate if this approach could be used to increase the response intensity and accuracy for specific target of high interest. The results show that artificial reflector can be successfully used to increase signal to noise ratio for measurements over structure for which knowledge of high accuracy displacement is critical. More information are available in Section 5.1 of the report attached in Appendix B.

After an additional 6 months of observation (end of November 2014) there was a marked improvement in the density of the measurements allowing for the following detections (once again the section numbers refer to the report attached in Appendix C):

- Signs of settlement were identified along primary roads:

  - Up to -45.5 mm of subsidence next to Mish Barn Road (Section 6.1.2).
  - -20 mm of subsidence near State Route 42 starting in early July 2014 (Section 6.1.3).
- Two unstable slopes along Route 600 and Greenville School Rd were observed (Sections 6.2.1 and 6.2.5).
- Movement was identified on riprap slopes along routes I-80 and I-61 within the AOI (Sections 6.2.2 and 6.2.3).
- No signs of movement were found in the area of two sinkholes that were active in September 2012 (Section 6.2.6).
- Pavement conditions were compared with InSAR results to identify possible correlations. InSAR results show more variability over repaved areas, but no clear trends were observed in the deformation time series (Section 6.4). An analysis of amplitude data may lead to further results.
- Measurement point density has more than doubled compared to the previous results (405 points per km2 vs 187 per km2).
- The three years and three months of data acquisition and processing led to an increase in the spatial coverage of the data over time and allowed monitoring updates at eight month intervals of the road network and potential Geohazard ground deformation in Virginia.

AOI2 – Northern Virginia and Washington, DC

For the Northern Virginia/Washington, DC area, the data was acquired for a shorter time since it could not be accumulated with previous data as for the central Virginia region. Nevertheless, there were very interesting findings. In particular, one area, Hill East and Capitol Hill in Washington, DC, where significant subsidence was detected in correspondence to an area where the DC Water and Sewer Authority started a tunneling work in early 2015 as part of the DC Water Clean Rivers Project:

https://www.dcwater.com/workzones/projects/anacostia_river_information_sheet.cfm

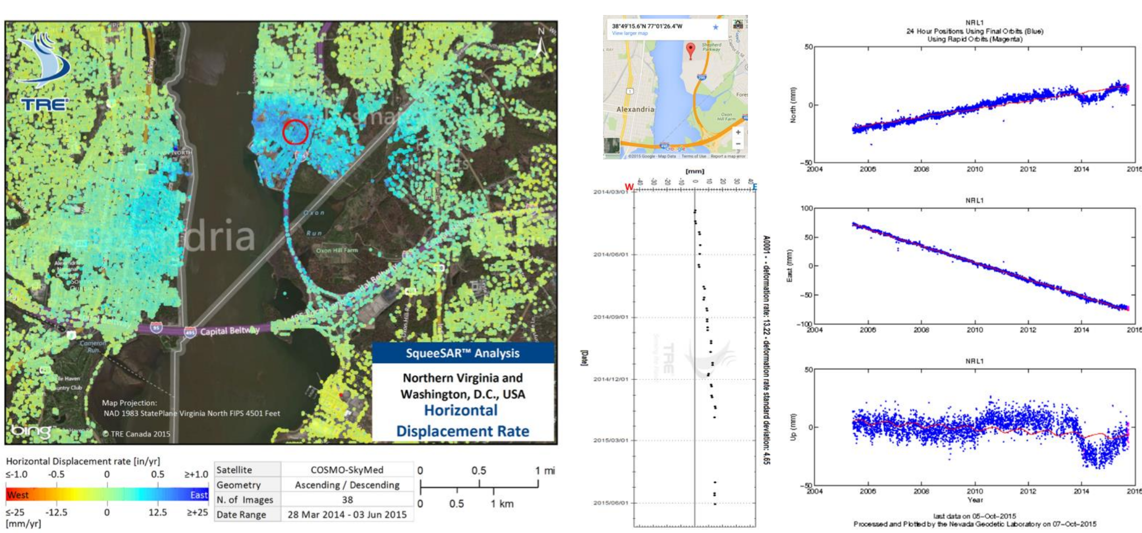

Figure 7 - Eastward movement north of Woodrow Wilson Bridge, Alexandria, VA (left); IGS08 GPS readings from GNSS NRL1 (right); source of uplift is currently under investigation.

The second region of uplift was detected in the region of Alexandria, VA, SW Washington, DC, and Forest Heights, MD. The causes behind this uplift are still unknown but, after further analysis and a second round of measurements, it was verified that the motion was not upward, but eastward. This was confirmed by the comparison with high resolution GPS measurements acquired by the GNSS NRL1 station located at the close by U.S. Naval Research Laboratory (Figure 7).

In October 2014 after 6 months of measurements, the following key findings were reported by TRE (the section numbers refer to the report attached in Appendix D):

- Up to -29 mm of subsidence was identified along primary roads, such as on the shoulder of US 29, Virginia State Route 237 Lee Highway and along Henry G Shirley Memorial Hwy (Section 5.2).
- The results show relative stability on the Woodrow Wilson Bridge, with the exception of a measurement point in the I-495 Express Lanes at the MD approach that indicates -20 mm of subsidence (Section 5.1.3).
- No significant subsidence was observed on the retaining wall along I-395 SB at King Street after the H-piles were built in early March (Section 5.1.2).
- No ground deformation on the bridge abutment along I-66 East Bound CD Road over Rte. 286 was observed. The surroundings of this bridge are stable. -30 mm of subsidence was detected on a landfill at the I-66 Transfer Station approximately 1 km east of the bridge.
- The slope failure along Piscataway Drive in Maryland is outside of the AOI, but measurement points close to this location indicate between -10 to -13 mm of movement.
- A total of 1.2 million measurement points was obtained from the data processing, providing a density of 781 points per square kilometer (2,022 points per square mile).
- The precision of the measurements is estimated at ±5.9 mm/year based on the displacement rate standard deviation. This value will improve with the acquisition of more images spanning a longer period of time.

After 15 months (June 2015), given increased temporal and spatial resolution resulting from the analysis of the larger stack, TRE reported the following key findings. More information are included in the attached report in Appendix E:

- Two areas exhibit interesting surface deformation patterns within the AOI.
  - Subsidence is observed in the area of Hill East and Capitol Hill, with rates of -12.4 mm/yr on average, and up to -33.7 mm/yr in the vicinity of RFK stadium and along the Anacostia River. The subsidence pattern appears to correspond with the path of the Anacostia River Tunnel project (Section 5.1.1).
  - An interesting uplift pattern with well-delineated boundaries is observed in the area of Alexandria, VA, SW Washington DC, and Forest Heights, MD, with up to +20.3 mm/yr (Section 5.1.2).
- No significant deformation was found over the following features indicated by UVA/VDOT:

    - The bridge of I-66 EB CD Road over Rte. 286 Fairfax County Pkwy.
    - The retaining wall along I-395 SB at King Street.
- A separate analysis was performed over the Woodrow Wilson Bridge (Section 5.1.3) to separate thermal contraction/expansion from other deformation signals. Compensation of the thermal effects highlights limited residual displacements.
- Subsidence was detected along the Silver Line metro in Vienna, VA (Section 5.2).
- A surface cross-section analysis highlights the evolution of horizontal profiles of the ground surface over time over certain features of interest (Section 5.3).
- A total of 3.6 million measurement points was obtained from the data processing, providing a density of 2,278 points per square kilometer (5,899 points per square mile).
- The precision of the measurements has improved from ±5.9 to ±2.3 mm/yr.

AOI3 – Afton mountain slope – I64

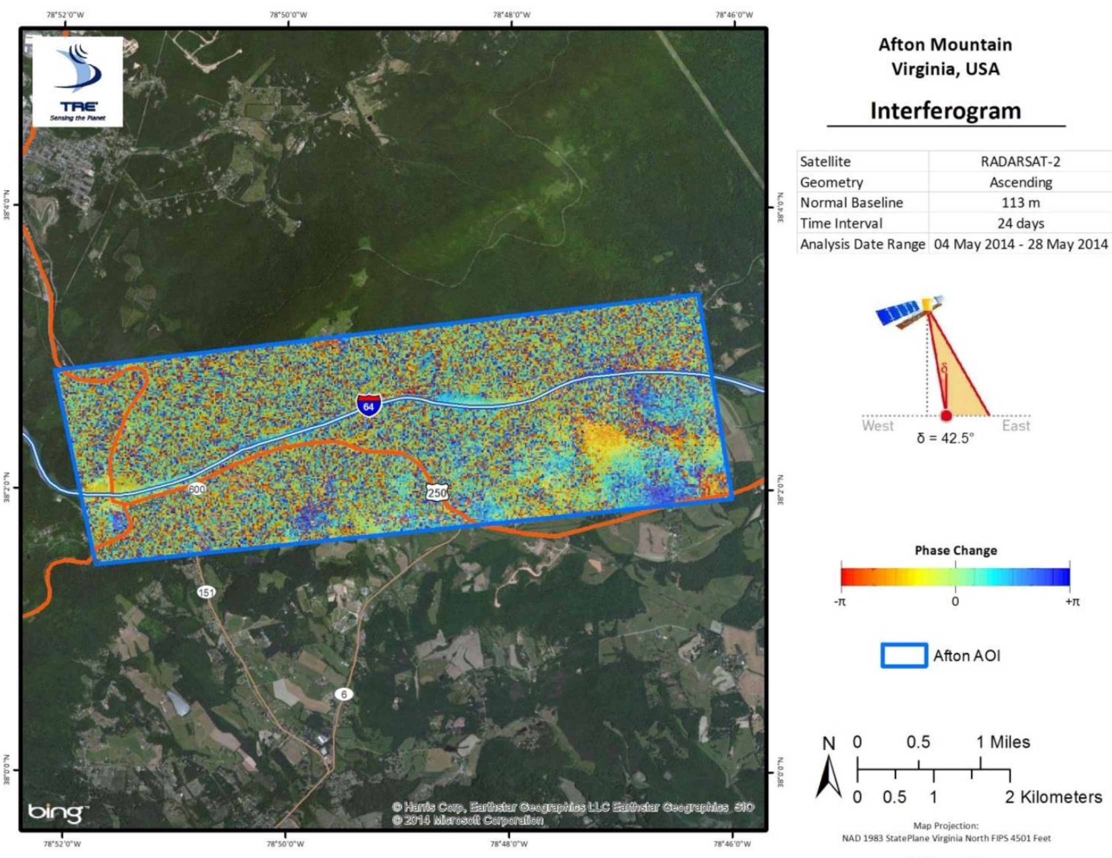

Figure 8 - Interferogram over the I-64 area of interest close to Afton Mountain (AOI3).

As described above, InSAR techniques can directly be used to identify motion. Since simple InSAR requires only two images to provide a rough analysis of the displacements, being able to utilize such technique to inspect larger area in order to identify regions requiring a closer look would provide a cheaper approach. To evaluate this option, we performed this type of analysis over AOI3 in a region adjacent to the I64 corridor and prone to landslides. The level of coherence over the exposed rock was high enough to perform a motion analysis. Although over the short period of time, no motion was detected, the high coherence of the measurements, underline the fact that this technique could be used to monitor slopes adjacent to transportation networks. The key findings, described in detail in Appendix A, are outlined here:

- An interferogram was produced from two Radarsat-2 satellite images acquired on 4 May 2014 and 28 May 2014.
- No movement was detected in the interferogram. It is possible that ground movement along the unstable slope was too small over the 24-day period to be detected.
- Both the interferogram and the associated coherence map are presented and discussed.
- The coherence map indicates that overall coherence of the area is low, with the
- exception of areas of exposed rock along the I-64 corridor.

CHAPTER 3: IMAGE ANALYSIS SOFTWARE DEVELOPMENT

Figure 9 illustrates the general analysis pipeline developed for this project. The first step consists of the acquisition and pre-processing of the remote sensing data. This part was performed by TRE and described in the previous section (CHAPTER 2: SATELLITE IMAGE ACQUISITION AND PRE-PROCESSING). After this step, the delivered data is the starting point for the individual analyses plugin/toolboxes. Each of the toolboxes, described in detail in this section, is targeted towards the detection of a specific issue:

- Subsidence detection
- Bridge motion analysis
- Coherent motion detection (pavement/slopes stability)
- Road smoothness analysis (distortion of pavement)

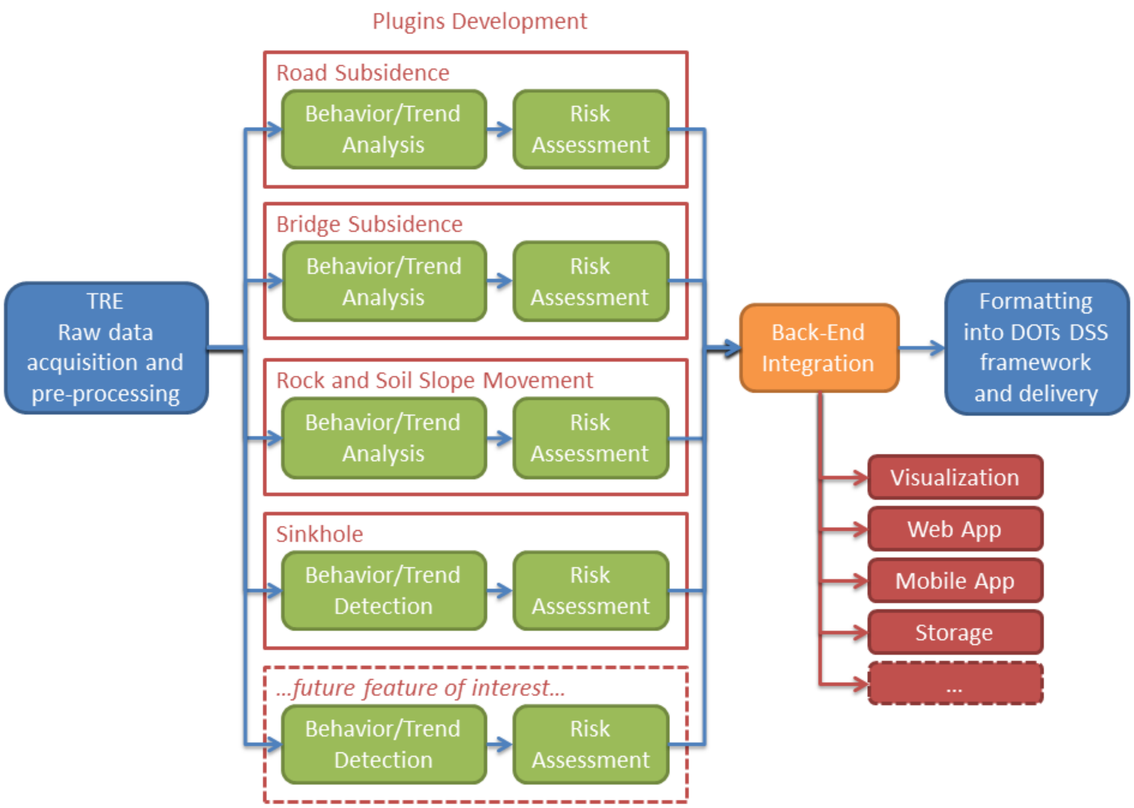

Figure 9 – Analysis pipeline.

The tools listed above were fully developed providing a full pipeline from pre-processed data all the way to back-end integration. The tools were implemented either directly as ArcGIS toolboxes or as standalone tools generating output that can be seamlessly imported into the ArcGIS environment (shapefiles or geo-referenced TIFF images). Furthermore, a Decision Support System web-based application was developed to integrate existing pavement quality assessment databases with the result of the tools analysis. This will be described in details in the next section (CHAPTER 4: GEOGRAPHICAL INFORMATION SYSTEMS (GIS) AND DECISION SUPPORT SYSTEM (DSS) DEVELOPMENT).

All the software developed for the project is under revision control and hosted on GitHub under the VIVA section: https://github.com/VIVAUVA. Further information is also available from the project website:

http://viva-lab.ece.virginia.edu/foswiki/InSAR/WebHome

Subsidence detection

Subsidence is a geohazard that is relevant not only for transportation since it can bring the closure of major highways, but also relevant for the population at large due to the often devastating consequences brought on by the development of sinkholes. Because of this, the development of an automated subsidence detection technique, played a major role in this as well as in previous projects supported by OST.

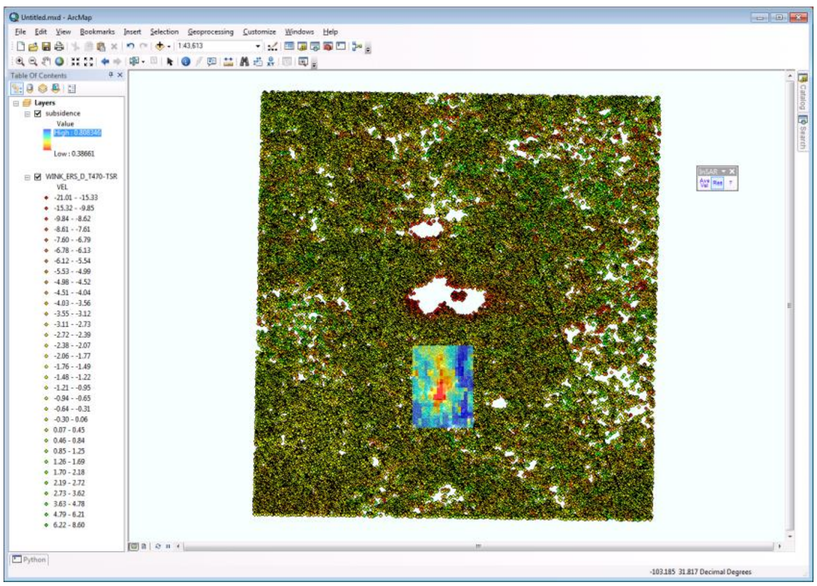

Figure 10 - Example of output from the subsidence ArcGIS add-in.

To this purpose, we couple the concept of matched filter and Hough transform to develop a spatiotemporal approach that could take advantage of the pointcloud nature of the SqueeSAR datasets. The fundamental steps followed by this approach can be summarized in:

1. Define a spatiotemporal model describing the expected changes in crustal elevation due to the feature of interest (this approach is not limited to subsidence and can be extended to detect other type of modelled deformations that might be of interest). Given the differential nature of the persistent scatterer interferometry (SPI), what we are interested in detecting, hence modeling, are the changes to the local elevation rather than the actual shape of the feature of interest.
2. Identify the key parameters that regulates the model behavior. In the case of subsidence due to sinkholes, some of the parameters of interest are size, orientation, growth velocity, *etc.*

3. Quantize and define the limits of the parameter space
4. For each set of parameters in the parameter space, generate a template from the model
5. Search the dataset for regions (group of scatterers) whose spatiotemporal behavior matches the template.

In case of sinkhole developing in a karst terrain, the model we developed, based on measurements performed on existing sinkholes, is that of a Gaussian of fixed width linearly growing in time:

$$g(\boldsymbol{x}, t) = \alpha t \exp[-(\boldsymbol{x} - \boldsymbol{x_0})^2 / 2\sigma^2] \tag{1}$$

For more information about this model and the results of the analysis, please refer to the project website: http://viva-lab.ece.virginia.edu/foswiki/InSAR/WebHome

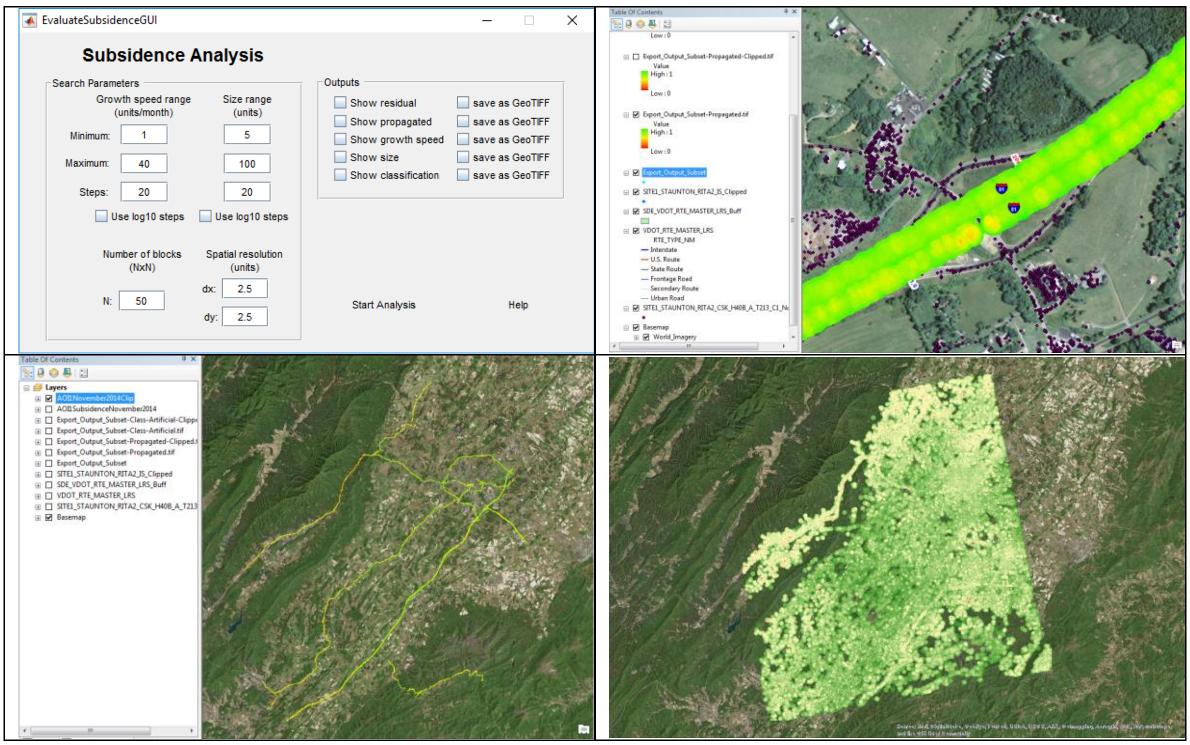

Figure 11 - Subsidence analysis application. User interface (top left). Result of analysis around interstate section (top right). Results over interstates and primaries in Area I (bottom left). Results over the entire Area I (bottom right). Warmer colors indicate potential subsidence development.

The main goal of the current project was to incorporate this a tool whose output could be easily incorporated within a decision support system. To this purpose we followed two routes. The first approach was to develop an ArcGIS add-in (Figure 10). The documentation on how to install and use this add-in is included in Appendix F.

After testing the developed ArcGIS implementation of the subsidence detection algorithm, we came to the conclusion that this format (ESRI ArcGIS add-in) did not provide a sufficient level of flexibility. One of the shortcomings of this approach was the fact that the analysis had to be run in foreground due to restrictions imposed by the

ArcGIS environment on the execution modality. This proved to be quite a limitation since areas containing regions with high scatterer density might require substantial execution time during which the ArcGIS environment would be locked, preventing the user from executing further tasks. Furthermore, the first version of the add-in, did not allow for fine tuning of the analysis parameters. Both the issues were addressed by converting the ESRI ArcGIS add-in into a more flexible external standalone application that could be fine-tuned without the restrictions imposed by the ArcGIS environment. The flexibility provided by this approach also allowed for a better integration with the web-based DSS.

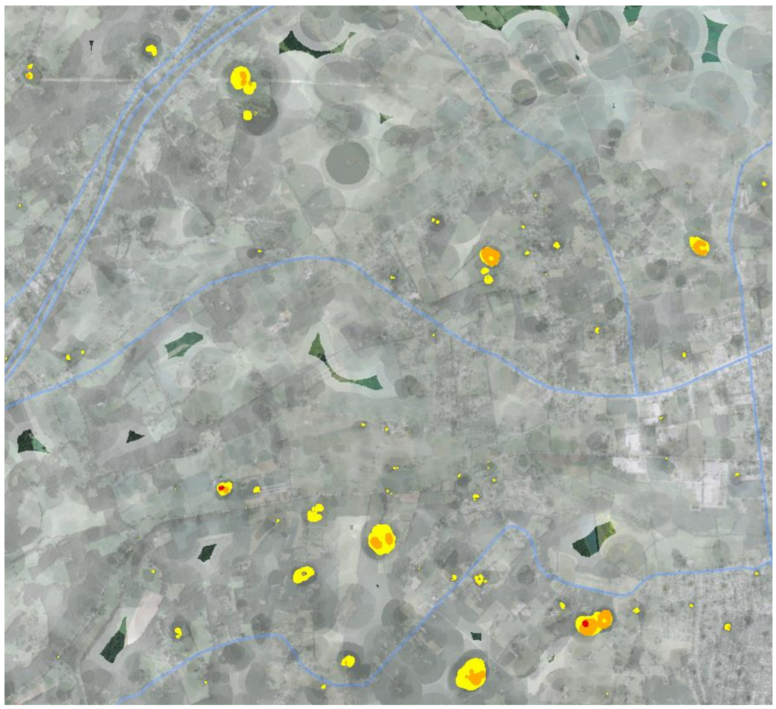

Figure 12 – Detail of post processing of subsidence analysis results within the ArcGIS environment. The gray scale image represents the results of the subsidence where the darker color indicates a higher degree of match with the subsidence model. The blue lines identify the primary roads in the region while the yellow, orange, and red areas indicate the top match identified by the subsidence algorithm.

The standalone application was designed to allow the user to have fine control on the analysis parameters while producing results seamlessly importable within the ArcGIS environment (Figure 11). The various output resulting from the analysis can be directly visualized within the application environment or exported as geo-referenced TIFF files. These files can be easily imported into ArcGIS for further analysis. For example in Figure 12 we show the top subsidence detections at the network level whereas in Figure 13 we show an example of integration with other layers. This is a section of I81 near which two top subsiding (yellow) regions were identified. In this case the other layer that were imported in ArcGIS to better analyze the area were the SqueeSAR (point features) and another raster layer including the temporary scatterers. By combining all these layers, it was possible to determine that some movement was occurring on the shoulder of the northbound lane of the interstate. It is interesting to notice that the sensitivity of the measurement allowed the clear detection of movements as small as half an inch (red dots region in the top right corner).

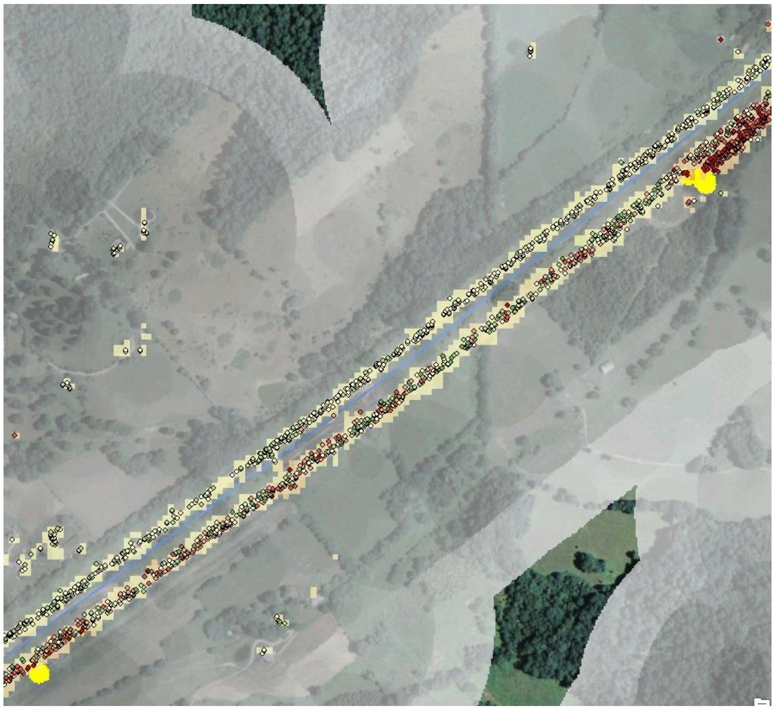

Figure 13 – This figure is a snapshot of an area of I81 where some subsidence activity was identify along the interstate (yellow and orange area in the bottom left and top right corner). This image show how several layers can be combined within ArcGIS to facilitate the decision making process by providing a wide set of focused information about a specific location.

The current release of the subsidence analysis application and links to the publications explaining the core algorithm are now available from Github and the project website. The plugin software was packaged as a standalone executable for both Windows- and OsX-based (Macintosh) machines. The target of the analysis can be an entire region, a road network, or smaller section of interest.

Bridge motion analysis

The Bridge Movements tool is needed for detecting conditions of bridges that are part of our extensive road networks. Currently, bridges are monitored in the same way that roads are monitored - physical inspection by transportation employees. Even with frequent inspection, problems often go undetected, leading to catastrophic bridge collapse. Bridge deterioration is arguably more dangerous than road disrepair, as bridges are often elevated structures with no support underneath. A collapse of a large bridge over a body of water or even other roads can be disastrous, leading to many deaths and millions of dollars in damages. We want to prevent these disasters before they occur. The Bridge Movements toolbox allows for remote monitoring of bridges that can be performed any time new satellite data is collected. This toolbox can accurately measure conditions for any bridge, and these results can be verified by on ground personnel.

Figure 14 - Example of auto-zoom to critical detection.

The Bridge Movements plug-in ArcGIS uses SqueeSAR data along bridges to detect vertical movement. These are the steps performed by the toolbox:

1. A shapefile of bridges, shown in Figure 15, is used with the SqueeSAR data points for analysis. Data points on the bridges are selected.
2. First, the points on a bridge are compared by height. The median height is taken for all points on a selected bridge. Then, all points within the selection are compared to this median height. Any points 3 meters or more below or above the median height are assumed to be on the road beside or below the bridge, and are removed from the selected data.
3. There are two thresholds used in the Bridge Movements toolbox: the warning threshold and the critical threshold. The critical threshold is movement at or above 0.5 inches per month. The displacements from month to month are used to calculate velocities for each month (for each point.) If any of these monthly velocities exceed 0.5 inches per month, then the critical alarm is raised, and the bridge is colored red.
4. The monthly velocities are then used to calculate whether or not the points on the bridge exceed the warning threshold. The warning threshold is set to movement at or above 1 inch per year. To calculate whether or not the bridge is moving at this rate, the monthly velocities are aggregated. The median velocity is calculated for each point on an array of the points' monthly velocities. If any of these median velocities exceed 1 inch/year movement, then the warning alarm is raised.

5. While the toolbox is running, a dialog box appears (Figure 16), detailing the coordinates of each bridge, how many points are being analyzed, and the condition of the bridge: good, warning, or critical. To give a sense of runtime, analyzing 17 bridges takes about 16.4 seconds on a stock Dell i7 desktop with. The coordinates and conditions for each bridge are also saved in an output file that can be accessed for later investigation.
6. Coloring of the bridges is done according to a symbology file. Depending on the amount of movement over time, the bridges of interest are colored one of three colors: red, yellow, or green. If there is minimal movement, the bridge is colored green, signifying a bridge that is in good condition. If there is moderate movement, the bridge is colored yellow, signifying a warning that the bridge may be in poor condition.
7. The bridge most recently found in critical condition is zoomed to on the map after running of the Bridge Movements toolbox, as shown in Figure 14. Points on the bridge are labeled with their height (mm) and average velocity (mm/year).

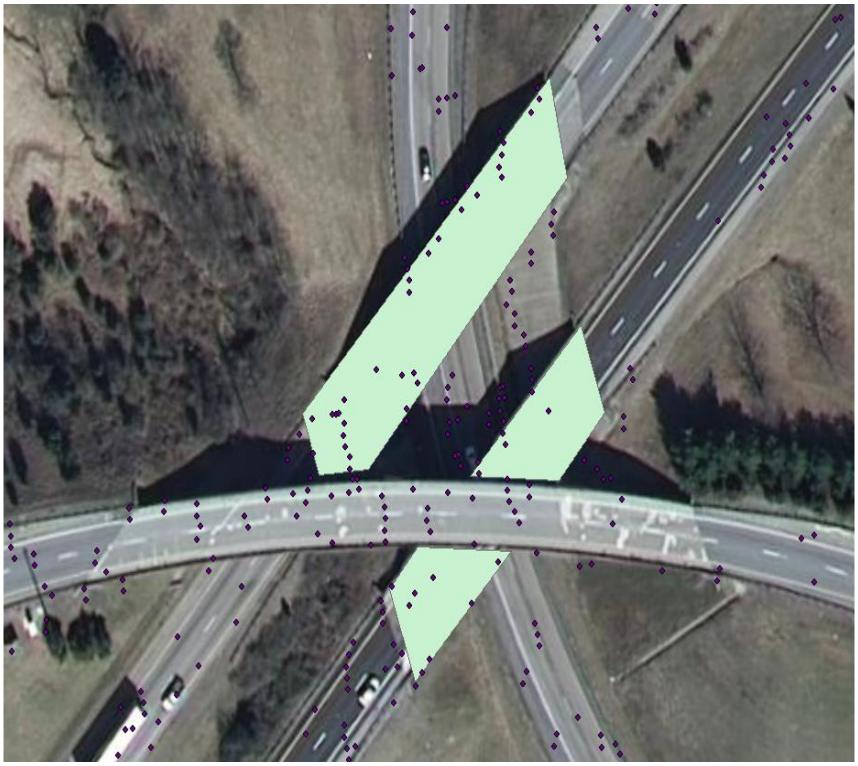

Figure 15 - Shapefile of bridges.

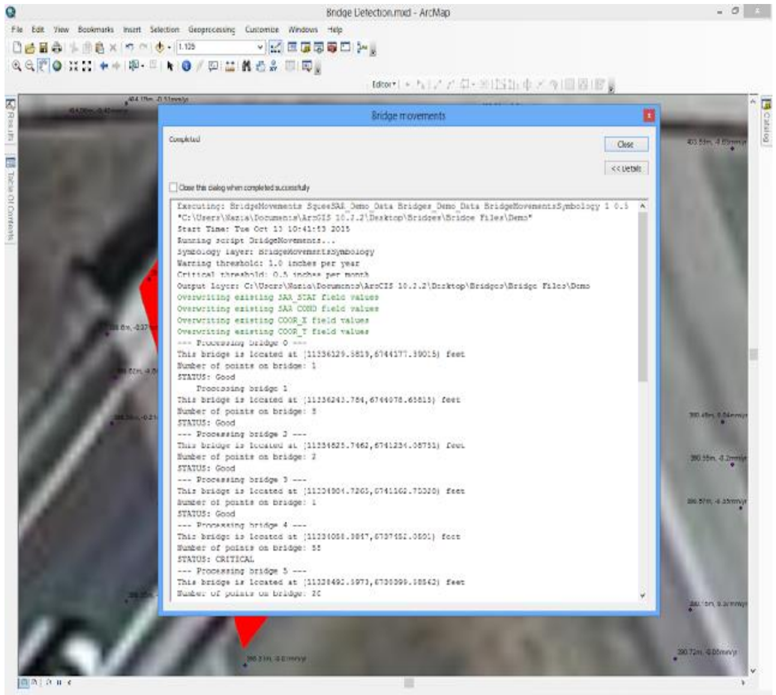

Figure 16 - Toolbox running.

To use the Bridge Movements toolbox, a shapefile of the bridges of interest must be created. When using the demo data, we have provided, you must save the folder containing the toolbox and the data in a convenient place. Open ArcMap and navigate to where you have saved the toolbox. First, drag the data files (the SqueeSAR layer and the bridge shapefile) to your map. Then click the plus icon next to the toolbox name to reveal the Bridge Movements tool underneath (Figure 17). Double click on this tool.

A dialog box will pop when the tool is double-clicked (Figure 18), with fields that can be filled out. The first field is the layer containing the SqueeSAR data layer. Next is the shapefile containing bridges of interest. The fields for the critical and warning thresholds are also provided, filled in with the suggested parameters. These can be tweaked according to user preferences. The output field can be filled according to where the user wishes the output file to be placed. Click OK, and the tool will run.

Two points to make about troubleshooting the plug-in. The file should not be placed in the Default GDB directory as using this directory with the current version of the toolbox results in errors. Also, if you have placed the toolbox in a Dropbox or any other type of syncing folder, please turn off the sync functionality of this folder before running the tool. Otherwise, the fields in the output will not be updated and the tool will not complete running.

The output file can take the form of a shapefile that can be viewed within ArcMap, or a GeoJSON file that can be used with a web interface. The locations of critical and warning bridges can be noted and physically inspected.

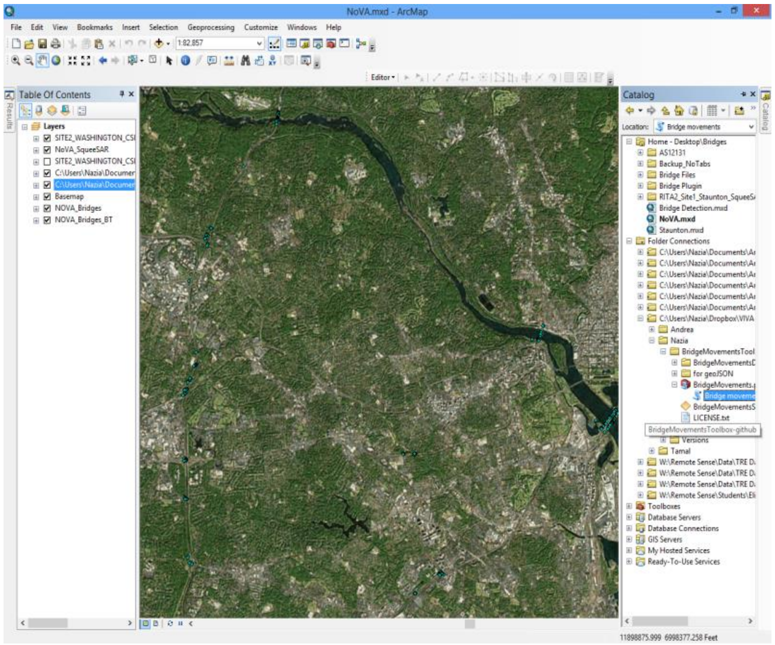

Figure 17 - Locating the tool.

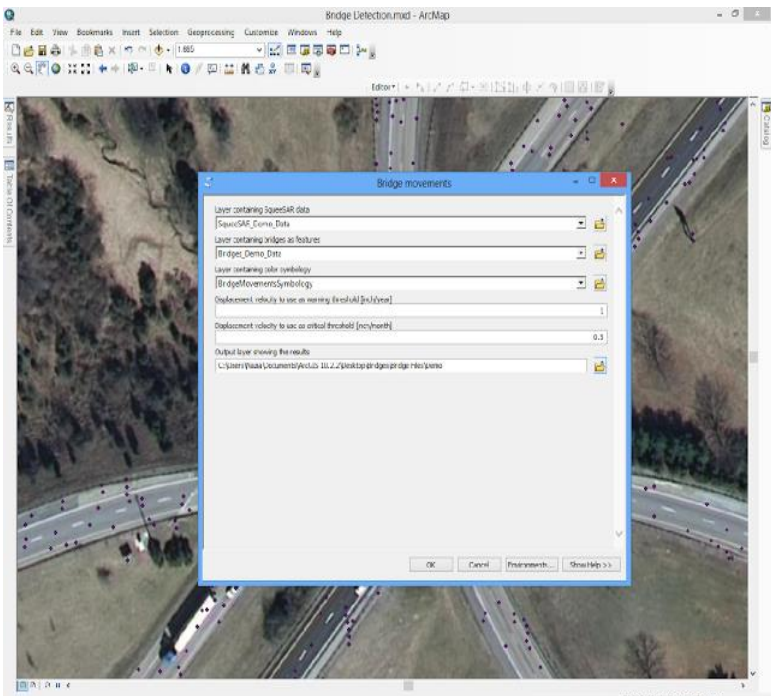

Figure 18 - Toolbox dialog.

Figure 19 and Figure 20 show examples of the bridge analysis toolbox outputs.

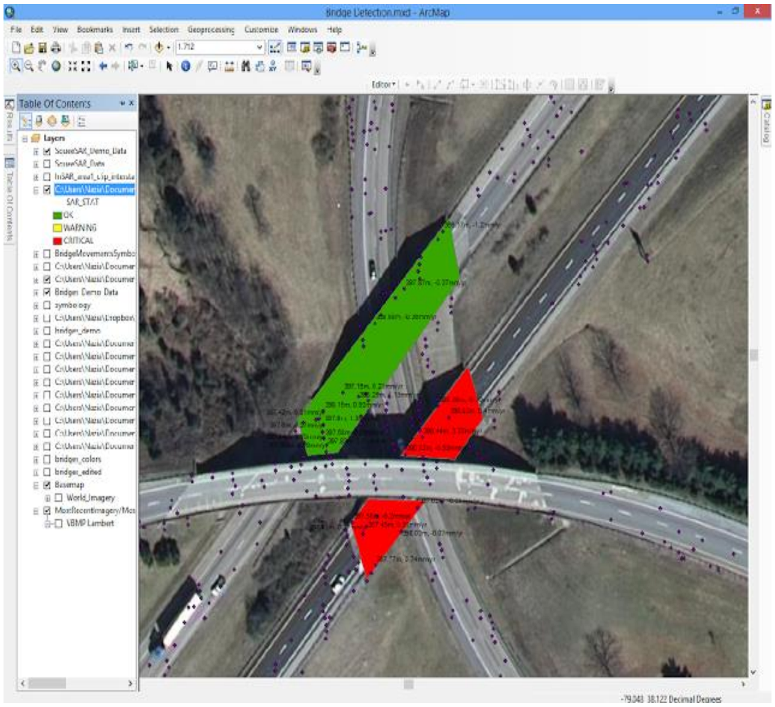

Figure 19 - Example of bridge analysis toolbox output.

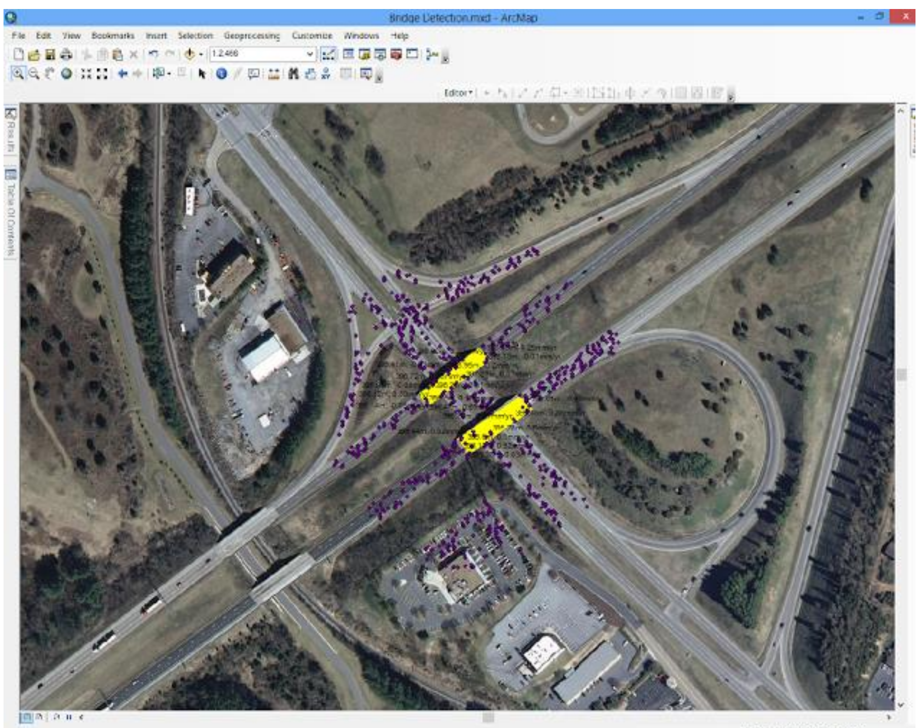

Figure 20 - Example of bridge analysis toolbox output.

Coherent motion detection

The coherent motion toolbox primarily aims at obtaining the elevation map of a specific location over time. The map is useful for detecting local events (grooves/ruts on a road/pavement) as well as large-area events (subsidence/sinkholes). In addition, this tool can be used for detecting the trends of topological changes on the Earth's surface.

The tool works on each point (geolocations) independent of other points in its neighborhood. The output is a scalar quantity, called median velocity. As the SqueeSAR data contains both additive and multiplicative noise drawn from unknown distributions, the median operation attempts to eliminate it and gives an approximate trend of displacements of a point over time.

This tool is scale-free, so it can be used for both local (pavement rut) and more extended (rock slope failure, sinkhole) analysis. The potentially "warning" and "critical" zones are detected using a threshold on median slopes. Care MUST be taken in the proper selection of thresholds. For a temporally slow activity (sinkhole), the thresholds must be on lower side of median slope. Otherwise, slow changes will be overridden and undetected by a locally-fast movement. Therefore, prior to using this tool, selection of the zone/area is expected to be done using selection tool in ArcGIS. Automatic detection of SqueeSAR points on building or construction areas is not developed inside the tool. So, there are false positives on construction areas and others. Below is the list of figures on

- Coherent Motion Toolbox location (Figure 21)
- Coherent Motion Toolbox dialog box with side notes (Figure 22)
- Coherent Motion Toolbox output path selection (Figure 23)
- Coherent Motion Toolbox output (Figure 24)

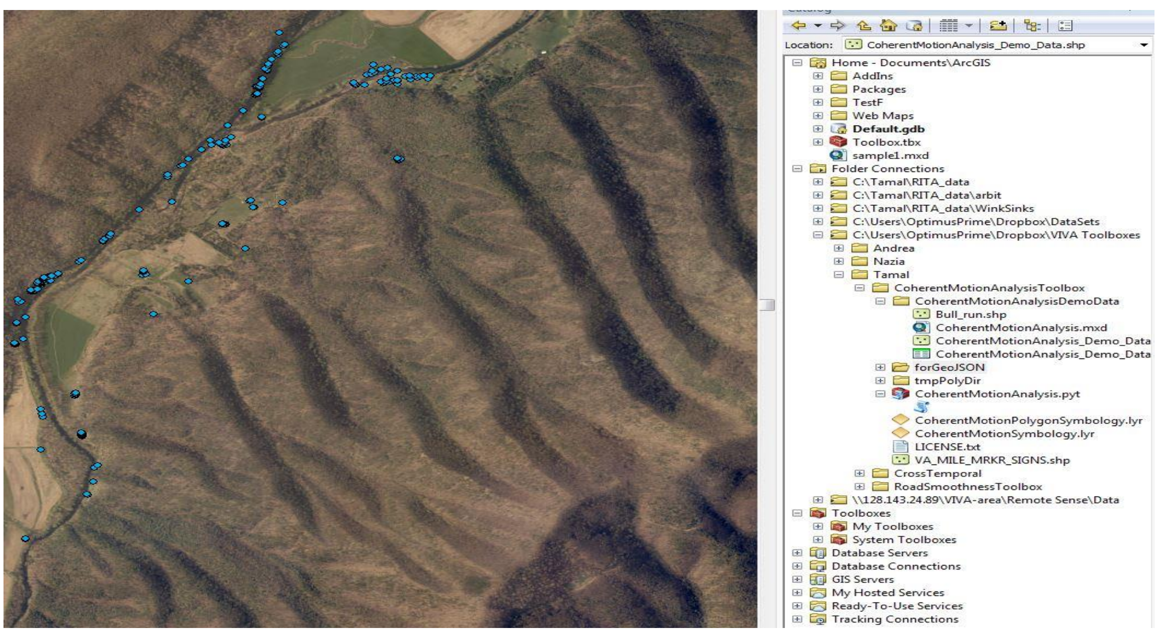

Figure 21 - Toolbox location with a demo data (CoherentMotionAnalysisDemoData) and Tool (CoherentMotionAnalysis.pyt). Click the blue icon in the tool.

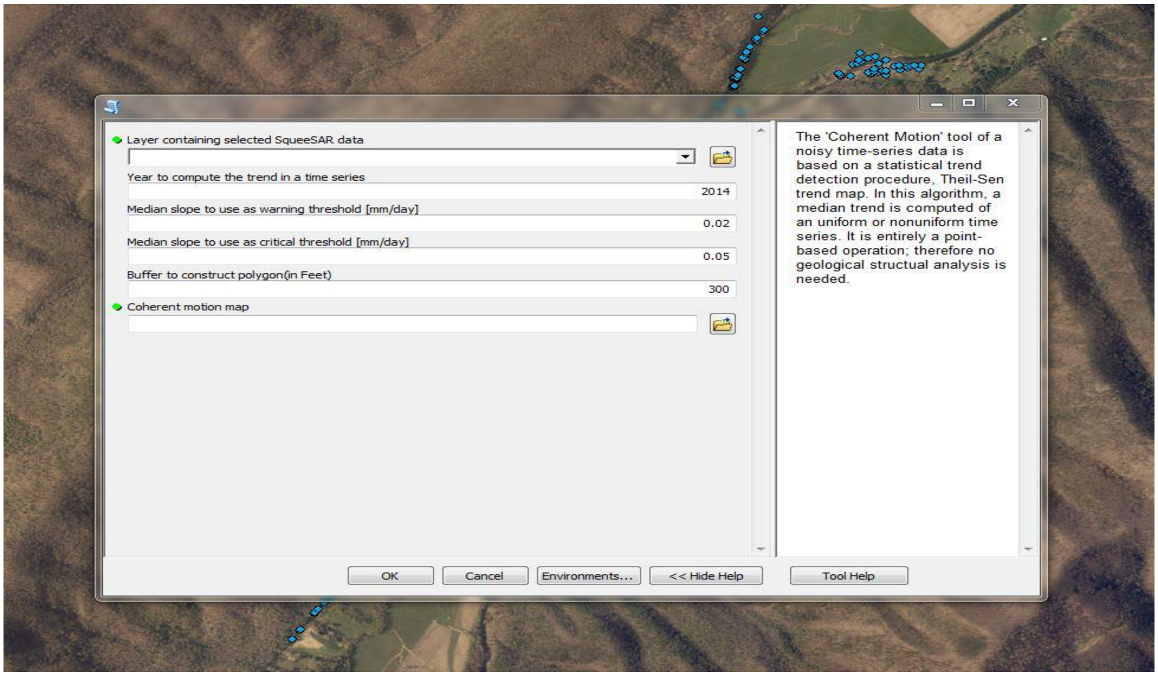

Figure 22 - Tool dialog box with side notes. The output is in "coherent motion map".

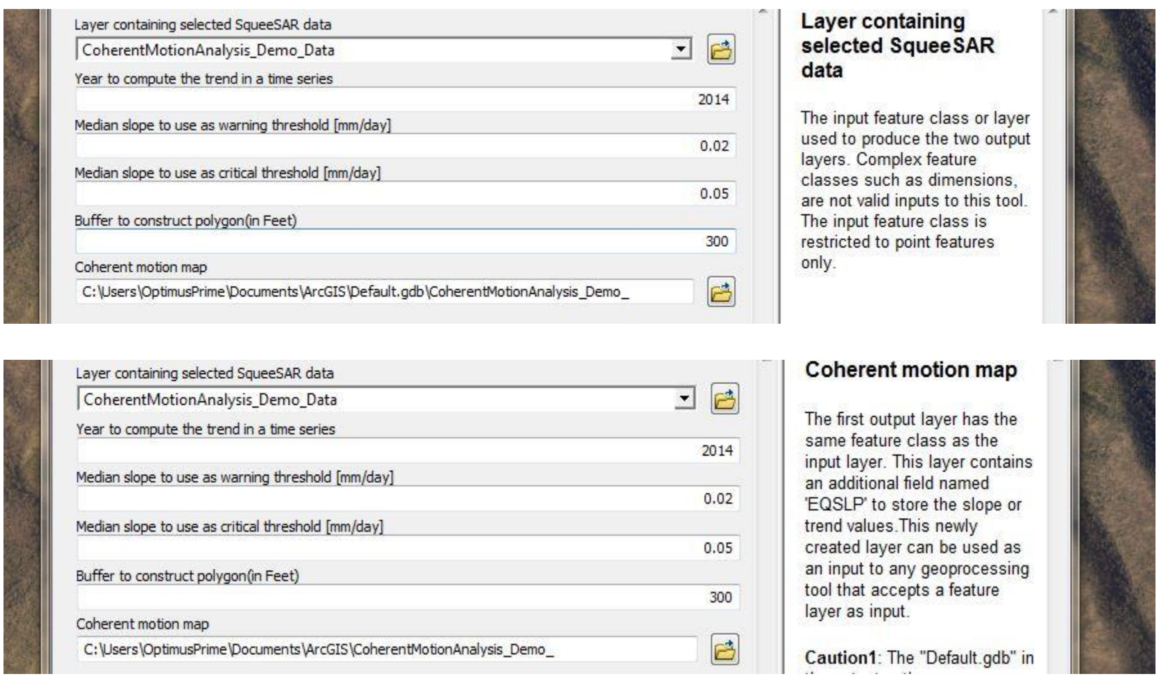

Figure 23 - The address in "coherent motion map" field is changed by manually deleting "Default.gdb" from the top one. Check Caution 1 below.

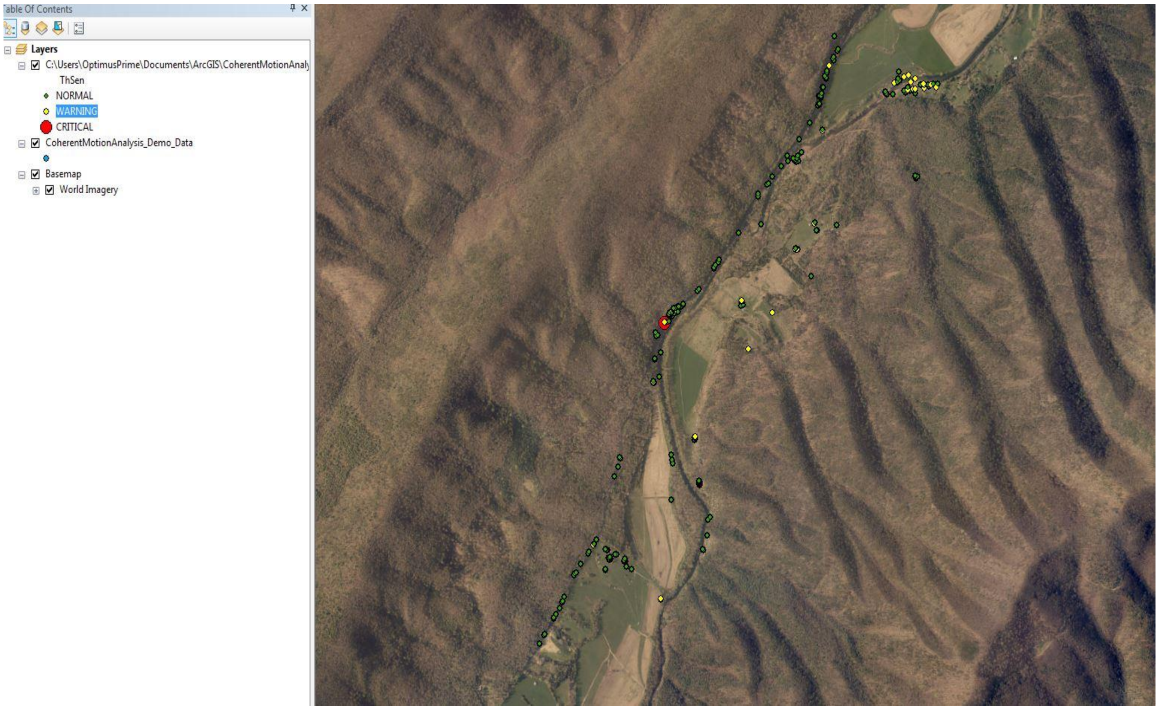

Figure 24 - The output of coherent motion toolbox. The input file is “CoherentMotionAnalysis_Demo_Data” and the output file is “C:\Users\..”. Yellow markers indicate “Warning” and red “Critical”. This is an impending slope failure on route600.

Caution:

1. The address path of output file pops up automatically depending on the environment (of ArcMap) settings. If the output file address path is “…./default.gdb/output.shp”, then manually erase “default.gdb”, which results into the output path “…/output.shp”. This deletion will ensure the output shape file(s) to show up in the “Table of Contents”
2. If the input and output shapefile locations are in a virtual storage (e.g. Dropbox, Google drive, *etc*.), make sure to turn off /pause sync. Otherwise, an error flag will pop up.

Road smoothness analysis

Road smoothness is a graph-based tool in a sense that it measures the behavior of a group of points/locations over time. In this method, a neighborhood of a point is selected first based on a distance threshold (scale). As the points are in general irregularly sampled, a graph framework is employed to perform the analysis. Therefore, the SqueeSAR points in the neighborhood are modeled as a set of vertices of a graph. A graph can be connected in numerous ways. For computational ease, we consider only fully-connected simple undirected graph. The connectivity is hard-coded in the package. Each point/location has a time series of displacements (in mm), which is considered as a signal on the point. Moreover, each edge weight is considered to be a function of inverse Euclidean distance between two SqueeSAR points that are connected by the edge.

Once the graph is constructed, a dimensionless quantity, called the smoothness value is computed at each time point. Low smoothness value indicates that the group of points moves up/down in similar fashion keeping the surface locally smooth. On the other hand, a high smoothness value can be directly correlated with the roughness of the surface.

Larger scale analysis encapsulates more points than such an analysis at a smaller scale. Because of the fact that the computation of smoothness is a weighted average operation, the value for large scale drifts towards low smoothness triggering false alarm about the road condition. On the other hand, points within a smaller scale (e.g. points on a crack of a surface) may not trigger the actual status flag. Therefore, flexibility is given to experiment with different scales, and thresholds to find a suitable status of road smoothness.

Dialog box: The toolbox takes a shapefile as an input. To investigate a predefined region, the region is preferred to be selected first or may be cropped as a separate shapefile. Next, a time point would have to be set from the drop-down list to visualize the smoothness. If not selected, a default time point is preset. This is followed by a scale selection. A default value is also provided there. To identify and thereby categorize potentially ‘Warning’ and ‘Critical’ neighborhoods, there are warning threshold and threshold in the dialog box. Default values are provided, which are tested based on the ground truth data provided by on-site personnel. The toolbox outputs two separate shapefiles with different geometries. The first output shows the smoothness value at each points/geolocations. The second shapefile is of polygon geometry giving the warning and critical tagged clusters. Below is the list of figures on

- Road Smoothness Toolbox location (Figure 25)
- Road Smoothness Toolbox dialog box with side notes (Figure 26)
- Road Smoothness Toolbox output path selection (Figure 27)
- Road Smoothness Toolbox output (Figure 28, Figure 29, and Figure 30)

Figure 25 - Toolbox location with a demo data (RoadSmoothnessDemoData) and Tool (RoadSmoothness.pyt). Click the blue icon in the tool.

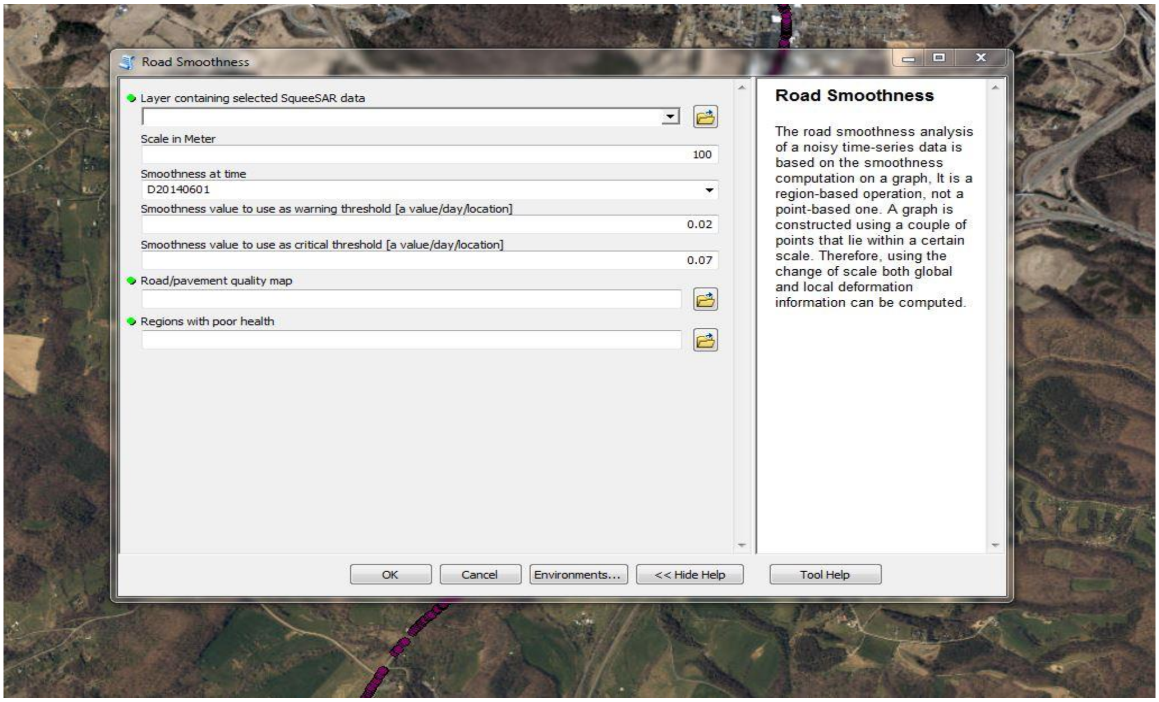

Figure 26 - Tool dialog box with side notes. The outputs are in "Road/pavement quality map" and "Regions with poor health". Default values are provided.

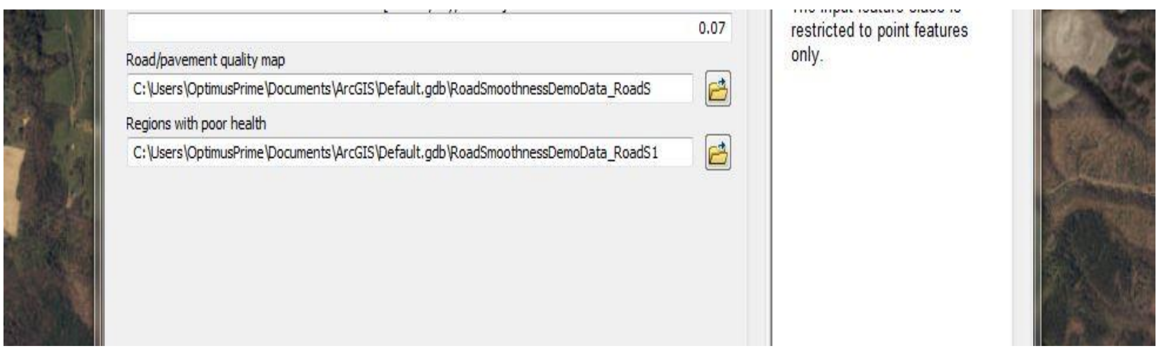

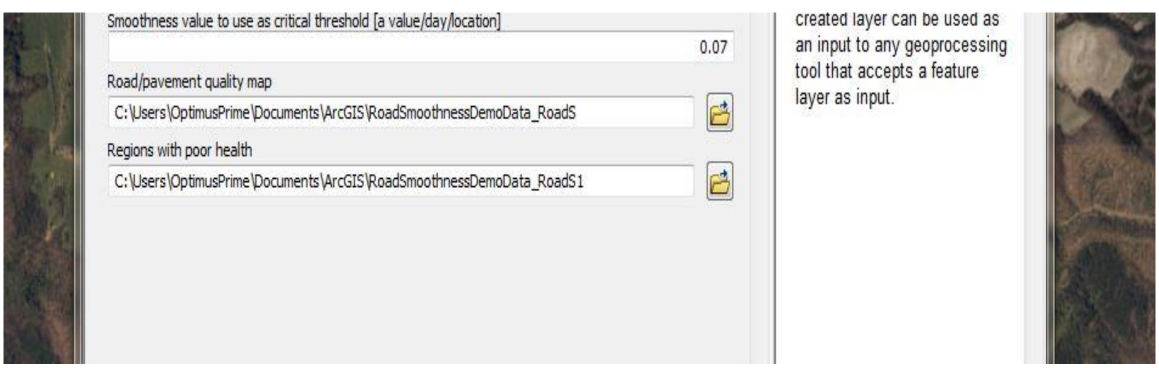

Figure 27 - The addresses in "Road/pavement quality map" and "Regions with poor health" fields are changed by manually deleting "Default.gdb" from the top one. Check Caution 1 below.

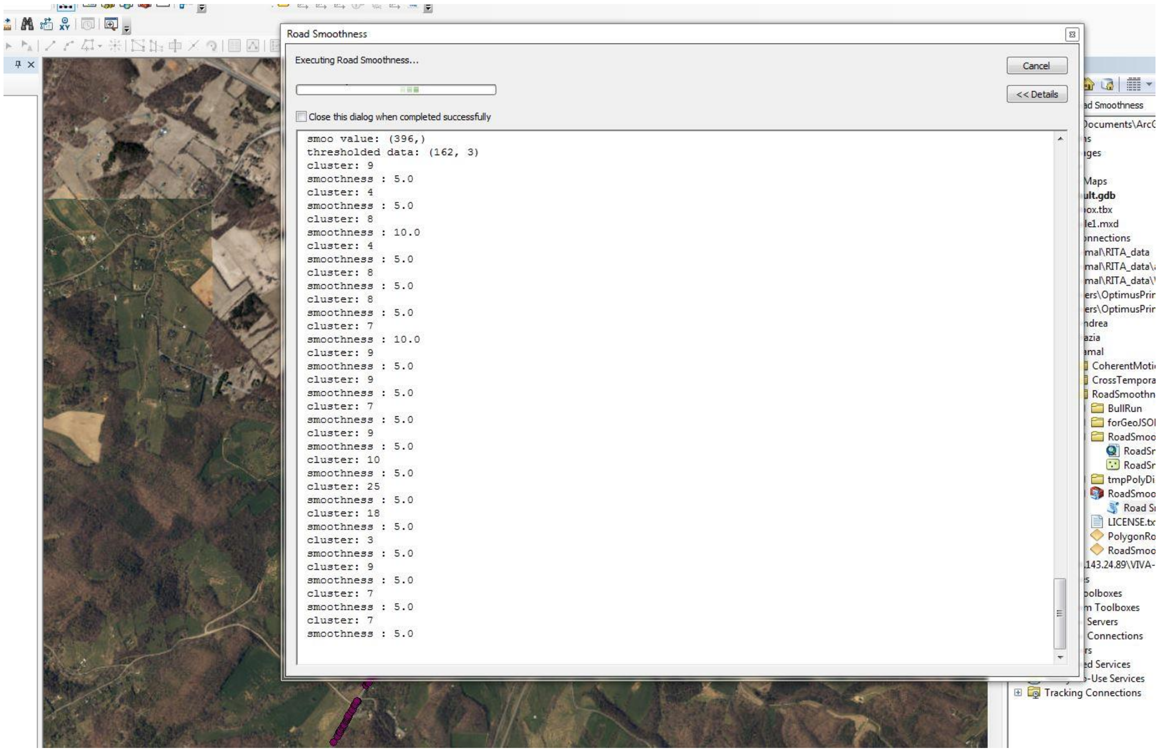

Figure 28 - Running dialog box with smoothness values shown for each neighborhood/cluster.

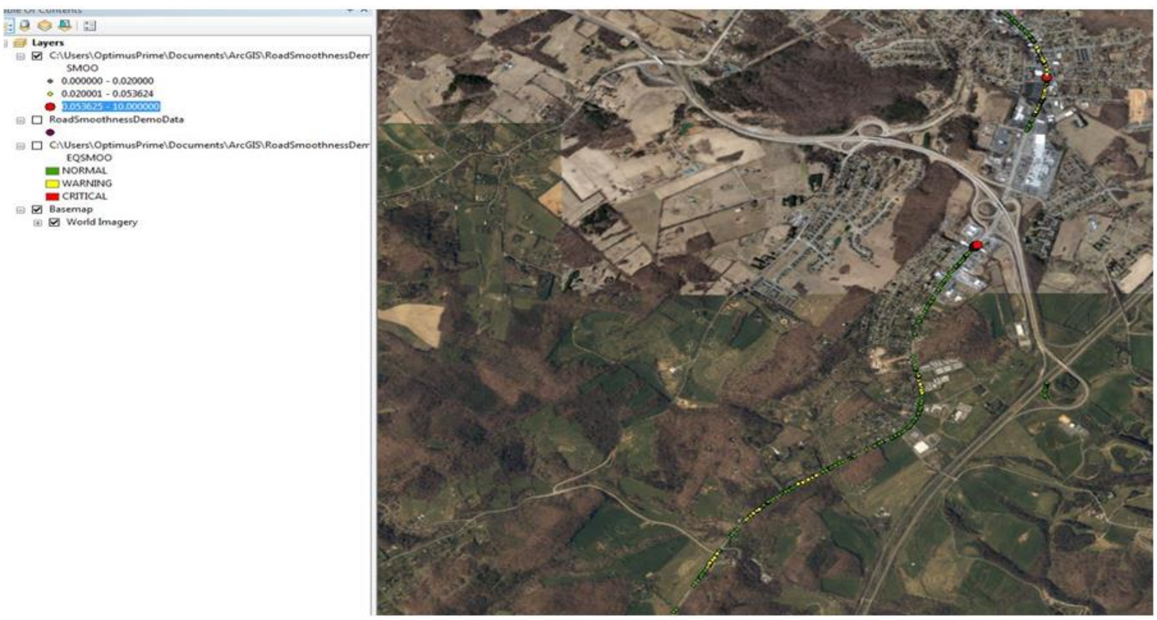

Figure 29 - The output of road smoothness toolbox. The input file is "RoadSmoothness_Demo_Data" and the output file shown here is "C:\Users\.." with "SMOO". Yellow markers indicate "Warning" and red "Critical" status.

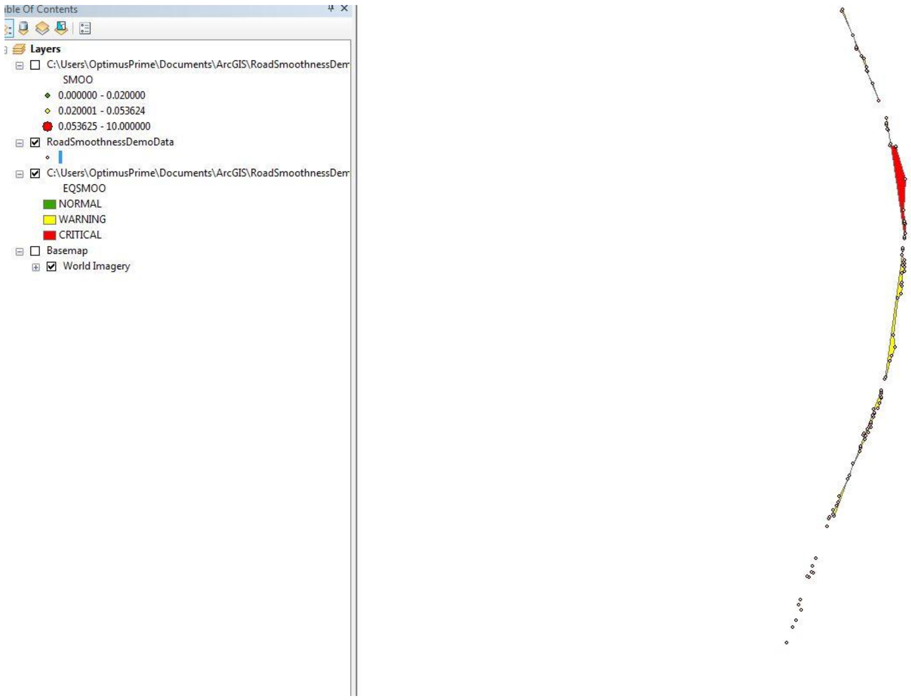

Figure 30 - The output file shown here is "C:\Users\.." with "EQSMOO" (a polygon layer). Yellow markers indicate "Warning" and red "Critical" status of polygons/clusters.

Caution:

1. The address path of output file(s) pops up automatically depending on the environment (of ArcMap) settings. If the output file address path is "…./default.gdb/output.shp", then manually erase "default.gdb", which results into the output path "…/output.shp". This deletion will ensure the output shape file(s) to show up in the "Table of Contents".
2. If the input and output shapefile locations are in a virtual storage (e.g. Dropbox, Google drive, *etc*.), make sure to turn off /pause sync. Otherwise, an error flag will pop up.

Amplitude images: pavement changes detection and absolute road quality quantification

Subcontracted by VDOT and in collaboration with both TRE and UVA, the team at University of Alaska Fairbanks (UAF) was tasked to analyze the role to Temporary Scatterers (TS) in a transportation infrastructure setting. The contract was then extended to evaluate the benefits of using SAR amplitude information tor transportation infrastructure monitoring as well as the development of an outreach plan for communication the benefits of InSAR to the DOT community (this part of the work will be addressed in the section: CHAPTER 6: TEAM MEETINGS, OUTREACH AND EDUCATION). The main findings are summarized below. For the complete report, please refer to Appendix G.

Motivated by the strong belief that SAR amplitude information carries relevant, yet typically untapped potential in transportation infrastructure monitoring, and that amplitude analysis requires less specialty knowledge about the SAR image formation process making it easier to implement by end-users such as DOTs, a research was carried to identify potential correlation between pavement quality and changes and SAR amplitude values.

The research showed that amplitude values from high resolution X-band (8-12GHz) sensors such as TerraSAR-X, TanDEM-X, and Cosmo-SkyMED, can indeed be used for:

1. Detecting changes in surface condition on roads, by leveraging the time-series analysis (trend) of the amplitude values
2. Measure absolute road surface condition when quantified by the International Rouchness Index (IRI). Best performance in this case was achieved when measuring secondary roads where higher levels of deterioration were observed.

CHAPTER 4: GEOGRAPHICAL INFORMATION SYSTEMS (GIS) AND DECISION SUPPORT SYSTEM (DSS) DEVELOPMENT

In this project, we provided two parallel approaches to the development of a DSS including the InSAR data. The first approach leverages the ubiquitous presence of ArcGIS within DOTs as well as the development of the novel ArcGIS Online for Organization platforms. The second approach is based on a web-app which does not required any special software a part from a standard web browser, which is now routinely shipped with any operating system.

ArcGIS Online for Organizations

The ubiquitous presence of ArcGIS within most of the organizations (mainly DOTs) that might be interested in including InSAR data within their decision-making process, makes it the ideal platform for data aggregation. With the appearance of the new ArcGIS Online for Organizations (AGO) product (available to all the owners or ArcGIS), several of the main issue of distribution of data and availability on mobile platforms were addressed.

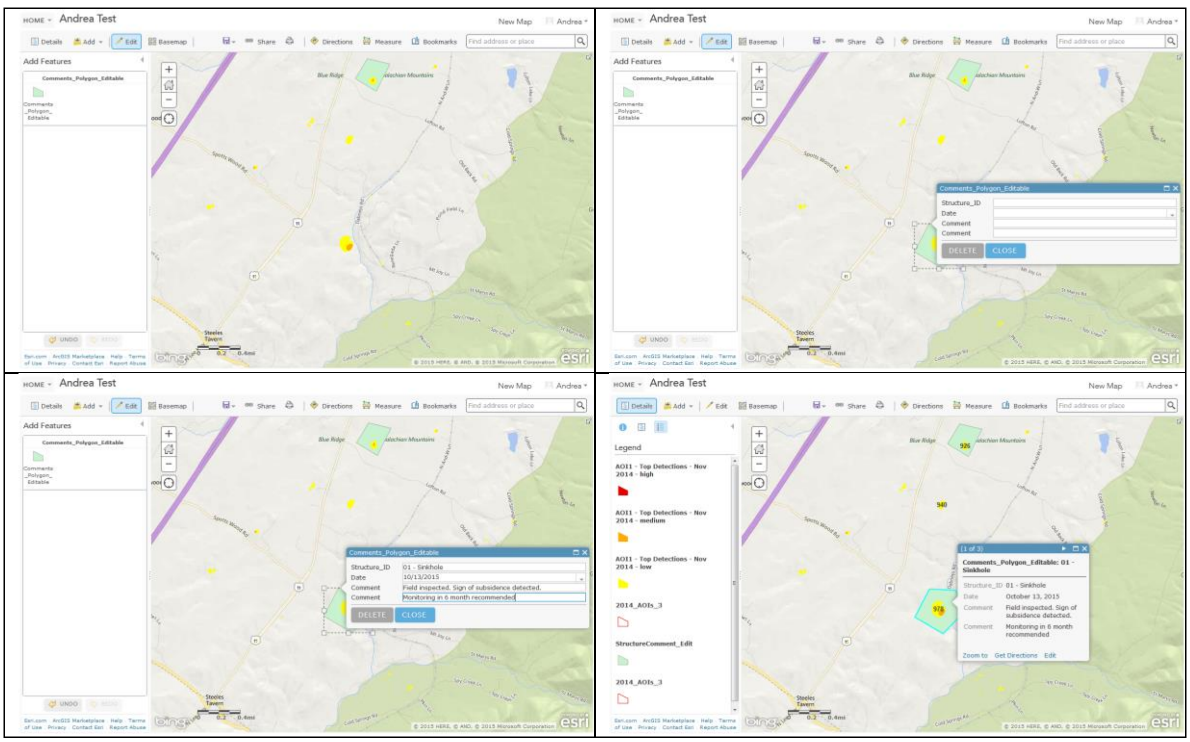

Figure 31 - Example of data flow within the ArcGIS Online environment.

We developed and tested a typical data-flow scenario where the InSAR data, preprocessed by the data provider (TRE) was delivered to the project teams as shapefiles stored within a special group defined within the AGO environment used by VDOT. VIVA, using the tools described above, analyzed the data and created final products identifying regions of interest. These products were once again posted on AGO in the form of either shapefiles or geo-referenced TIFF images. VDOT was able to import these products and, not only visualize them within their exiting environment, but also integrate them with newly developed occurrence models for karst and slope geohazards (Todd, 2014) to provide integrated datasets that were used for decision regarding, for example, the placement of storm water management stations (Brian Bruckno, 2015).

The use of the AGO environment allows for the data to be instantaneously available to subscribing users. Several different groups can be created and, based on the group privileges, different data can be delivered and/or different level of access granted. In Figure 31 we show an example of how the results of an analysis can were integrated and distributed allowing end user to both visualize the data and, if authorized, add comments. This would prove an incredibly flexible tool were different users, from the maintenance manager, to the geologist that performed the geohazard analysis, all the way to the ground crew that inspected the location, could enter comments to highlight issues or create a maintenance log. In the top left of the figure, we show a screenshot of the AGO interface, accessed through a web browser, where a subset of the top detections of the subsidence analysis conducted over the Staunton data (see previous report) are displayed. This is an example on how data can be distributed to any authorized user. In the top right, a user that was enabled to enter comments, identifies a specific region and, according to a predefined form, enters the results, for example, of the field inspection (bottom left). The data entered in the form is instantaneously available to all the other authorized users (bottom right) decreasing the time to decision.

Since AGO is a web-based environment, all the basic operations described above, can be conducted on any mobile internet client without the installation of any third-party software. Figure 32 show an example of how the same data flow will appear on an Android device.

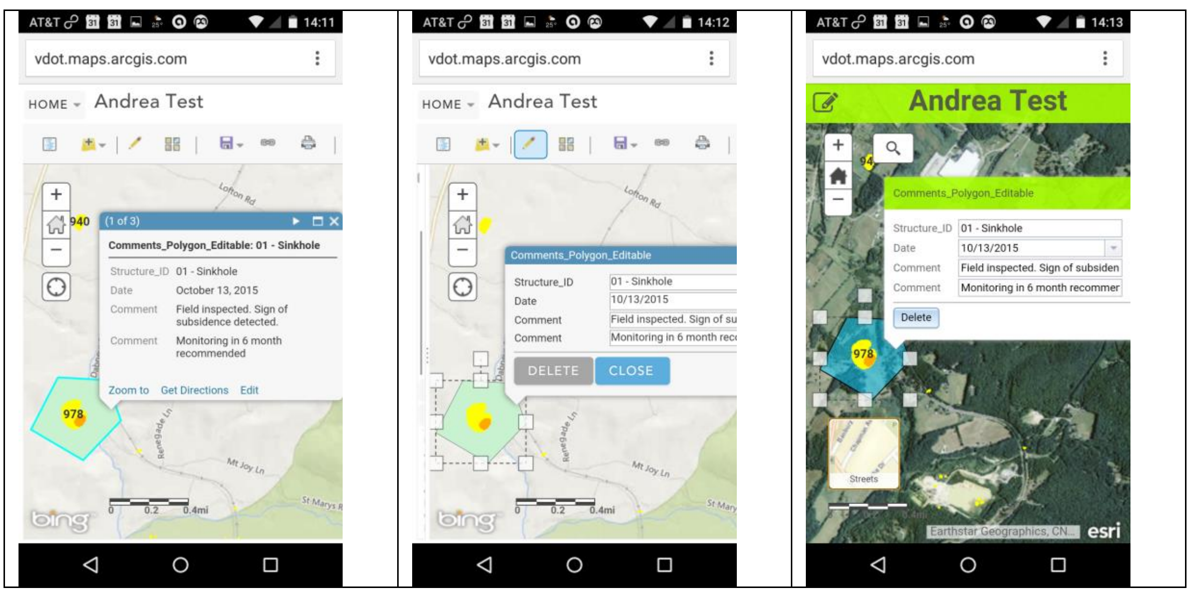

Figure 32 - ArcGIS Online data flow on Android device.

Details about installing and configuring ArcGIS Online to work as a cooperative framework from the introduction of InSAR data within existing ArcGIS environments, including details about its implementation within VDOT are included in Appendix H.

Network Level DSS Web Application

As previously mentioned, a parallel approach was followed to develop a standalone DSS based on freely available web-based tools. The basic idea behind this approach was to provide interested parties with a web-app that would allow them to experiment with the introduction and merging of InSAR and InSAR-derived data with existing dataset. In the case of VDOT, we provided a web-based GIS interface where the results of the analysis toolboxes described above could be visualized together with the existing pavement quality dataset.

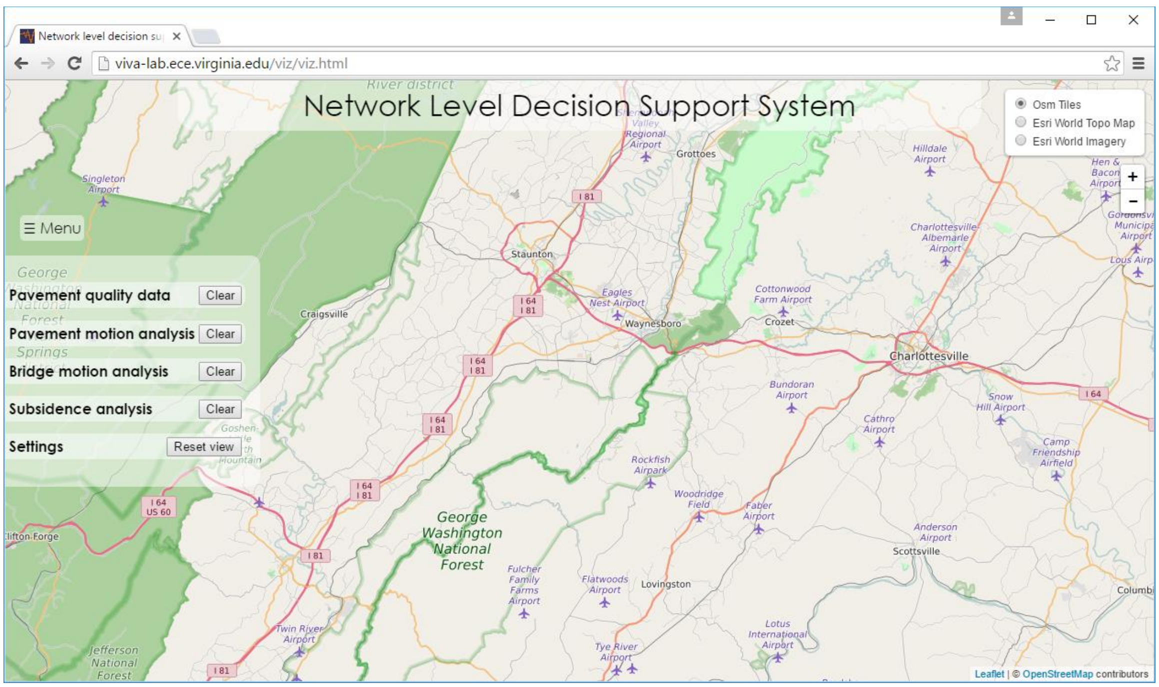

Figure 33 - Network Level DSS web application start up screen (as visualized by Google Chrome).

The web-app was developed in JavaScript (JS) making use of a few open source libraries: *leaflet (http://leafletjs.com)* the leading JS library for mobile-friendly interactive maps, *jquery (https://jquery.com)* a fast, small, and feature-rich JS library providing optimized access to HTML document manipulation, event handling, animation, and asynchronous Java access (Ajax) to large datasets, and *Chart.js (http://www.chartjs.org)* a simple and flexible JS charting library.

In Figure 33 we show the start-up screen centered on AOI1. Several option for the base map are available (top left corner). The base map is displayed using the standard tiling approach used by most mapping application hence it is easily extensible to include any standard base map a user might need. The menu on the left, typically hidden until selected, provide modular access to the results of the various analysis toolboxes as well as existing databases. In this example, we use the historic VDOT pavement quality data, with high resolution (0.1 miles), covering the satellite data acquisitions (2011-2015) to allow for direct comparison with the analysis results. The data format used by the application is *GeoJson (http://geojson.org)* a geospatial data interexchange standard format based on JS Object Notation (RFC7946). Since both GeoJson and shapefile are standards in the geospatial community, plenty of tools exists to convert the default output of our analysis toolboxes (shapefile) to the GeoJson format. For example, the basic license for ArcGIS for Desktop includes the *FeaturesToJSON_conversion()* function within the *conversion toolbox* that would allow a potential user to convert further data for easy inclusion within the DSS.

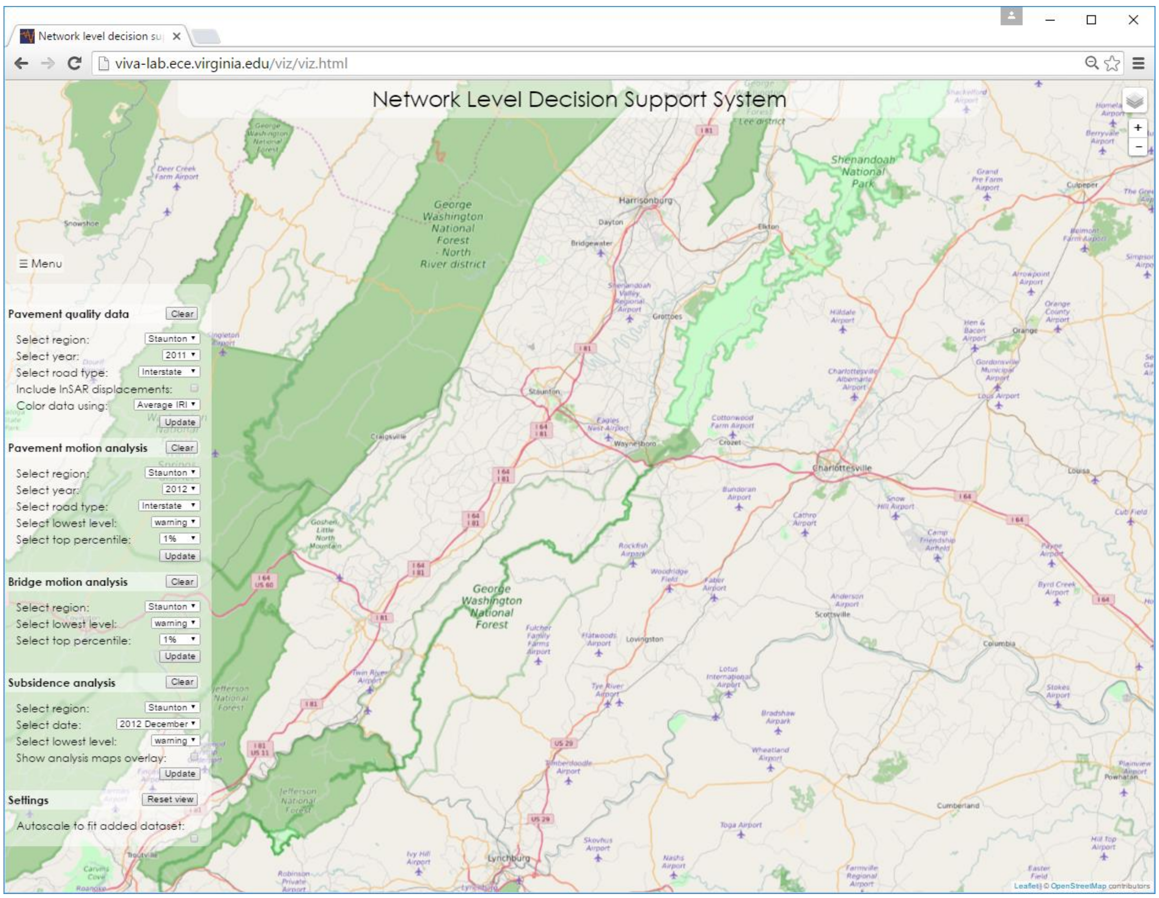

Figure 34 - Full expanded menus view.

As it can be seen in Figure 34, the current version of the DSS, a part from the *Settings* menu, includes other four datasets:

- Pavement quality data
- Pavement motion analysis
- Bridge motion analysis
- Subsidence analysis

Each one of this sections is implemented as a standalone module within the code and provides simple access to visualization options for the underlying data. Furthermore, each section is independent from the others so that they can be visualized simultaneously from a more accurate analysis of the overall situation of the transportation network.

Pavement quality data

This section allows the visualization of a high resolution pavement quality data database generated by VDOT each year. We have restricted the dataset to include the regions covered by the satellite (Staunton and NOVA), the years where satellite data was available (2011-2015), the type of road (interstate, primary, secondary, all) and two option for data coloring (IRI and CCI). All these parameters could be extended to include more data or more options depending on the user needs.

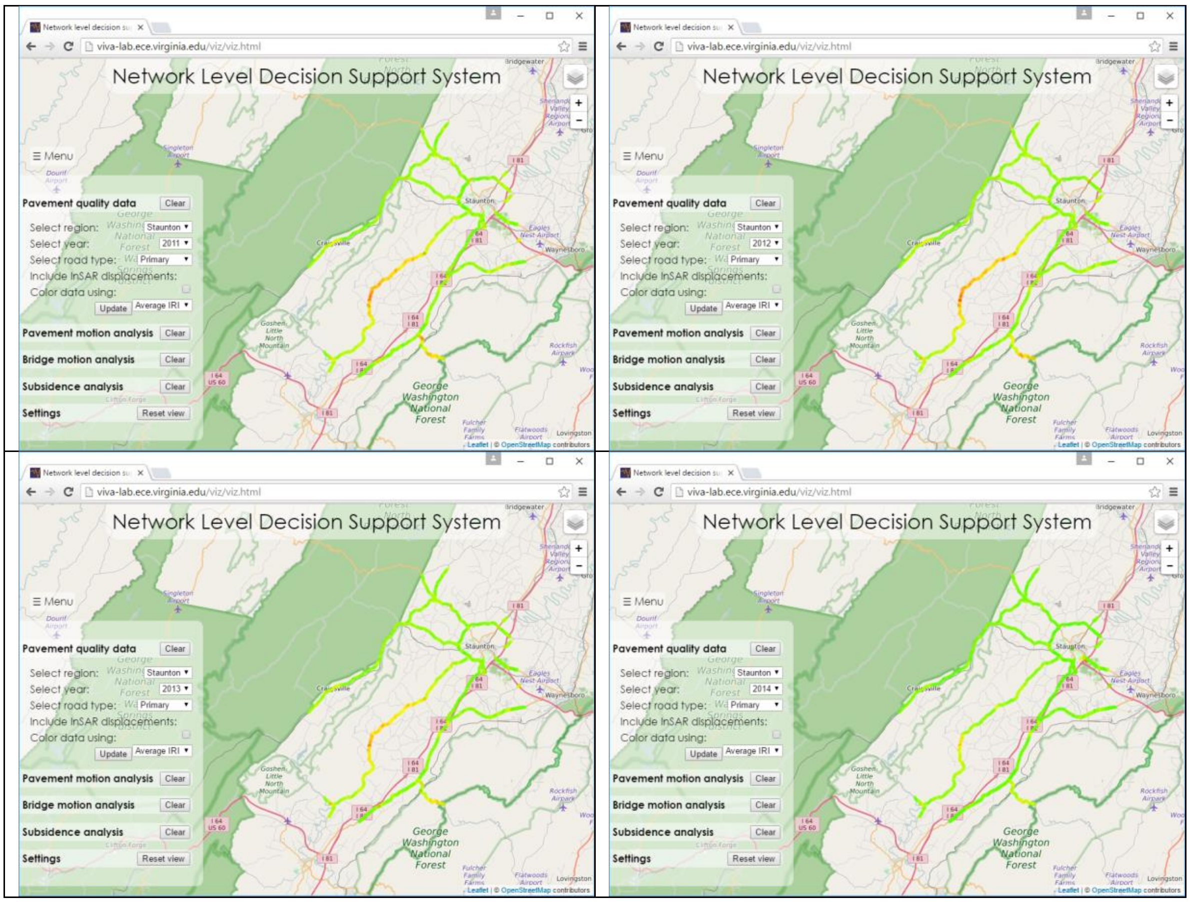

Figure 35 - Example of evolution of primaries pavement quality: 2011 (top left), 2012 (top right), 2013 (bottom left), and 2014 (bottom right).

The ability to visualize several years of data allows to identify regions where changes are occurring in the pavement quality. In Figure 35 we show and example where the pavement quality of the primary roads in AOI1 (Staunton) are visualized colored according the IRI (warmer colors indicated higher IRI corresponding to rougher road surfaces). It is possible to clearly notice that most of the warm colors slowly turn to green between 2011 (top left) and 2014 (bottom right) indicating a successful paving campaign.

The same approach could be used to quickly identify roads where the pavement is deteriorating.

To facilitate analysis of the pavement data, we have included the ability, for each 0.1 section of road, to list all the information included in the database as popup window. This is available by simply clicking on a section of the road and selecting the corresponding option. Furthermore, we have also added the option to visualize the Google Streetview for the selected location providing a direct visual inspection. In Figure 36 we show an example of both these features for a section of poor quality within AOI2.

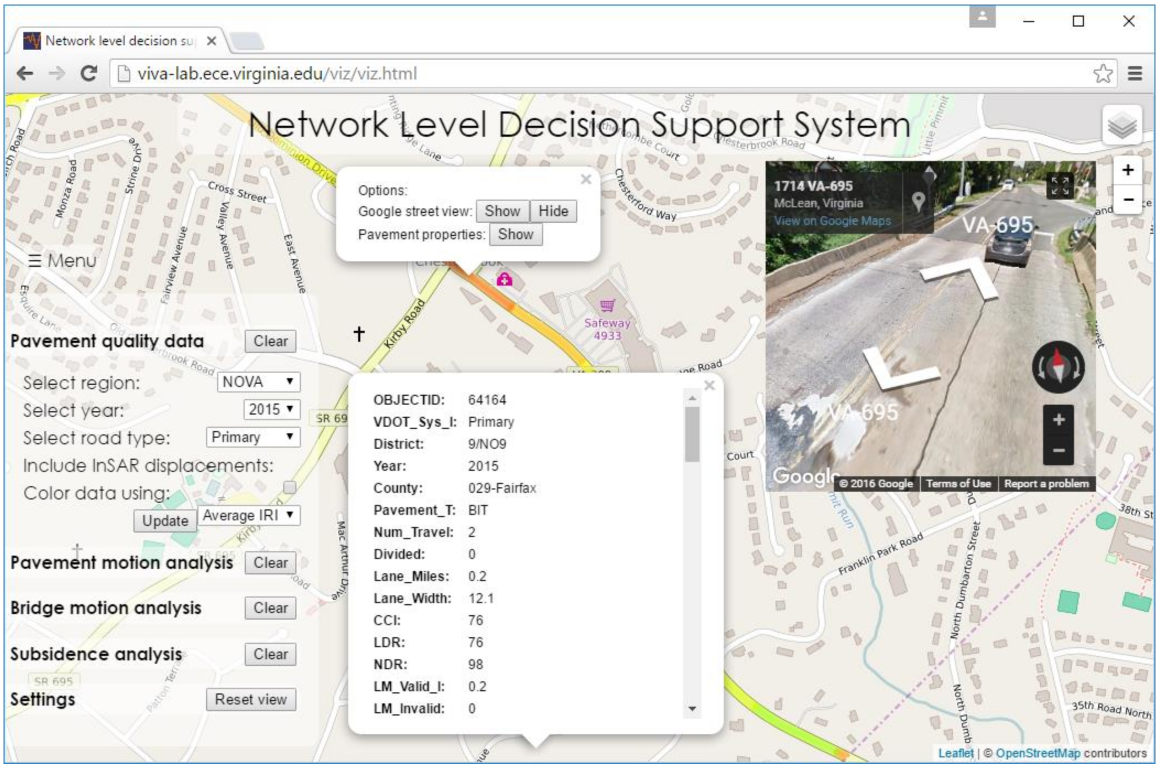

Figure 36 - Example of detailed information about pavement quality and Google Streetview.

To allow for a direct comparison with the satellite data, we included the option to merge the pavement data with the data obtained from the SqueeSAR analysis. This, to our knowledge, is the first time that such a rich dataset is made available. When the two datasets are merged, the map will visualize the scatterers identified along the roads and, for each of them, additional to the pavement data at that particular location and the Google Streetview, the SqueeSAR data is made available as popup window. Furthermore, we provided a facility that allows the user to visualize a chart showing the time series of the measured displacement as an overlay chart (Figure 37).

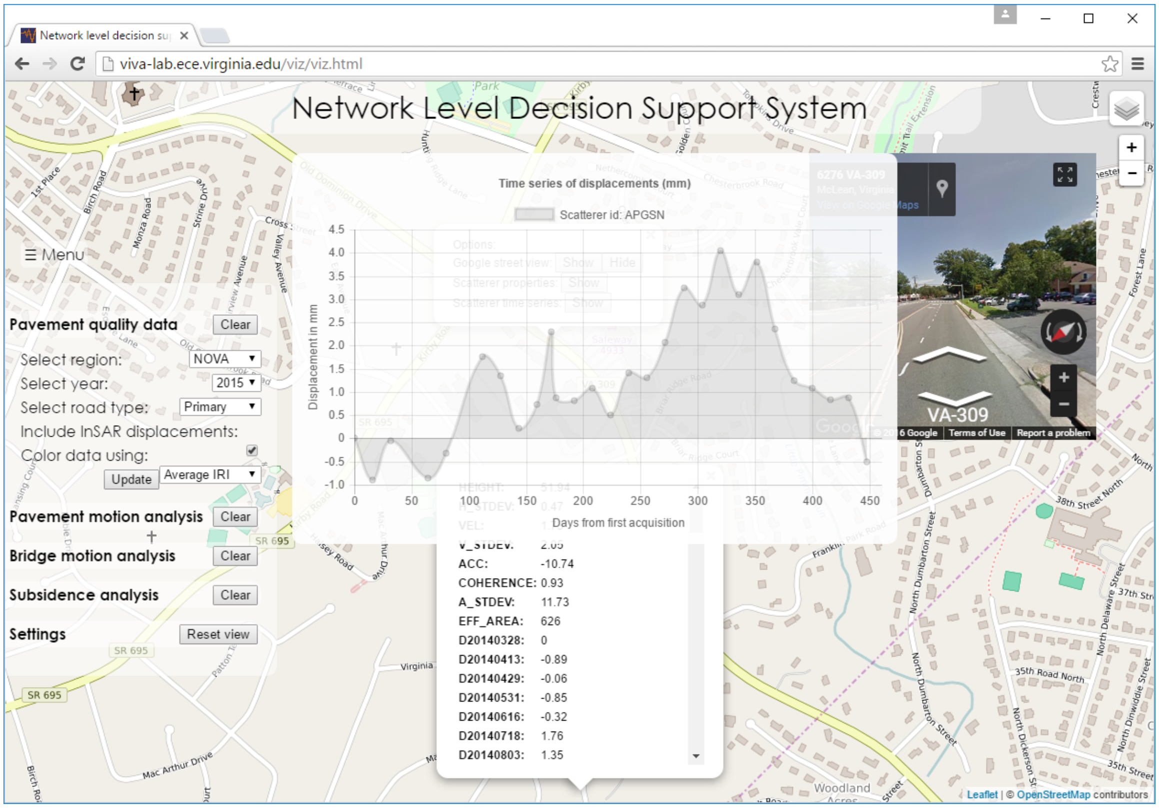

Figure 37 - Example of detailed analysis using the joint pavement data and SqueeSAR datasets.

Pavement motion analysis

The pavement motion analysis dataset was obtained using the coherence motion analysis toolbox. The approach we have taken for the visualization of the results of analysis performed using the satellite data is to exclusively identify location that presented issues using a semaphore-like approach. In this case, as well as for the other tools, yellow indicates a general warning whereas red indicates location where the analysis identified higher level of motion. The thresholds were selected based on discussion with VDOT road engineers (for pavement), bridge engineers (for bridges), and geologists (for subsidence).

Depending on the data available in the various datasets more or less options are going to be available for each modulus. In the case of the pavement motion, the user can select the region of interest, the year for which the analysis was performed (this depends on the availability of satellite data), the type of road on which the analysis was performed, the lowest level to visualize (warning or danger), and/or the top percentile of detections to visualize. The availability of this large set of options allows managers to quickly select what they are interested in (for example, the top 1%) and have a clear idea of how and where detections are distributed providing a quick overview of the current situation. In Figure 38 we provide an example of the visualization of all the detection over AOI1 primary roads for the year 2014. Once again, for each pin it is possible to have a Google Streetview visualization. When used in conjunction with the pavement quality and

SqueeSAR dataset, all the additional information described in the previous section are available for the location where the motion was detected.

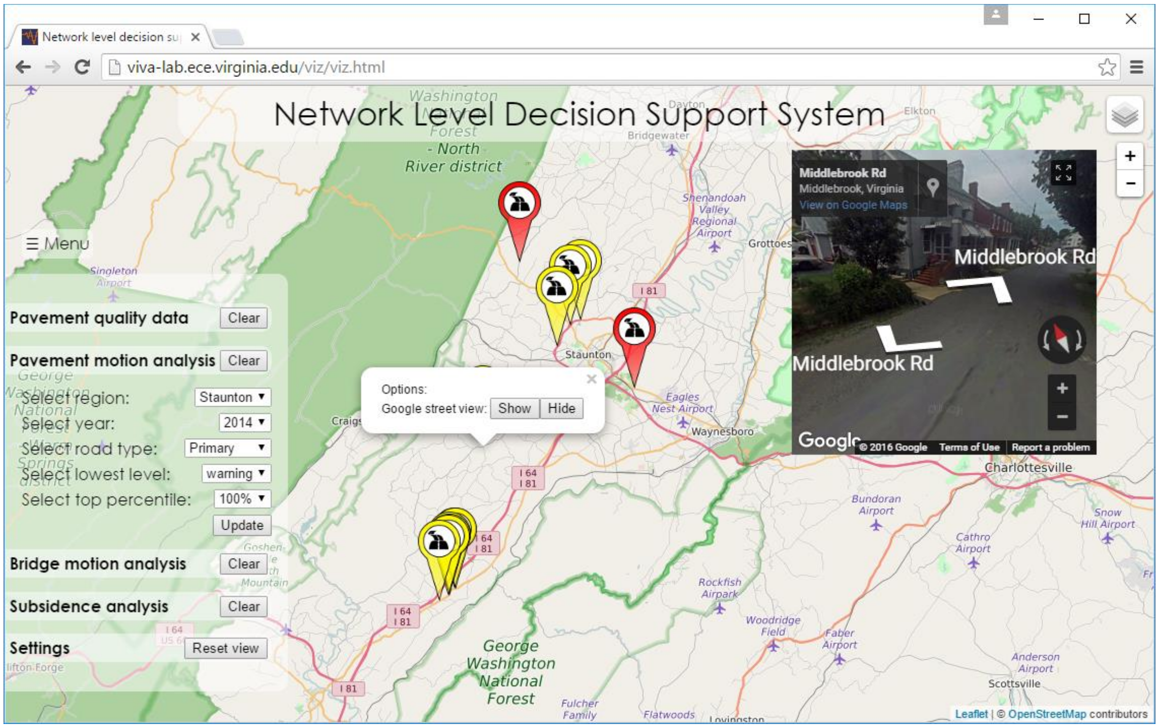

Figure 38 - Visualization of the pavement motion analysis results for AOI1.

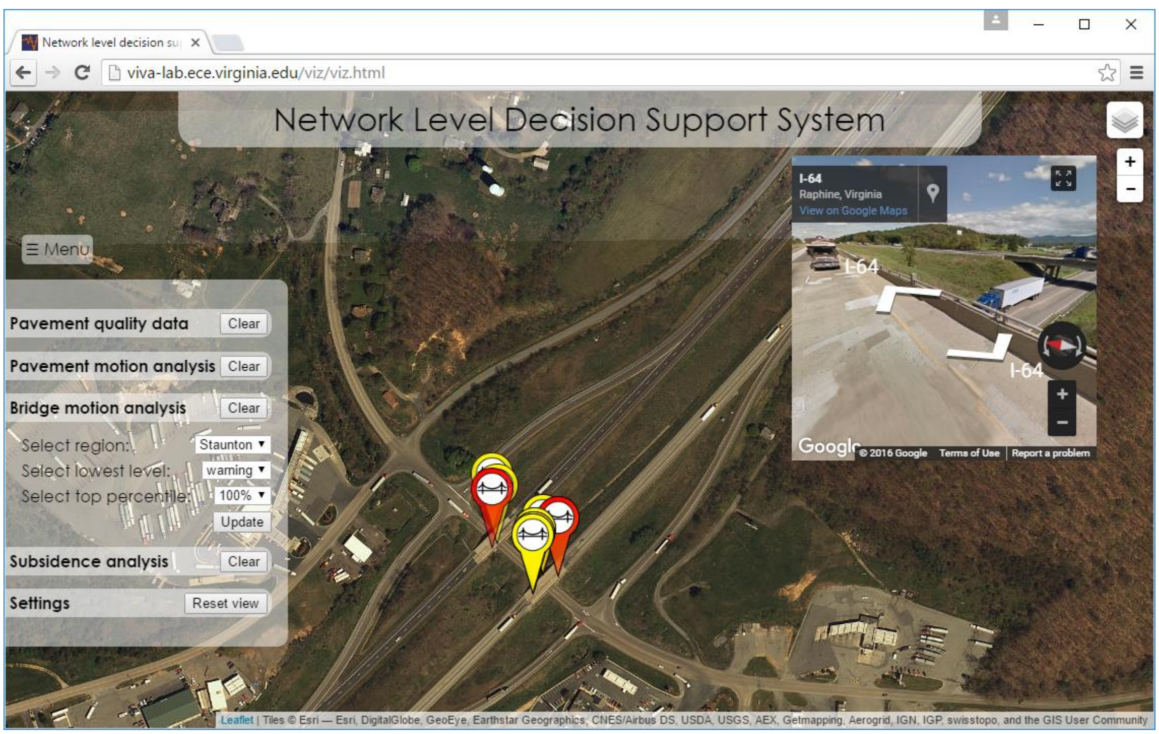

Figure 39 - Example of bridge motion analysis results displayed over a satellite view basemap.

This provides a very powerful tool that can allow DOT engineers to study correlations between the pavement quality, the satellite data and the detected motion while simultaneously having the ability to quickly identify the region thanks to the Google Streetview inset.

Bridge motion analysis

In Figure 39 we show an example of the visualization of the results obtained from the bridge motion analysis toolbox within the web based DSS.

Similar to the pavement motion analysis, the semaphore-style data visualization can be constrained by regions, level of gravity and top percentile detections. Once again, this data can be visualized together with Streetview and data from the previous modules to provide exhaustive information about the area surrounding the detection.

Subsidence analysis

The subsidence analysis module allows the visualization of the potential geohazards detected by the subsidence detection standalone software previously described. A script was developed that, taking the output of the detection software (geotiff) as input, performs a series of operations. First of all, the geotiff is compared to threshold values to identify regions showing signs of subsidence. The comparison is used to generate two shapefiles: one that provides the location and gravity of the detection, the other that provide a contour of the detected region. An example of the visualization of these two files for a small subset of AOI1 is shown in Figure 40.

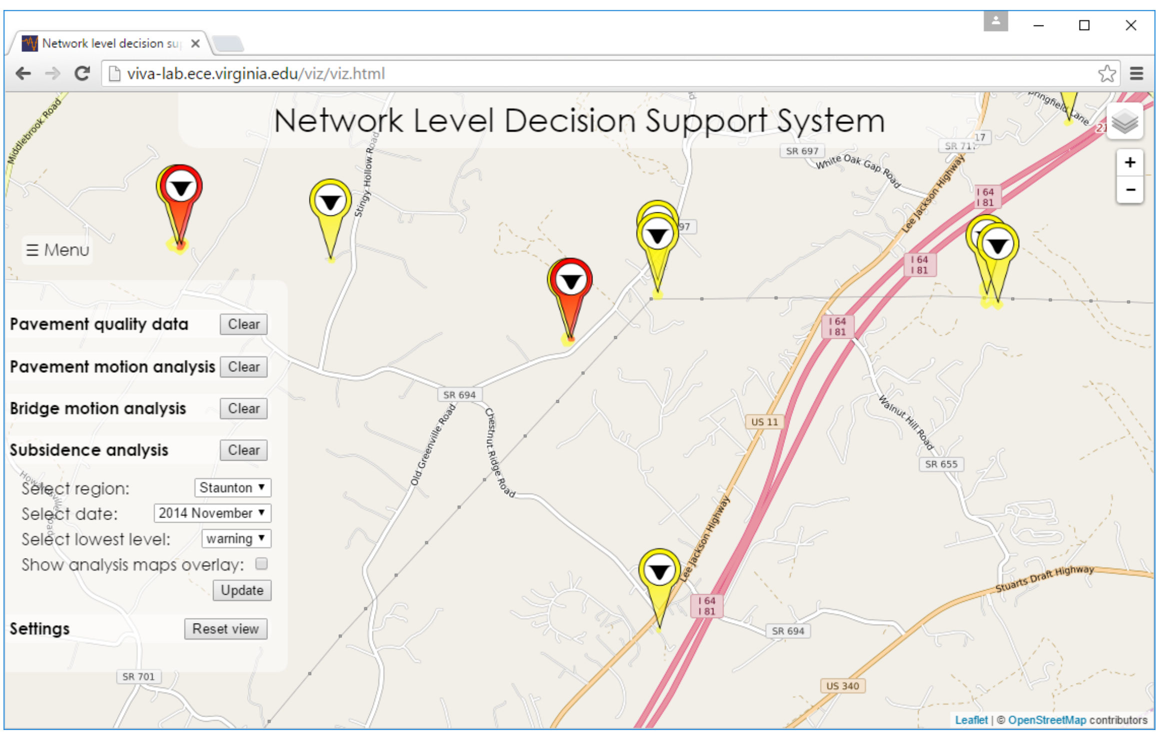

Figure 40 - Semaphore visualization of the location and contour of the detected subsiding regions. Subset of detections within AOI1.

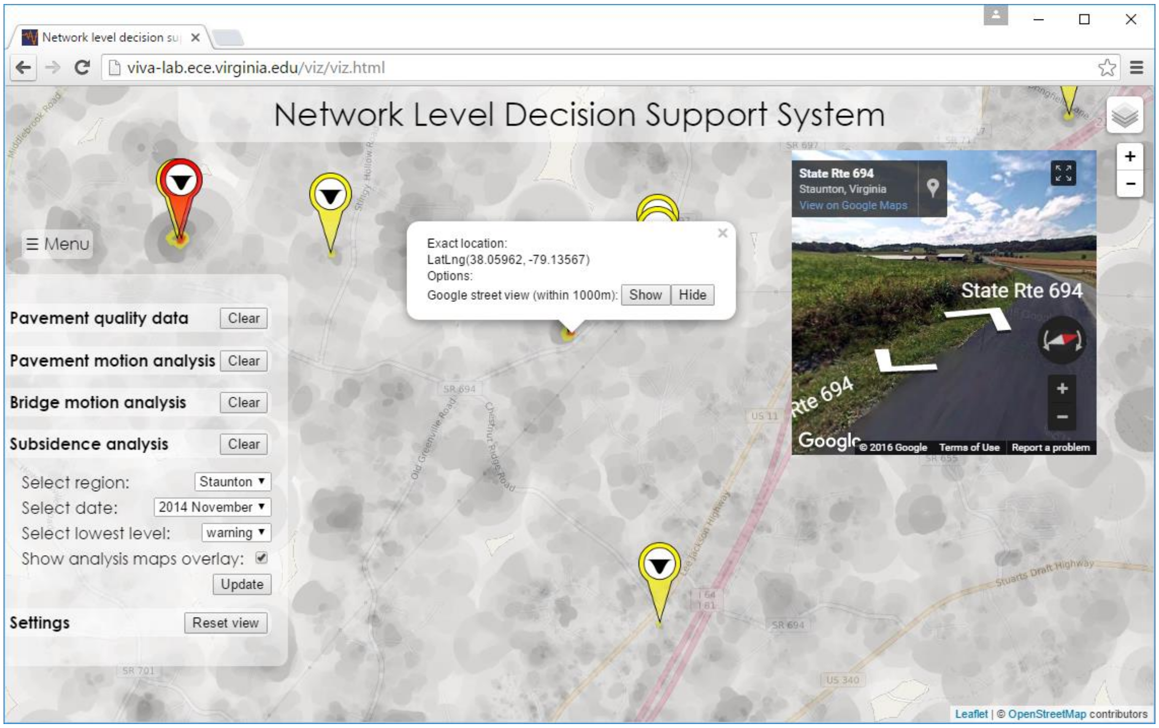

Figure 41 - Subsidence analysis visualization including analysis overlay, popup coordinates information for one of the detections as well as the closest Streetview available within 1km from the detection location.

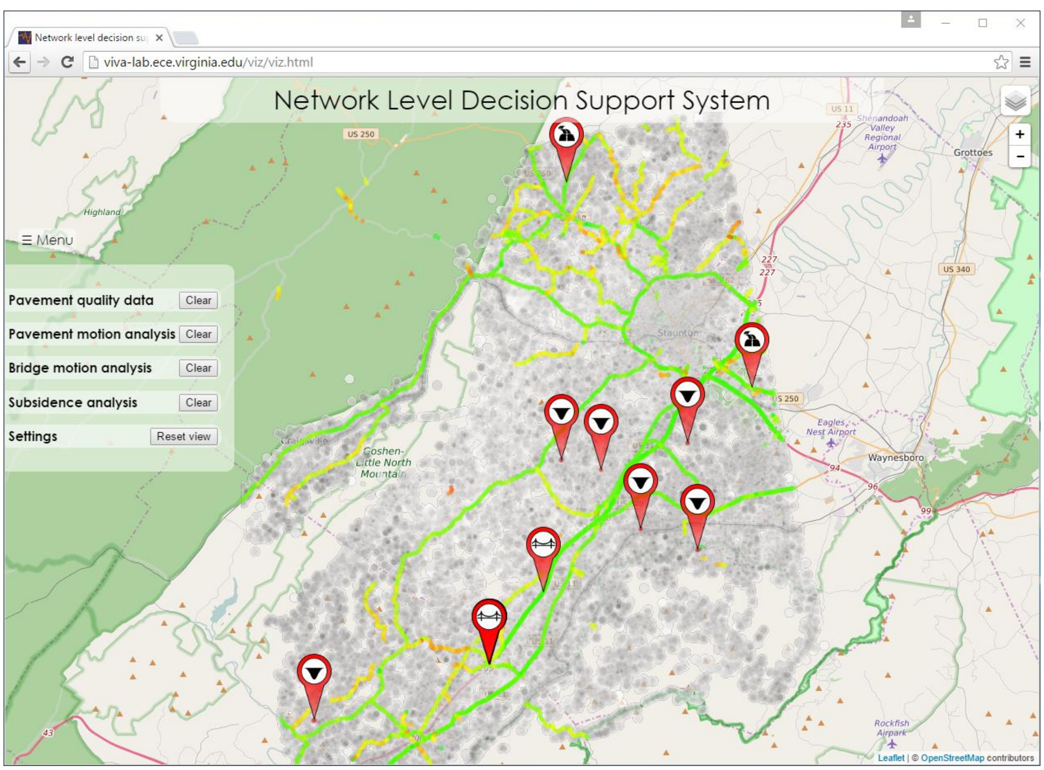

Figure 42 - Example of top danger detection visualized simultaneously together with pavement condition and subsidence analysis overlay.

A second output of the script is a tiled version of the actual geotiff showing the direct results of the subsidence analysis. This can be visualized as well within the DSS by selecting the appropriate checkbox. When this is selected, the geotiff is shown as a grayscale overlay on top of the basemap. Currently, the darker colors indicate regions where the detected motion more closely matches the subsidence model previously described whereas the brighter regions indicate areas where no subsidence matching the model was detected.

When one of the pin is selected, a popup window will display the exact coordinates (in latitude and longitude) of the location of the detection as well as the Google Streetview within 1km (Figure 41).

In Figure 42 we provide a final example of what a typical network level situation snapshot might look like. In this case we are visualizing the danger level detection from all the analysis tools (bridges, subsidence and pavement motion) together with the pavement quality data and the subsidence analysis overlay. This snapshot shows how the developed DSS could be used to give instantaneous information about what are the critical issue allowing better allocation of the available resources.

CHAPTER 5: REPORTING

After evaluating several content management systems (CMS), the team decided to use foswiki, a Wiki-based platform, to implement the permanent project site. This collaborative platform allowed the various member of the team to individually update the relevant parts of the site.

The project website is located at the following URL http://viva-lab.ece.virginia.edu/foswiki/InSAR and includes present and past projects sponsored by the DOT.

Every quarter, the team delivered a brief report highlighting the to-date accomplishments and business status, identifying the intended direction for the following quarter, and including all the relevant document as attachments.

The team met with the project management office for regular meetings at the end of both the first and the second year of the project.

CHAPTER 6: TEAM MEETINGS, OUTREACH AND EDUCATION

Team Meetings

After the kickoff on January 1st, 2014, the team members met with the advisory committee. The minutes are included in Appendix I.

The following individuals agreed to serve as advisory board members:

Chad A. Allen, P.E.
Vermont Agency of Transportation

Scott A. Anderson Ph.D., P.E.
FHWA Resource Center

Melba Crawford
Associate Dean of Engineering for Research/Professor of Agronomy, Civil and Electrical and Computer Engineering/Chair of Excellence in Earth Observation
Purdue University

Emmet Heltzel
State maintenance engineer and division administrator
VDOT Maintenance Division

Michael Mathioudakis
New York State DOT

Ty Ortiz, P.E.
Colorado Department of Transportation

For the duration of the project, the team members held regular meeting to tightly monitor the development of the project and insure that the guidelines suggested by the advisory committee were followed and their key issue addressed.

Outreach and Education

An important goal of the project was not only to develop tools that allow to incorporate the use of InSAR data within exiting DSS, but also to develop outreach material that could be used to promote the use of InSAR within the DOT community. To this end several initiatives were undertaken by the various project teams. Links to all these activities, the produced outreach and education material, as well as several academic publications are available through the project website:

http://viva-lab.ece.virginia.edu/foswiki/InSAR

Given his previous experience, Franz Meyer of the University of Alaska Fairbanks was tasked with the development of outreach material. Section 5 of the report included in Appendix G showcase the developed material. Notable are:

- A 90 minutes long webinar on "Discover Simplified SAR Solutions" was conducted on September 23, 2015 from 2pm – 3pm ET. The event was hosted by NASA Earthdata and was advertised broadly through their website:
  https://earthdata.nasa.gov/user-resources/webinars-and-tutorials/webinar-asf-daac-23-sept-2015)
  The event was attended by more than 120 participants from governmental organizations, academia, and industry. The event was recorded and is available at: https://www.youtube.com/watch?v=YC6gDdgZrOw.
- A four-day SAR training course on SAR principles and applications was held on the campus of AF, August 10-13, 2015. The course was designed to introduce students to the principle and application of microwave remote sensing, including transportation.
- The results of the project were presented at the 2015 NISAR (http://nisar.jpl.nasa.gov/nisarworkshop2015.html) application workshop (http://nisar.jpl.nasa.gov/nisarworkshop2015.html). NISAR is a dedicated U.S. and Indian InSAR mission, in partnership with ISRO, optimized for studying hazards and global environmental change.

An update version of the poster highlighting the use of this technology for the transportation infrastructure that was presented during the the "2015 NASA-ISRO SAR mission application workshop: linking the applied science community to mission data" was presented at the Transportation Research Arena 2016 conference during the Marketplace section (TRA is the European equivalent of TRB). This poster session focused on the "exhibit of case studies, interesting applications looking for transfer opportunities, or valuable projects in their inception phase".

During the Transportation Research Board – 95th Annual Meeting (TRB2016), the tem organized a half-day workshop (Workshop 879 - Interferometric Synthetic Aperture Radar: Promising New Tool for Networkwide Transportation Infrastructure Monitoring) showcasing the project results as well as a cost-benefit study for the implementation of InSAR monitoring technology within DOTs. The workshop was attended by several SAR companies as well as DOT representatives. The team developed and advertised a website hosting all the material presented at the workshop:
http://viva-lab.ece.virginia.edu/foswiki/InSAR/WorkshopTRB2016

Team members participated to the VDOT Geotechnical Engineering annual meeting (Geotech 2015) and showcased the current advancement in the use of InSAR for the transportation community as well as the current results of the project.

One of the main outreach efforts was provided by the VDOT team members. They not only were champions of the technology within VDOT (in multiple occasions they showed other members of the VDOT community how SAR data could be used to improve risk evaluation, for example in the placement of storm water management stations) but they also presented the advantages derived by the implementation of SAR monitoring techniques at various meeting and conferences within and outside the US including meeting with the US Army Corps of Engineers, TRB. Furthermore, the use of InSAR technologies will be included as part of the "Report on Structural Health Monitoring Technologies for Concrete Structure" under development by the American Concrete Institute.

As part of the outreach and education effort, a large portion of the project website was dedicated to the collection of relevant material covering both general information about satellite-based SAR technology and its application within the transportation framework:

http://viva-lab.ece.virginia.edu/foswiki/InSAR/RitaOutreach

http://viva-lab.ece.virginia.edu/foswiki/InSAR/RitaEducation

CHAPTER 7: COST-BENEFIT ANALYSIS

Economist Audrey Moruza of VDOT has performed a cost-benefit analysis that seeks to evaluate a novel use of an established technology (InSAR) and its potential savings for VDOT. In the analysis, benefits were defined as savings resulting from a reduction in the number of geohazard repairs occurring as emergencies which translated into benefits for both the public and for VDOT in the form of savings in user costs for emergency work zones as well as VDOT's liability exposure to claim, and material support costs.

An excel-based tool (tool's guide), that can be used by interested stakeholders to assess the economic advantages deriving from the implementation of InSAR techniques as part of maintenance flow, was developed together with the accompanying users' guide. The results of the analysis were presented, and the tool demonstrated, during TRB 2016, as part of the outreach effort.

The TRB presentation, the tool users' guide, the cost benefit analysis and a link to the tools are available both in Appendix J and on the workshop website:

http://viva-lab.ece.virginia.edu/foswiki/InSAR/WorkshopTRB2016

CHAPTER 8: COMMERCIALIZATION PLAN

During the 4th quarter, a commercialization plan was added to the RITARS-14-H-UVA by request of the project management.

As part of this effort TRE, the commercial partner in the project, hired a manager (Marie Josee Banwell) dedicated to the development of transportation and infrastructure projects within the US. Thanks to the results and the experience gained during the project, TRE was able to secure the following contracts:

- A new project with VDOT for an InSAR study of the West Point Bridge in Virginia
- For high speed rail line in California, TRE is providing InSAR measurements to determine subsidence risk as the proposed route runs through the San Joachim valley. Due to the heavy farming and oil extraction in the region, the valley has seen very high level of subsidence up to meters in some places. TRE will provide an historic analysis of the subsidence and there is a strong interest, by the rail system, to the possibility of ongoing monitoring
- The City of Seattle has contracted TRE to provide data to determine the exact timing and effects of the subsidence on specific areas and buildings due to the "big bertha" tunneling project. The tunnel is being bored right under Pike square in downtown Seattle and is expected to cause subsidence.

By leveraging the experience gained through these contract as well as the results of this project, TRE will continue to advertise the InSAR capabilities to State DOTs (in particular to VDOT) and will focus its efforts to bring onboard a DOT as client of this technology.

CHAPTER 9: CONCLUSION AND FINDINGS

After the years spanning this project, as well as RITARS-11-H-UVA, the teams involved (research, commercial and stakeholder) came to the conclusion that SAR and derived technology provide extremely valuable approaches with the capability to revolutionize the way the transportation infrastructure is monitored and assessed.

Just a single satellite pass can already provide amplitude information that research team members are in the process of correlating with the pavement international roughness index (IRI) of the imaged roads. The development of a robust correlation algorithm could potentially allow interested stakeholders to evaluate the pavement quality of the entire imaged network at every satellite pass. The approach currently developed by the University of Alaska at Fairbanks (Appendix G) provides very promising results in the separation between high and low IRI values thus allowing the identification of good vs bad roads.

With just two satellite passes it is possible to leverage the power of interferometric measurement by creating simple InSAR phase maps (Appendix A) which can be used to provide constant monitoring of detectable deformations, for example, in exposed slopes next to major highways or as post-event assessment. Thanks to the differential nature of the such measurement, these maps could provide not only the current phase status but also be updated at every satellite pass to create a historical record allowing for trend analysis.

Allowing for an extended acquisition campaign, the collected stack of SAR images can be analyzed with state of the art persistent scattering interferometric algorithms (Technology) bringing to fruition the tools developed during the project (CHAPTER 3: IMAGE ANALYSIS SOFTWARE DEVELOPMENT). Filtering the data using these powerful techniques allows the creation of datasets providing historical measurement of ground displacements with sub-centimeter resolution. These datasets are at the core of the tools the project made available online for the detection and analysis of subsidence, pavement smoothness and bridge settlement.

Stakeholders interested in the introduction of InSAR techniques within their agency decision support systems can, not only take advantage of the data analysis tools made available by the project, but also leverage the cost-benefit analysis example developed by and for the Virginia department of transportation included within this report (Appendix J). Furthermore, an interactive and customizable excel-based analysis spreadsheet is available for download from the project website to guide interested stakeholders in their analysis.

The above developments, together with the growing interest towards InSAR techniques witnessed in the past few years by the project commercial partner (TRE Altamira), which has brought the hiring of a manager entirely dedicated to the development of new business opportunities with US state and local agencies, and the open-data policy that will be adopted by several space agencies for the upcoming SAR missions, clearly identify InSAR as major player in the development of robust and resilient detection and monitor techniques for the transportation network of the future.

CHAPTER 10: FUTURE DEVELOPMENTS

During the past four years, the various members of the project team have gained a greater understanding not only about how remote sensing technology can be integrated within the transportation community framework, but also what is relevant to such a community. Thanks to the studies conducted during the two projects, the team had the ability to evaluate what type of analysis is relevant for the transportation community and what is the most efficient way to report and visualize the analysis findings.

We do believe that there is significant potential in InSAR data that could dramatically transform the way inspections are conducted and bring on an efficient and streamlined maintenance approach to the transportation infrastructure. Because of this, if given the opportunity, the team will be eager to continue the development of novel analysis techniques with the goal of not only provide the transportation stakeholders with an improved and extended DSS for network level hazards evaluation and post-event assessments, but also train the next generation of engineers to be champions in the implementation of remote sensing techniques.

PUBLICATIONS

An updated list of publications and public outreach initiatives, as well as media coverage, is maintained on the project website at the following URL:

http://viva-lab.ece.virginia.edu/foswiki/InSAR/RitaPublications

REFERENCES

Bartholomew, M. J. (1977). *Geology of the {Greenfield} and {Sherando} quadrangles, {Virginia}*. Richmond, VA: Commonwealth of Virginia, Dept. of Conservation and Economic Development, Division of Mineral Resources. Retrieved from http://www.dmme.virginia.gov/commercedocs/PUB_4.pdf

Bingham, E. (1991). Publication 105: Physiographic Diagram of {Virginia} [map]. 1:750,000. *Publication 105: Physiographic Diagram of {Virginia} [map]. 1:750,000*. Richmond, VA. Retrieved from https://www.dmme.virginia.gov/commerce/ProductDetails.aspx?ProductID=1435

Brian Bruckno, E. H. (2015). Integration of Interferometric Synthetic Aperture Radar Data into Geotechnical Planning and Deisgn. *Transportation Research Board 94th Annual Meeting.* Washington, DC.

Ferretti, A., Fumagalli, A., Novali, F., Prati, C., Rocca, F., & Rucci, A. (2011, Sep.). A New Algorithm for Processing Interferometric Data-Stacks: SqueeSAR. *IEEE Trans. on Geoscience and Remote Sensing, 49*(9), 3460-3470.

Ferretti, A., Prati, C., & Rocca, F. (2001, Jan.). Permanent scatterers in SAR interferometry. *IEEE Trans. on Geoscience and Remote Sensing, 39*(1), 8-20.

Rader, E. K., & Wilkesm, G. P. (2001). Publication 163: Geologic Map of the {Virginia} Portion of the {Staunton} 30x60-minute Quadrangle [map]. 1:100,000. *Publication 163: Geologic Map of the {Virginia} Portion of the {Staunton} 30x60-minute Quadrangle [map]. 1:100,000*. Richmond, VA. Retrieved from https://www.dmme.virginia.gov/commerce/ProductDetails.aspx?productID=1443

Todd, A. (2014). *A method of Mapping Sinkhole Susceptibility Using a Geographic information System: A Case Study for Interstates in the Karst Counties of Virginia. (Master's Thesis).* Charlottesville, VA: University of Virginia.

APPENDICES

Appendix A – AOI3 – Afton mountain report (June 2014)

TRE – **Interferogram analysis along I-64 in the area of Afton Mountain** [download][1]

[1] http://viva-lab.ece.virginia.edu/elecdocs/ritars14/Afton.pdf

Interferogram analysis along I-64 in the area of Afton Mountain

Report

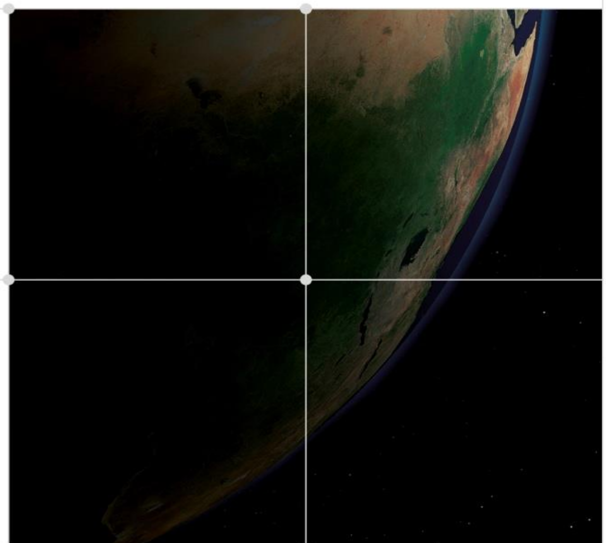

TRE®

Sensing the Planet

Submitted to:
Dr. Scott Acton
Dept. of Electrical & Computer Engineering
University of Virginia
351 McCormick Road
PO Box 400743
Charlottesville, VA, 22904-4743
USA

Prepared by:
TRE Canada Inc.
475 West Georgia Street, Suite 410
Vancouver, B.C., V6B 4M9
Canada

Doc. Ref.: JO14-3015-REP1.0
Confidential

30 June 2014

Prepared by: Vicky Hsiao __________________________
(signature)
GIS Analyst
TRE Canada Inc.

Approved by: Giacomo Falorni __________________________
(signature)
Operations Manager
TRE Canada Inc.

Executive Summary

This report describes the results of an analysis carried out to investigate the use of differential InSAR for monitoring of unstable slopes at Afton Mountain, VA. The following points summarize the key findings of the investigation:

- An interferogram was produced from two Radarsat-2 satellite images acquired on 4 May 2014 and 28 May 2014.
- No movement was detected in the interferogram. It is possible that ground movement along the unstable slope was too small over the 24-day period to be detected.
- Both the interferogram and the associated coherence map are presented and discussed.
- The coherence map indicates that overall coherence of the area is low, with the exception of areas of exposed rock along the I-64 corridor.

Table of Contents

1 Introduction

The University of Virginia has contracted TRE Canada Inc. (TRE) to perform an InSAR analysis using DInSAR at the Afton site within the Rita project “EN-EE InSAR Remote Sensing for Performance Monitoring of Transportation Infrastructure at the Network Level” (RITARS-14-H-UVA). This area experienced rockslides in 2013 that temporarily closed interstate highway I-64.

The objective of the analysis is to investigate the use of differential InSAR (DInSAR) techniques to map and monitor unstable slopes along transportation corridors. DInSAR only requires two radar images compared to multi-image Persistent Scatterer approaches and can therefore provide quick updates of ground deformation.

The area of interest (AOI) is located along I-64 in Afton, VA and covers an area of 8.63 square miles (22.3 km2, Figure 1).

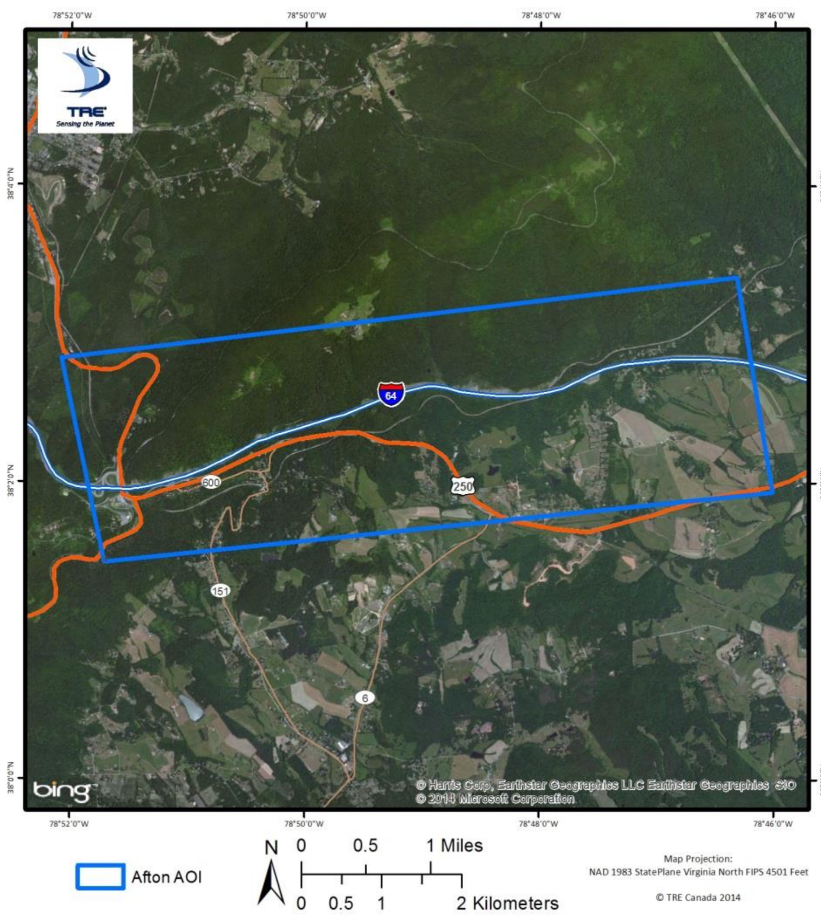

Figure 1: The Afton AOI.

2 Satellite Imagery

Radar imagery is acquired using a side-looking viewing geometry, with viewing angles that vary from 18° to 55° off the vertical. If the coupling of the viewing angle with local topography produces areas affected by radar errors, it is not possible to identify measurements in these locations. A viewing geometry analysis was conducted to select the optimal satellite viewing angle prior to the tasking of the satellite. The analysis took into account local topography and the different sensor viewing angles available over the area. A high resolution (1/3 arcsecond approximately equal to a 10 meter cell size) USGS National Elevation Dataset DEM was used to represent local topography.

The Canadian Space Agency Radarsat-2 (RSAT2) satellite was selected for the study. It provided the best solution in terms of satellite revisit time (24 days), viewing angles and spatial resolution.

The output of the viewing geometry analysis indicated that the optimal satellite beam mode was F3, corresponding to a viewing angle of approximately 42.5° off the vertical, as it minimizes the radar error (foreshortening) over the area (Figure 2). Very few areas are not visible to the satellite. Only small unfavourably oriented slopes along US-250 in the northwest of the AOI (indicated as red arrows in Figure 2) and very small areas on the steepest slopes (orange arrow in Figure 2) above I-64 are in foreshortening.

The two RSAT-2 images were acquired on 4 May and 28 May, 2014 from an ascending orbit. Characteristics of the imagery and the interferogram are shown in Table 1. Additional information on satellite acquisition parameters can be found in Appendix 3.

Report	Interferogram
Dates	04 - 28 May 2014
Temporal Baseline	24 days
Normal Baseline	113 m
Geometry	Ascending
Viewing Angle	Veritcal : 42.5º East-West: 11.1º
Resolution	5 x 7 [Rng x Az] m

Table 1: Imagery and interferogram parameters.

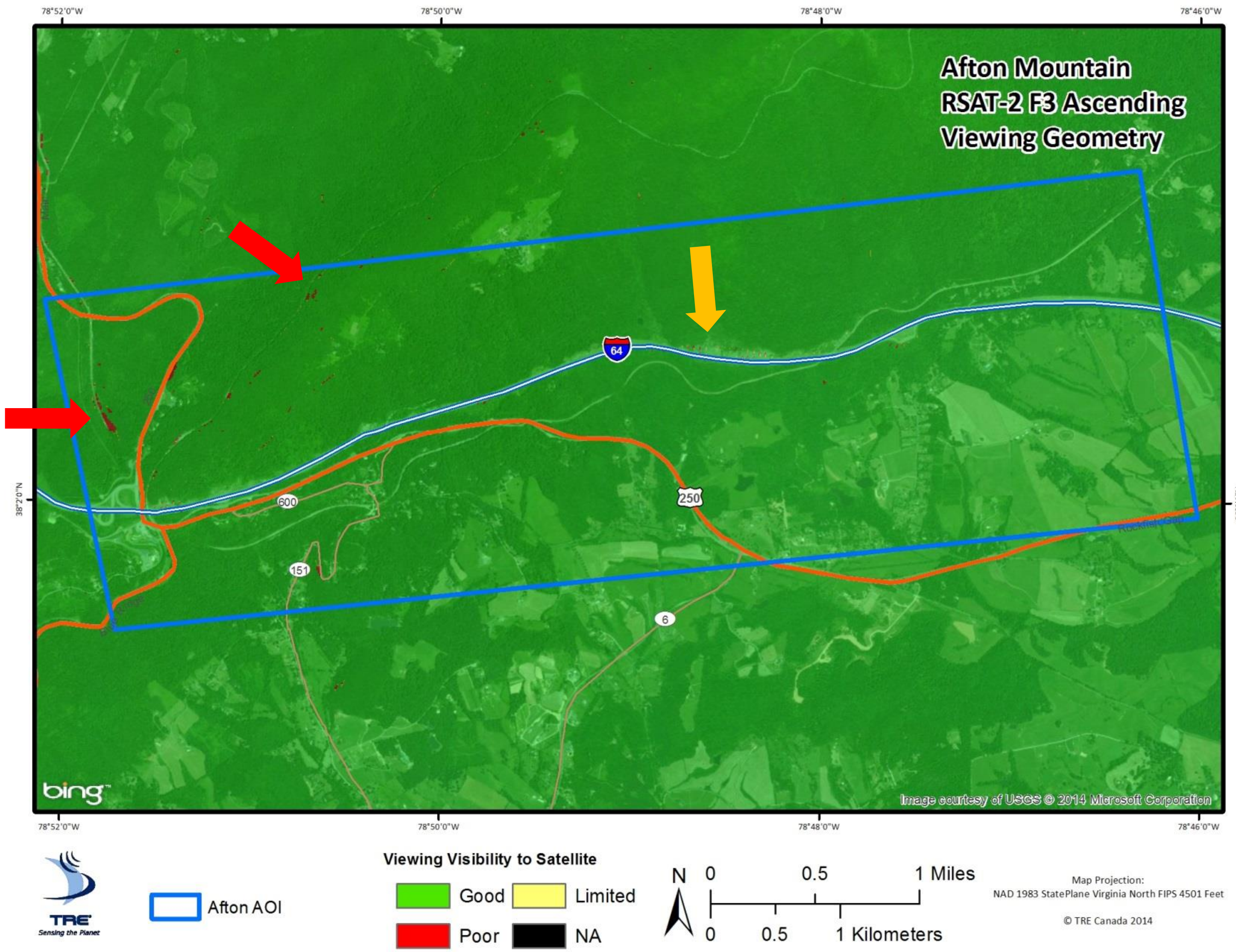

Figure 2: Visibility analysis results for the RSAT-2 data set over I-64. Three arrows point out the locations with the poor/limited visibility to satellite.

3 Interferogram

The interferogram over I-64 is shown in Figure 4. An interferogram is a visual representation of differences in phase between two radar images. As phase is measured in radians, interferogram values are enclosed between -π and +π. Pixel values are colour-coded and vary continuously between red (-π) and blue (+π). Areas with closely spaced fringes may indicate strong movement whereas areas with gradual colour changes represent areas where phase changes gradually over space. Note that the atmospheric contribution cannot be removed from interferograms, which limits the precision of movement measurements to approximately 1 cm. Any movement smaller than this amount will be difficult to detect.

The rock slope that originated the traffic disruptions in April 2013 is coherent but does not show signs of significant movement between the 4th and 28th of May, 2014, as seen in the close ups of two coherent areas in Figure 3. The lack of closely spaced colour fringes in the area indicate that no movement has been identified. The remainder of the area of interest has a grainy appearance in the interferogram, which indicates a low coherence of the radar signal (Figure 4). Low coherence, or decorrelation, is caused by changes in scattering characteristics between two images. This often occurs in vegetated areas.

Areas that have good coherence over time (e.g. arid sites) usually allow the production of deformation maps, in which convert signal phase values in an interferogram are converted to displacement. In the case of Afton Mountain the coherence is too low over much of the area to allow the generation of a deformation map.

It is likely that the temporal window (24 days) was too short to allow significant movement of the slope and/or that the ground was deforming too slowly in the monitored period. It is possible to cover longer of periods of time between images however, this usually produces further decreases in coherence, which over the Afton site is already reduced.

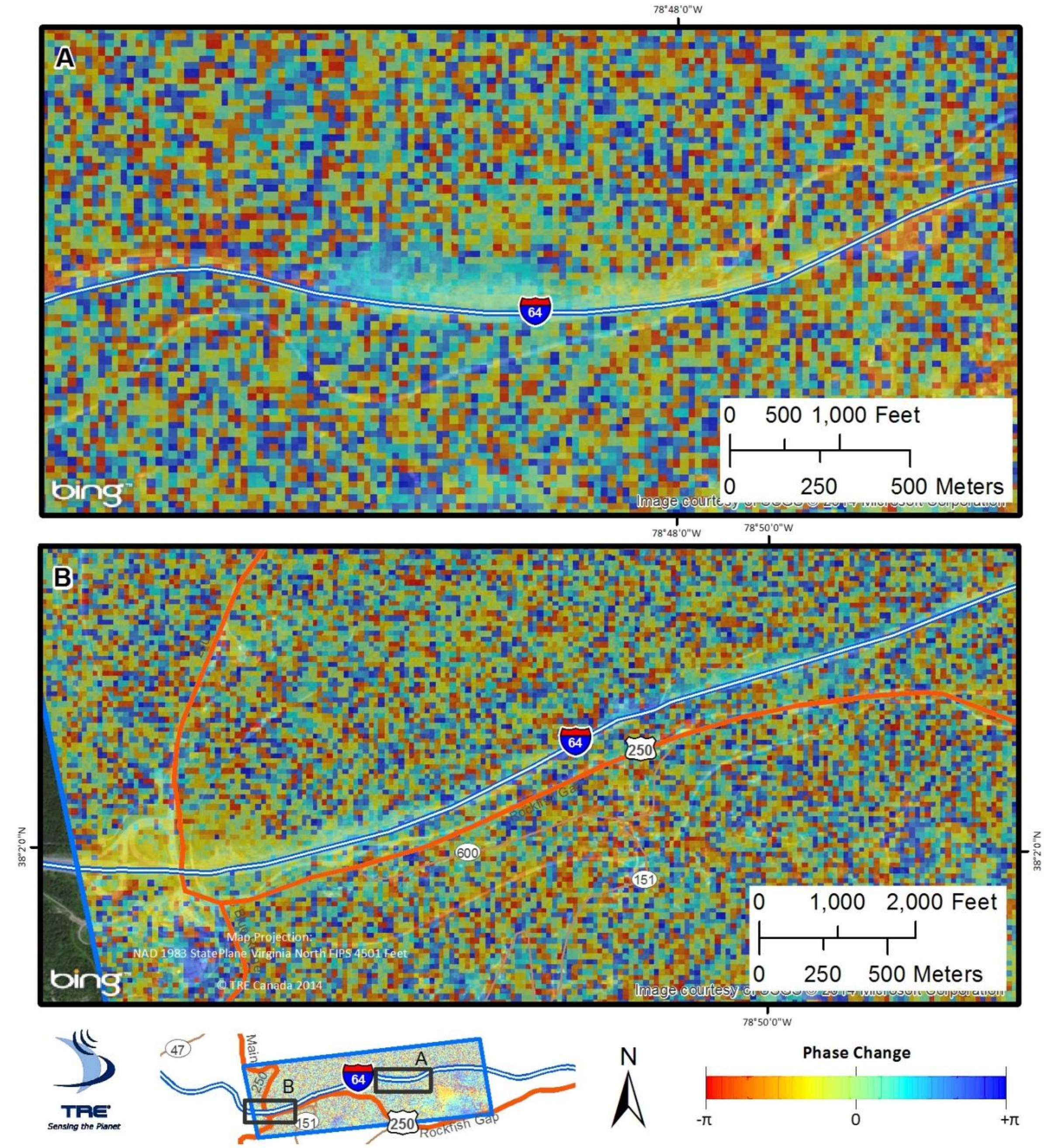

Figure 3: Close ups of two coherent areas. The top panel is centred on the unstable rock slope along I-64 and the bottom panel is in the intersection of I-64 and US-250.

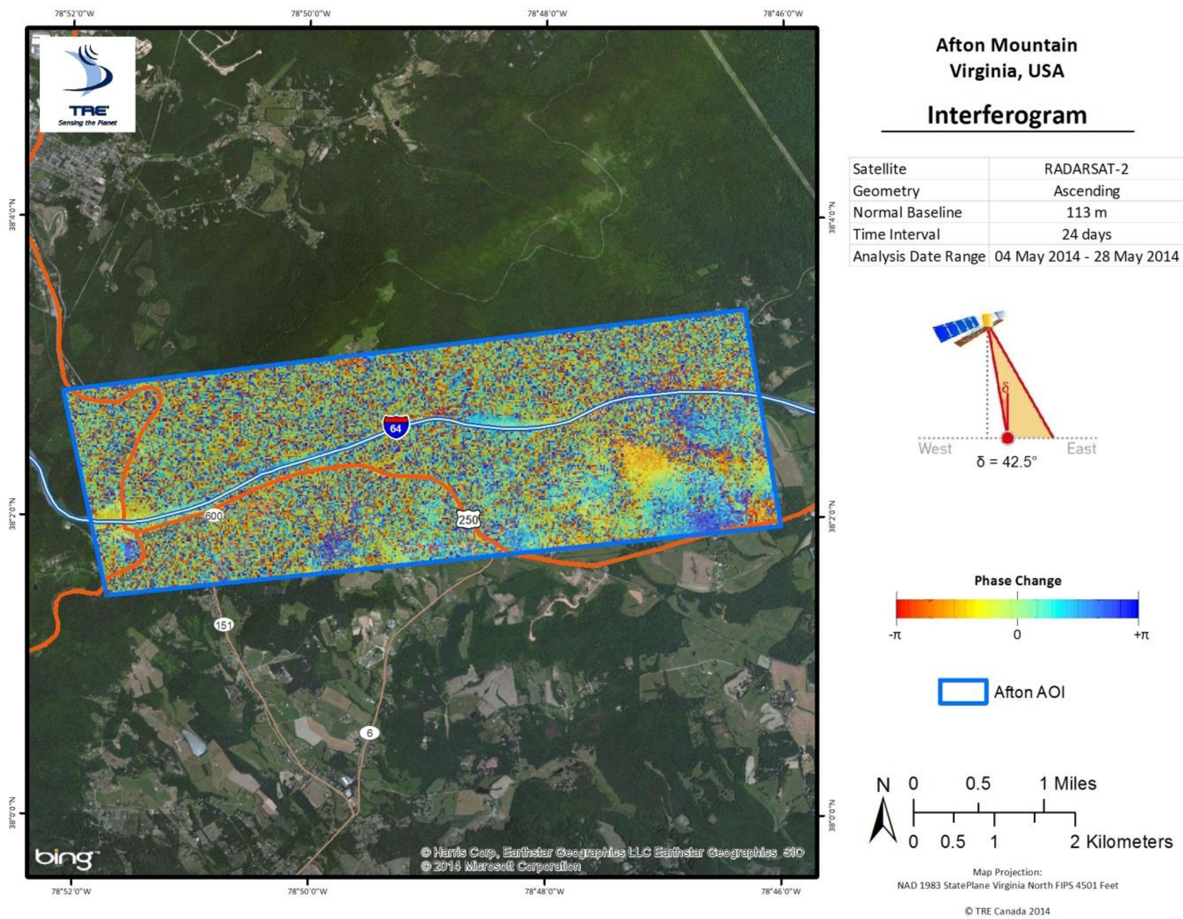

Figure 4: Interferogram over the I-64 area of interest.

4 Coherence map

A coherence map can assist with the interpretation of an interferogram by providing a clearer indication of coherent/incoherent areas. Coherence is a parameter used to describe the quality of the radar signal and is measured with an index that ranges from 0 to 1. A value of 1 indicates complete coherence, while 0 corresponds to complete decorrelation.

The average coherence for the Afton site is 0.4, as indicated by the prevalently orange colour in Figure 5. A few areas along I-64, including the unstable rock slope along I-64 at the centre of the image and the intersection of US 250 and I-64 intersection have coherence greater than 0.7. The southeastern section of the AOI, which has little vegetation, has coherence values between 0.7 and 0.9.

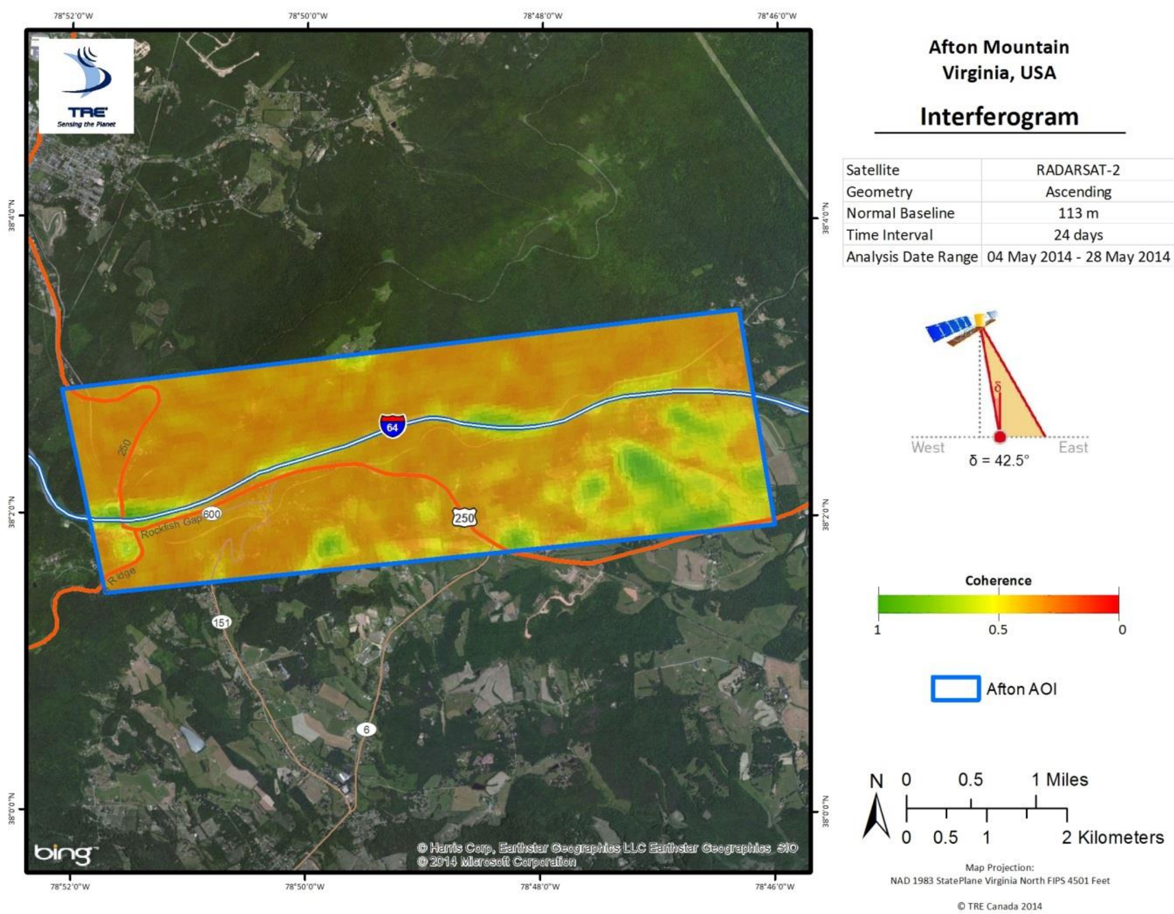

Figure 5: Coherence map over I-64.

5 Observations and recommendations

The careful selection of the appropriate viewing geometry ensured that the steep slope along I-64 where ground movement had been recorded in the past was visible to the satellite. However, the interferogram analysis did not detect any ground movement. This is likely due to the lack of strong ground motion in the 24-day interval and to the centimetre level precision of this type of InSAR (Differential InSAR). In theory it would be possible to select a longer interval between images (e.g 48 or 72 days, or even longer) but this typically leads to a trade-off with image coherence. In general the longer the time between image acquisitions the lower the coherence of the interferogram.

For future interferometric work on this area different approaches are possible:

1) Multi-image type analysis: This approach would provide the most useful results. The area is coherent and rates of movement are appropriate so that a technique such as SqueeSAR would provide a high density of millimetre precision points for monitoring deformation, detecting changes in movement rates and identifying movement boundaries. However, this type of approach requires a few months of lead time as the image stack is being built up to the required 15 images. After 15 images are acquired it would then be possible to perform SqueeSAR processing after any further acquisition, including on short notice. With the advent of low-cost or free radar satellite data from the new sensors that are being launched or that will be launched in the future, this approach would become more cost-effective.

2) DInSAR approach with different intervals between image acquisitions: In this case a trial and error approach would be required to identify the correct compromise between movement rates and coherence;

3) Use higher resolution radar satellite imagery: this would not resolve *per se* the issues encountered but it would enhance the quality of both a SqueeSAR and a DInSAR approach. In the former the higher resolution (e.g. moving from the current 7m x 5m to a 3m x 3m cell size) would generate a significantly higher number of measurement points, thereby allowing a better characterization of ground movement. In the case of DInSAR the higher resolution would possibly also improve coherence as it would reduce the number of scattering elements in each pixel;

4) Use L-band imagery: the longer wavelength of L-band sensors allows them to penetrate vegetation, increasing coherence in areas where vegetation is an obstacle to the shorter wavelength C- and X-band sensors. However, there are two main limitations to be considered: 1) there are currently no operational L-band satellites. In September 2014 the ALOS-2 satellite, which has already been successfully launched and is in the calibration stage, should become operational. It is not yet clear what the data acquisition policy will be but, as this satellite is owned by the Japanese Space Agency (JAXA), it may have a pre-scheduled acquisition plan. This

entails that it will not be possible to task the satellite to acquire over specific areas and it will be necessary to wait until a sufficient number of images have been acquired over the I-64 site; 2) The long wavelength (23 cm) of these sensors makes them less sensitive to movement, meaning that it would be necessary to wait for a longer interval before movement could be detected.

Appendix 1: Delivery of Data

The interferogram products accompanying the present report include a 24-day interferogram and a coherence map. These are provided both in geotiff format, which can be viewed in an ArcGIS environment, and in kmz format, which can be viewed using Google Earth. The following table contains the file names and descriptions.

File name	Description
Afton_20140504_20140528_Bn-113_Bt-24_Interferogram.tif	24-day interferogram in geotiff format
Afton_20140504_20140528_Bn-113_Bt-24_ Interferogram_RGB.tif	24-day interferogram in geotiff format with RGB colour scale
Afton_20140504_20140528_Bn-113_Bt-24_ Interferogram.kmz	24-day interferogram in kmz format
Afton_20140504_20140528_Bn-113_Bt-24_CoherenceMap.tif	24-day coherence map in geotiff format
Afton_20140504_20140528_Bn-113_Bt-24_ CoherenceMap_RGB.tif	24day coherence map in geotiff format with RGB colour scale
Afton_20140504_20140528_Bn-113_Bt-24_ CoherenceMap.tif	24-day coherence map in kmz format

Table 2: List of delivered files.

Appendix 2: TREmaps

The InSAR results presented here are also viewable using TREmaps™, a web-based portal developed by TRE, where they can be accessed through a secure client login (only authorized users will have access to the results). The InSAR data is superimposed onto a Google Maps background and data can be visualized on any device with an internet connection, including portable tablets.

Figure 6 shows an example dataset loaded into the web-based GIS TREmaps™ platform. Site and access details (username and password) are provided directly to the primary contact via email.

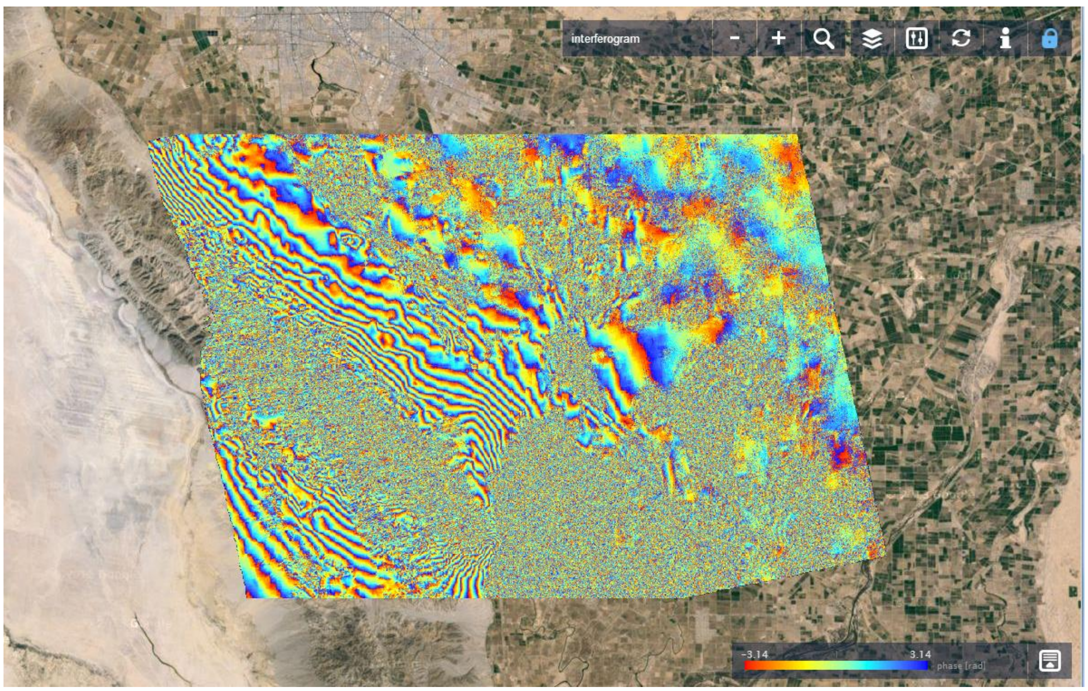

Figure 6: Example of Interferogram within TREmaps.

Appendix 3: Additional Properties of the RSAT2 Data Sets

InSAR-based approaches measure surface displacement in one dimension, known as the satellite line-of-sight (LOS). The LOS angle varies depending on the satellite and on the acquisition parameters.

The RSAT2 images for the present analysis were acquired from an ascending orbit (satellite travelling from south to north and imaging to the east) in beam mode F3. Table 3 lists the values of the angles for this study, while Figure 7 shows the geometry of the RSAT2 image acquisitions. The symbol δ (delta) represents the angle the LOS forms with the vertical and Θ (theta) the angle formed with the geographic north.

Orbit geometry	Symbol	Angle
Ascending	**δ**	42.5
Ascending	**Θ**	11.1

Table 3: Satellite Line-of-Sight viewing angle for the RSAT2 ascending orbit imagery over Afton.

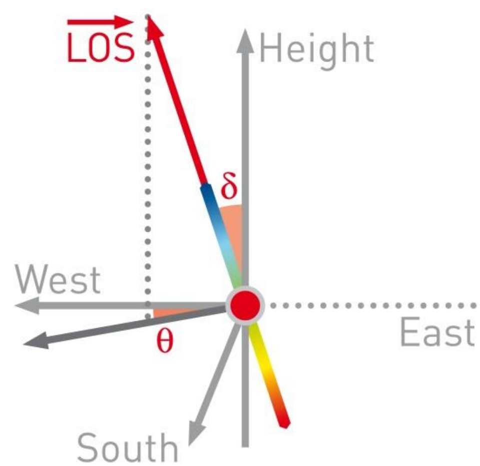

Line Of Sight

Figure 7: Geometry of the RSAT2 image acquisitions for an ascending orbit.

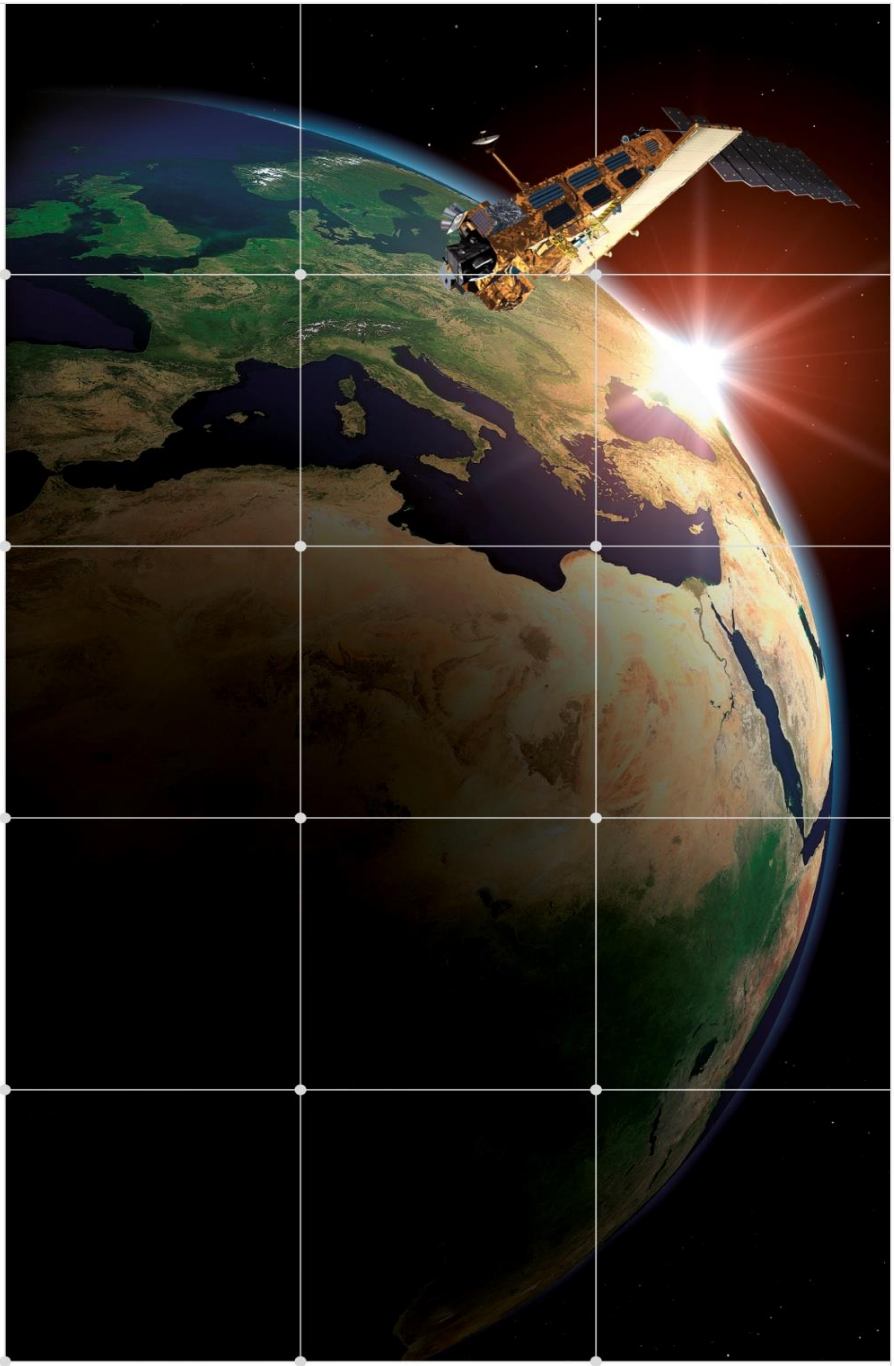

Appendix B – AOI1 – Staunton: SqueeSAR report (June 2014)

TRE – **Analysis of ground movements over Virginia using SqueeSAR – First Report** – June 2014 [download][2]

TRE – **Analysis of ground movements over Virginia using SqueeSAR – First Report - Technical Appendix** – June 2014 [download][3]

[2] http://viva-lab.ece.virginia.edu/elecdocs/ritars14/Staunton_Jun14.pdf
[3] http://viva-lab.ece.virginia.edu/elecdocs/ritars14/Staunton_Jun14_TA.pdf

Analysis of Ground Movement over Virginia using SqueeSAR

Site 1 First Report

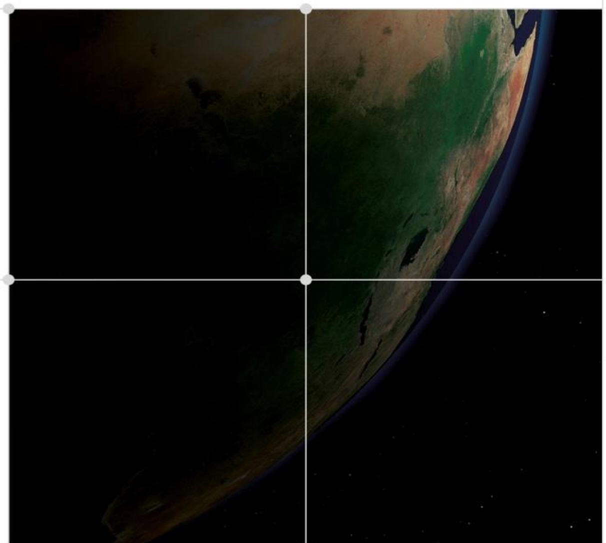

TRE®
Sensing the Planet

Submitted to:
University of Virginia
1001 N. Emmet St.
PO Box 400195
Charlottesville, Virginia 22904
USA

Prepared by:
TRE Canada Inc.
475 West Georgia Street, Suite 410
Vancouver, B.C., V6B 4M9
Canada

Doc. Ref.: JO14-3011-REP1.0
Confidential

31 October 2014

Prepared by: Vicky Chun-Yi Hsiao ___________________________
(signature)
GIS Analyst
TRE Canada Inc.

Approved by: Giacomo Falorni ___________________________
(signature)
Operations Manager
TRE Canada Inc.

Executive Summary

This report describes the approach and results of the InSAR analysis carried out to measure surface deformation in Virginia (Site1) for the project "InSAR remote sensing for performance monitoring of transportation infrastructure at the network level" (RITARS-14-H-UVA). The results provide an overview of ground movement occurring in the area over a 34-month period.

The following points summarize the key findings of this analysis and the features of this deliverable:

- Up to -30 mm of subsidence were identified along primary roads, such as at Jefferson Highway near Greenview Dr where sudden movement begins in early 2014 (Section 5.2.2). Displacement was also observed on the State Route 635 bridge overpass of I-81 (Section 5.2.1).
- A rock slope along Route 600 exhibited subsidence rates of up to -9.1 mm/year (Section 5.3.1).
- Movement was identified on riprap placed along several routes within the AOI (Sections 5.3.2, 5.3.3, 5.3.4).
- Observations in the area of two sinkholes active in the past do not show recent movement (Section 5.3.6).
- Measurement point density has more than doubled compared to the previous results (180 points per km^2 vs 83 per km^2).
- Three out of four reflectors installed on the Route 262 Bridge were visible. -4.6 mm of settlement was detected from reflector #2 on top of the parapet mid-span between March to June, 2014 (Section 5.1.2).

The deliverables for the project include the present report, which describes the results of the data processing, a technical appendix and a CD containing the displacement data.

Table of Contents

1 Introduction

The University of Virginia VIVA lab is leading a research project with the Virginia Research Transportation Council and TRE Canada entitled "InSAR remote sensing for performance monitoring of transportation infrastructure at the network level " (RITARS-14-H-UVA). The work was awarded to the University of Virginia as a research grant funded by the Commercial Remote Sensing and Spatial Information Technology Application Program, RITA Phase V.

One of the main objectives of this project is to systematically extract consistent and reliable information on road subsidence, bridge monitoring, slope stability, sinkhole development and pavement condition from InSAR data. TRE Canada Inc. (TRE) has been contracted to perform the InSAR work using our SqueeSAR algorithm. Cosmo-SkyMed (CSK) radar satellite imagery was used to build on the archive initiated in the previous phase of the project over the same area of interest. The increased temporal coverage will allow better delineation of ground subsidence trends and further refinement of a sinkhole detection model.

The AOI corresponds to a full CSK radar scene, approximately 1,600 km^2 (618 square miles) in size, covering most of Augusta county, Virginia (as well as a small portion of Rockbridge county). The AOI contains dense vegetation, active agriculture, fallow fields, exposed ground, infrastructure and towns (Figure 1). Mountainous terrain and areas of highly variable topography are present in the northwest and southeast corners of the scene. Man-made structures, as well as bare or sparsely vegetated ground, often yield a high number of measurement points. Areas of dense vegetation, active agriculture and steep slopes will produce a lower density of measurement points. Historically, portions of the area have been prone to sinkholes, landslides, and other instabilities.

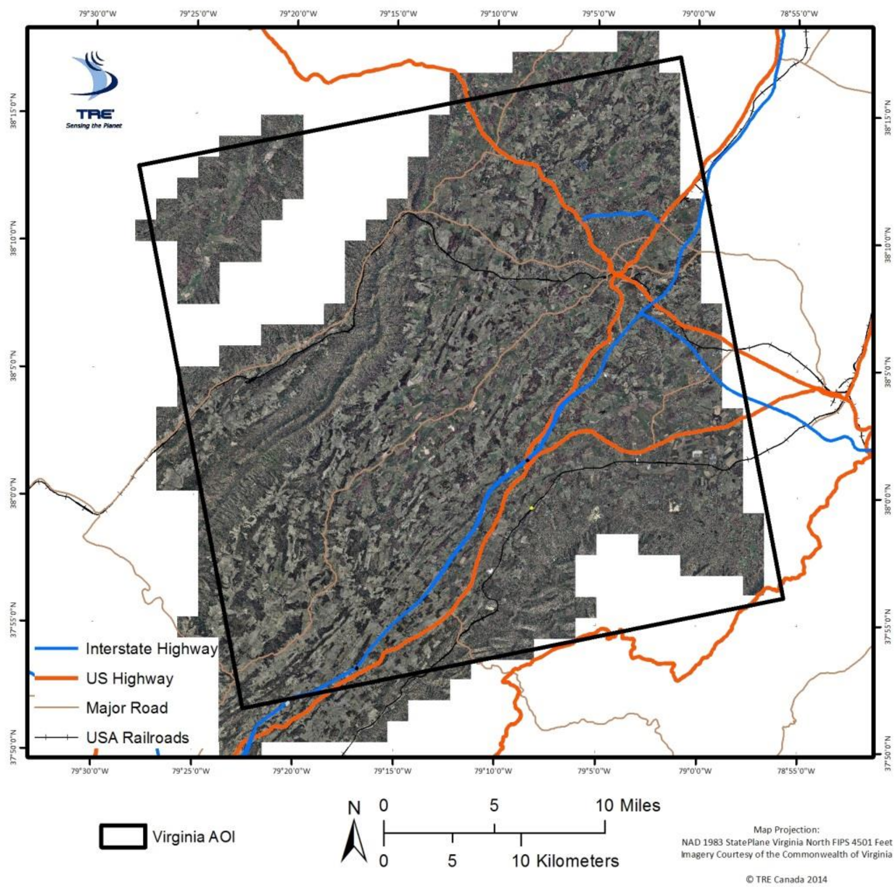

Figure 1: The Area of Interest (AOI). The background 2012 orthophotos used in the figures of this report were provided by the Commonwealth of Virginia.

2 Radar data

All images were acquired by the Cosmo-SkyMed (CSK) constellation from an ascending orbit along Track 213. Imagery is currently being acquired with a 16-day frequency. Fifty-seven images were acquired between 29 August 2011 and 17 June 2012, with five being discarded during the processing due to low coherence values (snow) in winter scenes. In total, 52 images have been processed covering a period of two years and 10 months (Table 1). Note that there was an interruption in image acquisitions for approximately eight months between October 2012 and June 2013, which resulted in a corresponding gap in all time series.

Additional information on the satellite parameters can be found in the Technical Appendix.

CSK Data					
No.	**Date**	**Interval**	**No.**	**Date**	**Interval**
1	29 Aug 2011		**28**	23 Sep 2012	16
2	05 Sep 2011	7	**29**	09 Oct 2012	32
3	13 Sep 2011	8	**30**	25 Oct 2012	16
4	21 Sep 2011	8	**31**	14 Jun 2013	16
5	29 Sep 2011	8	**32**	30 Jun 2013	232
6	07 Oct 2011	8	**33**	16 Jul 2013	16
7	15 Oct 2011	8	**34**	01 Aug 2013	16
8	31 Oct 2011	16	**35**	17 Aug 2013	16
	17 Nov 2011		**36**	02 Sep 2013	16
9	02 Dec 2011	32	**37**	18 Sep 2013	16
10	18 Dec 2011	16	**38**	04 Oct 2013	16
11	03 Jan 2012	16	**39**	20 Oct 2013	16
12	19 Jan 2012	16	**40**	21 Oct 2013	16
13	04 Feb 2012	16	**41**	05 Nov 2013	1
	20 Feb 2012		**42**	21 Nov 2013	15
14	07 Mar 2012	32	**43**	07 Dec 2013	16
15	23 Mar 2012	16		23 Dec 2013	
16	08 Apr 2012	16		08 Jan 2014	
17	16 Apr 2012	8		24 Jan 2014	
18	02 May 2012	16	**44**	09 Feb 2014	64
19	18 May 2012	16	**45**	25 Feb 2014	16
20	11 Jun 2012	24	**46**	13 Mar 2014	16
21	12 Jun 2012	1	**47**	29 Mar 2014	16
22	15 Jun 2012	3	**48**	14 Apr 2014	16
23	19 Jun 2012	4	**49**	30 Apr 2014	16
24	05 Jul 2012	16	**50**	16 May 2014	16
25	21 Jul 2012	16	**51**	01 Jun 2014	16
26	06 Aug 2012	16	**52**	17 Jun 2014	16
27	22 Aug 2012	16			

Table 1: Dates of the CSK image acquisitions. Image dates in orange were discarded during the data processing.

3 Data Processing

Due to the large size of the AOI and the large swath of densely vegetated terrain over the North Mountain and Great North Mountain in the northwest corner, the data set had to be divided into two separate clusters. Each cluster has its own reference point from which the displacement values are calculated. The larger area in each of the figures in this section corresponds to Cluster 1, while Cluster 2 refers to the smaller grouping in the northwest corner (Figure 2).

Reference Point

SqueeSAR™ is a differential technique meaning displacement is measured compared to a reference point that is assumed to be stable. The reference points used for the two clusters are both shown in Figure 2. The reference points were selected using an optimization procedure that performs a statistical analysis of all targets to select a point with optimal radar parameters including high coherence, low standard deviation and low temporal variability over time. The use of this procedure ensures the highest quality results are achieved. Reference point coordinates for the current analysis are listed in the Technical Appendix.

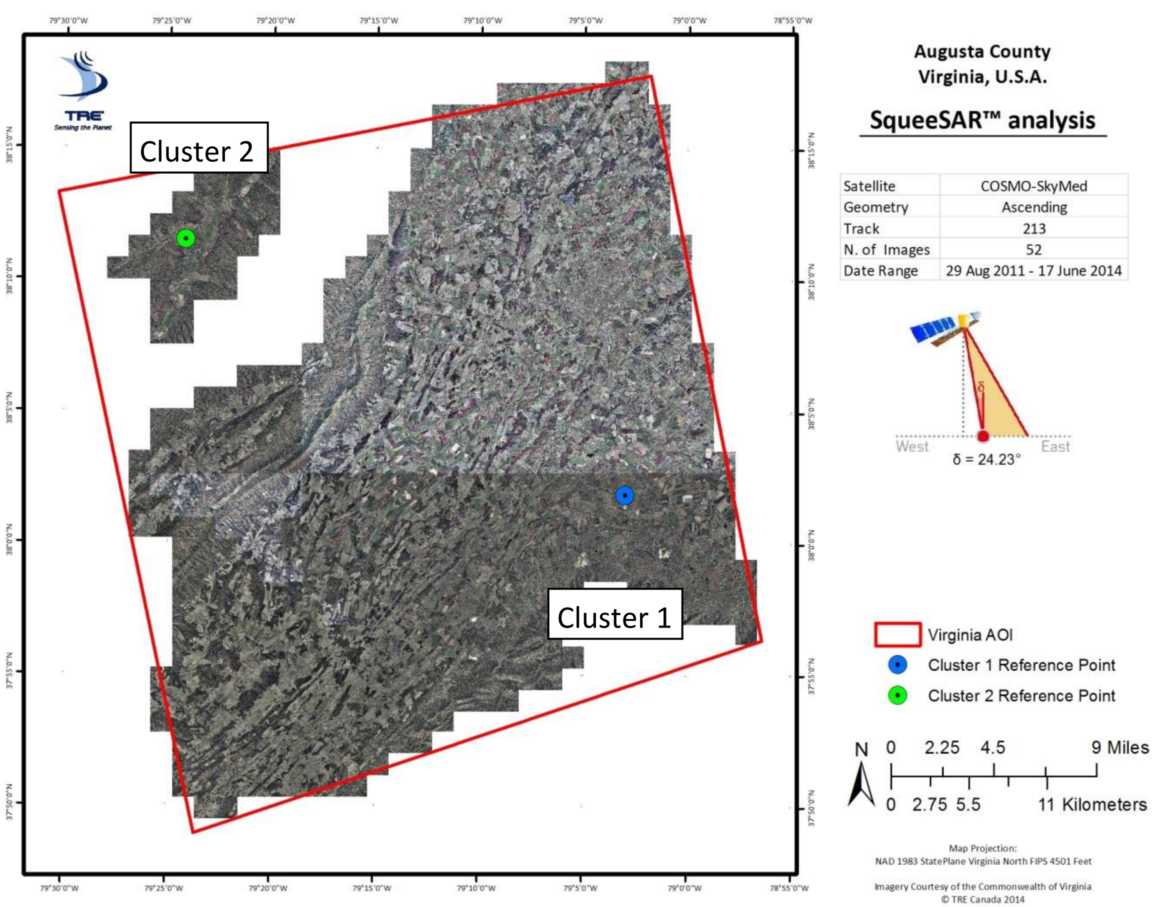

Figure 2: The location of the two data clusters and their associated reference points.

4 Results of the SqueeSAR™ analysis

4.1 Cumulative Displacement

The total amount of displacement measured during the 34-month period is shown below (Figure 3). Each point corresponds to a PS or DS, and is color-coded according to the magnitude and direction of total movement. Movement is measured along the satellite line-of-sight (LOS) relative to the first image (August 29 2011) of the data stack.

Cumulative displacement from August 2011 to June 2014 ranges from -74.4 to +47.8 mm within the AOI, as compared to -31.6 to +24.0 mm in the previous results (August 2011 to October 2012). Several localized areas of subsidence and uplift are found along major highways, railways, and open fields. More detailed analyses of the results are described in Section 5.

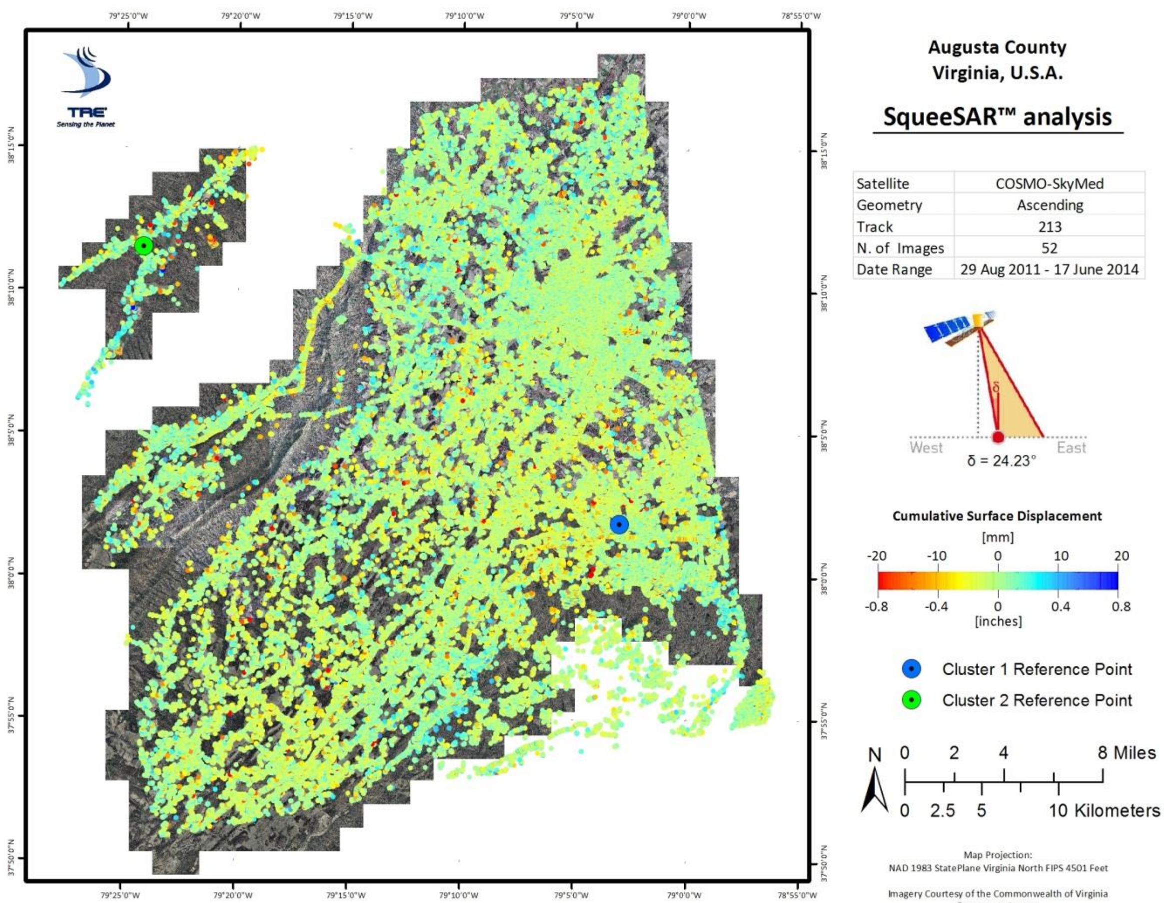

Figure 3: Cumulative deformation, expressed in millimeters, from August 29 2011 to June 17 2014.

4.2 Displacement rate

The line-of-sight (LOS) displacement rates, expressed in mm/year, as detected from the processing of all images are shown below (Figure 4). Each point corresponds to a Permanent Scatterer (PS) or a Distributed Scatterer (DS), and is color-coded according to its annual rate of movement. Average displacement values are calculated from a linear regression of the ground movement measured over the entire period covered by the satellite images. Detailed information on ground motion is also provided by means of displacement time series, which are provided for each PS and DS.

Displacement rates are low throughout the AOI, with 99% within -5 and +5 mm/yr. Overall, displacement rates range from -27.6 to 16.3 mm/yr.

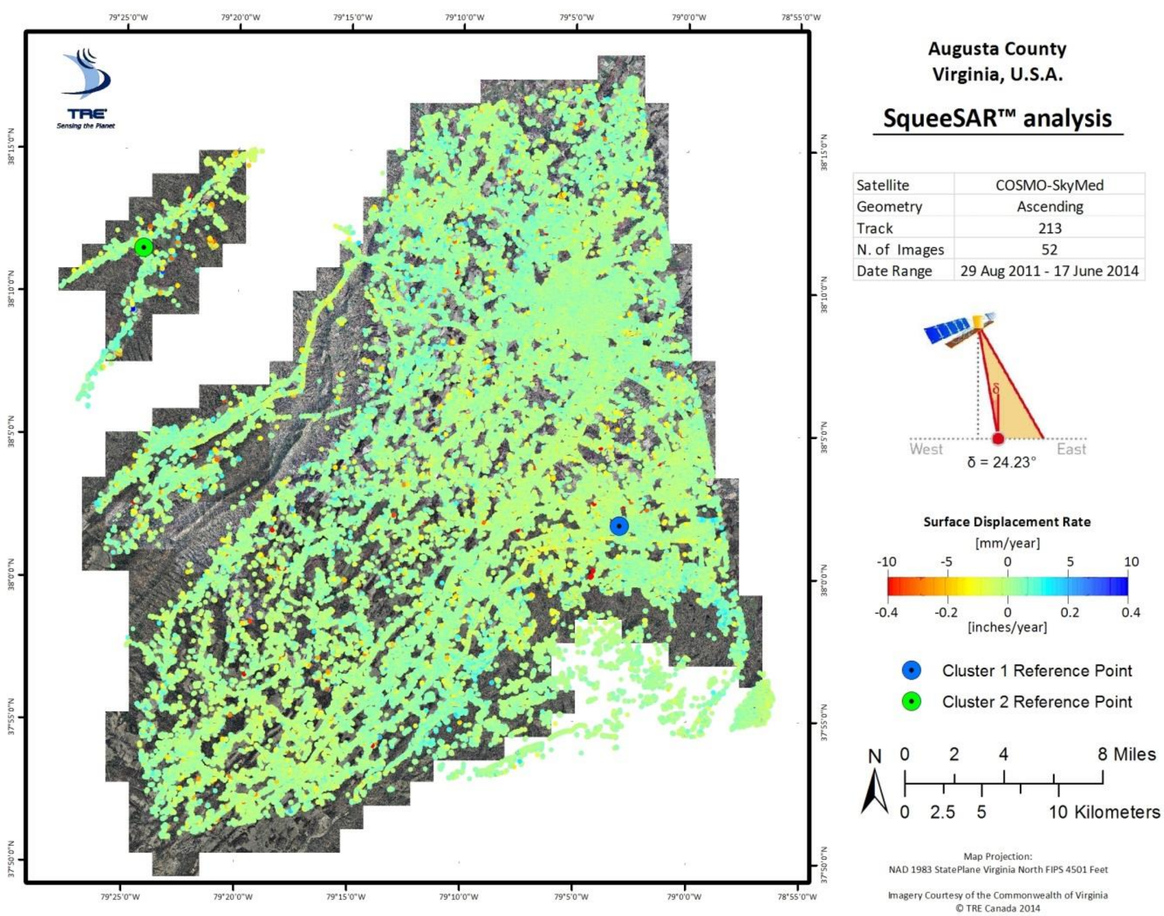

Figure 4: Deformation rates in mm/year.

4.3 Displacement Rate Standard Deviation

The standard deviation of the surface displacement data characterizes the error of the measurements (Figure 5). For this reason, any measurement should be interpreted in the form of Displacement Rate ± Standard Deviation. Standard deviation values tend to increase with distance from the reference point. Higher values indicate a greater variability in displacement rates and are often associated with areas of rapid and/or irregular ground movement.

Standard deviation values are low throughout the AOI, ranging from 0.04 to 1.21 mm/year. Slightly higher standard deviation values were identified over areas further away from the reference point. The average standard deviation value of all measurement points within this data set is ±0.56 mm/year for cluster 1 and ±0.40 mm/year for cluster 2.

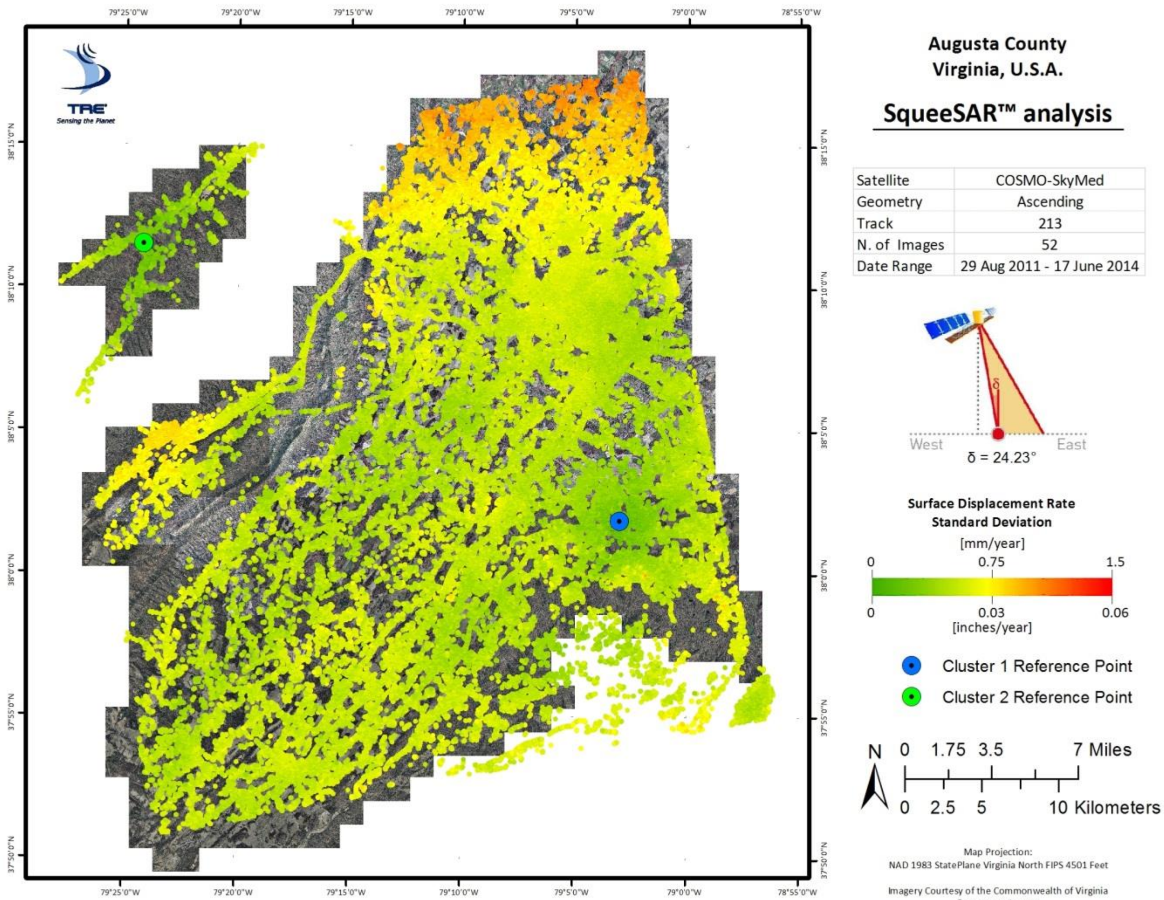

Figure 5: Standard deviation values of the displacement rates.

4.4 Temporary Scatterers (TS)

This technique developed by TRE is based upon the extraction of Temporary Scatterers (TS) from a radar image stack. Compared to PS and DS, TS represent measurement points identified within a subset of the image data set rather than the complete stack. This approach typically leads to a greater spatial coverage of the results as it often includes areas where PS and DS are not identified. The output is a raster map, with a 10 m x 10 m cell size, representing average surface displacement rates.

The results of the TS analysis in the Virginia data set are shown in Figure 6. A higher spatial coverage of deformation information is provided in certain regions of the AOI. The area near the intersection of Richmond Ave and Statler Blvd in Staunton, as shown in Figure 7, is an example of this increased spatial coverage. The left panel represents the results from the PS/DS and the right panel shows the same area when using the TS data. Three localized areas, two exhibiting subsidence and one showing uplift, are observable with the TS results but are not identified in the PS/DS results. Deformation rates of up to -15.8 to 6.3 mm/year were found for these three areas.

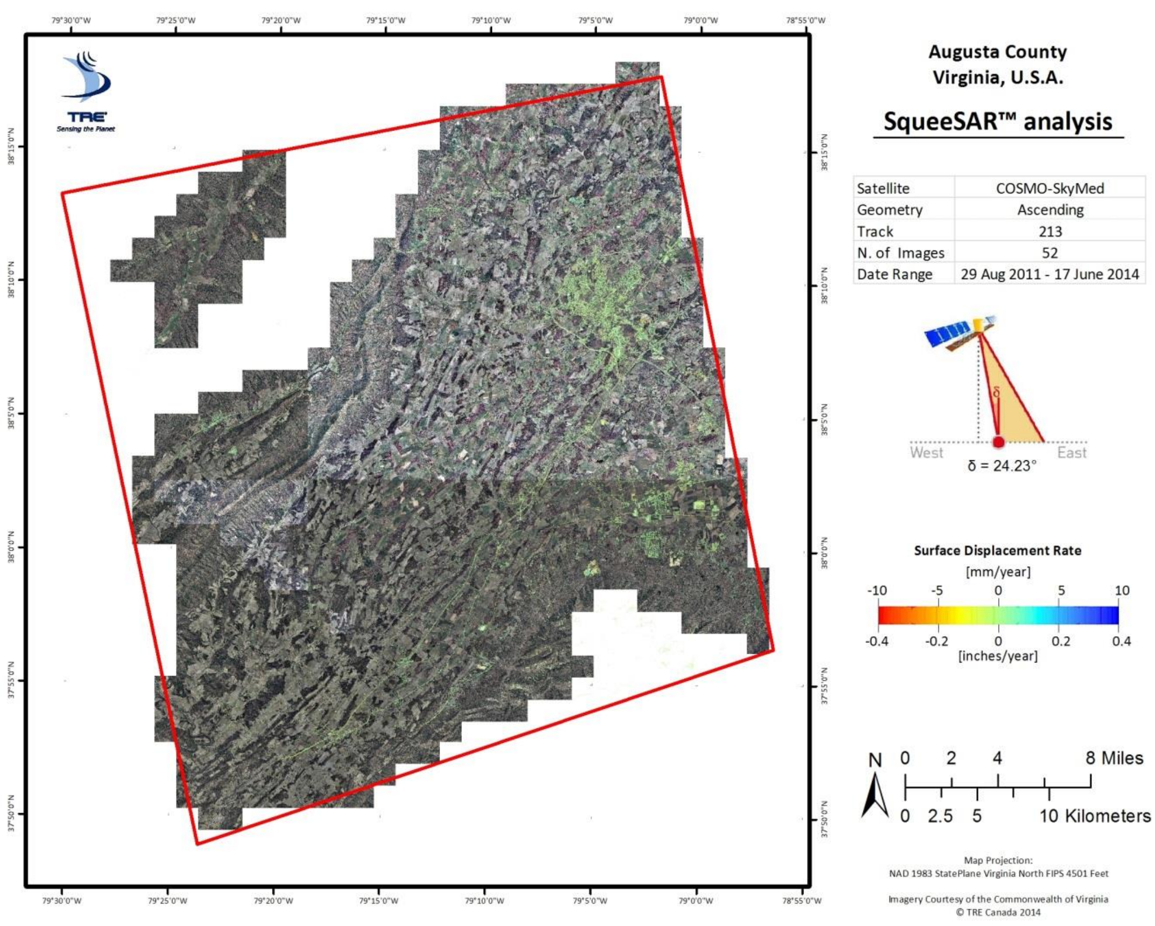

Figure 6: Surface displacement results identified from the TS, expressed in millimeters per year.

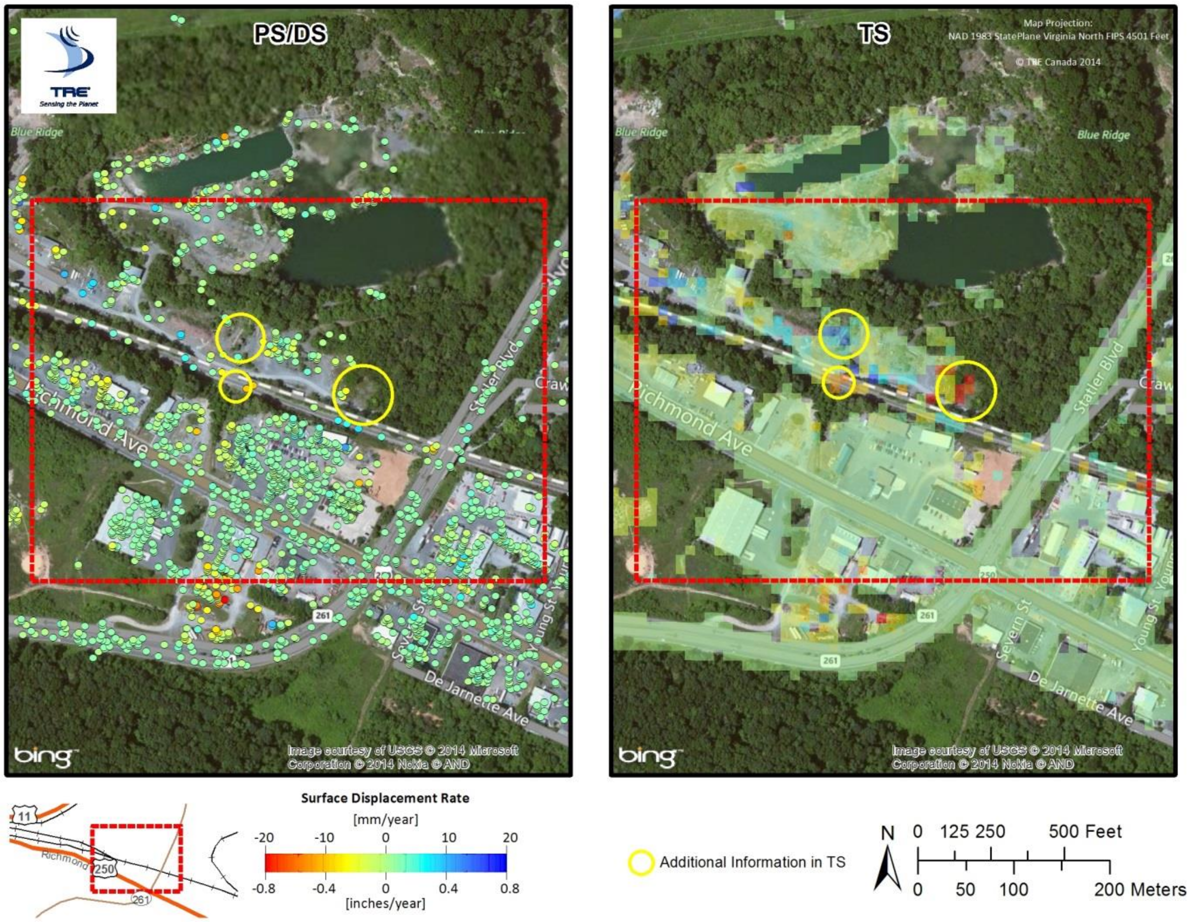

Figure 7: Comparison between PS/DS and TS results. Three areas where additional information was extracted using TS are highlighted with yellow circles.

5 Observations

The diverse nature of the AOI provides ample opportunities for the application of InSAR to detect ground movement at the locations where potential geohazards could occur, including sinkholes and unstable slopes, and to attempt to assess pavement conditions. The results of the reflector analysis over the Route 262 Bridge and City of Staunton Water Treatment Plant are detailed in Section 5.1. Movement detected over primary roads is described in Section 5.2. Several areas of localized movement were detected and those located close to potential geological instabilities are discussed in Section 5.3. Note that all of the individual and grouped measurement points highlighted in the figures in section 5 are labelled 'TS'. In this case, the acronym TS refers to the Time Series of the data, and not temporary scatterers as discussed in Section 4.4.

The processing of 52 CSK images over a 34-month time span produced a density of 180 PS and DS per square kilometre (1,049 PS/DS per square mile). With this larger data stack collected over a longer period of time, the precision of the results has reached sub-millimetre scale and the density of points has more than doubled compared to the previous results (Table 2).

Further statistics summarizing the results of the data processing can be found in Technical Appendix.

	2011		2012		2014	
Attribute	**Cluster 1 Results**	**Cluster 2 Results**	**Cluster 1 Results**	**Cluster 2 Results**	**Cluster 1 Results**	**Cluster 2 Results**
Dates	29 Aug 2011 – 20 Feb 2012		29 Aug 2011 – 25 Oct 2012		29 Aug 2011 – 17 Jun 2014	
Period covered (months)	6		14		33	
N. of images processed	16		32		52	
N. of PS	38,057 (20%)	336 (12%)	166,348 (56%)	1,453 (49%)	461,656 (72%)	3,975 (62%)
N. of DS	148,536 (80%)	2,486 (88%)	129,773 (44%)	1,512 (51%)	180,388 (28%)	2,469 (38%)
Total N. of Measured Points (PS and DS)	186,593	2,822	296,121	2,965	642,044	6,445
Average PS and DS Density (per square km) Cluster 1 and 2 combined	53 pts/km^2 (307 pts/mi^2)		83 pts/km^2 (484 pts/mi^2)		180 pts/km^2 (1049 pts/mi^2)	
Average Displacement Rate (mm/year)	2.1	0.6	0.2	-0.2	-0.2	-0.4
Average Displacement Rate Standard Deviation (mm/year)	3.4	8.7	1.5	1.4	0.6	0.4
Average Acceleration Rate (mm/$year^2$)	8.6	62.9	0.5	-3.5	-0.2	-0.7
Average Acceleration Rate Standard Deviation (mm/$year^2$)	50.3	129.4	9.6	8.7	1.7	1.2

Table 2. Statistics of the two clusters identified over the Virginia AOI.

5.1 Artificial Reflectors

A total of six artificial reflectors (AR) were installed within the Virginia AOI between December 2011 and January 2012 to highlight specific areas of interest for monitoring. Four of the ARs were installed on the Route 262 Bridge (top left in Figure 8), one was installed on the Staunton water treatment plant (top right in Figure 8), and the last one was installed at the Virginia Department of Transportation (VDOT) Materials building (bottom left in Figure 8). A location map of the reflectors is shown on the bottom right in Figure 8. The ARs on Route 262 were installed to determine whether InSAR could be used to detect movement during a bridge load test.

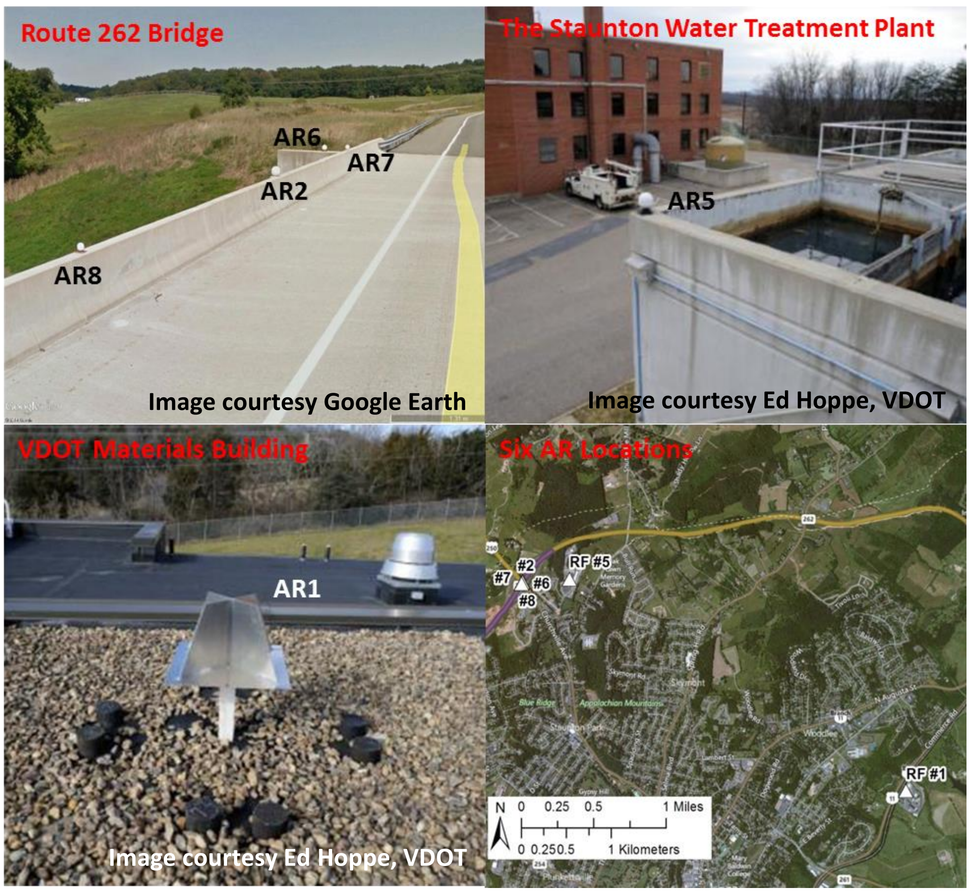

Figure 8: Top two and bottom left panels show close ups of the installed reflectors and the bottom right panel represents the locations of the six reflectors.

5.1.1 AR Visibility Analysis

A reflector visibility analysis was conducted in August 2014 to examine the amplitude values of radar imagery acquired before and after AR installation. A summary of the results is shown in Table 3. Three out of six reflectors (AR #2, AR #6, AR #5) were visible to the radar satellite compared to prior results, where only two were visible (AR5 has become visible). It is worth noting that AR #7 on the Route 262 Bridge is visible in the amplitude imagery. However, the reflectivity of the signal is not yet stable nor strong enough to allow the target to become a PS. AR #5, located at the City of Staunton Water Treatment Plant, was visible to the satellite until it was removed in September 2013. The removal of the reflector can be identified in the amplitude time series by the drop in value after 17 August 2013 (Figure 9). Similar to previous results, ARs #8 and #1 are not visible to the satellite. A complete listing of amplitude results for every reflector is provided in the Technical Appendix.

AR	Location	AR Type	RCS Value (m^2)	Visibility to Radar Satellite	Note
2	Rte 262 Bridge, top of parapet mid-span	Luneburg	10	Yes	PS (code: 0042E)
6	Rte 262 Bridge abutment wingwall	Luneburg	50	Yes	PS (code: 00471, reference)
7	Rte 262 Bridge, top of parapet at 1/4 span (north)	Luneburg	2	Yes	The radar signal is not yet stable enough for the point to become a PS.
8	Rte 262 Bridge, top of parapet at 1/4 span (south)	Luneburg	1	No	
5	City of Staunton Water Treatment Plant	Luneburg	6	Yes	PS (code: ADRXL, removed after Sep 2013)
1	Virginia DOT Roof	Double Geometry	172*	No	

Table 3: Summary of the visibility to the satellite of the six ARs installed within the RITA AOI. *This RCS value is based on TREs double geometry reflector design.

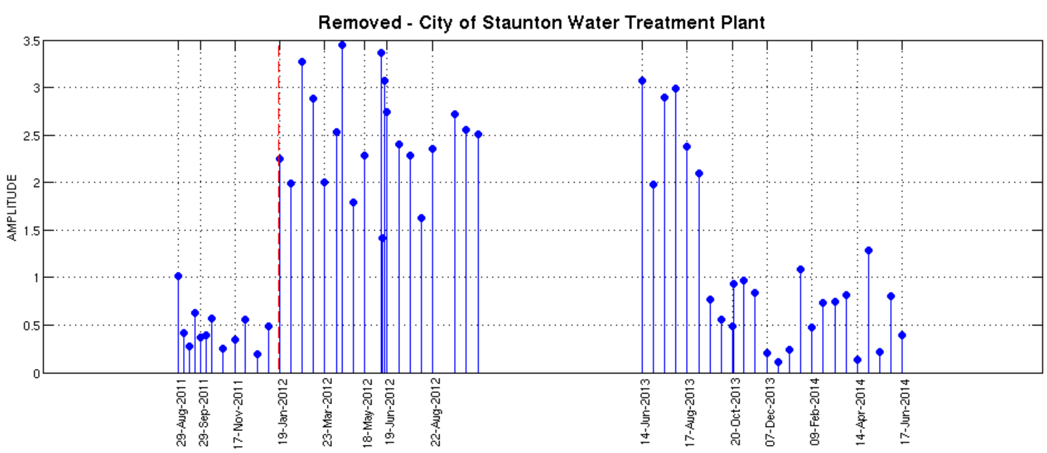

Figure 9: Time series of amplitude values for Reflector #5. The dashed red line corresponds to the date of installation while the drop in amplitude indicates removal of the reflector in September 2013.

5.1.2 AR Displacement Analysis

The strength of the reflected signals for reflectors #2, #6 and #5 was sufficient to perform deformation measurements. The results over the Route 262 Bridge are shown in Figure 10.

Reflector #6 was used as the reference, since it is positioned on a stable section of the bridge abutment wingwall where no deformation was expected. The time series for Reflector #2, located at mid-span, is shown in Figure 11, with the load test date highlighted.

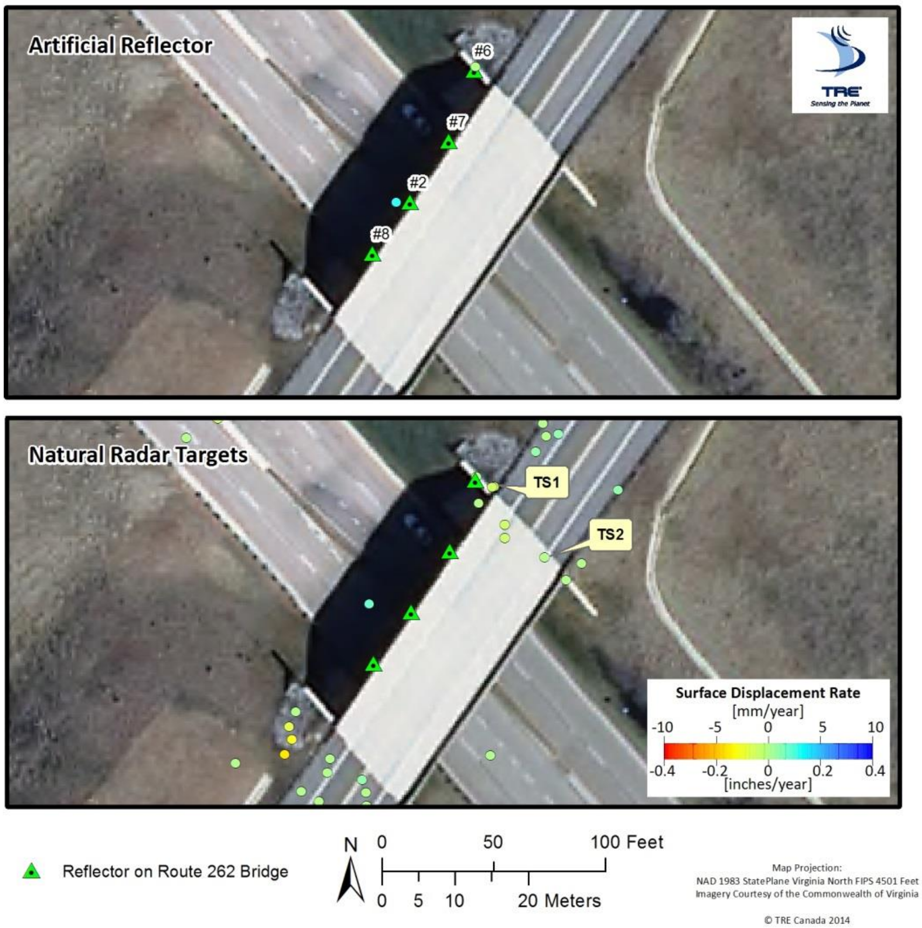

Figure 10: Displacement results on the bridge across route 262. The top panel represents the displacement of the reflectors and the bottom panel denotes displacement of natural radar targets.

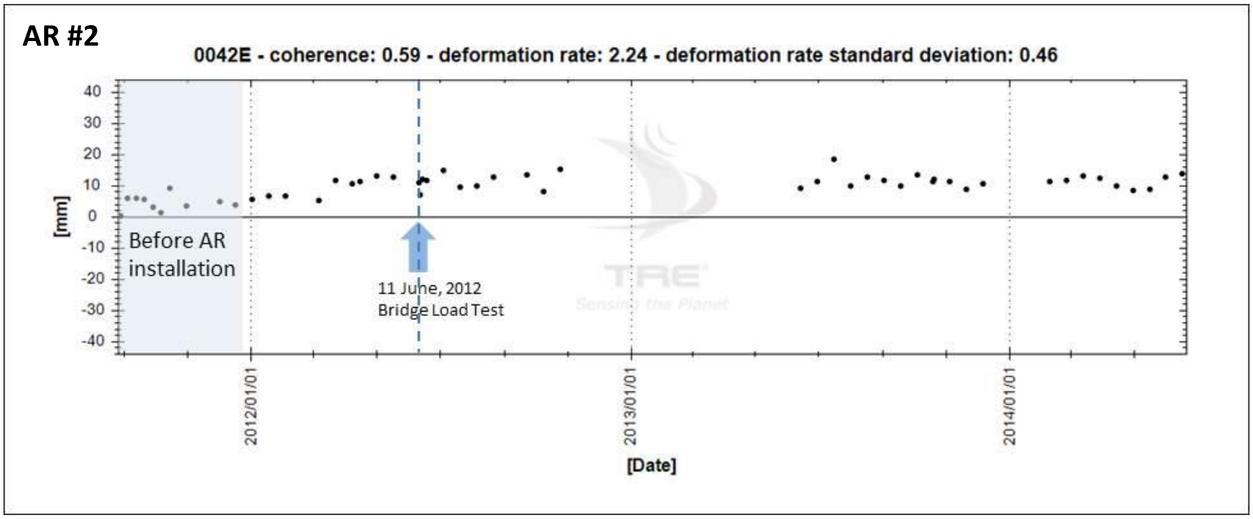

Figure 11: Time series of surface displacement for reflector #2 (a bridge load test conducted on 11 June 2012).

There are also a few measurements obtained from natural radar targets on the bridge (bottom panel in Figure 10), two of which were selected for further analysis. The first target was located on the abutment wingwall (TS1 in Figure 10) close to reflector #6 (Figure 12), and the second (TS2) was on the bridge at the north approach (Figure 13).

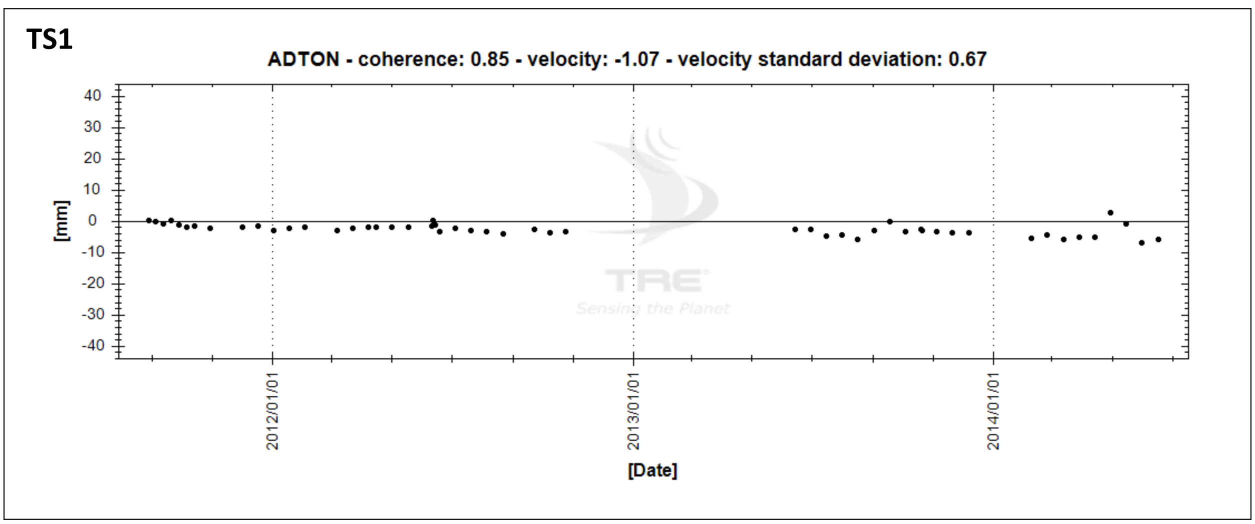

Figure 12: Time series of surface displacement for the measurement point identified as TS1 in Figure 10.

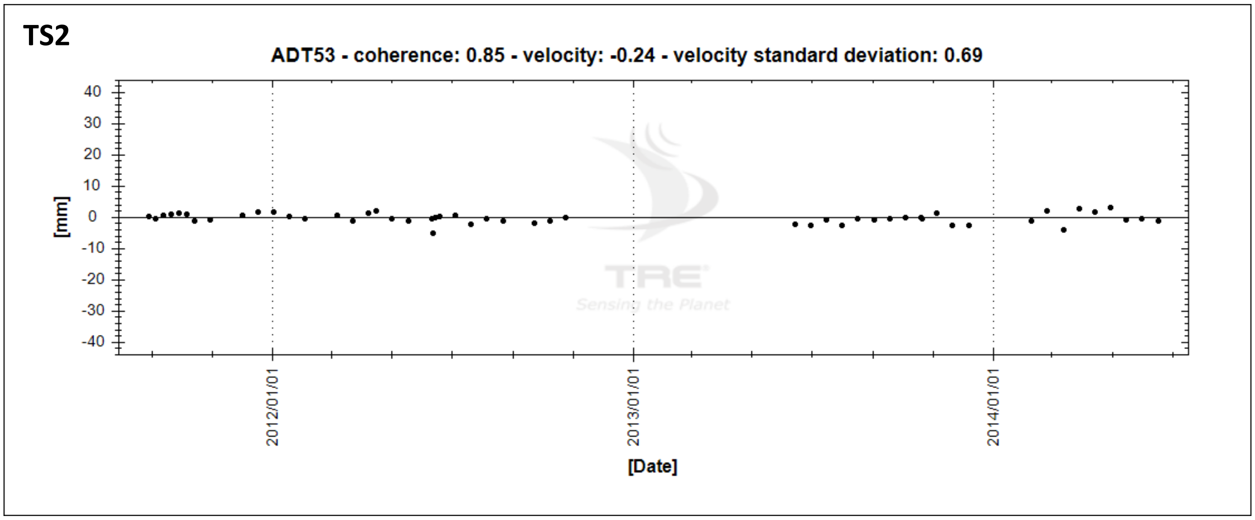

Figure 13: Time series of surface displacement for the measurement point identified as TS2 in Figure 10.

In addition to those on the Route 262 Bridge, AR #5 on the water treatment plant was also analyzed. With the addition of the extra images acquired since the previous processing the signal has become robust enough to become a PS. It will likely disappear again in the next processing as it has since been removed. The signal was consistent during the timeframe in which the reflector was present (Figure 14), but was noisier both before AR installation and after its removal.

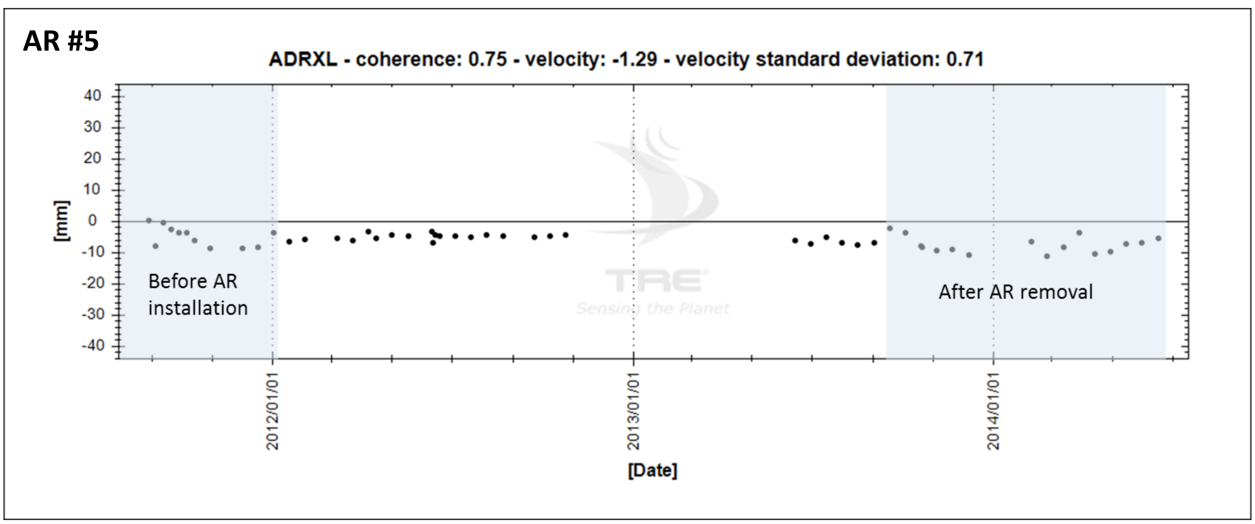

Figure 14: Time series of surface displacement for reflector #5.

5.2 Results over Primary Roads

Displacement rates for measurement points identified within a 30 m buffer around eight primary roads (I-81, I-64, Rt. 11, Rt. 250, Rt. 254, Rt. 262, Rt. 252 and Rt. 600) are shown in Figure 15. Nine sections of road are highlighted to focus on inspection of the ground displacement around the primary roads and their specific locations of subsidence are listed in Table 4.

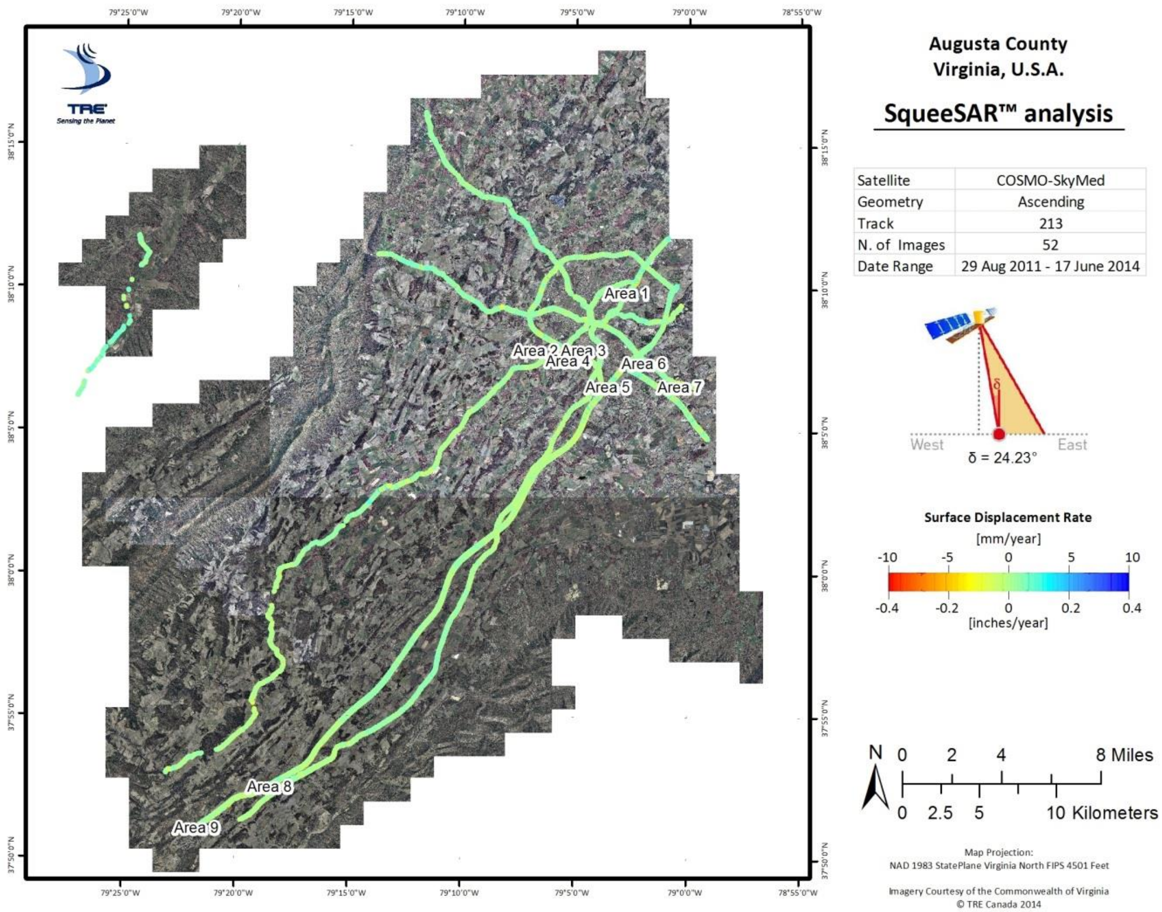

Figure 15: Surface displacement results identified within a 30 meter (100 foot) buffer of major roads within the AOI. Nine roads are indicated, with their specific locations listed in Table 4.

Area	Location	Brief Description of Subsiding Area	Maximum Displacement (mm/yr)
1	38°10'19.42" N; 79°2'15.82"W 38°9'58.21" N; 79°2'35.67"W	Railroad track running parallel to Lee Highway (Rt. 11)	-10.33 -4.8
2	38°7'57.82" N; 79°5'36.93"W	Slope along Route 262 approach to overpass of Middlebrook Ave (Rt 252)	-6.5
3	38°7'57.68" N; 79°5'30.17"W	Slope along an exit from Route 262 to Middle brook Ave	-7.0
4	38°7'34.72" N; 79°5'10.32"W	Exposed ground on the shoulder of Woodrow Wilson Parkway (Rt. 262)	-5.8
5	38°6'44.6" N; 79°3'24.6"W	State Route 635 bridge overpass above I-81	-7.03
6	38°7'24.95" N; 79°1'48.91"W	Railroad track running parallel to Jefferson Highway (Rt. 250)	-9.7
7	38°6'42.36" N; 79°0'14.69"W 38°6'41.94" N; 79°0'11.71"W	Jefferson Highway (Rt. 250) near Greenview Dr	-6.9
8	37°52'37.39" N; 79°18'13.34"W	Along shoulder of I-64	-6.6
9	37°51'8.50" N; 79°21'29.13"W	Along shoulder of I-64	-5.8

Table 4: Coordinates of the twelve highlighted locations indicated in Figure 15. All coordinates were obtained from PS points indicating subsidence within the areas of interest.

Area 5 and 7 correspond to small groups of two or three measurement points located on roads or bridges and are presented in further detail in the figures below. All of the measurement points highlighted in the time series below are of the PS type.

5.2.1 Area 5 - State Route 635 bridge overpass

Area 5 is located on the State Route 635 bridge overpass of I-81 (Figure 16). A measurement point with a displacement rate of -7.0 mm/yr is highlighted (Figure 17).

Figure 16: Displacement results on the State Route 635 bridge overpass (Identified as Area 5 in Figure 15).

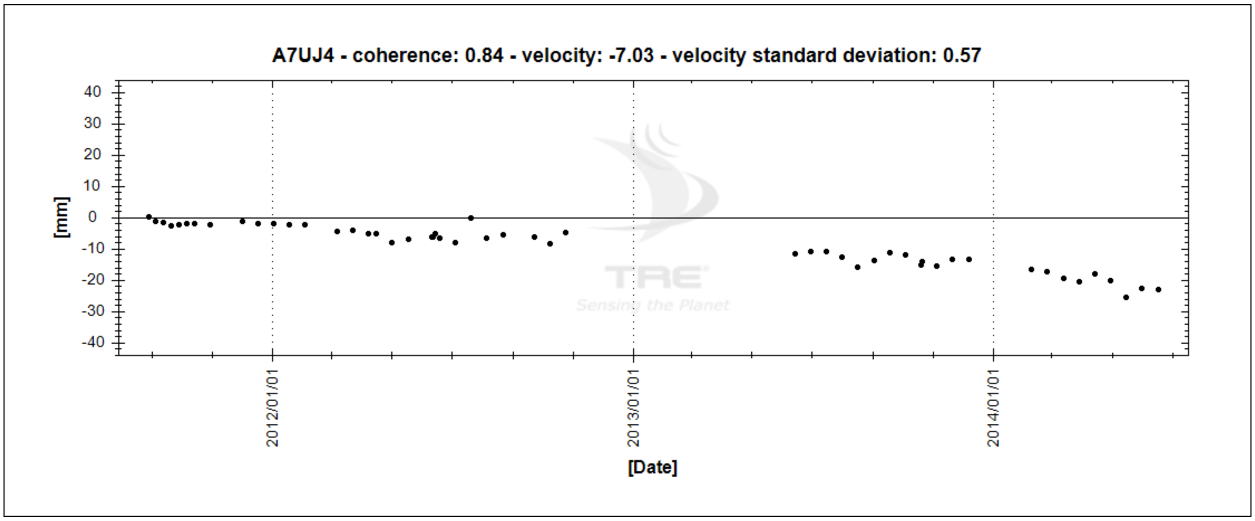

Figure 17: Time series of TS1 in Figure 16.

5.2.2 Area 7 - Jefferson Highway (Rt. 250) near Greenview Dr

Several measurement points indicate sudden displacement starting in 2014 in this area of Jefferson Highway (Figure 18). Movement begins in 2012 in TS1 (Figure 19) but starts later and more abruptly in TS2 and TS3 (Figure 20 and Figure 21).

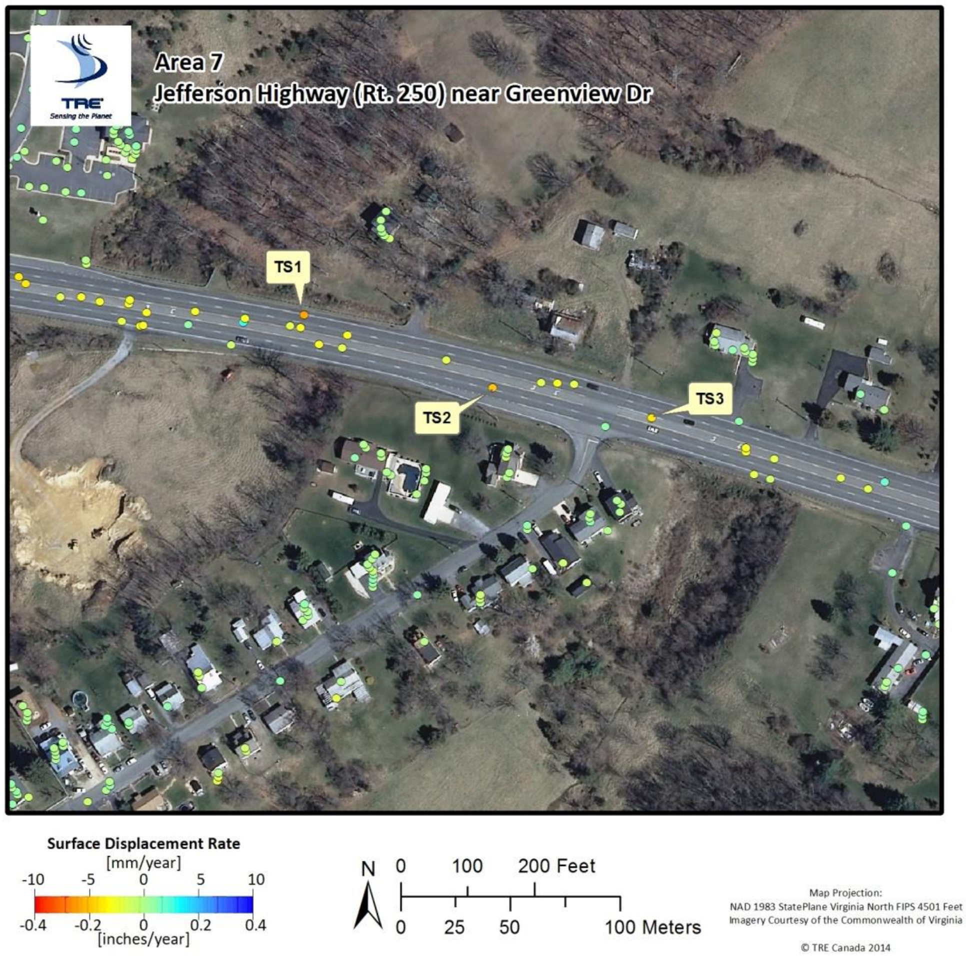

Figure 18: Displacement results over Jefferson Highway (Rt. 250) near the intersection with Greenview Dr (identified as Area 7 in Figure 15).

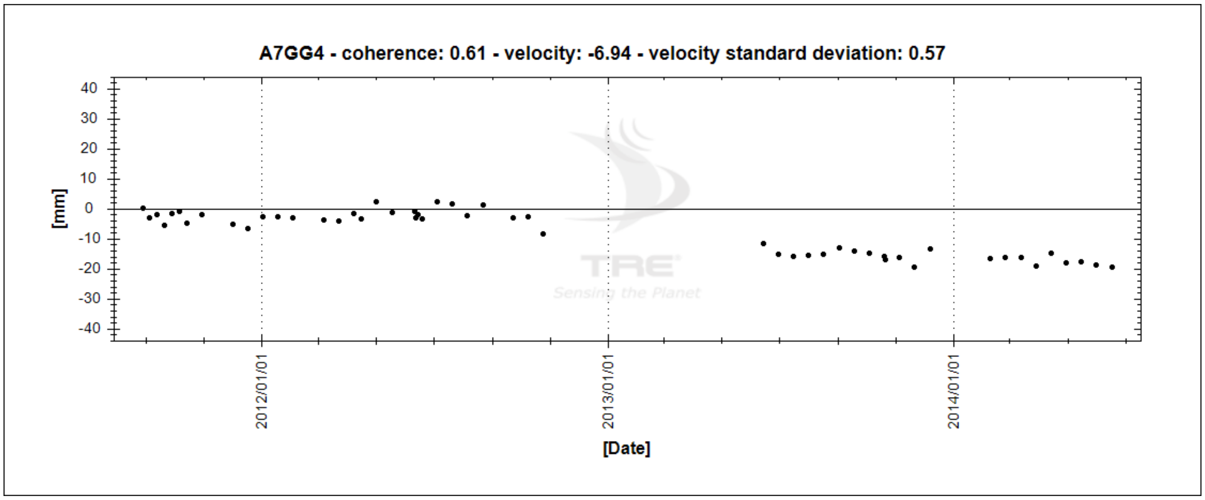

Figure 19: Time series of TS1 in Figure 18.

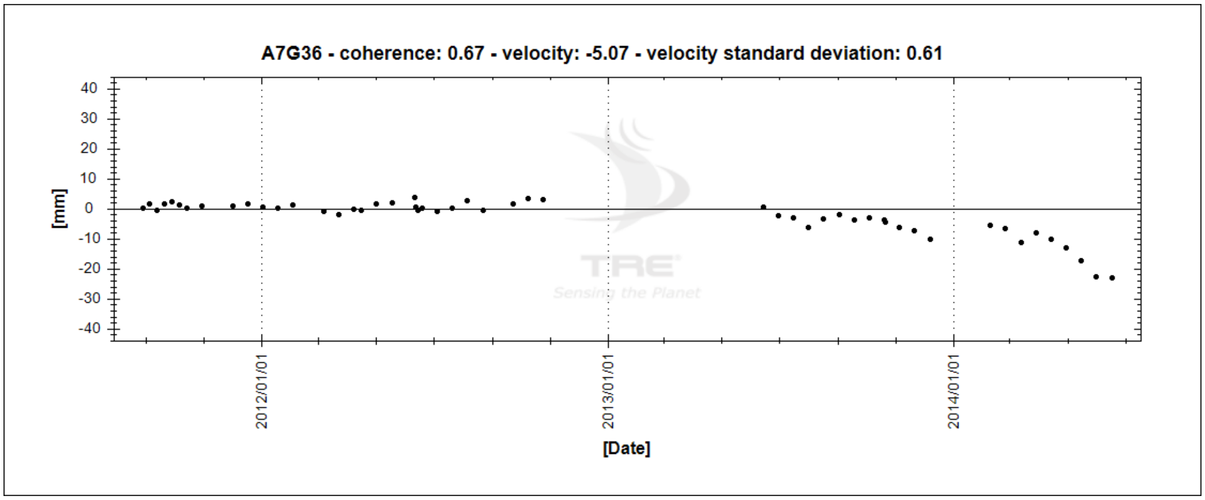

Figure 20: Time series of TS2 in Figure 18.

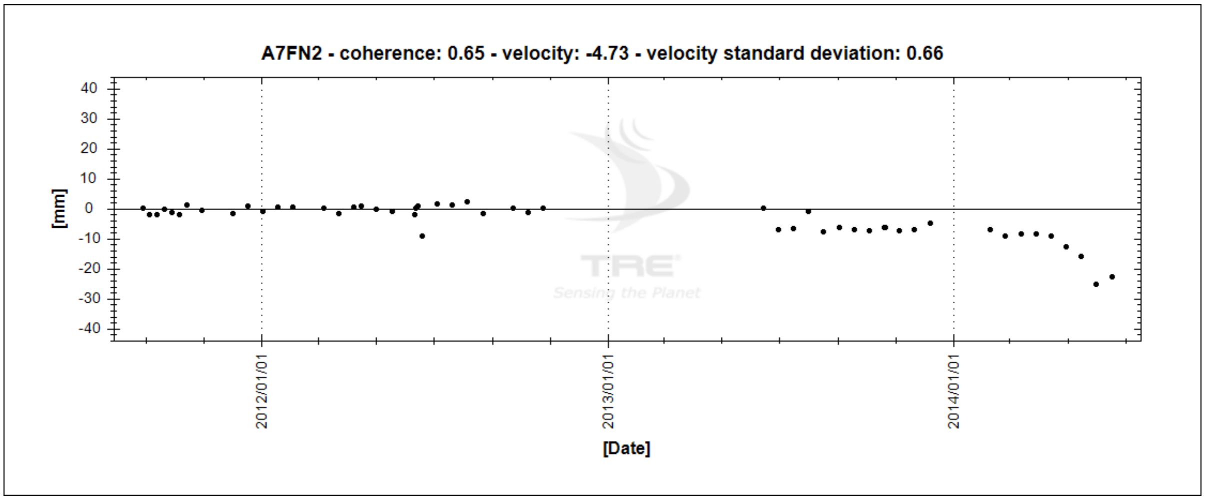

Figure 21: Time series of TS3 in Figure 18.

5.3 Comparison to Geohazards Data

Shown below are the displacement results overlaid with historic sinkholes, landslides and other geohazards data provided by the Commonwealth of Virginia (Figure 22). A total of 30 sinkholes, one slope failure, as well as 23 karst geohazards located along Interstate 81 are indicated. In the current analysis, continuous monitoring was completed for fifteen points of interest (POI) that are relevant to the University of Virginia and the Virginia Department of Transportation , specifically in relation to the detection of sinkholes, landslides and road/bridge monitoring. These points were also highlighted in previous report (Doc. Ref.: JO11-3011-REP2.0)

Five locations (Feature 1 to 5 in Figure 22) are analyzed further in the following section. These features were selected either because localized surface displacement was identified or they represent areas where known geohazards were identified in the field during the monitoring period.

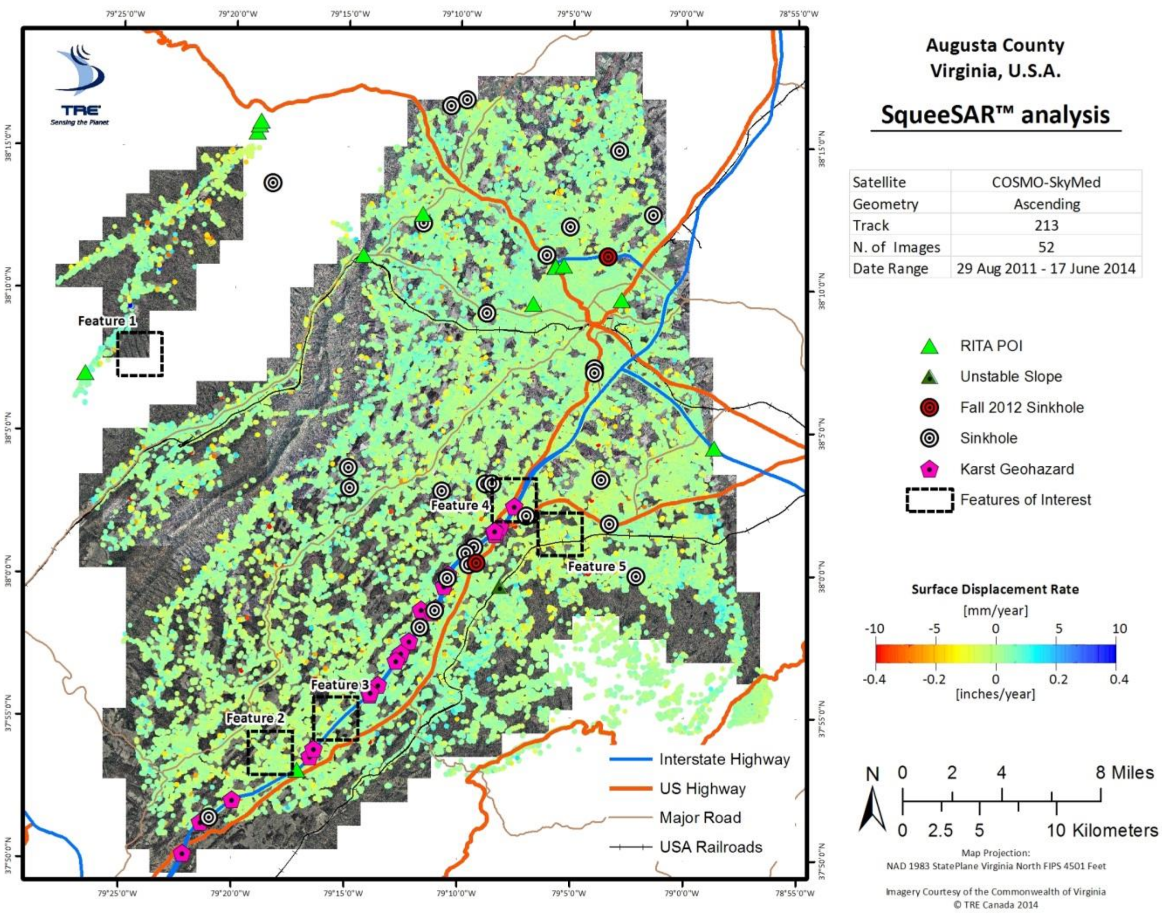

Figure 22: Historic geohazard event data and points of interest within the Virginia AOI overlaid on the surface displacement results.

5.3.1 Feature 1 – Rock Slope on Route 600

Feature 1, located on a rock slope along Route 600 (Figure 23), had subsidence rates of up to -9.1 mm/year. An average rate of -8.5 mm/yr was calculated using a group of measurement points located on the slope (Figure 24). Mild positive rates were detected at the bottom of the slope and on the road, possibly due to a rotational movement of the slope, which would produce a slight uplift of the road surface (Figure 25).

Figure 23: A close-up of displacement results over Feature 1 in Figure 22.

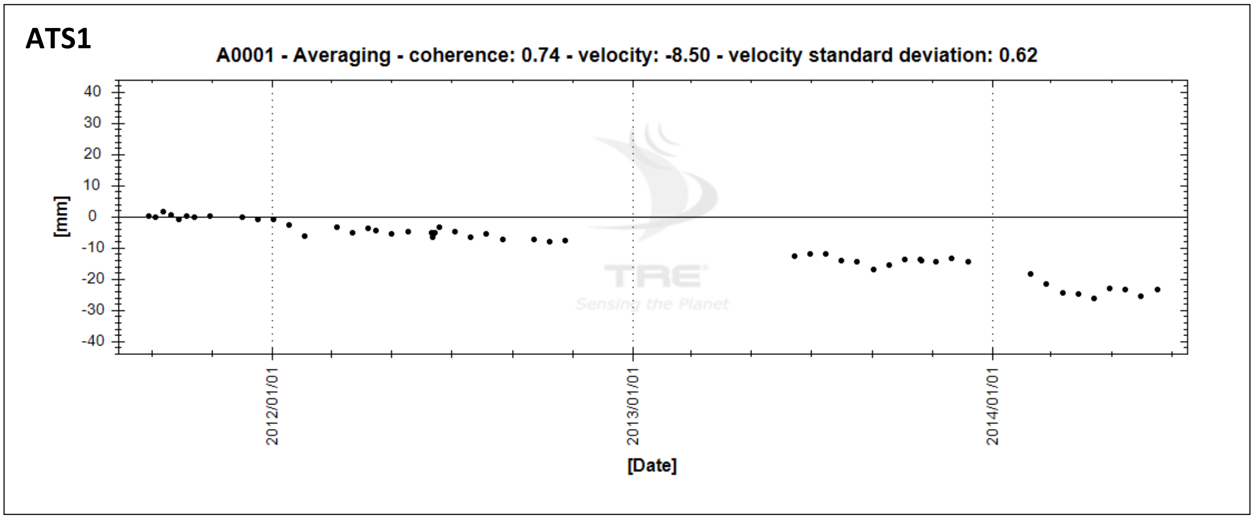

Figure 24: Average time series for ATS1 in Figure 23.

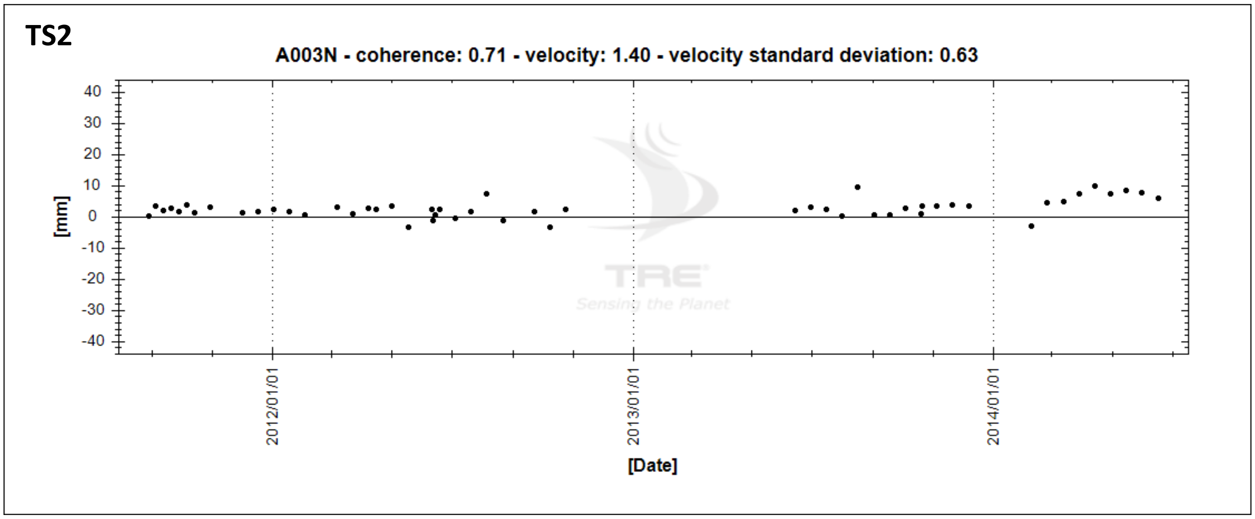

Figure 25: Time series of TS2 in Figure 23.

5.3.2 Feature 2 – I-81

Feature 2 consists of two locations on I-81 (Figure 26). An overpass of Route 710 shows slight subsidence on both approaches and TS1 indicates movement ranging from -7 mm to -17 mm in one month (June – July 2014, Figure 27). As this result is a single point and the movement occurs near the end of the time series, it should be interpreted with caution and verified with an on-site inspection. Roughly 365 metres northeast of this location, movement was also detected on a riprap slope (Figure 28).

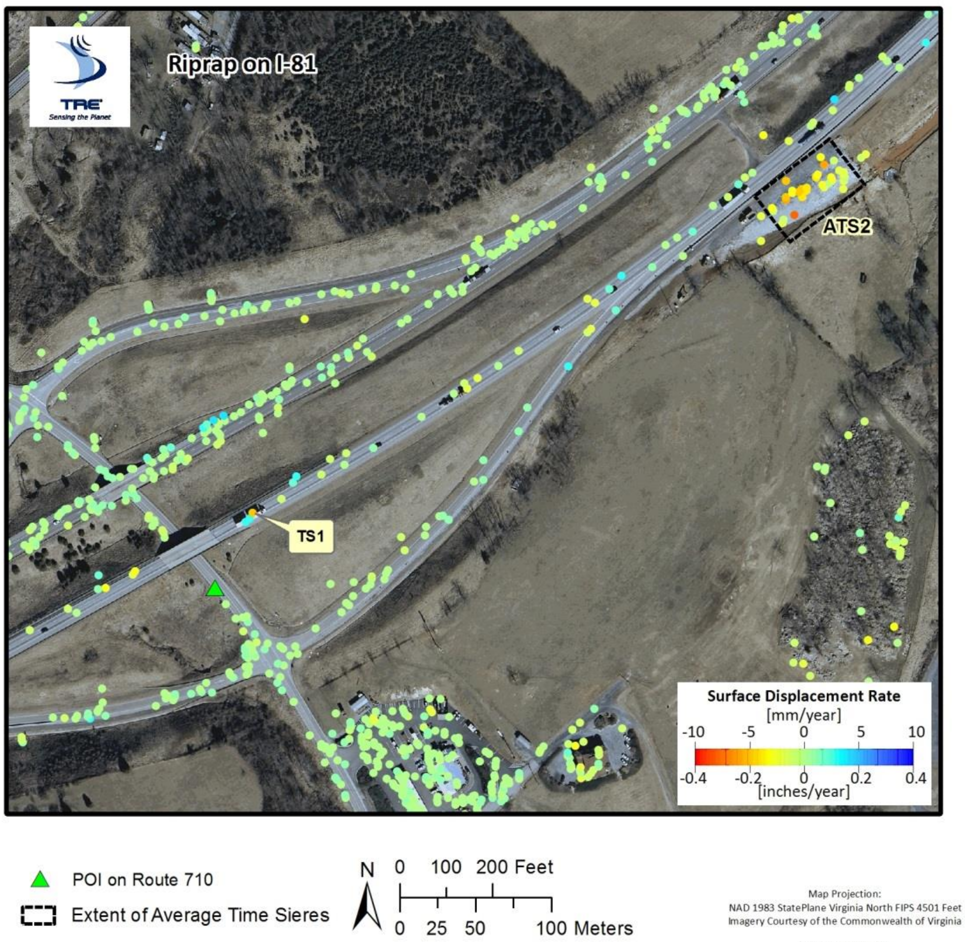

Figure 26: A close-up of displacement results over Feature 2 in Figure 22.

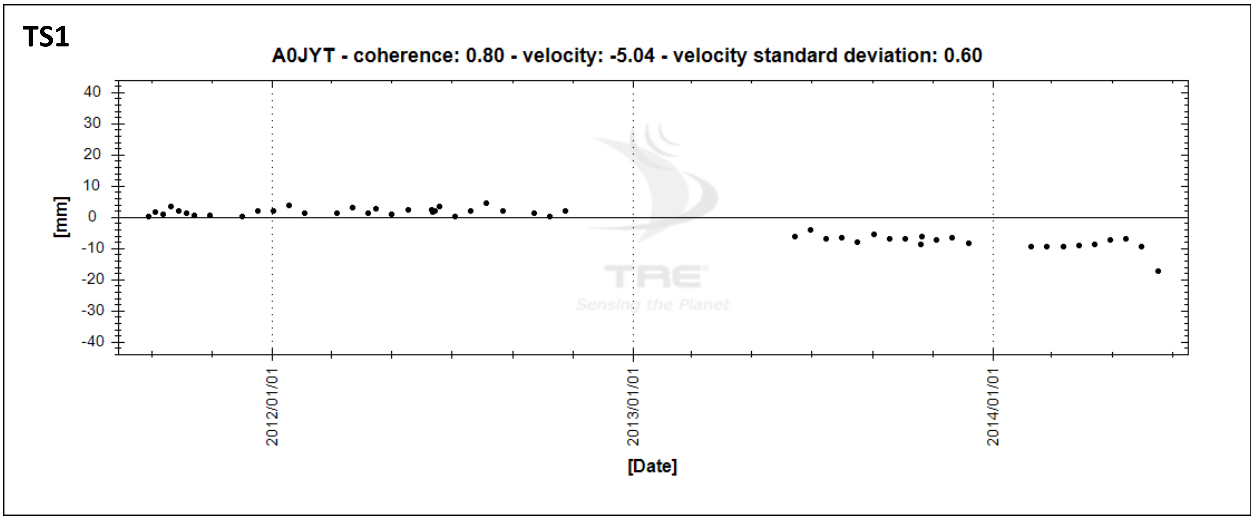

Figure 27: Time series of surface displacement for TS1 in Figure 26.

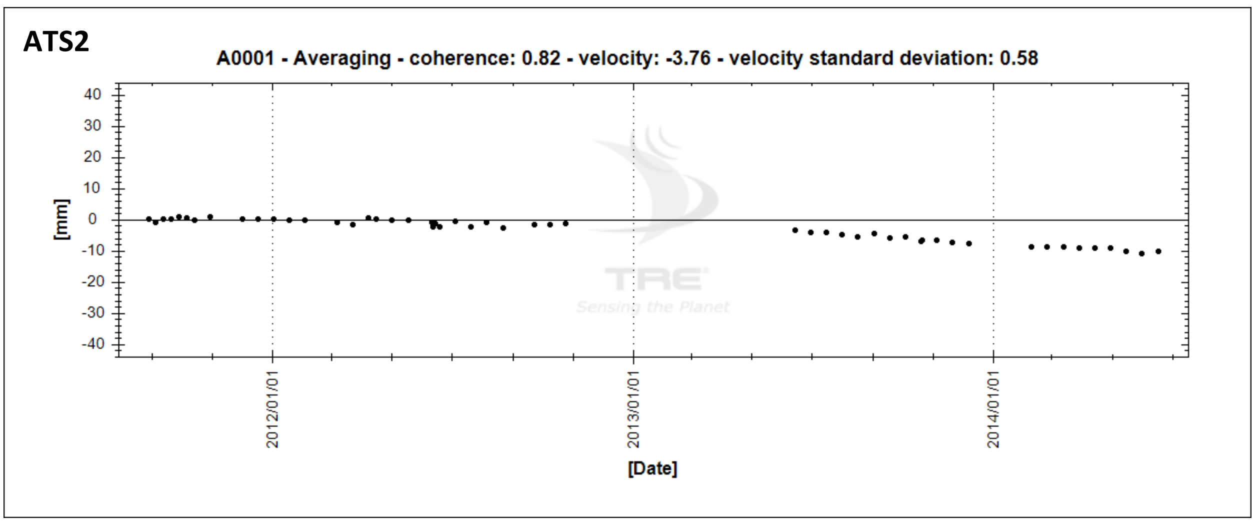

Figure 28: Average time series of surface displacement for ATS2 in Figure 26.

5.3.3 Feature 3 – Karst Geohazard and Riprap on I-64

Feature 3 is along I-64 in the southwest portion of the AOI (Figure 29). Subsidence rates up to -9.4 mm/yr and -14.7 mm/yr were identified approximately 115 metres (375 feet, TS1 in Figure 29) and 17 metres (55 feet, TS2 in Figure 29), respectively from a karst geohazard near I-64. TS1 indicates that subsidence started in July 2012 and appeared to stabilize after June 2013 (Figure 30). TS2 has a similar time series, with the exception of an additional movement from February to April 2014 (Figure 31).

Continuous movement was also identified on a riprap slope located along I-64 in this area (ATS3 in Figure 29), the average time series for which is shown in Figure 32.

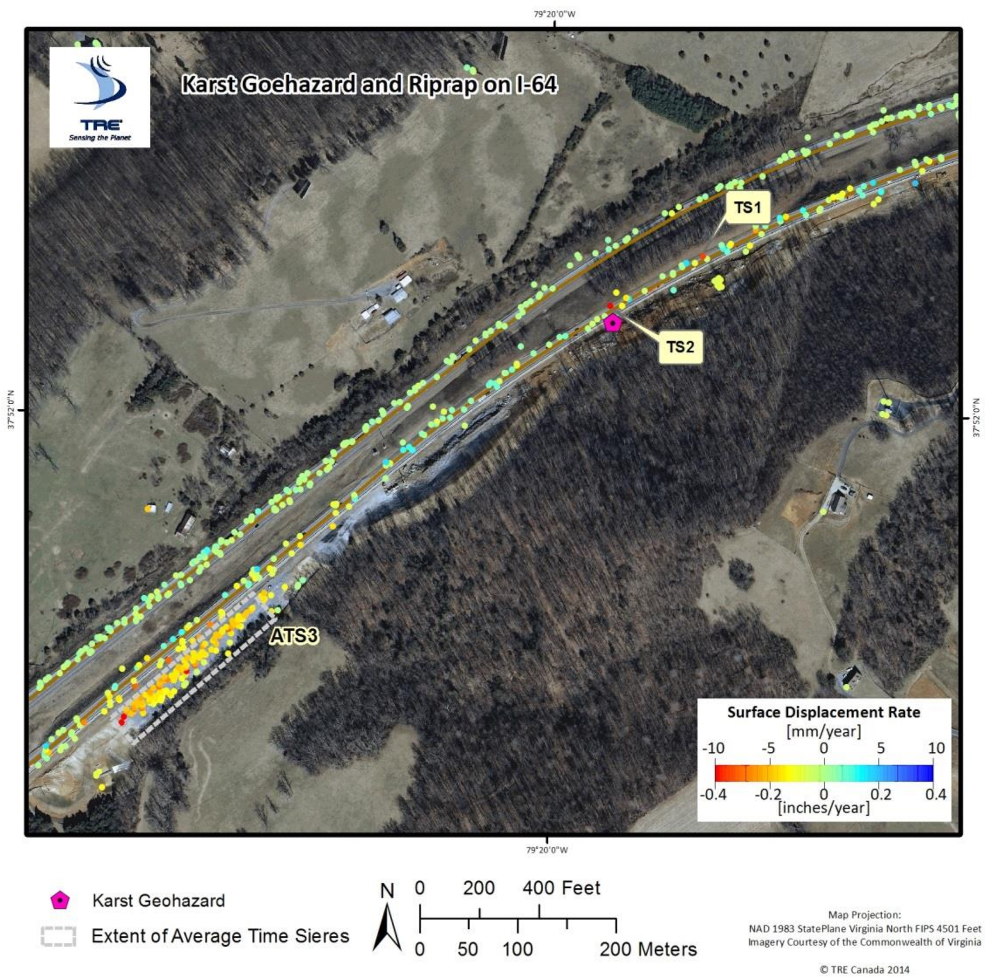

Figure 29: A close-up of displacement results over a karst geohazard and riprap slope on I-64.

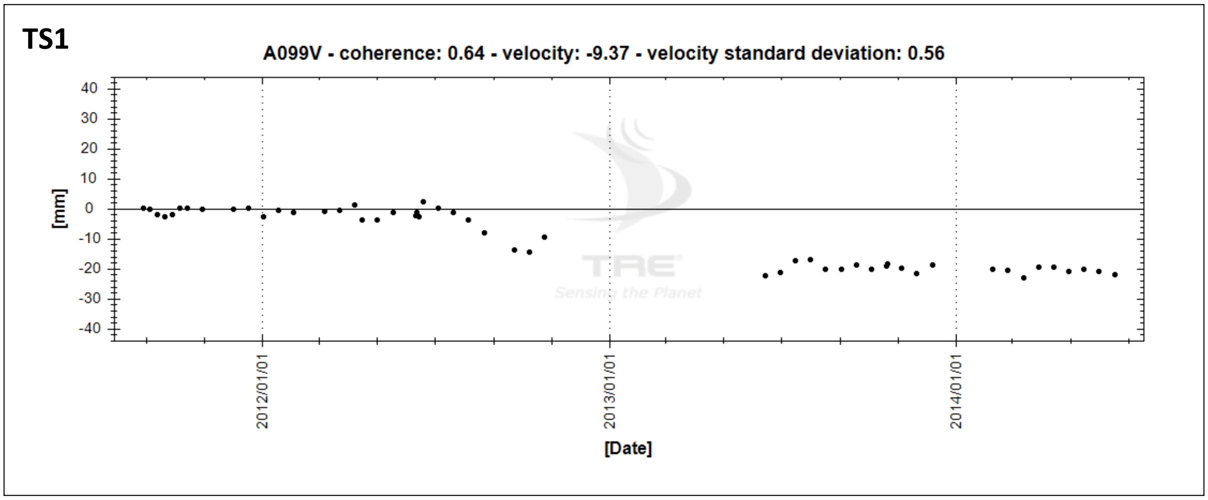

Figure 30: Time series of surface displacement for the measurement point identified as TS1 in Figure 29.

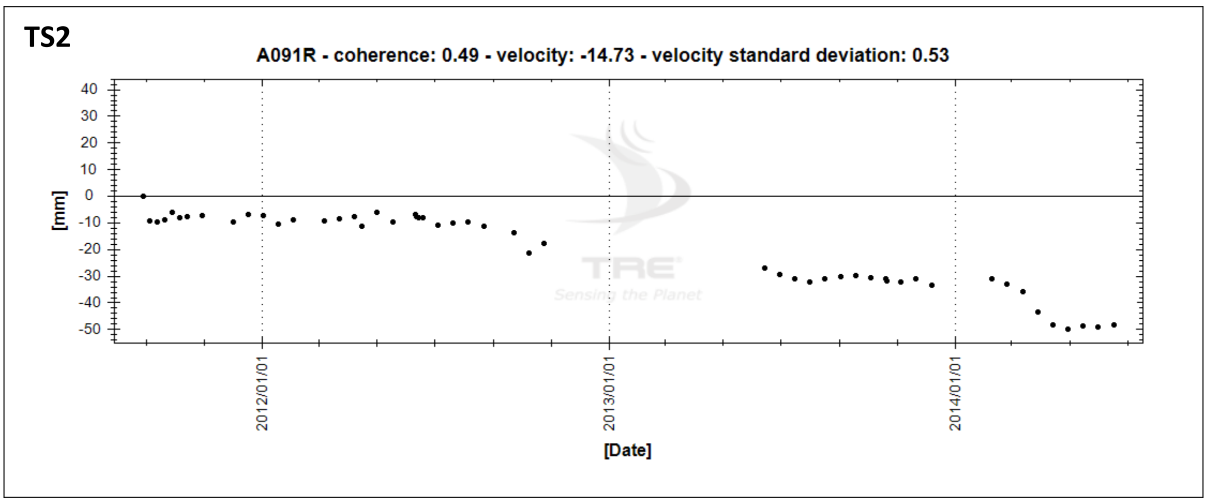

Figure 31: Time series of TS2 in Figure 29.

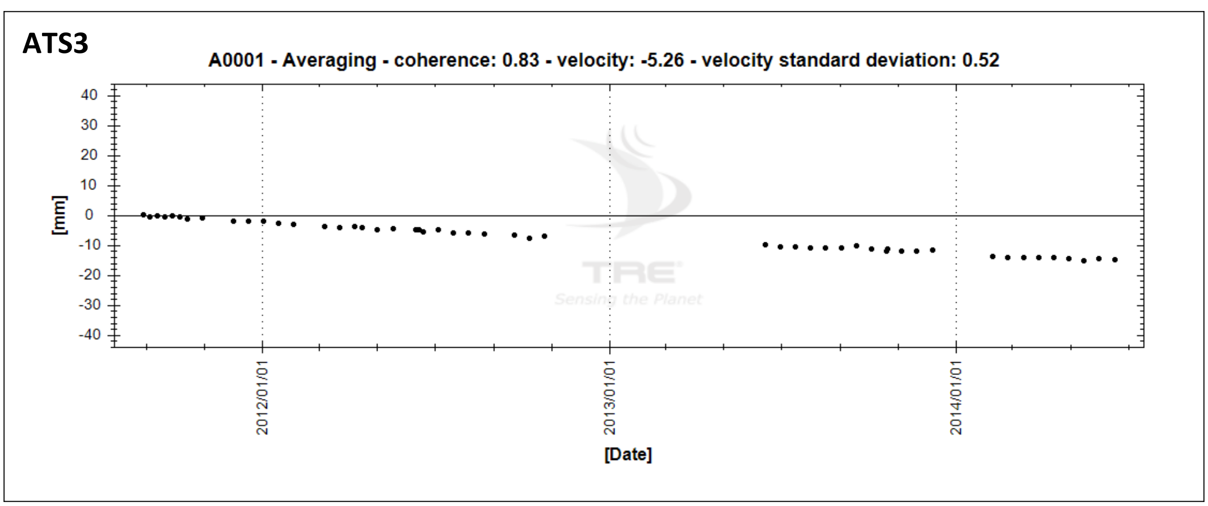

Figure 32: Average time series of ATS1 in Figure 29.

5.3.4 Feature 4 – Riprap on I-64

A riprap slope located close to the I-64 overpass of Highway 11 shows signs of deformation (Figure 33). The average time series indicates that movement did not occur until September 2013 (Figure 34). Three karst geohazard sites are also shown in Figure 33. Ground movement at these locations was less than -1.2 mm/yr.

Figure 33: A close-up of displacement results over a riprap slope on I-64.

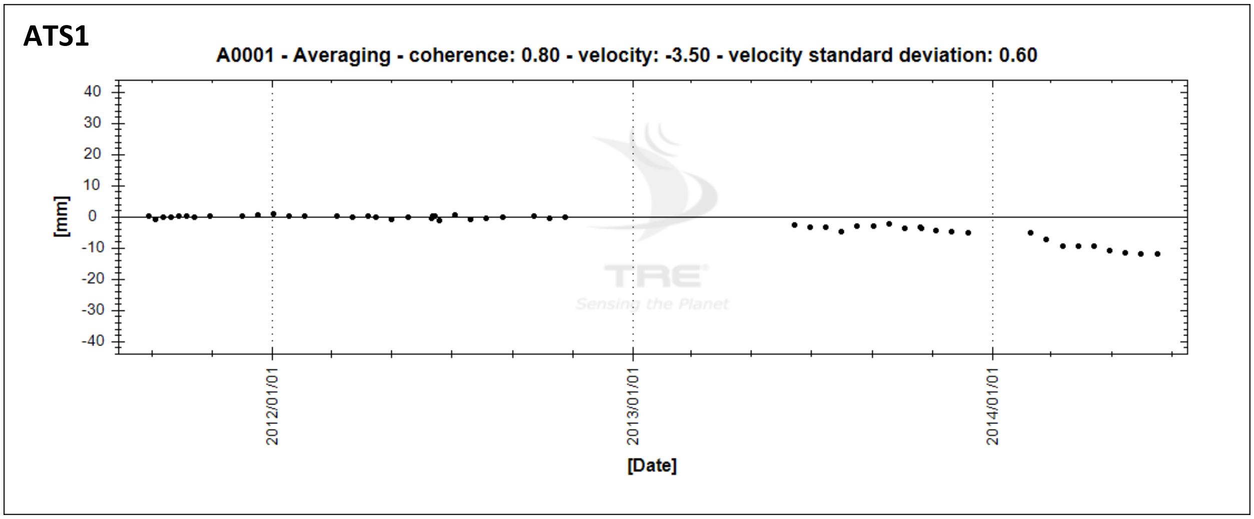

Figure 34: Average time series of ATS1 in Figure 33.

5.3.5 Feature 5 - Railway

Feature 5 is a stretch of railway between Greenville and Stuarts Draft in Augusta County (Figure 35) where a few locations with displacement rates up to -16 mm/yr were observed. Three individual points were highlighted from north to south and are labeled as TS1, TS2, and TS3, respectively (Figure 36 to Figure 38). Subsidence for TS1 was detected between February and October 2012, with gradual stabilization after June 2013. Subsidence in TS2 and TS3 started later and more abruptly in June 2013.

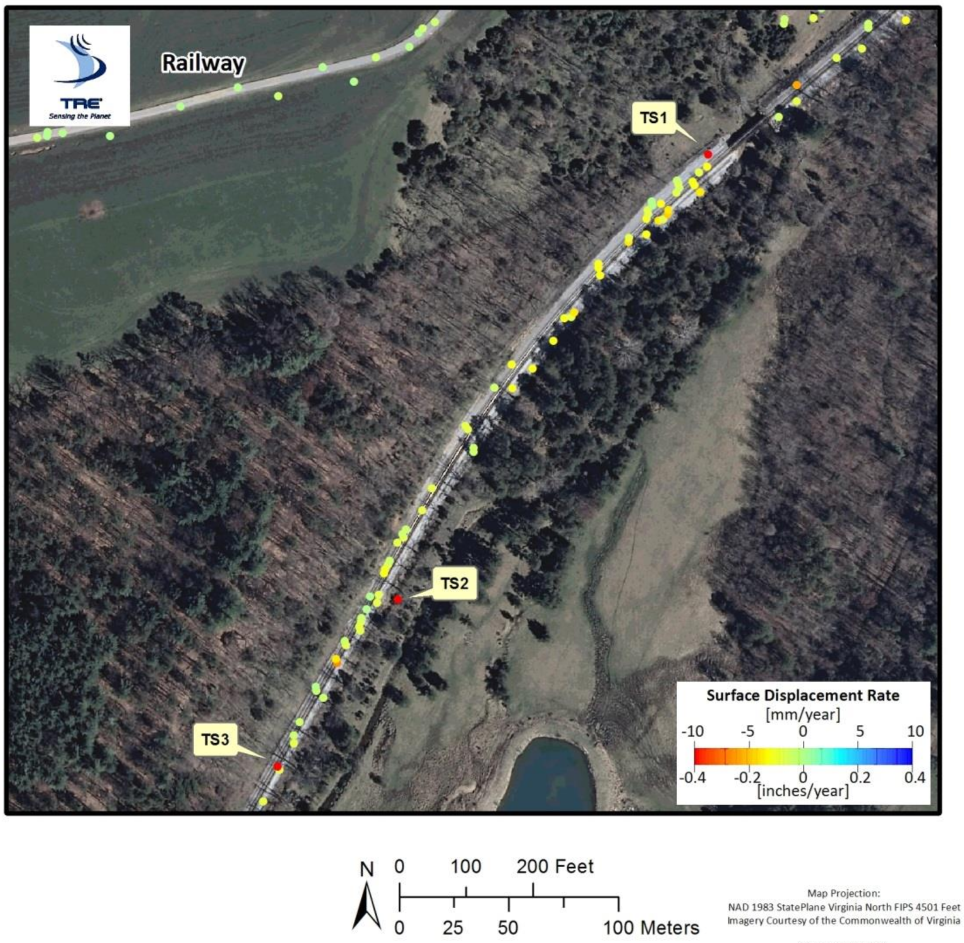

Figure 35: A close-up of displacement results along the railway between Greenville and Stuarts Draft in Augusta County.

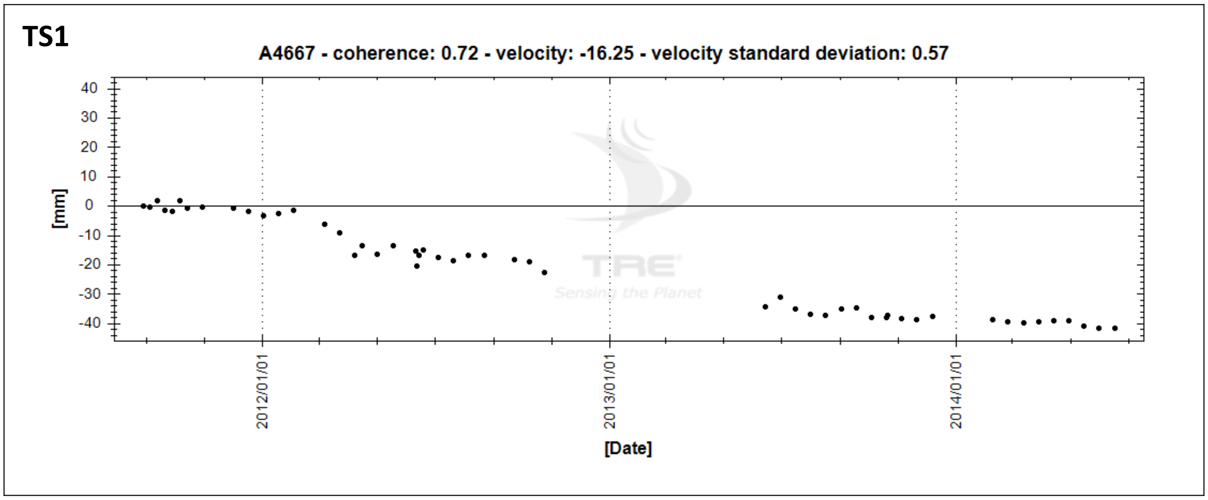

Figure 36: Time series of TS1 in Figure 35.

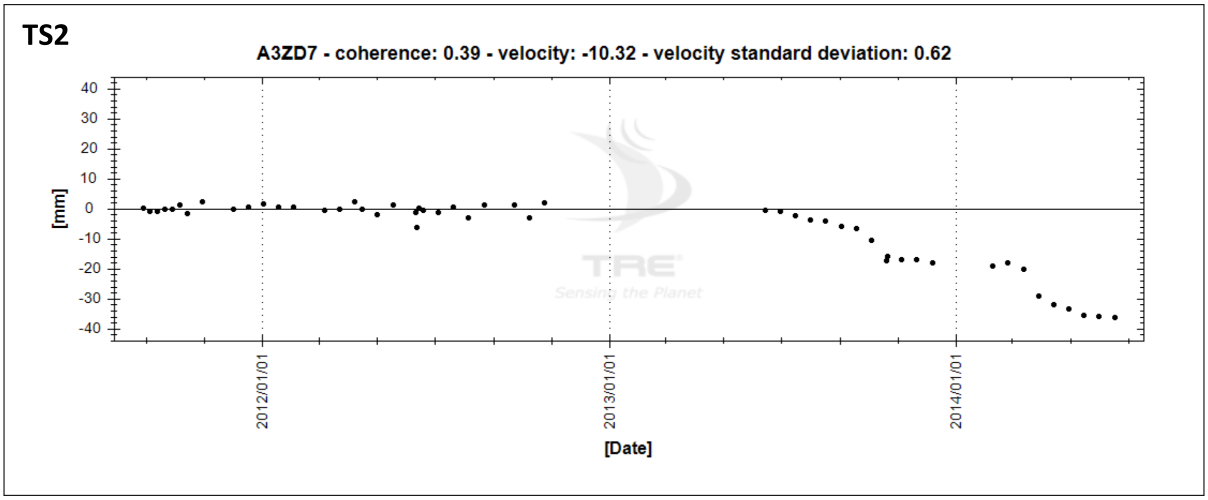

Figure 37: Time series of TS2 in Figure 35

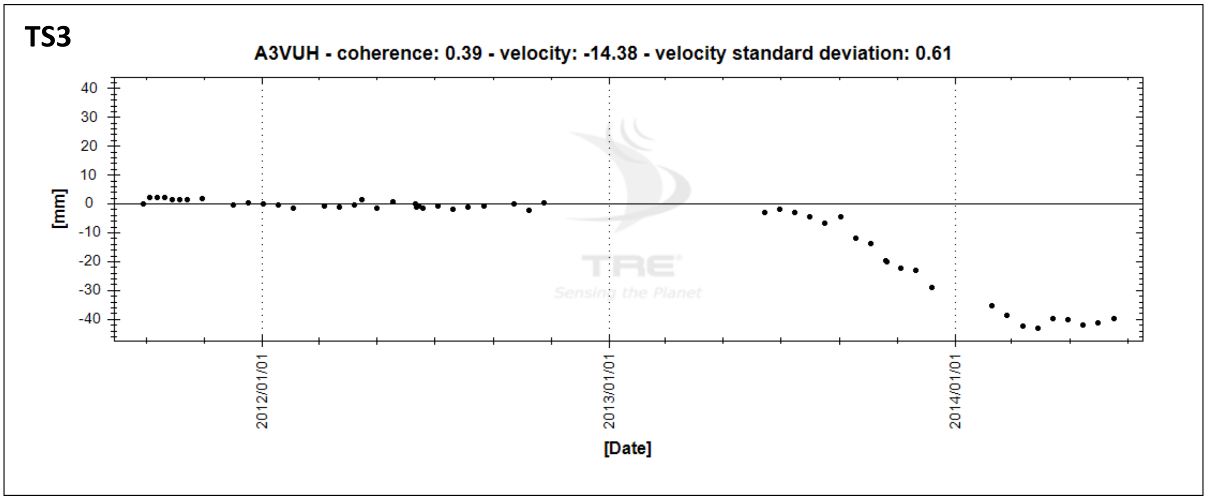

Figure 38: Time series of TS3 in Figure 35

5.3.6 Feature 6 - Sinkhole

A sinkhole was observed in September 2012 along Lee Jackson Highway in a vegetated area and is shown in the top panel of Figure 39 overlaid with Temporary Scatterers results. Similar to previous findings, the single DS measurement point identified in the vicinity of the sinkhole did not identify ground movement from PS/DS or Temporary Scatterers between 2013 to 2014 (Figure 40).

Another sinkhole that initially formed in July 2011 and which recurred in October 2012 is displayed in the bottom panel of Figure 39. Two measurement points close to the sinkhole are highlighted in Figure 41 and Figure 42. Due to the gap in image acquisitions from late October 2012 to early June 2013, the ground deformation during this period is not captured. No movement related to the sinkhole was found in the time series or Temporary Scatterers.

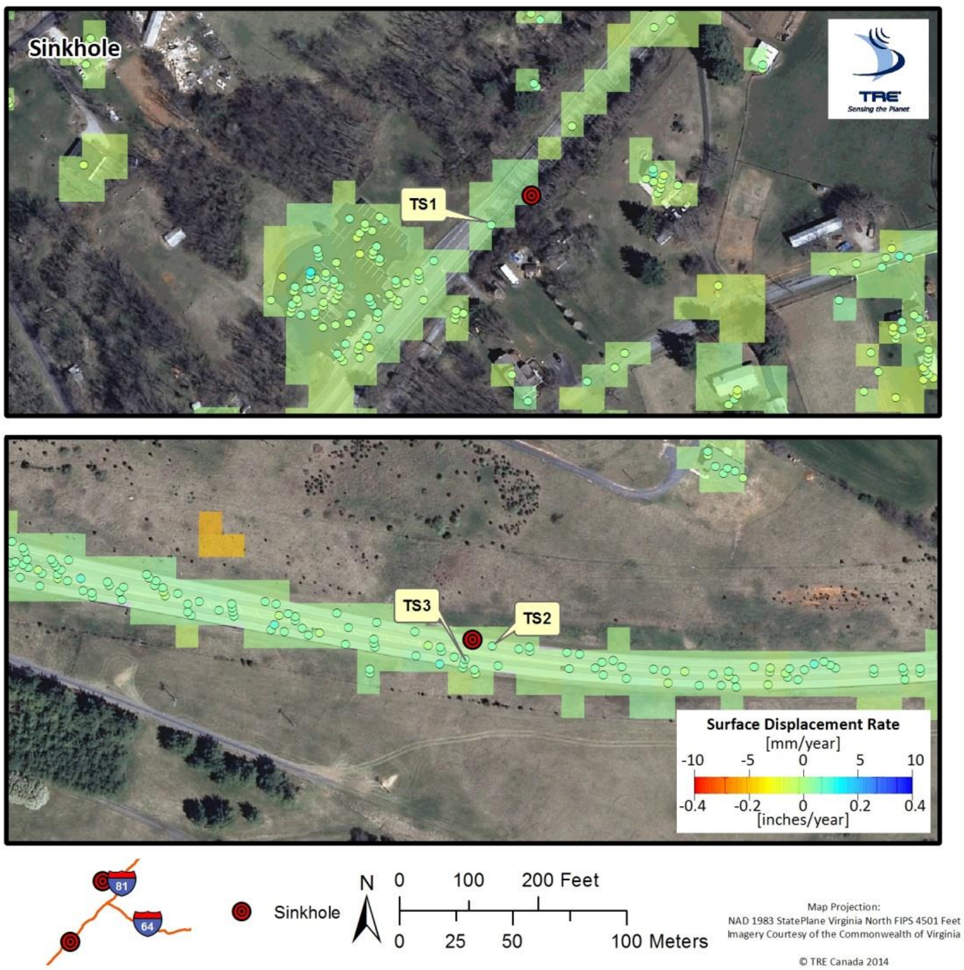

Figure 39: A close-up of displacement results over an area where a sinkhole developed in September 2012.

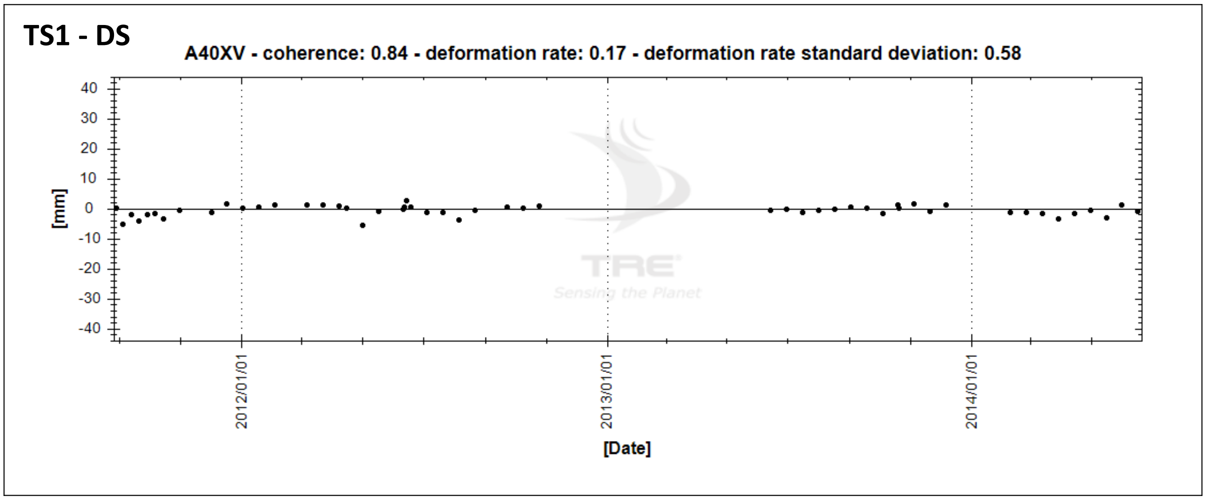

Figure 40: Time series of surface displacement for the measurement point identified as TS1 in Figure 39.

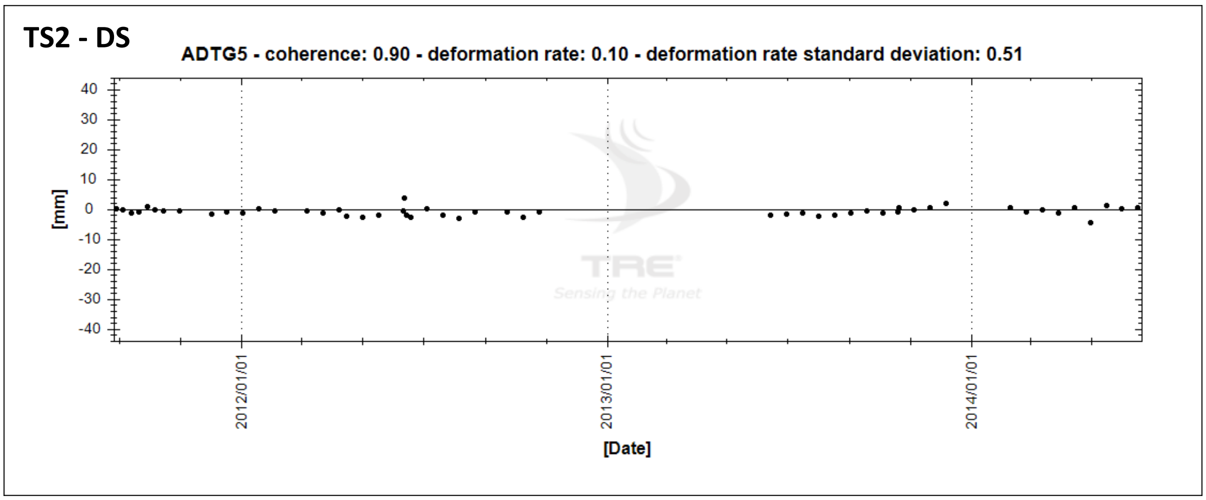

Figure 41: Time series of surface displacement for the measurement point identified as TS2 in Figure 39.

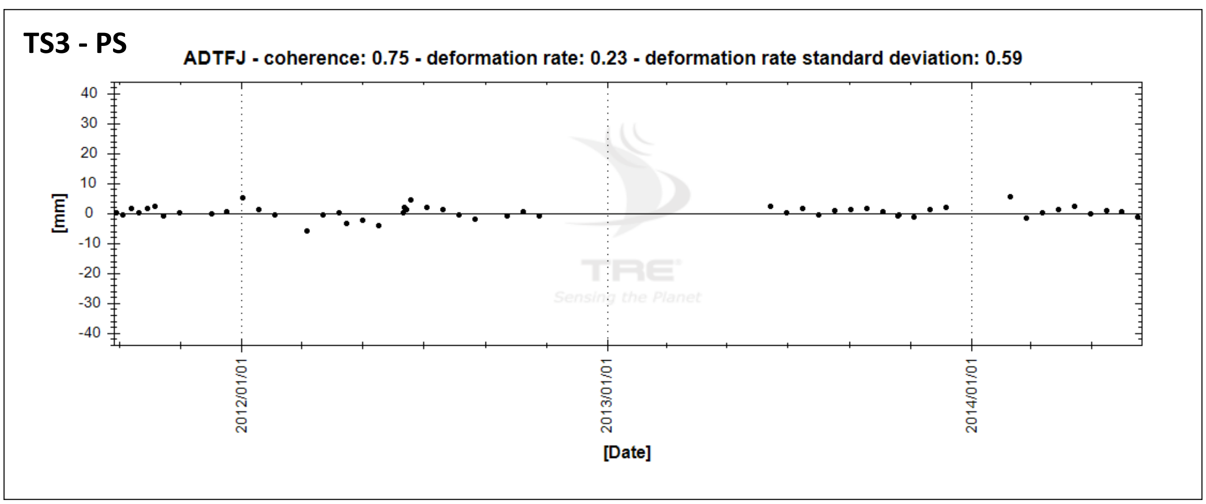

Figure 42: Time series of surface displacement for the measurement point identified as TS3 in Figure 39.

6 Summary

A total of 52 CSK images were processed, covering a 34-month period from August 2011 through June 2014. The increased temporal coverage improves the density of points from 83 to 180 points per square kilometer and allows better characterization of ground deformation trends in the AOI.

Several areas of deformation were observed along the primary roads (Section 5.2). In particular, up to -30 mm of sudden movement was identified at Jefferson Highway (Rt. 250) near Greenview Dr and on the State Route 635 bridge overpass of I-81. Several localized areas of subsidence were also identified on slopes, riprap and a railway. The analysis of reflectors installed on the Route 262 Bridge indicated that two out of four reflectors were visible. Reflector #2, located on top of the parapet mid-span on the bridge, yielded -4.6 mm of displacement from March to June 2014.

Along with this report, a technical appendix is included, which contains the list of delivered files, AR visibility check results and additional information regarding InSAR processing.

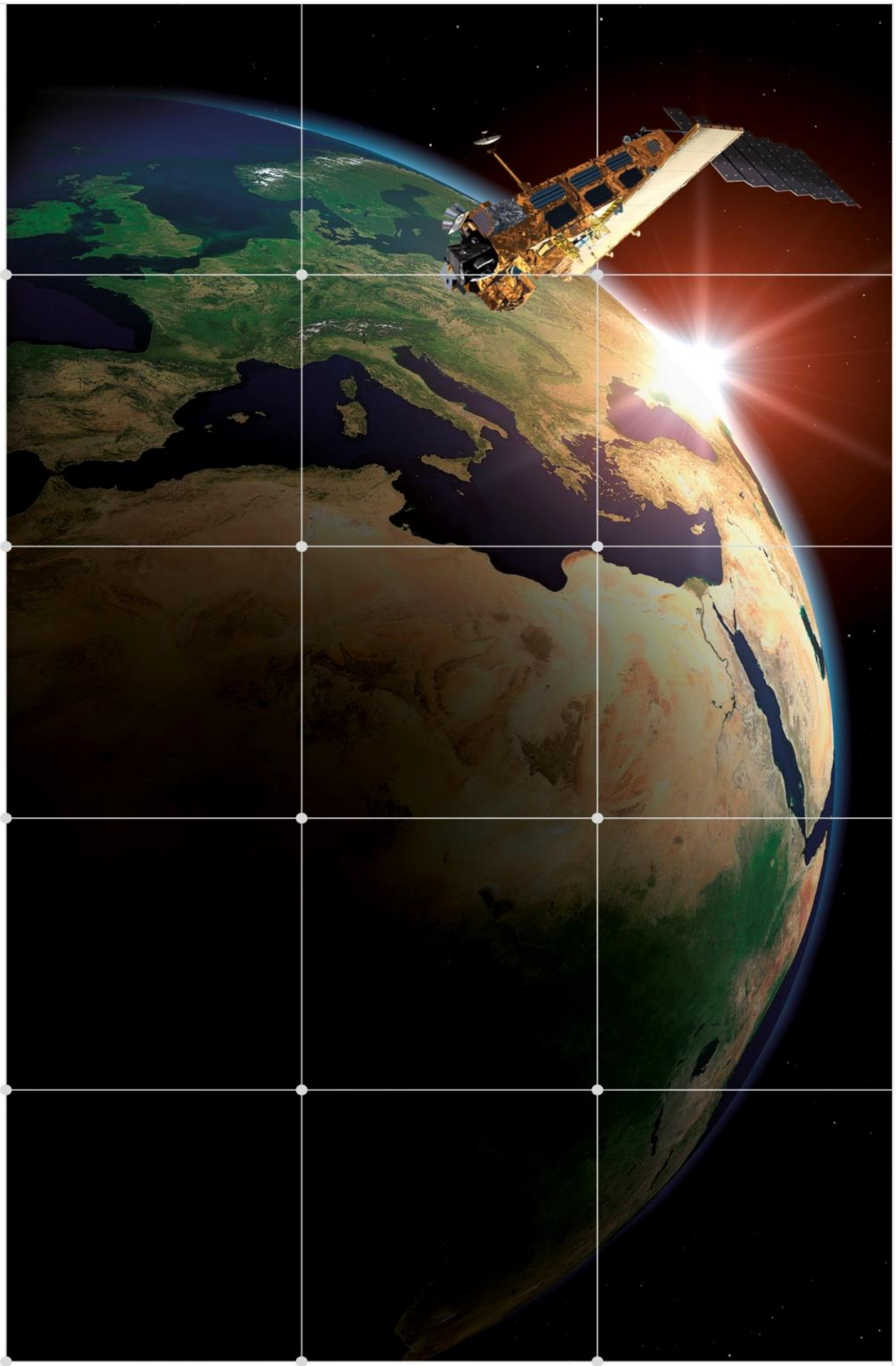

Analysis of Ground Movement using the SqueeSAR™ Algorithm at Virginia, VA

Site 1 First Report – Technical Appendix

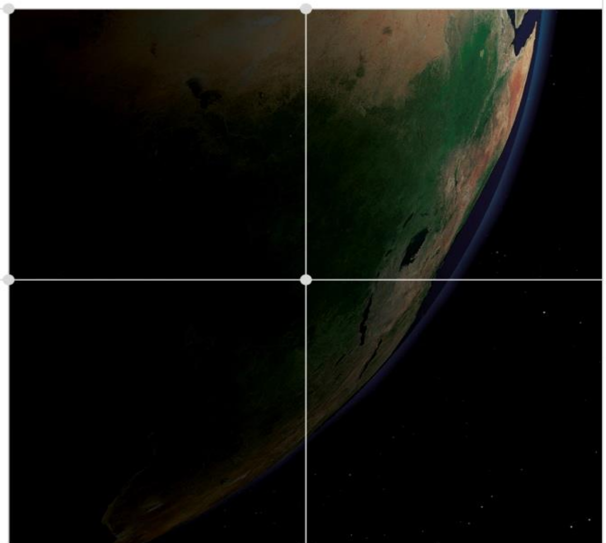

TRE®

Sensing the Planet

Submitted to:
University of Virginia
1001 N. Emmet St.
PO Box 400195
Charlottesville, Virginia 22904
USA

Prepared by:
TRE Canada Inc.
475 West Georgia Street, Suite 410
Vancouver, B.C., V6B 4M9
Canada

Doc. Ref.: JO14-3011-REP1.0
Confidential

31 October 2014

TRE
Sensing the Planet

Table of Contents

Appendix 1: List of delivered files

List of Delivered Files

The deliverables of the SqueeSAR™ analysis include the present report, the PS data files and a software tool for assisting with the loading, viewing and interrogation of the data in ESRI ArcGIS 10.x software. Table 1 and Table 2 list the files contained on the accompanying CD.

Data type	Description
-TSR.shp	ESRI Shapefile for displaying the database file (dbf) geospatially in a GIS environment.
-TSR.dbf	Table containing the height, velocity, velocity standard deviation, acceleration, coherence and time series of all the PS/DS identified.
-REF.shp	ESRI Shapefile for displaying the reference point file in a GIS environment.
-REF.dbf	The reference point used for the ascending and descending data processing.
.xml	An encoding document for each -TSR.shp, VERT.shp, EAST.shp file This file contains metadata for data processing and provides information for the TRE customer toolbar application
VEL.tif	TS raster maps of the surface displacement rate.
VEL_STDEV.tif	TS raster maps of the standard deviation of estimated surface displacement rate.
.mxd	A ESRI ArcGIS 10.2 project file contains the results.

Table 1: List of delivered file types.

		File Name
AOI	Cluster 1	Virginia_RITA2_CSK_H40B_A_T213_C1_Jun14-TSR
		Virginia_RITA2_CSK_H40B_A_T213_C1_Jun14-REF
		Virginia_RITA2_CSK_H40B_A_T213_C1 _VEL_Jun14
		Virginia_ RITA2_CSK_H40B_A_T213_C1_VEL_STDEV_Jun14
	Cluster 2	Virginia_RITA2_CSK_H40B_A_T213_C2_Jun14-TSR
		Virginia_RITA2_CSK_H40B_A_T213_C2_Jun14-REF
		Virginia_RITA2_CSK_H40B_A_T213_C2 _VEL_Jun14
		Virginia_ RITA2_CSK_H40B_A_T213_C2_VEL_STDEV_Jun14
Artificial Reflector		Virginia_RITA2_CSK_H40B_A_T213_AR_Jun14

Table 2: List of delivered files.

The ESRI ArcGIS 10.2 project file is included to make it easier to view the data. Once the data contained on the CD has been saved to the user's hard drive it will be sufficient to open the project file with ArcGIS and update the links to indicate the new locations of the data. The project also contains various layers for viewing the data, including: the AOI, the reference point, the shapefiles for the site and the AOI shapefile.

The Structure of the Database Files

Table 3 below, describes the attributes of each PS/DS data within the database.

Field	Description
CODE	Unique identification code.
SHAPE	Indicates type of geometry (point).
HEIGHT (m)	Elevation above sea level of the PS and DS.
H_STDEV (m)	Standard deviation of PS and DS elevation value.
VEL (mm/yr)	PS movement rate. Positive values correspond to movement toward the satellite (uplift); negative values correspond to motion away from the satellite (subsidence).
V_STDEV (mm/yr)	Standard deviation of PS and DS deformation rate.
ACC (mm/yr^2)	PS and DS acceleration rate.
A_STDEV (mm/yr2)	Standard deviation of PS and DS acceleration value.
COHERENCE	Quality measure [between 0 and 1].
SEASON_AMP (mm)*	Amplitude of seasonal cycles present within the data.
SEASON_PHS (days)*	Phase of seasonal cycles present within the data.
S_AMP_STD (mm)*	Standard deviation of the seasonal amplitude.
S_PHS_STD (days)*	Standard deviation of the seasonal phase.
EFF_AREA (m^2)	Size of the area belonging to the PS and DS. For PS EFF_AREA = 0, for DS EFF_AREA > 0.
D(year/month/day) (mm)	Following the EFF_AREA column are a series of fields that contain the displacement values of successive acquisitions relative to the Master, expressed in mm.

Table 3: Description of the fields contained in the LOS data Shapefile.

*Applicable only to data sets that span one year or longer.

TREmaps™

The SqueeSAR™ data are also available using TREmaps™, a web-based portal where they can be visualised through a secure client login (only authorised users will have access to the results). SqueeSAR™ data are superimposed onto a Google Maps background and time-series can be viewed.

Data can be visualised on any device with an internet connection, including portable tablets. Figure 28 shows an example dataset loaded into the web-based GIS TREmaps™ platform. Site and the access details (username and password) will be provided directly to the primary contact via email.

https://tremaps.treuropa.com/tremaps

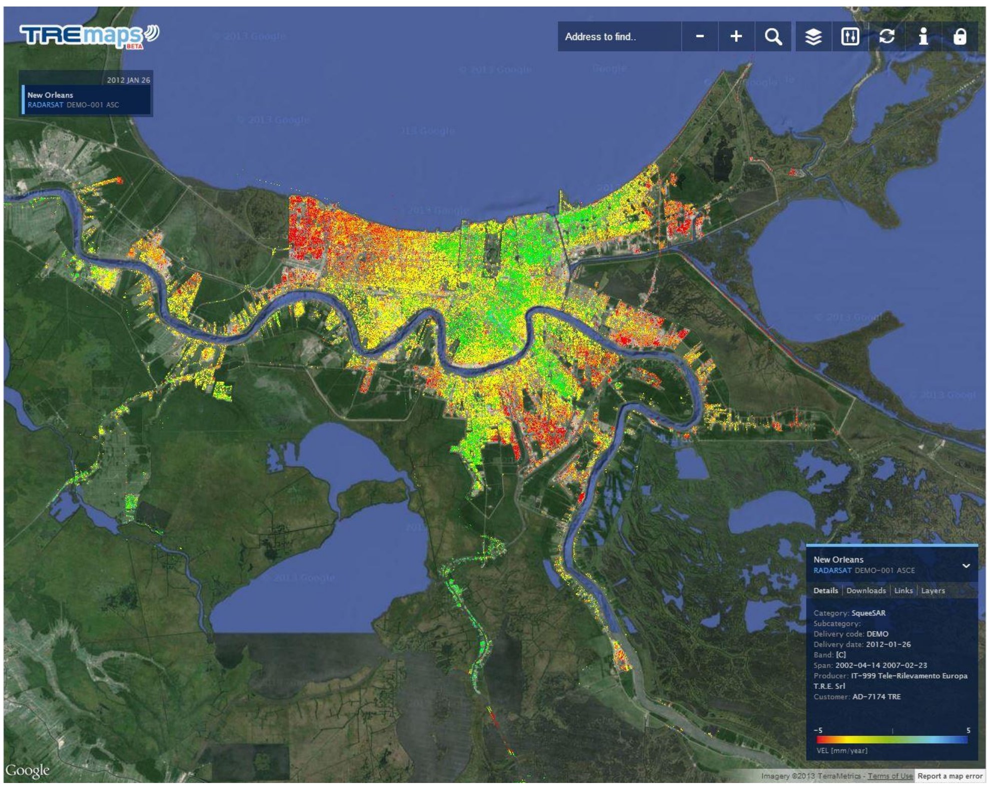

Figure 1: Example of SqueeSAR data within TREmaps.

Appendix 2: Reflectivity and Time Series of Artificial Reflector

Reflectivity of Artificial Reflector (conducted in August, 2014)

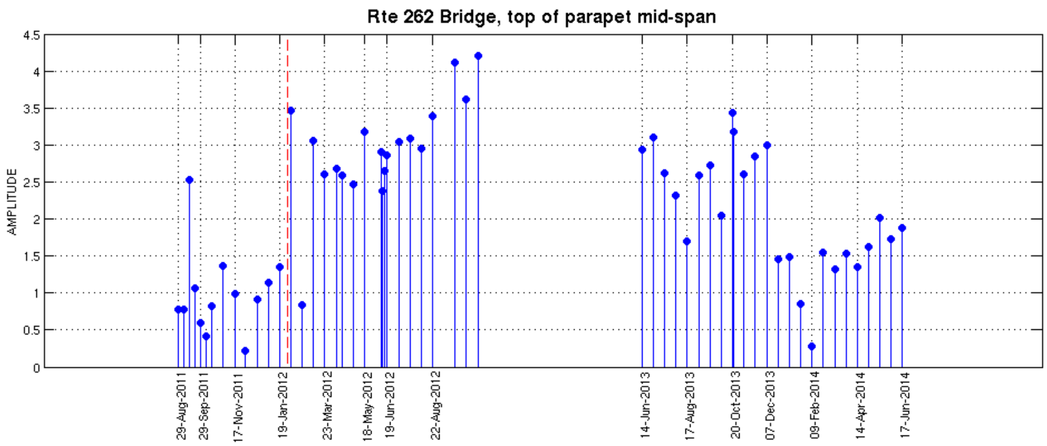

Figure 2: Reflectivity of AR2.

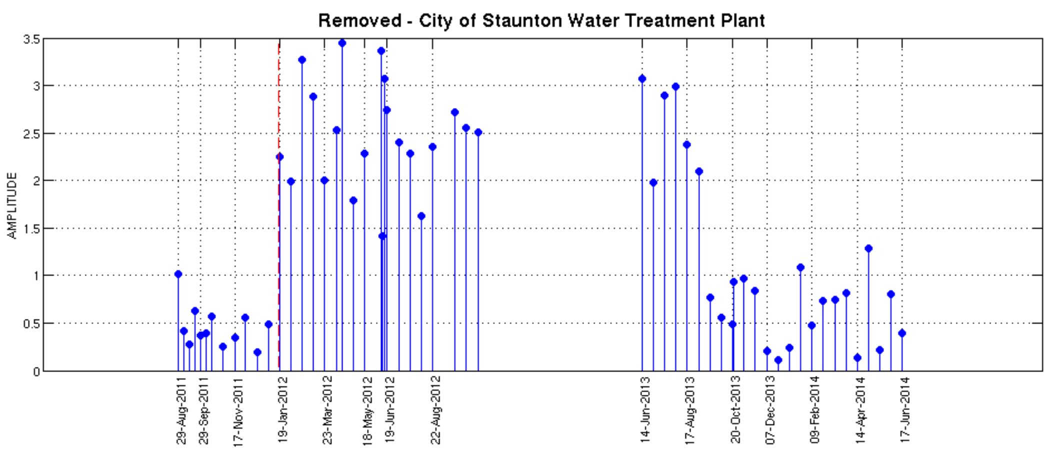

Figure 3: Reflectivity of AR5.

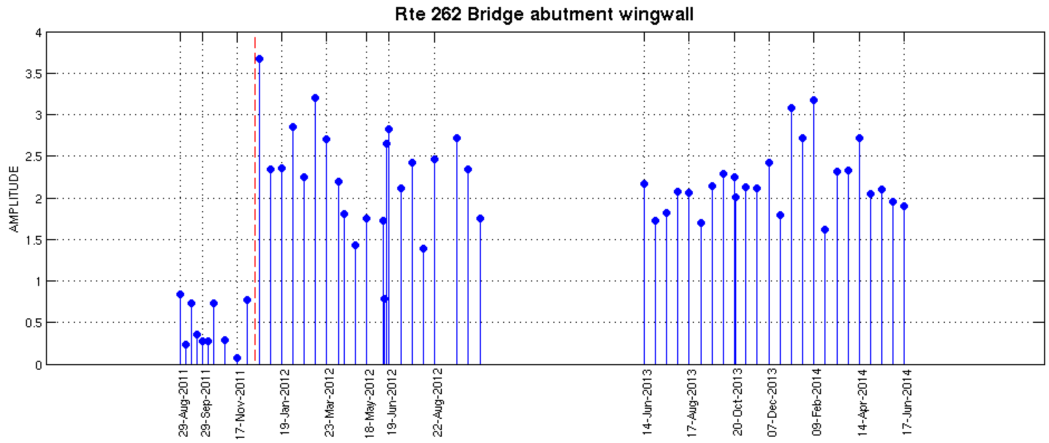

Figure 4: Reflectivity of AR6.

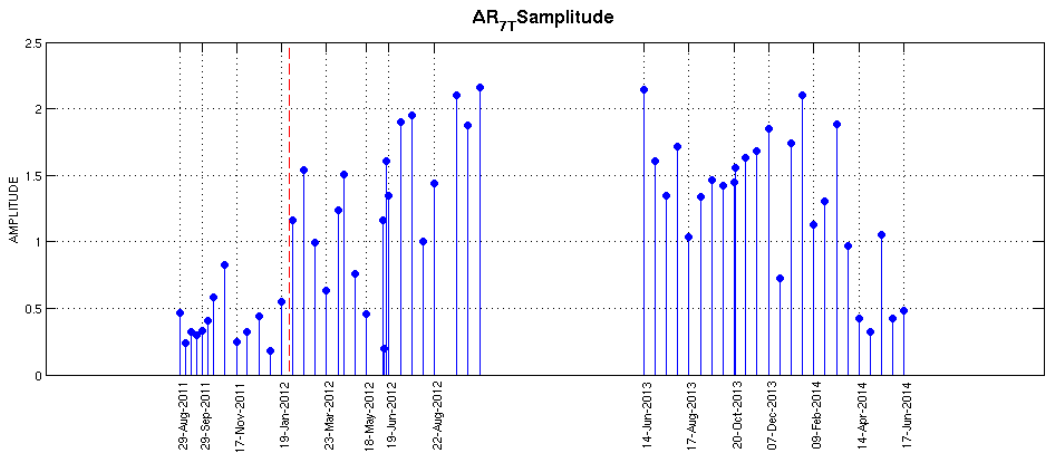

Figure 5: Reflectivity of AR7.

Time Series of Artificial Reflector (August 29, 2011 – 17 June, 2014)

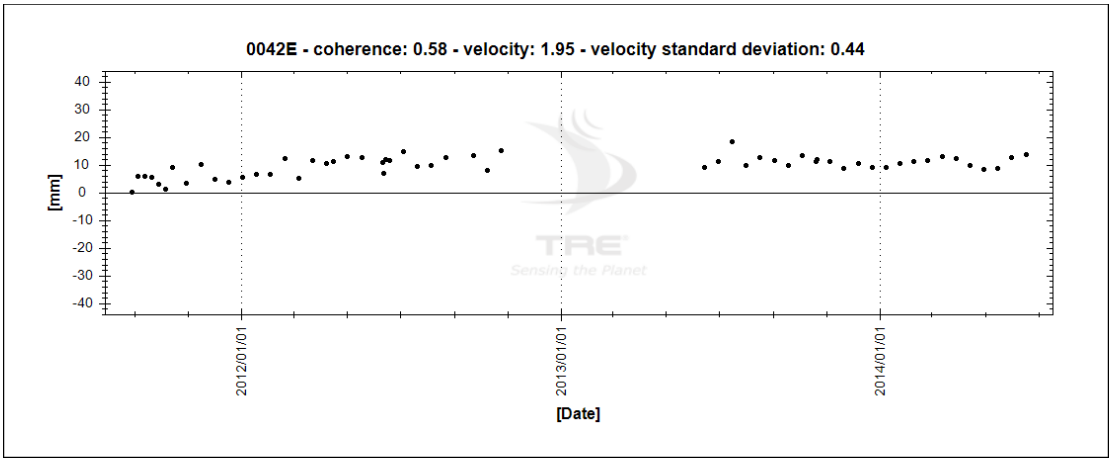

Figure 6: Time series of AR2.

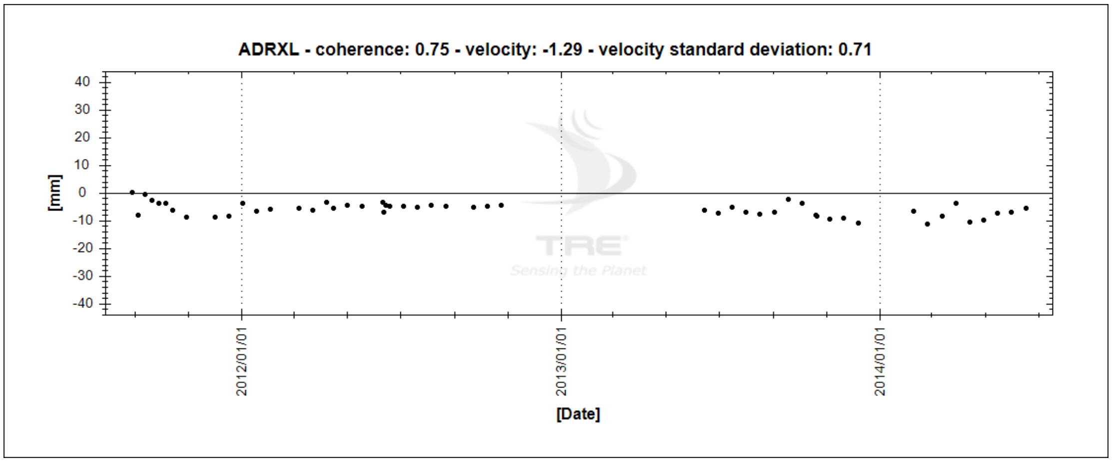

Figure 7: Time series of AR5.

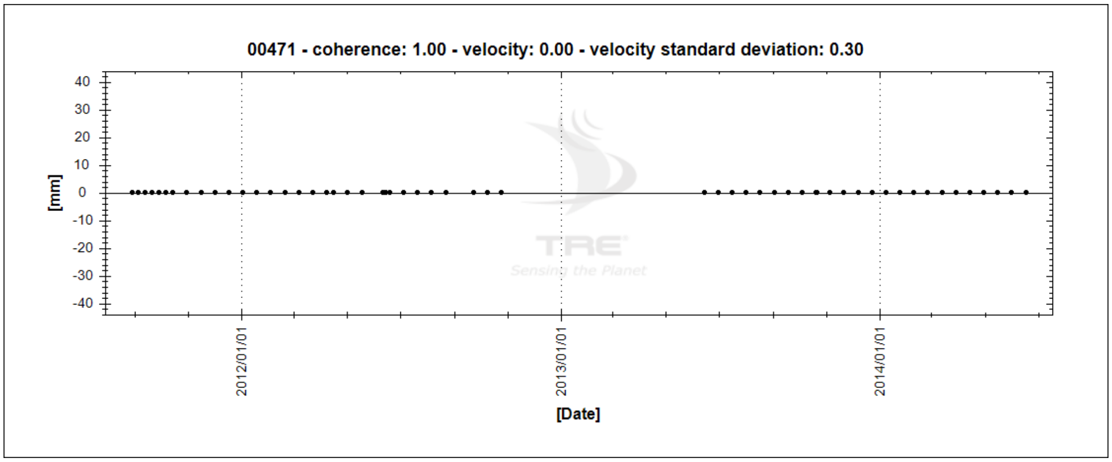

Figure 8: Time series of AR6.

Appendix 3: Additional Properties of the SqueeSAR™ results

Radar Data Acquisition Geometry

InSAR-based approaches measure surface displacement on a one-dimensional plane, along the satellite line-of-sight (LOS). The LOS angle varies depending on the satellite and on the acquisition parameters while another important angle, between the orbit direction and the geographic North, is nearly constant.

The images used for the historical analysis were acquired from the COSMO-SkyMed (CSK) satellite on an ascending orbit (satellite travelling from south to north and imaging to the east) along Track 213.

Table 4 lists the values of the angles for this study, while Figure 9 shows the geometry of the image acquisitions over the site for the ascending orbits, respectively. The symbol δ (delta) represents the angle the LOS forms with the vertical and Θ (theta) the angle formed with the geographic north.

Satellite	Orbit geometry	Symbol	Angle
CSK	Ascending	**δ**	24.23°
		θ	12.52°

Table 4: Satellite viewing angles for the CSK ascending orbit imagery.

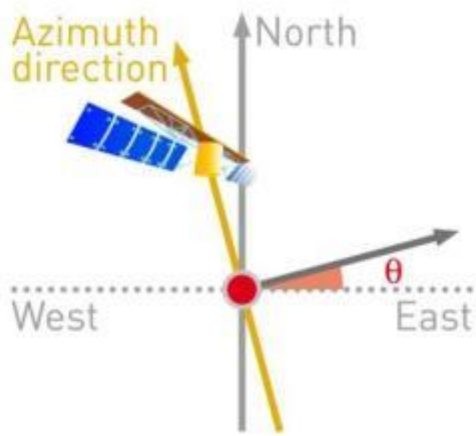

Θ Angle

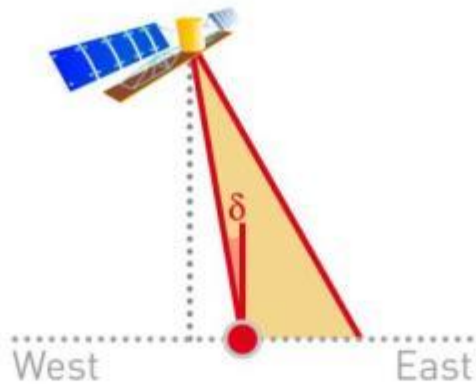

δ Angle

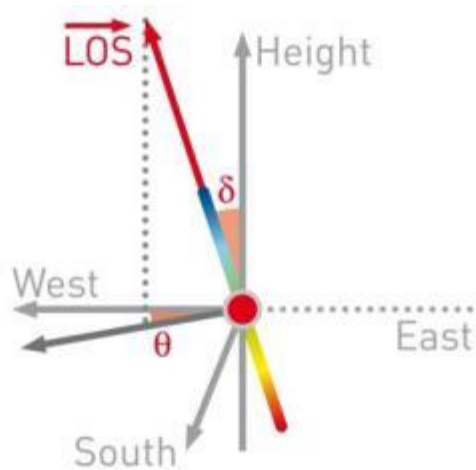

Line Of Sight

Figure 9: Geometry of the image acquisitions over the AOI for the ascending orbit.

Data Processing

Both permanent scatterers (PS) and distributed scatterers (DS) were identified at this site. Bare ground, roads, and infrastructure provide the basis for many PS points in the present SqueeSAR™ analysis. Many natural features such as rocks or exposed ground were also likely sources of stable PS targets.

DS correspond to large areas (up to hundreds of square meters) and were identified from exposed areas such as sparsely vegetated areas, exposed ground or rock. It is important to consider that while DS are represented as individual points for clarity of presentation and ease of interpretation, these measurements actually correspond to non-point features that are multiple pixels in size. The size of the DS within the AOI ranges from 76 to 889 m^2.

Table 5, shown below; provide a summary of the other properties relative to the data processing.

Satellite	COSMO-SkyMed (CSK)
Acquisition geometry	Ascending
Analysis time interval	29 August 2011 - 16 June 2014
Number of scenes processed	52
Georeferencing	PS aligned on 2012 orthophoto (1 foot resolution)
Projection system used / datum	State Plane Virginia North FIPS 4501 (Feet) / NAD 1983
Reference Point location (Cluster 1)	6694908.7191N;11324626.8532 E
Reference Point location (Cluster 2)	6754263.668 N; 11223287.8379 E
Area of interest	617.8 sq. mile (1,600 km^2)

Table 5: Statistics of the processed data.

Standard Deviation and Precision

Standard deviation values of the displacement measurements are a function of the factors listed below and of local ground movement dynamics.

- Spatial density of the PS and DS (higher densities produce higher precisions)
- Quality of the radar targets (signal-to-noise ratio levels)
- Distance from the reference point
- Number of images processed
- Period of time covered by the imagery
- Climatic conditions at the time of the acquisitions
- Distance between the measurement point and the reference

In addition to each measurement point having an associated standard deviation value to represent the error of the displacement measured, results can also be characterized by the accuracy of the technique. Specifically, three parameters are used to characterize the overall accuracy of the results:

- Precision of the estimated deformation rates;
- Precision of the estimated elevations;
- Precision of the geocoding.

Table 6 summarizes the typical precision values applicable to PS located within 2 km from the reference point when **at least 45 radar images** have been processed.

DEFORMATION RATE	< 1 [mm/yr]
DISPLACEMENT ERROR (single displacement between contiguous satellite images)	< 5 [mm]
ELEVATION	± 1.5 [m]
POSITIONING ERROR ALONG EAST DIRECTION	± 3 [m]
POSITIONING ERROR ALONG NORTH DIRECTION	± 2 [m]

Table 6: Measurement accuracies for PS located within 2 km of the reference point, based on the processing of at least 45 SAR images.

Appendix 4: InSAR Processing

InSAR

Interferometric Synthetic Aperture Radar, also referred to as SAR interferometry or InSAR, is the measurement of signal phase change (interference) between radar images. When a point on the ground moves, the distance between the sensor and the point changes, thereby producing a corresponding shift in signal phase. This shift is used to quantify the ground movement.

An interferogram is a 2D representation of the difference in phase values. Variations of phase in an interferogram are identified by fringes, colored bands that indicate areas where and how much movement is occurring. The precision with which the movement can be measured is usually in the centimetre (cm) range as the phase shift is also impacted by topographic distortions, atmospheric effects, and other sources of noise.

DInSAR

When InSAR is used to identify and quantify ground movement the process is referred to as Differential InSAR (DInSAR). In DInSAR topographic effects are removed by using a DEM of the area of interest to create a differential interferogram.

Differential InSAR is still impacted by atmospheric effects, as there is no method for removing this signal phase contribution. It is a useful tool for identifying footprints of progressing movement and creating deformation maps. The limitations of DInSAR are its relatively low precision (cm scale) and that it cannot distinguish between linear and non-linear motion.

PSInSAR™

Permanent Scatterer SAR Interferometry is an advanced form of DInSAR. The fundamental difference is that it uses multiple interferograms created from a stack of at least 15 radar images.

Permanent Scatterer SAR Interferometry was developed to overcome the errors produced by atmospheric artifacts on signal phase. The PSInSAR algorithm automatically searches the interferograms for pixels that display stable radar reflectivity characteristics throughout every image of the data set. In PSInSAR these pixels are referred to as Permanent Scatterers (PS). The result is the identification of a sparse grid of point-like targets on which an atmospheric correction procedure can be performed. Once these errors are removed, a history of motion can be created for each target, allowing the detection of both linear and non-linear motion.

The result is a sparse grid of PS that are color-coded according to their deformation rate and direction of movement. The information available for each PS includes its deformation rate, acceleration, total deformation, elevation, coherence as well as a time series of movement. The PSInSAR algorithm measures ground movement with millimetre accuracy.

SqueeSAR™

Permanent Scatterers are objects, such as buildings, fences, lampposts, transmission towers, crash barriers, rocky outcrops, etc, that are excellent reflectors of radar microwaves. However, TRE has noticed that many other signals are present in the processed data. These do not produce the same high signal-to-noise ratios of PS but are nonetheless distinguishable from the background noise. Upon further investigation it was found that the signals are reflected from extensive homogeneous areas where the back-scattered energy is less strong, but statistically consistent. These areas have been called distributed scatterers (DS) and correspond to rangeland, pastures, bare earth, scree, debris fields, arid environments, etc (Figure 10).

The SqueeSAR™ algorithm was developed to process the signals reflected from these areas. As SqueeSAR™ incorporates PSInSAR no information is lost and movement measurement accuracy is unchanged.

The SqueeSAR™ algorithm also produces improvements in the quality of the displacement time series. The homogeneous areas that produce DS normally comprise several pixels. The single time series attributed to each DS is estimated by averaging the time series of all pixels within the DS, effectively reducing noise in the data.

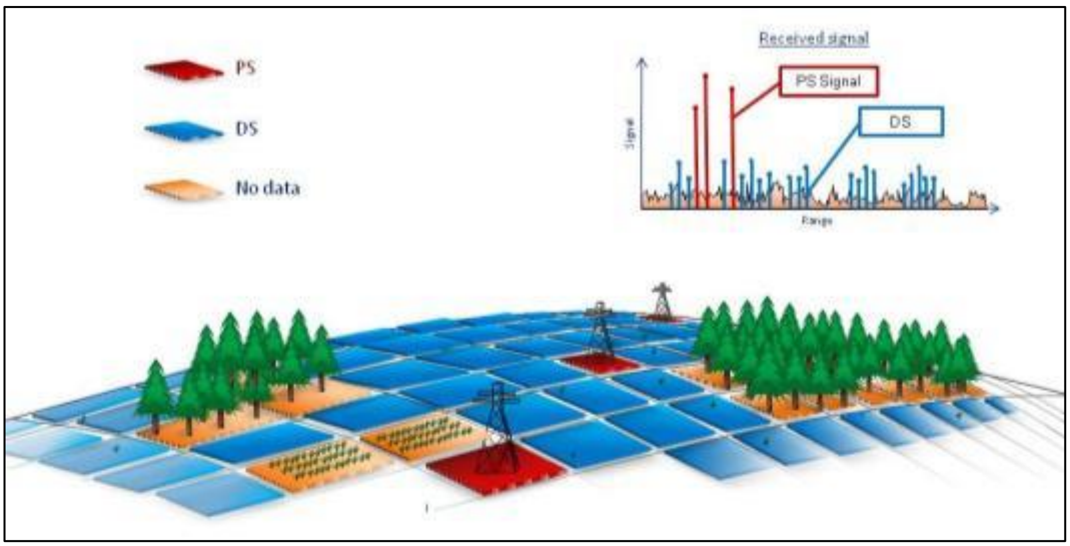

Figure 10: Illustration of the identification of permanent (PS) and distributed scatterers (DS) by the SqueeSAR™ algorithm.

Appendix 5: Data Processing

Methodology

The identification of PS and DS in a series of radar images comprises a sequence of steps.

First, all radar data archives are screened to determine the most suitable source of raw data for the particular area of interest and to select all the high quality images within the chosen data set.

As the signal echo from a single point target contains many returning radar pulses it appears defocused in a synthetic aperture radar (SAR) raw image. The first processing step is therefore to focus all the received energy from a target in one pixel. The images are then precisely aligned to each other, or co-registered, and analyzed for their suitability for interferometry. The parameters that are analyzed are the normal baseline and the temporal distribution of the images.

There then follows a number of statistical analyses on the phase and amplitude characteristics of the backscattered radar signal that return to the satellite. If a concentrated number of signals reflect off a particular feature within a pixel and backscatter to the satellite, the feature is referred to as a 'scatterer'. When the same scatterer appears in all, or most, of a data set of SAR images of a particular location, then the scatterer is deemed to be 'permanent'.

At this stage it is possible to identify a subset of pixels, referred to as Permanent Scatterer Candidates (PSC), that are used to estimate the impact on signal phase of ionospheric, tropospheric and atmospheric effects, as well as possible orbit errors.

Once the signal phase has been corrected for these effects, any remaining changes in signal phase directly reflect ground movement.

Master Image Selection

SqueeSAR™ requires that one image (or scene) in each data set has to become both a geometric and temporal reference to which all the other images are then related. This image is referred to as the master image and those that remain are slave images.

The master image should be chosen according to the following criteria:

- it minimizes the spread of normal baseline values for the slave images;
- similarly, it minimizes the temporal baseline values between the master and each slave image; and
- it minimizes the effects of signal noise arising from changes in vegetation cover and/or small changes in the look angle of the satellite from one scene to another.

Signal Phase and Amplitude Analysis

General

Each pixel of a SAR image contains information on the amplitude of signals that are backscattered toward the satellite, as well as on the signal phase. The amplitude is a measure of the amount of the radar pulse energy reflected, while the phase is related to the length of the path of the electromagnetic wave, from the platform to the ground and back again.

Analyses of both amplitude and phase of the SAR image provide an indication of the stability of each pixel, over time, whereby it is possible to identify those pixels that are most likely to behave as Permanent Scatterers. Statistical methods are used extensively in this process.

Among the different statistical parameters that can be computed two are of particular interest: the Phase Stability Index (PSI), obtained from the phases of the images within the data set, and the Multi Image Reflectivity (MIR) map, derived from the amplitude values of the available acquisitions.

Radar phase and coherence

The phase stability is strongly linked to the concept of coherence. Pixels that consistently display high phase stability are said to be coherent. Coherence is measured by an index that ranges from 0 to 1. When a pixel is completely coherent, it will have a coherence value of 1. Correspondingly, if a pixel has a low phase stability, its coherence index will be 0. In general, interferometry is successful when the coherence index lies between 0.5 and 1.0.

Radar amplitude and multi-image reflectivity

The amplitude of a pixel within a SAR image is the aggregate of the backscattered energy toward the satellite from within the pixel's equivalent land area. This equivalent land area is referred to as the radar resolution, and in the case of the CSK satellite, it measures about 3 m by 3 m. It is necessary to look into the amplitude values of all the images in the data set, in order to understand exactly what was seen by the satellite at the time of each acquisition.

If a target has experienced significant change in its surface characteristics it will exhibit variation in its reflectivity (electromagnetic response) between two acquisitions. In such circumstances, the possibility of detecting movement by means of SAR interferometry is seriously compromised. The signal phase difference between the two images now contains not only the contribution due to displacement, but also that due to the change in the reflectivity of the target. This prevents, in the worst case, the obtaining of any useful information on ground movement.

Accordingly, it is necessary to look into the amplitude values of all the images in the data set, in order to understand exactly what was seen by the satellite at the time of each acquisition.

Another artifact linked to amplitude is known as speckle. Speckle is random noise that appears as a grainy salt and pepper texture in an amplitude image. This is caused by random interference from the multiple scattering returns that occur within each resolution cell. Speckle

has an adverse impact on the quality and usefulness of SAR images. However, the higher the number of images has taken of the same area at different times or from slightly different 'look' angles, the easier it is to reduce speckle. This increases the quality and level of details of the amplitude image enabling it to be used as a background layer for observing the presence of PS results.

The Multi Image Reflectivity (MIR) map is the means by which speckle reduction is accomplished. Averaging a number of images tends to negate the random amplitude variability, leaving the uniform amplitude level unchanged (Figure 11).

It should be emphasised that the information in the MIR map is the reflectivity of each pixel, i.e. the ability to backscatter the incident wave toward the satellite. Flat surfaces (roads, highway, rivers, and lakes) act like a mirror, meaning that if their orientation is not exactly perpendicular to the incident wave negligible energy is reflected back to the sensor; they appear dark in the image. On the other hand, because of their irregular physical shape, metal structures or buildings reflect a significant portion of the incident signal back to the radar, resulting in very bright pixels in the MIR map.

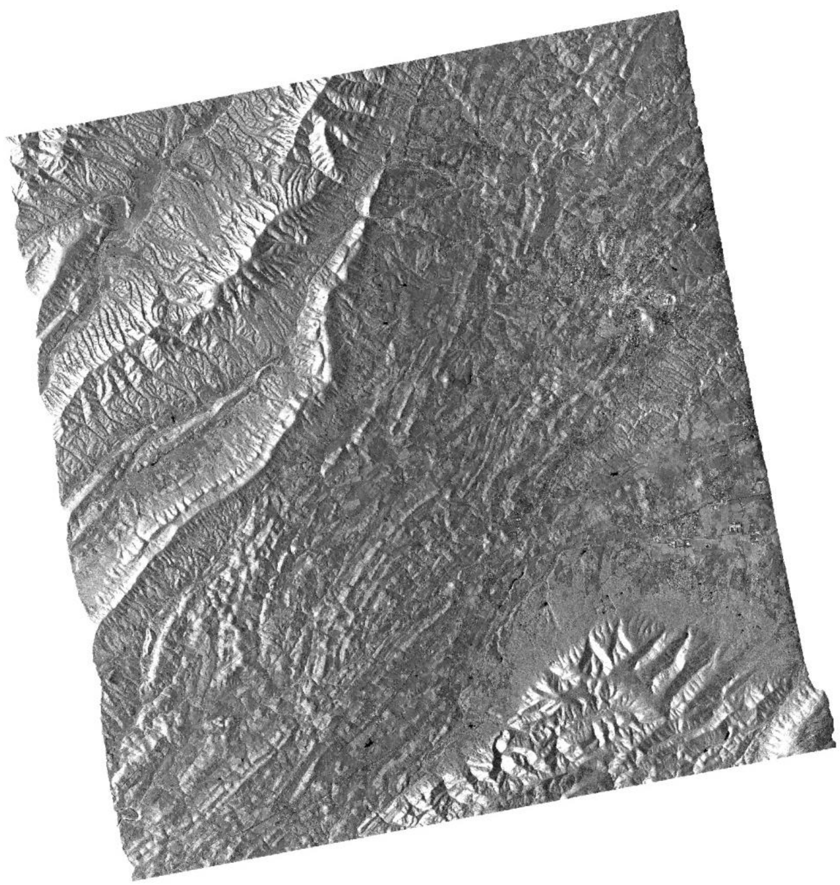

Figure 11: Multi-image reflectivity map of the ascending CSK data set over Virginia.

Interferograms

After the statistical analyses of the SAR images have been completed, a set of differential interferograms is generated. This entails subtracting the phase of each slave image from the phase of the master image. In doing so, the difference in signal path length between the two images is calculated. This difference is related to possible ground motion.

In any SAR image, there are embedded topographic distortions that arise during image acquisition. These are removed using a reference Digital Elevation Model (DEM), leaving ground movement and the signal phase distortions arising from atmospheric effects as the only embedded variables.

The differential interferograms represent the starting point for applying the PSInSAR approach.

Estimation of the Atmospheric Effects

When a radar signal enters and exits a moisture-bearing layer in the atmosphere, its wavelength can be affected, introducing potential errors into the signal path length. The removal of atmospheric impacts is fundamental for increasing the precision of ground movement measurement.

A sub-set of pixels, usually corresponding to buildings, lampposts, antennas, small structures and exposed rocks, is chosen from among those that have high PSI values. These are referred to as PS Candidates (PSC). PSC density is, of course, higher in towns and cities rather than in forests and vegetated areas. However, it is often possible to obtain good PSC density in rural areas.

For each image, the atmospheric impacts are estimated at each PSC location. The process is statistically based and benefits in accuracy by the greater the number of available images for the analysis. By comparing the atmospheric contribution on neighboring pixels that would be experiencing the same atmospheric conditions, the atmospheric contribution can be reconstructed over the whole image.

The processed data set allows identification of a PSC cluster dense enough to identify and extract the atmospheric contribution over the entire area of interest.

Post-processing

In this stage the processed data undergoes a thorough quality control following ISO 9001:2000 guidelines. The PS data is checked for anomalies, aligned on an optical image layer usually provided by the client and the final report is prepared.

Appendix 6: Abbreviations and Acronyms

AOI	Area Of Interest
DInSAR	Differential Interferometry
DS	Distributed Scatterer (s)
GIS	Geographic Information System
InSAR	Interferometric SAR
LOS	Line Of Sight
MIR	Multi-Image Reflectivity
PS	Permanent Scatterer(s)
PSInSAR™	Permanent Scatterer SAR Interferometry is a worldwide Polytechnic University of Milan Trademark
SAR	Synthetic Aperture Radar
SqueeSAR™	The most recent InSAR algorithm patented by TRE
TRE	Comprehensive term for Tele-Rilevamento Europa and TRE Canada
TS	(Permanent Scatterer Displacement) Time Series

Appendix C – AOI1 – Staunton: SqueeSAR report (November 2014)

TRE – **Analysis of ground movements over Virginia using SqueeSAR – Final Report** – November 2014 [download][4]

TRE – **Analysis of ground movements over Virginia using SqueeSAR – Final Report - Technical Appendix** – November 2014 [download][5]

[4] http://viva-lab.ece.virginia.edu/elecdocs/ritars14/Staunton_Nov2014.pdf
[5] http://viva-lab.ece.virginia.edu/elecdocs/ritars14/Staunton_Nov2014_TA.pdf

Analysis of Ground Movement over Virginia using SqueeSAR

Site 1 Final Report

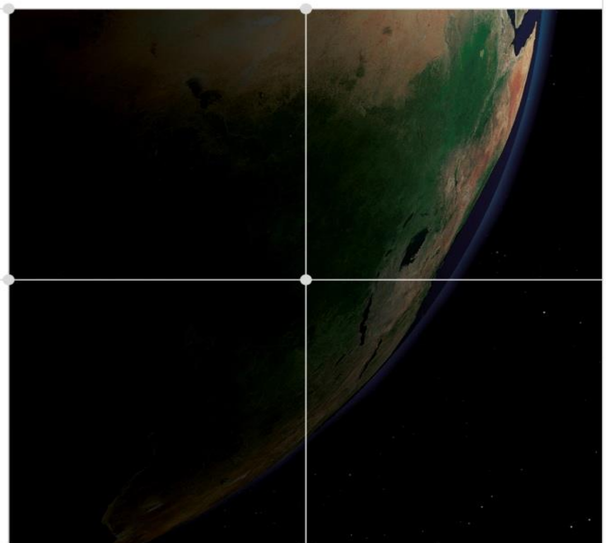

TRE

Sensing the Planet

Submitted to:
University of Virginia
1001 N. Emmet St.
PO Box 400195
Charlottesville, Virginia 22904
USA

Prepared by:
TRE Canada Inc.
Suite 410, 475 West Georgia Street
Vancouver, B.C., V6B 4M9
Canada

Prepared by: Vicky Hsiao
GIS Analyst
TRE Canada Inc.
____
(signature)

Approved by: Giacomo Falorni
Operations Manager
TRE Canada Inc.
____
(signature)

Doc. Ref.: JO14-3011-REP2.0
February 25 2014

Executive Summary

This report describes the approach and results of the InSAR analysis carried out to measure surface deformation in Virginia (Site1) for the project "InSAR remote sensing for performance monitoring of transportation infrastructure at the network level" (RITARS-14-H-UVA). The results provide an overview of ground movement occurring in the area over a 39-month period.

The following points summarize the key findings and features of this deliverable:

- Signs of settlement were identified along primary roads:
    - Up to -45.5 mm of subsidence next to Mish Barn Road (§6.1.2).
    - -20 mm of subsidence near State Route 42 starting in early July 2014 (§6.1.3).
- Two unstable slopes along Route 600 and Greenville School Rd were observed (§6.2.1 and §6.2.5).
- Movement was identified on riprap slopes along routes I-80 and I-61 within the AOI (§6.2.2 and 6.2.3).
- No signs of movement were found in the area of two sinkholes that were active in September 2012 (§6.2.6).
- Pavement conditions were compared with InSAR results to identify possible correlations. InSAR results show more variability over repaved areas, but no clear trends were observed in the deformation time series (§6.4). An analysis of amplitude data may lead to further results.
- Measurement point density has more than doubled compared to the previous results (405 points per km^2 vs 187 per km^2).
- The three years and three months of data acquisition and processing led to an increase in the spatial coverage of the data over time and allowed monitoring updates at eight month intervals of the road network and potential Geohazard ground deformation in Virginia.

The deliverables for the project include the present report, which describes the results of the data processing, a technical appendix and a CD containing the displacement data.

Table of Contents

1 Introduction

The University of Virginia VIVA lab is leading a research project with the Virginia Research Transportation Council and TRE Canada entitled "InSAR remote sensing for performance monitoring of transportation infrastructure at the network level " (RITARS-14-H-UVA). The work was awarded to the University of Virginia as a research grant funded by the Commercial Remote Sensing and Spatial Information Technology Application Program, RITA Phase V.

One of the main objectives of this project is to systematically extract consistent and reliable information on road subsidence, bridge monitoring, slope stability, sinkhole development and pavement condition from InSAR data. TRE Canada Inc. (TRE) has been contracted to perform the InSAR work using our SqueeSAR algorithm. Cosmo-SkyMed (CSK) radar satellite imagery was acquired to build on the archive initiated in the previous phase of the project over the same area of interest. The increased temporal coverage will allow better delineation of ground subsidence trends and further refinement of a sinkhole detection model.

The AOI corresponds to a full CSK radar scene, approximately 1,600 km^2 (618 square miles) in size, covering most of Augusta County, Virginia (as well as a small portion of Rockbridge County). The AOI contains dense vegetation, active agriculture, fallow fields, exposed ground, infrastructure and towns (Figure 1). Mountainous terrain and areas of highly variable topography are present in the northwest and southeast corners of the scene. Man-made structures, as well as bare or sparsely vegetated ground, often yield a high number of measurement points. Areas of dense vegetation, active agriculture and steep slopes will produce a lower density of measurement points. Historically, portions of the area have been prone to sinkholes, landslides, and other instabilities.

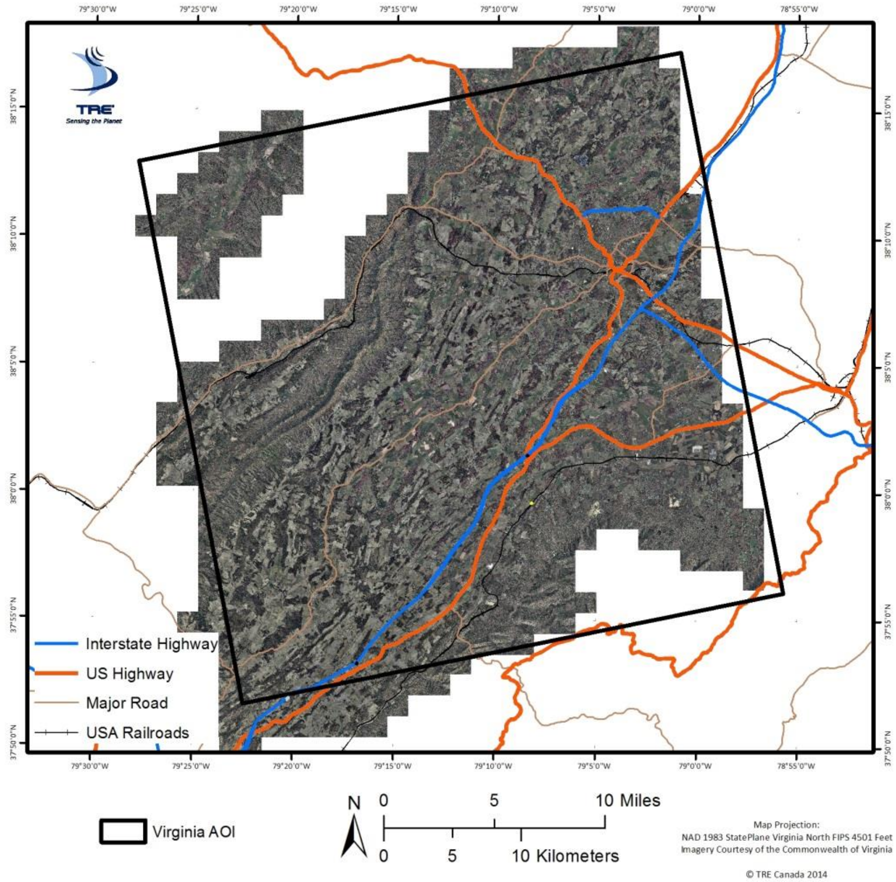

Figure 1: The Area of Interest (AOI). The background 2012 orthophotos used in the figures of this report were provided by the Commonwealth of Virginia.

2 Radar data

Sixty-seven images were acquired between 29 August 2011 and 24 November 2014, with five being discarded during processing due to low coherence values in winter scenes where snow was present (see Table 1 for more information regarding the radar imagery). In total, 62 images covering a period of three years and three months were processed (Table 2). Note that there was an eight-month interruption in image acquisitions between October 2012 and June 2013, which resulted in a corresponding gap in all time series.

Additional information on the satellite parameters can be found in the Technical Appendix.

Radar Data Information	
Constellation	Cosmo-SkyMed (CSK)
Resolution	3m x 3m
LOS Off-Nadir Angle	24.23°
Orbit Direction	Ascending
Track	213
Revisit Frequency	16 days
Period Covered by Imagery	29 August 2011 – 24 November 2014
Number of Processed Images	62

Table 1: Information regarding the radar imagery used in the analysis.

CSK Data								
No.	**Date**	**Interval**	**No.**	**Date**	**Interval**	**No.**	**Date**	**Interval**
1	29 Aug 2011		**23**	19 Jun 2012	4	**44**	09 Feb 2014	64
2	05 Sep 2011	7	**24**	05 Jul 2012	16	**45**	25 Feb 2014	16
3	13 Sep 2011	8	**25**	21 Jul 2012	16	**46**	13 Mar 2014	16
4	21 Sep 2011	8	**26**	06 Aug 2012	16	**47**	29 Mar 2014	16
5	29 Sep 2011	8	**27**	22 Aug 2012	16	**48**	14 Apr 2014	16
6	07 Oct 2011	8	**28**	23 Sep 2012	16	**49**	30 Apr 2014	16
7	15 Oct 2011	8	**29**	09 Oct 2012	32	**50**	16 May 2014	16
8	31 Oct 2011	16	**30**	25 Oct 2012	16	**51**	01 Jun 2014	16
	17 Nov 2011		**31**	14 Jun 2013	16	**52**	17 Jun 2014	16
9	02 Dec 2011	32	**32**	30 Jun 2013	232	**53**	03 Jul 14	16
10	18 Dec 2011	16	**33**	16 Jul 2013	16	**54**	19 Jul 14	16
11	03 Jan 2012	16	**34**	01 Aug 2013	16	**55**	04 Aug 14	16
12	19 Jan 2012	16	**35**	17 Aug 2013	16	**56**	24 Aug 14	20
13	04 Feb 2012	16	**36**	02 Sep 2013	16	**57**	05 Sep 14	16
	20 Feb 2012		**37**	18 Sep 2013	16	**58**	21 Sep 14	16
14	07 Mar 2012	32	**38**	04 Oct 2013	16	**59**	07 Oct 14	16
15	23 Mar 2012	16	**39**	20 Oct 2013	16	**60**	23 Oct 14	16
16	08 Apr 2012	16	**40**	21 Oct 2013	16	**61**	08 Nov 14	16
17	16 Apr 2012	8	**41**	05 Nov 2013	1	**62**	24 Nov 14	16
18	02 May 2012	16	**42**	21 Nov 2013	15			
19	18 May 2012	16	**43**	07 Dec 2013	16			
20	11 Jun 2012	24		23 Dec 2013				
21	12 Jun 2012	1		08 Jan 2014				
22	15 Jun 2012	3		24 Jan 2014				

Table 2: Dates of the CSK image acquisitions. Image dates in orange were discarded during data processing.

3 Delivery of Data

3.1 List of Delivered Files

The deliverables of the SqueeSAR™ analysis include the present report, the PS data files and a software tool for assisting with the loading, viewing and interrogation of the data in ESRI ArcGIS 10.3 software. Table 3 and Table 4 list the files contained on the accompanying CD.

Data type	Description
-TSR.shp	ESRI Shapefile for displaying the database file (dbf) geospatially in a GIS environment.
-TSR.dbf	Table containing the height, velocity, velocity standard deviation, acceleration, coherence and time series of all the PS/DS identified.
-REF.shp	ESRI Shapefile for displaying the reference point file in a GIS environment.
-REF.dbf	The reference point used for the ascending and descending data processing.
.xml	An encoding document for each -TSR.shp, VERT.shp, EAST.shp file. This file contains metadata for data processing and provides information for the TRE customer toolbar application
.mxd	An ESRI ArcGIS 10.3 project file containing the results.

Table 3: List of delivered types.

	File Name
Full Data	SITE1_STAUNTON_RITA2_CSK_H40B_A_T213_C1_Nov14-TSR SITE1_STAUNTON_RITA2_CSK_H40B_A_T213_C1_Nov14-REF SITE1_STAUNTON_RITA2_CSK_H40B_A_T213_C2_Nov14-TSR SITE1_STAUNTON_RITA2_CSK_H40B_A_T213_C2_Nov14-REF
Artificial Reflector	SITE1_STAUNTON_RITA2_CSK_H40B_A_T213_AR_Nov14

Table 4: List of delivered files

The ESRI ArcGIS 10 project file is included to make it easier to view the data. Once the data on the CD has been saved to the user's hard drive, it will be sufficient to open the project file with ArcGIS and update the links to indicate the new locations of the data.

3.2 The Structure of the Database Files

Table 5 below, describes the attributes of each PS within the database.

Field	Description
CODE	Unique identification code.
SHAPE	Indicates type of geometry (point).
HEIGHT (m)	Elevation above sea level of the PS.
H_STDEV (m)	Standard deviation of PS elevation value.
VEL (mm/yr)	PS movement rate. Positive values correspond to movement toward the satellite (uplift); negative values correspond to motion away from the satellite (subsidence).
V_STDEV (mm/yr)	Standard deviation of PS deformation rate.
ACC (mm/yr^2)	PS acceleration rate.
A_STDEV (mm/yr2)	Standard deviation of PS acceleration value.
COHERENCE	Quality measure [between 0 and 1].
EFF_AREA (m^2)	Size of the area belonging to the PS. For PS EFF_AREA = 0, for DS EFF_AREA > 0.
D (year/month/day) (mm)	Following the EFF_AREA column are a series of fields that contain the displacement values of successive acquisitions relative to the Master, expressed in mm.

Table 5: Description of the fields contained in the Shapefile.

3.3 TREmaps™

The SqueeSAR data are also available on TREmaps™, a web-based portal accessed via a secure client login (only authorized users have access to the results) for viewing and interrogating deformation data online. The SqueeSAR data is superimposed on a Google Maps background and the individual time-series of each point can be viewed by point-and-click.

Data can be visualized on any device with an internet connection, including portable tablets. User credentials (username and password) will be provided via email.

TREmaps link: https://tremaps.treuropa.com/tremaps

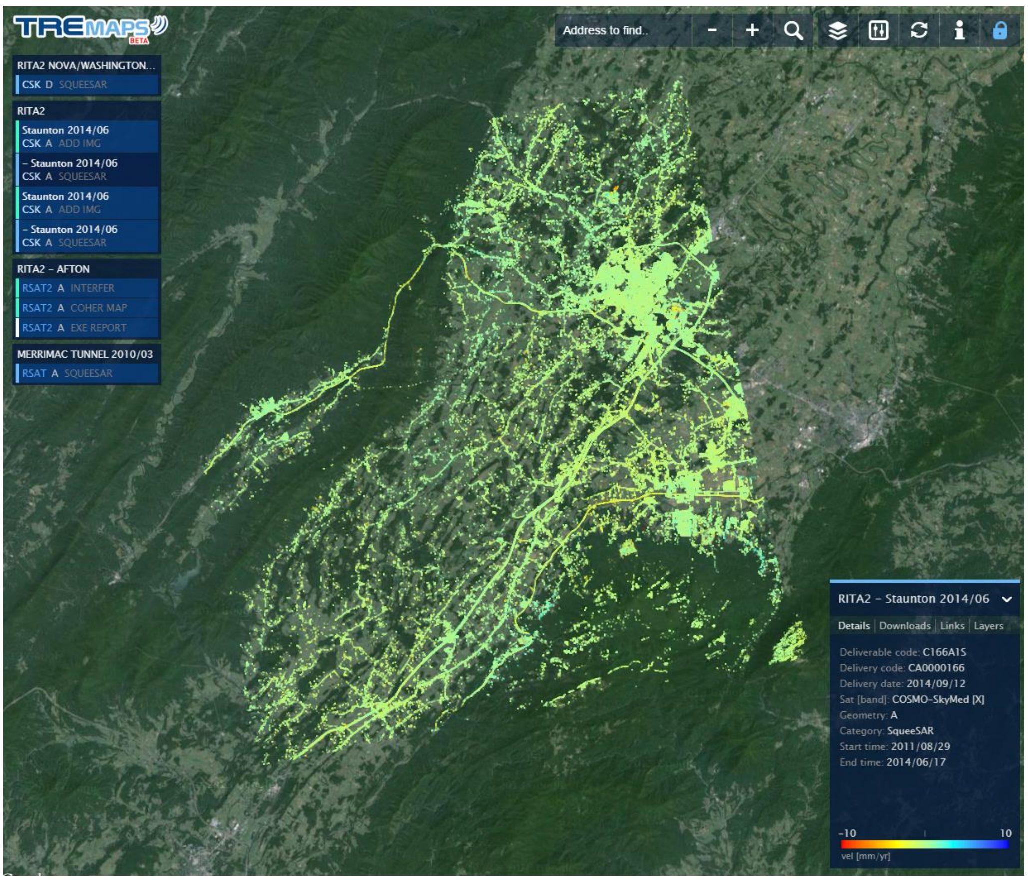

shows an example dataset loaded into the web-based GIS TREmaps™ platform.

4 Data Processing

The data set is provided in two separate clusters as the large swath of densely vegetated terrain over the North Mountain and Great North Mountain in the northwest corner makes it difficult to link the two clusters together. Each cluster has its own reference point from which the displacement values are calculated. The larger area in each of the figures corresponds to Cluster 1, while Cluster 2 refers to the smaller grouping in the northwest corner (Figure 2).

Reference Point

SqueeSAR™ is a differential technique meaning displacement is measured compared to a reference point that is assumed to be stable. The reference points used for the two clusters are both shown in Figure 2. The reference points were selected using an optimization procedure that performs a statistical analysis of all targets to select a point with optimal radar parameters including high coherence, low standard deviation and low temporal variability over time. The use of this procedure ensures the highest quality results are achieved. Reference point coordinates for the current analysis are listed in the Technical Appendix.

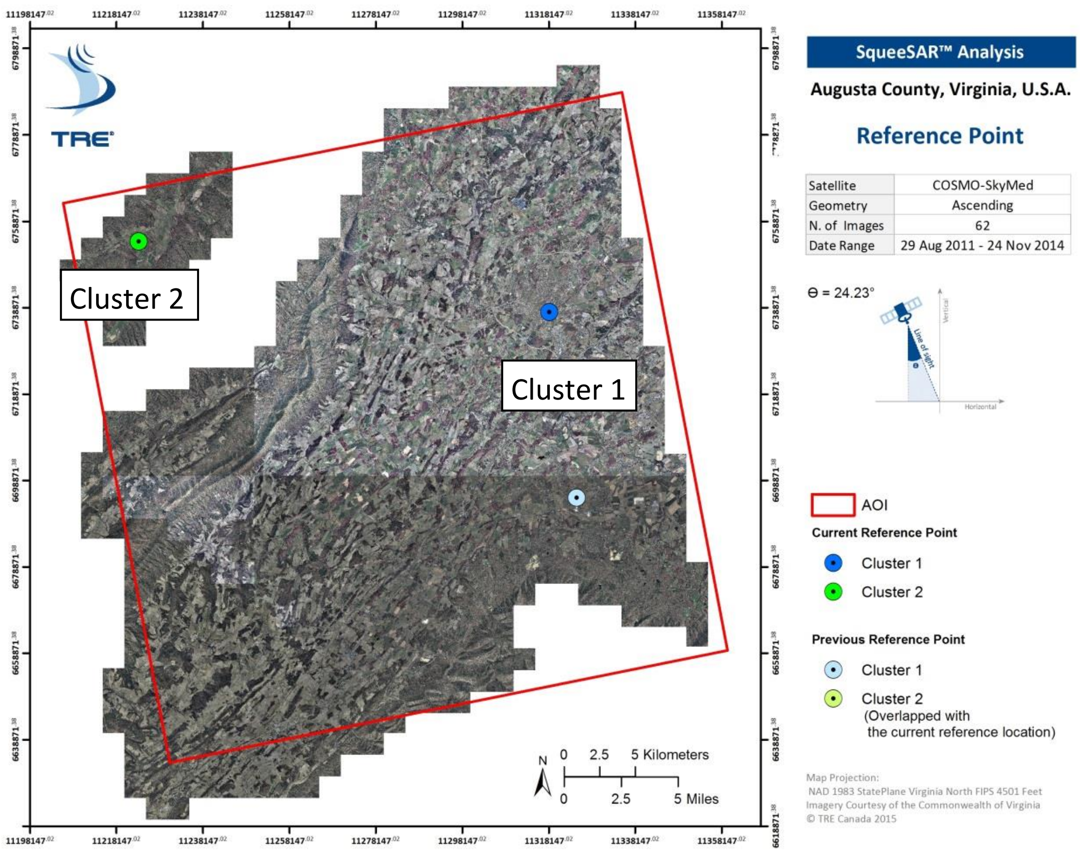

Figure 2: The location of the two data clusters and their associated reference points.

(Cluster 1: E 11318282.23 N 6737916.39, Cluster 2: E 11223288.75 N 6754263.96)

5 Results of the SqueeSAR™ analysis

5.1 Cumulative Displacement

The total amount of displacement measured over the 39-month period is shown below (Figure 3). Each point corresponds to a PS or DS, and is color-coded according to the magnitude and direction of total movement. Movement is measured along the satellite line-of-sight (LOS) relative to the first image (August 29 2011) of the data stack.

Cumulative displacement from August 2011 to November 2014 ranges from -110.0 to +59.0 mm within the AOI, as compared to -74.4 to +47.8 mm in the previous results (August 2011 to June 2014). More detailed analyses of the results along major roads are described in Section 6.

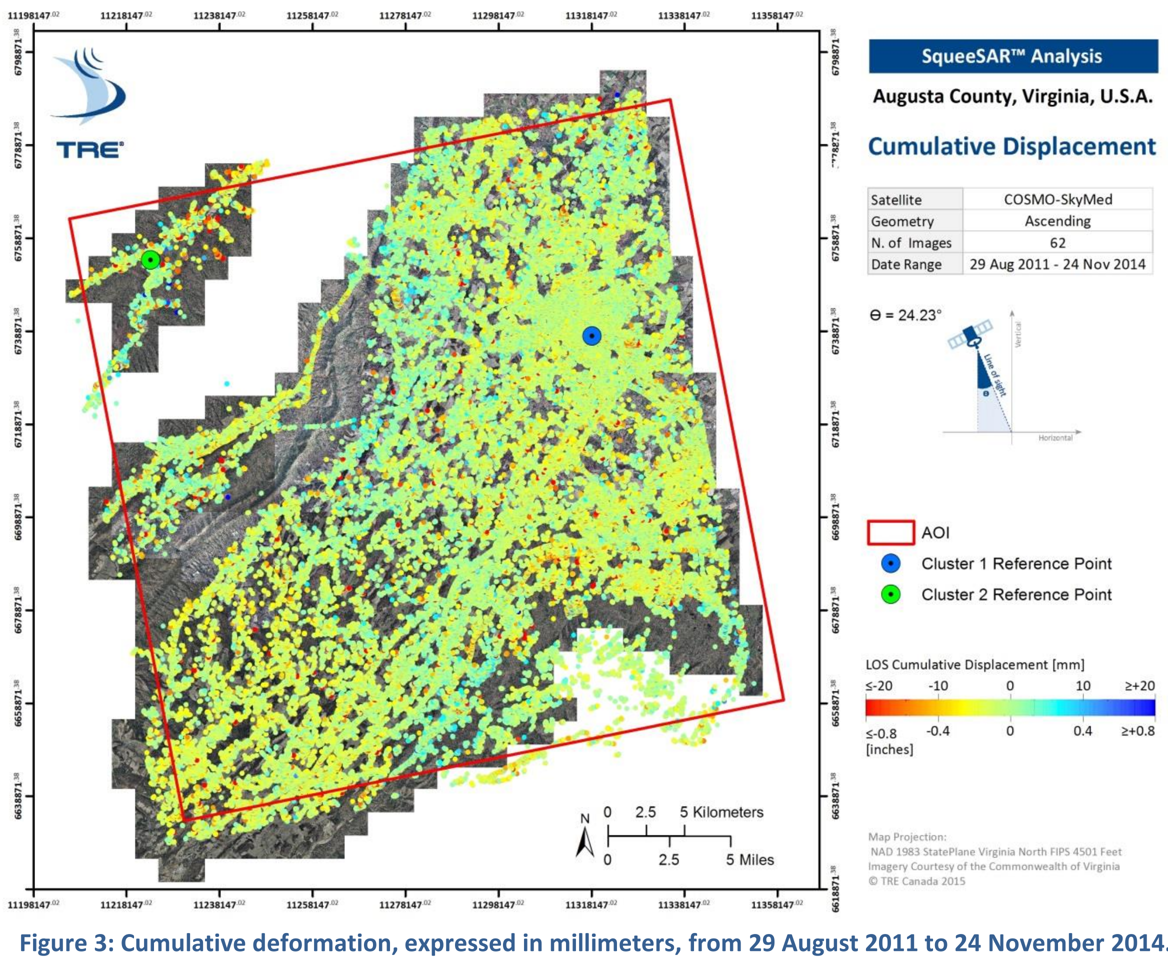

Figure 3: Cumulative deformation, expressed in millimeters, from 29 August 2011 to 24 November 2014.

5.2 Displacement rate

The line-of-sight (LOS) displacement rates, expressed in mm/year, as detected from the processing of all images, are shown below (Figure 4). Each point corresponds to a Permanent Scatterer (PS) or a Distributed Scatterer (DS), and is color-coded according to its annual rate of movement. Average displacement values are calculated from a linear regression of the ground movement measured over the entire period covered by the satellite images. Detailed information on ground motion is also provided by means of displacement time series, which are provided for each PS and DS.

Displacement rates are low throughout the AOI, with 94% and 85% of the points constrained to within -2 and +2 mm/yr. Overall, displacement rates range from -35.5 to 17.0 mm/yr.

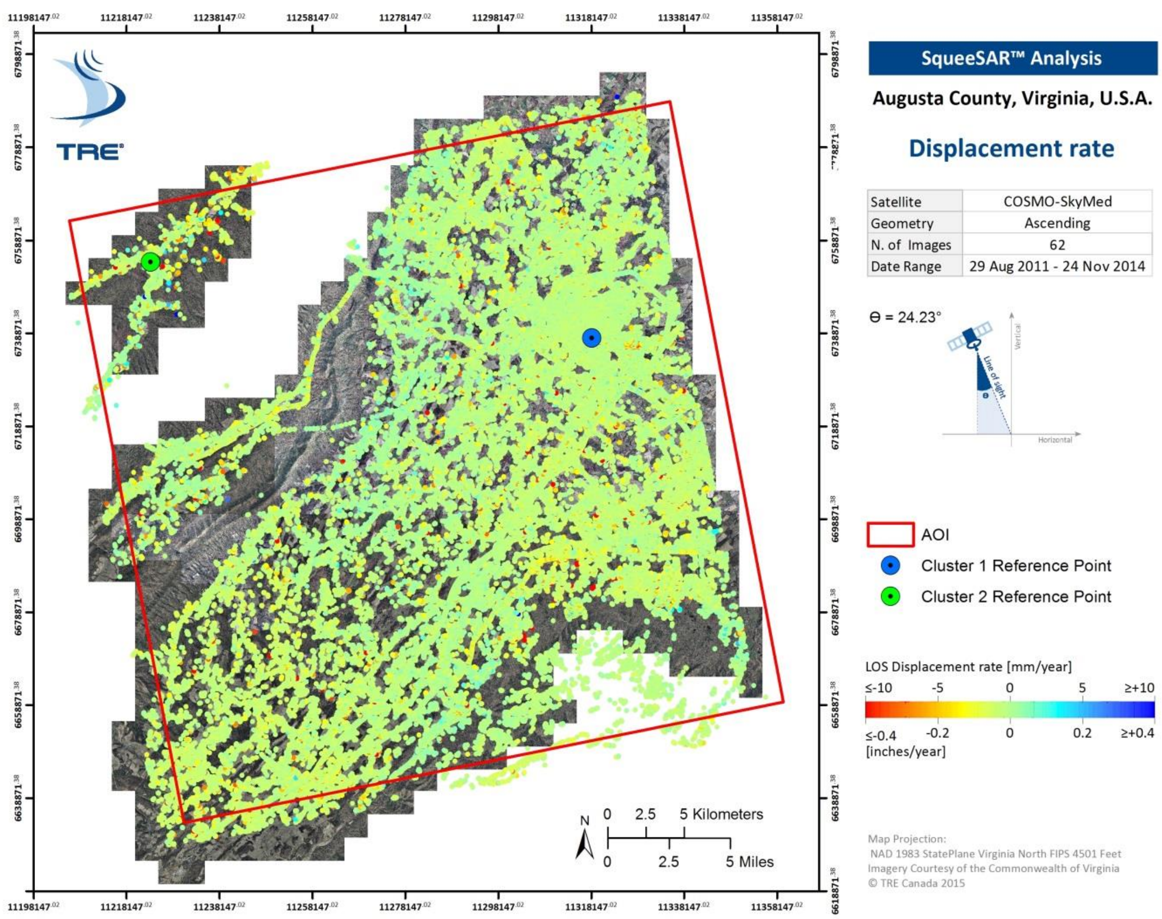

Figure 4: Displacement rates in mm/year.

5.3 Displacement Rate Standard Deviation

The standard deviation of the surface displacement data characterizes the error of the measurements (Figure 5). For this reason, any measurement should be interpreted in the form of Displacement Rate ± Standard Deviation. Standard deviation values tend to increase with distance from the reference point. Higher values indicate a greater variability in displacement rates and are often associated with areas of rapid and/or irregular ground movement.

Standard deviation values range from 0.04 to 0.93 mm/year. The average standard deviation value of all measurement points within this data set is ±0.45 mm/year for cluster 1 and ±0.38 mm/year for cluster 2.

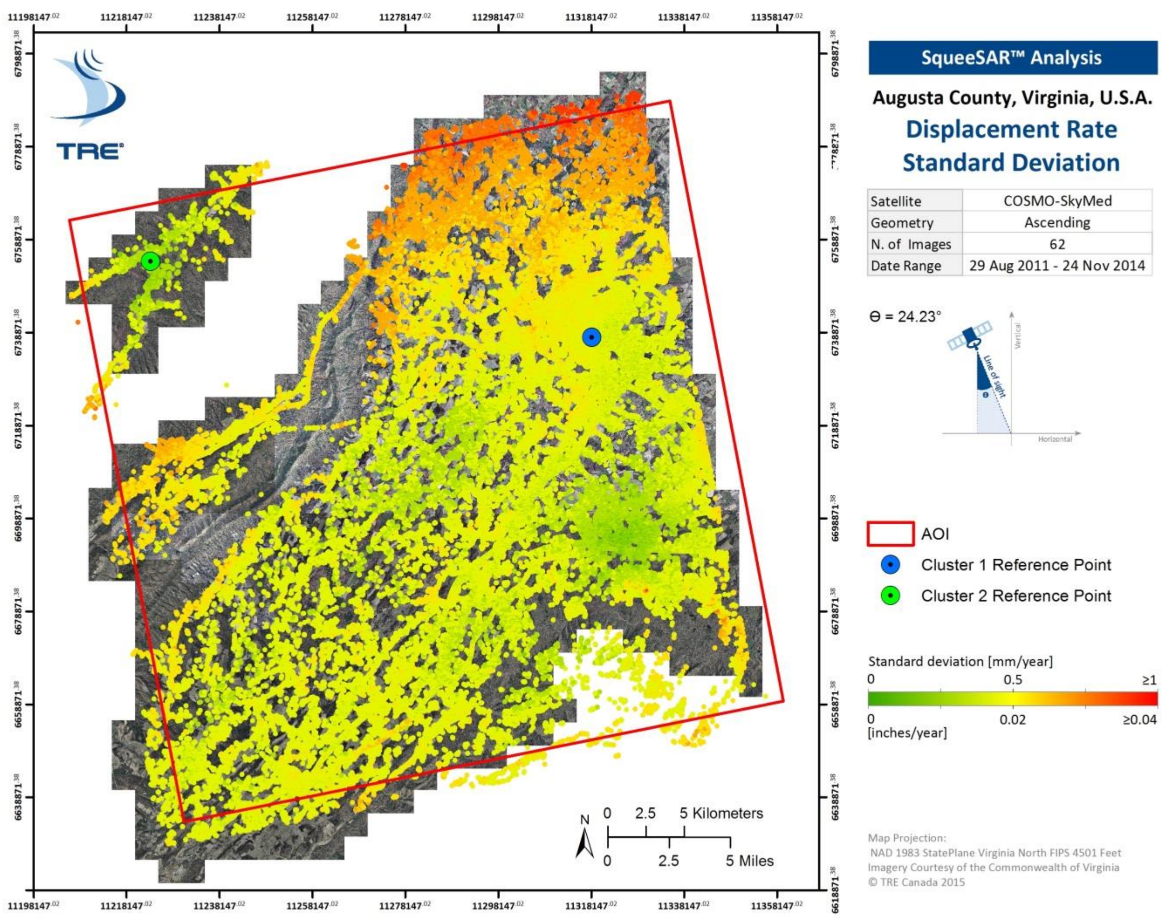

Figure 5: Standard deviation values of the displacement rates.

5.4 Temporary Scatterers (TS)

This technique developed by TRE is based upon the extraction of Temporary Scatterers (TS) from a radar image stack. Compared to PS and DS, TS represent measurement points identified within a subset of the image data set rather than the complete stack. This approach typically leads to a greater spatial coverage of the results as it often includes areas where PS and DS are not identified. The output is a raster map, with a 10 m x 10 m cell size, representing average surface displacement rates.

The results of the TS analysis in the Virginia data set are shown in Figure 6. As expected, the TS approach provides a higher spatial coverage of deformation information in certain regions of the AOI compared to the SqueeSAR results. However, the increased density of measurement points in the SqueeSAR results now makes the results comparable in many areas.

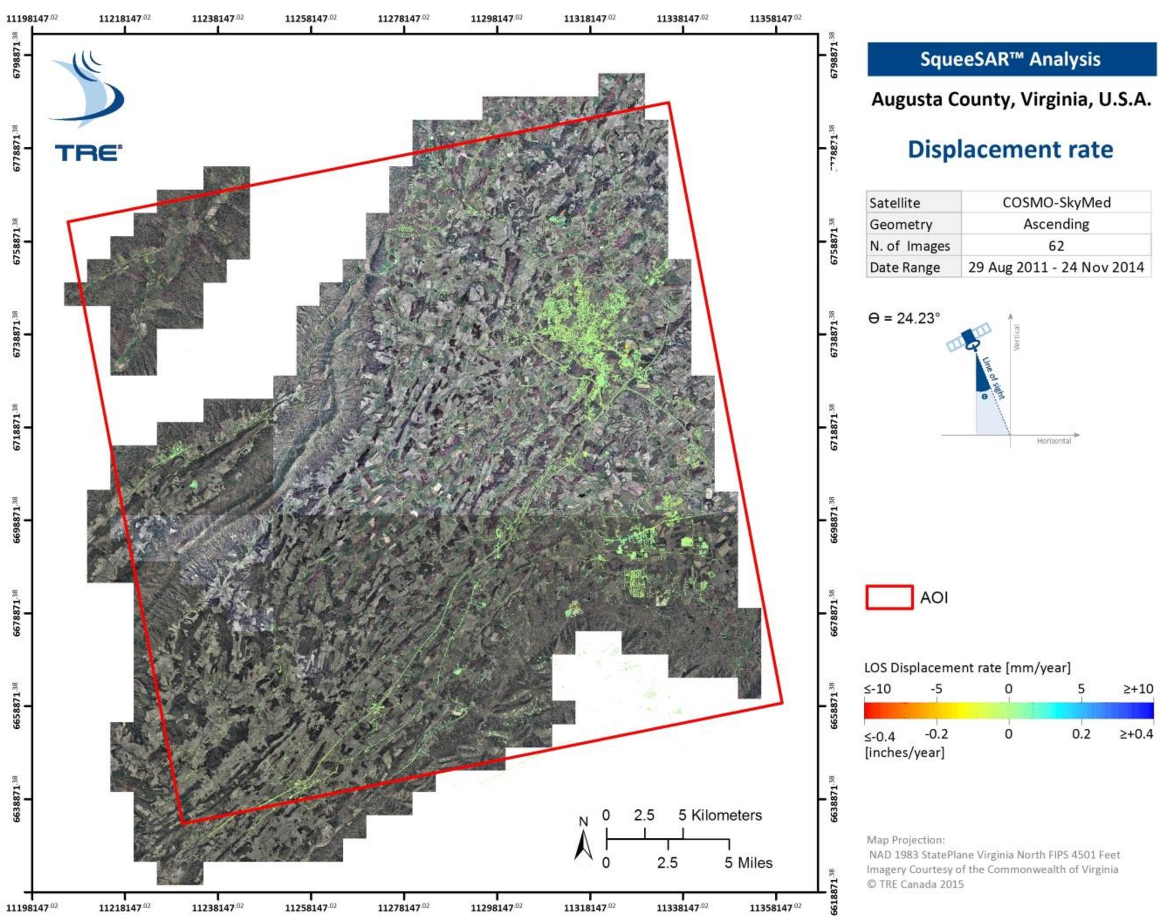

Figure 6: Surface displacement results identified from the TS, expressed in millimeters per year.

6 Observations

The InSAR results spanning 39 months provide comprehensive ground deformation information. As the focus of the project is on potential geohazards near transportation assets, several section detail different aspects related to transportation in the next sections. Section 6.1 describes settlement over primary and secondary roads while Section 6.2. analyzes several areas of localized movement located close to potential geological instabilities. The results of the reflector analysis over the Route 262 Bridge are detailed in Section 6.3. Finally, Pavement conditions and an InSAR results comparison are described in Section 6.4

Note that all of the individual and grouped measurement points highlighted in the figures in Section 6 are labelled 'TS'. In this case, the acronym TS refers to the Time Series of the data, and not temporary scatterers as discussed in Section 5.4.

The processing of 62 CSK images over the 39-month period produced a density of 497 PS and DS per square kilometre (1,287 PS/DS per square mile, Table 6) compared to 405 points per square kilometre in the previous processing.

Further statistics summarizing the results of the data processing can be found in the Technical Appendix.

	2011		2012		2014		2014	
Attribute	**Cluster 1 Results**	**Cluster 2 Results**	**Cluster 1 Results**	**Cluster 2 Results**	**Cluster 1 Results**	**Cluster 2 Results**	**Cluster 1 Results**	**Cluster 2 Results**
Dates	29 Aug 2011 – 20 Feb 2012		29 Aug 2011 – 25 Oct 2012		29 Aug 2011 – 17 Jun 2014		29 Aug 2011 – 24 Nov 2014	
Period covered (months)	6		14		33		39	
N. of images processed	16		32		52		62	
N. of PS	38,057 (20%)	336 (12%)	166,348 (56%)	1,453 (49%)	461,656 (72%)	3,975 (62%)	699,070 (89%)	7,705 (89%)
N. of DS	148,536 (80%)	2,486 (88%)	129,773 (44%)	1,512 (51%)	180,388 (28%)	2,469 (38%)	89,745 (11%)	919 (11%)
Total N. of Measured Points (PS and DS)	186,593	2,822	296,121	2,965	642,044	6,445	788,815	8,624
Average PS and DS Density (per square km) Cluster 1 and 2 combined	118 pts/km^2 (307 pts/sq. mi)		187 pts/km^2 (484 pts/sq. mi)		405 pts/km^2 (1,049 pts/sq. mi)		497 pts/km^2 (1,287 pts/sq. mi)	
Average Displacement Rate (mm/year)	2.1	0.6	0.2	-0.2	-0.2	-0.4	-0.5	-0.8
Average Displacement Rate Standard Deviation (mm/year)	3.4	8.7	1.5	1.4	0.6	0.4	0.4	0.4
Average Acceleration Rate (mm/year^2)	8.6	62.9	0.5	-3.5	-0.2	-0.7	-0.9	-1.4
Average Acceleration Rate Standard Deviation (mm/year^2)	50.3	129.4	9.6	8.7	1.7	1.2	1.2	1.0

Table 6. Statistics of the two clusters identified over the Staunton AOI.

6.1 Results over Primary Roads

Displacement rates for measurement points identified within a 30 m buffer around eight primary roads and partial secondary roads (I-81, I-64, Rt. 11, Rt. 250, Rt. 254, Rt. 262, Rt. 252 and Rt. 600) are shown in Figure 7. The eight sections of road used in the inspection of the ground displacement around primary roads and the specific subsidence locations are listed in Table 7.

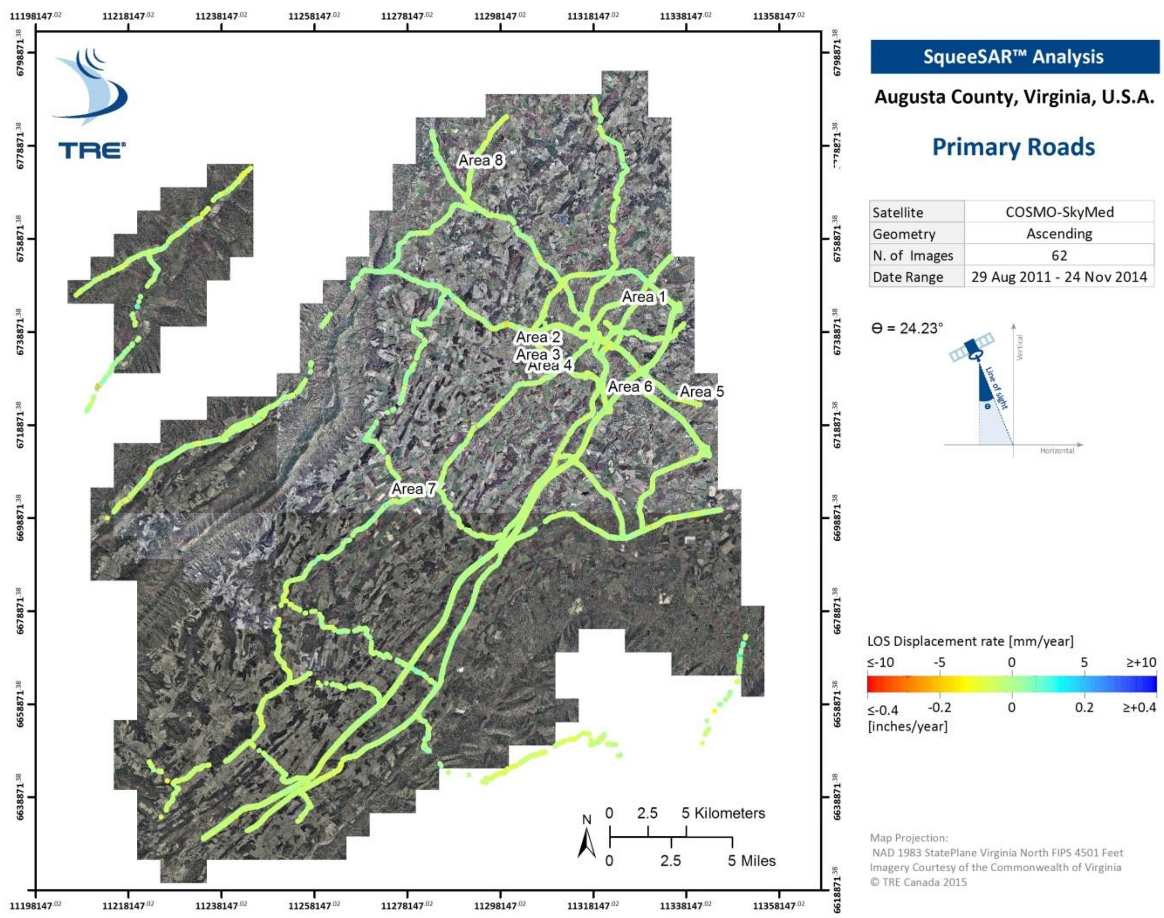

Figure 7: Surface displacement results identified within a 30 meter (100 foot) buffer of major roads within the AOI. Eight roads are indicated, with their specific locations listed in Table 7.

Area	Location (E, N)	Brief Description of Subsiding Area	Maximum Displacement (mm/yr)
1	(-79.043251, 38.166152) (-79.043245, 38.166167)	Railroad track running parallel to Lee Highway (Rt. 11)	-14.2 -5.6
2	(-79.093591, 38.132709)	Slope along Route 262 approach to overpass of Middlebrook Ave (Rt 252)	-7.5
3	(-79.092755 38.130462)	Slope along an exit from Route 262 to Middle brook Ave	-8.6
4	(-79.086683 38.126387)	Exposed ground on the shoulder of Woodrow Wilson Parkway (Rt. 262)	-8.0
5	(-78.998735, 38.110664)	On Jefferson Hwy (Rte250). Close to the intersection with Idlewood Blvd	-11.1
6*	(-79.064883, 38.120738)	VA 262 W to US 11	-3.1
7*	(-79.213444, 38.052683)	10 Metres (33 ft) to Mish Barn Rd Between Middlebrook Rd and Whispering Ln	-16.9
8*	(-79.164962, 38.247153)	On VA 42 between Massey Mill Ln and McCray Ln	-2.4

Table 7: Coordinates of the twelve highlighted locations indicated in Figure 7. All coordinates were obtained from PS points indicating subsidence within the areas of interest. *Displacement over the area is highlighted in more detail in the next section.

Areas 6, 7 and 8 correspond to small groups of two or three measurement points located on or near roads and are presented in further detail in the figures below. All of the measurement points highlighted in the time series below are of the PS type.

6.1.1 Area 6 – VA-262 Westbound to US-11

Area 6 is located on State Route 262 Westbound (WB) to U.S. Route 11 (TS1 in Figure 8) and U.S. Route 11 Northbound (NB) to the State Route 262 Westbound (TS2 in Figure 8). Two measurement points with a displacement rate of -3.1 mm/yr and -7.3 mm/yr are highlighted (Figure 9 and Figure 10). The TS1 time series indicates that up to -15.9 mm of subsidence occurred during May to September 2014 before subsequently rebounding.

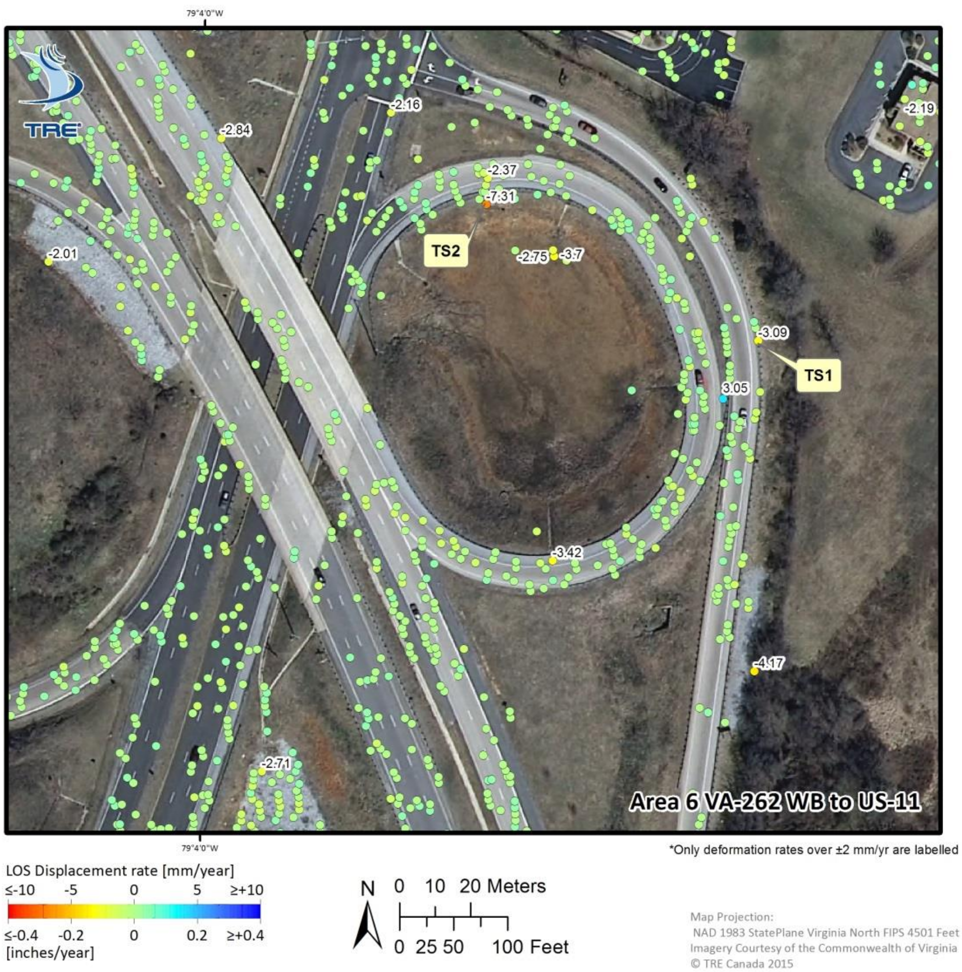

Figure 8: Displacement results on VA-262 and US-11 (Identified as Area 6 in Figure 7).

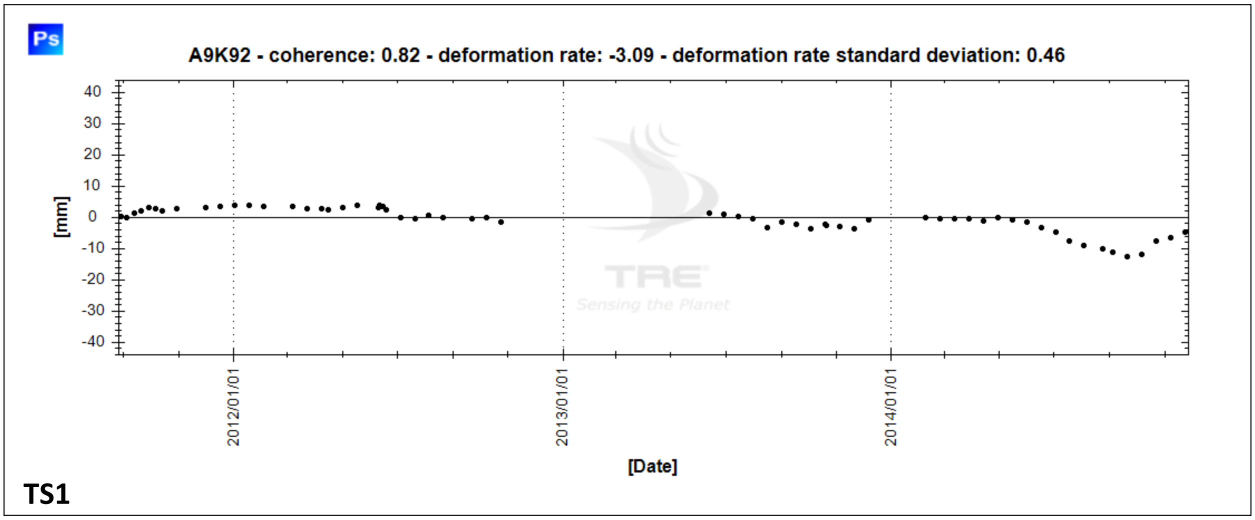

Figure 9: Time series of TS1 in Figure 8.

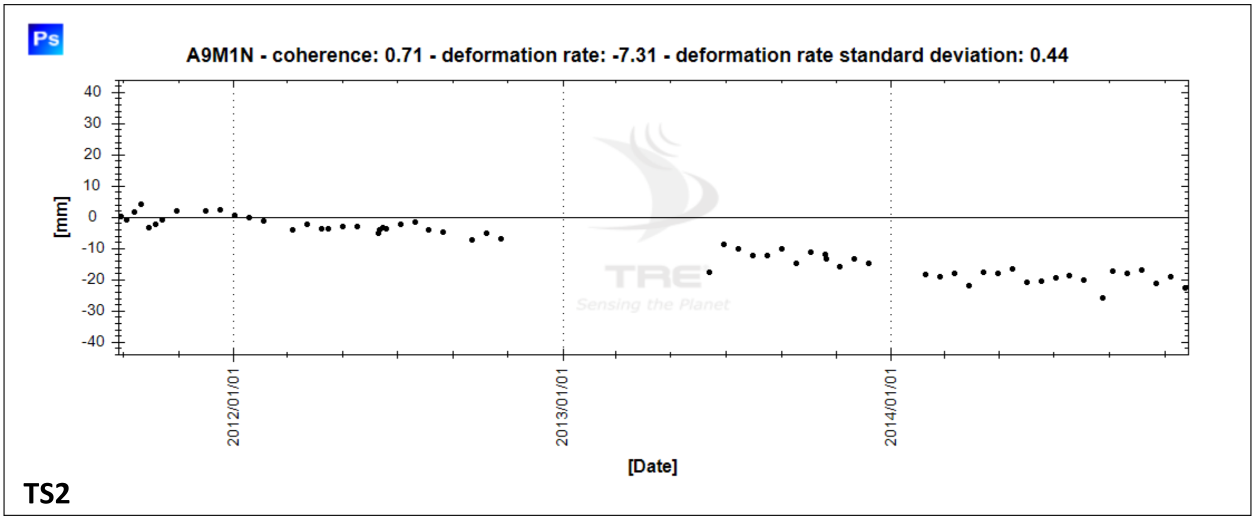

Figure 10: Time series of TS2 in Figure 8.

6.1.2 Area 7 - Mish Barn Road

A measurement point indicated continuous displacement since 2012 near Mish Barn Road between Middlebrook Rd and Whispering Ln (TS1 in Figure 11). Movement of up to -45.5 mm was measured several metres west of the road (Figure 12) while the road itself appears stable (ATS2 in Figure 11, time series in Figure 13).

Figure 11: Displacement results near Mish Barn Road between Middlebrook Rd and Whispering Ln (identified as Area 7 in Figure 7).

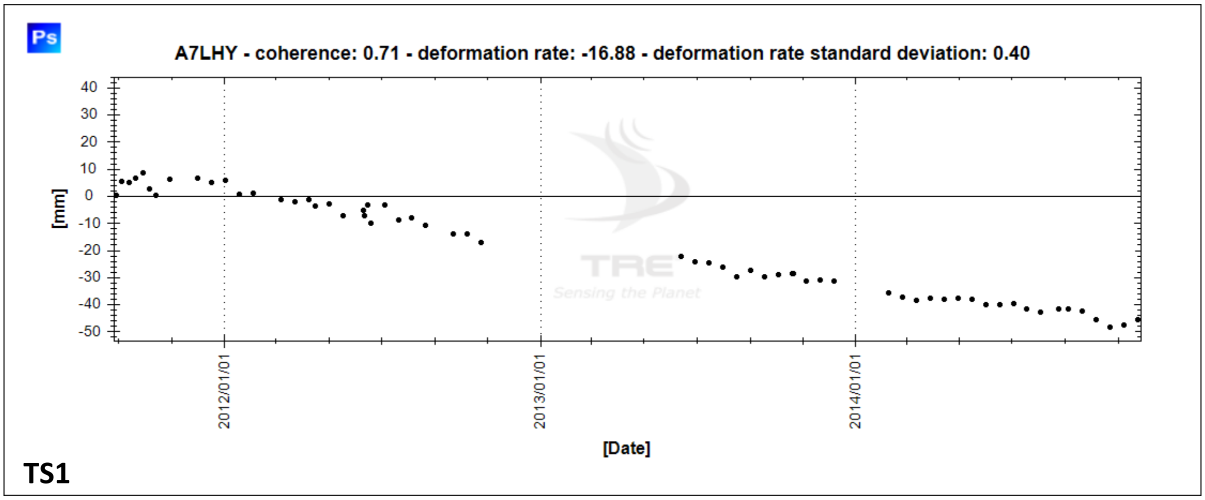

Figure 12: Time series of TS1 in Figure 11.

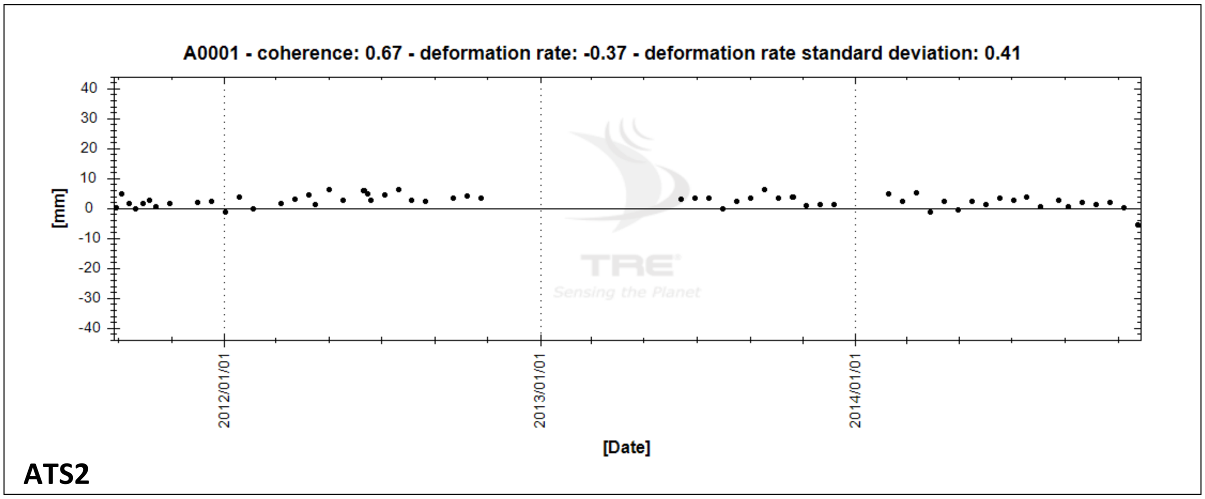

Figure 13: Average time series of ATS2 in Figure 11.

6.1.3 Area 8 – VA-42

Possible subsidence relative to a single point (TS1 in Figure 14) was detected on State Route 42 between Massey Mill Ln and McCray Ln. The change in movement trend started in early July 2014 (Figure 15). The neighbouring area over VA-42 (ATS2 in Figure 16) appears to be stable.

Figure 14: Displacement results over State Route 42 between Massey Mill Ln and McCray Ln (identified as Area 8 in Figure 7).

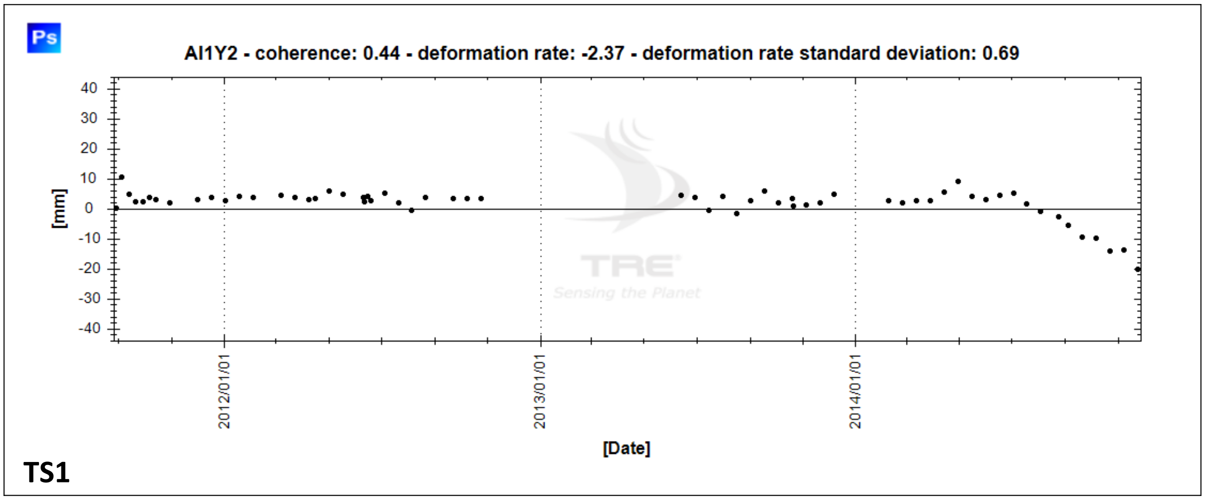

Figure 15: Time series of TS1 in Figure 14.

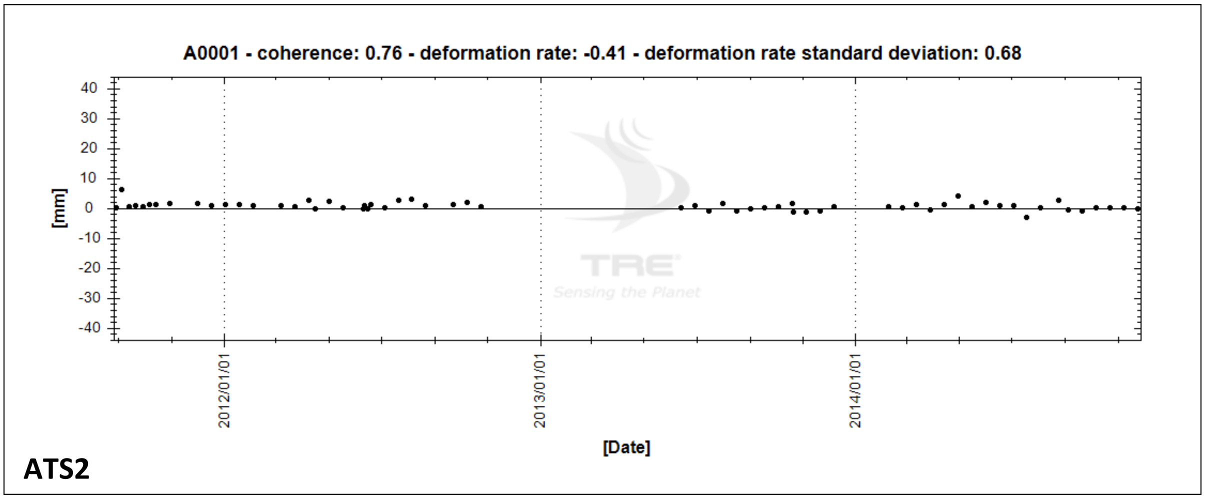

Figure 16: Average time series of ATS2 in Figure 14.

6.2 Comparison to Geohazards Data

Shown below are the displacement results overlaid with historic sinkholes, landslides and other geohazard data provided by the Commonwealth of Virginia (Figure 17). A total of 30 sinkholes, one slope failure, as well as 23 karst geohazards located along Interstate 81 are indicated. In the current analysis, fifteen points of interest (POI) that are relevant to the University of Virginia and the Virginia Department of Transportation have continued to be monitored, specifically in relation to the detection of sinkholes and landslides as well as road/bridge condition. These points were also highlighted in the previous report (Doc. Ref.: JO11-3011-REP2.0)

Five locations (Feature 1 to 5 in Figure 17) are analyzed further in the following section. These features were selected either because localized surface displacement was identified or they are areas where geohazards were identified in the field during the monitoring period.

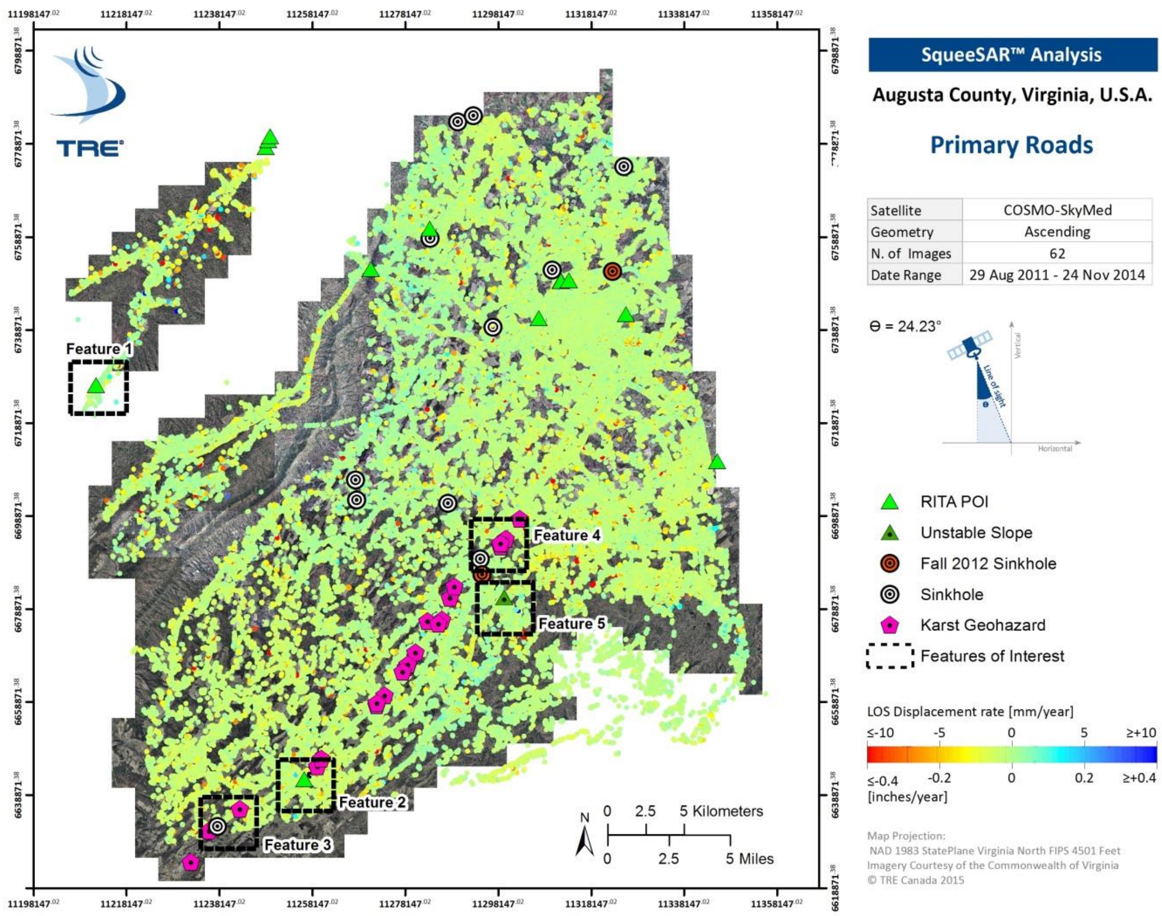

Figure 17: Historical geohazard events and points of interest overlaid on the surface displacement results.

6.2.1 Feature 1 – Rock Slope on Route 600

Feature 1, located on a rock slope along Route 600 (Figure 18), has experienced subsidence rates of up to -14.3 mm/year. Two average rates of -9.6 mm/yr and -2.7 mm/yr were calculated using groups of measurement points located on the slope (ATS1, Figure 19 and ATS2, Figure 20, respectively).

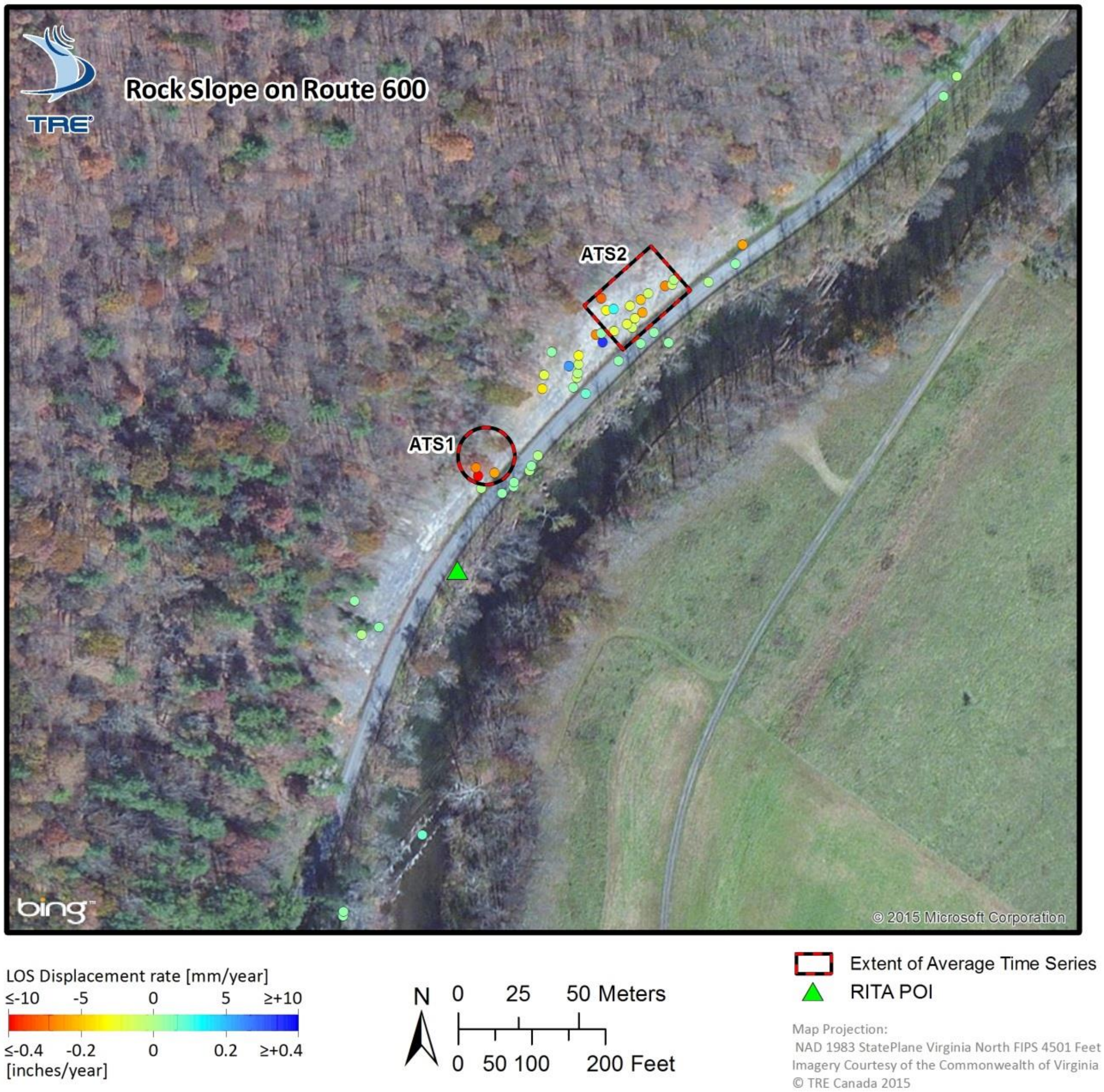

Figure 18: Displacement results over the rock slope on Route 600 (Feature 1 in Figure 17).

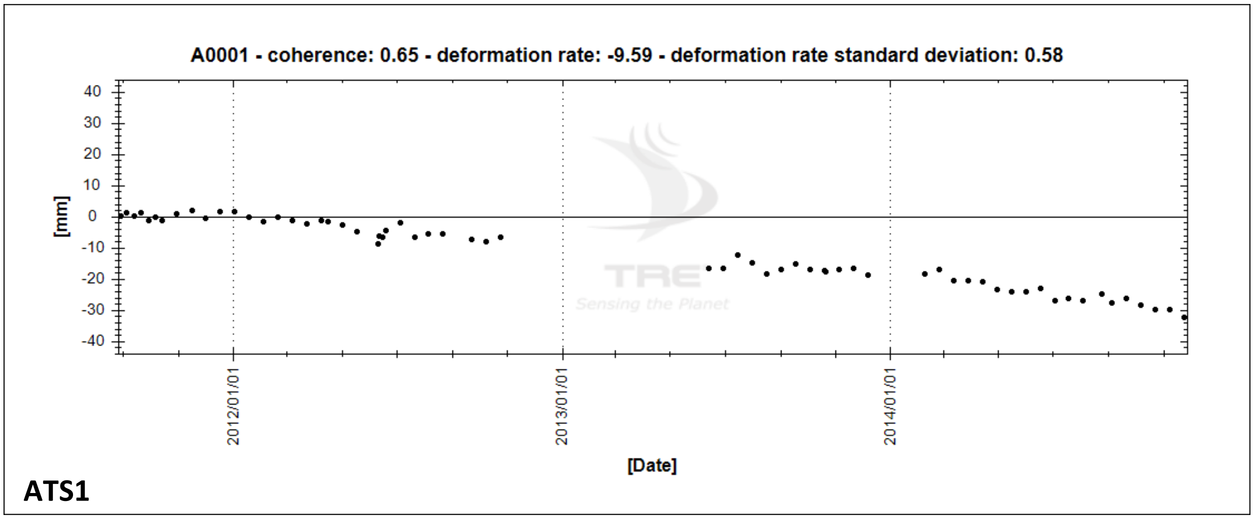

Figure 19: Average time series for ATS1 in Figure 18.

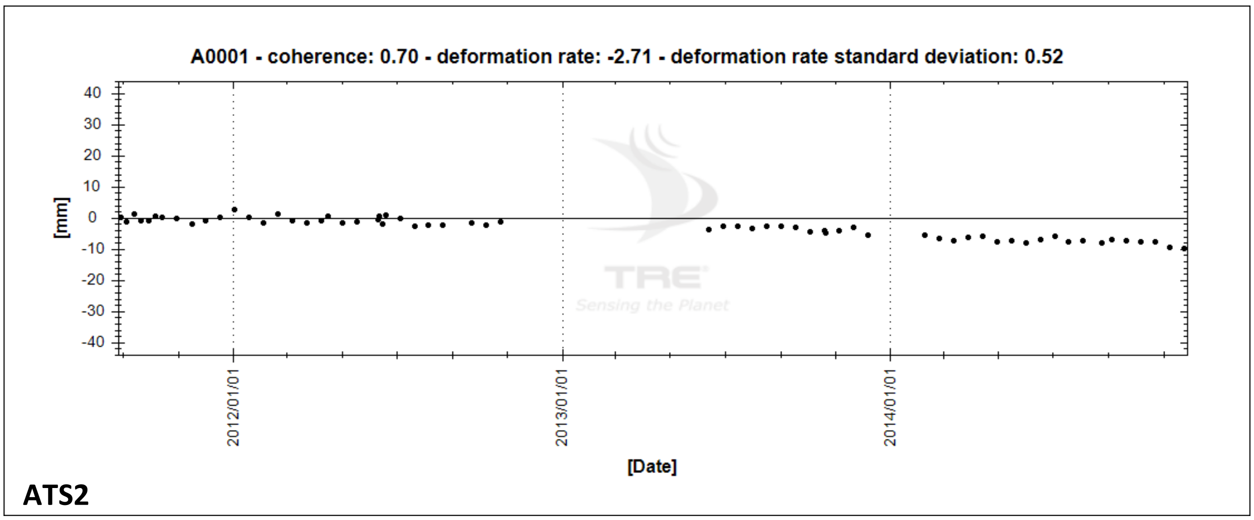

Figure 20: Time series of TS2 in Figure 18.

6.2.2 Feature 2 – I-81 Northbound / I-64 Eastbound

Feature 2 consists of two locations along I-81 NB and I-64 EB (Figure 21). The Sterrett Road overpass of Route 710 shows signs of subsidence on both approaches: -13.5 mm/yr for a single point on the east (TS1, Figure 22) and -7.1 mm/yr on the west (ATS2, Figure 23). In both of these cases, the movement stabilized after August 2014. Points east of TS1, however, do not indicate movement (ATS3, Figure 24). Roughly 365 metres northeast of this overpass, movement was also detected on a riprap slope (ATS4, Figure 25).

It is also interesting to observe that I-81 SB is significantly more stable than the northbound lane. This may indicate that I-81 NB was experiencing construction or post-construction distress during the InSAR monitoring period.

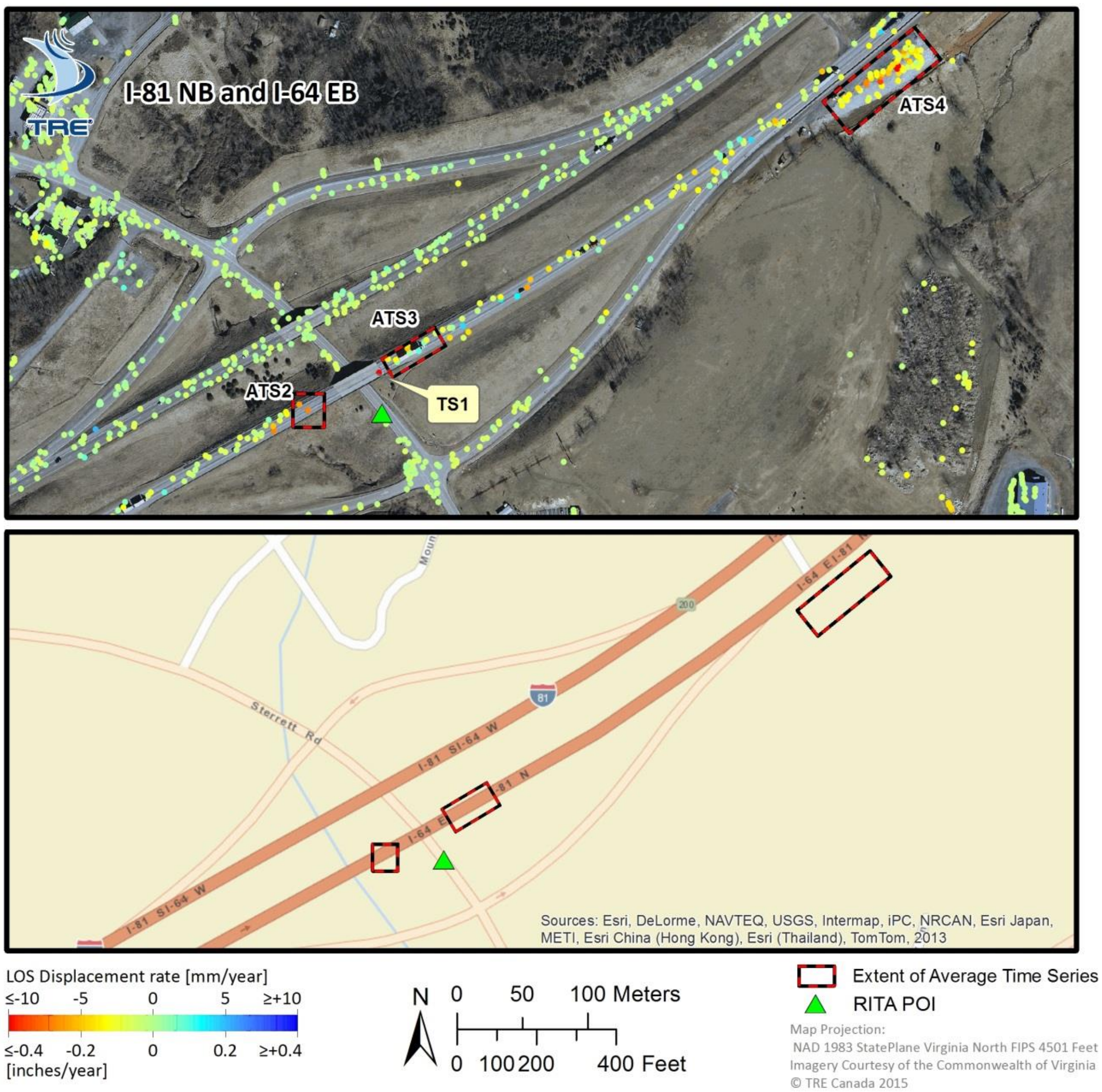

Figure 21: Displacement results along I-81 NB / I-64 EB (Feature 2 in Figure 17). The top panel shows InSAR data overlaid on an aerial image. The bottom panel contains a street map to help identify the highlighted roads.

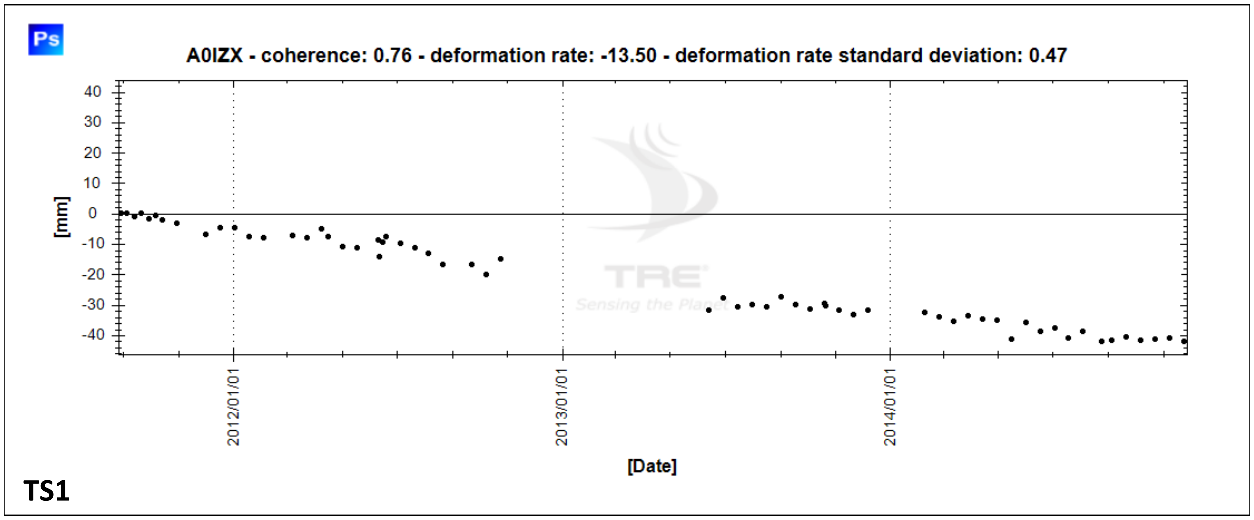

Figure 22: Time series of surface displacement for TS1 in Figure 21.

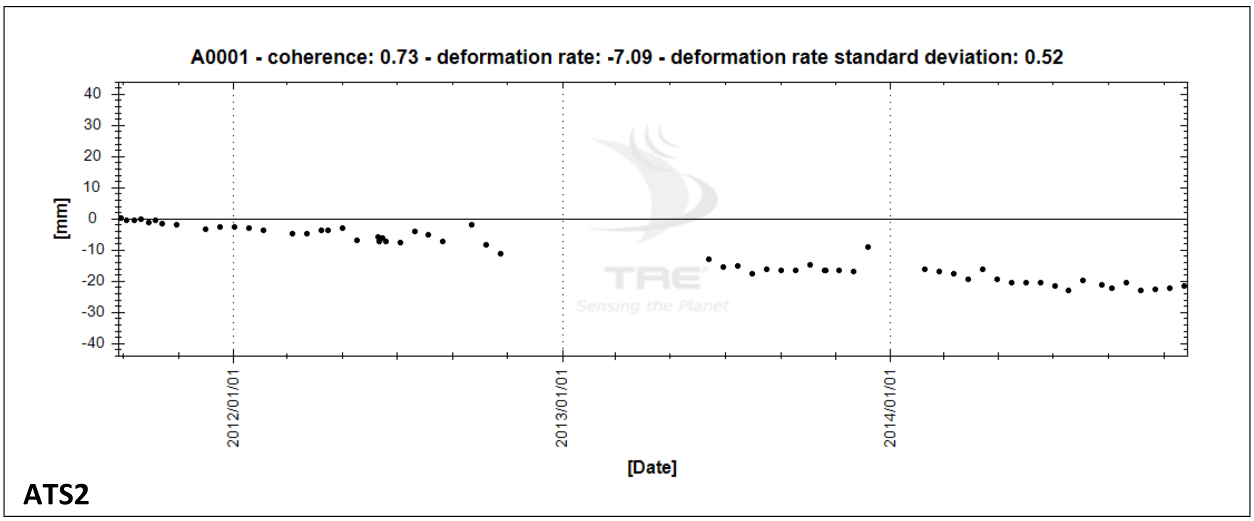

Figure 23: Average time series of surface displacement for ATS2 in Figure 21.

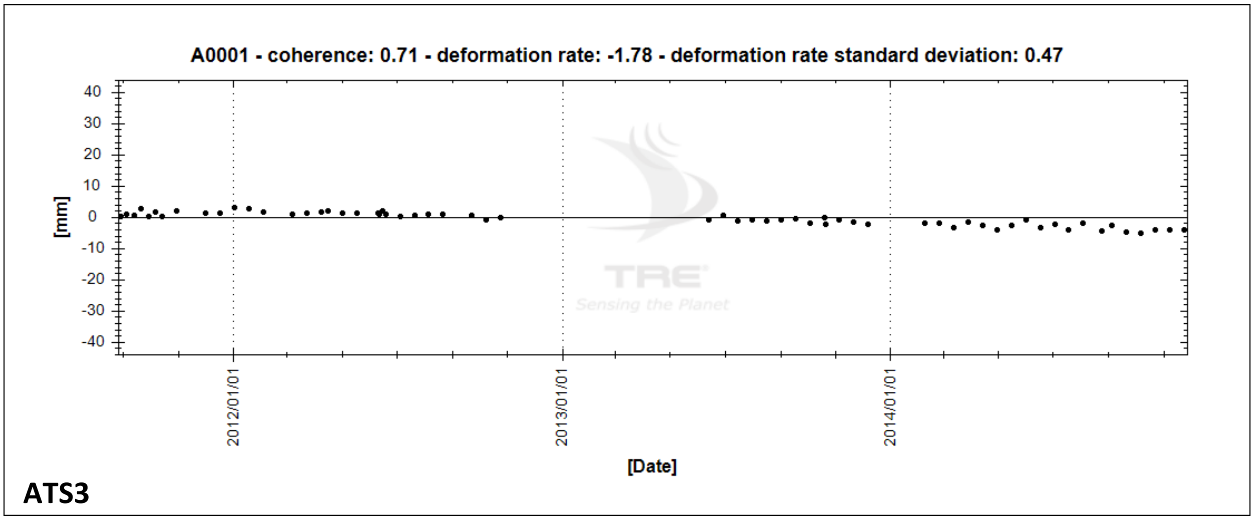

Figure 24: Average time series of surface displacement for ATS3 in Figure 21.

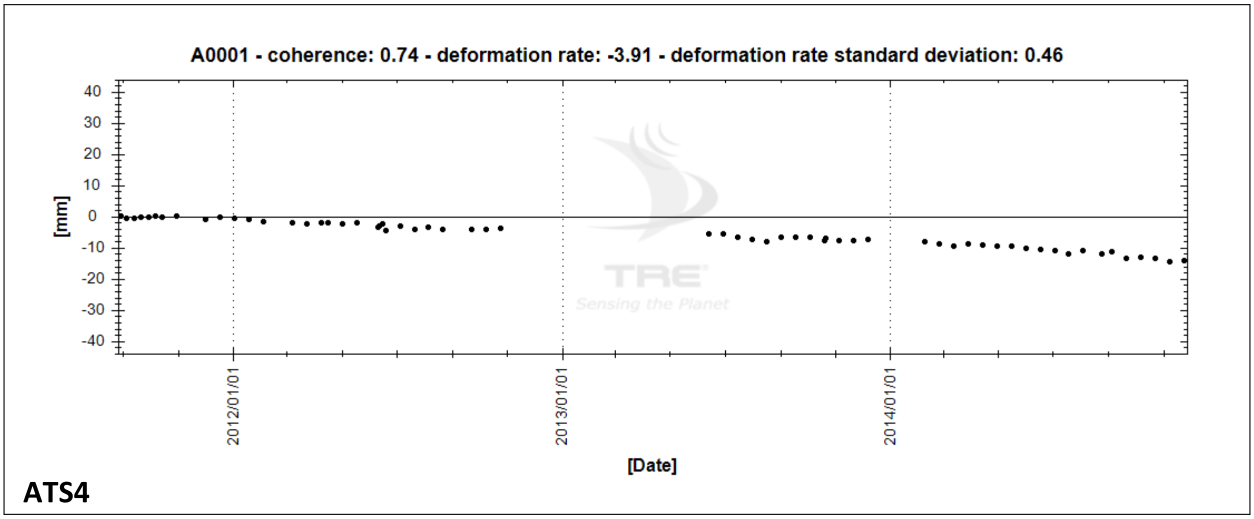

Figure 25: Average time series of surface displacement for ATS4 in Figure 21.

6.2.3 Feature 3 – Karst Geohazard and Riprap along I-81 Northbound

Feature 3 is along I-81 NB in the southwest portion of the AOI (Figure 26). Three sub-areas were highlighted here: a riprap slope with an average deformation rate of -4.9 mm/yr (Area A in Figure 26), which was similar to previous results; a karst geohazard location near I-81 NB exhibited mild movement (Area B in Figure 26) and; a second riprap slope close to I-81 SB with a deformation rate of -6.7 mm/yr along Decatur Rd. The time series for Feature 3 are shown in Figure 27 to Figure 29.

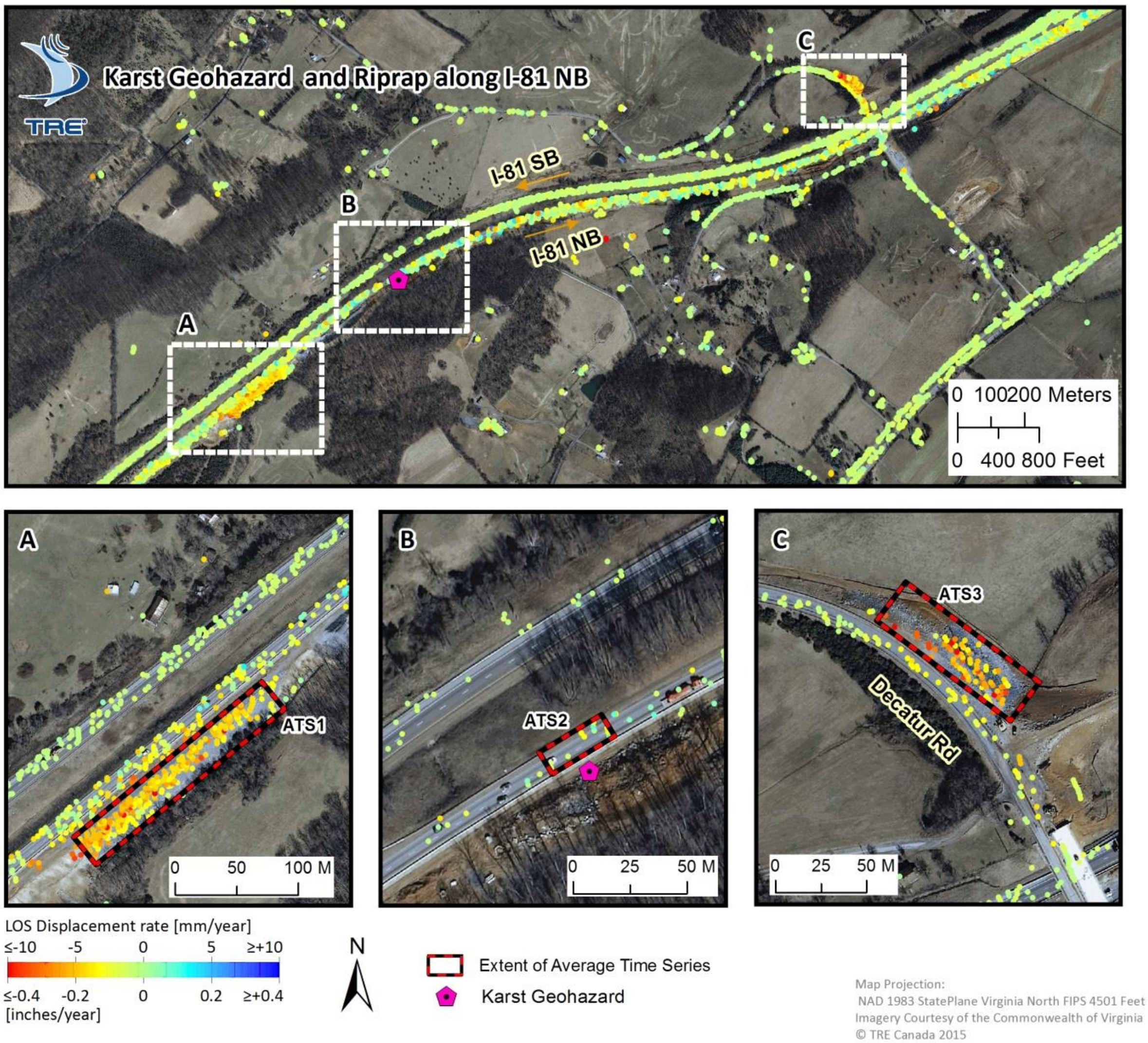

Figure 26: Displacement results over a karst geohazard and two riprap slopes along I-81. The top panel provides an overview of the highlighted areas and the bottom panels illustrates the three subareas.

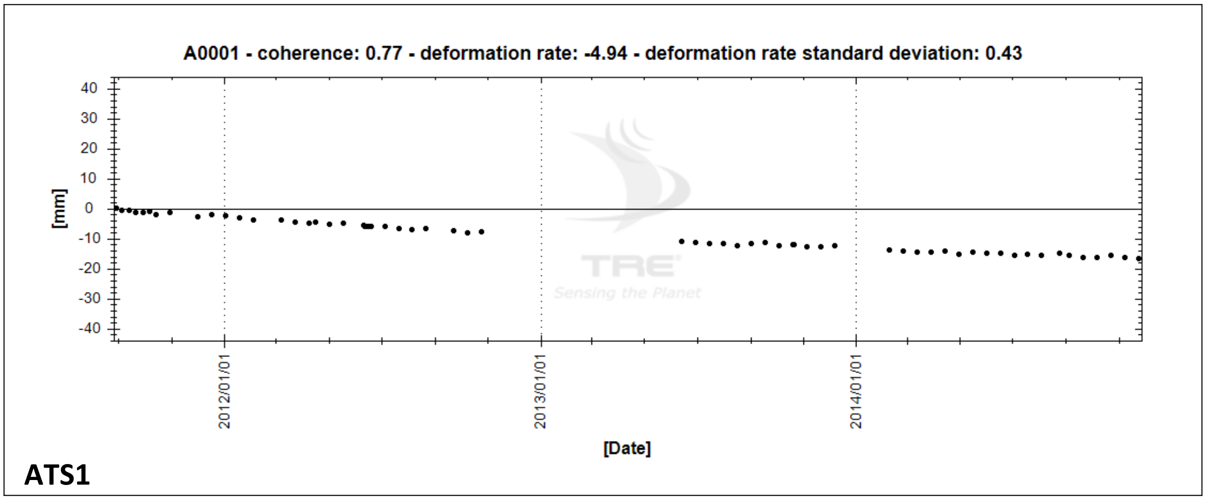

Figure 27: Average time series of surface displacement for ATS1 in Figure 26.

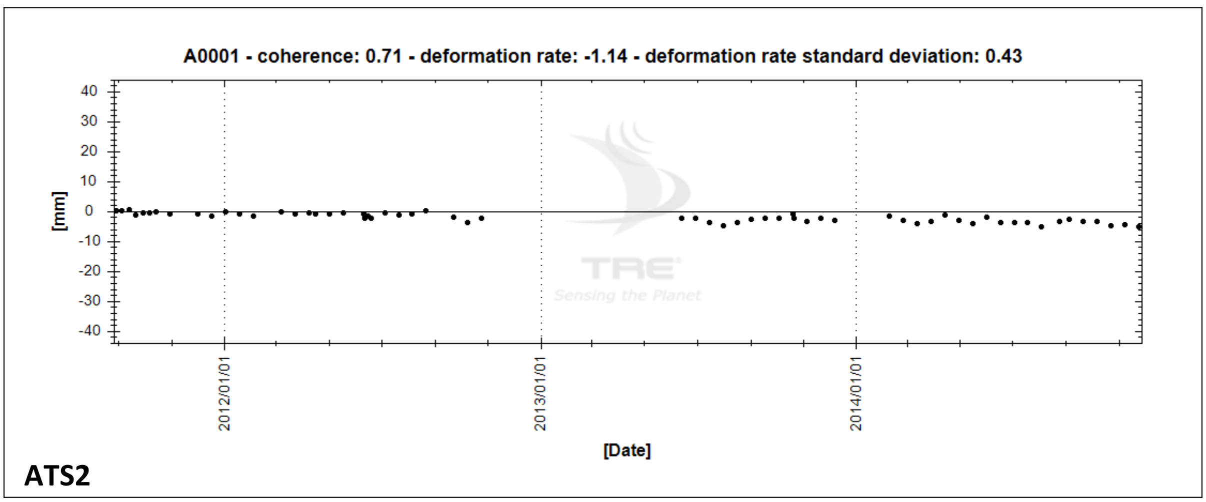

Figure 28: Average time series of surface displacement for ATS2 in Figure 26.

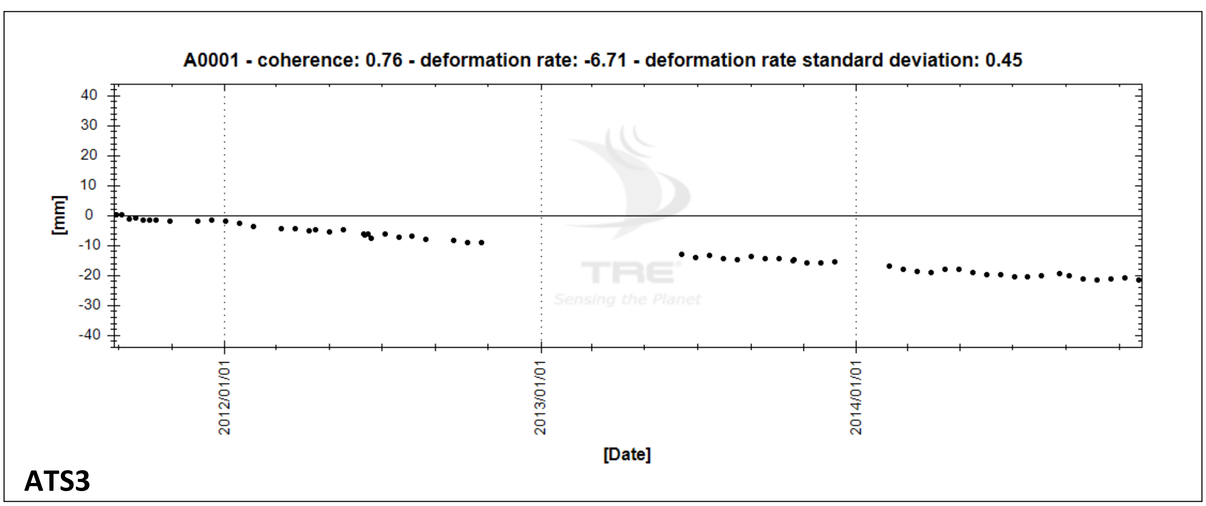

Figure 29: Average time series of surface displacement for ATS3 in Figure 26.

6.2.4 Feature 4 – Riprap on I-64

A riprap slope located close to the I-81 NB (I-64 EB) overpass of Highway 11 shows mild settlement (Figure 30) of -2.2 mm/yr. Three karst geohazard sites are also shown in Figure 30. In each case ground movement is less than ±1 mm/yr.

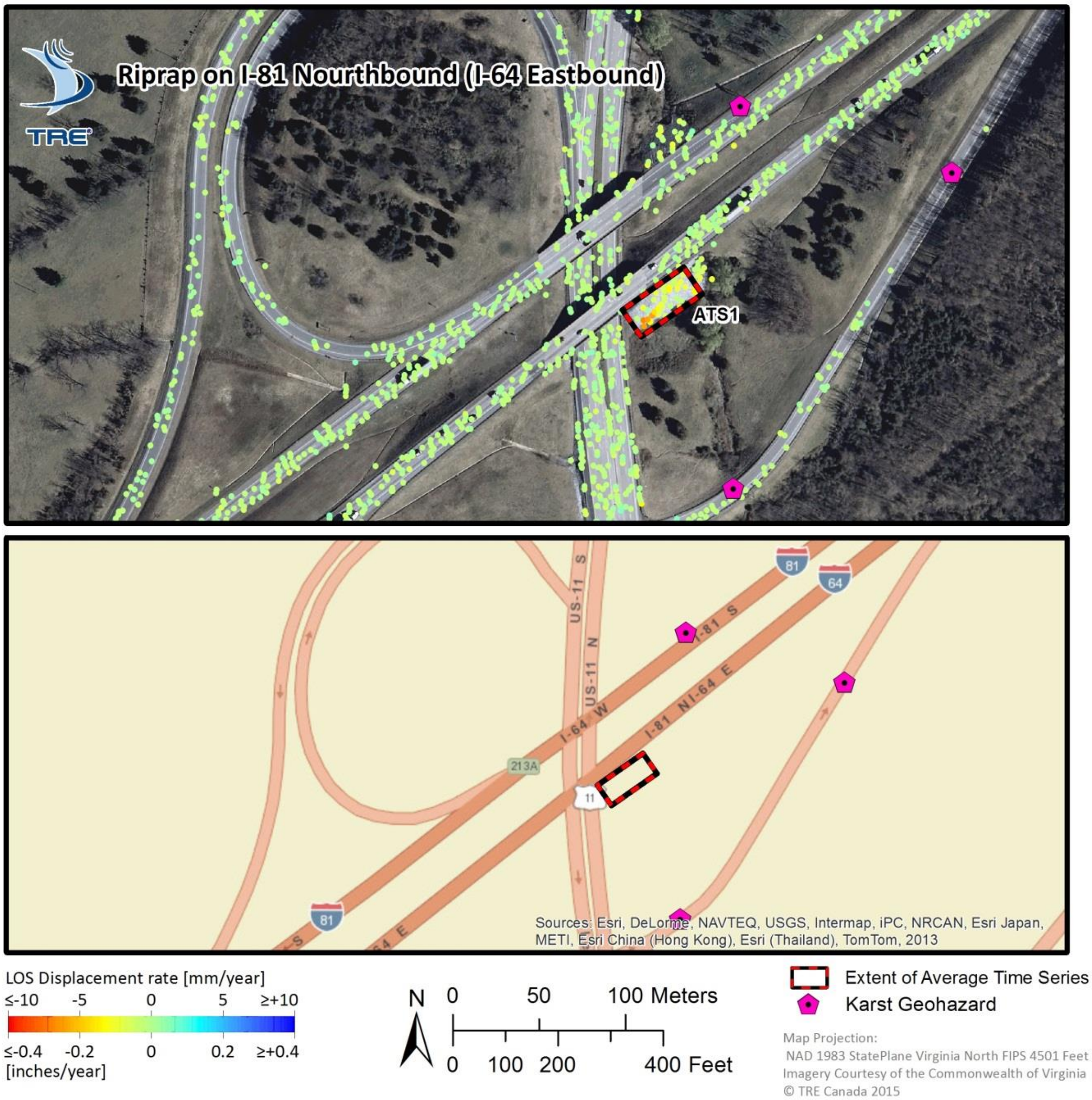

Figure 30: Displacement results over a riprap slope on I-64. The top panel shows InSAR data overlaid on an aerial image and the bottom panel contains a street map to help identify the highlighted roads.

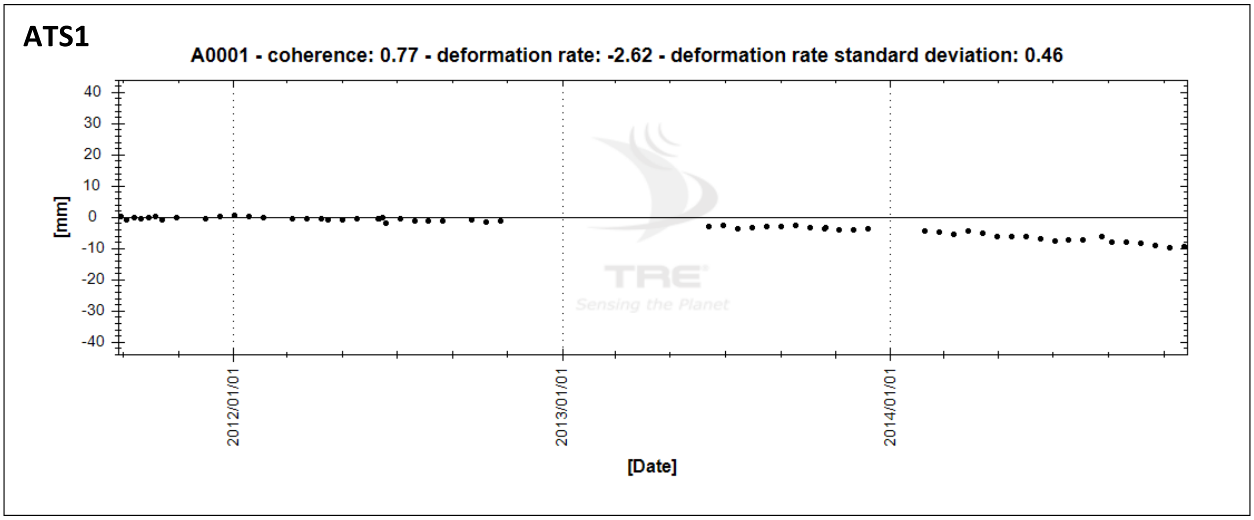

Figure 31: Average time series of ATS1 in Figure 30.

6.2.5 Feature 5 - Unstable Slope along Greenville School Rd

Feature 5 is a slope along Greenville School Rd between Penmerryl Dr. and Cold Springs Rd. (Figure 32). An average displacement rate of -3.8 mm/yr was observed (Figure 33) with a maximum of -10.3 mm/yr. The time series stabilize gradually after April 2014.

Figure 32: Displacement results for a slope along Greenville School Rd.

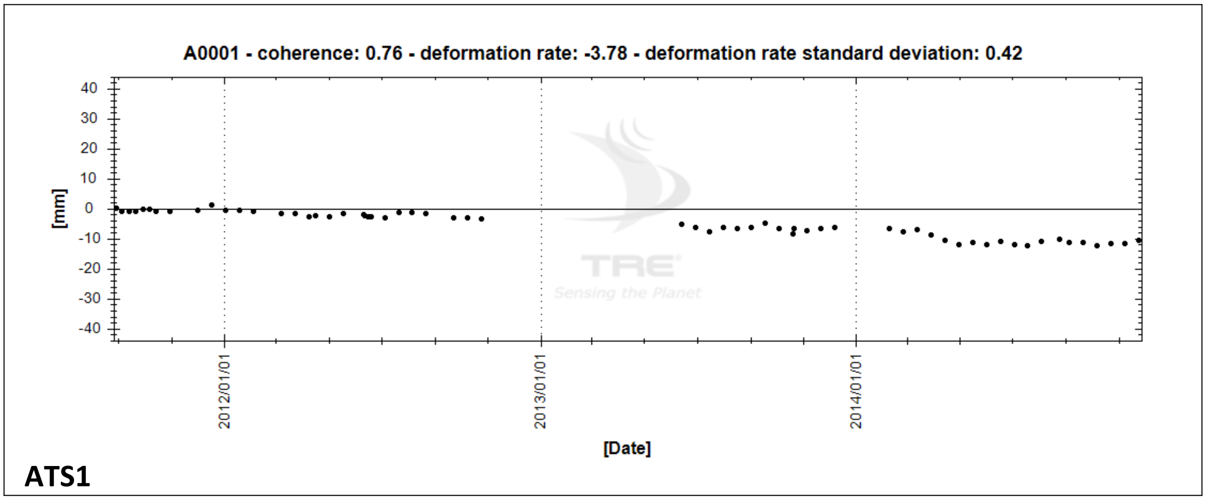

Figure 33: Average time series of ATS1 in Figure 32.

6.2.6 Feature 6 - Sinkhole

A sinkhole was observed in September 2012 along Lee Jackson Highway in a vegetated area and is shown in the top panel of Figure 34 together with Temporary Scatterer results. Neither the TS nor the single DS measurement point identified in the vicinity of the sinkhole identified ground movement between 2013 and 2014 (Figure 35 and Figure 36).

Another sinkhole that initially formed in July 2011 and which recurred in October 2012 is displayed in the bottom panel of Figure 34. The average displacement of the measurement points within 20 metres (66 ft) of the sinkhole do not identify movement (Figure 37). The TS also do not show any movement in the area.

Figure 34: Displacement results over two areas where sinkholes developed in September 2012.

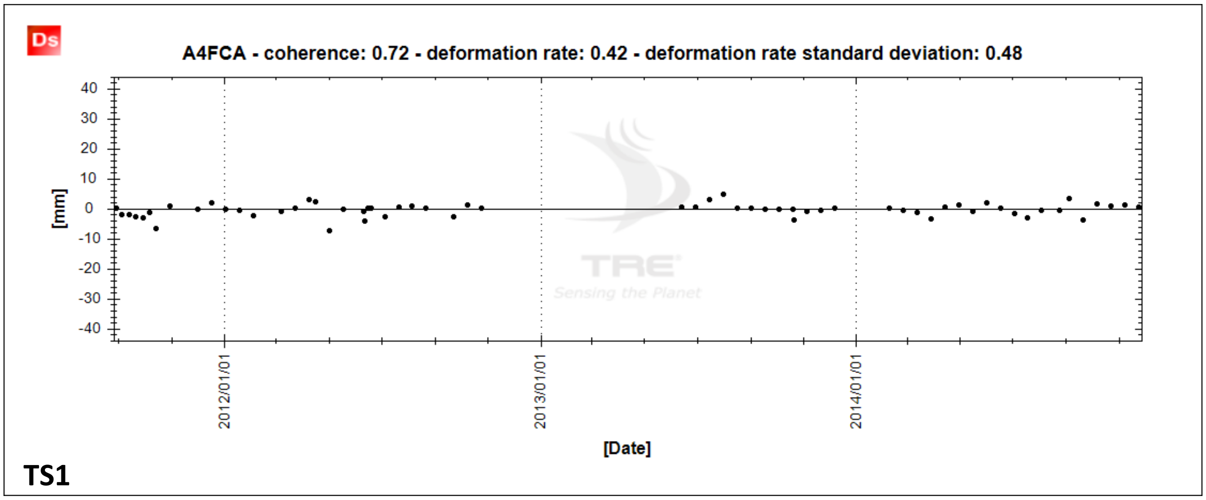

Figure 35: Time series of surface displacement for the measurement point identified as TS1 in Figure 34.

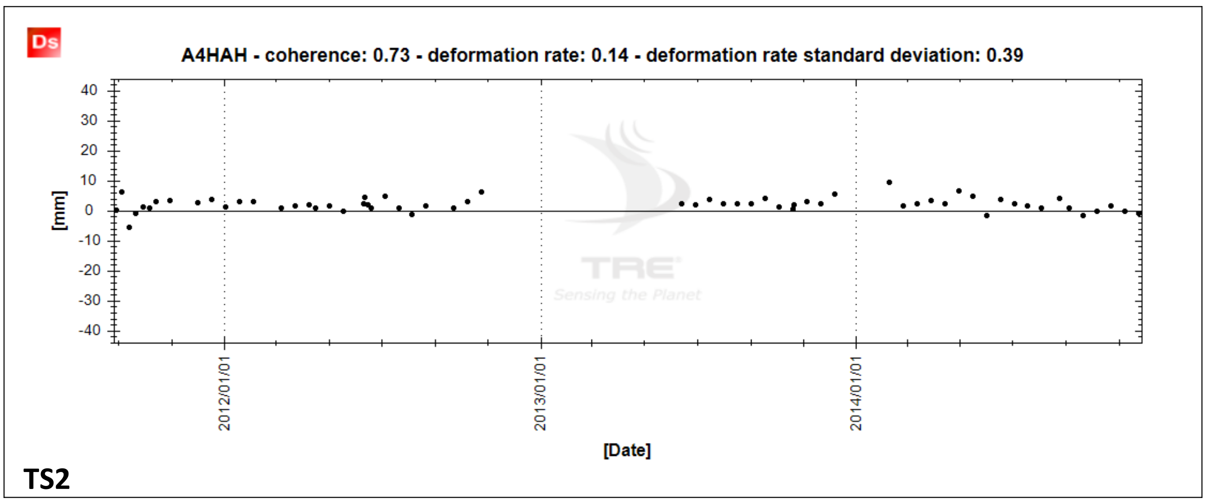

Figure 36: Time series of surface displacement for the measurement point identified as TS2 in Figure 34.

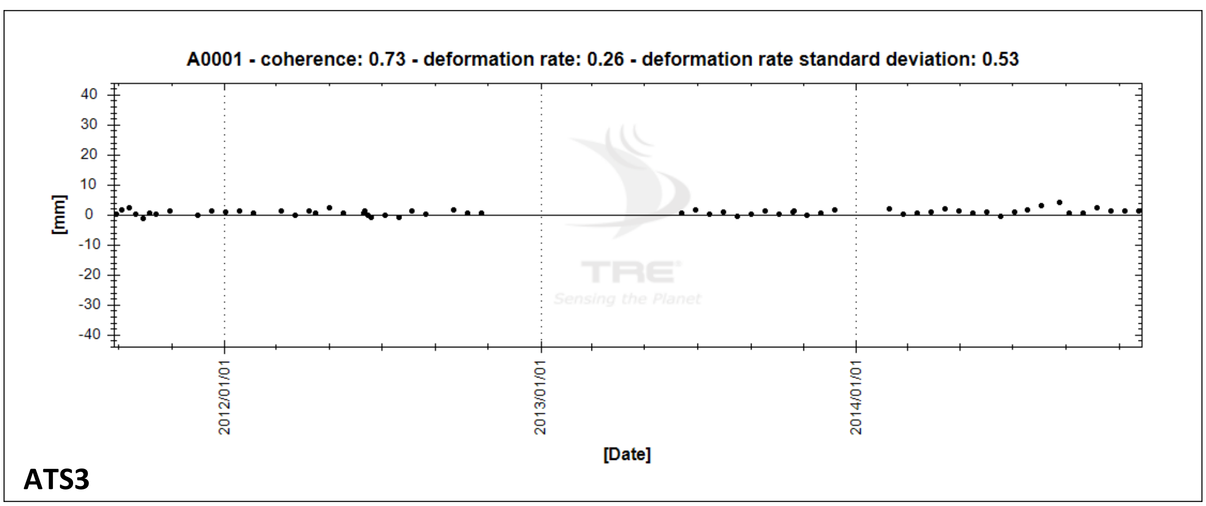

Figure 37: Time series of surface displacement for the measurement point identified as TS3 in Figure 34.

6.3 AR Displacement Analysis

Four ARs (AR #2, 6, 7, 8) were installed to determine whether InSAR could be used to detect movement during a Route 262 bridge load test on 11 June 2012. As the signals of AR #7 and #8 were too weak, only AR #2 and #6 became PS and were utilized for deformation measurements. The results over the Route 262 Bridge are shown in Figure 38.

Reflector #6 was used as the reference and the time series for Reflector #2, located at mid-span, is shown in Figure 39, with the load test date highlighted. A few measurements on the bridge were obtained from natural radar targets (bottom panel in Figure 38), two of which were selected for further analysis. The first target was located on the abutment wingwall (TS1 in Figure 38) close to Reflector #6 (Figure 40) and the second (TS2) was on the bridge at the north approach (Figure 41).

Figure 38: Displacement results on the Route 262 bridge. The top panel shows the reflectors while the bottom panel denotes displacement of natural radar targets.

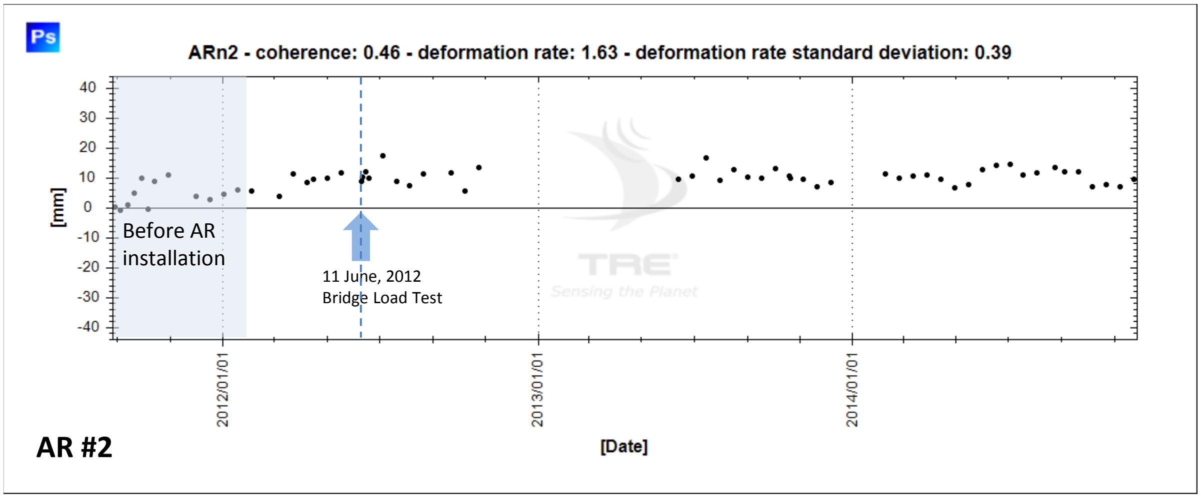

Figure 39: Time series of surface displacement for Reflector #2 (bridge load test conducted on 11 June 2012).

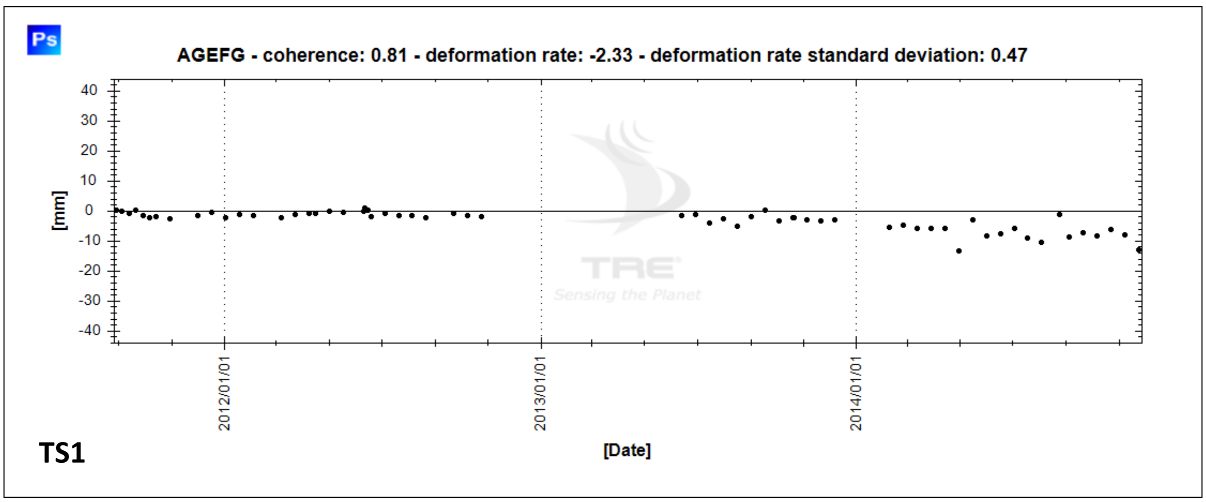

Figure 40: Time series of surface displacement for the measurement point identified as TS1 in Figure 38.

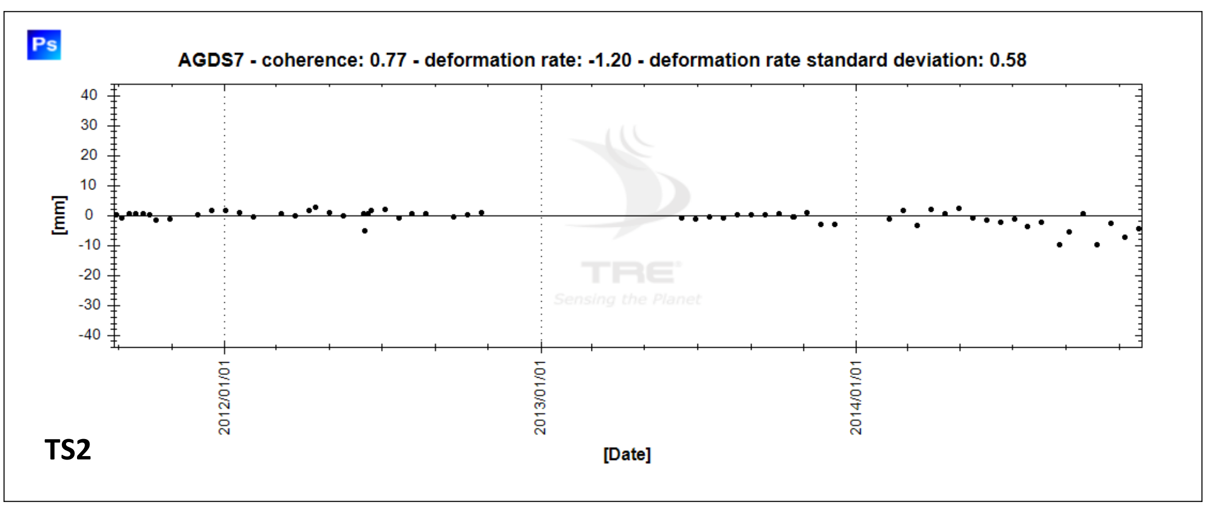

Figure 41: Time series of surface displacement for the measurement point identified as TS2 in Figure 38.

6.4 Pavement Conditions

One aim of the project is to investigate whether InSAR results can provide information on road pavement conditions. For this purpose VDOT has provided annual pavement condition data from 2011 to 2014 for the Staunton area. Data is collected between October of the previous year and March of the current year. Roads are rated on a scale of 1 to 100, with 100 being Excellent Condition, and assigned a qualitative description of Very Poor, Poor, Fair, Good, Excellent and Not Rated, based on the ratings values.

To investigate a possible relationship between pavement conditions and surface deformation, the stretch of Route 262 (white rectangle in Figure 42) between I-81 and Barterbrook Rd was selected. This area has been repaved between October 2012 – March 2013. Figure 42 provides a side-by-side comparison of road pavement conditions and surface deformation.

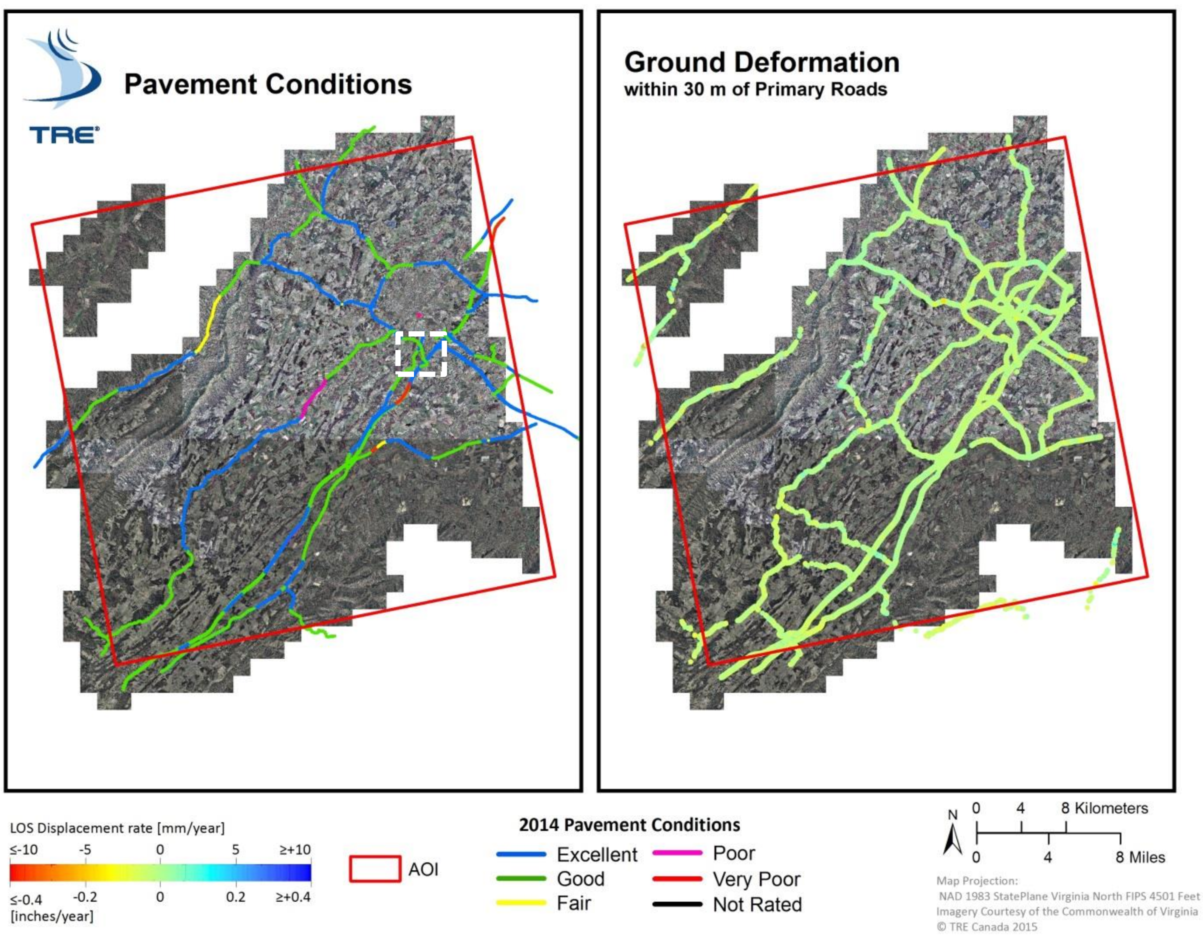

Figure 42: The left panel represents the pavement conditions along primary roads over the AOI. The right panel indicates ground deformation results within 30 meters of primary roads.

A close up of pavement conditions for the selected area is shown in Figure 43. Based on the pavement conditions database, Route 262 east bound was rated as poor in 2011 and very poor in 2012. The road was then repaved in 2013, which improved the conditions ratings to excellent for both 2013 and 2014. In the InSAR results, this translates to an increased variability of the deformation measurements over the repaved area (ATS1 in Figure 43) compared to the non-repaved area (ATS2 in Figure 43). However, despite the differing pavement conditions over time, no substantial differences in average ground deformation values between the two stretches of road can be observed.

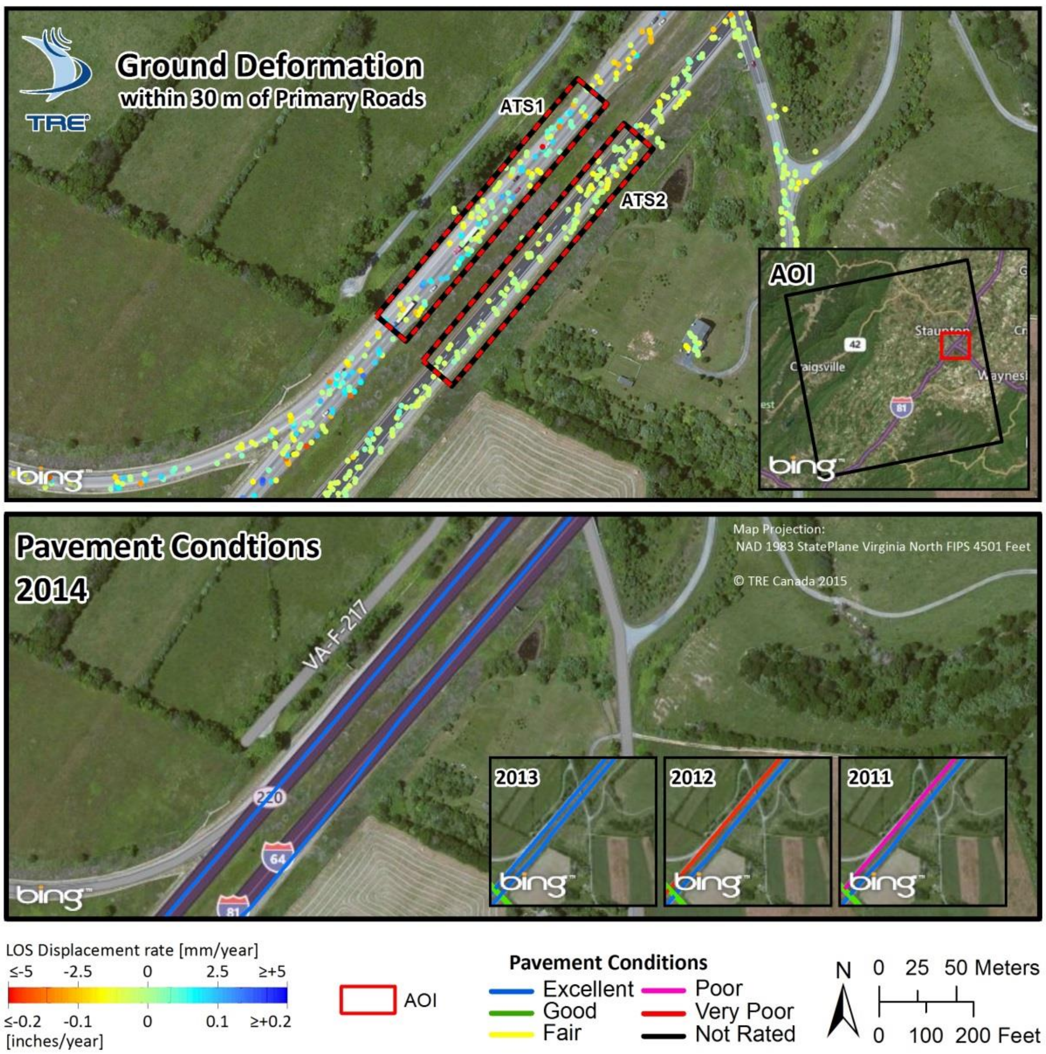

Figure 43: A close up of the pavement conditions along Middlebrook Rd. The top panel represents InSAR data overlaid with Temporary Scatterers, while the bottom panel shows the pavement conditions from 2011 to 2014.

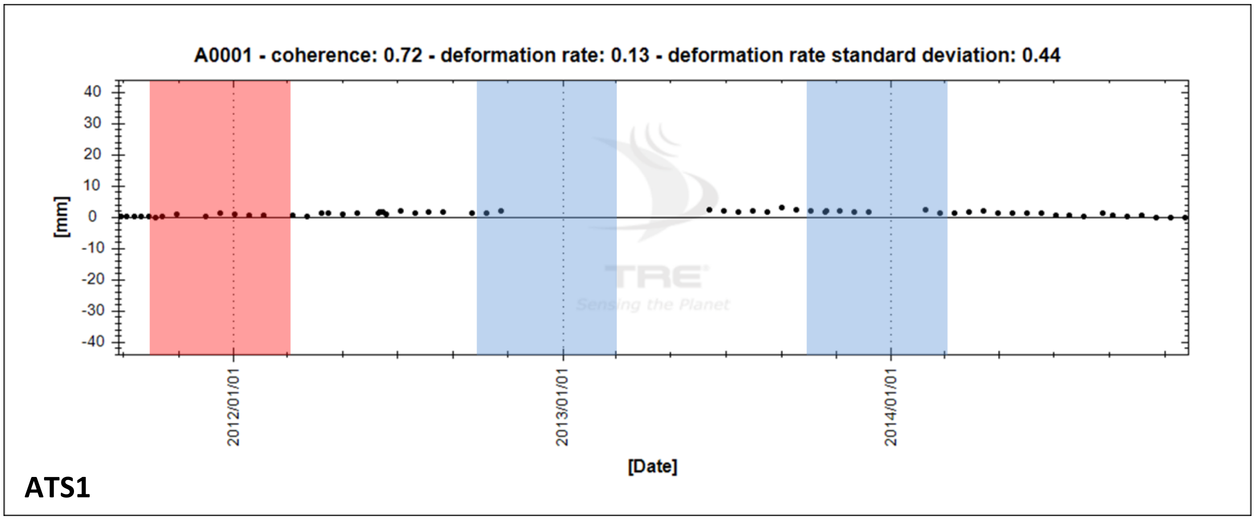

Figure 44: Average time series of surface displacement for the measurement point identified as ATS1 in Figure 43. The background colour matches the colour according to the pavement conditions in the time series.

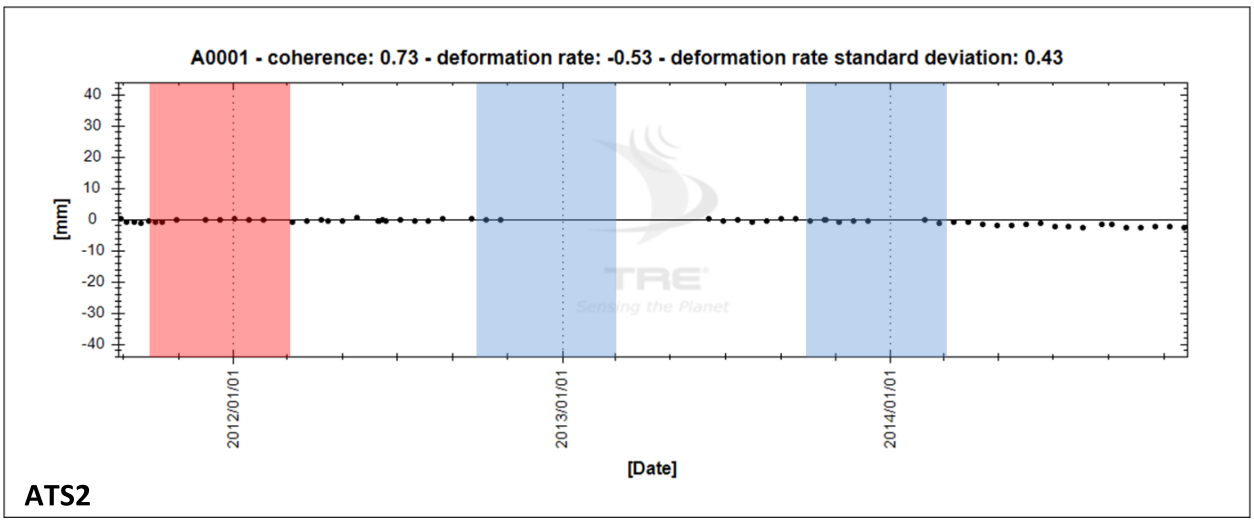

Figure 45: Average time series of surface displacement for the measurement point identified as ATS2 in Figure 43. The background colour matches the colour according to the pavement conditions in the time series.

7 Summary

The advanced SqueeSAR processing of satellite imagery spanning the period of August 2011 - September 2014 produced ground deformation measurements over a 40 km x 40 km area. Locations with signs of settlement were selected for further analysis as were areas where known geohazards had occurred in the past. No signs of movement were found around the sinkhole locations provided by VDOT or those discovered in September 2012.

Pavement conditions for the interstate and primary roads were compared with the InSAR results. A higher variability of displacement rates was observed over the repaved area than non-repaved area in the InSAR results, but no clear relationship was observed in the time series. Another area that remains to be explored is the coupling of amplitude data with pavement conditions.

Along with this report, a technical appendix is included, which contains AR visibility check results and additional information regarding InSAR processing.

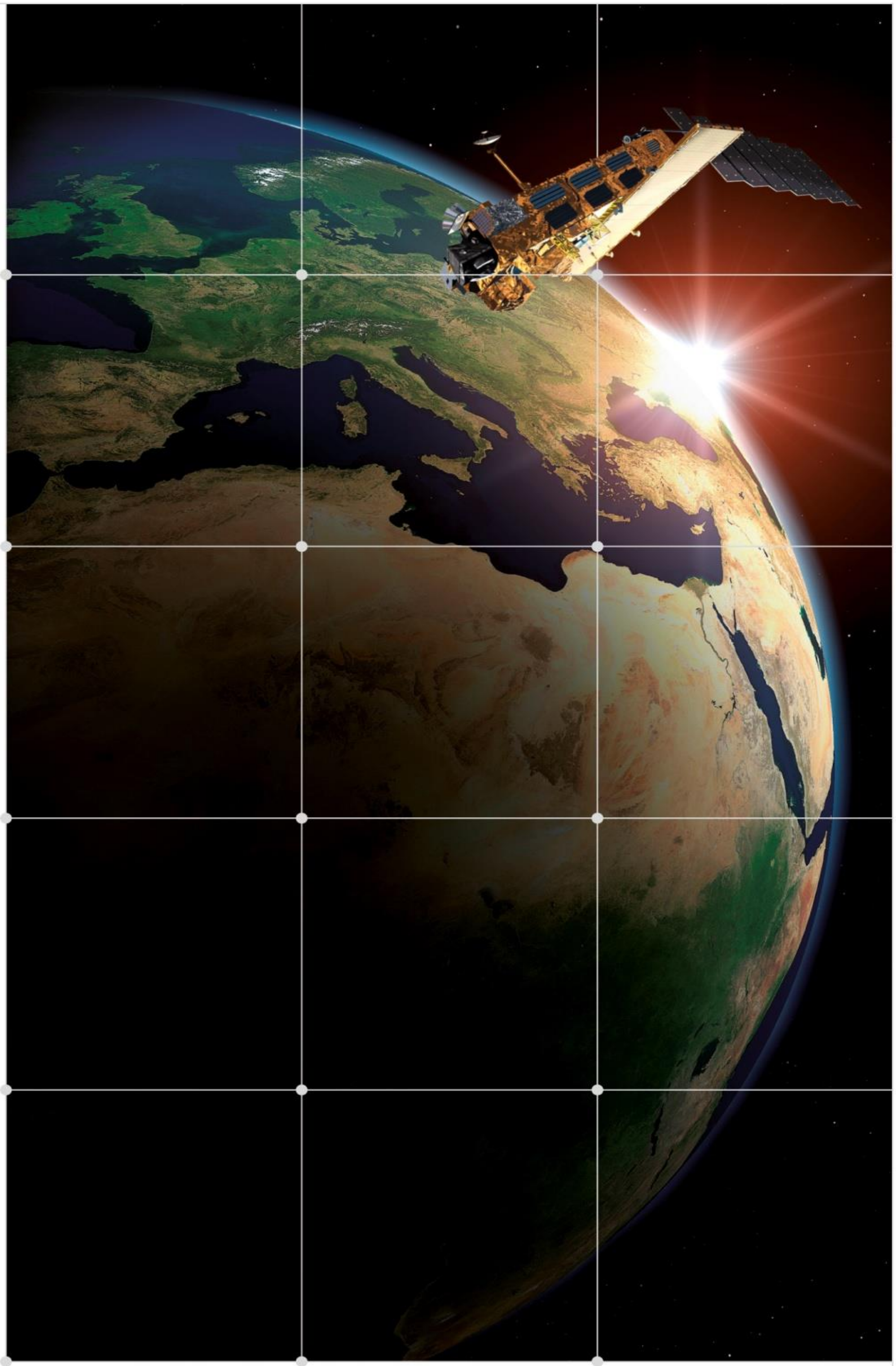

TRE®
Sensing the Planet

Tele-Rilevamento Europa T.R.E. s.r.l.
Ripa di Porta Ticinese, 79
20143 Milano - Italy
Tel. +39.02.4343.121
Fax +39.02.4343.1230

treuropa.com
tre@treuropa.com

TRE Canada Inc.
#410 - 475 West Georgia Street
Vancouver, BC V6B 4M9 - Canada
Tel. +1.604.331.2512
Fax +1.604.331.2513

trecanada.com
info@trecanada.com

Analysis of Ground Movement over Virginia using SqueeSAR

Site 1 Final Report – Technical Appendix

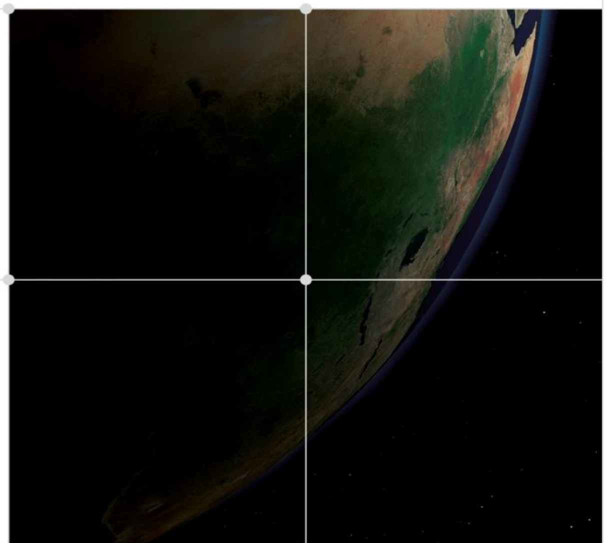

TRE®
Sensing the Planet

Submitted to:
University of Virginia
1001 N. Emmet St.
PO Box 400195
Charlottesville, Virginia 22904
USA

Prepared by:
TRE Canada Inc.
Suite 410, 475 West Georgia Street
Vancouver, B.C., V6B 4M9
Canada

Prepared by: Vicky Hsiao
GIS Analyst
TRE Canada Inc.
(signature)

Approved by: Giacomo Falorni
Operations Manager
TRE Canada Inc.
(signature)

Doc. Ref.: JO14-3011-REP2.0
February 25 2014

Table of Contents

Appendix 1: Reflectivity and Time Series of Artificial Reflector

Reflectivity of Artificial Reflector (conducted in January, 2015)

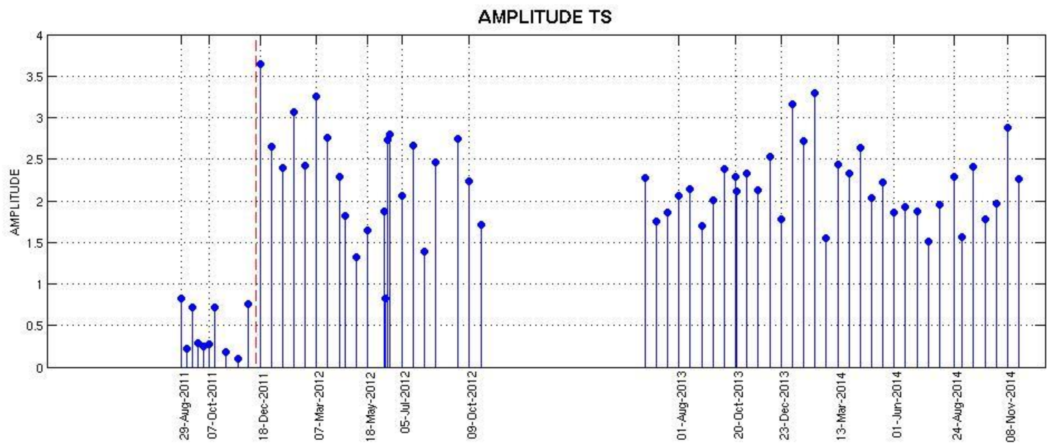

Figure 1: Reflectivity of AR2.

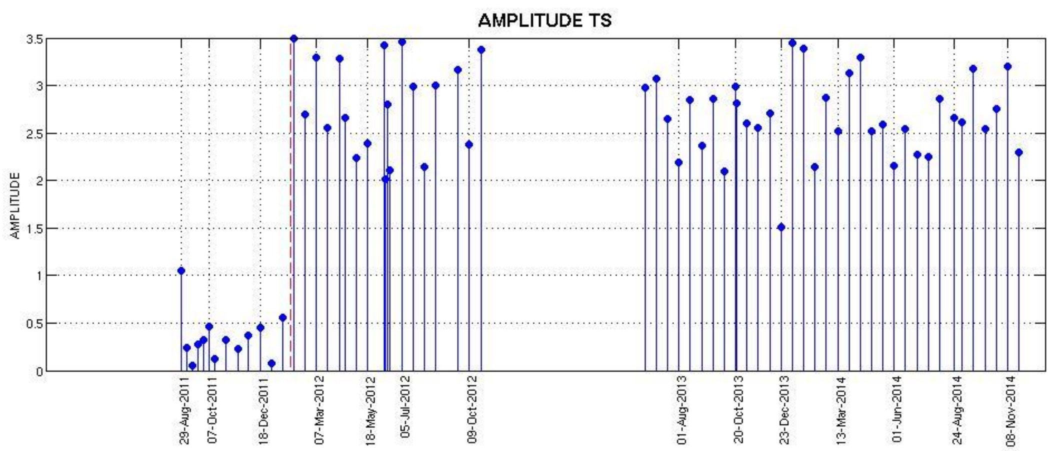

Figure 2: Reflectivity of AR6.

Time Series of Artificial Reflector (August 29, 2011 – 24 November, 2014)

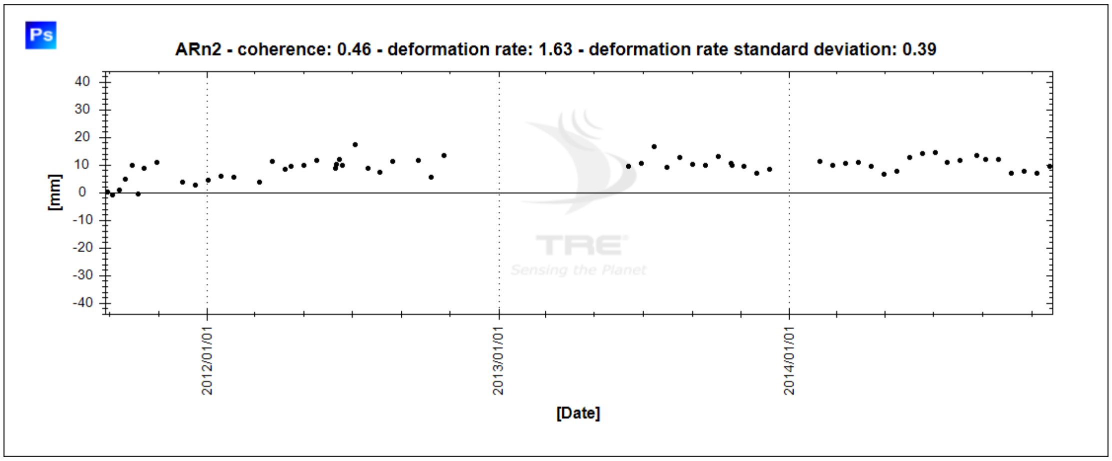

Figure 3: Time series of AR2.

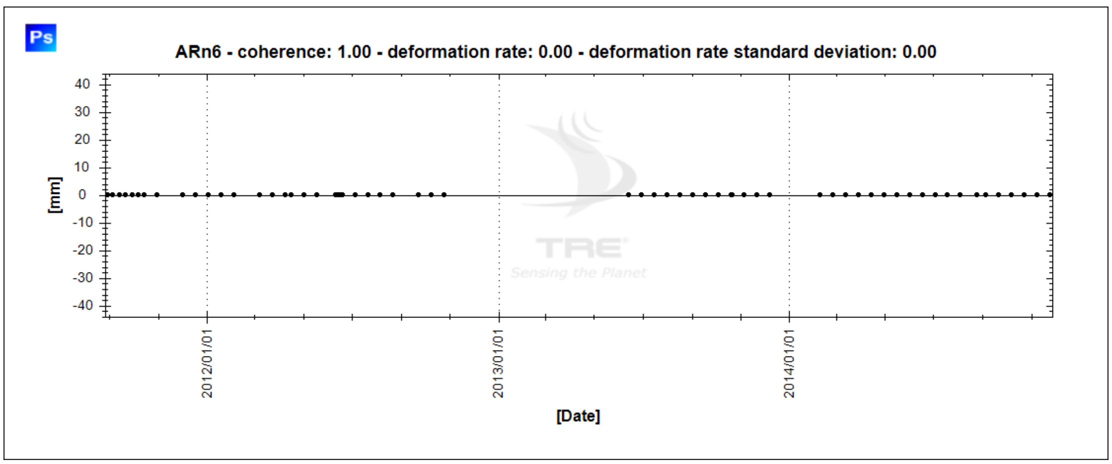

Figure 4: Time series of AR6.

Appendix 3: Additional Properties of the SqueeSAR™ results

Radar Data Acquisition Geometry

InSAR-based approaches measure surface displacement on a one-dimensional plane, along the satellite line-of-sight (LOS). The LOS angle varies depending on the satellite and on the acquisition parameters while another important angle, between the orbit direction and the geographic North, is nearly constant.

The images used for the historical analysis were acquired from the COSMO-SkyMed (CSK) satellite on an ascending orbit (satellite travelling from south to north and imaging to the east) along Track 213.

Table 1 lists the values of the angles for this study, while Figure 5 shows the geometry of the image acquisitions over the site for the ascending orbits, respectively. The symbol δ (delta) represents the angle the LOS forms with the vertical and Θ (theta) the angle formed with the geographic north.

Satellite	Orbit geometry	Symbol	Angle
CSK	Ascending	**δ**	12.52°
		θ	24.23°

Table 1: Satellite viewing angles for the CSK ascending orbit imagery.

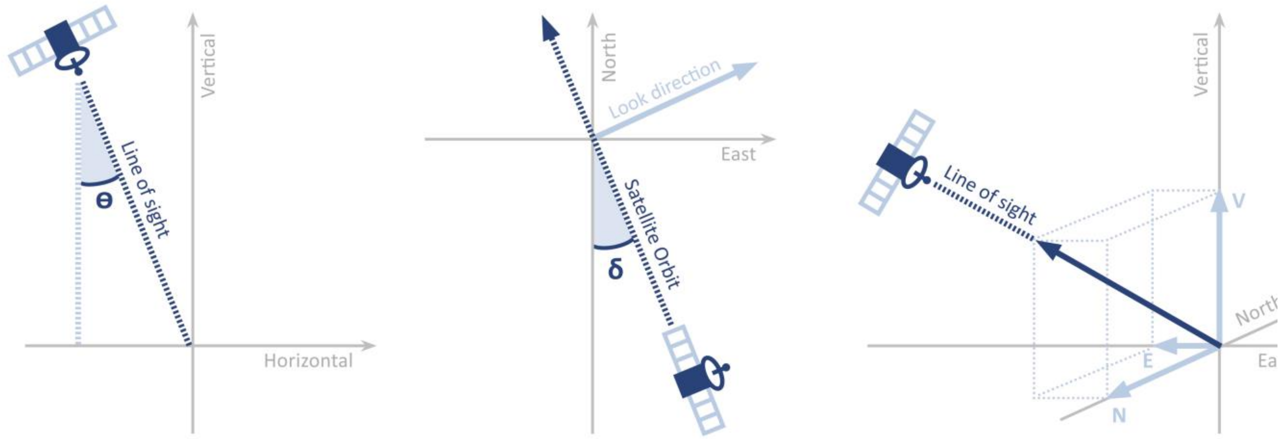

Figure 5: Geometry of the image acquisitions over the AOI for the ascending orbit.

Data Processing

Both permanent scatterers (PS) and distributed scatterers (DS) were identified at this site. Bare ground, roads, and infrastructure provide the basis for many PS points in the present SqueeSAR™ analysis. Many natural features such as rocks or exposed ground were also likely sources of stable PS targets.

DS correspond to large areas (up to hundreds of square meters) and were identified from exposed areas such as sparsely vegetated areas, exposed ground or rock. It is important to consider that while DS are represented as individual points for clarity of presentation and ease of interpretation, these measurements actually correspond to non-point features that are multiple pixels in size. The size of the DS within the AOI ranges from 76 to 889 m^2.

Table 2, shown below; provide a summary of the other properties relative to the data processing.

Satellite	COSMO-SkyMed (CSK)
Acquisition geometry	Ascending
Analysis time interval	29 August 2011 - 24 November 2014
Number of scenes processed	62
Georeferencing	PS aligned on 2012 orthophoto (1 foot resolution)
Projection system used / datum	State Plane Virginia North FIPS 4501 (Feet) / NAD 1983
Reference Point location (Cluster 1)	E 11318282.23; N 6737916.39
Reference Point location (Cluster 2)	E 11223288.75; N 6754263.96
Area of interest	617.8 sq. mile (1,600 km^2)

Table 2: Statistics of the processed data.

Standard Deviation and Precision

Standard deviation values of the displacement measurements are a function of the factors listed below and of local ground movement dynamics.

- Spatial density of the PS and DS (higher densities produce higher precisions)
- Quality of the radar targets (signal-to-noise ratio levels)
- Distance from the reference point
- Number of images processed
- Period of time covered by the imagery
- Climatic conditions at the time of the acquisitions
- Distance between the measurement point and the reference

In addition to each measurement point having an associated standard deviation value to represent the error of the displacement measured, results can also be characterized by the accuracy of the technique. Specifically, three parameters are used to characterize the overall accuracy of the results:

- Precision of the estimated deformation rates;
- Precision of the estimated elevations;
- Precision of the geocoding.

Table 3 summarizes the typical precision values applicable to PS located within 2 km from the reference point when **at least 45 radar images** have been processed.

DEFORMATION RATE	< 1 [mm/yr]
DISPLACEMENT ERROR (single displacement between contiguous satellite images)	< 5 [mm]
ELEVATION	± 1.5 [m]
POSITIONING ERROR ALONG EAST DIRECTION	± 3 [m]
POSITIONING ERROR ALONG NORTH DIRECTION	± 2 [m]

Table 3: Measurement accuracies for PS located within 2 km of the reference point, based on the processing of at least 45 SAR images.

Appendix 4: InSAR Processing

InSAR

Interferometric Synthetic Aperture Radar, also referred to as SAR interferometry or InSAR, is the measurement of signal phase change (interference) between radar images. When a point on the ground moves, the distance between the sensor and the point changes, thereby producing a corresponding shift in signal phase. This shift is used to quantify the ground movement.

An interferogram is a 2D representation of the difference in phase values. Variations of phase in an interferogram are identified by fringes, colored bands that indicate areas where and how much movement is occurring. The precision with which the movement can be measured is usually in the centimetre (cm) range as the phase shift is also impacted by topographic distortions, atmospheric effects, and other sources of noise.

DInSAR

When InSAR is used to identify and quantify ground movement the process is referred to as Differential InSAR (DInSAR). In DInSAR topographic effects are removed by using a DEM of the area of interest to create a differential interferogram.

Differential InSAR is still impacted by atmospheric effects, as there is no method for removing this signal phase contribution. It is a useful tool for identifying footprints of progressing movement and creating deformation maps. The limitations of DInSAR are its relatively low precision (cm scale) and that it cannot distinguish between linear and non-linear motion.

PSInSAR™

Permanent Scatterer SAR Interferometry is an advanced form of DInSAR. The fundamental difference is that it uses multiple interferograms created from a stack of at least 15 radar images.

Permanent Scatterer SAR Interferometry was developed to overcome the errors produced by atmospheric artifacts on signal phase. The PSInSAR algorithm automatically searches the interferograms for pixels that display stable radar reflectivity characteristics throughout every image of the data set. In PSInSAR these pixels are referred to as Permanent Scatterers (PS). The result is the identification of a sparse grid of point-like targets on which an atmospheric correction procedure can be performed. Once these errors are removed, a history of motion can be created for each target, allowing the detection of both linear and non-linear motion.

The result is a sparse grid of PS that are color-coded according to their deformation rate and direction of movement. The information available for each PS includes its deformation rate, acceleration, total deformation, elevation, coherence as well as a time series of movement. The PSInSAR algorithm measures ground movement with millimetre accuracy.

SqueeSAR™

Permanent Scatterers are objects, such as buildings, fences, lampposts, transmission towers, crash barriers, rocky outcrops, etc, that are excellent reflectors of radar microwaves. However, TRE has noticed that many other signals are present in the processed data. These do not produce the same high signal-to-noise ratios of PS but are nonetheless distinguishable from the background noise. Upon further investigation it was found that the signals are reflected from extensive homogeneous areas where the back-scattered energy is less strong, but statistically consistent. These areas have been called distributed scatterers (DS) and correspond to rangeland, pastures, bare earth, scree, debris fields, arid environments, etc (Figure 6).

The SqueeSAR™ algorithm was developed to process the signals reflected from these areas. As SqueeSAR™ incorporates PSInSAR no information is lost and movement measurement accuracy is unchanged.

The SqueeSAR™ algorithm also produces improvements in the quality of the displacement time series. The homogeneous areas that produce DS normally comprise several pixels. The single time series attributed to each DS is estimated by averaging the time series of all pixels within the DS, effectively reducing noise in the data.

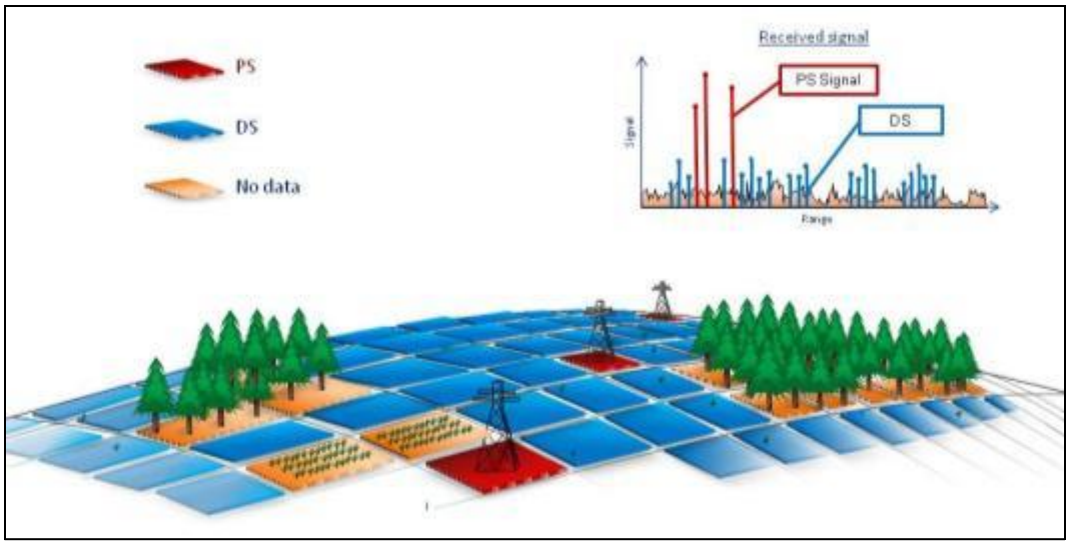

Figure 6: Illustration of the identification of permanent (PS) and distributed scatterers (DS) by the SqueeSAR™ algorithm.

Appendix 5: Data Processing

Methodology

The identification of PS and DS in a series of radar images comprises a sequence of steps.

First, all radar data archives are screened to determine the most suitable source of raw data for the particular area of interest and to select all the high quality images within the chosen data set.

As the signal echo from a single point target contains many returning radar pulses it appears defocused in a synthetic aperture radar (SAR) raw image. The first processing step is therefore to focus all the received energy from a target in one pixel. The images are then precisely aligned to each other, or co-registered, and analyzed for their suitability for interferometry. The parameters that are analyzed are the normal baseline and the temporal distribution of the images.

There then follows a number of statistical analyses on the phase and amplitude characteristics of the backscattered radar signal that return to the satellite. If a concentrated number of signals reflect off a particular feature within a pixel and backscatter to the satellite, the feature is referred to as a ‘scatterer’. When the same scatterer appears in all, or most, of a data set of SAR images of a particular location, then the scatterer is deemed to be ‘permanent’.

At this stage it is possible to identify a subset of pixels, referred to as Permanent Scatterer Candidates (PSC), that are used to estimate the impact on signal phase of ionospheric, tropospheric and atmospheric effects, as well as possible orbit errors.

Once the signal phase has been corrected for these effects, any remaining changes in signal phase directly reflect ground movement.

Master Image Selection

SqueeSAR™ requires that one image (or scene) in each data set has to become both a geometric and temporal reference to which all the other images are then related. This image is referred to as the master image and those that remain are slave images.

The master image should be chosen according to the following criteria:

- it minimizes the spread of normal baseline values for the slave images;
- similarly, it minimizes the temporal baseline values between the master and each slave image; and
- it minimizes the effects of signal noise arising from changes in vegetation cover and/or small changes in the look angle of the satellite from one scene to another.

Signal Phase and Amplitude Analysis

General

Each pixel of a SAR image contains information on the amplitude of signals that are backscattered toward the satellite, as well as on the signal phase. The amplitude is a measure of the amount of the radar pulse energy reflected, while the phase is related to the length of the path of the electromagnetic wave, from the platform to the ground and back again.

Analyses of both amplitude and phase of the SAR image provide an indication of the stability of each pixel, over time, whereby it is possible to identify those pixels that are most likely to behave as Permanent Scatterers. Statistical methods are used extensively in this process.

Among the different statistical parameters that can be computed two are of particular interest: the Phase Stability Index (PSI), obtained from the phases of the images within the data set, and the Multi Image Reflectivity (MIR) map, derived from the amplitude values of the available acquisitions.

Radar phase and coherence

The phase stability is strongly linked to the concept of coherence. Pixels that consistently display high phase stability are said to be coherent. Coherence is measured by an index that ranges from 0 to 1. When a pixel is completely coherent, it will have a coherence value of 1. Correspondingly, if a pixel has a low phase stability, its coherence index will be 0. In general, interferometry is successful when the coherence index lies between 0.5 and 1.0.

Radar amplitude and multi-image reflectivity

The amplitude of a pixel within a SAR image is the aggregate of the backscattered energy toward the satellite from within the pixel's equivalent land area. This equivalent land area is referred to as the radar resolution, and in the case of the CSK satellite, it measures about 3 m by 3 m. It is necessary to look into the amplitude values of all the images in the data set, in order to understand exactly what was seen by the satellite at the time of each acquisition.

If a target has experienced significant change in its surface characteristics it will exhibit variation in its reflectivity (electromagnetic response) between two acquisitions. In such circumstances, the possibility of detecting movement by means of SAR interferometry is seriously compromised. The signal phase difference between the two images now contains not only the contribution due to displacement, but also that due to the change in the reflectivity of the target. This prevents, in the worst case, the obtaining of any useful information on ground movement.

Accordingly, it is necessary to look into the amplitude values of all the images in the data set, in order to understand exactly what was seen by the satellite at the time of each acquisition.

Another artifact linked to amplitude is known as speckle. Speckle is random noise that appears as a grainy salt and pepper texture in an amplitude image. This is caused by random interference from the multiple scattering returns that occur within each resolution cell. Speckle

has an adverse impact on the quality and usefulness of SAR images. However, the higher the number of images has taken of the same area at different times or from slightly different ‘look’ angles, the easier it is to reduce speckle. This increases the quality and level of details of the amplitude image enabling it to be used as a background layer for observing the presence of PS results.

The Multi Image Reflectivity (MIR) map is the means by which speckle reduction is accomplished. Averaging a number of images tends to negate the random amplitude variability, leaving the uniform amplitude level unchanged (Figure 7).

It should be emphasised that the information in the MIR map is the reflectivity of each pixel, i.e. the ability to backscatter the incident wave toward the satellite. Flat surfaces (roads, highway, rivers, and lakes) act like a mirror, meaning that if their orientation is not exactly perpendicular to the incident wave negligible energy is reflected back to the sensor; they appear dark in the image. On the other hand, because of their irregular physical shape, metal structures or buildings reflect a significant portion of the incident signal back to the radar, resulting in very bright pixels in the MIR map.

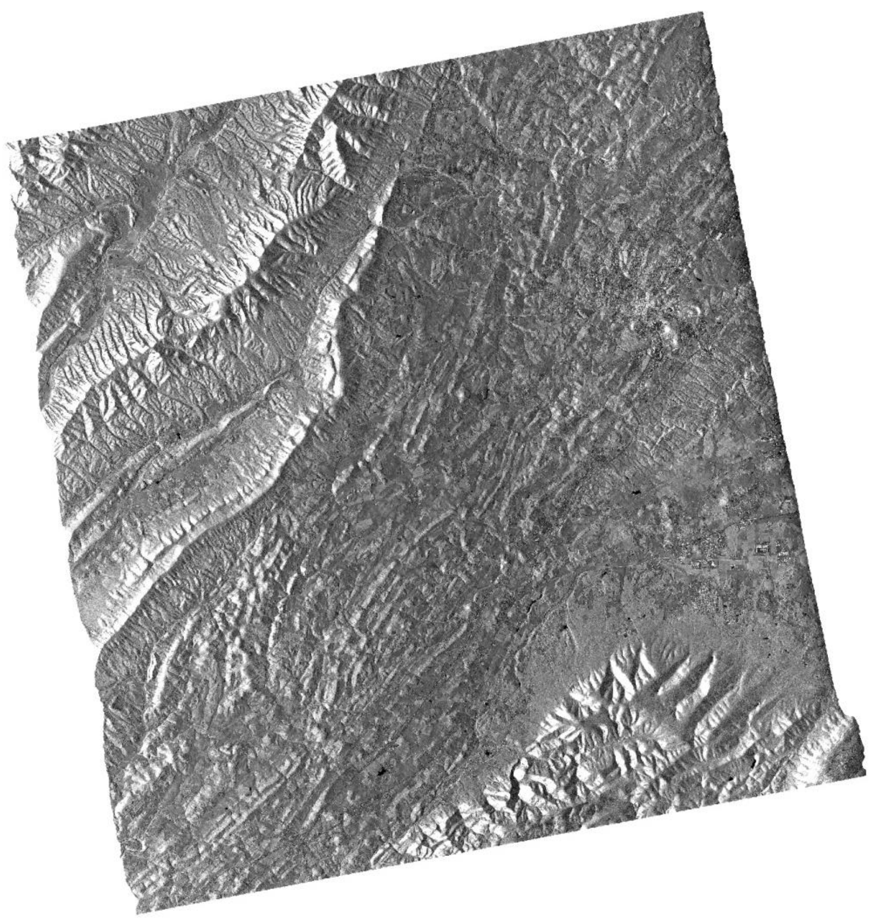

Figure 7: Multi-image reflectivity map of the ascending CSK data set over Virginia Site 1.

Interferograms

After the statistical analyses of the SAR images have been completed, a set of differential interferograms is generated. This entails subtracting the phase of each slave image from the phase of the master image. In doing so, the difference in signal path length between the two images is calculated. This difference is related to possible ground motion.

In any SAR image, there are embedded topographic distortions that arise during image acquisition. These are removed using a reference Digital Elevation Model (DEM), leaving ground movement and the signal phase distortions arising from atmospheric effects as the only embedded variables.

The differential interferograms represent the starting point for applying the PSInSAR approach.

Estimation of the Atmospheric Effects

When a radar signal enters and exits a moisture-bearing layer in the atmosphere, its wavelength can be affected, introducing potential errors into the signal path length. The removal of atmospheric impacts is fundamental for increasing the precision of ground movement measurement.

A sub-set of pixels, usually corresponding to buildings, lampposts, antennas, small structures and exposed rocks, is chosen from among those that have high PSI values. These are referred to as PS Candidates (PSC). PSC density is, of course, higher in towns and cities rather than in forests and vegetated areas. However, it is often possible to obtain good PSC density in rural areas.

For each image, the atmospheric impacts are estimated at each PSC location. The process is statistically based and benefits in accuracy by the greater the number of available images for the analysis. By comparing the atmospheric contribution on neighboring pixels that would be experiencing the same atmospheric conditions, the atmospheric contribution can be reconstructed over the whole image.

The processed data set allows identification of a PSC cluster dense enough to identify and extract the atmospheric contribution over the entire area of interest.

Post-processing

In this stage the processed data undergoes a thorough quality control following ISO 9001:2000 guidelines. The PS data is checked for anomalies, aligned on an optical image layer usually provided by the client and the final report is prepared.

Appendix 6: Abbreviations and Acronyms

AOI	Area Of Interest
DInSAR	Differential Interferometry
DS	Distributed Scatterer (s)
GIS	Geographic Information System
InSAR	Interferometric SAR
LOS	Line Of Sight
MIR	Multi-Image Reflectivity
PS	Permanent Scatterer(s)
PSInSAR™	Permanent Scatterer SAR Interferometry is a worldwide Polytechnic University of Milan Trademark
SAR	Synthetic Aperture Radar
SqueeSAR™	The most recent InSAR algorithm patented by TRE
TRE	Comprehensive term for Tele-Rilevamento Europa and TRE Canada
TS	(Permanent Scatterer Displacement) Time Series

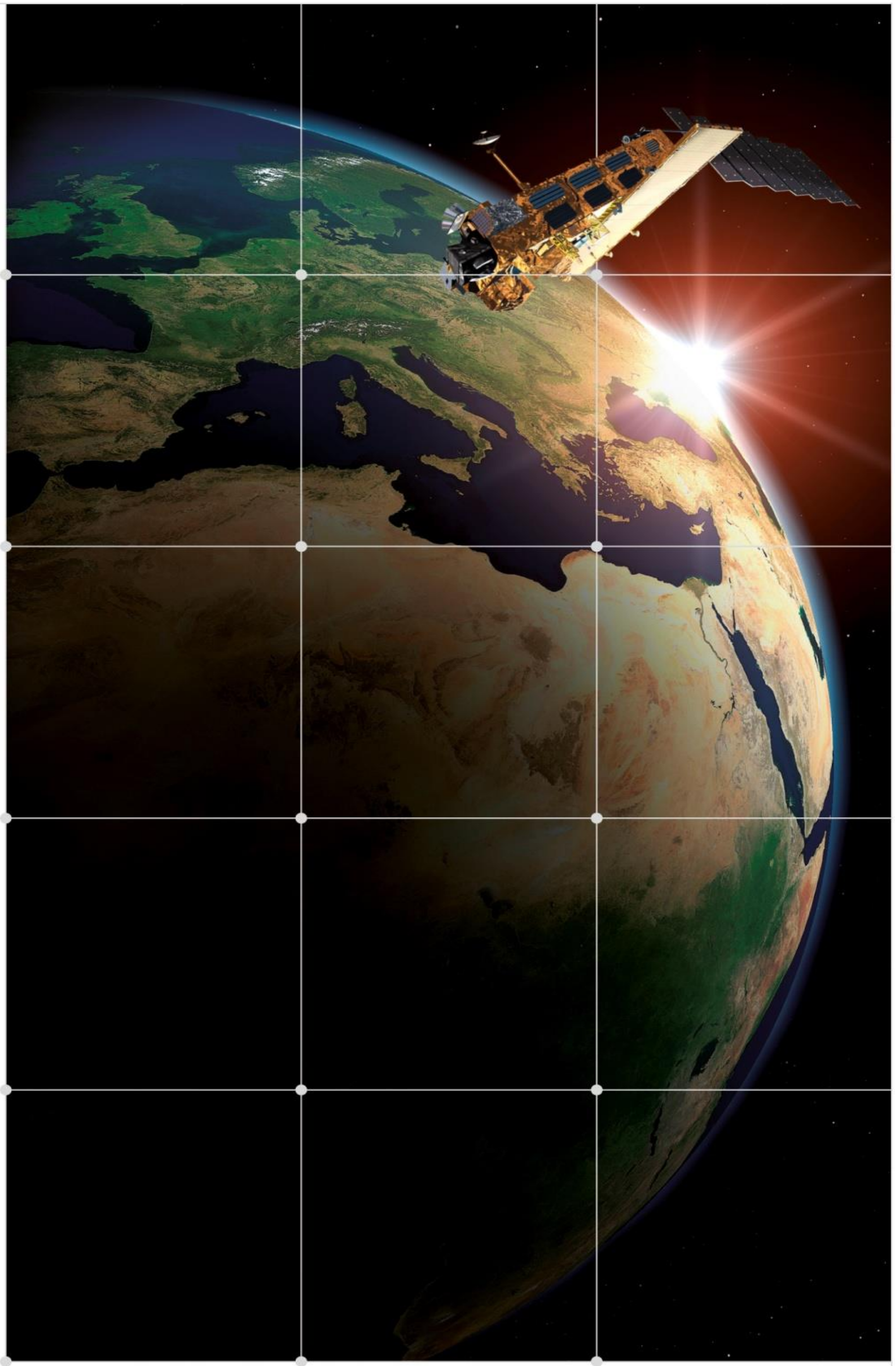

Appendix D – AOI2 – NOVA: SqueeSAR report (October 2014)

TRE – **Analysis of ground movements over Northern Virginia and Washington DC using SqueeSAR – First Report** – October 2014 [download][6]

TRE – **Analysis of ground movements over Northern Virginia and Washington DC using SqueeSAR – First Report - Technical Appendix** – October 2014 [download][7]

[6] http://viva-lab.ece.virginia.edu/elecdocs/ritars14/NOVA_Oct14.pdf
[7] http://viva-lab.ece.virginia.edu/elecdocs/ritars14/NOVA_Oct14_TA.pdf

Analysis of Ground Movement over Northern Virginia and Washington D.C. using SqueeSAR

Site 2 First Report

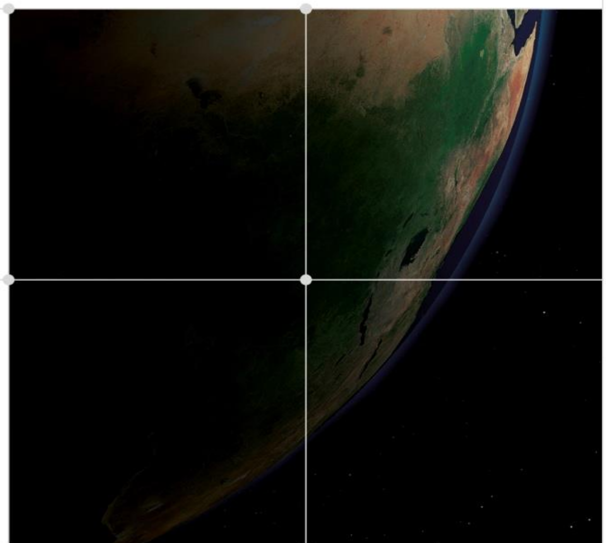

TRE®

Sensing the Planet

Submitted to:
University of Virginia
1001 N. Emmet St.
PO Box 400195
Charlottesville, Virginia 22904
USA

Prepared by:
TRE Canada Inc.
Suite 410, 475 West Georgia Street
Vancouver, B.C., V6B 4M9
Canada

Prepared by: Vicky Hsiao
GIS Analyst
TRE Canada Inc.
____
(signature)

Approved by: Giacomo Falorni
Operations Manager
TRE Canada Inc.
____
(signature)

Doc. Ref.: JO14-3014-REP1.0
December 11 2014

Executive Summary

This report describes the approach and results of the InSAR analysis carried out to measure surface deformation in Northern Virginia and most of Washington D.C. (Site2) for the project "InSAR remote sensing for performance monitoring of transportation infrastructure at the network level" (RITARS-14-H-UVA). The results provide an overview of ground movement occurring in the area over a seven-month period.

The following points summarize the key findings of the analysis:

- Up to -29 mm of subsidence were identified along primary roads, such as on the shoulder of US 29, Virginia State Route 237 Lee Highway and along Henry G Shirley Memorial Hwy (Section 5.2).
- The results show relative stability on the Woodrow Wilson Bridge, with the exception of a measurement point in the I-495 Express Lanes at the MD approach that indicates -20 mm of subsidence (5.1.3).
- No significant subsidence was observed on the retaining wall along I-395 SB at King Street after the H-piles were built in early March (5.1.2).
- No ground deformation on the bridge abutment along I-66 East Bound CD Road over Rte. 286 was observed. The surroundings of this bridge are stable. -30 mm of subsidence was detected on a landfill at the I-66 Transfer Station approximately 1 km east of the bridge.
- The slope failure along Piscataway Drive in Maryland is outside of the AOI, but measurement points close to this location indicate between -10 to -13 mm of movement.
- A total of 1.2 million measurement points was obtained from the data processing, providing a density of 781 points per square kilometre (2,022 points per square mile).
- The precision of the measurements is estimated at ±5.9 mm/year based on the displacement rate standard deviation. This value will improve with the acquisition of more images spanning a longer period of time.

The deliverables for the project include the present report, which describes the results of the data processing, a technical appendix and a CD containing the displacement data.

Table of Contents

1 Introduction

The University of Virginia VIVA lab is leading a research project with the Virginia Research Transportation Council and TRE Canada entitled "InSAR remote sensing for performance monitoring of transportation infrastructure at the network level " (RITARS-14-H-UVA). The work was awarded to the University of Virginia as a research grant funded by the Commercial Remote Sensing and Spatial Information Technology Application Program, RITA Phase V.

One of the main objectives of this project is to systematically extract consistent and reliable information on road subsidence, bridge monitoring, slope stability, sinkhole development and pavement condition from InSAR data. TRE Canada Inc. (TRE) has been contracted to perform the InSAR work using our SqueeSAR algorithm. Cosmo-SkyMed (CSK) radar satellite imagery has been acquired on a 16-day interval over the site 2 area of interest (AOI) in Northern Virginia.

The AOI corresponds to a full CSK radar scene, approximately 1,600 km^2 (618 square miles) in size, covering northern Virginia (NOVA), and includes most of the Washington, D.C. metropolitan area (Figure 1). The AOI contains a high density of urban and transportation infrastructure including numerous bridges, areas with slope stability issues, and some of the highest volume traffic routes in Virginia, which facilitates the evaluation of road response to high traffic loading (subsidence and pavement conditions). These man-made structures often yield a high number of measurement points while areas of dense vegetation, active agriculture and steep slopes tend to produce a lower density of measurement points.

Figure 1: The Area of Interest (AOI).

2 Radar data

All images were acquired by the Cosmo-SkyMed (CSK) constellation from a descending orbit along Track 88. Imagery is currently being acquired with a 16-day frequency. See Table 1 for more information regarding the radar imagery. Fifteen images were acquired between March 17 and October 22 2014; however, two of these images were discarded during data processing due to the presence of strong atmospheric noise. In total, 13 images were processed, covering a period of 7 months (Table 2). Additional information on the satellite parameters can be found in the Technical Appendix.

Radar Data Information	
Constellation	Cosmo-SkyMed (CSK)
Resolution	3m x 3m
LOS Off-Nadir Angle	23.99°
Orbit Direction	Descending
Track	88
Revisit Frequency	16 days
Period Covered by Imagery	17 March 2014 – 22 October 2014
Number of Processed Images	13

Table 1: Information regarding the radar imagery used in the analysis.

No.	Date	Interval
1	28 Mar 14	
2	13 Apr 14	16
3	29 Apr 14	16
	15 May 14	
4	31 May 14	32
5	16 Jun 14	16
	02 Jul 14	
	10 Jul 14	24
6	18 Jul 14	8
7	03 Aug 14	16
8	19 Aug 14	16
9	04 Sep 14	16
10	16 Sep 14	12
11	20 Sep 14	4
12	06 Oct 14	16
13	22 Oct 14	16

Table 2: Dates of the CSK image acquisitions. Image dates in orange were discarded during the data processing, in red were not acquired, and in blue were additional images acquired.

3 Data Processing

The processing of the 13 CSK images provides an initial overview of displacement trends within the AOI and of the distribution and density of measurement points. Point density and measurement precision is satisfactory based on our experience for this number of images. Overall measurement point distribution can also be considered normal for this type of area, although no points were identified in the SE corner due to the relevant width of the Potomac River. This constitutes a physical barrier that impeded the linkage of the few identified points to the main data cluster. There are too few points identified in the area to produce a second, independent cluster (e.g. as seen for the site 1 in Staunton). It is expected that data density, distribution and precision will improve at the next processing when another eight months of images will be available. It is recommended that the current results be considered as preliminary.

Reference Point

SqueeSAR™ is a differential technique meaning displacement is measured compared to a reference point that is assumed to be stable. The reference points used is shown in Figure 2. The reference points were selected using an optimization procedure that performs a statistical analysis of all targets to select a point with optimal radar parameters including high coherence, low standard deviation and low temporal variability over time. The use of this procedure ensures the highest quality results are achieved.

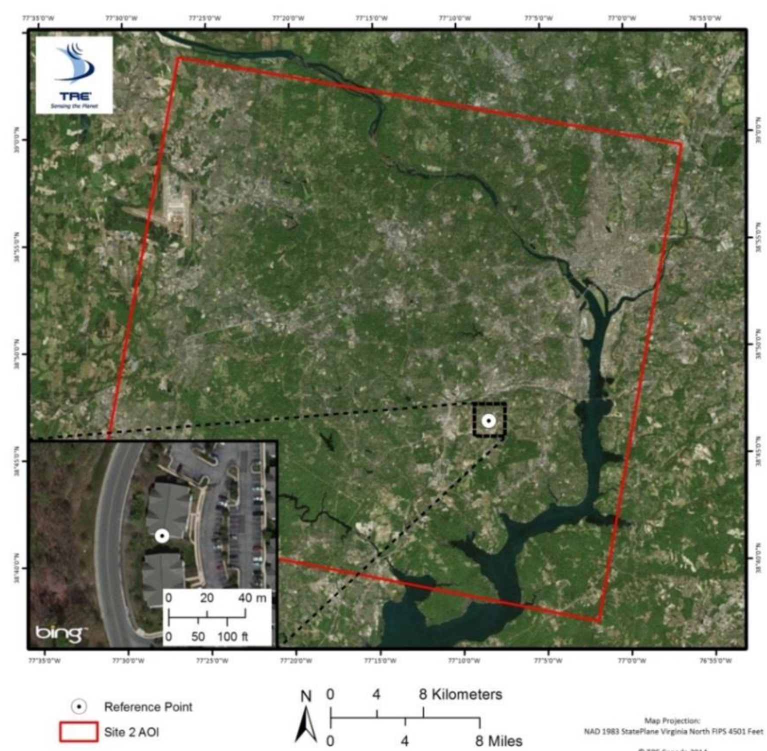

Figure 2: The location of the reference point (E: -77.139100, N: 38.777196).

4 Results of the SqueeSAR™ analysis

4.1 Cumulative Displacement

The total amount of displacement measured during the seven-month period is shown below (Figure 3). Each point corresponds to a PS or DS, and is color-coded according to the magnitude and direction of total movement. Movement is measured along the satellite line-of-sight (LOS) relative to the first image (March 28 2014) of the data stack.

Cumulative displacement from March 2014 to October 2014 ranges from -36.9 to +28.8 mm within the AOI. Measurement point coverage of the AOI is satisfactory with lower point densities in areas that are heavily vegetated, including the Potomac River in the SW corner and along the Occoquan Reservoir.

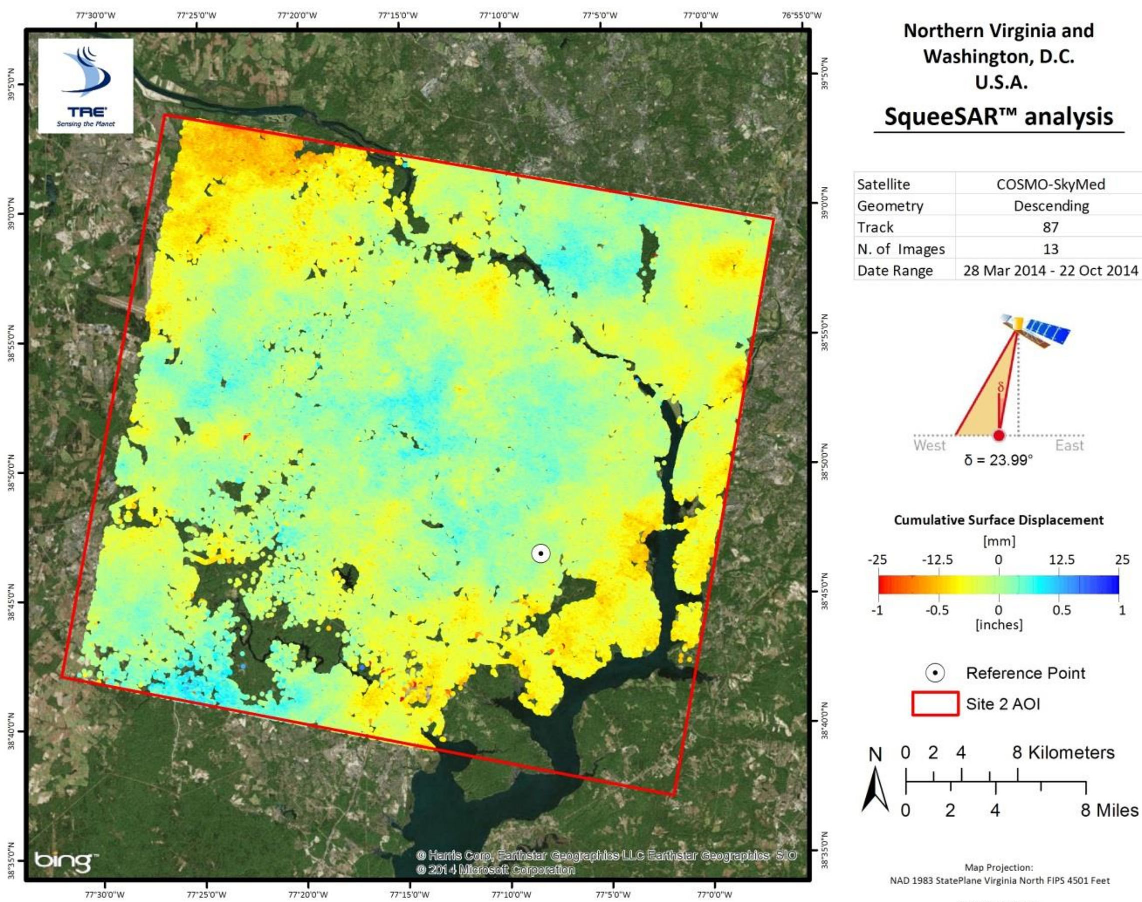

Figure 3: Cumulative deformation, expressed in millimeters, from March 28 2014 to October 22 2014.

4.2 Displacement rate

The line-of-sight (LOS) displacement rates, expressed in mm/year, as detected from the processing of all images are shown below (Figure 4). Each point corresponds to a Permanent Scatterer (PS) or a Distributed Scatterer (DS), and is color-coded according to its annual rate of movement. Average displacement values are calculated from a linear regression of the ground movement measured over the entire period covered by the satellite images. Detailed information on ground motion is also provided by means of displacement time series, which are provided for each PS and DS.

Displacement rate distribution is very similar to that of the cumulative displacement, given the short period of time covered by the imagery. Deformation rates range from -65.1 to +40.5 mm/yr.

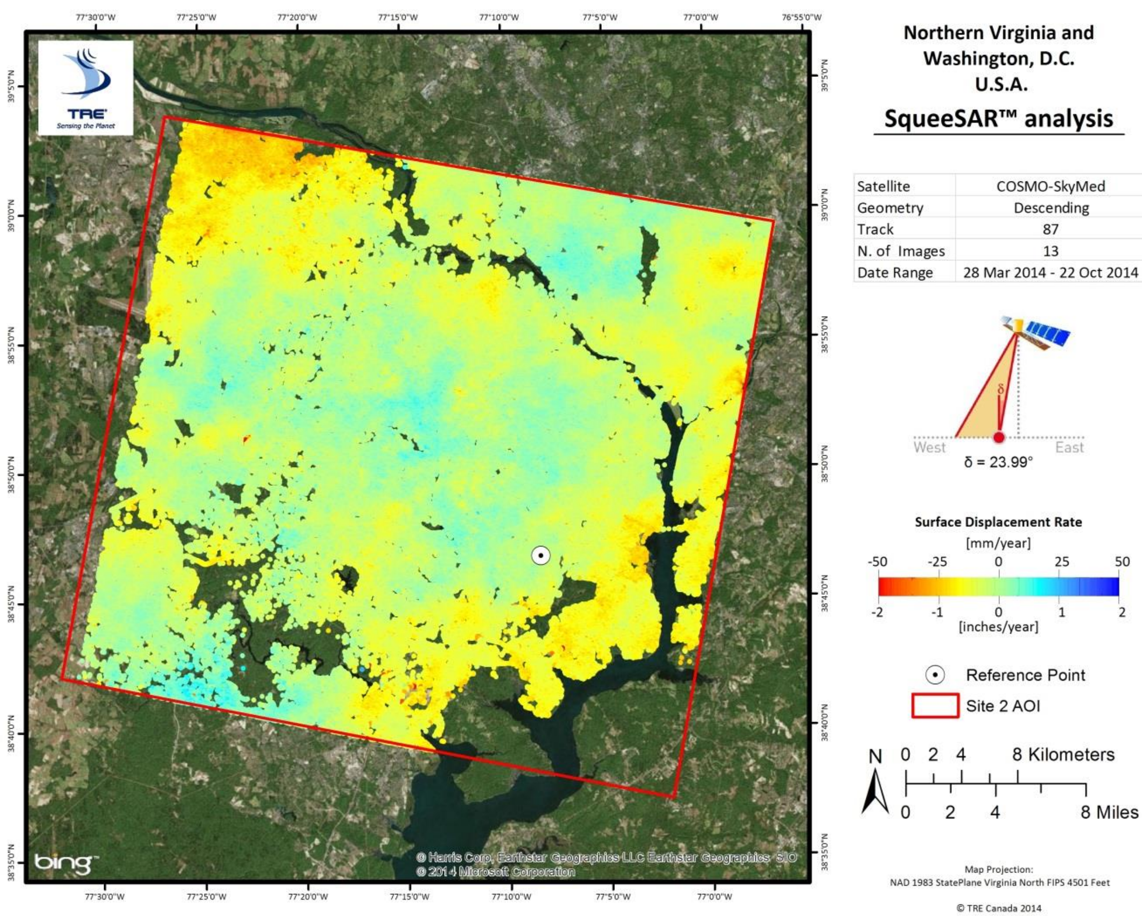

Figure 4: Deformation rates in mm/year.

4.3 Displacement Rate Standard Deviation

The standard deviation of the surface displacement data characterizes the error of the measurements (Figure 5). For this reason, any measurement should be interpreted in the form of Displacement Rate ± Standard Deviation. Standard deviation values tend to increase with distance from the reference point. Higher values indicate a greater variability in displacement rates and are often associated with areas of rapid and/or irregular ground movement.

The average standard deviation value of all measurement points within this data set is ±5.9 mm/year.

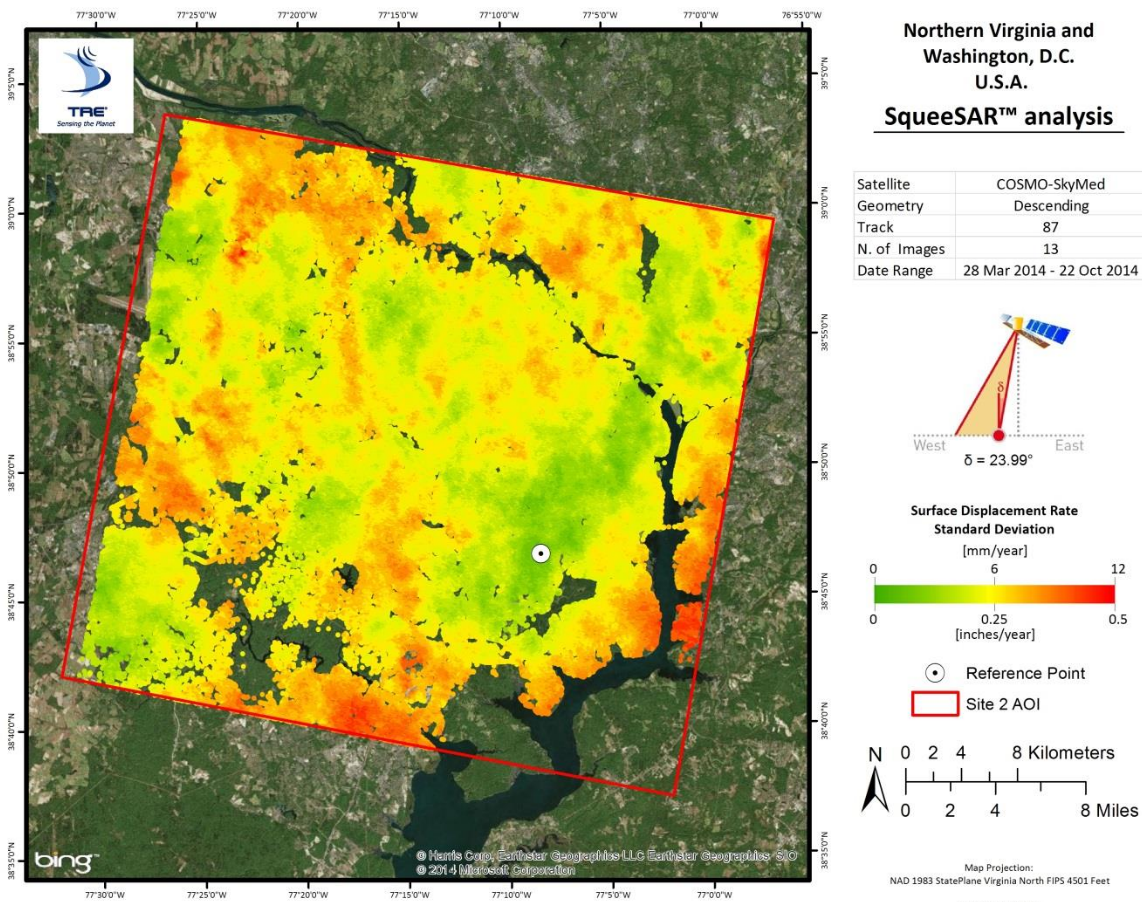

Figure 5: Standard deviation values of the displacement rates.

5 Observations

A total of 13 images were processed for the first monitoring period, leading to the identification of over 1.2 million measurement points and a density of 781 points per square kilometre (2,022 points per square mile). Table 3 summarize the statistics of the results.

The results provide an overview of the displacement trends throughout the AOI. However, it is worth noting that all displacements should be interpreted considering the ±6 mm/yr measurement precision. Furthermore, within the seven-month time span of the data it is not possible to discern and separate long-term deformation trends from seasonal signatures induced by soil moisture variations, temperature fluctuations, etc.

In the present report, only areas exhibiting localized ground deformation that occurs in or near the transportation network are highlighted. The results over four features of interest with a history of prior settlement are discussed in 5.1 while movement detected over primary roads is described in Section 5.2. Further statistics summarizing the results of the data processing can be found in the Technical Appendix.

Attribute	First Monitoring Analysis
Dates	28 Mar 2014 – 22 Oct 2014
Period covered (months)	7
N. of images processed	13
N. of PS	962,627 (77%)
N. of DS	148,536 (23%)
Total N. of Measured Points (PS and DS)	1,249,506
Average PS and DS Density (per square km) Cluster 1 and 2 combined	781 pts/km^2 (2022 pts/sq. mi)
Average Displacement Rate (mm/year)	-5.2
Average Displacement Rate Standard Deviation (mm/year)	±5.9
Average Acceleration Rate (mm/year^2)	5.8
Average Acceleration Rate Standard Deviation (mm/year^2)	±78.8

Table 3: Statistics of the results obtained over the site 2 AOI.

5.1 Feature of Interest

There are four featured areas specified by Virginia Department of Transportation (VDOT) and University of Virginia (UVA) that are highlighted in this section (Figure 6). The features from west to east are: the bridge of I-66 EB CD Road over Rte. 286 Fairfax County Pkwy; the retaining wall on I-395 SB at King Street in Shirlington VA; the Woodrow Wilson Bridge; and the slope failure along Piscataway Drive in MD, respectively.

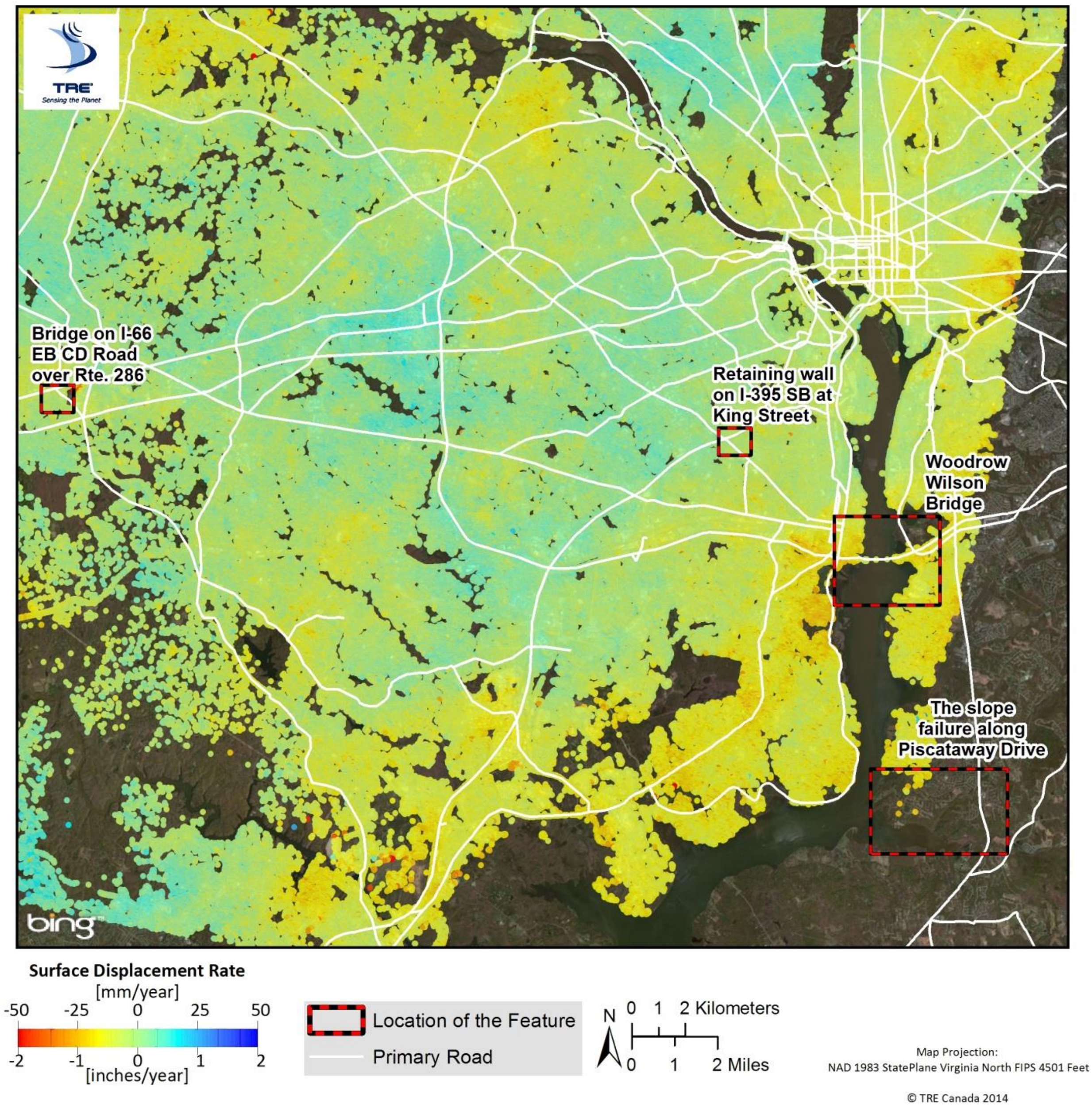

Figure 6: The locations of the features with a prior movement history.

5.1.1 The bridge of I-66 EB CD Road over Rte. 286 Fairfax County Pkwy

According to the Bridge Inspection Report from July 2014 provided by VDOT, there is a known settlement of up to 76.2 mm (3 inches) of MSE panels on the Abutment A side of the bridge (bottom left panel in Figure 7) on I-66 East Bound CD Road over Rte. 286 Fairfax County Pkwy. The SqueeSAR results over this area are shown in Figure 7. The MSE panels are located beneath the bridge and are thus not directly visible to the satellite. However, no perceptible ground deformation is observed on the bridge or in the surrounding area over the seven-month period (Figure 8 to Figure 12). Unrelated ground deformation was detected on a landfill at the I-66 Transfer Station approximately 1 km east of the bridge, where up to -30 mm of subsidence was observed (Figure 13 to Figure 16).

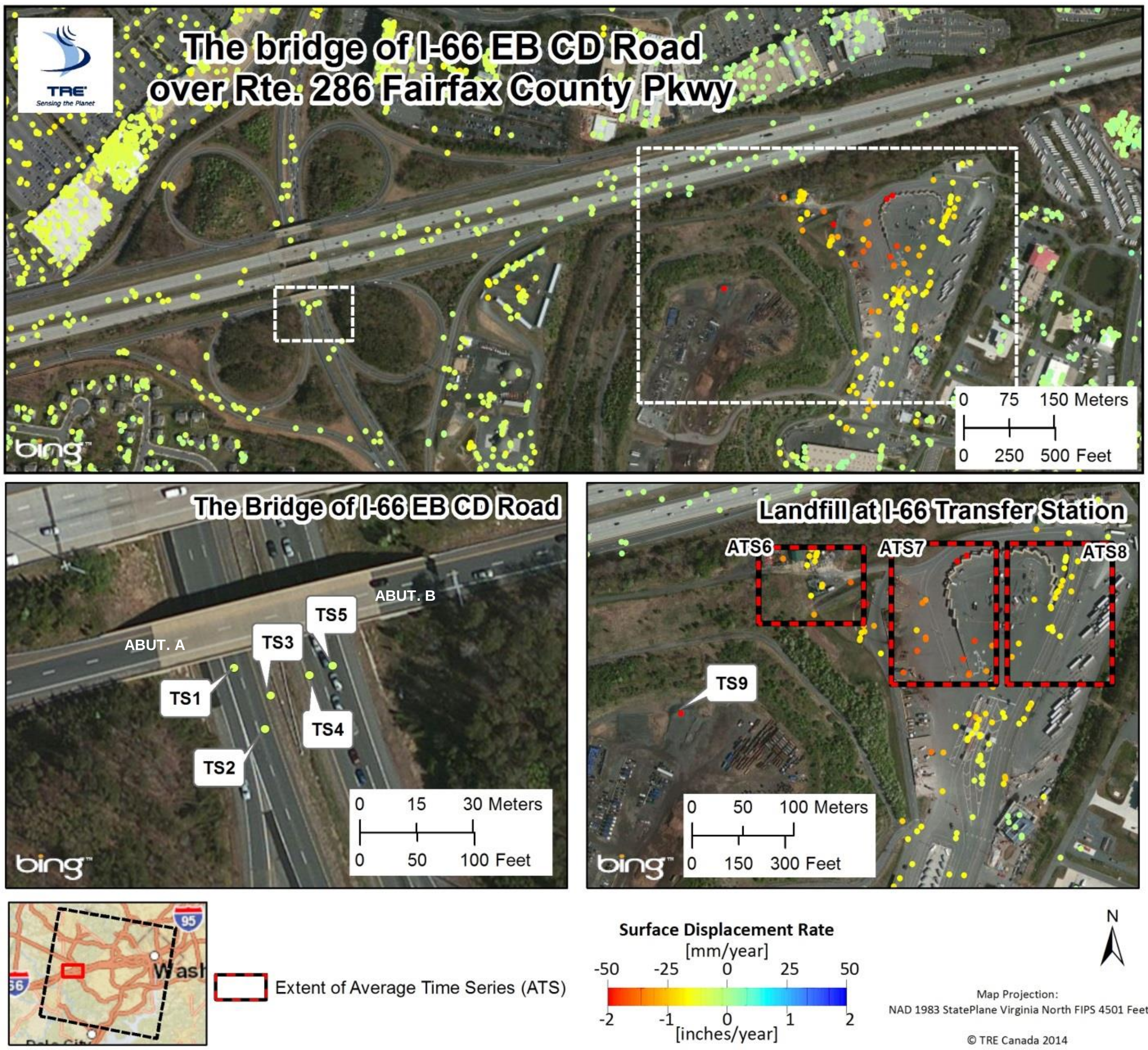

Figure 7: The SqueeSAR results over the bridge on I-66 EB CD Road. Top panel shows the bridge and its surroundings, while the bottom left panel and bottom right panel represent close ups of the bridge and a landfill 1 km east of the bridge, respectively.

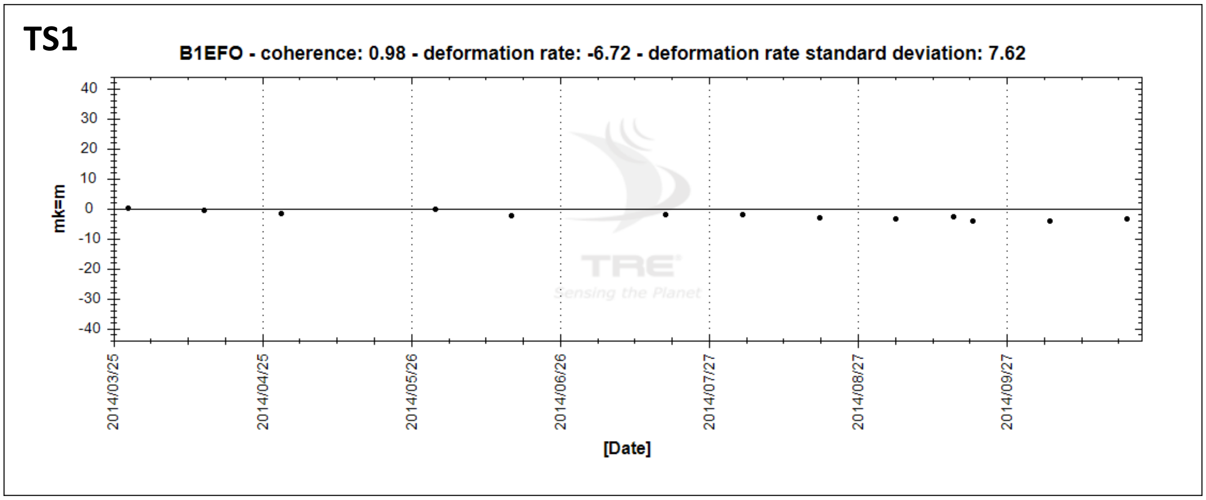

Figure 8: Time series of TS1 in Figure 7.

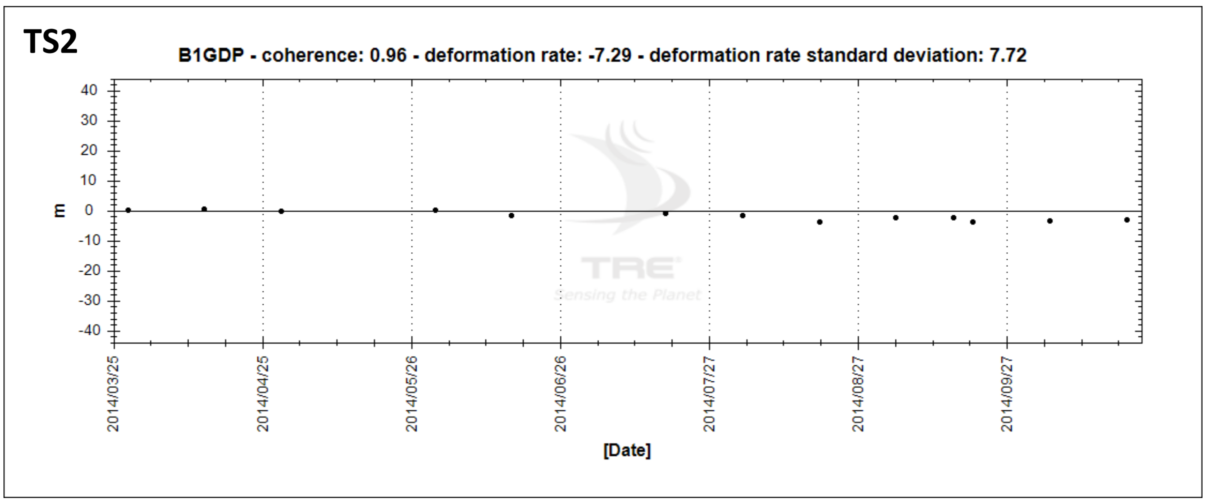

Figure 9: Time series of TS2 in Figure 7.

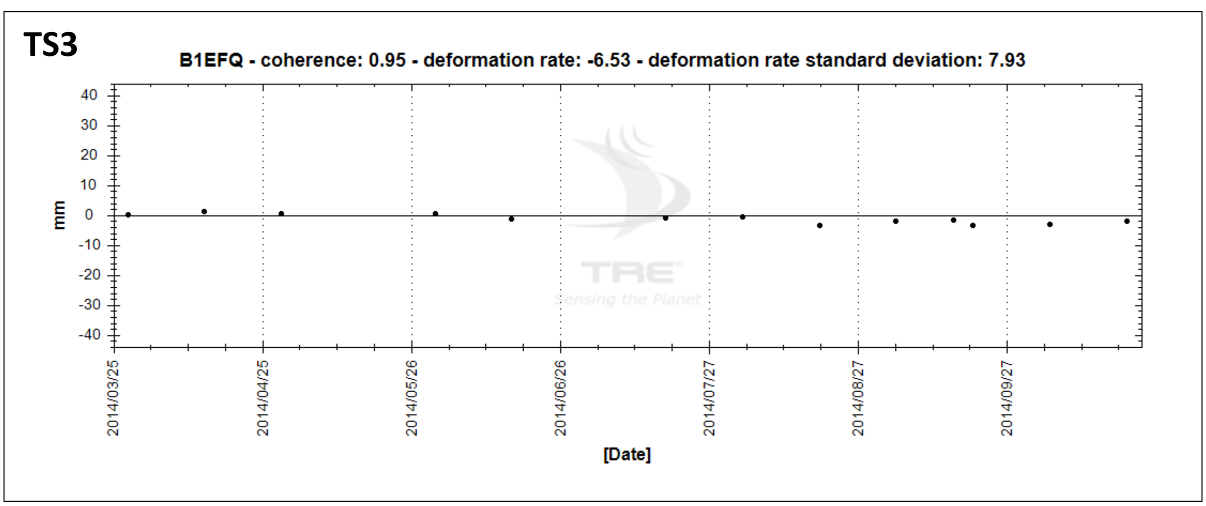

Figure 10: Time series of TS3 in Figure 7.

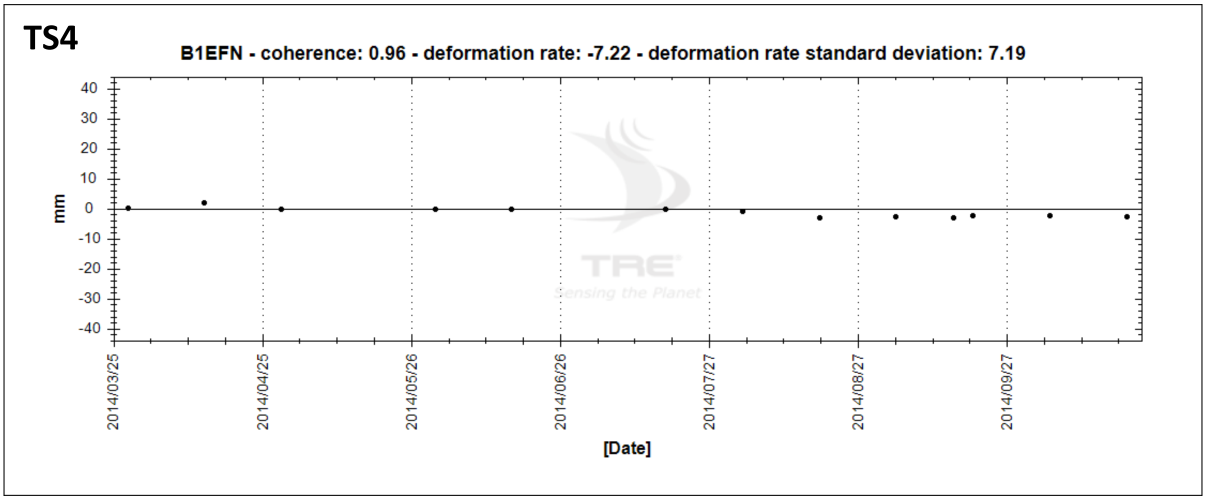

Figure 11: Time series of TS4 in Figure 7.

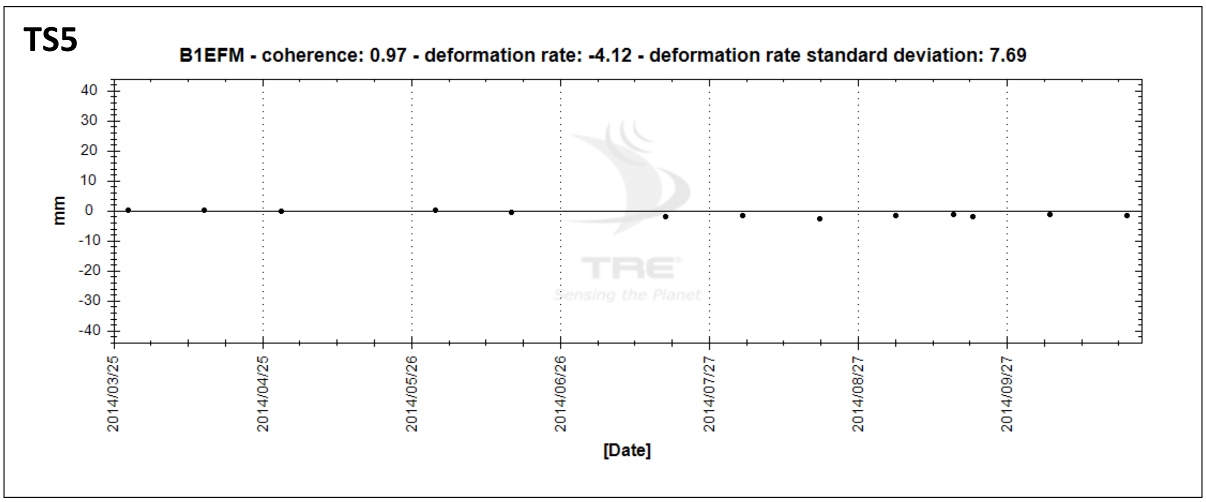

Figure 12: Time series of TS5 in Figure 7.

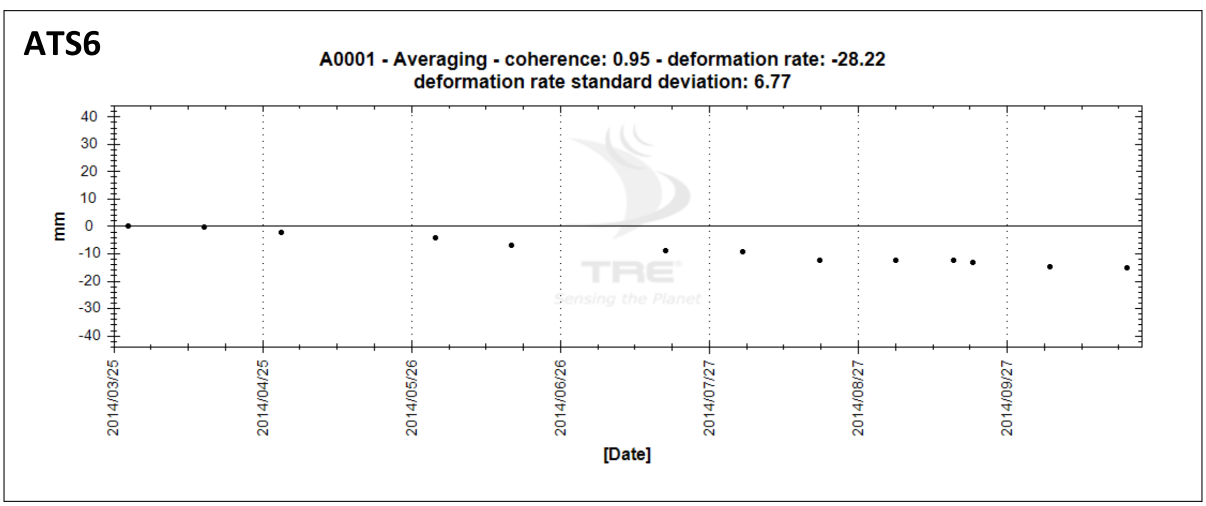

Figure 13: Average time series of ATS6 in Figure 7.

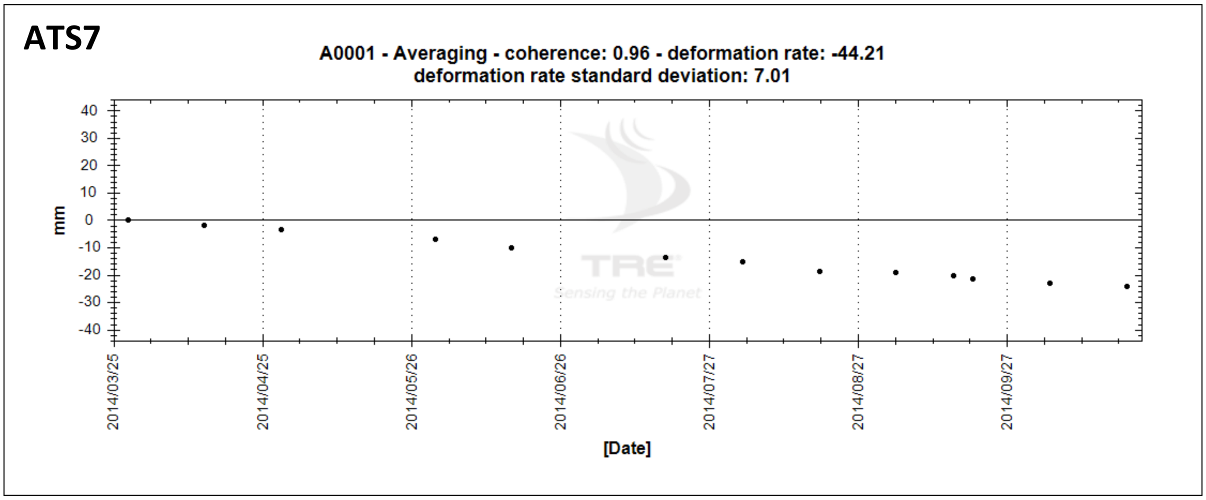

Figure 14: Average time series of ATS7 in Figure 7.

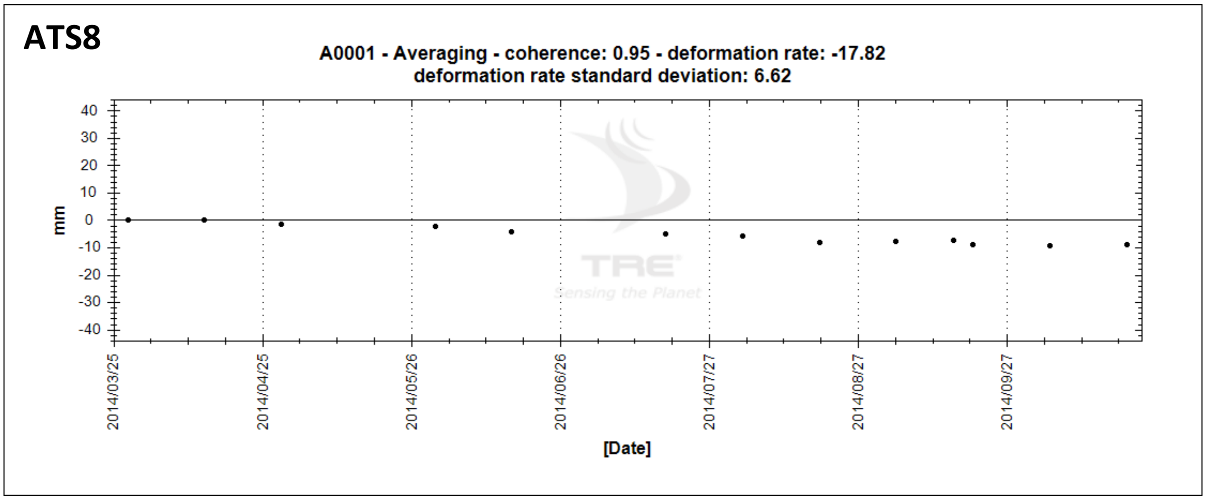

Figure 15: Average time series of ATS8 in Figure 7.

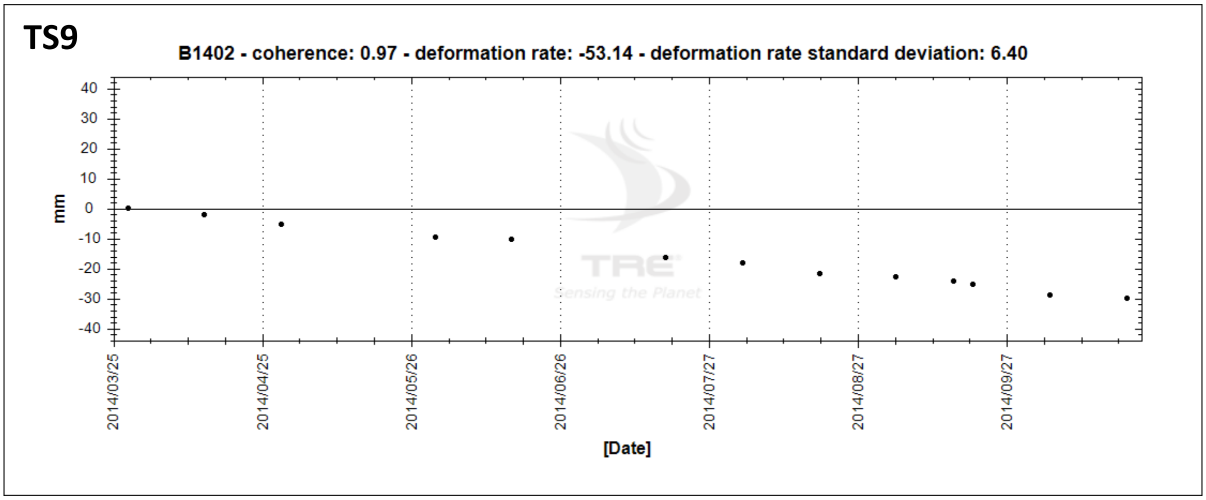

Figure 16: Time series of TS9 in Figure 7.

5.1.2 The retaining wall on I-395 SB at King Street in Shirlington VA

H-piles (vertical steel beams) were built in early March 2014 to stabilize a retaining wall that failed on I-395 South Bound at King Street (Figure 17). Seven measurement points, all of the PS type, were identified on the retaining wall, and none exhibited signs of significant subsidence (Figure 18 to Figure 24). Four average time series were calculated from the results in the residential area above the slope of the retaining wall for comparison and no clear indication of settlement was observed between late March to October 2014.

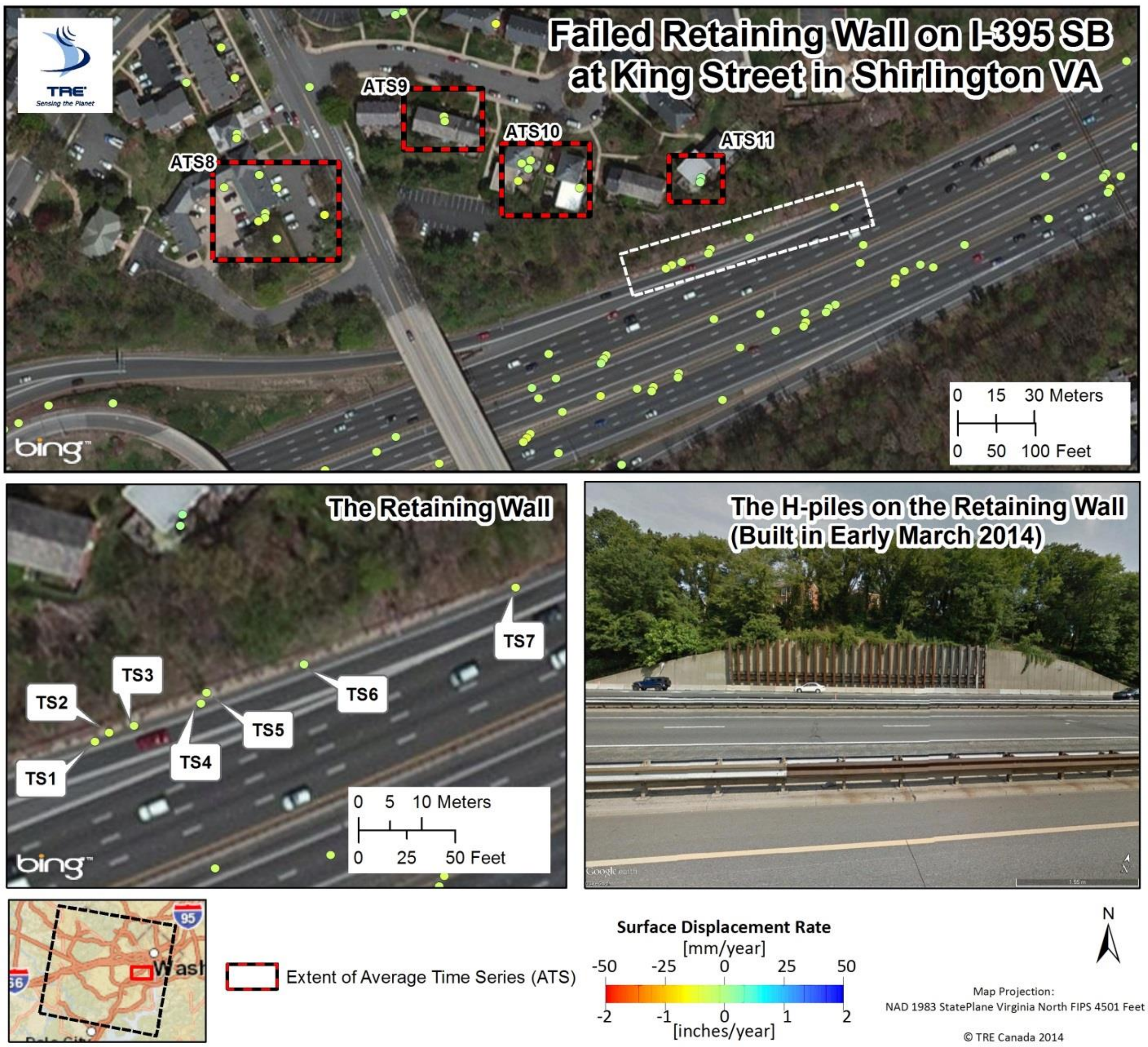

Figure 17: The SqueeSAR results over the retaining wall on I-395 South Bound at King Street in Shirlington VA. Top panel shows the retaining wall and the slope above, while the bottom left panel displays the PS points on the retaining wall. The bottom right panel depicts a photo taken after the H-piles were built in early March 2014 (photo credits: Google Earth, taken in August 2014).

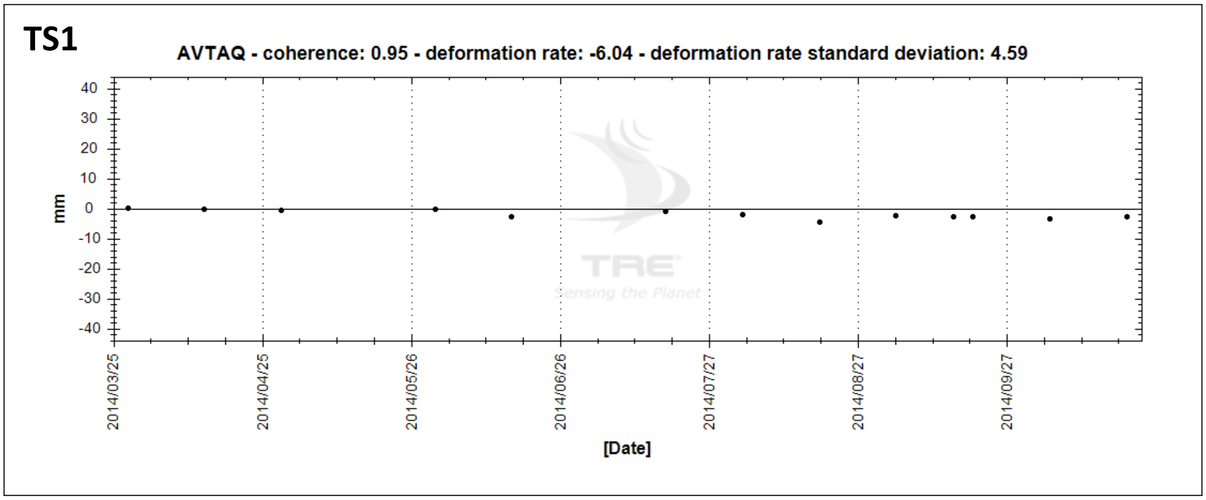

Figure 18: Time series of TS1 in Figure 17.

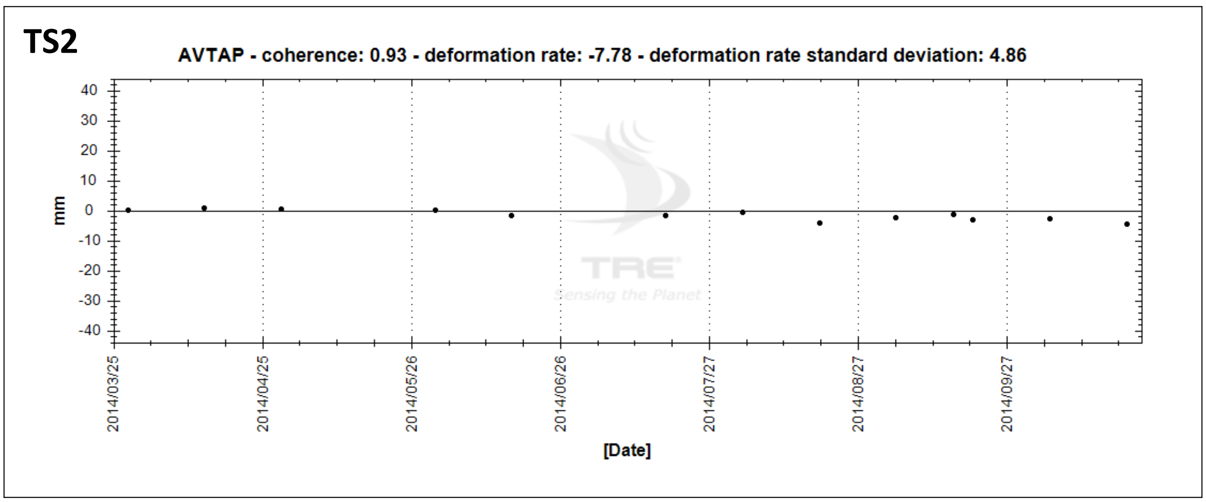

Figure 19: Time series of TS2 in Figure 17.

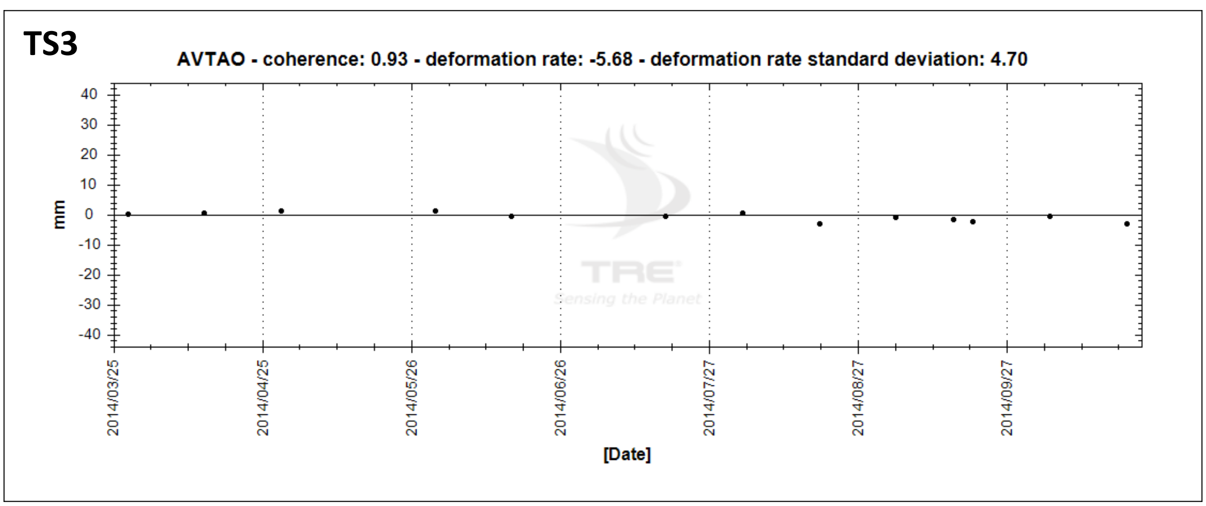

Figure 20: Time series of TS3 in Figure 17.

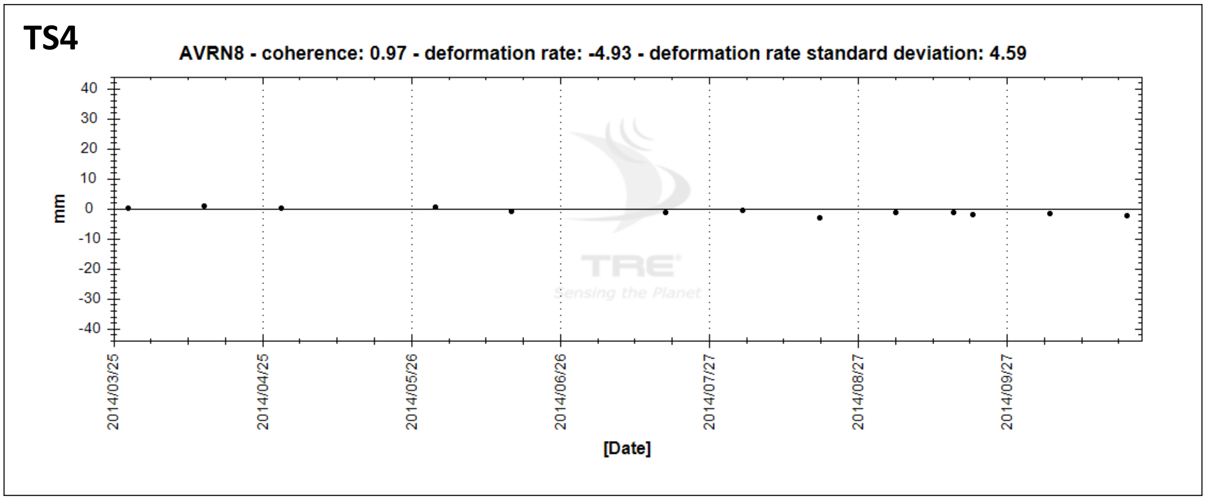

Figure 21: Time series of TS4 in Figure 17.

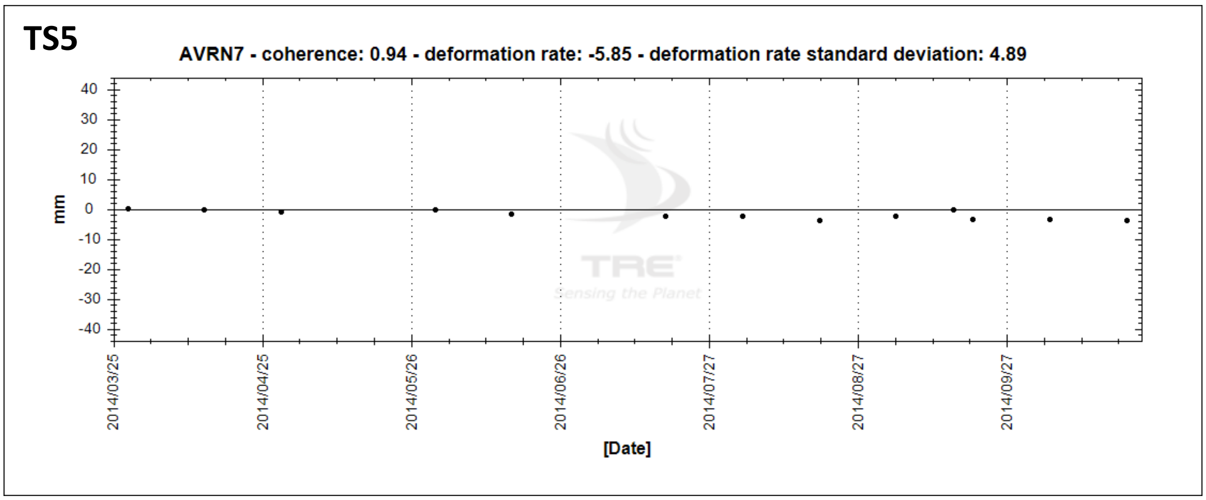

Figure 22: Time series of TS5 in Figure 17.

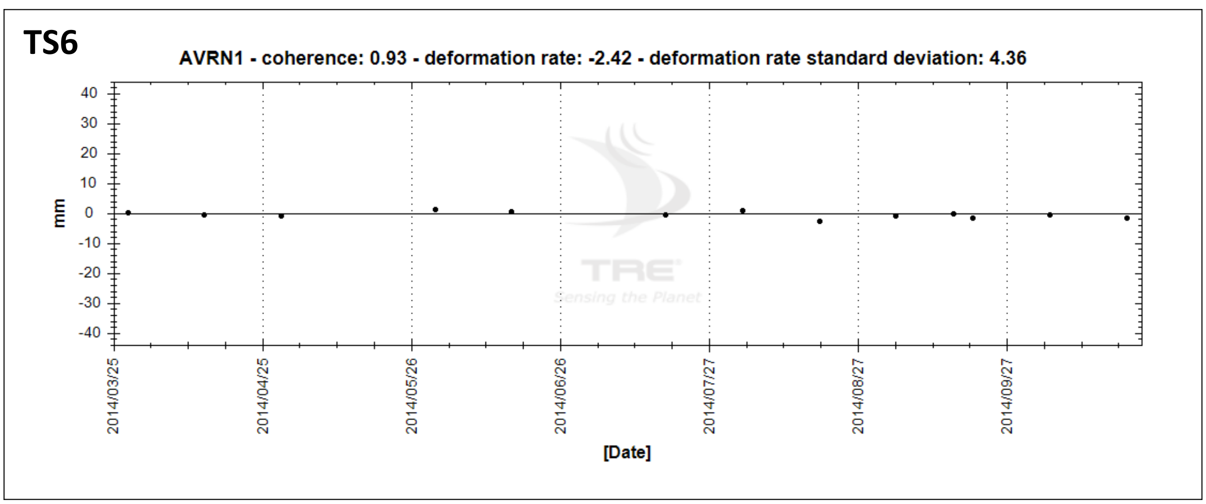

Figure 23: Time series of TS6 in Figure 17.

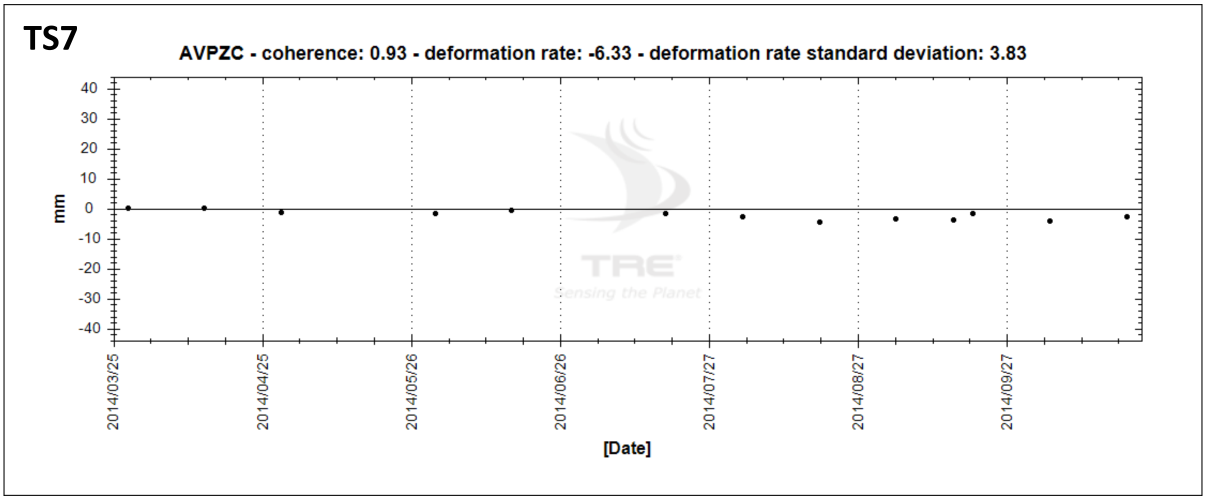

Figure 24: Time series of ATS7 in Figure 17.

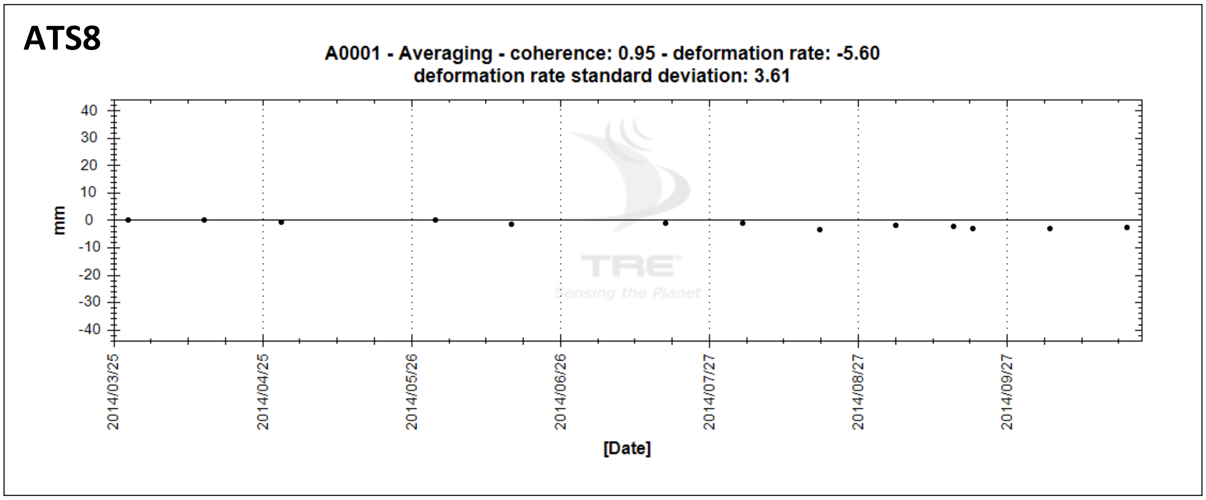

Figure 25: Average time series of ATS8 in Figure 17.

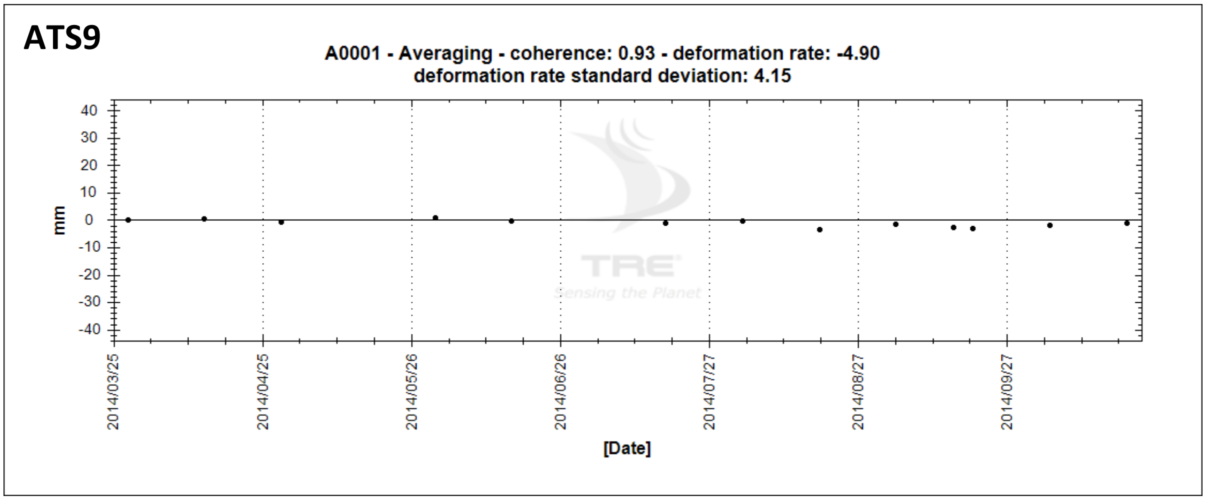

Figure 26: Average time series of ATS9 in Figure 17.

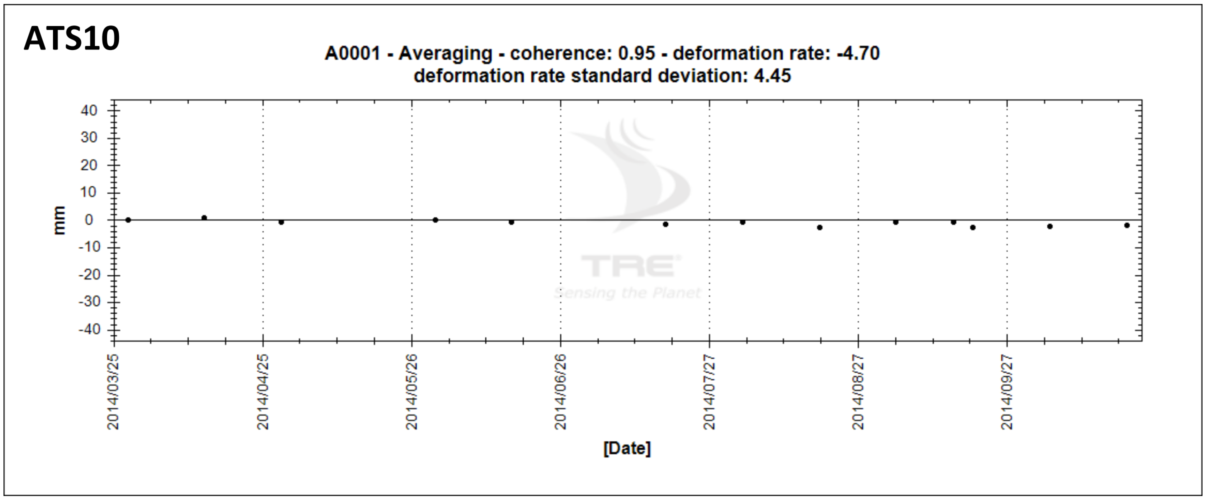

Figure 27: Average time series of ATS10 in Figure 17.

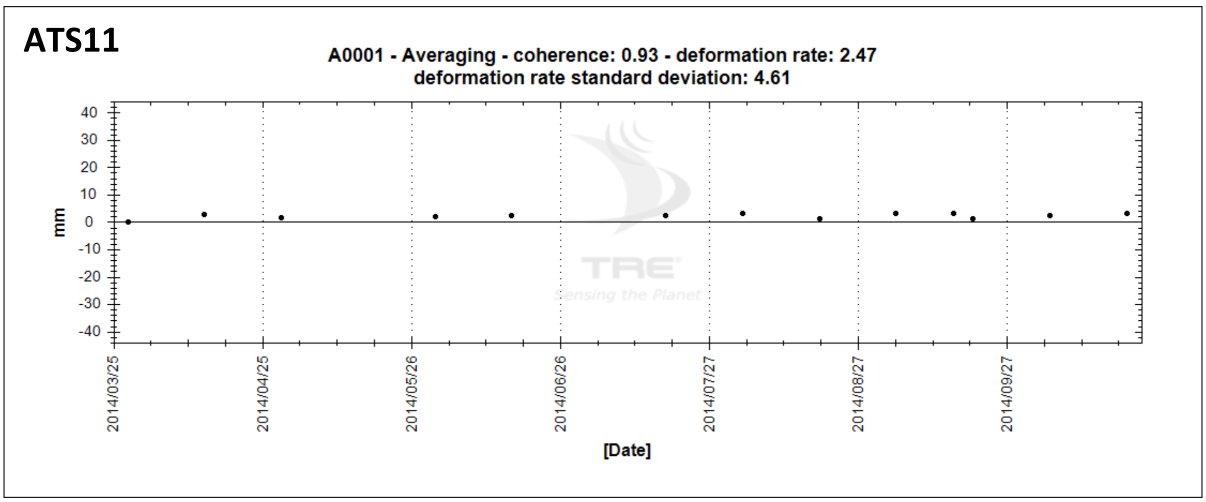

Figure 28: Average time series of ATS11 in Figure 17.

5.1.3 The Woodrow Wilson Bridge

Construction began on the new Woodrow Wilson Bridge (Wilson Bridge) in 2000 and it opened in 2006 as a replacement of the original Woodrow Wilson Bridge. The new Wilson Bridge crosses the Potomac River, has 12 lanes and is part of I-95/I-495. An overview of the results is shown in Figure 29 and several time series located on the bridge are provided in Figure 30 to Figure 37. The InSAR results indicate approximately -10 mm of subsidence from June to October 2014. A single Permanent Scatterer (PS) on the I-495 Express Lanes (labelled as TS8 in Figure 29, time series in Figure 37) exhibited relatively high subsidence (-20 mm) compared to its surroundings. In general, however, generalized subsidence was observed in the areas of Alexandria, VA and Oxon Hill. MD. With a longer time span of processed images, better comprehension of ground deformation in this area will be possible.

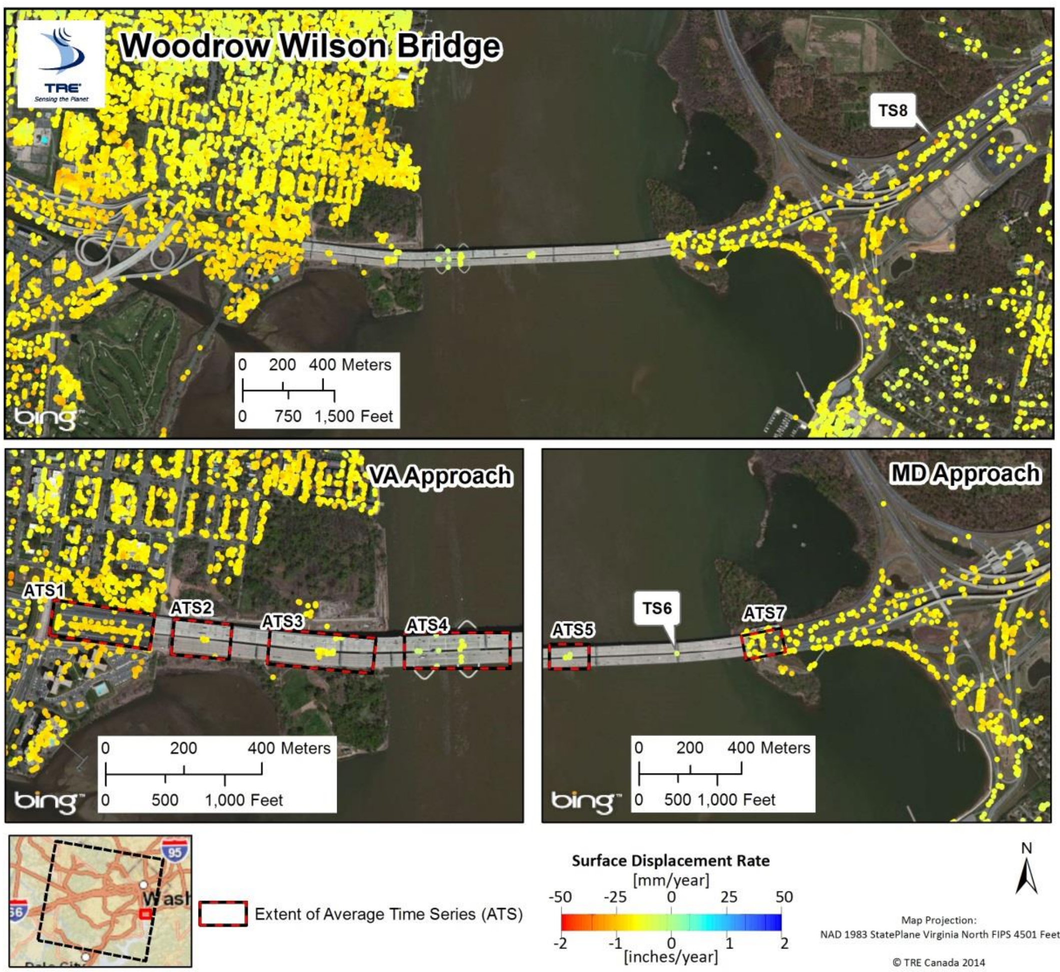

Figure 29: The SqueeSAR results over the Wilson Bridge. Top panel shows the entire Wilson Bridge; while the bottom left panel and bottom right panel represent the Virginia approach and Maryland approach of the Wilson Bridge, respectively.

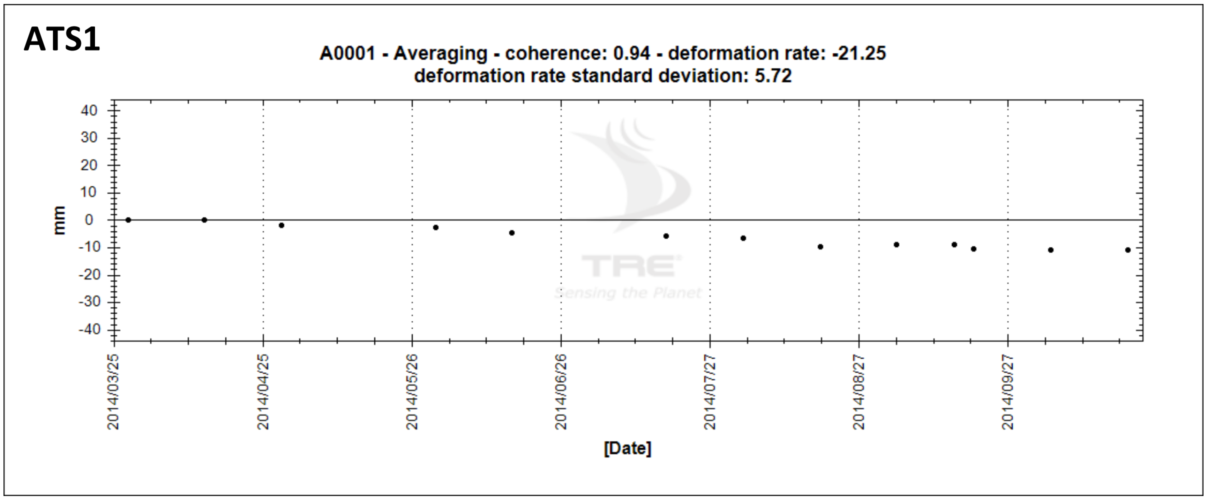

Figure 30: Average time series of ATS1 in Figure 29.

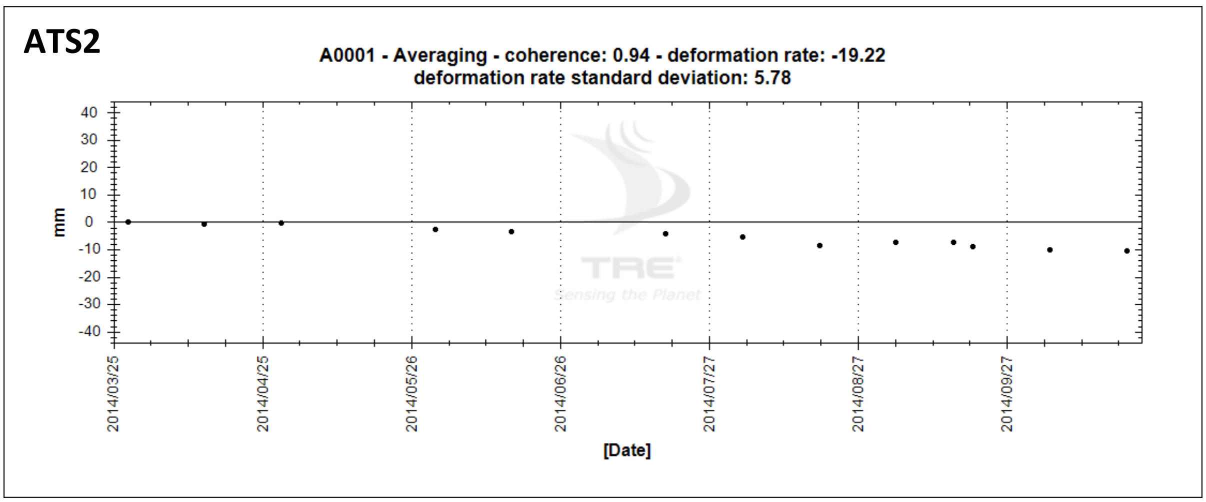

Figure 31: Average time series of ATS2 in Figure 29.

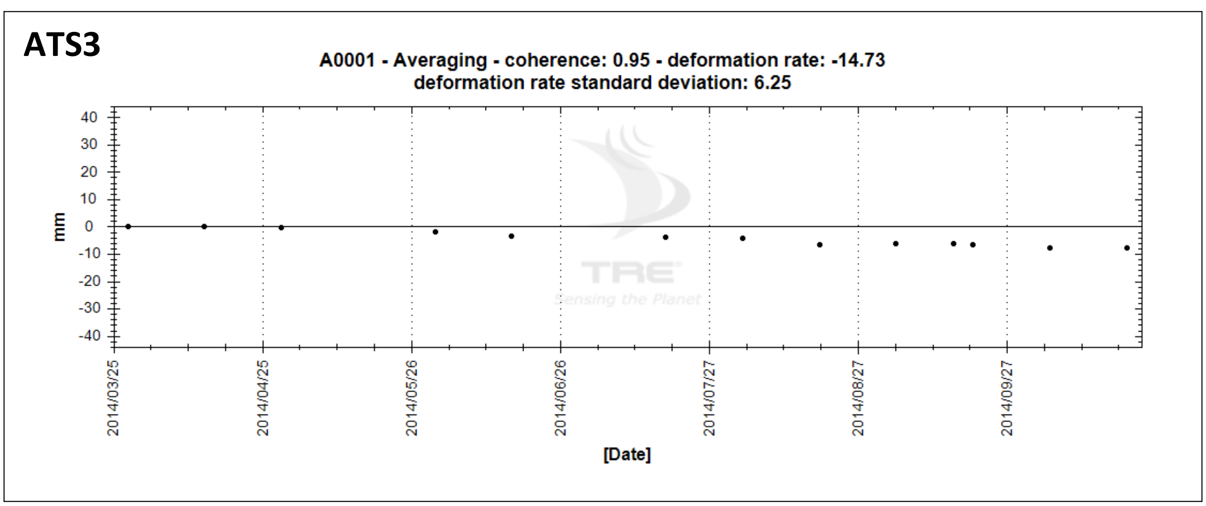

Figure 32: Average time series of ATS3 in Figure 29.

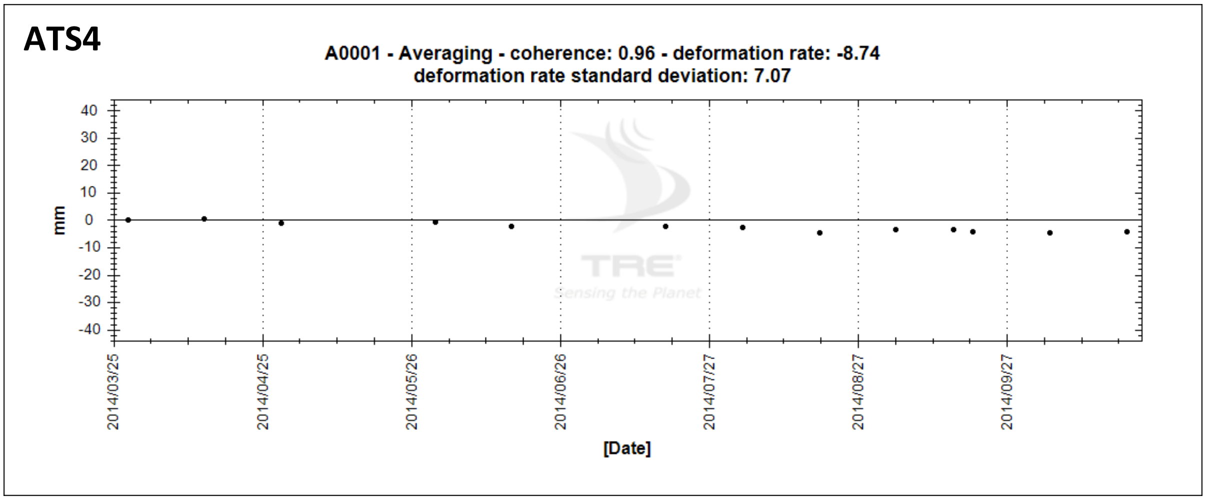

Figure 33: Average time series of ATS4 in Figure 29.

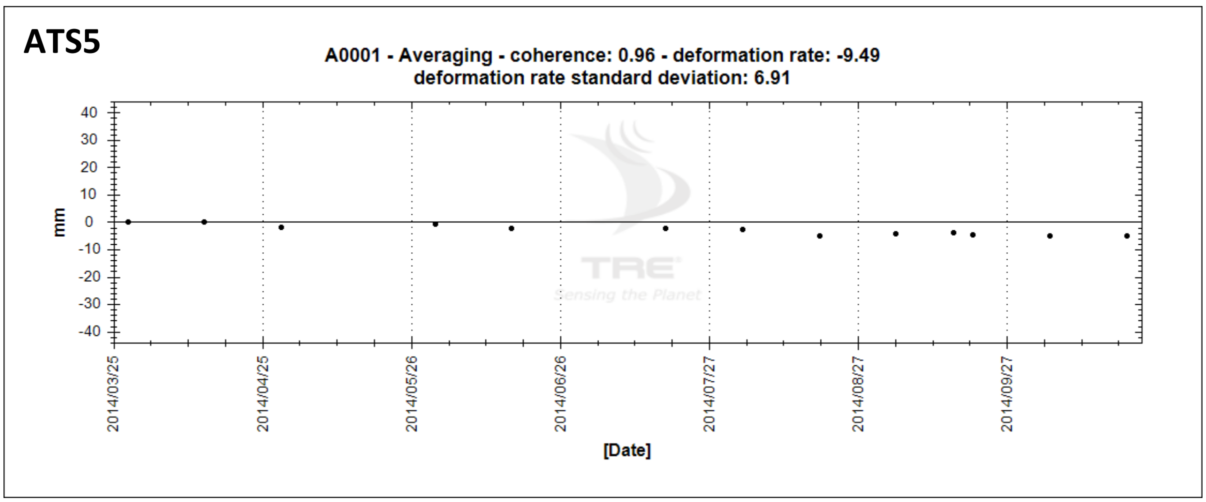

Figure 34: Average time series of ATS5 in Figure 29.

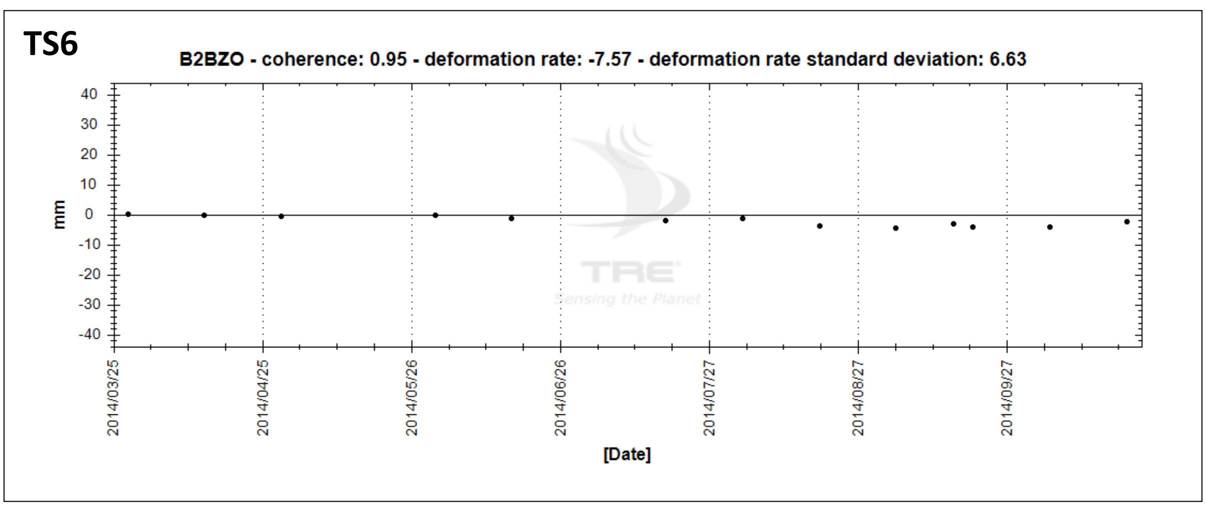

Figure 35: Time series of TS6 in Figure 29.

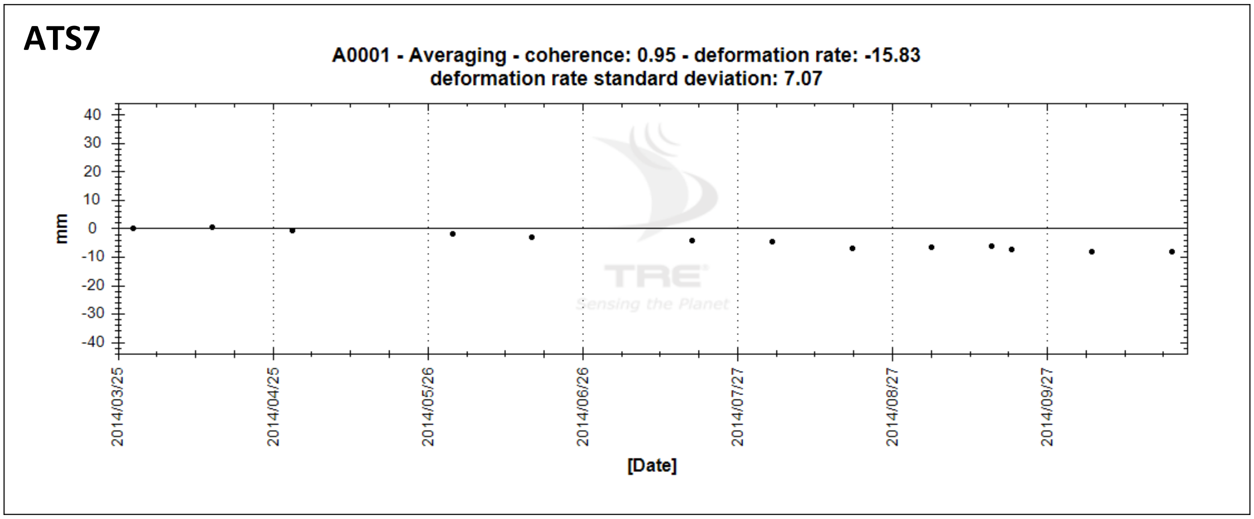

Figure 36: Average time series of ATS7 in Figure 29.

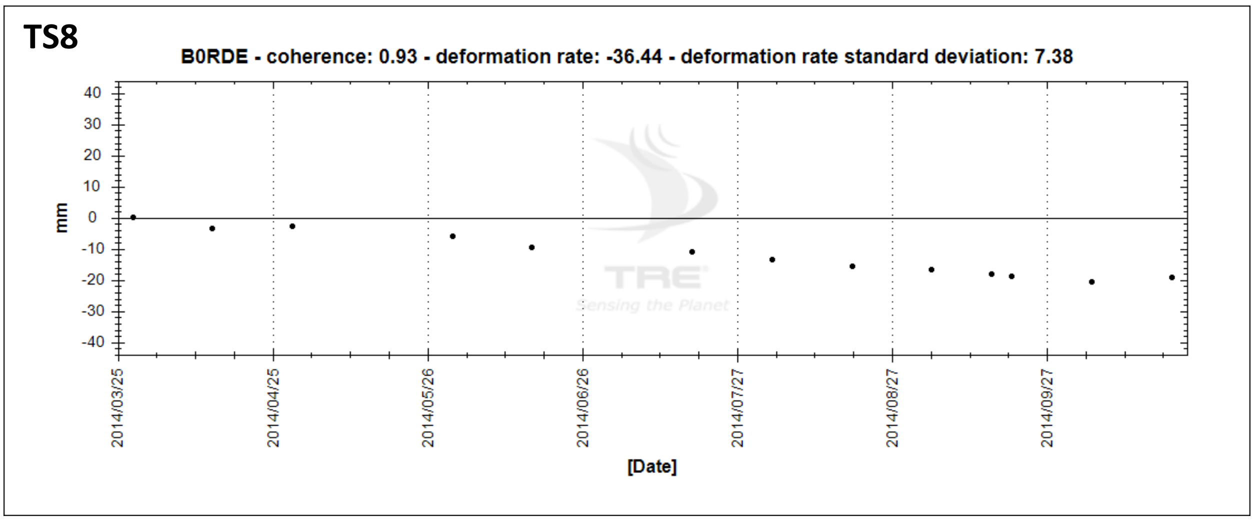

Figure 37: Time series of TS8 in Figure 29 (-77.01, 38.798).

5.1.4 The slope Failure along Piscataway Drive

An approximately 460-metre (1,500-foot) area of ground movement along Piscataway Drive, Fort Washington, Maryland was reported in early May 2014. Although this area is located outside of the AOI, the main soil layer causing the instability extends to the shore along the Potomac River on the Virginia side and is known as Marlboro clay. The InSAR results near the slope failure are displayed in Figure 38, and four selected measurement points closest to the slope failure indicate -10 to -13 mm of subsidence between March to October (Figure 39 to Figure 42). A general subsidence trend of approximately -7 mm was also observed in the region along Potomac River in the Southwest portion of the AOI. A geological map of the area is provided (bottom left panel in Figure 38) to attempt to correlate ground deformation trends with geological formations. With a longer image stack, it will be possible to analyze more closely the relationship between rock type and ground deformation.

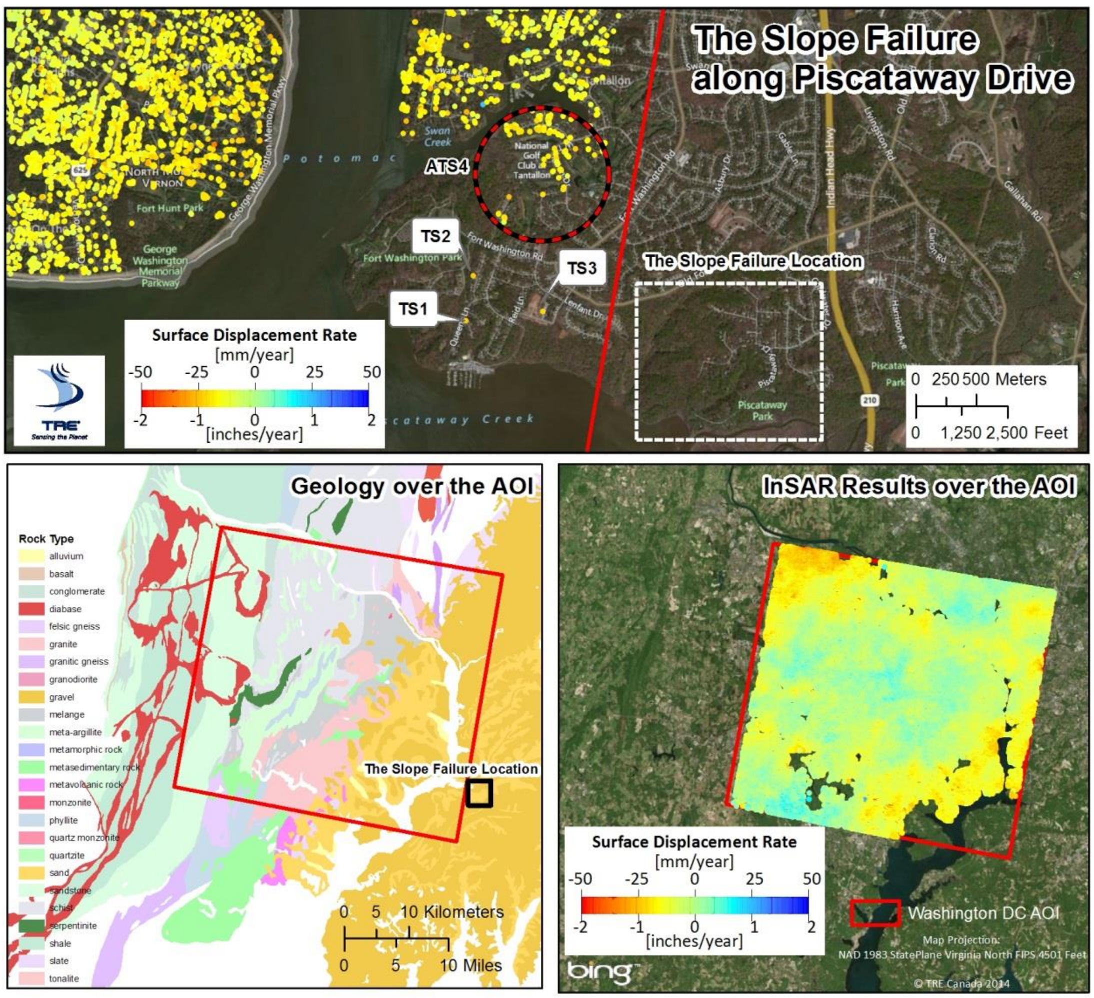

Figure 38: Top panel shows the SqueeSAR results near the slope failure along Piscataway Drive in Maryland. The bottom left panel illustrates the geology over the AOI and the bottom right panel represents the InSAR results over the AOI, respectively.

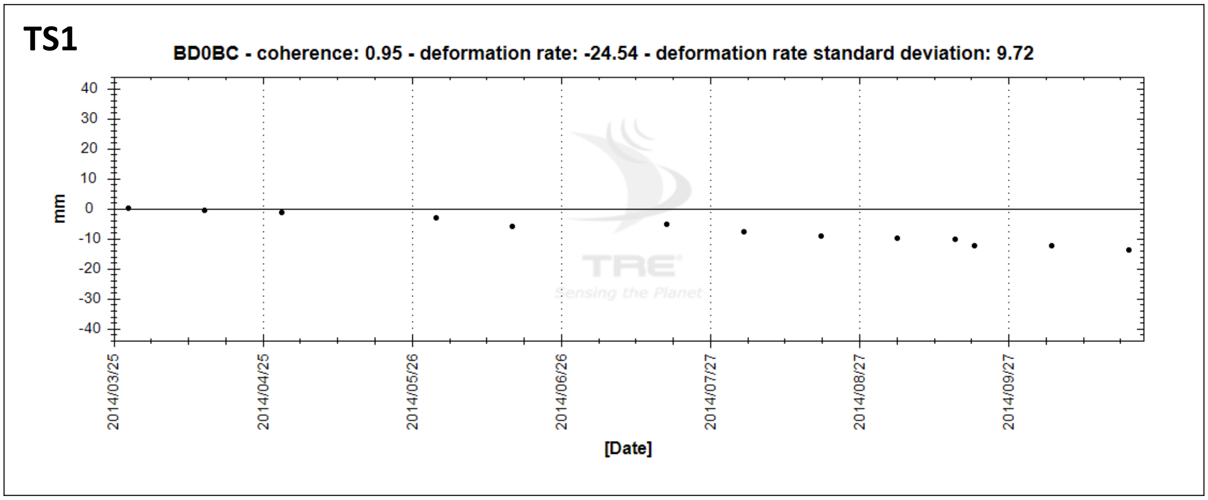

Figure 39: Time series of TS1 in Figure 38.

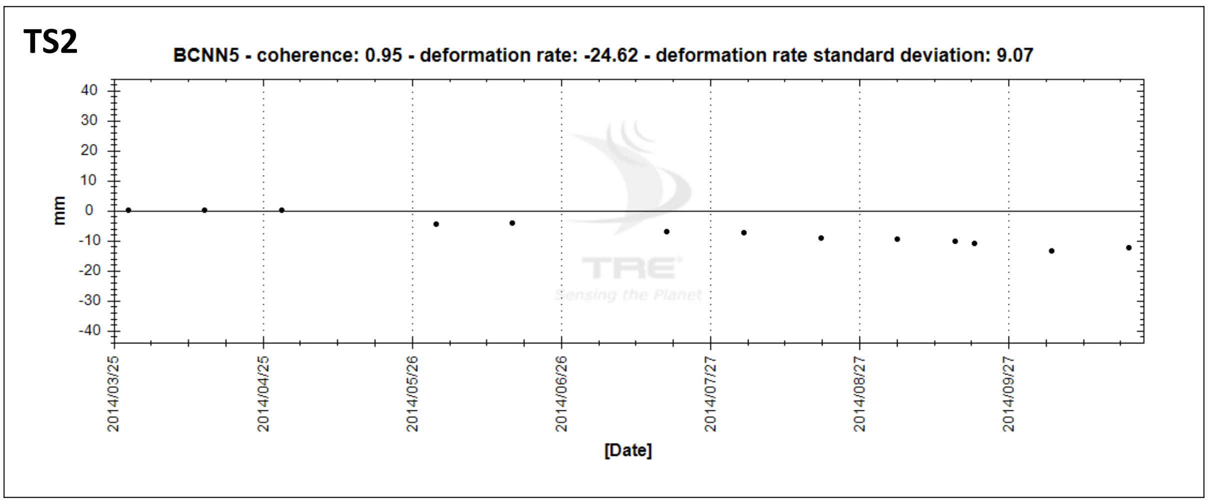

Figure 40: Time series of TS2 in Figure 38.

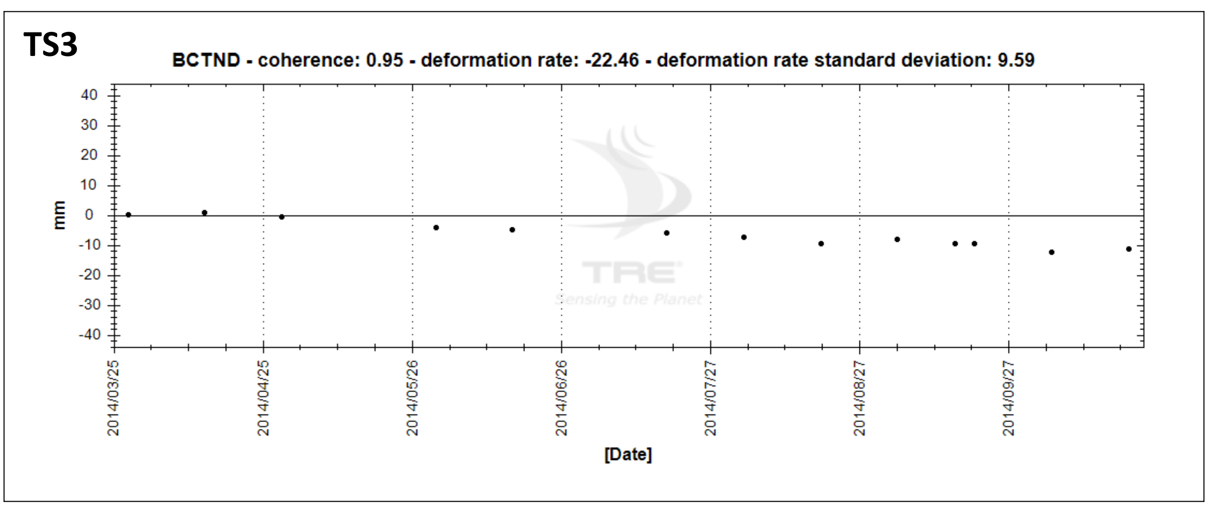

Figure 41: Time series of TS3 in Figure 38.

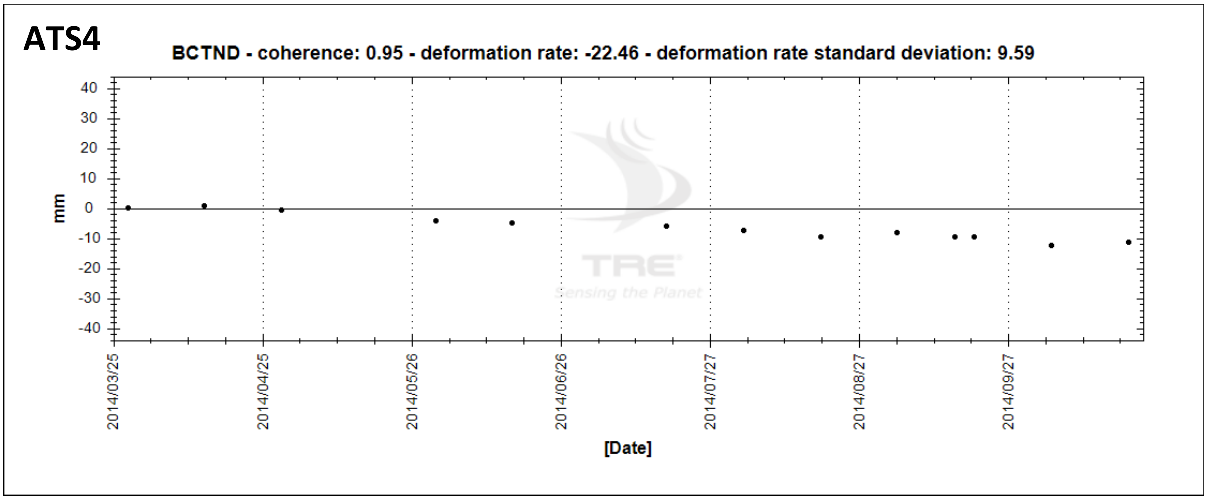

Figure 42: Average time series of ATS4 in Figure 38.

5.2 Results over Primary Roads

There is interest in identifying any subsidence detected on, or in close proximity to any major road within the AOI. A focused inspection of the data was therefore carried out to isolate and highlight any movement occurring within a 50 meter (164 foot) buffer around primary roads, including the Capital Beltway, I-95, I-64, I-66, I-295, the Henry G Shirley Memorial Hwy, and the Jackson Memorial Hwy.

Displacement rates for measurement points identified within a 50 m buffer around primary roads are shown in Figure 43. The seven sections of road highlighted in the figure are listed in Table 4 with a focused analysis of their ground deformation and specific locations of subsidence. These areas represent portions of the AOI with movement patterns that may be of interest to VDOT and UVA, particularly in relation to the detection of sinkholes, landslides and road/bridge monitoring. Results over these features will be revisited in the next data processing.

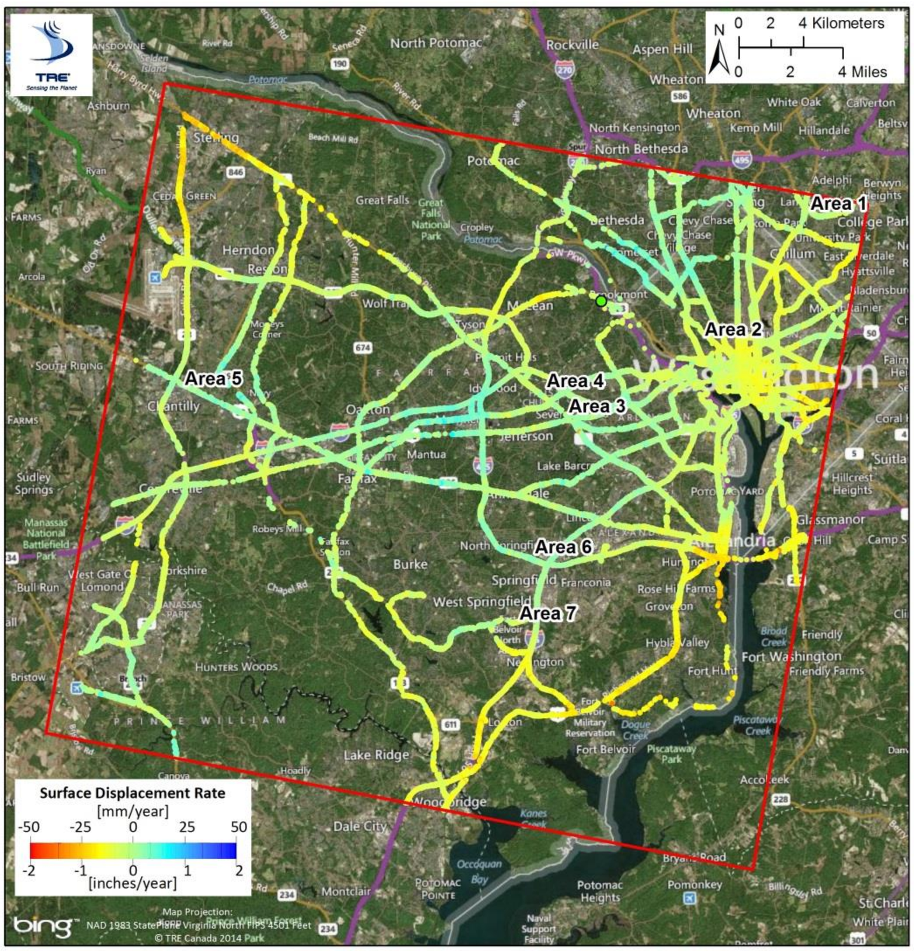

Figure 43: Surface displacement results identified within a 50 meter (164 foot) buffer of major roads in the AOI.

Area	Location (W,N)	Brief Description of Subsiding Area	Maximum Displacement (mm/yr)	Cumulative Displacement (mm)
1	(-76.972, 38.983)	On the EB of University Blvd E in MD, approx. 75m (246ft) to the intersection of 23rd Ave	-57.9	-33.7
2	(-77.052, 38.913)	Slope along Rock Creek and Potomac Pky NW	-62.9	-34.7
3	(-77.156, 38.872) (-77.151, 38.866)	In the intersection of Leesburg Pike and Sleepy Hollow Rd In the intersection of Leesburg Pike and Patrick Henry Dr	-35.5 -31.6	-19.1 -18.6
4	*(-77.163, 38.887)	On US 29, VA 237 Lee Highway	-53.5	-29.3
5	-77.421951 38.890323	On Lee Jackson Memorial Hwy	-36.8	-19.1
6	*(-77.173, 38.795)	On Henry G Shirley Memorial Hwy to Capital Beltway	-44.7	-26.0
7	(-77.184, 38.758)	On Backlick Rd	-37.2	-21.1

Table 4: Coordinates of the seven highlighted locations indicated in Figure 43. All coordinates were obtained from PS points indicating subsidence within the areas of interest. *Displacement over the area is highlighted in more detail in the next section.

Area 4 and 6 correspond to small groups of two or three measurement points located on roads or bridges and are presented in further detail in the figures below. All of the measurement points highlighted in the time series below are of the PS type.

5.2.1 Area 4 - US 29, VA 237 Lee Highway

Area 4 is located on the shoulder of US 29, Virginia State Route 237 Lee Highway (Figure 44). A measurement point with a -29.3 mm of cumulative displacement is highlighted (Figure 45).

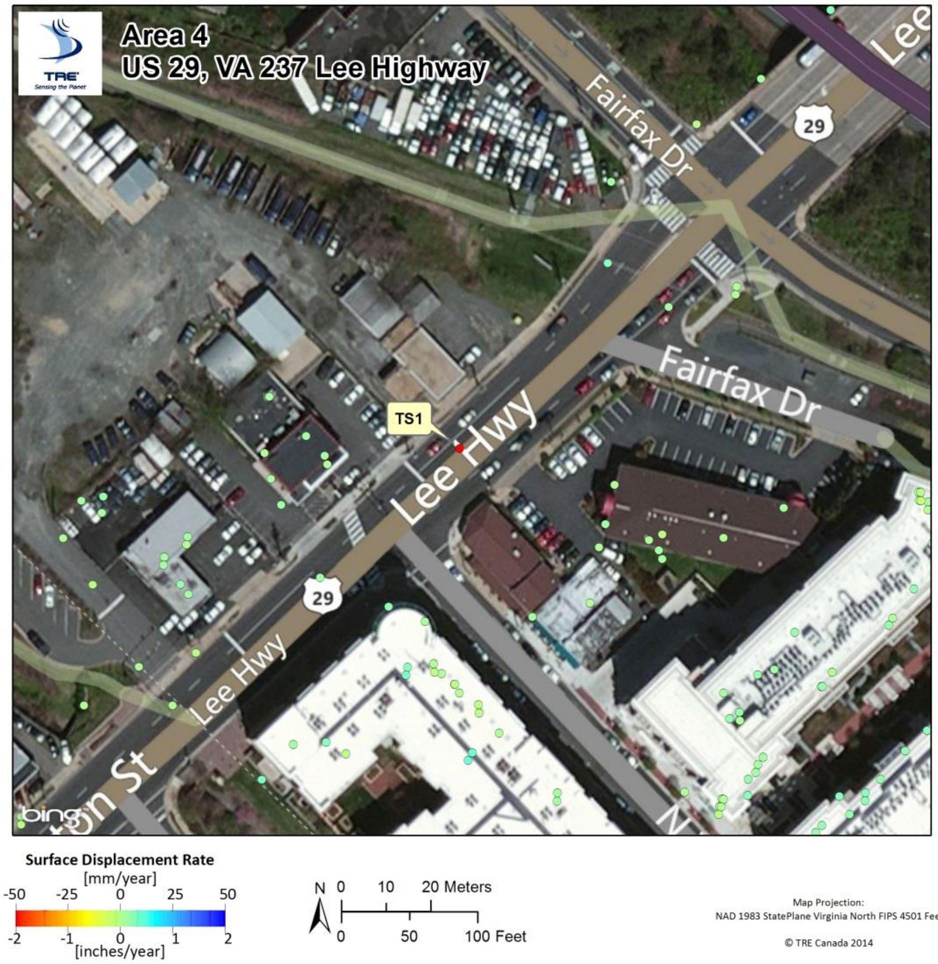

Figure 44: Displacement results on US 29, VA 237 Lee Highway (Identified as Area 4 in Figure 43).

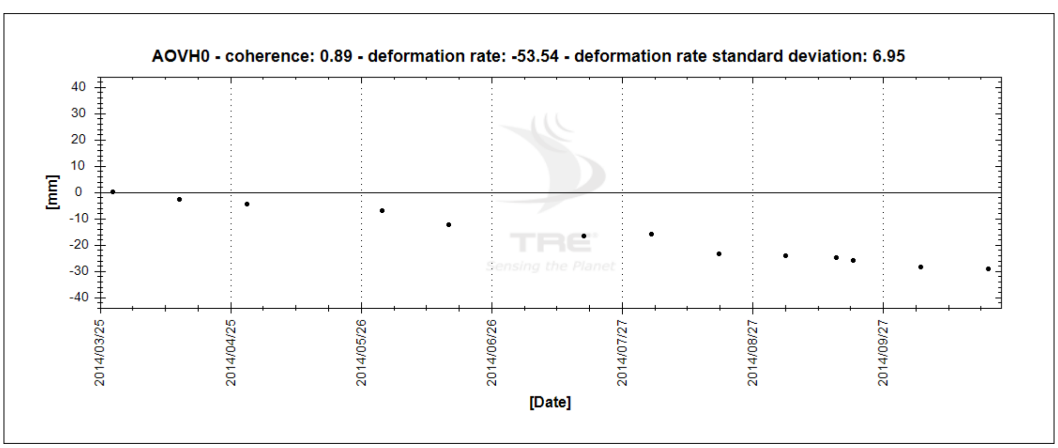

Figure 45: Time series of TS1 in Figure 44.

5.2.2 Area 6 - Henry G Shirley Memorial Hwy to Capital Beltway

A PS indicating -26 mm of cumulative subsidence was detected on the Henry G Shirley Memorial Hwy (Figure 46 and Figure 47).

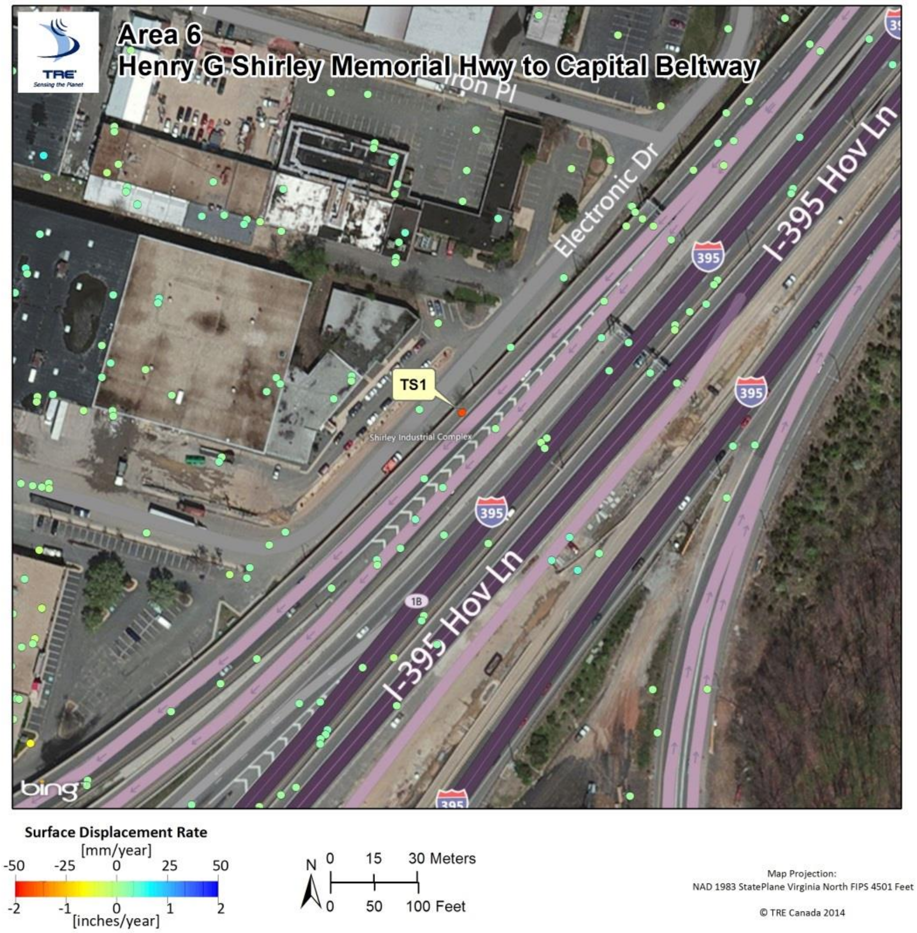

Figure 46: Displacement results over Jefferson Highway (Rt. 250) near the intersection with Greenview Dr (identified as Area 6 in Figure 43).

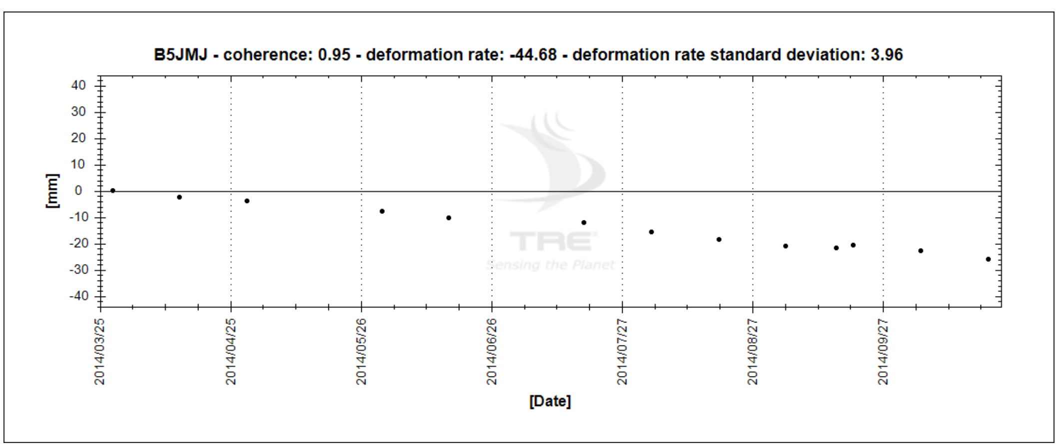

Figure 47: Time series of TS1 in Figure 46.

5.3 Pavement Conditions

One aim of the project is to investigate whether InSAR results can provide information on road pavement conditions. Figure 48 provides a side-by-side comparison of road pavement conditions and surface deformation. The pavement condition data is from early 2013 and was provided by VDOT. It rates roads on a scale of 1 to 100, with 100 being in Excellent Condition. The roads are also given a qualitative description of Very Poor, Poor, Fair, Good, Excellent and Not Rated based on their ratings. A close up of pavement conditions along the Capital Beltway in Virginia is shown in Figure 49.

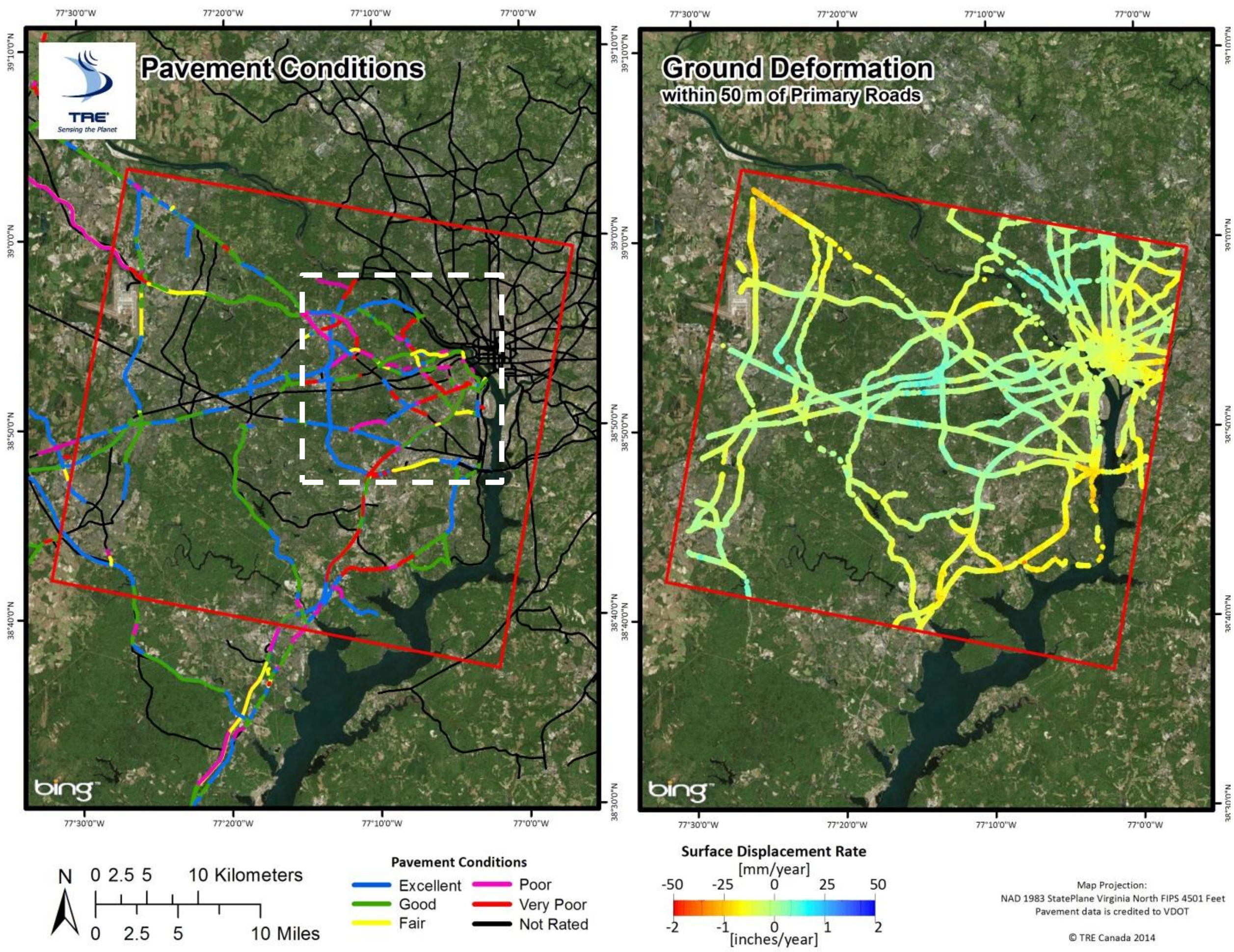

Figure 48: Left panel represents the pavement conditions over primary roads over the AOI in Virginia. Right panel indicates the ground deformation results within 50 meters of primary roads.

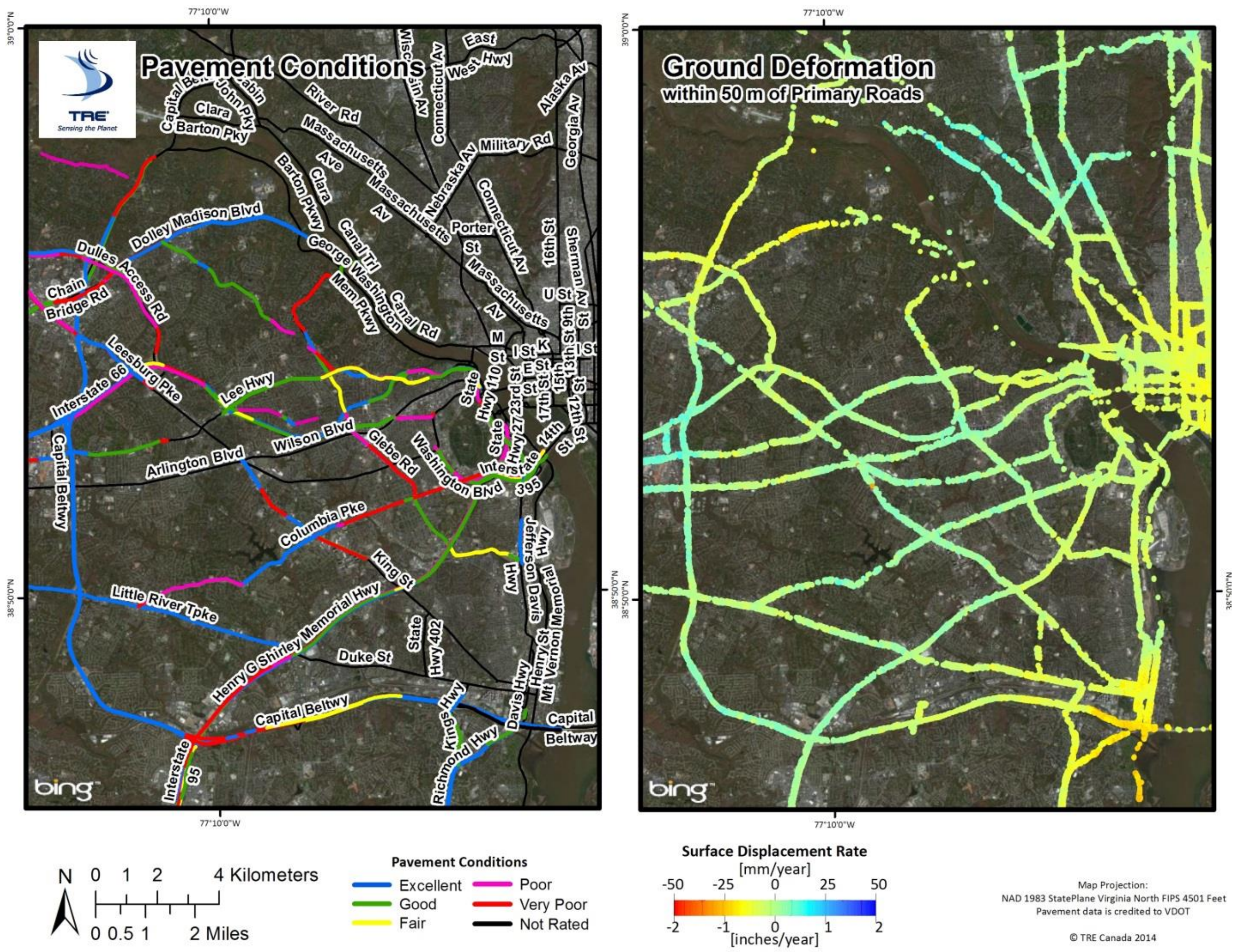

Figure 49: A close up of the pavement conditions along the Capital Beltway versus ground deformation indicated in the dashed white polygon in Figure 48.

6 Summary

A total of 1.2 million measurement points were obtained over the AOI, with a density of 781 points per square kilometre (2,022 points per square mile). As only 13 images covering seven months were processed, it is recommended to interpret results with caution and to bear in mind the ± 5.9 mm precision of the measurements.

This report highlighted ground deformation over the I-66 EB CD Road bridge over Rte. 286 Fairfax County Pkwy, the retaining wall on I-395 SB at King Street in Shirlington VA, and the slope failure along Piscataway Drive in MD. No significant subsidence was detected in these areas compared to their surroundings. One PS on the I-495 Express Lanes indicated -20 mm of subsidence close to the Woodrow Wilson Bridge.

An analysis focused on ground deformation over primary roads within the AOI was carried out. A list of findings is recorded in Table 4. Two areas experienced subsidence of -29.3 mm and -26.0 mm, on the shoulder of US 29, Virginia State Route 237 Lee Highway and along Henry G Shirley Memorial Hwy, respectively.

All of the highlighted locations in the current report will be revisited and a further analysis of the relationship between pavement conditions and ground deformation will be carried out in the next report.

Along with this report, a technical appendix is included, which contains the list of delivered files and additional information regarding InSAR processing.

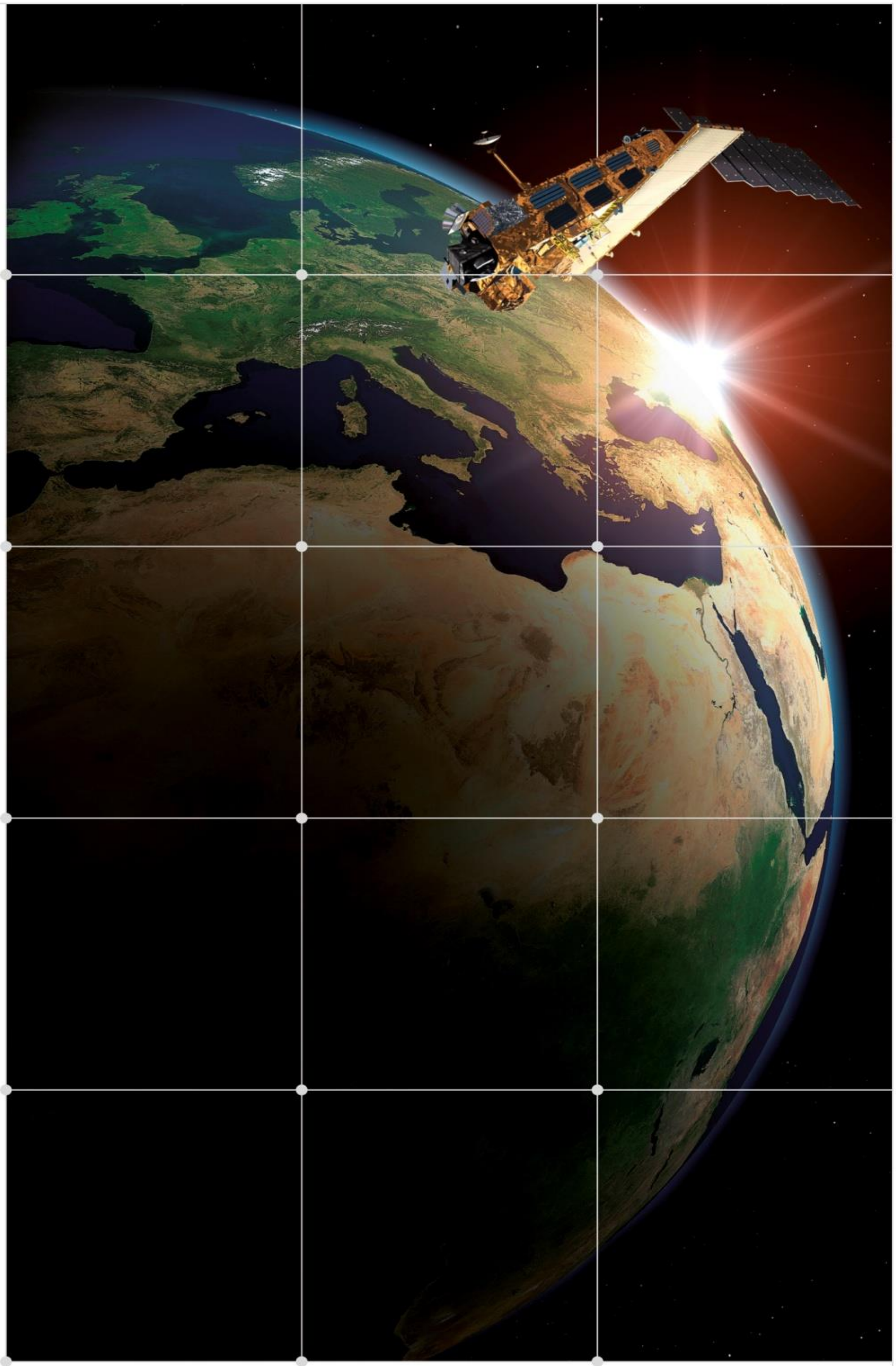

Analysis of Ground Movement over Northern of Virginia and Washington D.C. using SqueeSAR

Site 2 First Report

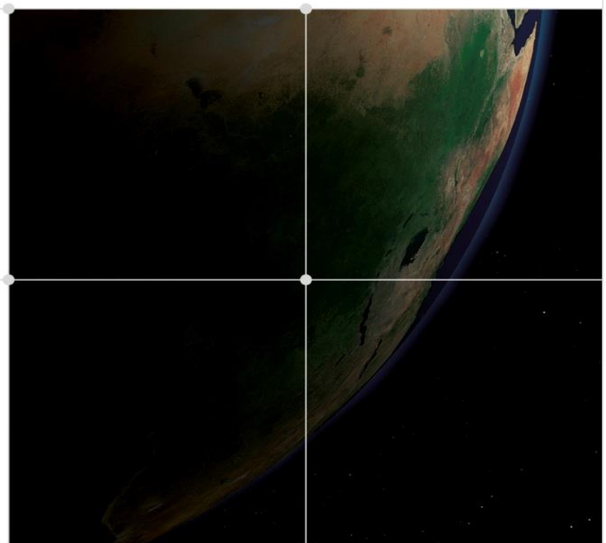

TRE®

Sensing the Planet

Submitted to:
University of Virginia
1001 N. Emmet St.
PO Box 400195
Charlottesville, Virginia 22904
USA

Prepared by:
TRE Canada Inc.
Suite 410, 475 West Georgia Street
Vancouver, B.C., V6B 4M9
Canada

Prepared by:	Vicky Hsiao GIS Analyst TRE Canada Inc.	______________________ (signature)
Approved by:	Giacomo Falorni Operations Manager TRE Canada Inc.	______________________ (signature)

Doc. Ref.: JO14-3014-REP1.0
December 11 2014

Table of Contents

Appendix 1: List of delivered files

List of Delivered Files

The deliverables of the SqueeSAR™ analysis include the present report, the PS data files and a software tool for assisting with the loading, viewing and interrogation of the data in ESRI ArcGIS 10.x software. Table 1 and Table 2 list the files contained on the accompanying CD.

Data type	Description
-TSR.shp	ESRI Shapefile for displaying the database file (dbf) geospatially in a GIS environment.
-TSR.dbf	Table containing the height, velocity, velocity standard deviation, acceleration, coherence and time series of all the PS/DS identified.
-REF.shp	ESRI Shapefile for displaying the reference point file in a GIS environment.
-REF.dbf	The reference point used for the ascending and/or descending data processing.
.xml	An encoding document for each -TSR.shp, VERT.shp, EAST.shp file This file contains metadata for data processing and provides information for the TRE customer toolbar application
.mxd	A ESRI ArcGIS 10.2 project file contains the results.

Table 1: List of delivered file types.

File Name		
Site 2 – NOVA and Washington D.C.	Full Resolution	SITE2_WASHINGTON_CSK_H40B_D_T87_Oct14-TSR SITE2_WASHINGTON_CSK_H40B_D_T87_Oct14 -REF
	Subsampled to 100 m X 100 m	SITE2_WASHINGTON_CSK_H40B_D_T87_SUB100_Oct14-TSR SITE2_WASHINGTON_CSK_H40B_D_T87_SUB100_Oct14 -REF

Table 2: List of delivered files.

The ESRI ArcGIS 10.2 project file is included to make it easier to view the data. Once the data contained on the CD has been saved to the user's hard drive it will be sufficient to open the project file with ArcGIS and update the links to indicate the new locations of the data. The project also contains various layers for viewing the data, including: the AOI, the reference point, the shapefiles for the site and the AOI shapefile.

The Structure of the Database Files

Table 3 below, describes the attributes of each PS/DS data within the database.

Field	Description
CODE	Unique identification code.
SHAPE	Indicates type of geometry (point).
HEIGHT (m)	Elevation above sea level of the PS and DS.
H_STDEV (m)	Standard deviation of PS and DS elevation value.
VEL (mm/yr)	PS movement rate. Positive values correspond to movement toward the satellite (uplift); negative values correspond to motion away from the satellite (subsidence).
V_STDEV (mm/yr)	Standard deviation of PS and DS deformation rate.
ACC (mm/yr^2)	PS and DS acceleration rate.
A_STDEV (mm/yr2)	Standard deviation of PS and DS acceleration value.
COHERENCE	Quality measure [between 0 and 1].
SEASON_AMP (mm)*	Amplitude of seasonal cycles present within the data.
SEASON_PHS (days)*	Phase of seasonal cycles present within the data.
S_AMP_STD (mm)*	Standard deviation of the seasonal amplitude.
S_PHS_STD (days)*	Standard deviation of the seasonal phase.
EFF_AREA (m^2)	Size of the area belonging to the PS and DS. For PS EFF_AREA = 0, for DS EFF_AREA > 0.
D(year/month/day) (mm)	Following the EFF_AREA column are a series of fields that contain the displacement values of successive acquisitions relative to the Master, expressed in mm.

Table 3: Description of the fields contained in the LOS data Shapefile.

*Applicable only to data sets that span one year or longer.

TREmaps™

The SqueeSAR™ data are also available using TREmaps™, a web-based portal where they can be visualised through a secure client login (only authorised users will have access to the results). SqueeSAR™ data are superimposed onto a Google Maps background and time-series can be viewed.

Data can be visualised on any device with an internet connection, including portable tablets. Figure 28 shows an example dataset loaded into the web-based GIS TREmaps™ platform. Site and the access details (username and password) will be provided directly to the primary contact via email.

https://tremaps.treuropa.com/tremaps

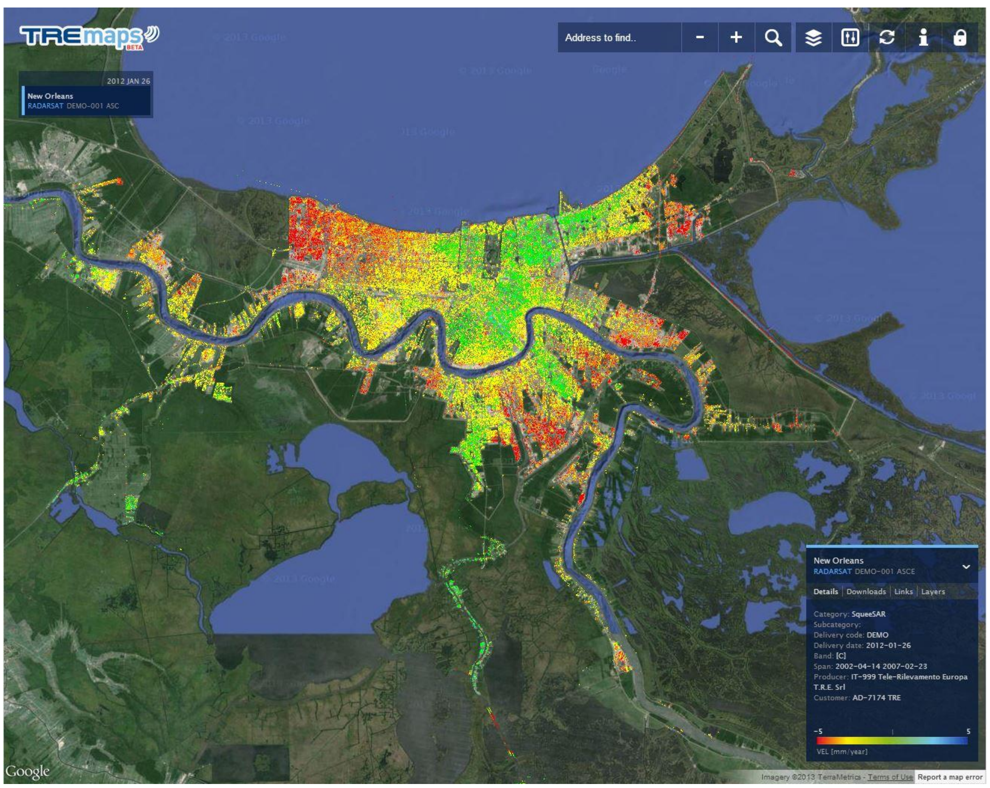

Figure 1: Example of SqueeSAR data within TREmaps.

Appendix 2: Additional Properties of the SqueeSAR™ results

Radar Data Acquisition Geometry

InSAR-based approaches measure surface displacement on a one-dimensional plane, along the satellite line-of-sight (LOS). The LOS angle varies depending on the satellite and on the acquisition parameters while another important angle, between the orbit direction and the geographic North, is nearly constant.

The images used for the historical analysis were acquired from the COSMO-SkyMed (CSK) satellite on an descending orbit (satellite travelling from north to south and imaging to the west) along Track 87.

Table 4 lists the values of the angles for this study, while Figure 2 shows the geometry of the image acquisitions over the site for the descending orbits, respectively. The symbol δ (delta) represents the angle the LOS forms with the vertical and Θ (theta) the angle formed with the geographic north.

Satellite	Orbit geometry	Symbol	Angle
CSK	Descending	**δ**	23.99º
		θ	12.87º

Table 4: Satellite viewing angles for the CSK descending orbit imagery.

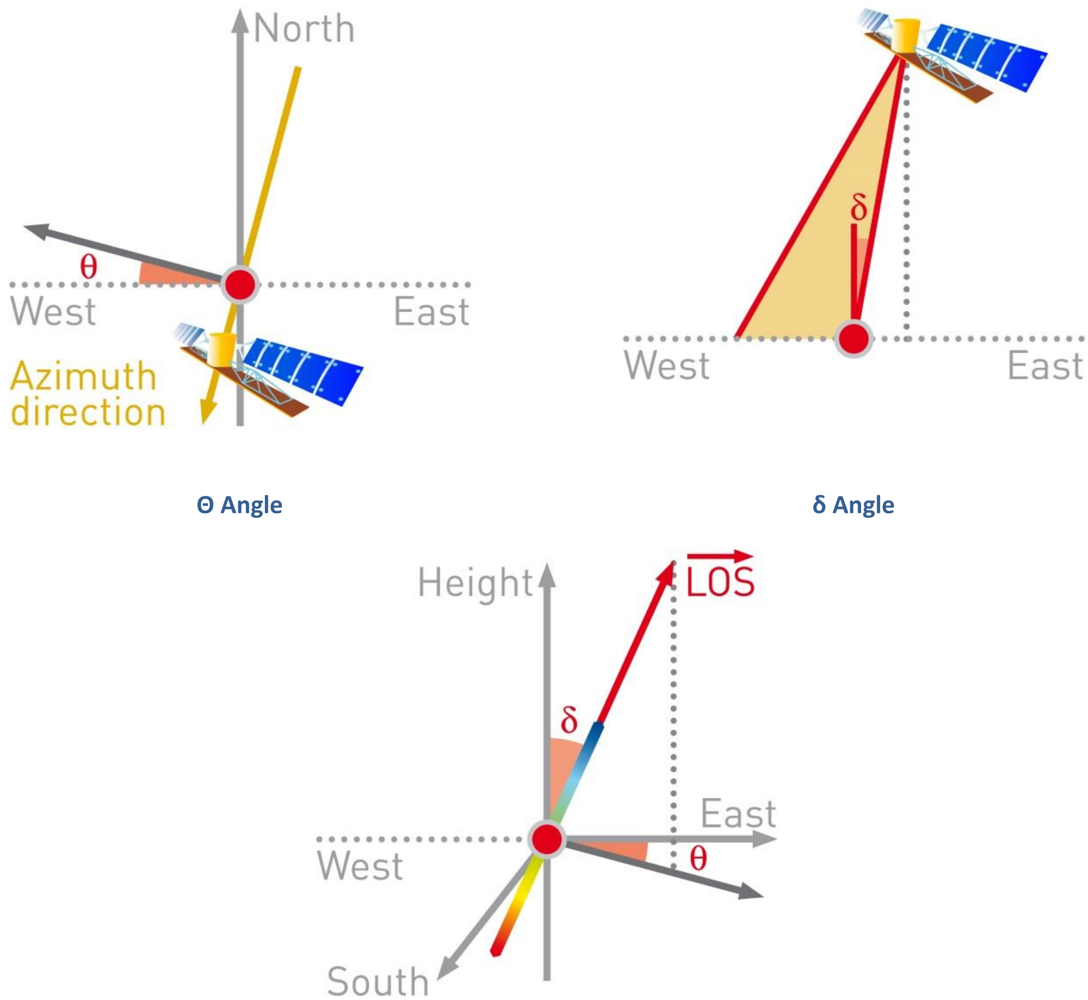

Θ Angle **δ Angle**

Line Of Sight

Figure 2: Geometry of the image acquisitions over the AOI for the descending orbit.

Data Processing

Both permanent scatterers (PS) and distributed scatterers (DS) were identified at this site. Bare ground, roads, and infrastructure provide the basis for many PS points in the present SqueeSAR™ analysis. Many natural features such as rocks or exposed ground were also likely sources of stable PS targets.

DS correspond to large areas (up to hundreds of square meters) and were identified from exposed areas such as sparsely vegetated areas, exposed ground or rock. It is important to consider that while DS are represented as individual points for clarity of presentation and ease of interpretation, these measurements actually correspond to non-point features that are multiple pixels in size. The size of the DS within the AOI ranges from 75 to 881 m^2.

Table 5, shown below; provide a summary of the other properties relative to the data processing.

Satellite	COSMO-SkyMed (CSK)
Acquisition geometry	Descending
Analysis time interval	28 March 2014 - 22 October 2014
Number of scenes processed	13
Georeferencing	Bing Map
Projection system used / datum	State Plane Virginia North FIPS 4501 (Feet) / NAD 1983
Reference Point location	EAST: 11870940.16 NORTH: 6968871.59
Area of interest	617.8 sq. mile (1,600 km^2)

Table 5: Statistics of the processed data.

Standard Deviation and Precision

Standard deviation values of the displacement measurements are a function of the factors listed below and of local ground movement dynamics.

- Spatial density of the PS and DS (higher densities produce higher precisions)
- Quality of the radar targets (signal-to-noise ratio levels)
- Distance from the reference point
- Number of images processed
- Period of time covered by the imagery
- Climatic conditions at the time of the acquisitions
- Distance between the measurement point and the reference

In addition to each measurement point having an associated standard deviation value to represent the error of the displacement measured, results can also be characterized by the accuracy of the technique. Specifically, three parameters are used to characterize the overall accuracy of the results:

- Precision of the estimated deformation rates;
- Precision of the estimated elevations;
- Precision of the geocoding.

Table 6 summarizes the typical precision values applicable to PS located within 2 km from the reference point when **at least 45 radar images** have been processed.

DEFORMATION RATE	< 1 [mm/yr]
DISPLACEMENT ERROR (single displacement between contiguous satellite images)	< 5 [mm]
ELEVATION	± 1.5 [m]
POSITIONING ERROR ALONG EAST DIRECTION	± 3 [m]
POSITIONING ERROR ALONG NORTH DIRECTION	± 2 [m]

Table 6: Measurement accuracies for PS located within 2 km of the reference point, based on the processing of at least 45 SAR images.

Appendix 4: InSAR Processing

InSAR

Interferometric Synthetic Aperture Radar, also referred to as SAR interferometry or InSAR, is the measurement of signal phase change (interference) between radar images. When a point on the ground moves, the distance between the sensor and the point changes, thereby producing a corresponding shift in signal phase. This shift is used to quantify the ground movement.

An interferogram is a 2D representation of the difference in phase values. Variations of phase in an interferogram are identified by fringes, colored bands that indicate areas where and how much movement is occurring. The precision with which the movement can be measured is usually in the centimetre (cm) range as the phase shift is also impacted by topographic distortions, atmospheric effects, and other sources of noise.

DInSAR

When InSAR is used to identify and quantify ground movement the process is referred to as Differential InSAR (DInSAR). In DInSAR topographic effects are removed by using a DEM of the area of interest to create a differential interferogram.

Differential InSAR is still impacted by atmospheric effects, as there is no method for removing this signal phase contribution. It is a useful tool for identifying footprints of progressing movement and creating deformation maps. The limitations of DInSAR are its relatively low precision (cm scale) and that it cannot distinguish between linear and non-linear motion.

PSInSAR™

Permanent Scatterer SAR Interferometry is an advanced form of DInSAR. The fundamental difference is that it uses multiple interferograms created from a stack of at least 15 radar images.

Permanent Scatterer SAR Interferometry was developed to overcome the errors produced by atmospheric artifacts on signal phase. The PSInSAR algorithm automatically searches the interferograms for pixels that display stable radar reflectivity characteristics throughout every image of the data set. In PSInSAR these pixels are referred to as Permanent Scatterers (PS). The result is the identification of a sparse grid of point-like targets on which an atmospheric correction procedure can be performed. Once these errors are removed, a history of motion can be created for each target, allowing the detection of both linear and non-linear motion.

The result is a sparse grid of PS that are color-coded according to their deformation rate and direction of movement. The information available for each PS includes its deformation rate, acceleration, total deformation, elevation, coherence as well as a time series of movement. The PSInSAR algorithm measures ground movement with millimetre accuracy.

SqueeSAR™

Permanent Scatterers are objects, such as buildings, fences, lampposts, transmission towers, crash barriers, rocky outcrops, etc, that are excellent reflectors of radar microwaves. However, TRE has noticed that many other signals are present in the processed data. These do not produce the same high signal-to-noise ratios of PS but are nonetheless distinguishable from the background noise. Upon further investigation it was found that the signals are reflected from extensive homogeneous areas where the back-scattered energy is less strong, but statistically consistent. These areas have been called distributed scatterers (DS) and correspond to rangeland, pastures, bare earth, scree, debris fields, arid environments, etc (Figure 3).

The SqueeSAR™ algorithm was developed to process the signals reflected from these areas. As SqueeSAR™ incorporates PSInSAR no information is lost and movement measurement accuracy is unchanged.

The SqueeSAR™ algorithm also produces improvements in the quality of the displacement time series. The homogeneous areas that produce DS normally comprise several pixels. The single time series attributed to each DS is estimated by averaging the time series of all pixels within the DS, effectively reducing noise in the data.

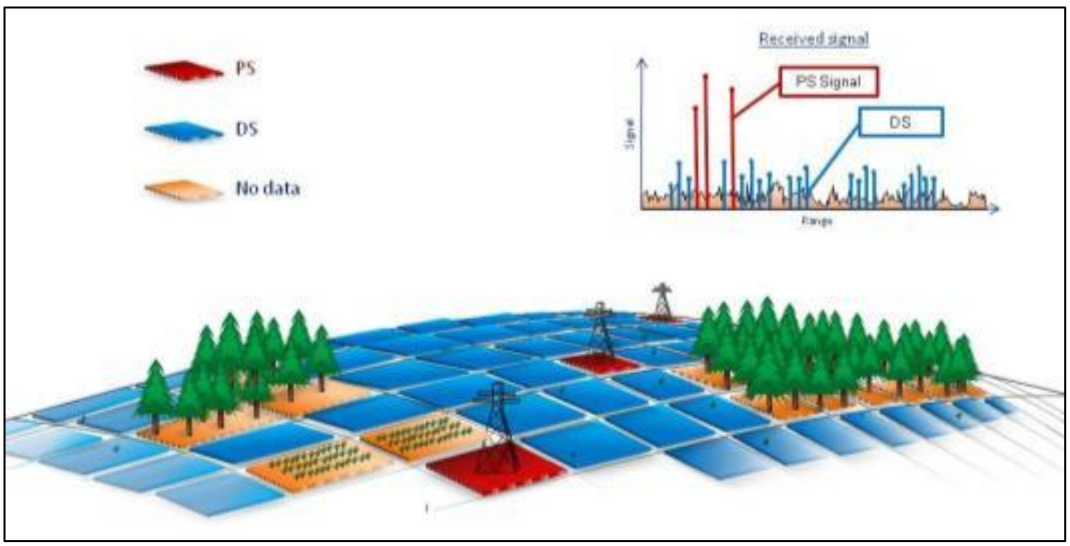

Figure 3: Illustration of the identification of permanent (PS) and distributed scatterers (DS) by the SqueeSAR™ algorithm.

Appendix 5: Data Processing

Methodology

The identification of PS and DS in a series of radar images comprises a sequence of steps.

First, all radar data archives are screened to determine the most suitable source of raw data for the particular area of interest and to select all the high quality images within the chosen data set.

As the signal echo from a single point target contains many returning radar pulses it appears defocused in a synthetic aperture radar (SAR) raw image. The first processing step is therefore to focus all the received energy from a target in one pixel. The images are then precisely aligned to each other, or co-registered, and analyzed for their suitability for interferometry. The parameters that are analyzed are the normal baseline and the temporal distribution of the images.

There then follows a number of statistical analyses on the phase and amplitude characteristics of the backscattered radar signal that return to the satellite. If a concentrated number of signals reflect off a particular feature within a pixel and backscatter to the satellite, the feature is referred to as a ‘scatterer’. When the same scatterer appears in all, or most, of a data set of SAR images of a particular location, then the scatterer is deemed to be ‘permanent’.

At this stage it is possible to identify a subset of pixels, referred to as Permanent Scatterer Candidates (PSC), that are used to estimate the impact on signal phase of ionospheric, tropospheric and atmospheric effects, as well as possible orbit errors.

Once the signal phase has been corrected for these effects, any remaining changes in signal phase directly reflect ground movement.

Master Image Selection

SqueeSAR™ requires that one image (or scene) in each data set has to become both a geometric and temporal reference to which all the other images are then related. This image is referred to as the master image and those that remain are slave images.

The master image should be chosen according to the following criteria:

- it minimizes the spread of normal baseline values for the slave images;
- similarly, it minimizes the temporal baseline values between the master and each slave image; and
- it minimizes the effects of signal noise arising from changes in vegetation cover and/or small changes in the look angle of the satellite from one scene to another.

Signal Phase and Amplitude Analysis

General

Each pixel of a SAR image contains information on the amplitude of signals that are backscattered toward the satellite, as well as on the signal phase. The amplitude is a measure of the amount of the radar pulse energy reflected, while the phase is related to the length of the path of the electromagnetic wave, from the platform to the ground and back again.

Analyses of both amplitude and phase of the SAR image provide an indication of the stability of each pixel, over time, whereby it is possible to identify those pixels that are most likely to behave as Permanent Scatterers. Statistical methods are used extensively in this process.

Among the different statistical parameters that can be computed two are of particular interest: the Phase Stability Index (PSI), obtained from the phases of the images within the data set, and the Multi Image Reflectivity (MIR) map, derived from the amplitude values of the available acquisitions.

Radar phase and coherence

The phase stability is strongly linked to the concept of coherence. Pixels that consistently display high phase stability are said to be coherent. Coherence is measured by an index that ranges from 0 to 1. When a pixel is completely coherent, it will have a coherence value of 1. Correspondingly, if a pixel has a low phase stability, its coherence index will be 0. In general, interferometry is successful when the coherence index lies between 0.5 and 1.0.

Radar amplitude and multi-image reflectivity

The amplitude of a pixel within a SAR image is the aggregate of the backscattered energy toward the satellite from within the pixel's equivalent land area. This equivalent land area is referred to as the radar resolution, and in the case of the CSK satellite, it measures about 3 m by 3 m. It is necessary to look into the amplitude values of all the images in the data set, in order to understand exactly what was seen by the satellite at the time of each acquisition.

If a target has experienced significant change in its surface characteristics it will exhibit variation in its reflectivity (electromagnetic response) between two acquisitions. In such circumstances, the possibility of detecting movement by means of SAR interferometry is seriously compromised. The signal phase difference between the two images now contains not only the contribution due to displacement, but also that due to the change in the reflectivity of the target. This prevents, in the worst case, the obtaining of any useful information on ground movement.

Accordingly, it is necessary to look into the amplitude values of all the images in the data set, in order to understand exactly what was seen by the satellite at the time of each acquisition.

Another artifact linked to amplitude is known as speckle. Speckle is random noise that appears as a grainy salt and pepper texture in an amplitude image. This is caused by random interference from the multiple scattering returns that occur within each resolution cell. Speckle

has an adverse impact on the quality and usefulness of SAR images. However, the higher the number of images has taken of the same area at different times or from slightly different ‘look’ angles, the easier it is to reduce speckle. This increases the quality and level of details of the amplitude image enabling it to be used as a background layer for observing the presence of PS results.

The Multi Image Reflectivity (MIR) map is the means by which speckle reduction is accomplished. Averaging a number of images tends to negate the random amplitude variability, leaving the uniform amplitude level unchanged (Figure 4).

It should be emphasised that the information in the MIR map is the reflectivity of each pixel, i.e. the ability to backscatter the incident wave toward the satellite. Flat surfaces (roads, highway, rivers, and lakes) act like a mirror, meaning that if their orientation is not exactly perpendicular to the incident wave negligible energy is reflected back to the sensor; they appear dark in the image. On the other hand, because of their irregular physical shape, metal structures or buildings reflect a significant portion of the incident signal back to the radar, resulting in very bright pixels in the MIR map.

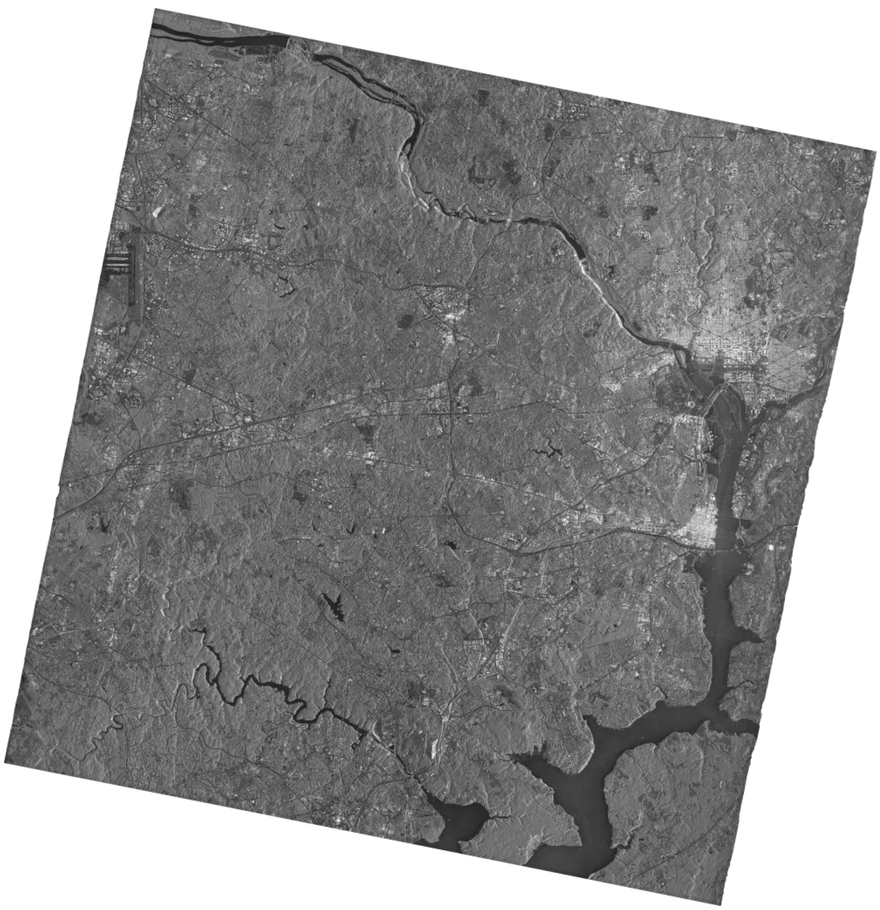

Figure 4: Multi-image reflectivity map of the descending CSK data set over NOVA and most of Washington D.C areas.

Interferograms

After the statistical analyses of the SAR images have been completed, a set of differential interferograms is generated. This entails subtracting the phase of each slave image from the phase of the master image. In doing so, the difference in signal path length between the two images is calculated. This difference is related to possible ground motion.

In any SAR image, there are embedded topographic distortions that arise during image acquisition. These are removed using a reference Digital Elevation Model (DEM), leaving ground movement and the signal phase distortions arising from atmospheric effects as the only embedded variables.

The differential interferograms represent the starting point for applying the PSInSAR approach.

Estimation of the Atmospheric Effects

When a radar signal enters and exits a moisture-bearing layer in the atmosphere, its wavelength can be affected, introducing potential errors into the signal path length. The removal of atmospheric impacts is fundamental for increasing the precision of ground movement measurement.

A sub-set of pixels, usually corresponding to buildings, lampposts, antennas, small structures and exposed rocks, is chosen from among those that have high PSI values. These are referred to as PS Candidates (PSC). PSC density is, of course, higher in towns and cities rather than in forests and vegetated areas. However, it is often possible to obtain good PSC density in rural areas.

For each image, the atmospheric impacts are estimated at each PSC location. The process is statistically based and benefits in accuracy by the greater the number of available images for the analysis. By comparing the atmospheric contribution on neighboring pixels that would be experiencing the same atmospheric conditions, the atmospheric contribution can be reconstructed over the whole image.

The processed data set allows identification of a PSC cluster dense enough to identify and extract the atmospheric contribution over the entire area of interest.

Post-processing

In this stage the processed data undergoes a thorough quality control following ISO 9001:2000 guidelines. The PS data is checked for anomalies, aligned on an optical image layer usually provided by the client and the final report is prepared.

Appendix 6: Abbreviations and Acronyms

AOI	Area Of Interest
DInSAR	Differential Interferometry
DS	Distributed Scatterer (s)
GIS	Geographic Information System
InSAR	Interferometric SAR
LOS	Line Of Sight
MIR	Multi-Image Reflectivity
PS	Permanent Scatterer(s)
PSInSAR™	Permanent Scatterer SAR Interferometry is a worldwide Polytechnic University of Milan Trademark
SAR	Synthetic Aperture Radar
SqueeSAR™	The most recent InSAR algorithm patented by TRE
TRE	Comprehensive term for Tele-Rilevamento Europa and TRE Canada
TS	(Permanent Scatterer Displacement) Time Series

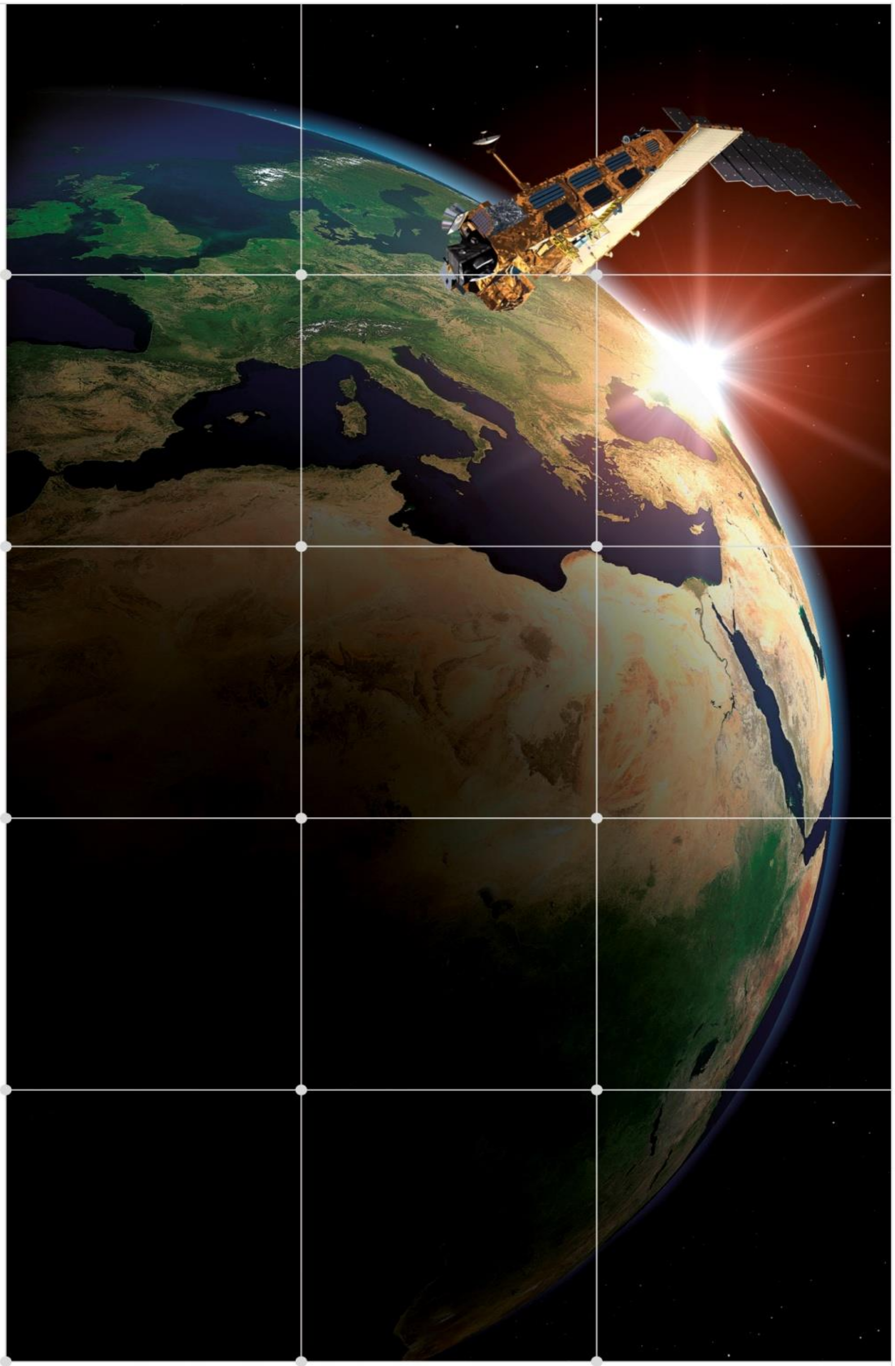

Appendix E – AOI2 – NOVA: SqueeSAR report (June 2015)

TRE – **Analysis of ground movements over Northern Virginia and Washington DC using SqueeSAR – Final Report** – June 2015 [download][8]

TRE – **Analysis of ground movements over Northern Virginia and Washington DC using SqueeSAR – Final Report - Technical Appendix** – June 2015 [download][9]

[8] http://viva-lab.ece.virginia.edu/elecdocs/ritars14/NOVA_Jun15.pdf
[9] http://viva-lab.ece.virginia.edu/elecdocs/ritars14/NOVA_Jun15_TA.pdf

Analysis of Ground Movement over Northern Virginia and Washington D.C. using SqueeSAR

Site 2 - Second Report

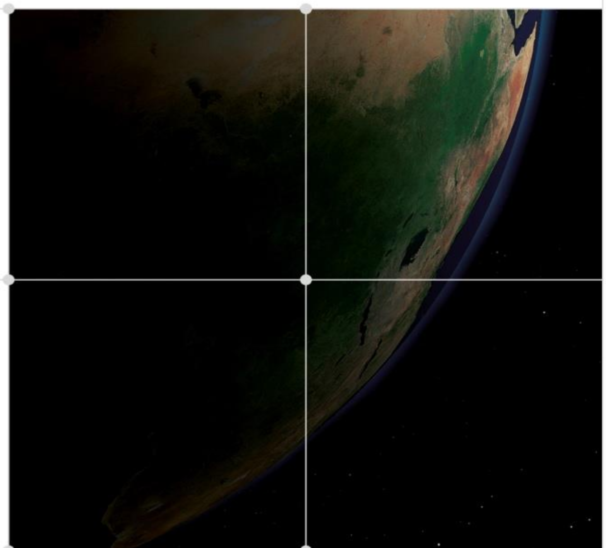

TRE®
Sensing the Planet

Submitted to:
University of Virginia
1001 N. Emmet St.
PO Box 400195
Charlottesville, Virginia 22904
USA

Prepared by:
TRE Canada Inc.
Suite 410, 475 West Georgia Street
Vancouver, B.C., V6B 4M9
Canada

Prepared by: Vicky Hsiao
GIS Analyst
TRE Canada Inc.
(signature)

Approved by: Giacomo Falorni
Operations Manager
TRE Canada Inc.
(signature)

Doc. Ref.: JO14-3014-REP2.0
4th September 2015

Executive Summary

This report describes the approach and results of the InSAR analysis carried out to measure surface deformation in Northern Virginia and a portion of Washington D.C. (Site 2) for the project "InSAR remote sensing for performance monitoring of transportation infrastructure at the network level" (RITARS-14-H-UVA). The results provide an overview of ground movement over a 15-month period.

The following points summarize the key findings of the analysis:

- Two areas exhibit interesting surface deformation patterns within the AOI.
    - Subsidence is observed in the area of Hill East and Capitol Hill, with rates of -12.4 mm/yr on average, and up to -33.7 mm/yr in the vicinity of RFK stadium and along the Anacostia River. The subsidence pattern appears to correspond with the path of the Anacostia River Tunnel project (§5.1.1).
    - An interesting uplift pattern with well-delineated boundaries is observed in the area of Alexandria, VA, SW Washington DC, and Forest Heights, MD, with up to +20.3 mm/yr (§5.1.2).
- No significant deformation was found over the following features indicated by UVA/VDOT:
    - The bridge of I-66 EB CD Road over Rte. 286 Fairfax County Pkwy.
    - The retaining wall along I-395 SB at King Street.
- A separate analysis was performed over the Woodrow Wilson Bridge (§5.1.3) to separate thermal contraction/expansion from other deformation signals. Compensation of the thermal effects highlights limited residual displacements.
- Subsidence was detected along the Silver Line metro in Vienna, VA (§5.2).
- A surface cross-section analysis highlights the evolution of horizontal profiles of the ground surface over time over certain features of interest (5.3).
- A total of 3.6 million measurement points was obtained from the data processing, providing a density of 2,278 points per square kilometre (5,899 points per square mile).
- The precision of the measurements has improved from ±5.9 to ±2.3 mm/yr.

The deliverables for the project include the present report, which describes the results of the data processing, a technical appendix and a CD containing the displacement data.

Table of Contents

1 Introduction

The University of Virginia VIVA lab is leading a research project with the Virginia Research Transportation Council and TRE Canada entitled "InSAR remote sensing for performance monitoring of transportation infrastructure at the network level " (RITARS-14-H-UVA). The work was awarded to the University of Virginia as a research grant funded by the Commercial Remote Sensing and Spatial Information Technology Application Program, RITA Phase V.

One of the main objectives of this project is to systematically extract consistent and reliable information on road subsidence, bridge monitoring, slope stability, sinkhole development and pavement conditions from InSAR data. TRE Canada Inc. (TRE) has been contracted to perform the InSAR work using our SqueeSAR algorithm. Cosmo-SkyMed (CSK) radar satellite imagery has been acquired on a 16-day interval over the site 2 area of interest (AOI) in Northern Virginia.

The AOI corresponds to a full CSK radar scene, approximately 1,600 km^2 (618 square miles) in size, covering northern Virginia (NOVA), and includes most of the Washington, D.C. metropolitan area (Figure 1). The AOI contains a high density of urban and transportation infrastructure, including numerous bridges, areas with slope stability issues, and routes with some of the highest traffic volumes in Virginia, which facilitates the evaluation of road response to high traffic loading (subsidence and pavement conditions). These man-made structures often yield a high number of measurement points, while areas of dense vegetation such as active agriculture and steep slopes tend to produce a lower density of measurement points.

Figure 1: The Area of Interest (AOI).

2 Radar data

All images were acquired by the Cosmo-SkyMed (CSK) constellation from a descending orbit with a 16-day frequency. See Table 1 for more information regarding the radar imagery. A total of 28 images were processed between 17 March 2014 and 19 June 2015, covering a period of 15 months (Table 2). Additional information on the satellite parameters can be found in the Technical Appendix.

Radar Data Information	
Constellation	Cosmo-SkyMed (CSK)
Resolution	3m x 3m
LOS Off-Nadir Angle	24.03°
Orbit Direction	Descending
Track	87
Revisit Frequency	16 days
Period Covered by Imagery	28 March 2014 – 19 June 2015
Number of Processed Images	28

Table 1: Information regarding the radar imagery used in the analysis.

No.	Date	Interval	No.	Date	Interval
1	28 Mar 14		**14**	07 Nov 14	16
2	13 Apr 14	16	**15**	23 Nov 14	16
3	29 Apr 14	16	**16**	09 Dec 14	16
	15 May 14		**17**	25 Dec 14	16
4	31 May 14	32	**18**	10 Jan 15	16
5	16 Jun 14	16	**19**	26 Jan 15	16
	02 Jul 14		**20**	11 Feb 15	16
	10 Jul 14	24	**21**	27 Feb 15	16
6	18 Jul 14	8	**22**	15 Mar 15	16
7	03 Aug 14	16	**23**	31 Mar 15	16
8	19 Aug 14	16	**24**	16 Apr 15	16
9	04 Sep 14	16	**25**	02 May 15	16
10	16 Sep 14	12	**26**	18 May 15	16
11	20 Sep 14	4	**27**	03 Jun 15	16
12	06 Oct 14	16	**28**	19 Jun 15	16
13	22 Oct 14	16			

Table 2: Dates of the CSK image acquisitions. Image dates in orange were discarded during the data processing due to strong atmospheric noise, while those in red were not acquired, and those in blue indicate dates where additional images were acquired. Image dates shaded in gray are new images for this data processing.

3 Data Processing

A total of 28 images were processed for the second monitoring period, leading to a significant increase in the number (over 3.6 million) and density (2,278 per square kilometre - 5,899 per square mile) of measurement points. Measurement precision improved from ±5.9 to ±2.3 mm/yr. Table 3 summarizes the statistics of the results.

The current data processing has led to an increased coverage in terms of measurement point distribution, including the SE corner of the AOI. While in the previous processing no points were identified in this area, the increased number of available radar images and corresponding increase in statistical robustness of the data has led to the identification of a substantial number of points. The data sets are divided into two clusters separated by the Potomac River, each with its own reference point. Further statistics summarizing the results of the data processing can be found in the Technical Appendix.

Attribute	1st Monitoring Analysis	2nd Monitoring Analysis	
		Cluster 1	Cluster 2
Dates	28 Mar 2014 – 22 Oct 2014	28 Mar 2014– 19 Jun 2015	
Period covered (months)	7	15	
N. of images processed	13	28	
N. of PS	962,627 (77%)	2,450,337 (68%)	10,296 (54%)
N. of DS	148,536 (23%)	1,174,712 (32%)	8,765 (46%)
Total N. of Measured Points (PS and DS)	1,249,506	3,625,049	19,061
Average PS and DS Density (per square km) Cluster 1 and 2 combined in the 1600 km^2 AOI	781 pts/km^2 (2022 pts/sq. mi)	2278 pts/km^2 (5899 pts/sq. mi)	
Average Displacement Rate (mm/year)	-5.2	-0.15	0.00
Average Displacement Rate Standard Deviation (mm/year)	±5.9	±2.3	±1.0
Average Acceleration Rate (mm/$year^2$)	5.8	-0.2	-1.3
Average Acceleration Rate Standard Deviation (mm/$year^2$)	±78.8	±13.1	±5.9

Table 3: Data processing statistics.

Reference Point

SqueeSAR™ is a differential technique, meaning displacement is measured compared to a reference point that is assumed to be stable. The reference points were selected using an optimization procedure that performs a statistical analysis of all targets and selects a point with optimal radar parameters including high coherence, low standard deviation and low temporal variability over time. The use of this procedure ensures the highest possible measurement quality is obtained. The reference points selected for this analysis are shown in Figure 2.

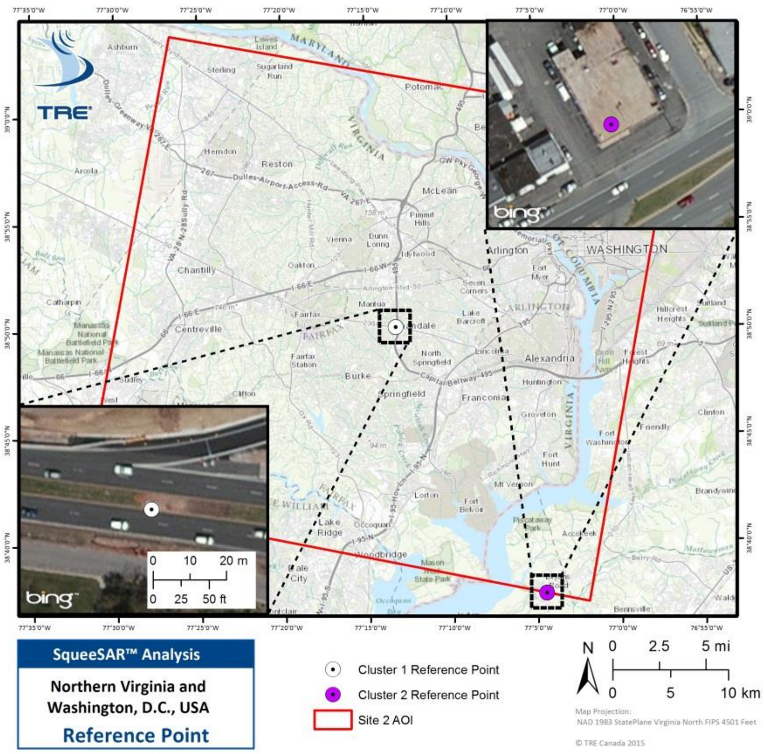

Figure 2: The location of the reference points.

Cluster 1 (E: -77.221521, N: 38.83506), Cluster 2 (E: -77.074654, N: 38.626708).

4 Results of the SqueeSAR™ analysis

4.1 Cumulative Displacement

The total amount of displacement measured during the 15-month period is shown below (Figure 3). Each point corresponds to a PS or DS, and is color-coded according to the magnitude and direction of total movement. Movement is measured along the satellite line-of-sight (LOS) relative to the first image (28 March 2014) of the data stack.

Cumulative displacement ranges from 89.5 mm of subsidence to 31.0 mm of uplift. Areas of deformation were identified at Hill East (Washington, DC), Alexandria (VA), and Forest Heights (MD), with average cumulative displacements of -13.5 mm, +6.8 mm, and +10.8 mm, respectively.

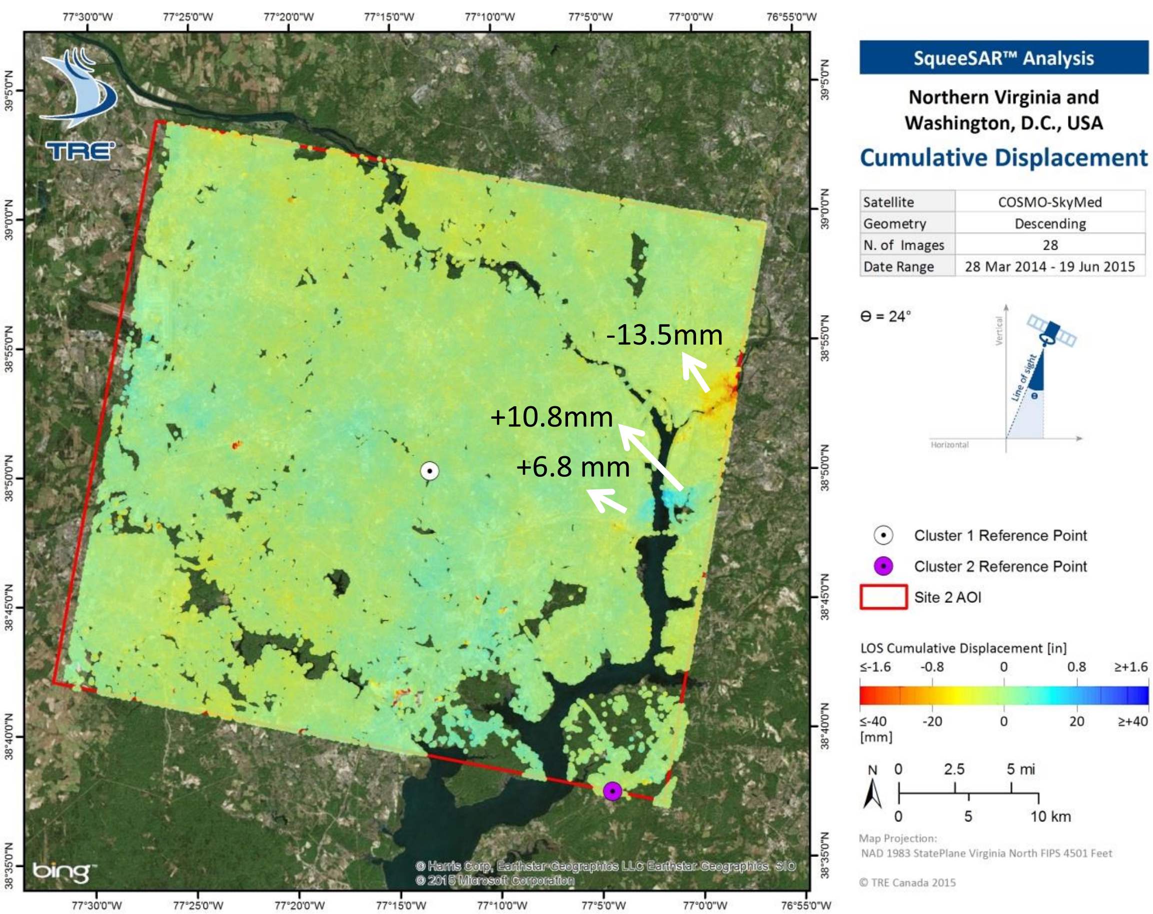

Figure 3: Cumulative deformation, expressed in millimeters, from 28 March, 2014 to 29 June, 2015.

4.2 Displacement rate

The line-of-sight (LOS) displacement rates, expressed in mm/year, as detected from the processing of all images are shown below (Figure 4). Each point corresponds to a Permanent Scatterer (PS) or a Distributed Scatterer (DS), and is color-coded according to its annual rate of movement. Average displacement values are calculated from a linear regression of the ground movement measured over the entire period covered by the satellite images. Detailed information on ground motion is also provided by means of displacement time series, which are provided for each PS and DS.

The displacement rate distribution mirrors that of the cumulative displacement. Deformation rates range from -70.3 to +24.8 mm/yr.

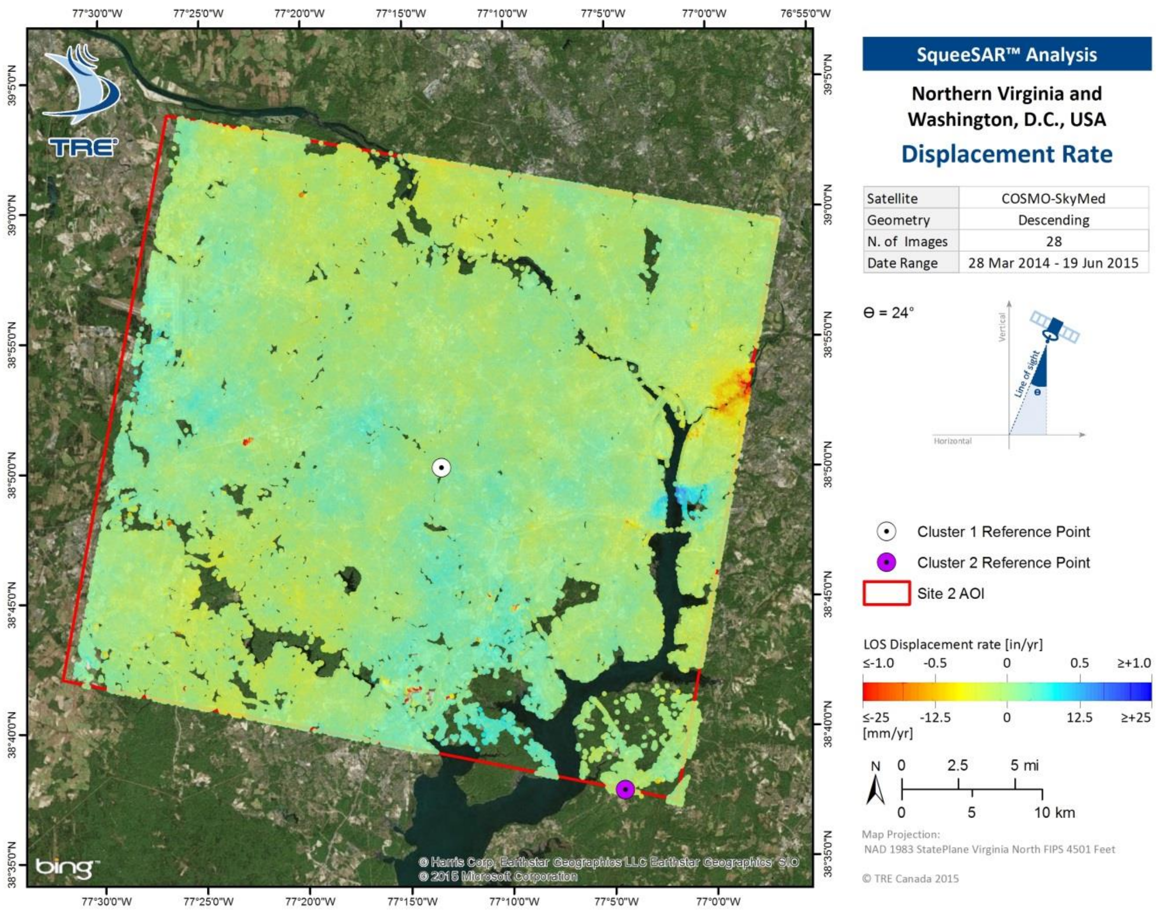

Figure 4: Deformation rates in mm/year.

4.3 Displacement Rate Standard Deviation

The standard deviation of the surface displacement data characterizes the error of the measurements (Figure 5). For this reason, any measurement should be interpreted in the form of Displacement Rate ± Standard Deviation. Standard deviation values tend to increase with distance from the reference point. Higher values indicate a greater variability in displacement rates and are often associated with areas of rapid and/or irregular ground movement.

The average standard deviation value of all measurement points within this data set is ±2.3 mm/year. Marginally higher values are concentrated in the SW portion of the AOI.

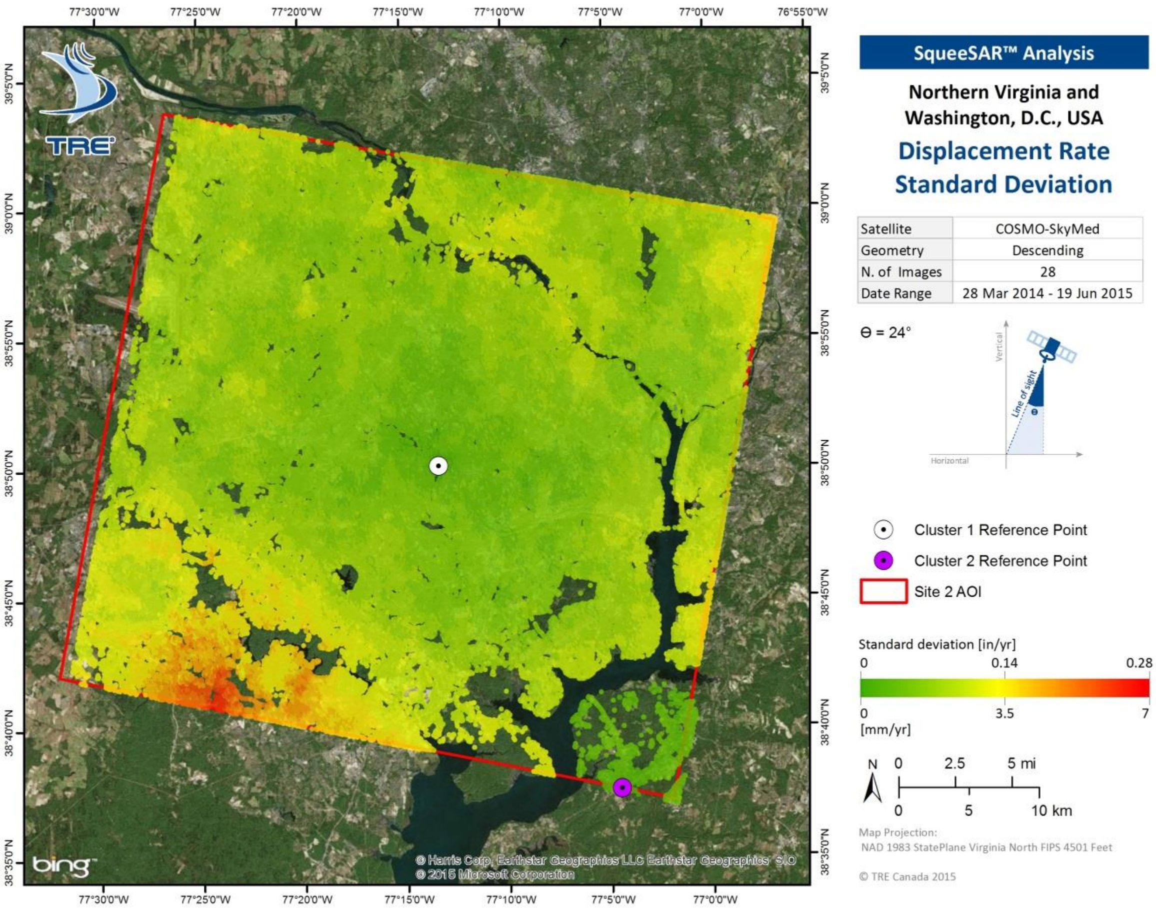

Figure 5: Standard deviation values of the displacement rates.

5 Observations

The observations focus on areas exhibiting particular deformation patterns or localized ground movement that occurred in proximity of the transportation network. The former include larger areas such as Hill East and Capitol Hill, Washington, DC, Alexandria, VA and Forest Heights, MD(§5.1). Local deformation was detected along infrastructure, such as the Silver Line Metro and Capital Beltway (§5.2). A cross-section analysis highlights the evolution of horizontal profiles of the ground surface over time in areas of interest (§5.3).

5.1 Features of Interest

The features comprise areas specified by the Virginia Department of Transportation (VDOT) and University of Virginia (UVA) as well as areas with unique deformation patterns (Figure 6). The features from west to east are: the bridge of I-66 EB CD Road over Rte. 286 Fairfax County Pkwy; the retaining wall on I-395 SB at King Street in Shirlington VA; Hill East and Capitol Hill in D. C.; Alexandria, VA, SW Washington DC, and Forest Heights, MD and the Woodrow Wilson Bridge respectively. A summary of the findings is organized in Table 4 and Table 5, with selected locations highlighted in detail in §5.1.1 to §5.1.3.

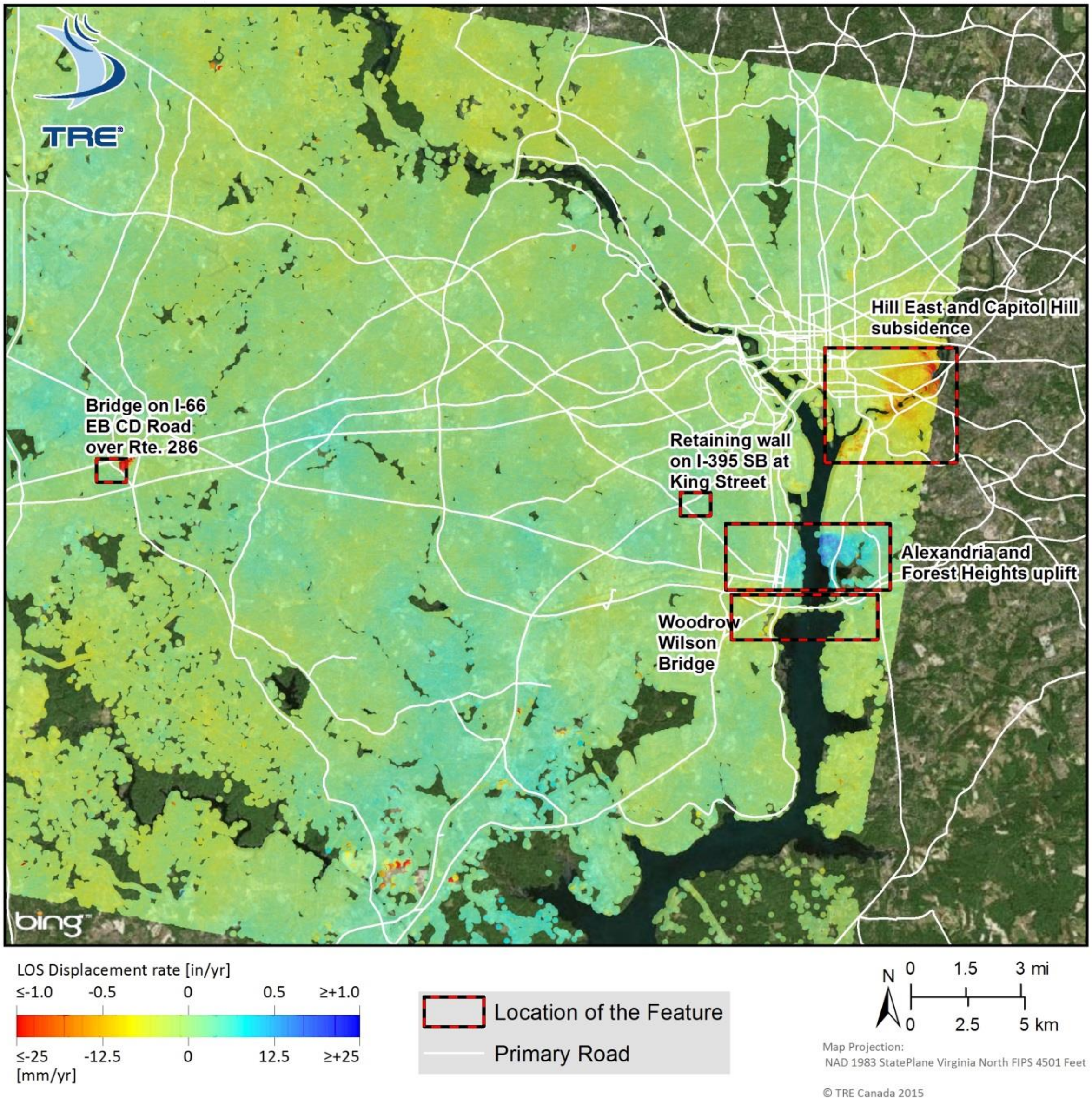

Figure 6: The locations of the features of interest.

Feature	Coordinates (N, E)	Description and Summary of Findings	Displacement Rate Range (mm/yr)
I-66 Bridge over Rte. 286 Fairfax County Pkwy	(38.854, -77.389)	According to a Bridge Inspection Report from July 2014, MSE panels settled up to 76.2 mm (3 inches) on an abutment of the I-66 bridge. No measurement points were obtained on the MSE wall due to the satellite geometry. Two points on the bridge show rates of -0.2 and -0.6 mm/yr. Unrelated ground deformation was detected on a landfill at the I-66 Transfer Station approximately 1 km east of the bridge, where deformation rates up to -70.3 mm/yr were observed.	-1.2 to +2.3
Retaining wall on I-395 SB at King Street in Shirlington, VA	(38.836, -77.094)	H-piles (vertical steel beams) were built in early March 2014, just prior to the start of the InSAR monitoring, to stabilize a failing retaining wall. InSAR indicated that no discernible movement occurred on the retailing wall, the slope, or the residential area behind the wall since the repair.	-0.1 to +5.0
Hill East and Capitol Hill in D. C. **§5.1.1**	(38.886, -76.985) along Independence Ave SE (38.887, -76.970) along Anacostia River close to RFK Stadium	An interesting subsidence pattern was observed in the Hill East and Capitol Hill areas. Subsidence rates of up to -33.7 mm/yr were identified. The highest subsidence occurred in the RFK stadium area and along the Anacostia River. The subsidence trend along the Anacostia River appears to agree with the path of the Anacostia River Tunnel that is currently under construction.	-33.7 to +1.65

Table 4: Summary of the features found in the InSAR results. The first set of coordinates in column two provides the general location of the feature itself, while subsequent coordinates in the same cell indicate the locations of measurement points with major ground deformation.

Feature	Coordinates (N, E)	Description and Summary of Findings	Displacement Rate Range (mm/yr)
Alexandria, VA, SW Washington DC, and Forest Heights, MD **§5.1.2**	(38.812, -77.039) (38.818, -77.027)	An interesting uplift pattern was observed in Alexandria, VA, SW Washington DC, and Forest Heights, MD. Rates between +8.9 and +14 mm/yr were observed in Rivergate City Park and Marbury Point.	-1.3 to +20.3
Woodrow Wilson Bridge **§5.1.3**	(-77.156, 38.872) (-77.068, 38.799) Subsidence along Mill Rd on VA approach to WWB	Thermal expansion and contraction of the bridge was identified in the deformation time series. A separate detailed analysis was carried out over the WWB with the intent of removing the thermal effects in the time series. No significant residual deformation was detected on the bridge. A ramp 2 km (1.27 miles) from the bridge experienced subsidence.	-5.8 to +8.3 (on the bridge) -28.1to -0.7 (Ramp to the bridge)

Table 5: (Continues from Table 4) Summary of the features found in the InSAR results. The first set of coordinates in column two provides the general location of the feature itself while subsequent coordinates in the same cell indicate the locations of measurement points with major ground deformation.

5.1.1 Subsidence in Hill East and Capitol Hill, Washington, DC

An interesting subsidence pattern with deformation rates of over -12.4 mm/yr was identified at Hill East and Capitol Hill in Washington, DC. The subsidence starts in the RFK stadium area and covers North Carolina Ave SE to the embankment of the Anacostia River and extends to the Anacostia Fwy across the River (Figure 7). A ring-like pattern experiencing rates between -12.4 to -22.5 mm/yr was identified within this area (ATS 1 to ATS 5 in Figure 7, time series in Figure 9 and Figure 10). TRE suspects that at least a part of the observed subsidence derives from tunneling activities related to the DC Water Clean Rivers Project (https://www.dcwater.com/workzones/projects/anacostia_river_information_sheet.cfm), including the Anacostia River Tunnel that is currently under construction (Figure 8). Two localized areas (the Navy Housing Welcome Center and a parking lot (38.856 N, -77.007 W)) are also subsiding (ATS6 and ATS7 in Figure 7, time series in Figure 10 and Figure 11).

An area where construction appears to have started in early 2015, according to the DC Water and Sewer Authority, is adjacent to Nationals Park, the ballpark of the Washington Nationals. Here work is under way to build two diversion chambers and the main Pumping Station Drop Shaft. An average time series over the area of construction (ATS8 in Figure 12) appears to indicate the start of subsidence in March 2015 (Figure 13).

Detailed tunnel location maps and construction dates is required to perform a more precise analysis and correlate surface movement with the tunnelling activities.

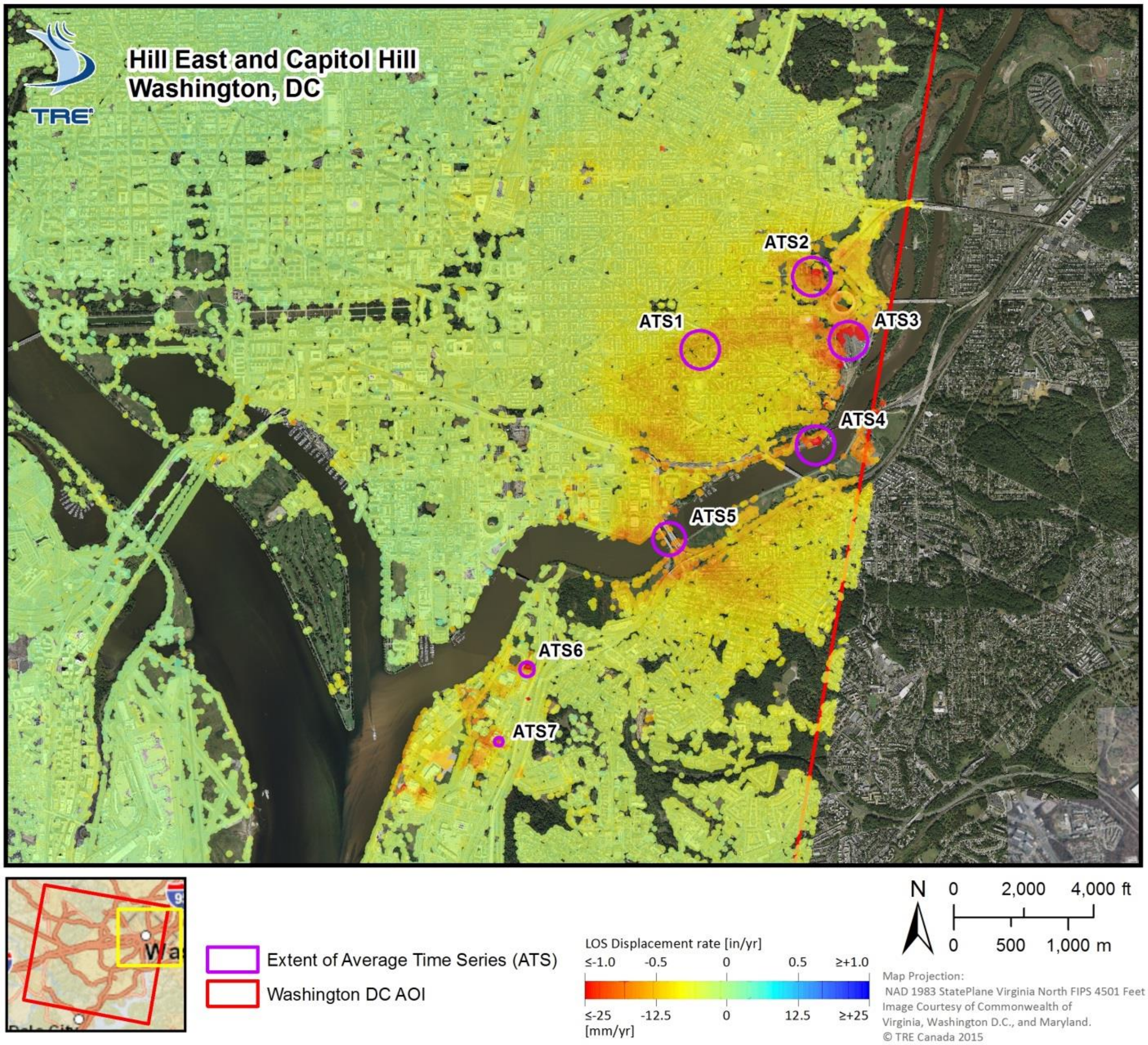

Figure 7: The SqueeSAR results over Hill East and Capitol Hill, Washington, DC.

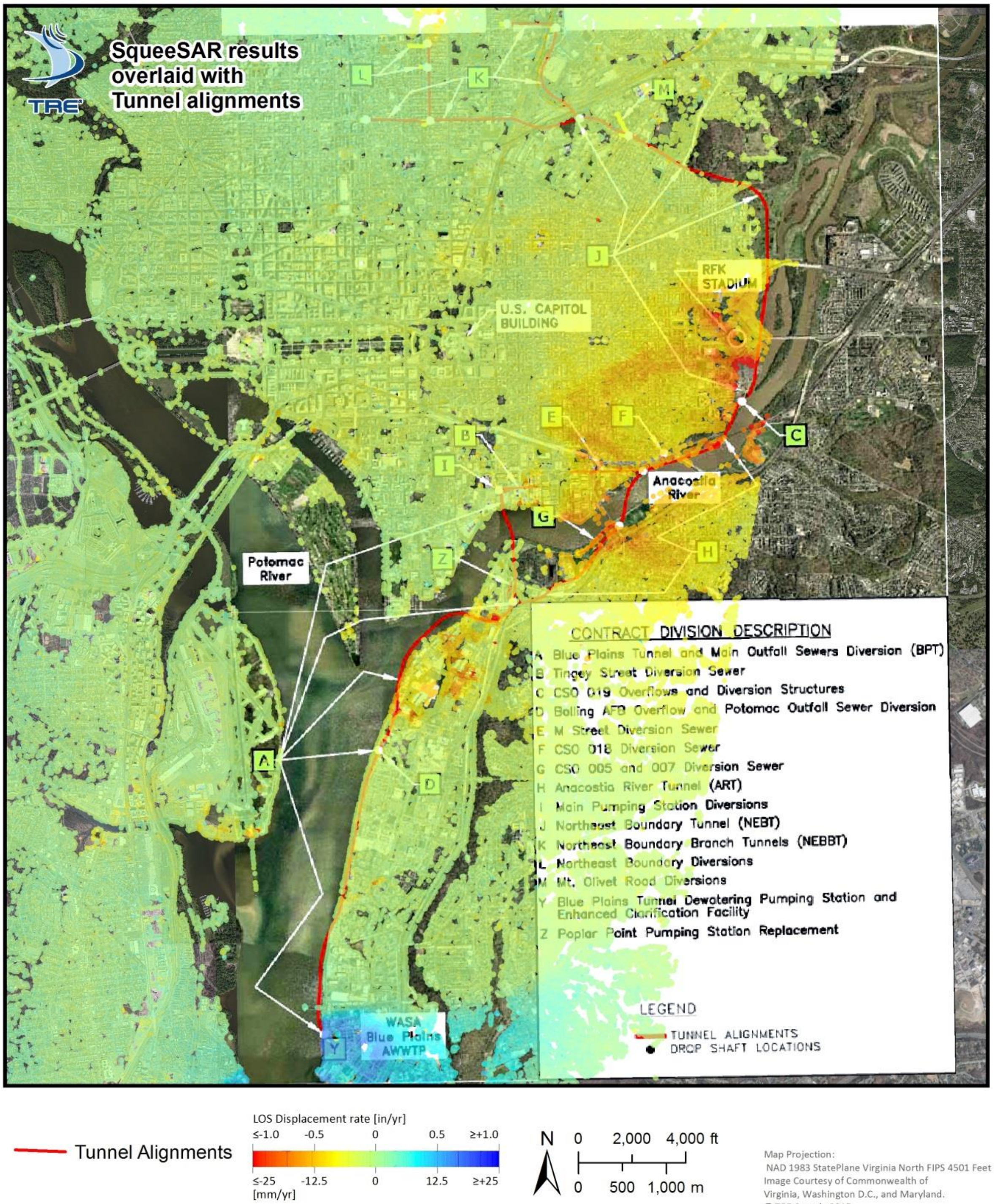

Figure 8: SqueeSAR results overlaid with Tunnel alignments. The estimated tunnel path is georeferenced from the Geotechnical Investigations for the Anacostia River Projects document.

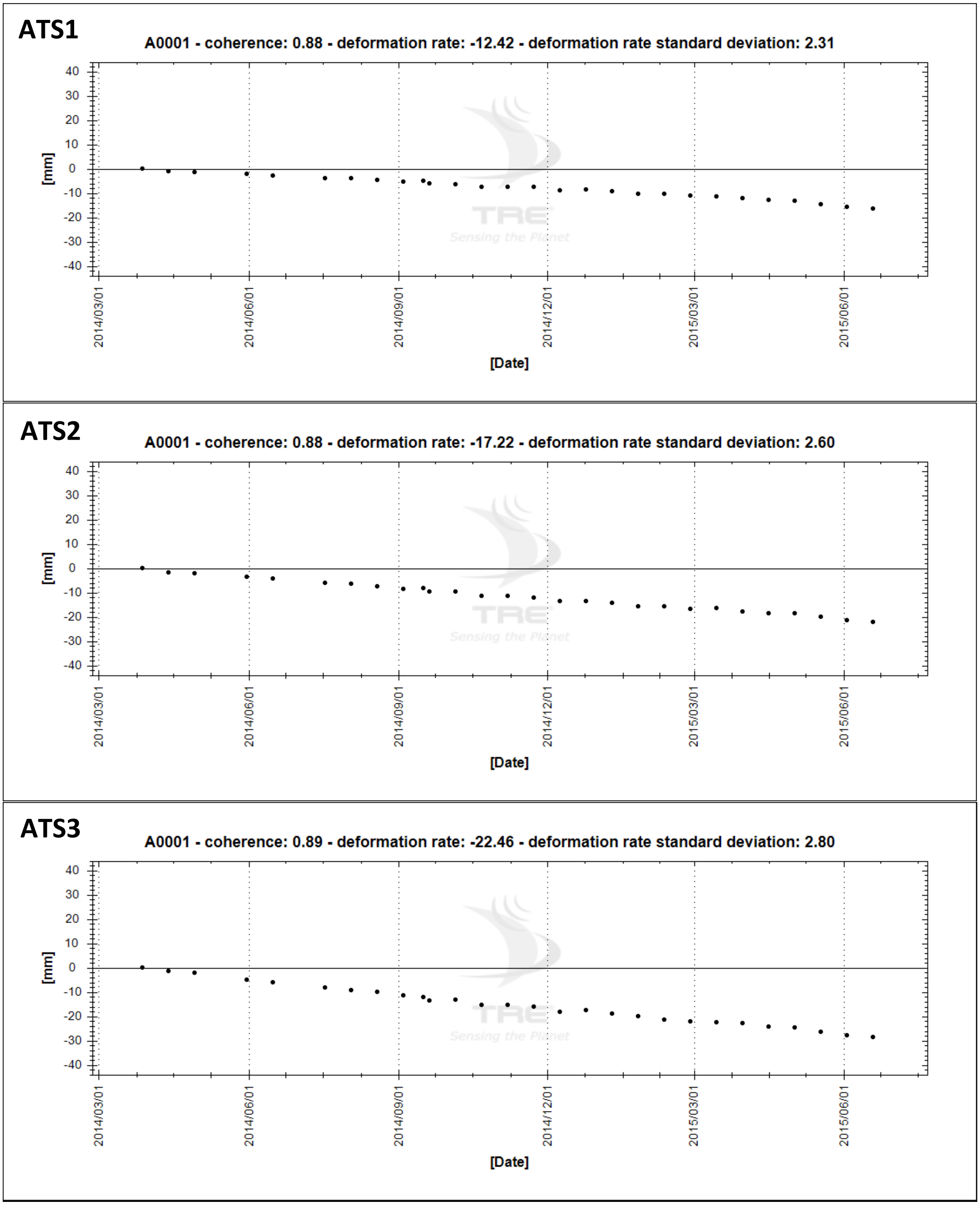

Figure 9: Average time series of ATS1 to ATS3 in Figure 7.

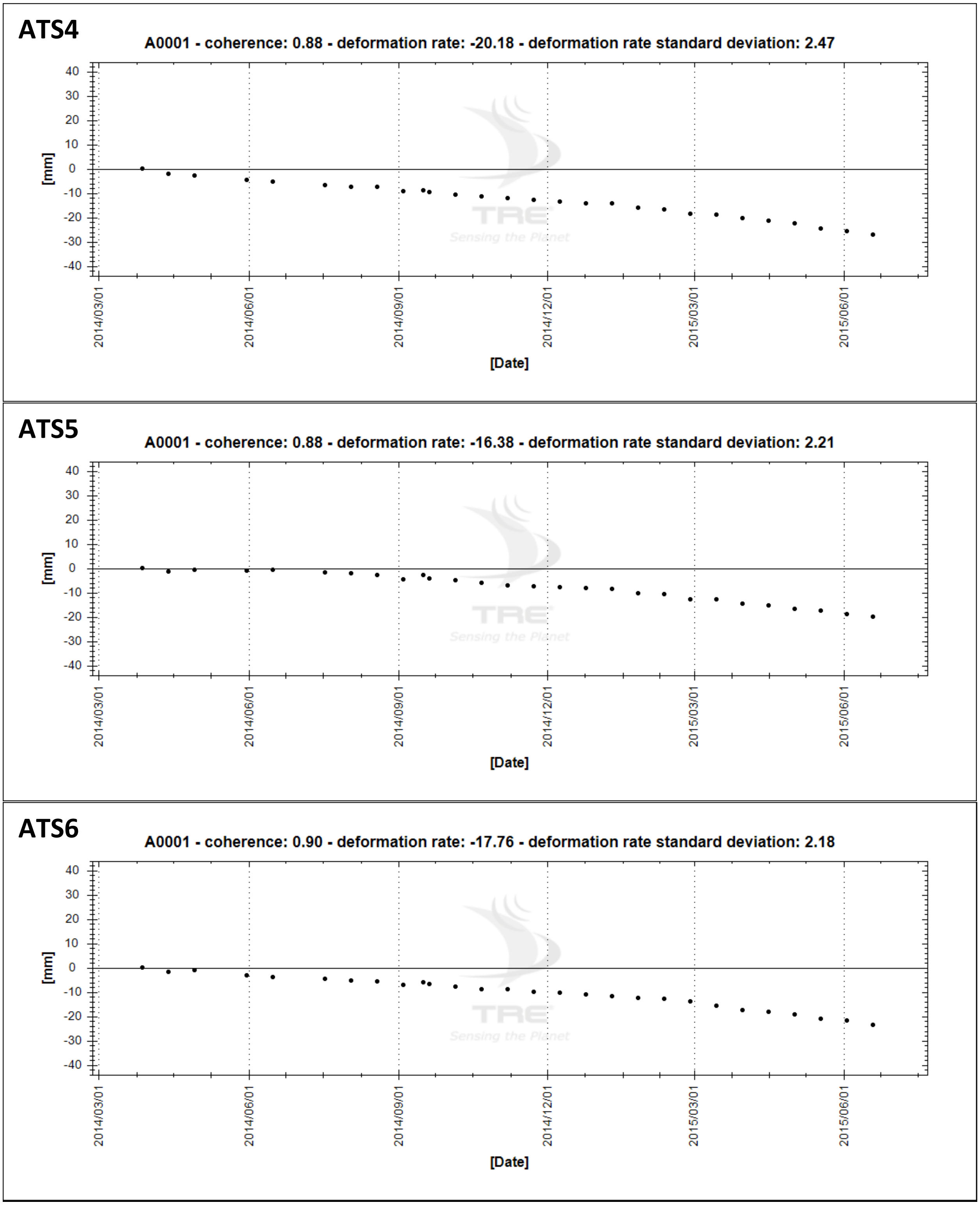

Figure 10: Average time series of ATS4 to ATS6 in Figure 7.

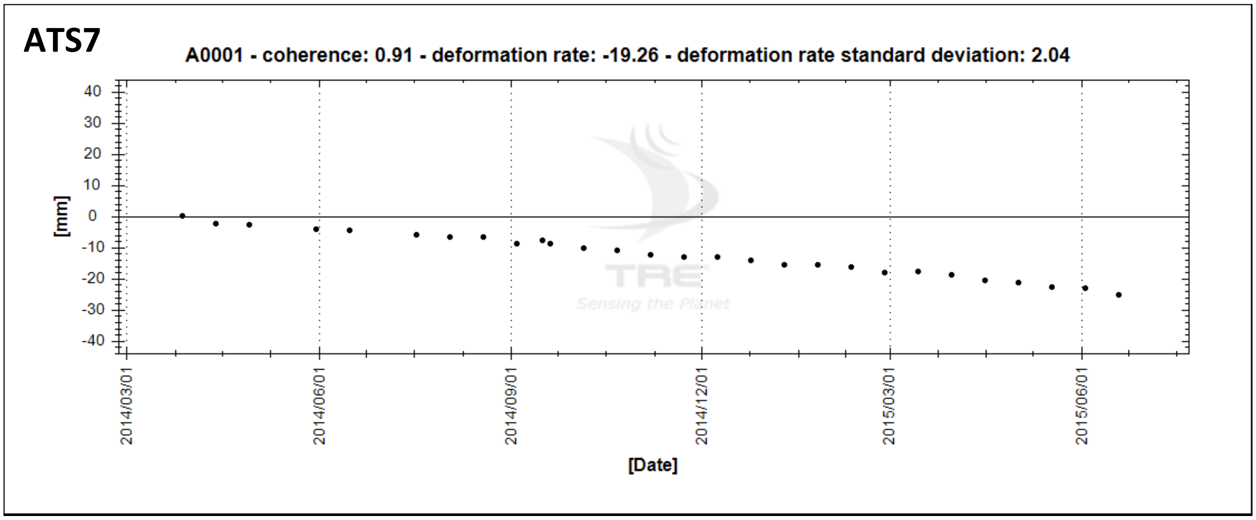

Figure 11: Average time series of ATS7 in Figure 7.

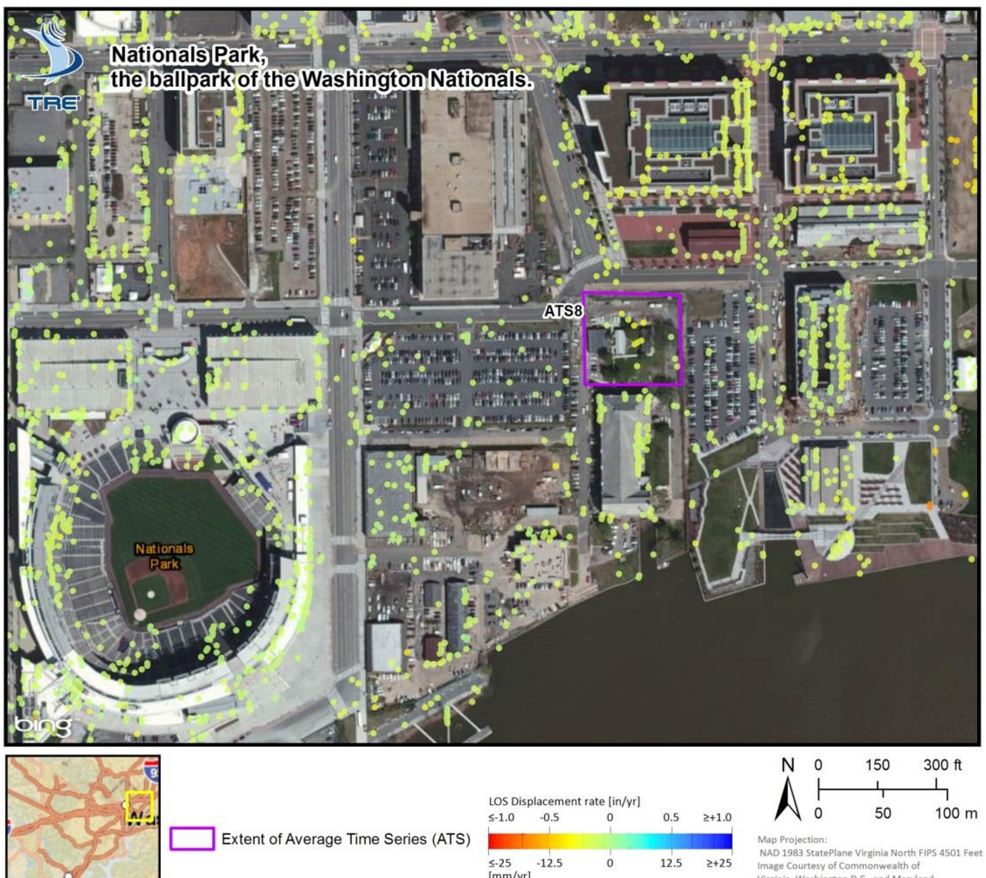

Figure 12: The SqueeSAR results over the area near the ballpark of the Washington Nationals.

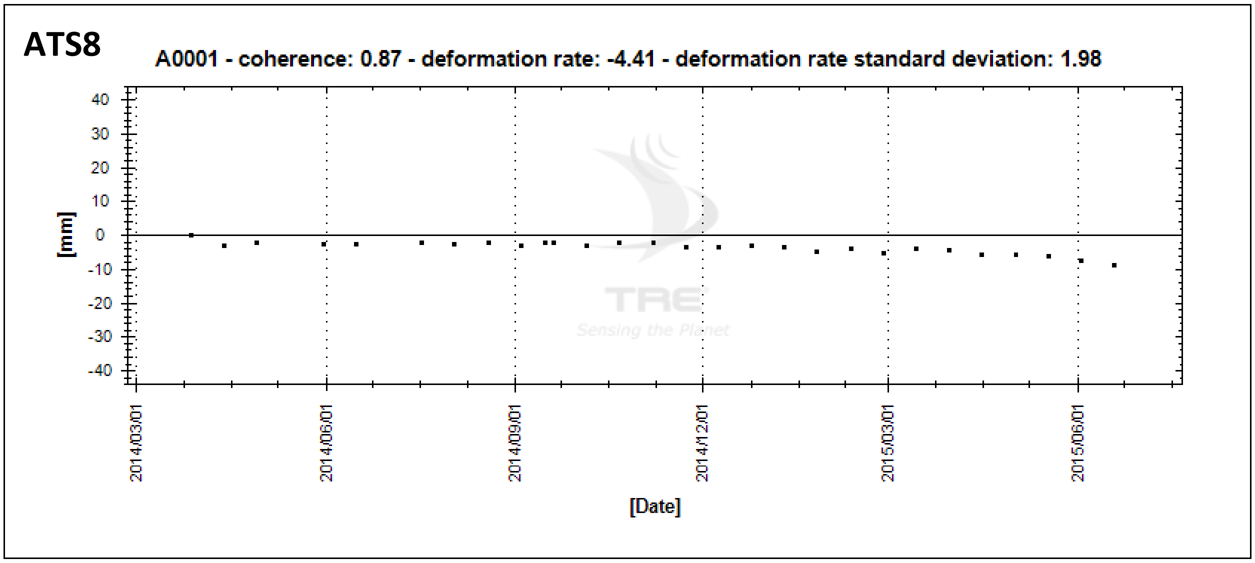

Figure 13: Average time series of ATS8 in Figure 12.

Snapshots of cumulative displacement taken at three month intervals from September 2014 to June 2015 show that the subsidence started in the RFK Stadium area and gradually extended west and along the Anacostia River over time (Figure 14). An animation file (.gif/ppt) illustrating the ground deformation over the AOI is included with the report.

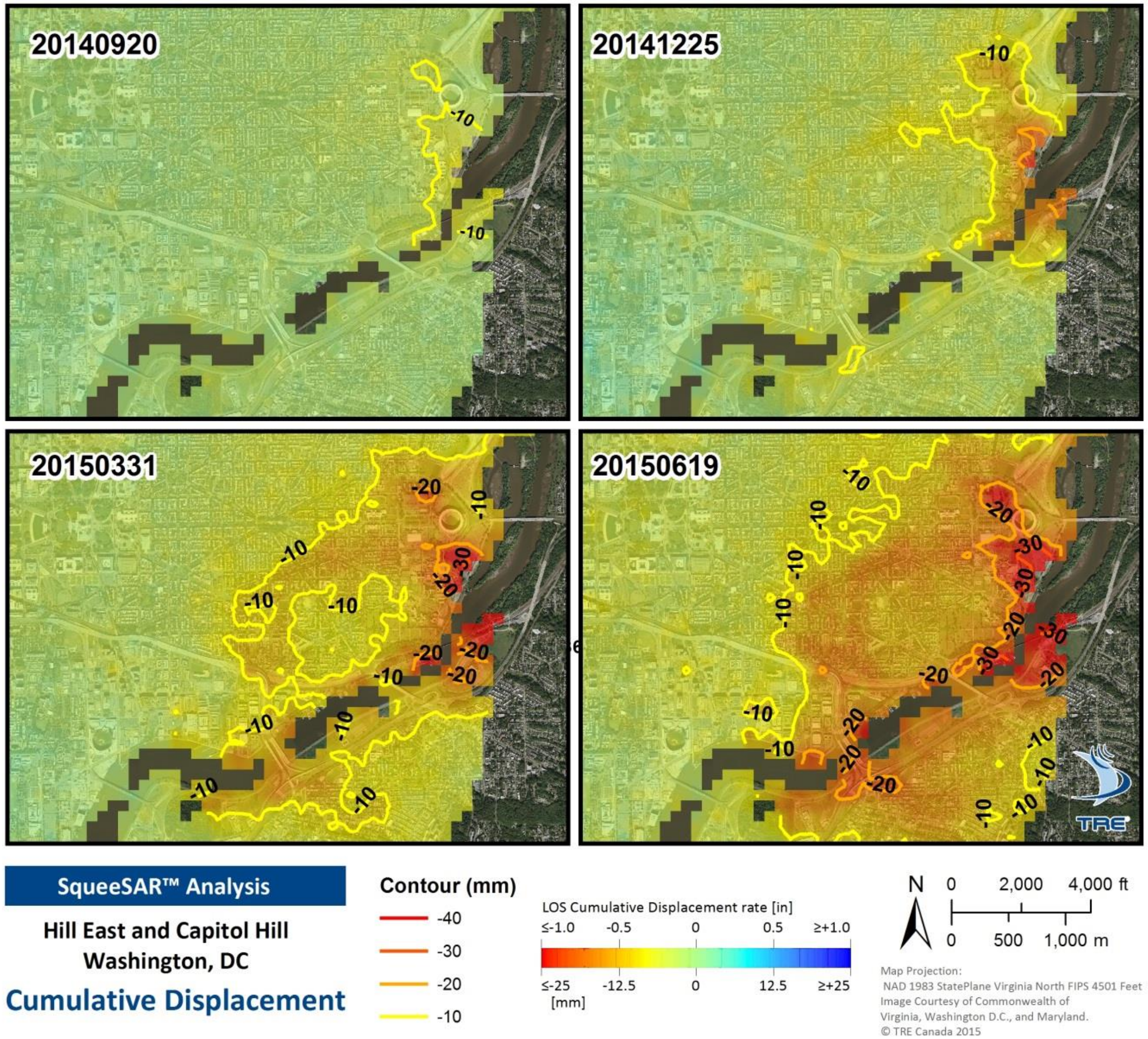

Figure 14: Cumulative displacement at 3-month intervals over Hill East and Capitol Hill, Washington, DC from September 2014 to June 2015.

5.1.2 Uplift in Alexandria, VA, SW Washington DC, and Forest Heights, MD

Apparent uplift (considering the 24 degree viewing angle of the satellite is mainly sensitive to vertical movement) was detected in Alexandria, VA, SW Washington DC, and Forest Heights, MD (Figure 15). The deformation began in late 2014, with the greatest movement observed close to Rivergate City Park in Alexandria, VA and in Marbury Point, Washington DC, with rates of +8.9 and +14.1 mm/yr, respectively (ATS1 and ATS2 in Figure 15, time series in Figure 16). Ground deformation was also measured on the Anacostia Fwy (I-295) connecting Washington DC and Maryland, with rates of +8.6 mm/yr (ATS3 in Figure 15, time series in Figure 16).

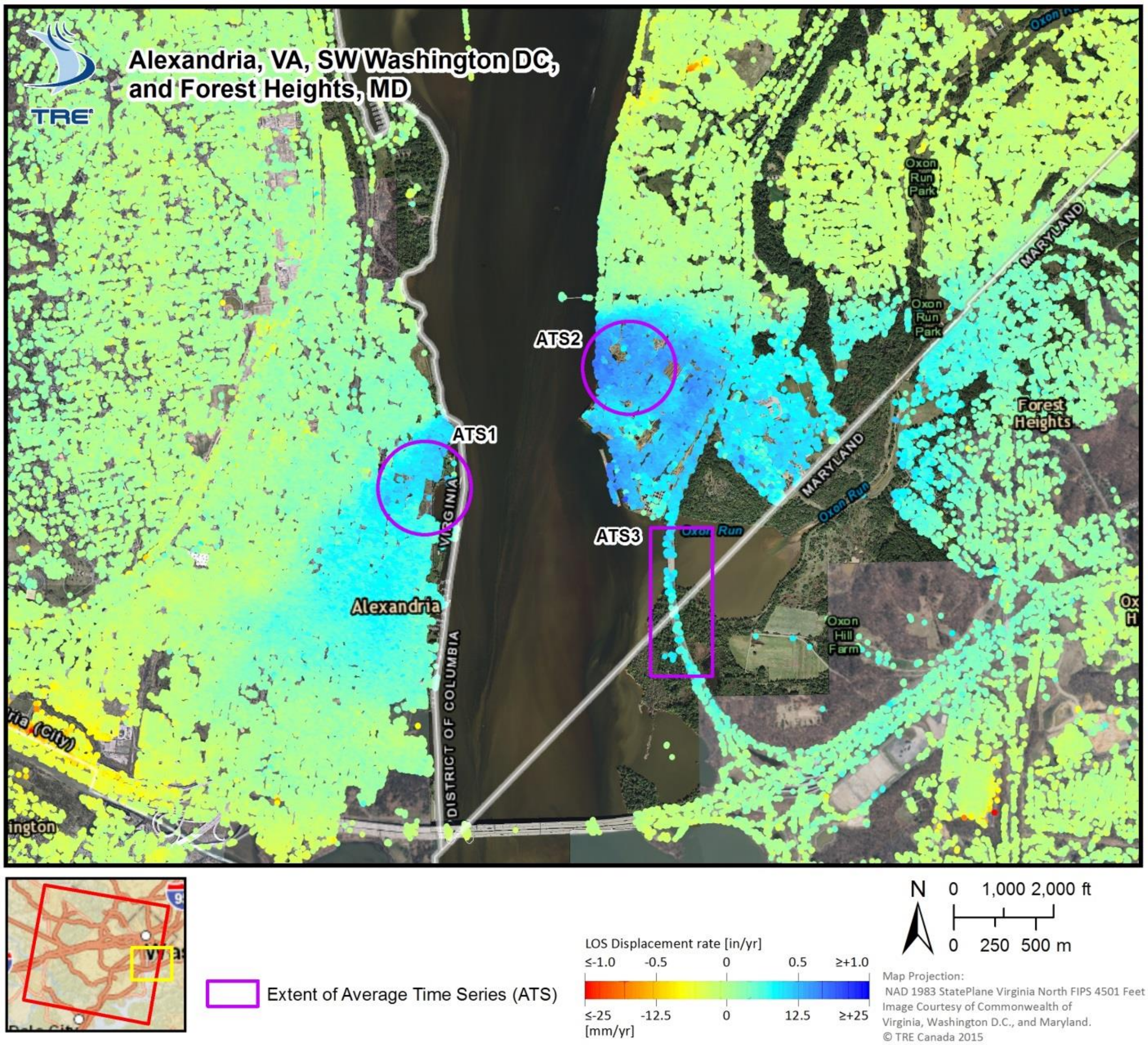

Figure 15: The SqueeSAR results over Alexandria, VA, SW Washington DC, and Forest Heights, MD.

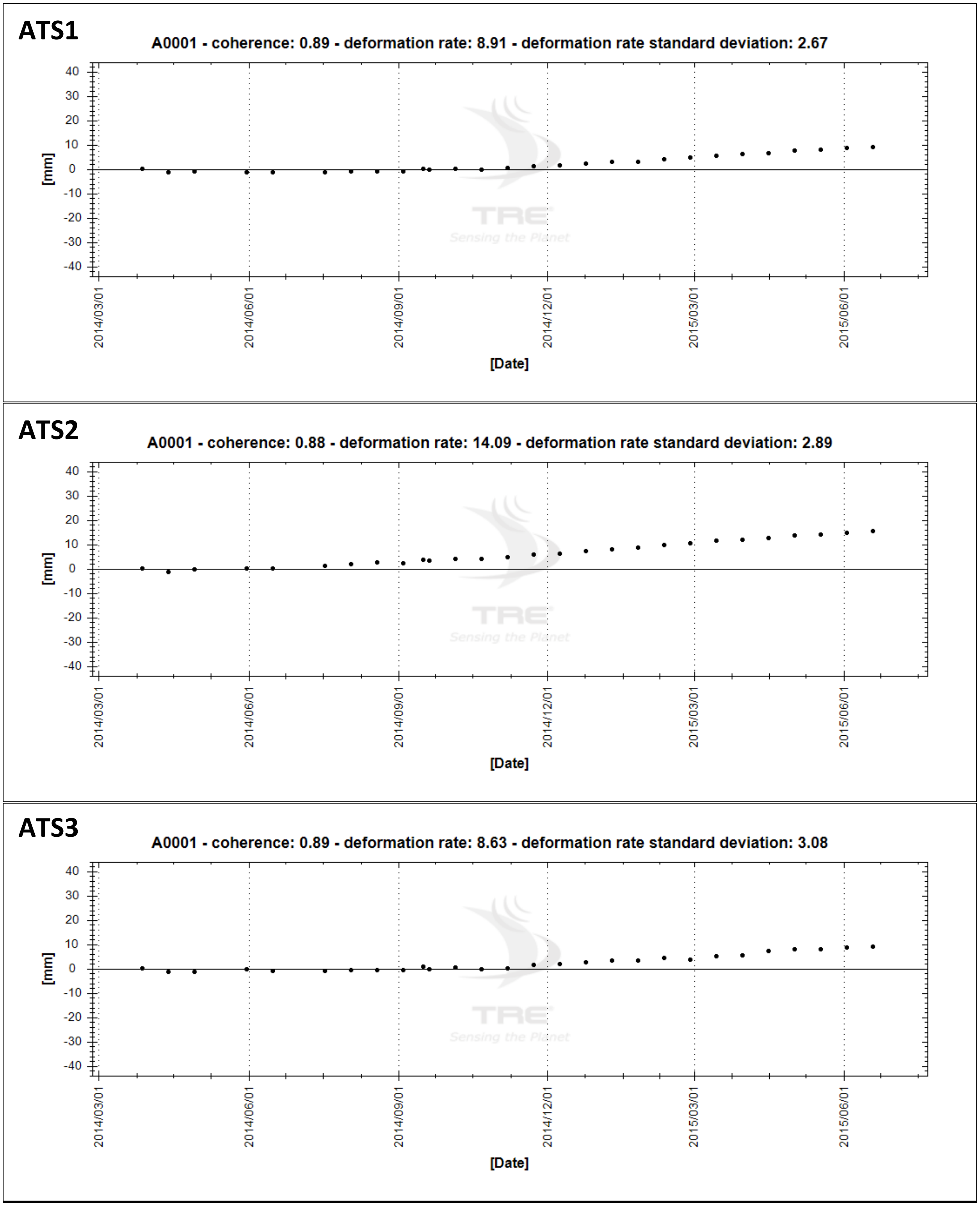

Figure 16: Average time series of ATS1 to ATS3 in Figure 15.

5.1.3 Woodrow Wilson Bridge

A separate analysis was performed on the Woodrow Wilson Bridge (WWB) to demonstrate the capabilities of InSAR for bridge monitoring. Bridges are linear infrastructure that expand and contract according to variations in temperature. This thermal expansion can produce significant deformation of the structure that can be measured by SAR interferometry. In the deformation results, the thermal expansion of the bridge is visible in the measurement point time series; as a result, this movement tends to mask any potential residual movement due to settling or other types of deformation. TRE attempted to compensate the thermal expansion/contraction cycles by correlating the average daily temperature with the deformation cycles and then removing this signal from the deformation time series. This led to the creation of a new parameter, VEL_TEMP, that should only contain the residual deformation.

An overview of the results over the Woodrow Wilson Bridge is shown in Figure 17. The top panel shows the deformation rate which contains the thermal expansion/contraction and exhibits a distinct pattern that oscillates between positive and negative values. Although measurements are 1-D (along the satellite line-of-sight) it is likely that this signature is caused by horizontal movement of the bridge structure as it expands and contracts thermally. In this case, negative rates indicate movement away (westward horizontal movement) from the satellite and positive rates are movement toward (eastward horizontal movement) the satellite.

The bottom panel in Figure 17 shows the residual deformation rate after removal of the thermal expansion component from the displacement time series. Several time series from polygons located on the bridge are shown in Figure 18 to Figure 20 with rates between -2.1 to +1.1 mm/yr. Deformation rates of -5.1 to +3.5 mm/yr were identified for individual measurement points on the bridge.

Figure 17: The SqueeSAR results over the Woodrow Wilson Bridge. Top panel represents results from the local bridge data processing with deformation rate with thermal expansion and contraction effects in the results and bottom panel shows deformation rate with thermal expansion and contraction effects removed, respectively. Note that this figure used a smaller colourbar (-10 mm/yr to +10 mm/yr) to display deformation rates changing between positive and negative values.

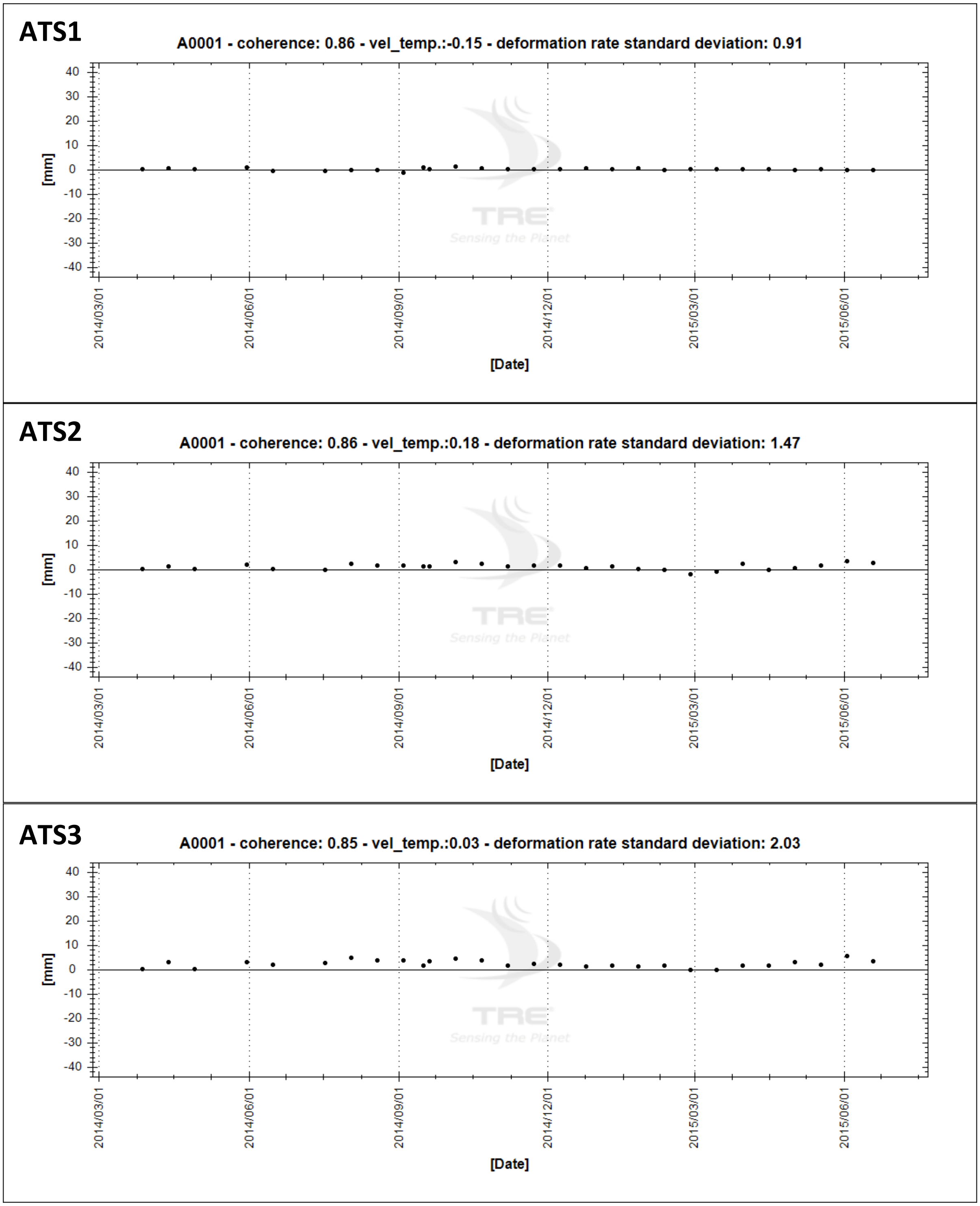

Figure 18: Average time series of ATS1 to ATS3 in Figure 17.

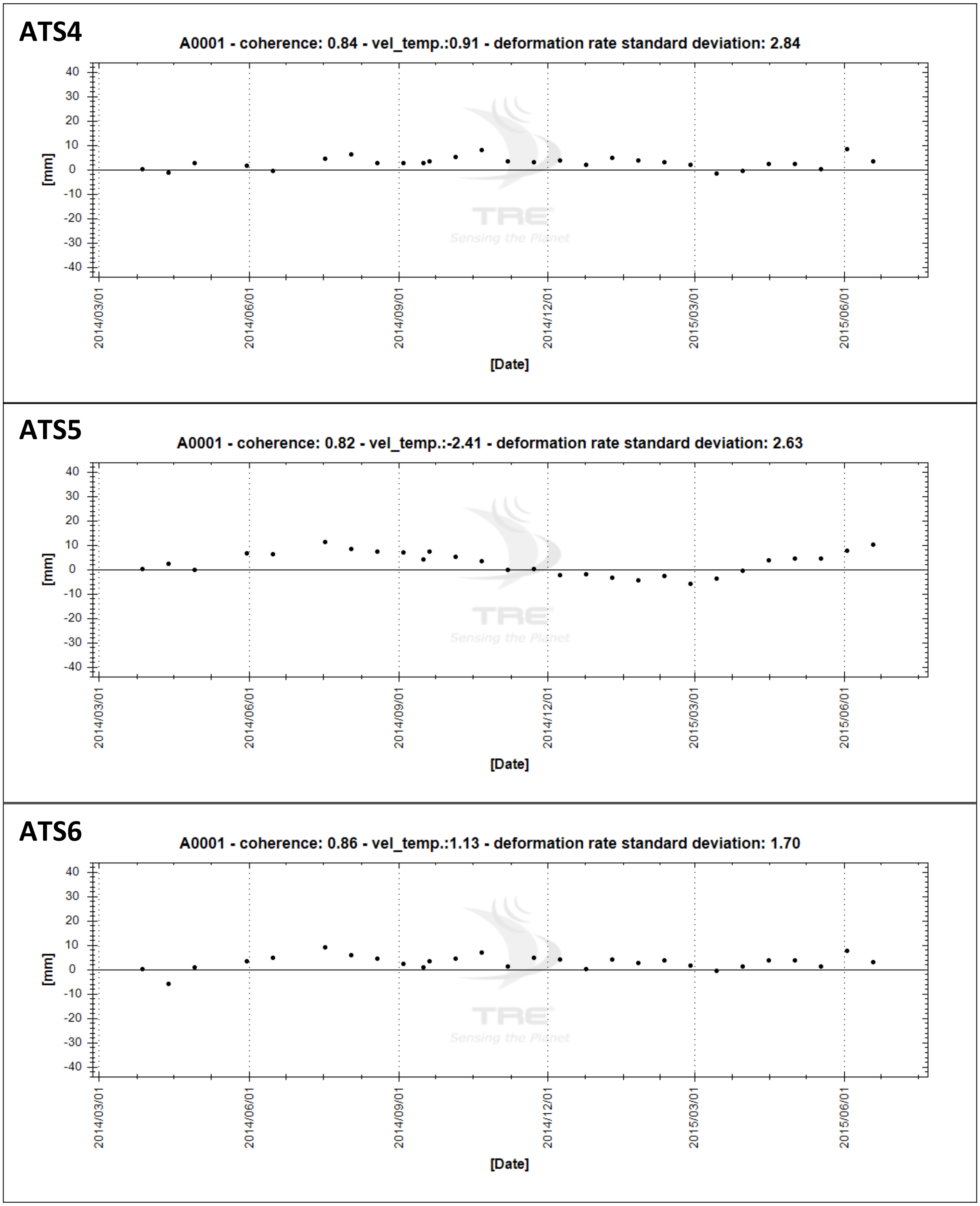

Figure 19: Average time series of ATS4 to ATS6 in Figure 17.

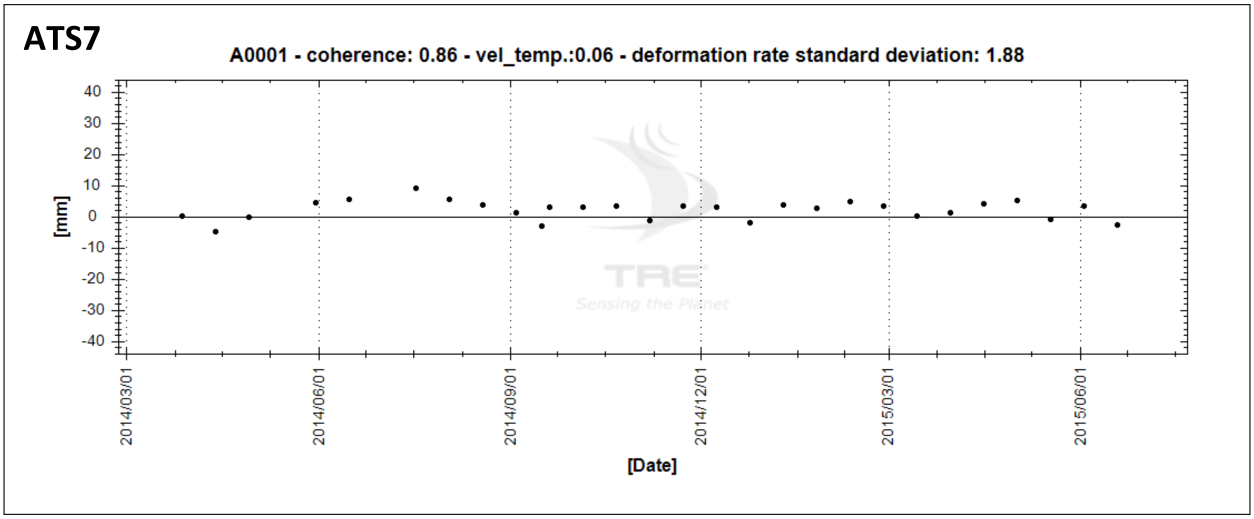

Figure 20: Average time series of ATS7 in Figure 17.

5.2 Results over Primary Roads

An inspection of subsidence on, or in close proximity of, major roads within the AOI was carried out to identify movement occurring within 50 meters (164 ft) of the primary roads.

Displacement rates for measurement points within the 50 m buffers are shown in Figure 21 for four sections of road. These may be of potential interest to VDOT and are described in Table 6.

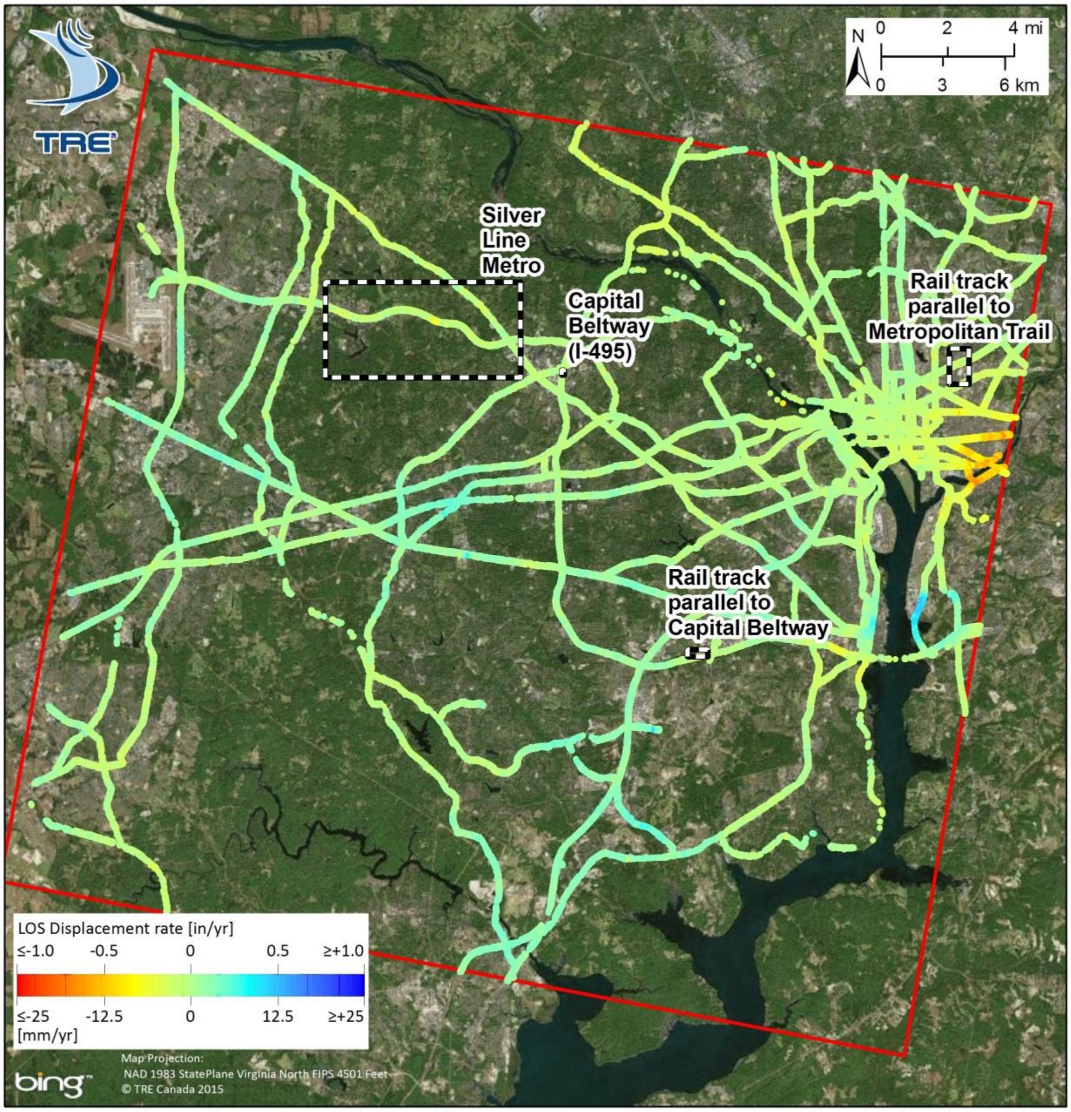

Figure 21: Surface displacement results identified within 50 m of major roads.

Feature	Coordinates (N, E)	Description and Summary of Findings	Displacement Rate (mm/yr)	Cumulative Displacement (mm)
Silver Line Metro	(38.945, -77.292) (38.945, -77.321)	Subsidence detected along the Silver Line metro, with an extent of approx. 0.4 km (0.25 mi). The results are displayed in Figure 22. Four highlighted areas with time series shown in Figure 23 and Figure 24. The deformation is possibly caused by post-construction settlement.	Up to -14.3	-16.7
Capital Beltway (I-495)	(38.920, -77.217)	Subsidence observed between Dolley Madison Blvd and Leesburg Pike along Capital Beltway (Figure 25 and Figure 26)	Up to -10.0	-12.5
Rail track parallel to Capital Beltway	(38.797, -77.147)	A 0.5 km (0.31 mi) segment of track experiencing subsidence.	Up to -19.1	-23.2
Rail track parallel to Metropolitan Trail	(- 38.914 -76.994)	A 1 km (0.62 mi.) stretch of rail track close to Rhode Island Metro station, parallel to the Metropolitan Trail, showing signs of subsidence.	Up to -31.5	-37.6

Table 6: Coordinates of the highlighted locations indicated in Figure 21 and the summary of the InSAR results over these locations.

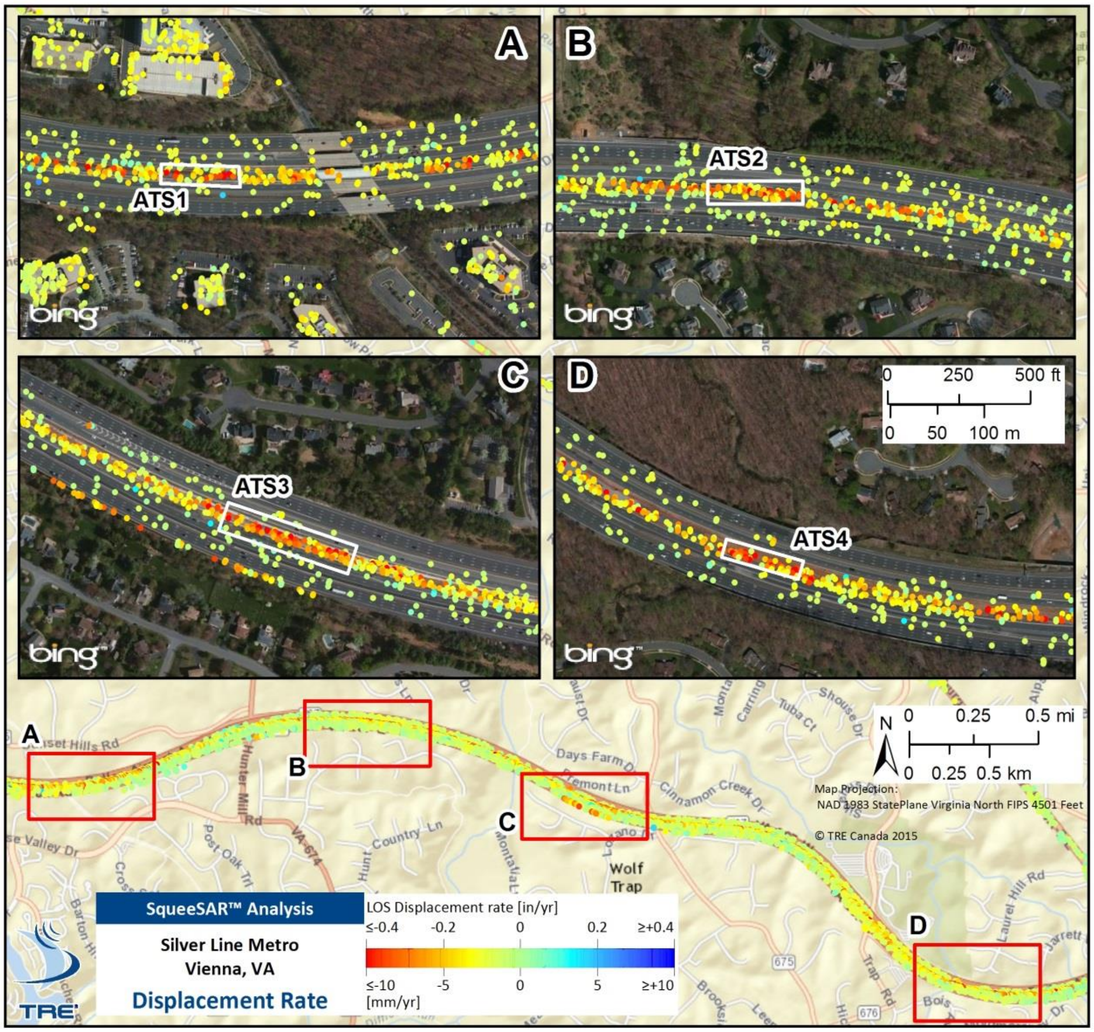

Figure 22: Subsidence observed along Silver Line Metro between Wiehle Ave and Leesburg Pike. A different scale (-10 mm/yr to +10 mm/yr) is used here to display deformation rates.

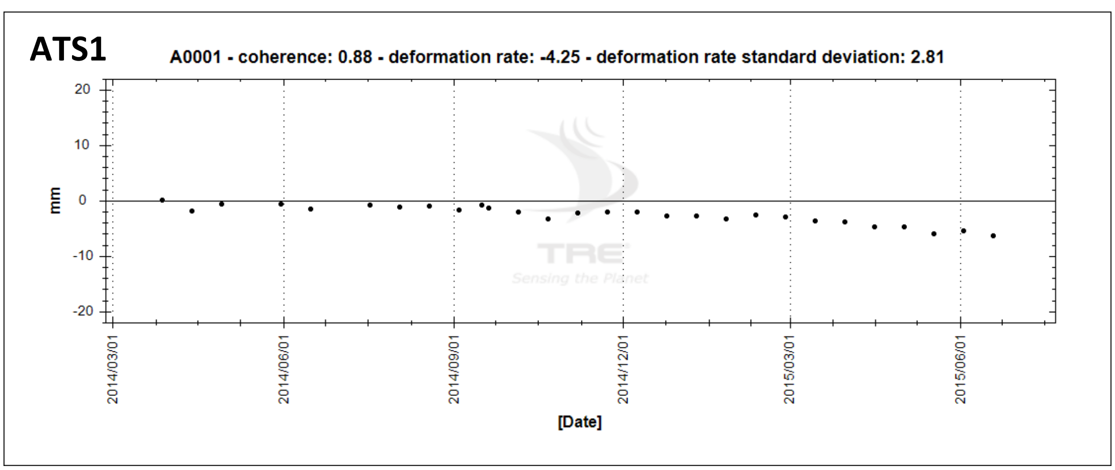

Figure 23: Average time series of ATS1 in Figure 22.

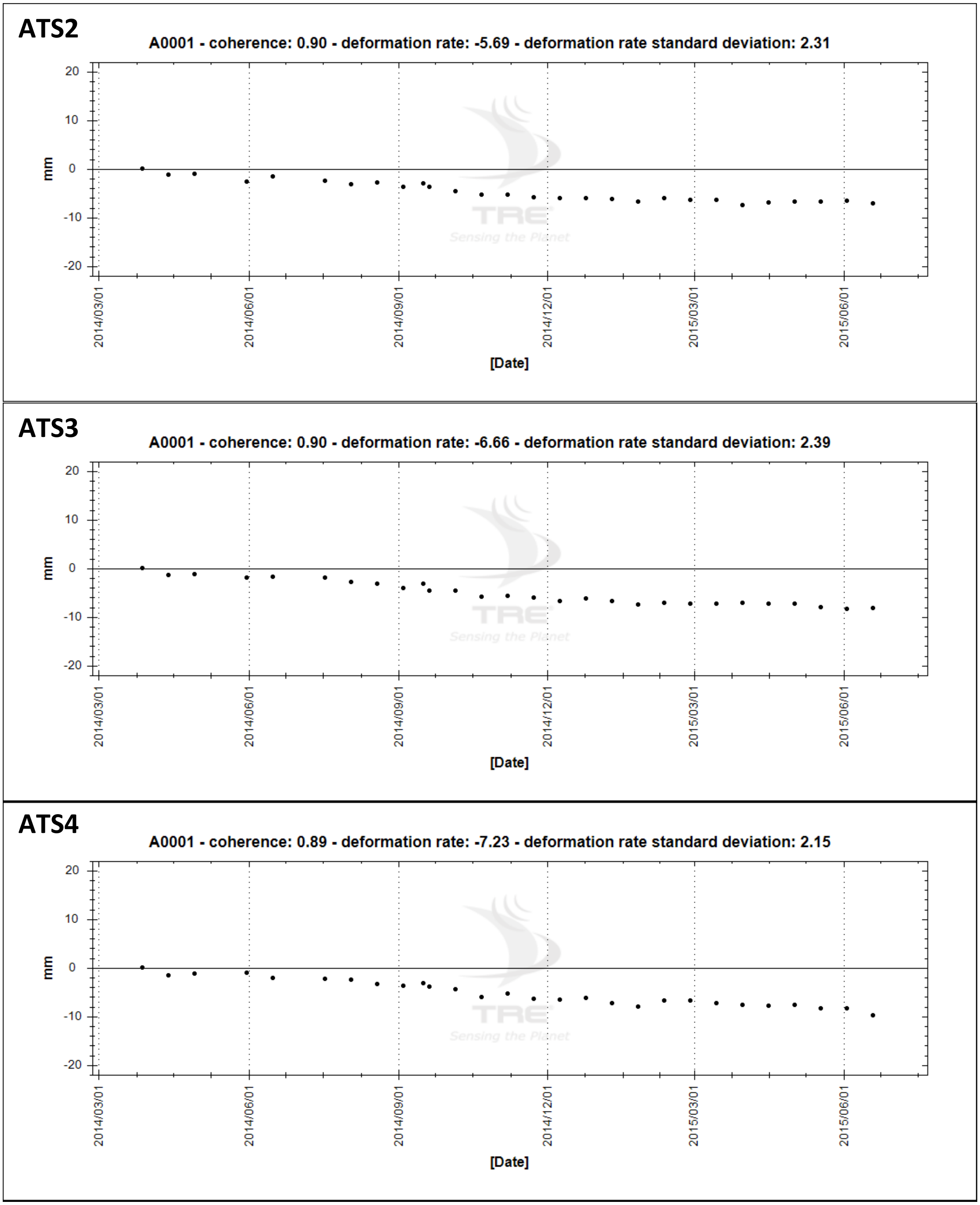

Figure 24: Average time series of ATS2 to ATS4 in Figure 22.

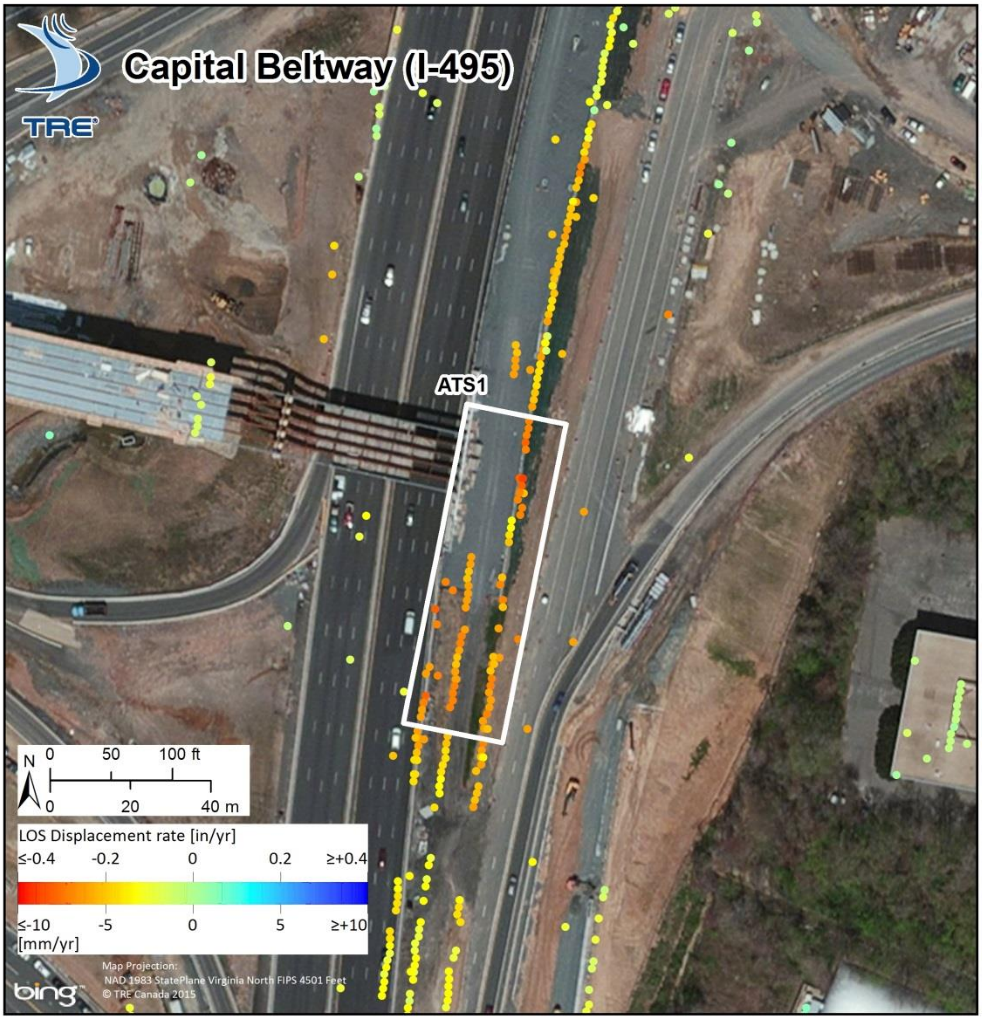

Figure 25: Displacement results over the Capital Beltway between Dolley Madison Blvd and Leesburg Pike.

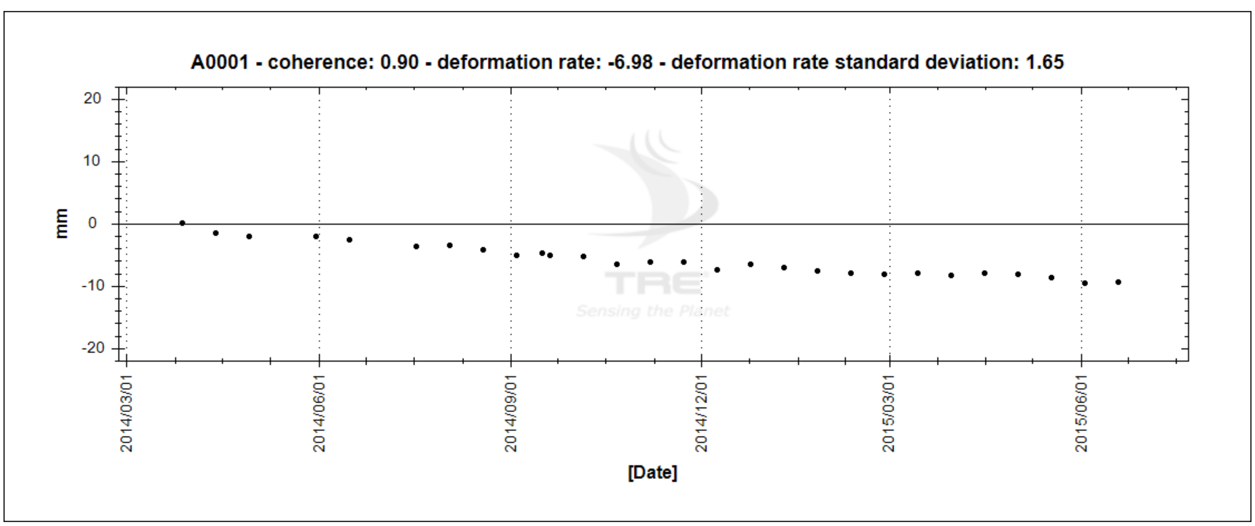

Figure 26: Average time series of ATS1 in Figure 25.

5.3 Surface Profile Cross-section Analysis

Surface cross-sections represent the evolution of horizontal profiles of the ground surface over time, with each individual profile line corresponding to ground displacement compared to a reference image (the first acquired image). The surface cross-section profiles were produced using a coherence-weighted average of all measurement points within a distance of 100 metres of the cross-section line.

Four cross-sections in the areas of the RFK stadium subsidence and of the uplift feature in Forest Heights, MD and Alexandria, VA were prepared (Figure 27) to illustrate the evolution of ground movement from March 2014 to June 2015. The results are shown in Figure 28 and Figure 29. CS1 and CS2 indicate that the maximum subsidence was detected close to shore (CS1 in Figure 38), in the area of RFK stadium, with over 35 mm of subsidence. CS3, which runs from SW Washington DC to Forest Heights, MD, and CS4 from Diagonal Rd to N Patrick St then to Tide Lock Park in Alexandria, indicate over 10 mm of uplift, with the uplift trend increasing gradually close to the Potomac River.

Animations illustrating the changes to the ground surface profiles over these areas were produced and are included in the associated deliverables for this project. The cross-section function is implemented in the latest version of the toolbar provided with this delivery.

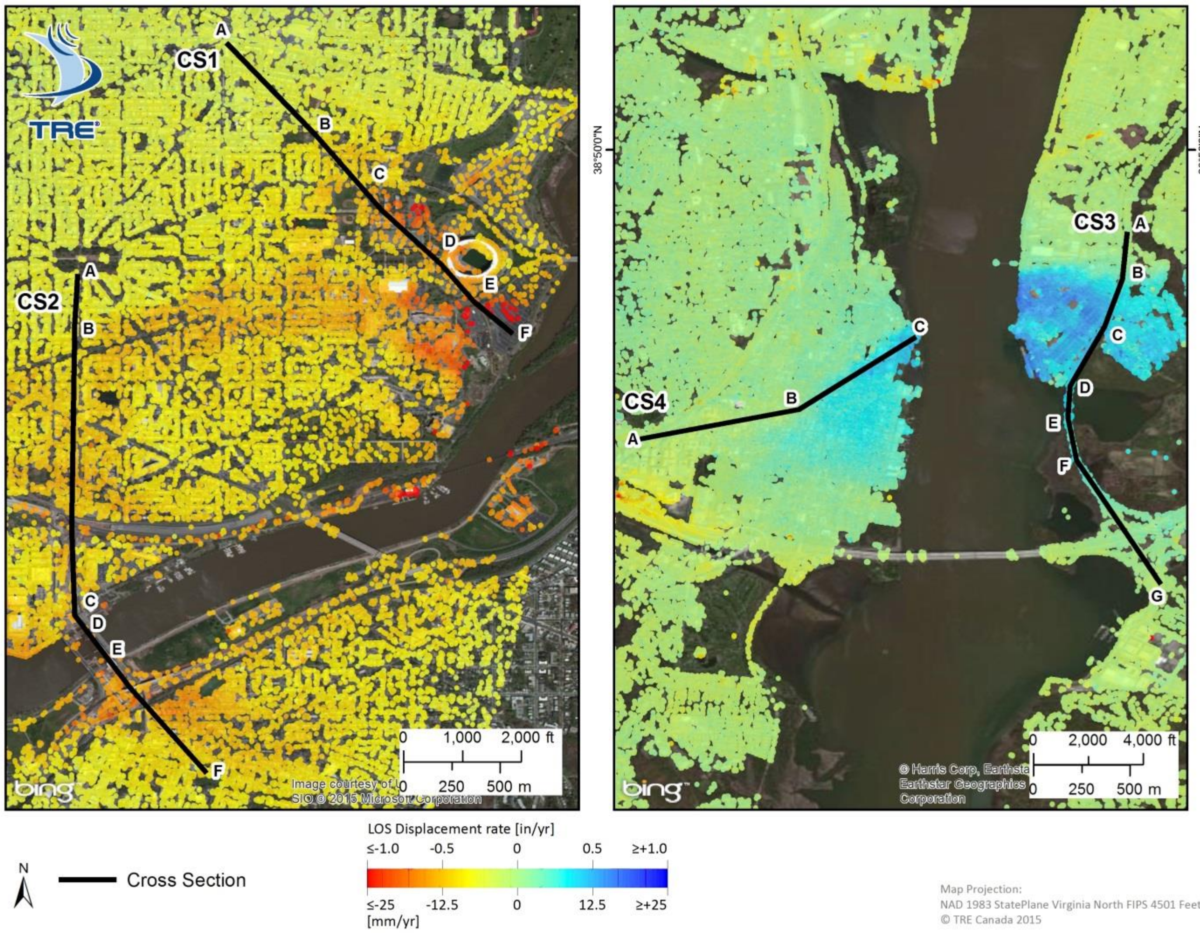

Figure 27: Traces of the four surface profile cross-sections over Hill East and Capitol Hill, Washington, DC (CS1 and CS2) and SW Washington DC and Alexandria, VA (CS3 and CS4).

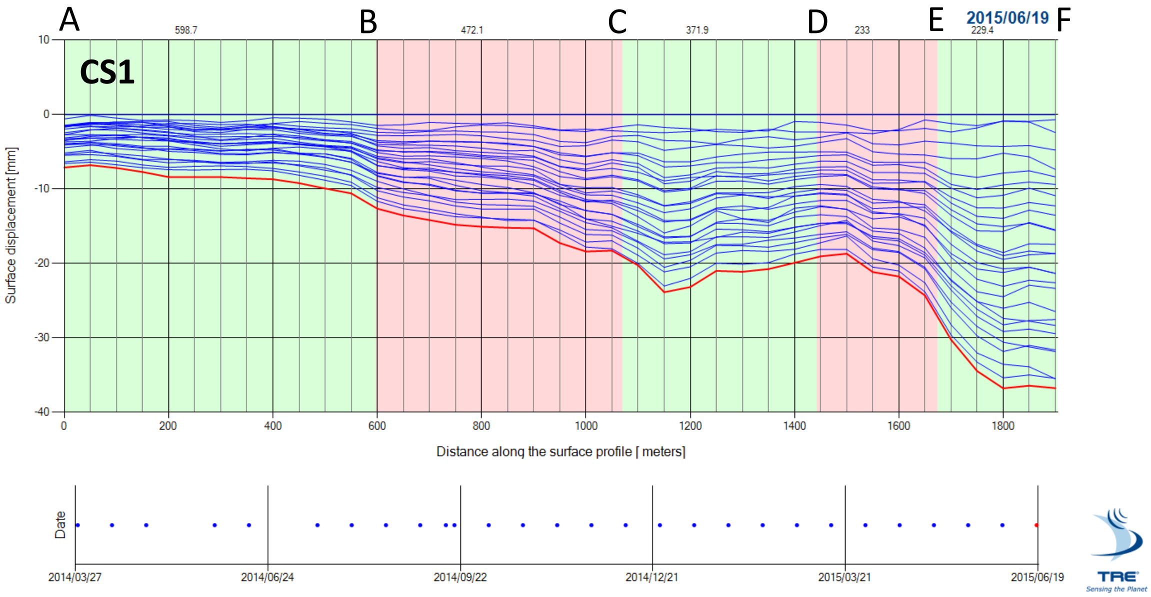

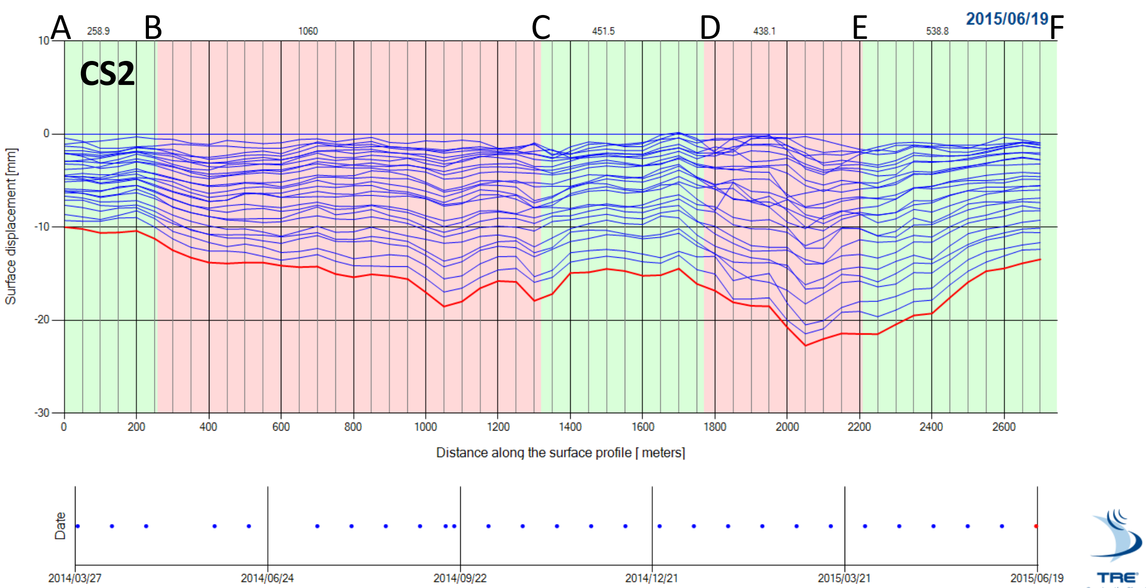

Figure 28: Two-dimensional representation of the surface cross-section. Top: From Starburst Intersection Plaza to RFK Stadium (CS1 in Figure 27). Bottom: Lincoln Park to 11th Street Bridge (CS2 in Figure 27).

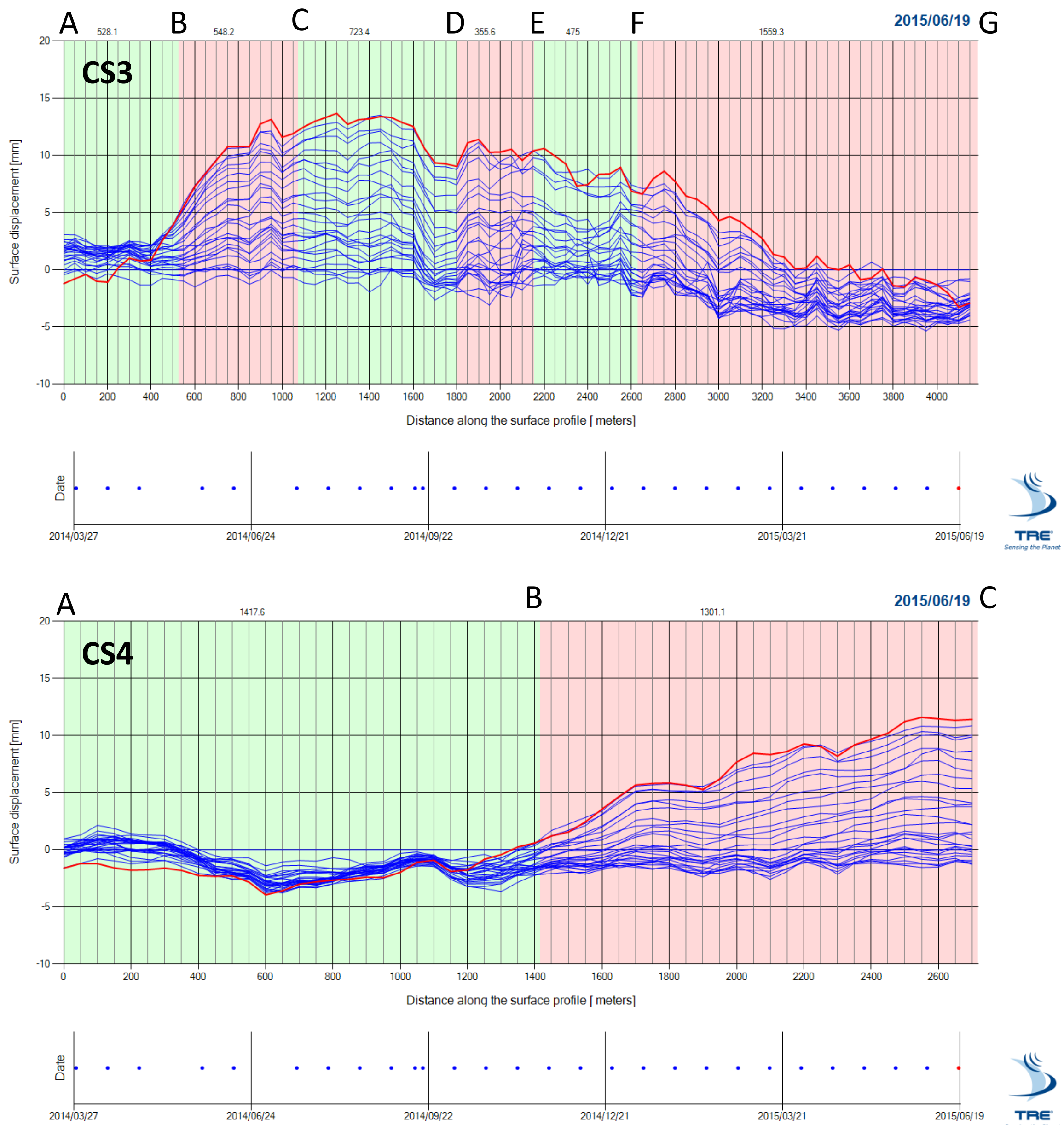

Figure 29: Two-dimensional representation of the surface cross-section. Top: From SW Washington DC to Forest Heights, MD (CS3 in Figure 27). Bottom: Diagonal Rd to N Patrick St then to Tide Lock Park in Alexandria (CS4 in Figure 27).

6 Summary

The second data processing over this site has identified several ground deformation trends of interest. Subsidence was observed in the Hill East and Capitol Hill areas with deformation patterns along the Anacostia River seeming to correspond with the Anacostia River Tunnel project. An area of uplift was observed in Alexandria, VA, SW Washington DC, and Forest Heights, MD. No known causes were identified from available sources for this ground movement.

No deformation was observed at the locations indicated by UVA/VDOT: the MSE wall of the bridge on I-66 EB CD Road over Rte. 286 Fairfax County Pkwy or the retaining wall along I-395 SB at King Street.

A detailed deformation analysis was carried out on the Woodrow Wilson Bridge, including the compensation of thermal expansion/contraction effects to highlight any residual movement of the bridge structure.

Analysis of ground movement along transportation corridors highlighted movement along the Silver Line Metro in Vienna, VA and a few subsiding locations along major roads.

Along with this report, a technical appendix is included, which contains the list of delivered files and additional information regarding InSAR processing.

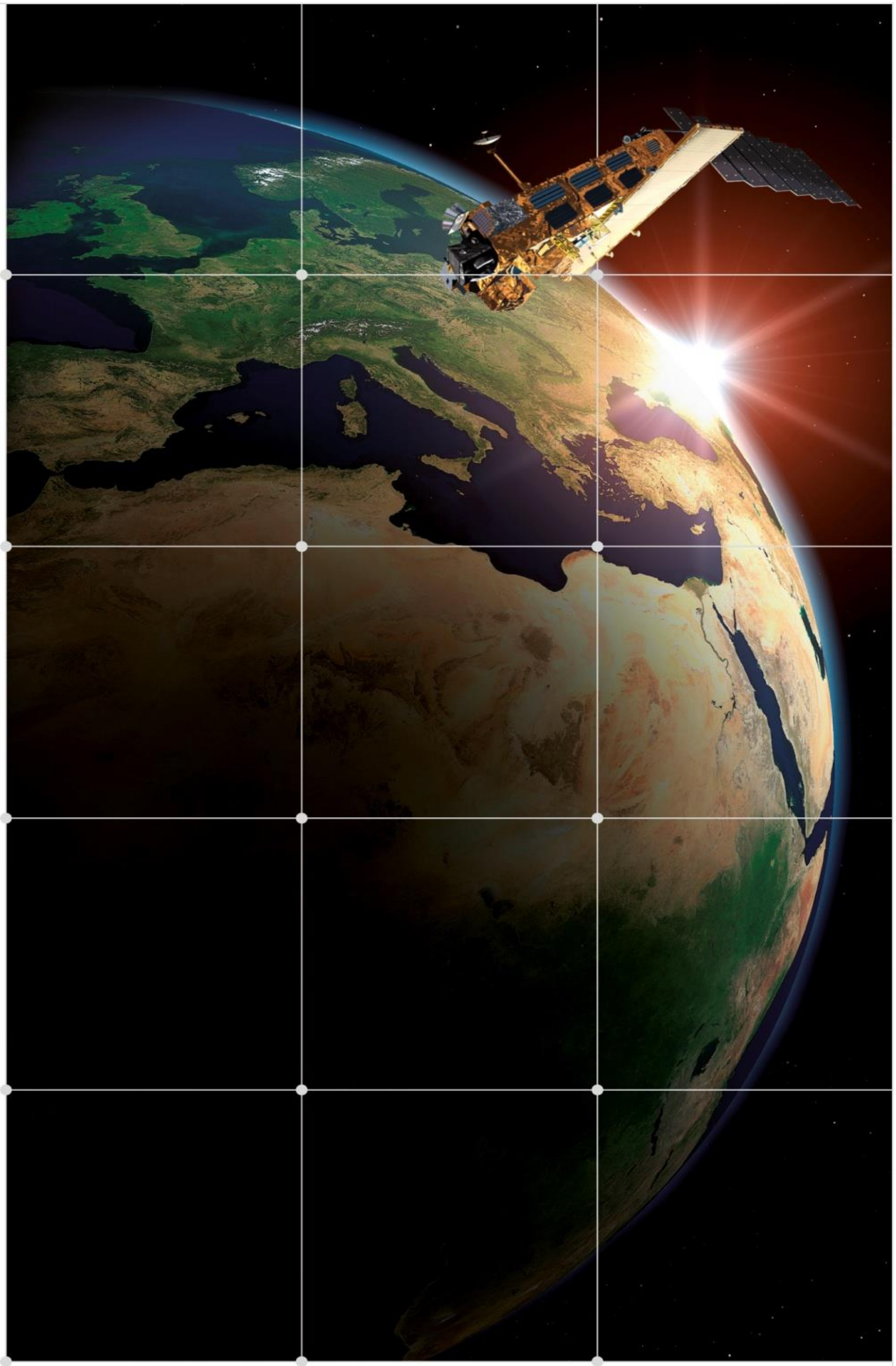

Analysis of Ground Movement over Northern Virginia and Washington D.C. using SqueeSAR

Site 2 Second Report– Technical Appendix

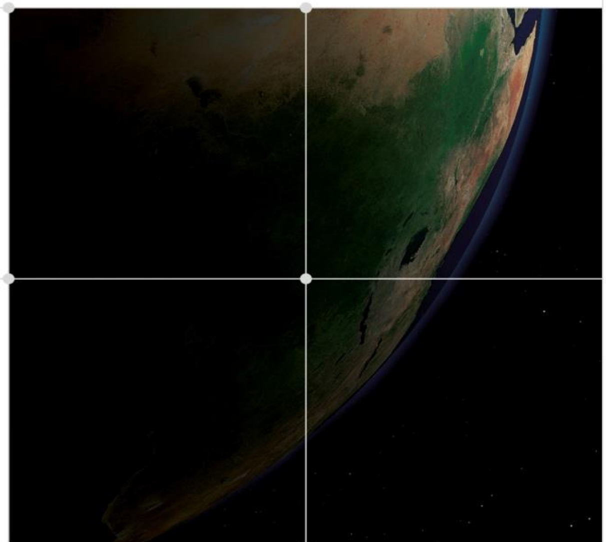

TRE®

Sensing the Planet

Submitted to:
University of Virginia
1001 N. Emmet St.
PO Box 400195
Charlottesville, Virginia 22904
USA

Prepared by:
TRE Canada Inc.
Suite 410, 475 West Georgia Street
Vancouver, B.C., V6B 4M9
Canada

Prepared by: Vicky Hsiao
GIS Analyst
TRE Canada Inc.
____
(signature)

Approved by: Giacomo Falorni
Operations Manager
TRE Canada Inc.
____
(signature)

Doc. Ref.: JO14-3014-REP2.0
4th September 2015

Table of Contents

Appendix 1: List of delivered files

List of Delivered Files

The deliverables of the SqueeSAR™ analysis include the present report, the PS data files and a software tool for assisting with the loading, viewing and interrogation of the data in ESRI ArcGIS 10.x software. Table 1 and Table 2 list the files contained on the accompanying CD.

Data type	Description
.shp	ESRI Shapefile for displaying the database file (dbf) geospatially in a GIS environment.
.dbf	Table containing the height, velocity, velocity standard deviation, acceleration, coherence and time series of all the PS/DS identified.
.xml	An encoding document for each .shp file This file contains metadata for data processing and provides information for the TRE customer toolbar application
.mxd	A ESRI ArcGIS (10.0 and 10.3) project file contains the results.

Table 1: List of delivered file types. Reference point is included in each .shp file.

<table>
<tr><th colspan="3">File Name</th></tr>
<tr><td rowspan="2">Site 2 –
NOVA and Washington D.C.</td><td>Full Resolution</td><td>SITE2_WASHINGTON_CSK_H40B_D_T87_Jun15
SITE2_ACCOKEEK_CSK_H40B_D_T87_Jun15</td></tr>
<tr><td>Subsampled to
100 m X 100 m</td><td>SITE2_WASHINGTON_CSK_H40B_D_T87_Jun15_SUB100</td></tr>
<tr><td>Woodrow Wilson Bridge</td><td>Full Resolution</td><td>WOODROW_WILSON_BRIDGE_CSK_T87_D_JUN2015_I1591A3S</td></tr>
</table>

Table 2: List of delivered files.

The ESRI ArcGIS 10.0 project file is included to make it easier to view the data. Once the data contained on the CD has been saved to the user's hard drive it will be sufficient to open the project file with ArcGIS and update the links to indicate the new locations of the data. The project also contains various layers for viewing the data, including: the AOI, the reference point, the shapefiles for the site and the AOI shapefile.

The Structure of the Database Files

Table 3 below, describes the attributes of each PS/DS data within the database.

Field	Description
CODE	Unique identification code.
SHAPE	Indicates type of geometry (point).
HEIGHT (m)	Elevation above sea level of the PS and DS.
H_STDEV (m)	Standard deviation of PS and DS elevation value.
VEL (mm/yr)	PS movement rate. Positive values correspond to movement toward the satellite (uplift); negative values correspond to motion away from the satellite (subsidence).
V_STDEV (mm/yr)	Standard deviation of PS and DS deformation rate.
ACC (mm/yr^2)	PS and DS acceleration rate.
A_STDEV (mm/yr2)	Standard deviation of PS and DS acceleration value.
COHERENCE	Quality measure [between 0 and 1].
SEASON_AMP (mm)*	Amplitude of seasonal cycles present within the data.
SEASON_PHS (days)*	Phase of seasonal cycles present within the data.
S_AMP_STD (mm)*	Standard deviation of the seasonal amplitude.
S_PHS_STD (days)*	Standard deviation of the seasonal phase.
EFF_AREA (m^2)	Size of the area belonging to the PS and DS. For PS EFF_AREA = 0, for DS EFF_AREA > 0.
VEL_TEMP (mm/yr)†	Displacement rate with thermal expansion and extraction effects removed from the displacement time series
COEF_TEMP (mm/ Celsius degree)†	A coefficient relates the LOS displacement to temperature variation.
D(year/month/day) (mm)	Following the EFF_AREA column are a series of fields that contain the displacement values of successive acquisitions relative to the Master, expressed in mm.

Table 3: Description of the fields contained in the LOS data Shapefile.

*Applicable only to data sets that span one year or longer. †Applicable only to the additional data processing over Woodrow Wilson Bridge data sets.

TREmaps™

The SqueeSAR™ data are also available using TREmaps™, a web-based portal where they can be visualised through a secure client login (only authorised users will have access to the results). SqueeSAR™ data are superimposed onto a Google Maps background and time-series can be viewed.

Data can be visualised on any device with an internet connection, including portable tablets. Figure 28 shows an example dataset loaded into the web-based GIS TREmaps™ platform. Site and the access details (username and password) will be provided directly to the primary contact via email.

https://tremaps.treuropa.com/tremaps

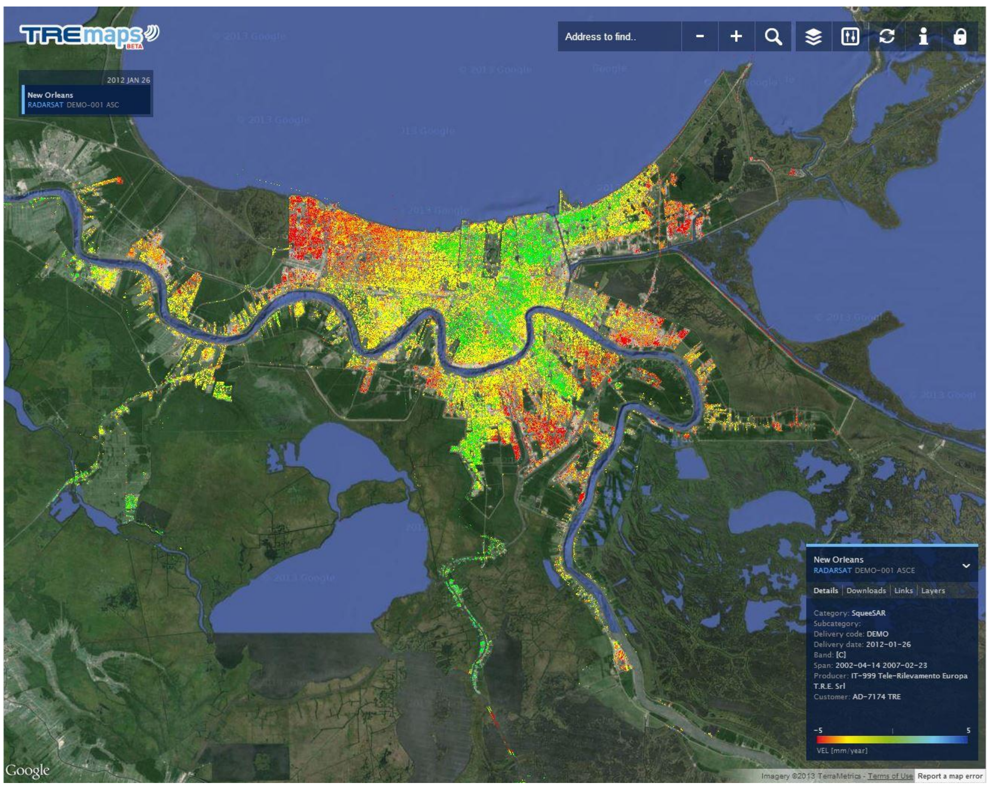

Figure 1: Example of SqueeSAR data within TREmaps.

Appendix 2: Additional Properties of the SqueeSAR™ results

Radar Data Acquisition Geometry

InSAR-based approaches measure surface displacement on a one-dimensional plane, along the satellite line-of-sight (LOS). The LOS angle varies depending on the satellite and on the acquisition parameters while another important angle, between the orbit direction and the geographic North, is nearly constant.

The images used for the historical analysis were acquired from the COSMO-SkyMed (CSK) satellite on an descending orbit (satellite travelling from north to south and imaging to the west) along Track 87.

Table 4 lists the values of the angles for this study, while

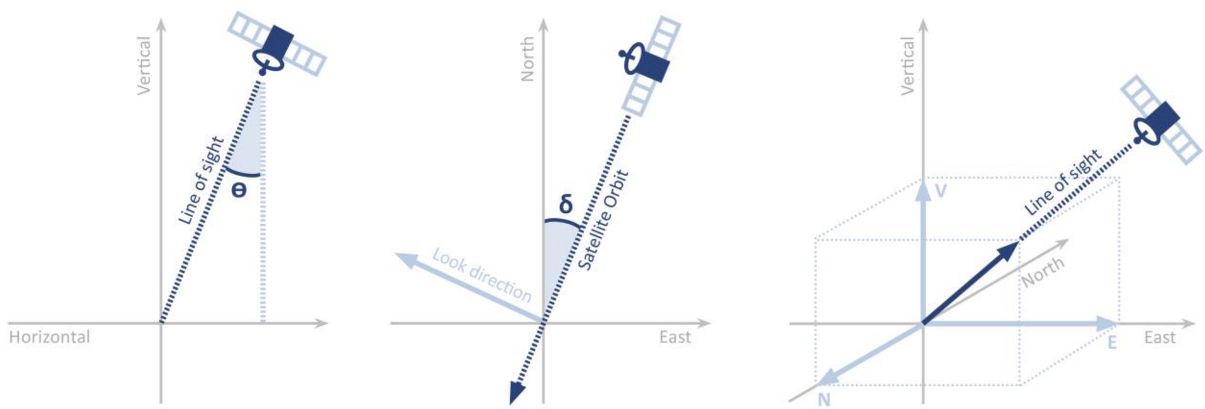

Θ Angle **δ Angle** **Line Of Sight**

Figure 2 shows the geometry of the image acquisitions over the site for the descending orbits, respectively. The symbol δ (delta) represents the angle the LOS forms with the vertical and Θ (theta) the angle formed with the geographic north.

Satellite	Orbit geometry	Symbol	Angle
CSK	Descending	**δ**	24.03°
		θ	12.87°

Table 4: Satellite viewing angles for the CSK descending orbit imagery.

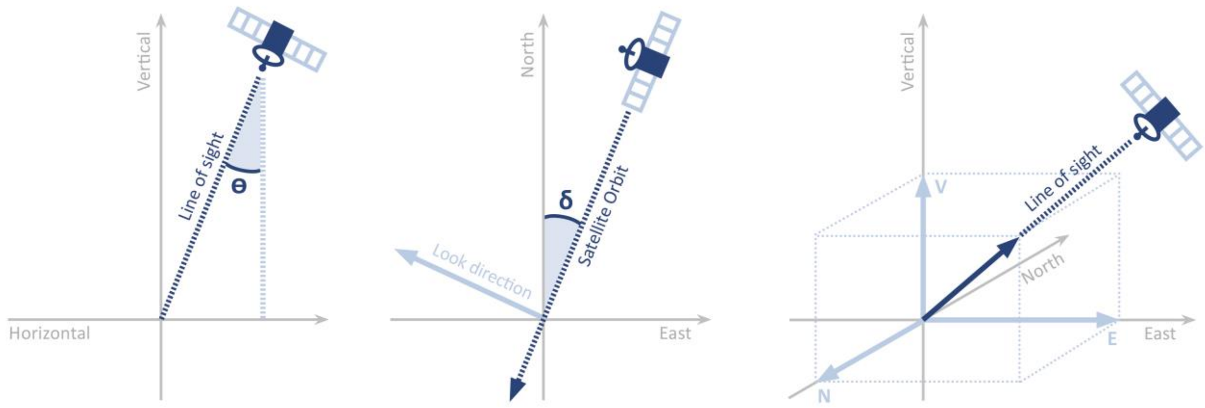

Θ Angle **δ Angle** **Line Of Sight**

Figure 2: Geometry of the image acquisitions over the AOI for the descending orbit.

Data Processing

Both permanent scatterers (PS) and distributed scatterers (DS) were identified at this site. Bare ground, roads, and infrastructure provide the basis for many PS points in the present SqueeSAR™ analysis. Many natural features such as rocks or exposed ground were also likely sources of stable PS targets.

DS correspond to large areas (up to hundreds of square meters) and were identified from exposed areas such as sparsely vegetated areas, exposed ground or rock. It is important to consider that while DS are represented as individual points for clarity of presentation and ease of interpretation, these measurements actually correspond to non-point features that are multiple pixels in size. The size of the DS within the AOI ranges from 75 to 881 m^2.

Table 5, shown below; provide a summary of the other properties relative to the data processing.

Satellite	COSMO-SkyMed (CSK)
Acquisition geometry	Descending
Analysis time interval	28 March 2014 – 19 June 2015
Number of scenes processed	28
Georeferencing	Bing Map
Projection system used / datum	State Plane Virginia North FIPS 4501 (Feet) / NAD 1983
Reference Point location	Code: BGX4H EAST: 11847083.91 NORTH: 6989695.03
Area of interest	617.8 sq. mile (1,600 km^2)

Table 5: Statistics of the processed data.

Standard Deviation and Precision

Standard deviation values of the displacement measurements are a function of the factors listed below and of local ground movement dynamics.

- Spatial density of the PS and DS (higher densities produce higher precisions)
- Quality of the radar targets (signal-to-noise ratio levels)
- Distance from the reference point
- Number of images processed
- Period of time covered by the imagery
- Climatic conditions at the time of the acquisitions
- Distance between the measurement point and the reference

In addition to each measurement point having an associated standard deviation value to represent the error of the displacement measured, results can also be characterized by the accuracy of the technique. Specifically, three parameters are used to characterize the overall accuracy of the results:

- Precision of the estimated deformation rates;
- Precision of the estimated elevations;
- Precision of the geocoding.

Table 6 summarizes the typical precision values applicable to PS located within 2 km from the reference point when **at least 45 radar images** have been processed.

DEFORMATION RATE	< 1 [mm/yr]
DISPLACEMENT ERROR (single displacement between contiguous satellite images)	< 5 [mm]
ELEVATION	± 1.5 [m]
POSITIONING ERROR ALONG EAST DIRECTION	± 3 [m]
POSITIONING ERROR ALONG NORTH DIRECTION	± 2 [m]

Table 6: Measurement accuracies for PS located within 2 km of the reference point, based on the processing of at least 45 SAR images.

Appendix 4: InSAR Processing

InSAR

Interferometric Synthetic Aperture Radar, also referred to as SAR interferometry or InSAR, is the measurement of signal phase change (interference) between radar images. When a point on the ground moves, the distance between the sensor and the point changes, thereby producing a corresponding shift in signal phase. This shift is used to quantify the ground movement.

An interferogram is a 2D representation of the difference in phase values. Variations of phase in an interferogram are identified by fringes, colored bands that indicate areas where and how much movement is occurring. The precision with which the movement can be measured is usually in the centimetre (cm) range as the phase shift is also impacted by topographic distortions, atmospheric effects, and other sources of noise.

DInSAR

When InSAR is used to identify and quantify ground movement the process is referred to as Differential InSAR (DInSAR). In DInSAR topographic effects are removed by using a DEM of the area of interest to create a differential interferogram.

Differential InSAR is still impacted by atmospheric effects, as there is no method for removing this signal phase contribution. It is a useful tool for identifying footprints of progressing movement and creating deformation maps. The limitations of DInSAR are its relatively low precision (cm scale) and that it cannot distinguish between linear and non-linear motion.

PSInSAR™

Permanent Scatterer SAR Interferometry is an advanced form of DInSAR. The fundamental difference is that it uses multiple interferograms created from a stack of at least 15 radar images.

Permanent Scatterer SAR Interferometry was developed to overcome the errors produced by atmospheric artifacts on signal phase. The PSInSAR algorithm automatically searches the interferograms for pixels that display stable radar reflectivity characteristics throughout every image of the data set. In PSInSAR these pixels are referred to as Permanent Scatterers (PS). The result is the identification of a sparse grid of point-like targets on which an atmospheric correction procedure can be performed. Once these errors are removed, a history of motion can be created for each target, allowing the detection of both linear and non-linear motion.

The result is a sparse grid of PS that are color-coded according to their deformation rate and direction of movement. The information available for each PS includes its deformation rate, acceleration, total deformation, elevation, coherence as well as a time series of movement. The PSInSAR algorithm measures ground movement with millimetre accuracy.

SqueeSAR™

Permanent Scatterers are objects, such as buildings, fences, lampposts, transmission towers, crash barriers, rocky outcrops, etc, that are excellent reflectors of radar microwaves. However, TRE has noticed that many other signals are present in the processed data. These do not produce the same high signal-to-noise ratios of PS but are nonetheless distinguishable from the background noise. Upon further investigation it was found that the signals are reflected from extensive homogeneous areas where the back-scattered energy is less strong, but statistically consistent. These areas have been called distributed scatterers (DS) and correspond to rangeland, pastures, bare earth, scree, debris fields, arid environments, etc (Figure 3).

The SqueeSAR™ algorithm was developed to process the signals reflected from these areas. As SqueeSAR™ incorporates PSInSAR no information is lost and movement measurement accuracy is unchanged.

The SqueeSAR™ algorithm also produces improvements in the quality of the displacement time series. The homogeneous areas that produce DS normally comprise several pixels. The single time series attributed to each DS is estimated by averaging the time series of all pixels within the DS, effectively reducing noise in the data.

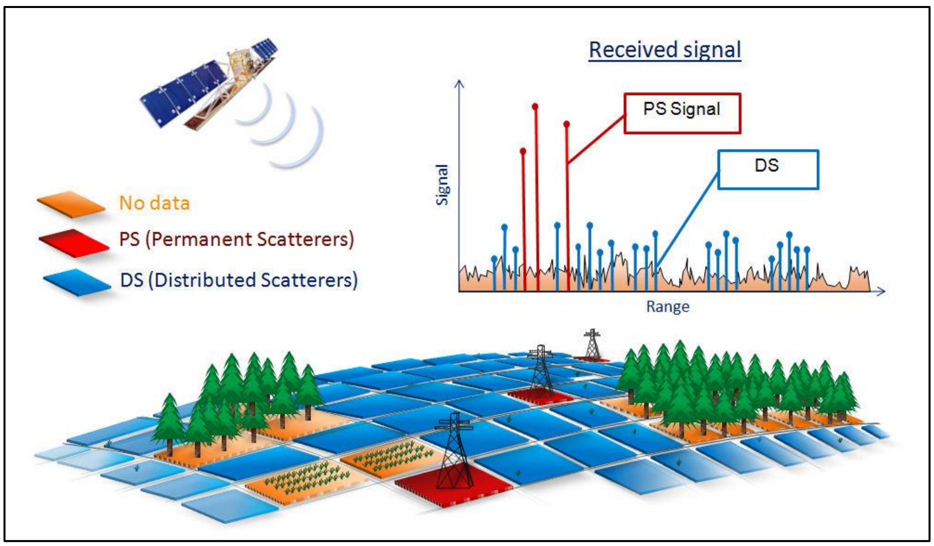

Figure 3: Illustration of the identification of permanent (PS) and distributed scatterers (DS) by the SqueeSAR™ algorithm.

Appendix 5: Data Processing

Methodology

The identification of PS and DS in a series of radar images comprises a sequence of steps.

First, all radar data archives are screened to determine the most suitable source of raw data for the particular area of interest and to select all the high quality images within the chosen data set.

As the signal echo from a single point target contains many returning radar pulses it appears defocused in a synthetic aperture radar (SAR) raw image. The first processing step is therefore to focus all the received energy from a target in one pixel. The images are then precisely aligned to each other, or co-registered, and analyzed for their suitability for interferometry. The parameters that are analyzed are the normal baseline and the temporal distribution of the images.

There then follows a number of statistical analyses on the phase and amplitude characteristics of the backscattered radar signal that return to the satellite. If a concentrated number of signals reflect off a particular feature within a pixel and backscatter to the satellite, the feature is referred to as a ‘scatterer’. When the same scatterer appears in all, or most, of a data set of SAR images of a particular location, then the scatterer is deemed to be ‘permanent’.

At this stage it is possible to identify a subset of pixels, referred to as Permanent Scatterer Candidates (PSC), that are used to estimate the impact on signal phase of ionospheric, tropospheric and atmospheric effects, as well as possible orbit errors.

Once the signal phase has been corrected for these effects, any remaining changes in signal phase directly reflect ground movement.

Master Image Selection

SqueeSAR™ requires that one image (or scene) in each data set has to become both a geometric and temporal reference to which all the other images are then related. This image is referred to as the master image and those that remain are slave images.

The master image should be chosen according to the following criteria:

- it minimizes the spread of normal baseline values for the slave images;
- similarly, it minimizes the temporal baseline values between the master and each slave image; and
- it minimizes the effects of signal noise arising from changes in vegetation cover and/or small changes in the look angle of the satellite from one scene to another.

Signal Phase and Amplitude Analysis

General

Each pixel of a SAR image contains information on the amplitude of signals that are backscattered toward the satellite, as well as on the signal phase. The amplitude is a measure of the amount of the radar pulse energy reflected, while the phase is related to the length of the path of the electromagnetic wave, from the platform to the ground and back again.

Analyses of both amplitude and phase of the SAR image provide an indication of the stability of each pixel, over time, whereby it is possible to identify those pixels that are most likely to behave as Permanent Scatterers. Statistical methods are used extensively in this process.

Among the different statistical parameters that can be computed two are of particular interest: the Phase Stability Index (PSI), obtained from the phases of the images within the data set, and the Multi Image Reflectivity (MIR) map, derived from the amplitude values of the available acquisitions.

Radar phase and coherence

The phase stability is strongly linked to the concept of coherence. Pixels that consistently display high phase stability are said to be coherent. Coherence is measured by an index that ranges from 0 to 1. When a pixel is completely coherent, it will have a coherence value of 1. Correspondingly, if a pixel has a low phase stability, its coherence index will be 0. In general, interferometry is successful when the coherence index lies between 0.5 and 1.0.

Radar amplitude and multi-image reflectivity

The amplitude of a pixel within a SAR image is the aggregate of the backscattered energy toward the satellite from within the pixel's equivalent land area. This equivalent land area is referred to as the radar resolution, and in the case of the CSK satellite, it measures about 3 m by 3 m. It is necessary to look into the amplitude values of all the images in the data set, in order to understand exactly what was seen by the satellite at the time of each acquisition.

If a target has experienced significant change in its surface characteristics it will exhibit variation in its reflectivity (electromagnetic response) between two acquisitions. In such circumstances, the possibility of detecting movement by means of SAR interferometry is seriously compromised. The signal phase difference between the two images now contains not only the contribution due to displacement, but also that due to the change in the reflectivity of the target. This prevents, in the worst case, the obtaining of any useful information on ground movement.

Accordingly, it is necessary to look into the amplitude values of all the images in the data set, in order to understand exactly what was seen by the satellite at the time of each acquisition.

Another artifact linked to amplitude is known as speckle. Speckle is random noise that appears as a grainy salt and pepper texture in an amplitude image. This is caused by random interference from the multiple scattering returns that occur within each resolution cell. Speckle

has an adverse impact on the quality and usefulness of SAR images. However, the higher the number of images has taken of the same area at different times or from slightly different 'look' angles, the easier it is to reduce speckle. This increases the quality and level of details of the amplitude image enabling it to be used as a background layer for observing the presence of PS results.

The Multi Image Reflectivity (MIR) map is the means by which speckle reduction is accomplished. Averaging a number of images tends to negate the random amplitude variability, leaving the uniform amplitude level unchanged (Figure 4).

It should be emphasised that the information in the MIR map is the reflectivity of each pixel, i.e. the ability to backscatter the incident wave toward the satellite. Flat surfaces (roads, highway, rivers, and lakes) act like a mirror, meaning that if their orientation is not exactly perpendicular to the incident wave negligible energy is reflected back to the sensor; they appear dark in the image. On the other hand, because of their irregular physical shape, metal structures or buildings reflect a significant portion of the incident signal back to the radar, resulting in very bright pixels in the MIR map.

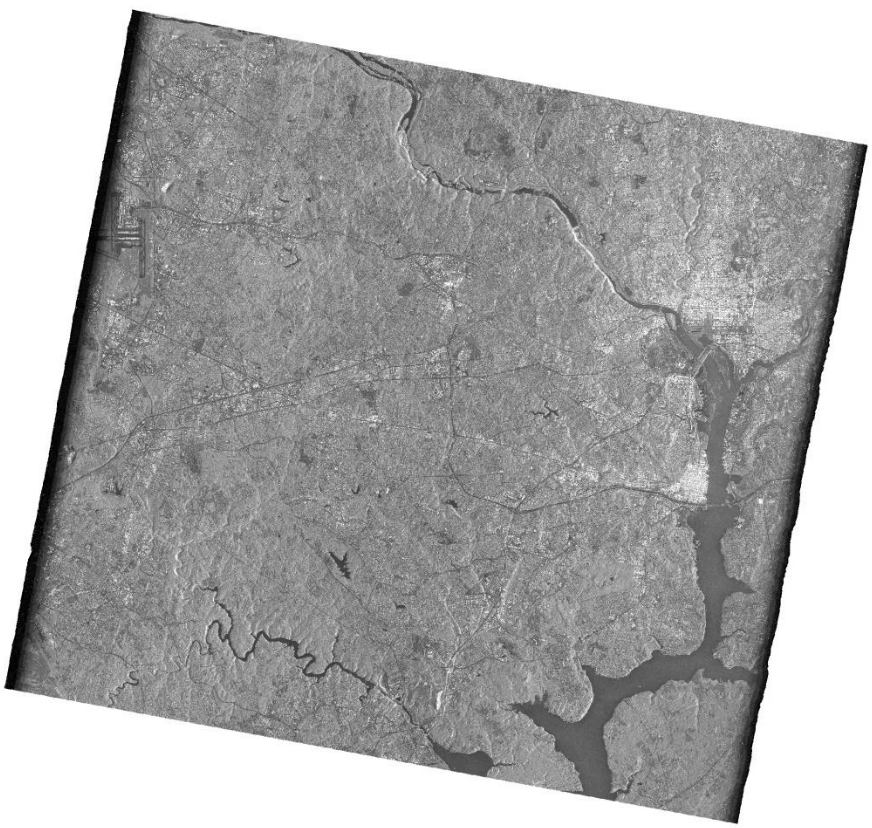

Figure 4: Multi-image reflectivity map of the descending CSK data set over NOVA and most of Washington D.C areas.

Interferograms

After the statistical analyses of the SAR images have been completed, a set of differential interferograms is generated. This entails subtracting the phase of each slave image from the phase of the master image. In doing so, the difference in signal path length between the two images is calculated. This difference is related to possible ground motion.

In any SAR image, there are embedded topographic distortions that arise during image acquisition. These are removed using a reference Digital Elevation Model (DEM), leaving ground movement and the signal phase distortions arising from atmospheric effects as the only embedded variables.

The differential interferograms represent the starting point for applying the PSInSAR approach.

Estimation of the Atmospheric Effects

When a radar signal enters and exits a moisture-bearing layer in the atmosphere, its wavelength can be affected, introducing potential errors into the signal path length. The removal of atmospheric impacts is fundamental for increasing the precision of ground movement measurement.

A sub-set of pixels, usually corresponding to buildings, lampposts, antennas, small structures and exposed rocks, is chosen from among those that have high PSI values. These are referred to as PS Candidates (PSC). PSC density is, of course, higher in towns and cities rather than in forests and vegetated areas. However, it is often possible to obtain good PSC density in rural areas.

For each image, the atmospheric impacts are estimated at each PSC location. The process is statistically based and benefits in accuracy by the greater the number of available images for the analysis. By comparing the atmospheric contribution on neighboring pixels that would be experiencing the same atmospheric conditions, the atmospheric contribution can be reconstructed over the whole image.

The processed data set allows identification of a PSC cluster dense enough to identify and extract the atmospheric contribution over the entire area of interest.

Post-processing

In this stage the processed data undergoes a thorough quality control following ISO 9001:2000 guidelines. The PS data is checked for anomalies, aligned on an optical image layer usually provided by the client and the final report is prepared.

Appendix 6: Abbreviations and Acronyms

AOI	Area Of Interest
DInSAR	Differential Interferometry
DS	Distributed Scatterer (s)
GIS	Geographic Information System
InSAR	Interferometric SAR
LOS	Line Of Sight
MIR	Multi-Image Reflectivity
PS	Permanent Scatterer(s)
PSInSAR^{TM}	Permanent Scatterer SAR Interferometry is a worldwide Polytechnic University of Milan Trademark
SAR	Synthetic Aperture Radar
SqueeSAR^{TM}	The most recent InSAR algorithm patented by TRE
TRE	Comprehensive term for Tele-Rilevamento Europa and TRE Canada
TS	(Permanent Scatterer Displacement) Time Series

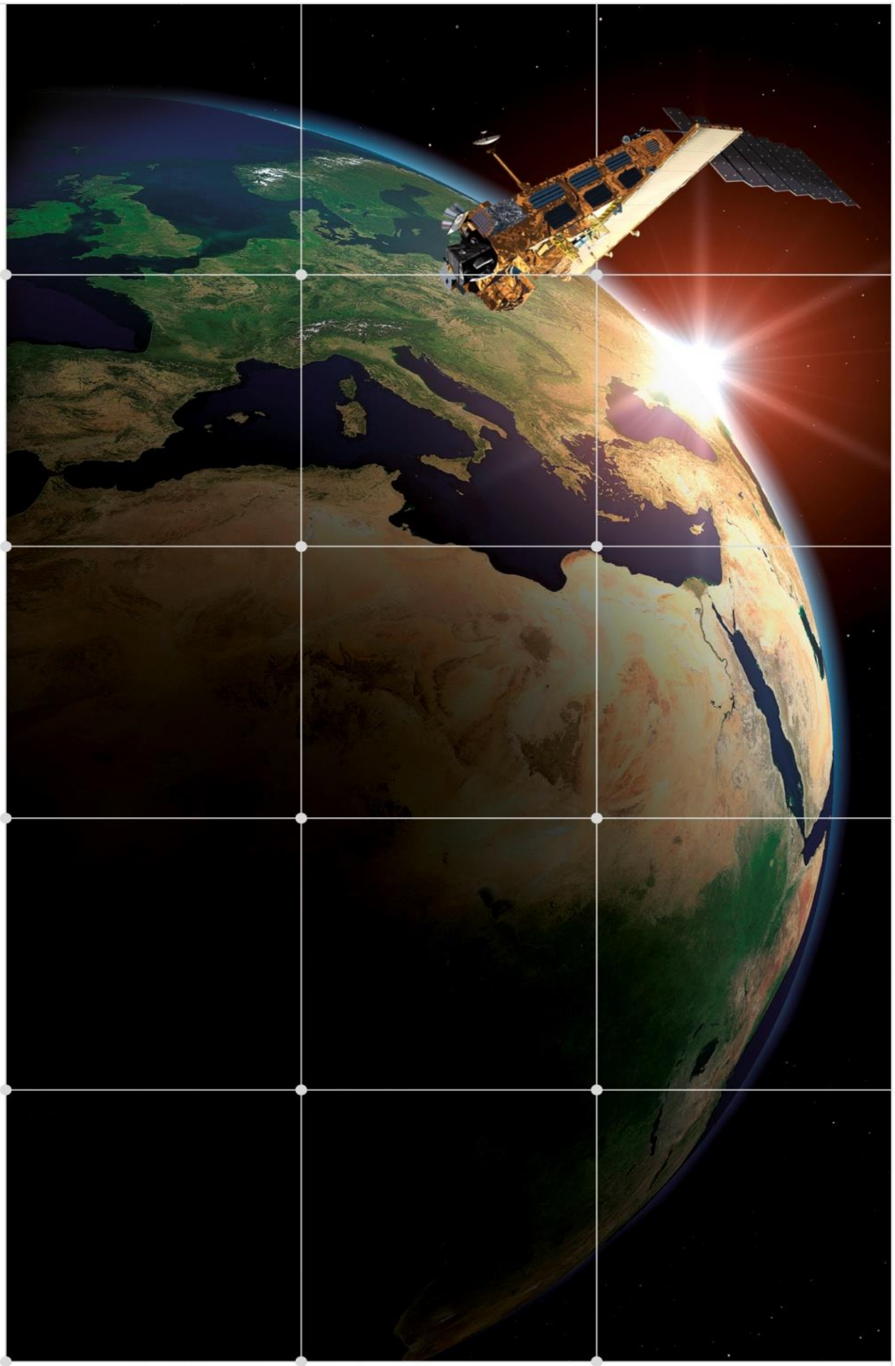

Appendix F – InSAR ArcGIS add-in documentation

VIVA – **InSAR Add-in Documentation** – October 2014 [download][10]

[10] http://viva-lab.ece.virginia.edu/elecdocs/ritars14/InSAR_Add-in.pdf

InSAR Add-in Documentation

Release [0.0.2alpha]

Andrea Vaccari (viva.uva@gmail.com)

October 20, 2014

CONTENTS

This manual describes the installation and the use of the add-in developed to implement, withing the ArcGIS environment, in particular ArcMap.

> **Caution:** The current documentation describes the ArcGIS test add-in developed as prototype for displacement data analysis directly within the ArcMAP environment. As *prototype* the current add-in is still under development and should be considered an **alpha** release.

CHAPTER ONE

INSTALLATION

The add-in is currently delivered as a single package file with extension `.esriaddin` (the current filename of the package is `InSAR_Add-in.esriaddin`).

Once the file has been downloaded it can be save to any directory for installation (In Fig. 1.1 we show the file in the directory where it was generated).

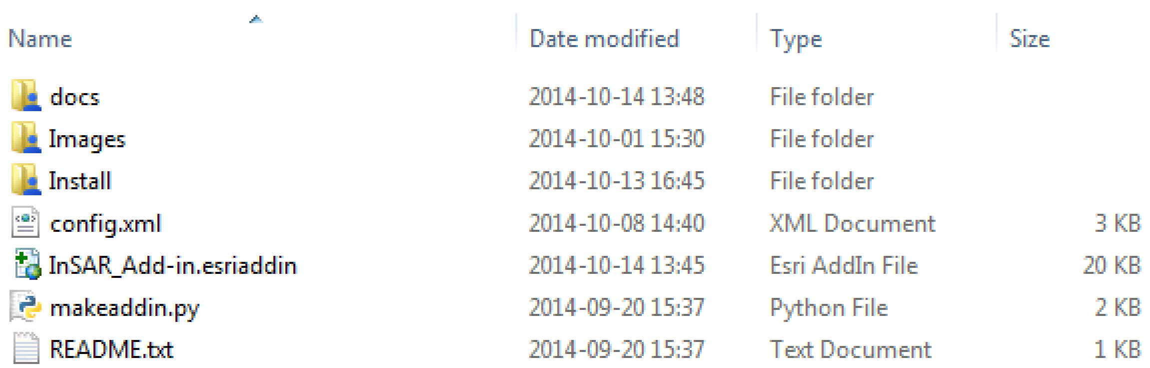

Figure 1.1: Example of hwo the `InSAR_Add-in.esriaddin` file should appear before installation.

All is required to install the add-in is to double-click on the file `InSAR_Add-in.esriaddin`. If the ArcGIS environment has been correctly installed, this will run the *ESRI ArcGIS Add-In Installation Utility* and prompt the use with a confirmation window (Fig. 1.2).

Once the installation is complete, if everything goes well, the user is notified by a pop-up window (Fig. 1.3).

At this point the user should start ArcMAP to verify the correct installation of the add-in. After starting the ArcMAP, the toolbar might or might not appear depending on the current user configuration. If the toolbar is visible, it might be *docked* (Fig. 1.4) or *floating* (Fig. 1.5).

Is the toolbar is not visible, the user should verify that the add-in was correctly installed by selecting *Add-In Manager...* from the *Customize* menu. This will present the user with the *Add-In Manager* window (Fig. 1.6) where the user can verify if the add-in was correctly installed. If the *InSAR Add-in* is present in the list on the left of the screes, it was correctly installed. Selecting the add-in will provide further information on the detais window to the right.

If the add-in was correctly installed and the toolbar is still not visible, then it should be possible to turn it on by enabling it under the *Customize -> Toolbars* menu.

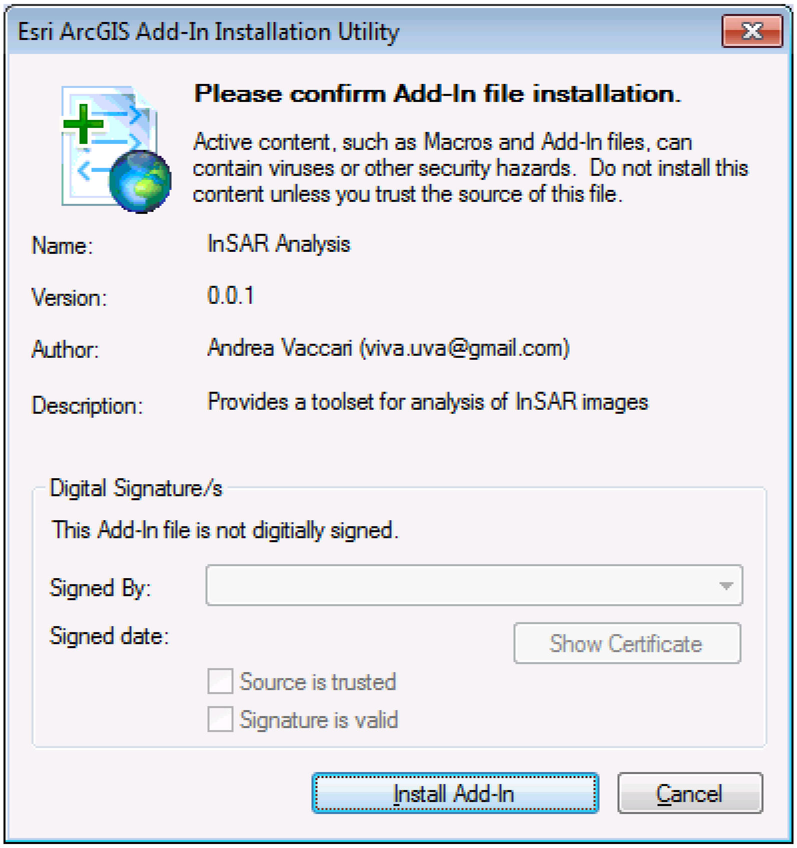

Figure 1.2: ESRI ArcGIS Add-In Instalaltion Utility prompt.

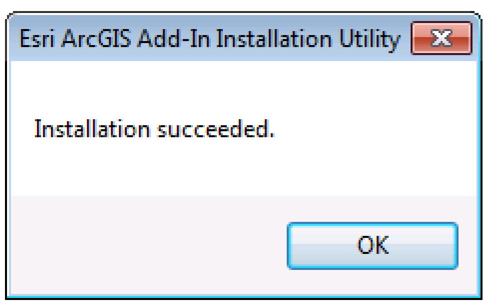

Figure 1.3: Notification of correct installation of add-in.

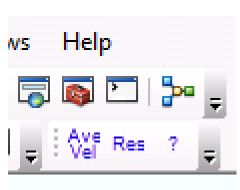

Figure 1.4: Example of *docked* toolbar.

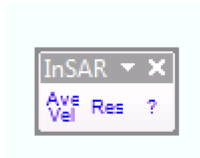

Figure 1.5: Example of *floating* toolbar.

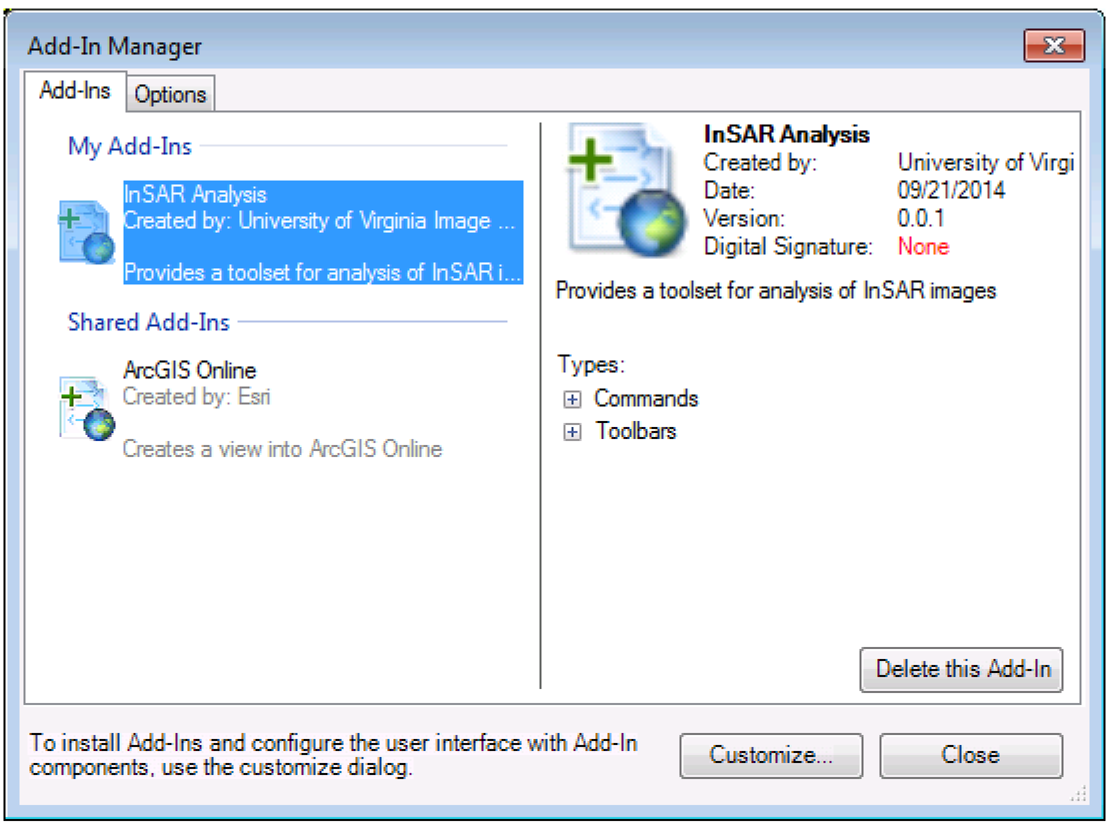

Figure 1.6: ArcMAP *Add-In Manager* window.

CHAPTER

TWO

OPERATION

Note: Since the current implementation was developed to provide an add-in for ArcMAP, all the different tools are run *in process*. This means that while the algorithm is executed, ArcMAP is locked and cannot be used. This can be quite a disadvantage sice, for certain analyses, the computation time can be quite long. For this reason is recommended that only a few hundred scatteres are selected when evaluating the subsidence residual map. For the following releases we are evaluating the possibility of implementing the analysis as tool within toolboxes that can then be called by the add-in. This would allow the tools to be run in background thus unlocking access to ArcMAP.

Currently there are two tools and one information button implemented in the add-in:

- Average Displacement Velocity
- Subsidence Residual
- About

2.1 Average Displacement Velocity (Ave Vel)

The *average displacement velocity* tool evaluates the average displacement velocity of all the scatterers within an area selected by the user. The evaluation is done by averaging the values within the `VEL` field within the dataset.

In order to use this tool, the layer containing the SqueeSAR dataset should be selected and the Ave Vel button pressed as illustrated in Fig. 2.1.

The tool will notify the user if no layer is selected of if the selected layer does not contain a SqueeSAR dataset.

Once the layer and the tool have been selected, the user can identify a rectangular area by clicking and dragging the cursor over the map. This will automatically select all the SqueeSAR scatterers within the area and evaluate the average displacement. A pop-up window will provide the user with information about the extent of the selected area, the number of scatterers identified, and the average displacement velocity observed in *mm/year* (Fig. 2.2).

2.2 Subsidence Residual (Res)

The *subsidence residual* tool provides a simple way to implement the residual analysis thechnique that was developed by the Virginia Image and Video Analysis (VIVA) laboratory at the University of Virginia.

The technique is fully described in the following paper (available for download here):

Vaccari, A.; Stuecheli, M.; Bruckno, B.; Hoppe, E.; Acton, S.T.; **"Detection of geophysical features in InSAR point cloud data sets using spatiotemporal models,"** *International Journal of Remote Sensing,* vol.34, no.22, pp.8215-8234. doi: 10.1080/01431161.2013.833357.

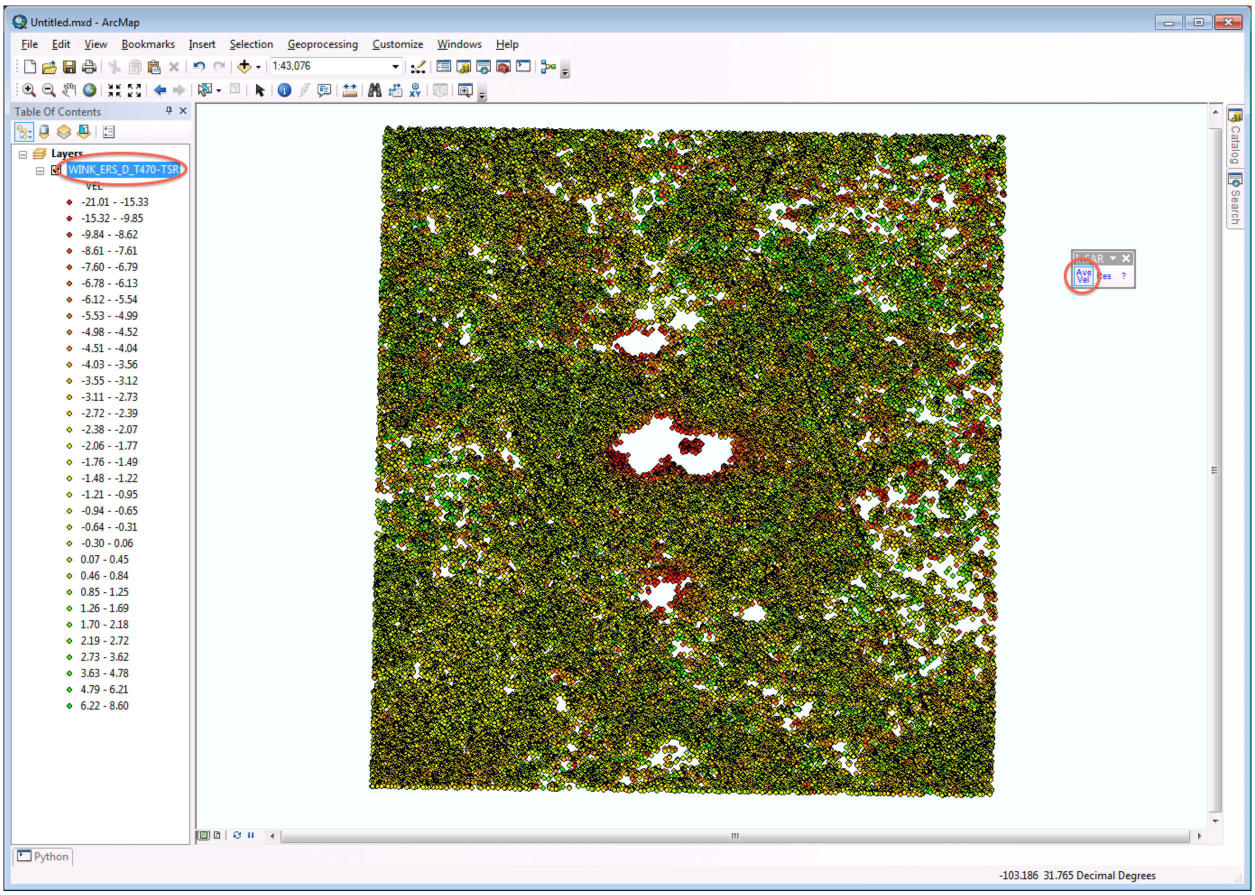

Figure 2.1: When using the *average displacement velocity* tool, make sure to select the layer containg the SqueeSAR data.

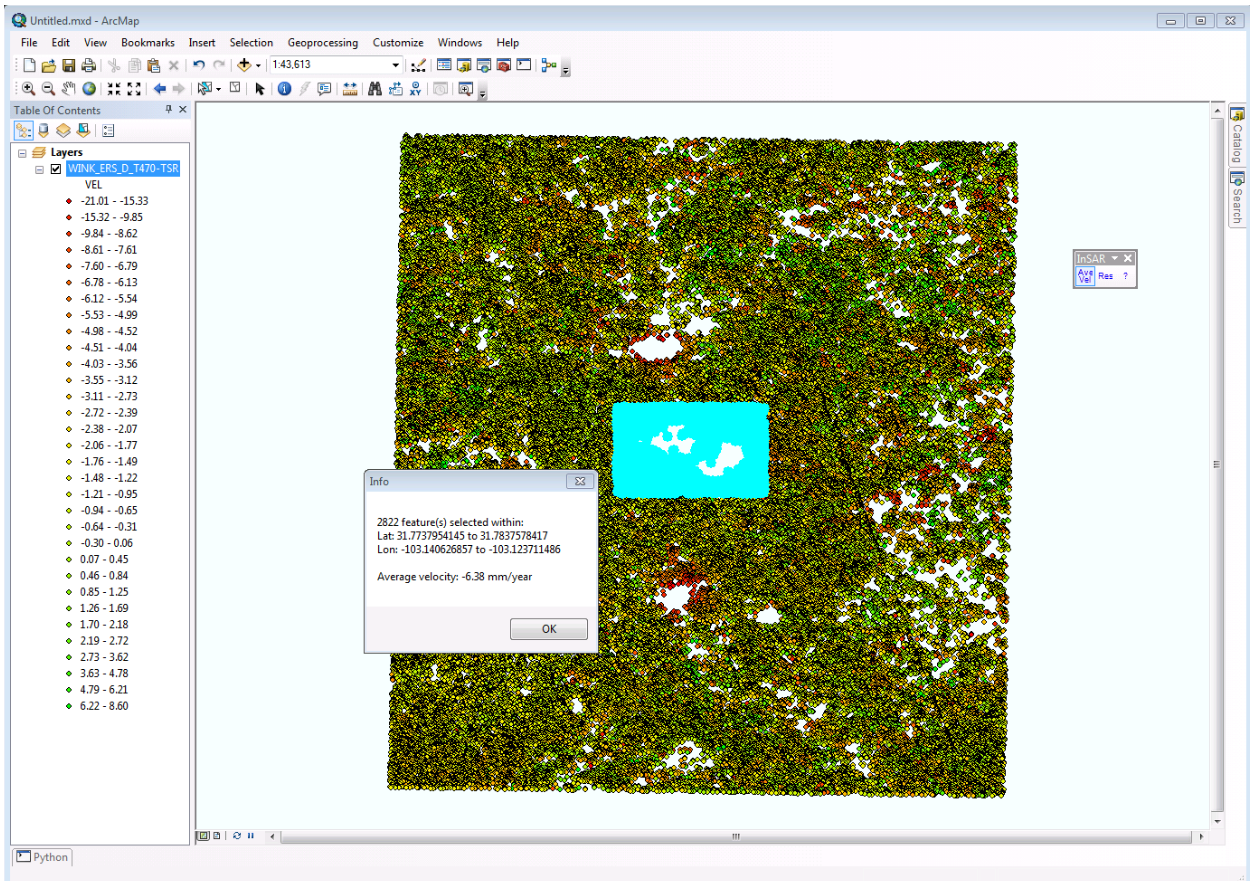

Figure 2.2: Example of the pup-up windows providing informations about the scatterers within the selected area.

The fundamental idea is search the data for regions behaving according to a specific spatiotemporal model. In the case of this tool, the model describes the expected behavior of a developing subsidence. The *subsidence residual* tool will look within the region selected by the user and, for each point on a currently pre-selected grid, will evaluate the difference between measured displacements and those predicted by a series of models obtained by varying size and growth-speed of the modeled subsidence.

As for the *average displacement velocity* tool, in order to perform the subsidence analysis, both the tool and the layer containing the SqueeSAR dataset should be selected and the Res button pressed as illustrated in Fig. 2.3.

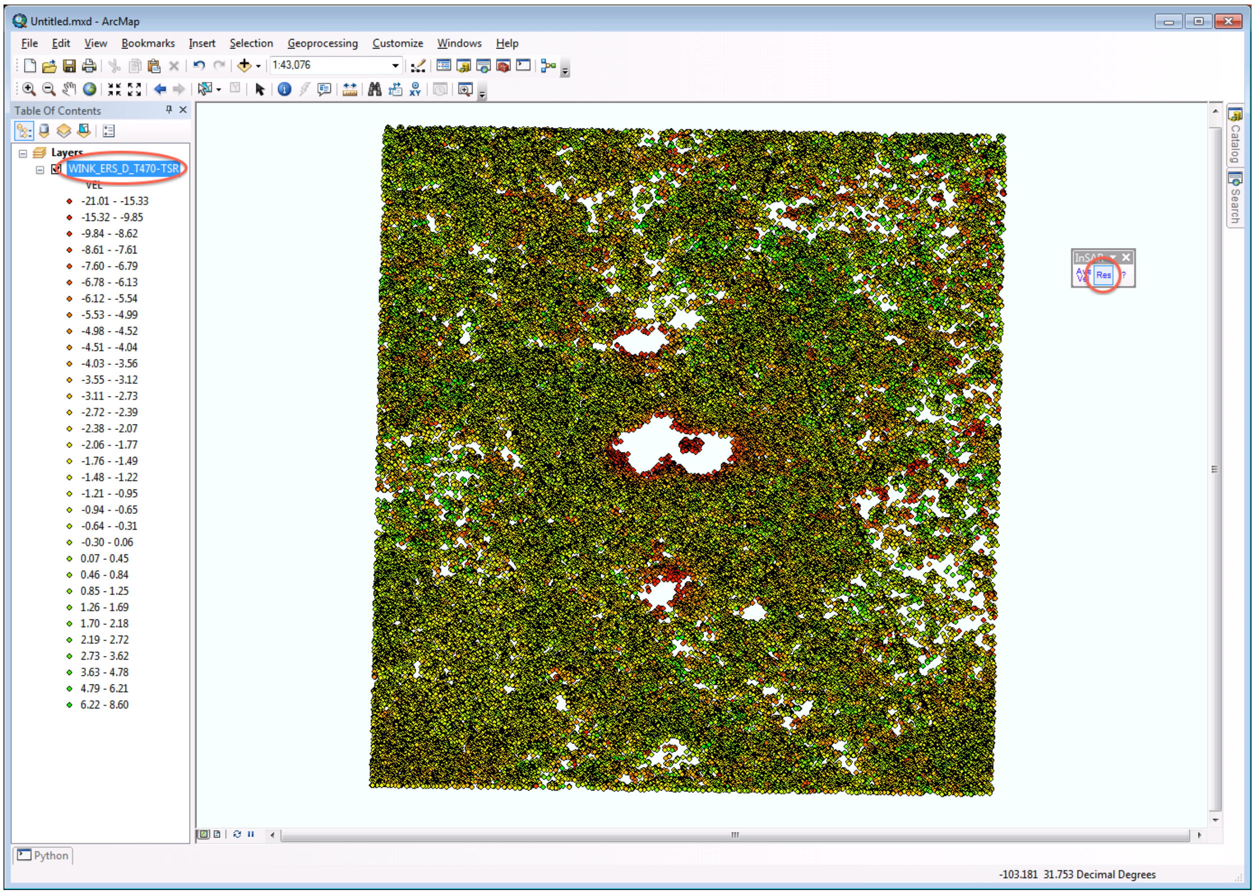

Figure 2.3: When using the *subsidence residual* tool, make sure to select the layer containing the SqueeSAR data.

A raster layer is generated containing, for each cell, the minimum residual obtained dusing the analysis. The raster layer is then stored, with the name of *subsidence*, in both the default geodatabase and as a layer within the map of the first available dataframe. An example of the result is showed in Fig. 2.4.

2.3 About (?)

The *about* button simply returns infromation about the add-in (Fig. 2.5).

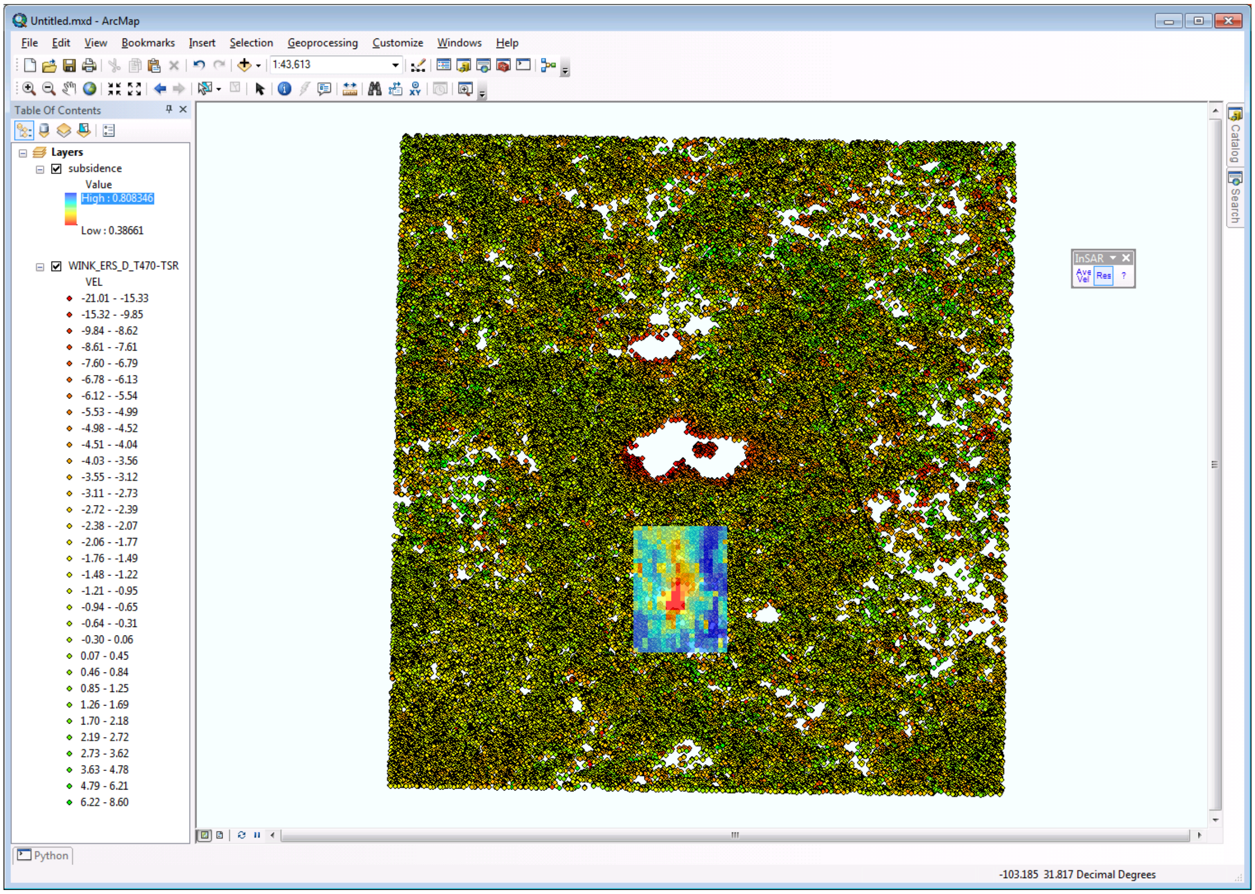

Figure 2.4: Example of the results of running the *subsidence residual* analysis tool within an area specified by the user. The result is a semi-transparent layer overlapped to the selected area. The lowes residual indicates the highest probability that the surrounding region is undergoing a subsiding process.

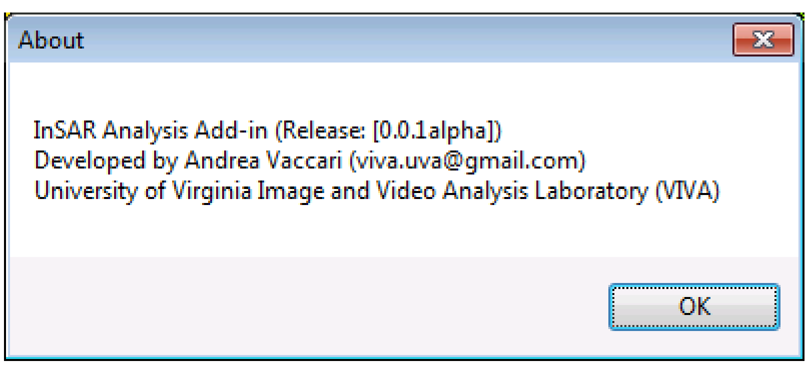

Figure 2.5: Example of infromation provided byt the *About* button.

CHAPTER THREE

DETAILED CODE DESCRIPTION

3.1 InSAR_addin module

This is the main entry point for the InSAR Add-In.

For each tool defined in the `config.xml` file, there is a corresponding class in this file and, for each class, the enabled method.

Things to keep in mind:

- This add-in is not a standalone application but it is supposed to be run from within the ArcMAP environment. As such it assumes the availability of the `arcpy` package and the `pythonaddins` modules which are part of the ArcGIS distribution.
- The initialization of each class occurs when arcmap starts and the addin is loaded.
- The code assumes that only homogenous data is selected and that the fields correspond to the one used by TRE in their data.
- At start time, ArcMAP instantiates an object for each of the classes using a name corresponding to the ID specified in the `config.xml` file. This requires extra caution when defining the name of modules since a duplication of the name will cause the add-in to mulfunction at runtime. Furthermore, the name is only defined in the `config.xml` file hence not visible from within the development environment. Extra care should be placed in naming packages and modules.
- Because of the above point, the `__init__` method of each class defined for each tool in the `config.xml` file is run at program start up.

Note: TODOs:

- Since the add-in is run *in process*, we might want to move the functionality into toolbox/tools, import them when the add-in is initialized, and then call the tools from within the plugin. This would also allow the user to enter parameters.
- Would be nice to use an extension to only enable the toolbar if a SqueeSAR layer is available. How do we determine if one is indeed available? How do we keep looking if a layer is added? `itemAdded(self, new_item)` method in the extension?
- The checking could be extended to allow individual tools depending on the environment conditions.
- There should be more trapping of potential errors with the `try` construct
- If any error occurs whie loading the add-in during startup, the entire ArcMAP will crash and will not start. This *HAS* to be fixed.

> **Caution:** The add-ins run *in process*. Since the evaluation takes a long time, ArcMAP will be locked for the duration of the processing. The algorithm should be moved to a toolbox and then called from the addin. Toolboxes can run in background!

class `InSAR_addin.`**`AboutButton`**

Bases: `object`

The class `AboutButton` is the implementation for the *about* button.

`onClick``()`

The `onClick()` method is called when the button is clicked.

This method displays a pop-up windows including information about the add-in.

class `InSAR_addin.`**`AverageDisplacementVelocity`**

Bases: `object`

The class `AverageDisplacementVelocity` is the implementation of the *average displacement velocity* tool.

`deactivate``()`

The `deactivate()` method is called when ArcGIS deactivates the tool. It cannot be called programmatically. This is where cleanup should happen. In this particular case, the user selection is cleared.

`onRectangle``(`*rectangle_geometry*`)`

The `onRectangle()` method is called after the user has activated the tool and selected an area of interest. This is where the main part of the tool is executed.

This method calls the `common.avevel.evaluate()` function where the average displacement velocity is computed.

After popping-up a window with the result, the selection is cleared and the method returns.

Args:

rectangle_geometry (Extent): the extent of the selection. This argument is passed directly by the ArcMAP enviromnment upon execution of the add-in.

class `InSAR_addin.`**`SubsidenceResidual`**

Bases: `object`

The class `SubsidenceResidual` is the implementation of the *subsidence residual* tool.

`deactivate``()`

The `deactivate()` method is called when ArcGIS deactivates the tool. It cannot be called programmatically. This is where cleanup should happen. In this particular case, the user selection is cleared.

`onRectangle``(`*rectangle_geometry*`)`

The `onRectangle()` method is called after the user has activated the tool and selected an area of interest. This is where the main part of the tool is executed.

In order for the evaluation to be carried on, there should be *at least 3 scatterers* selected.

This method calls the `common.subres.evaluate()` function where the subsidence residual map is computed.

The result of the residual evaluation is stored in a raster file (named *subsidence*) within the default geodatabase. The raster is also added as a layer (with the same name) and overlayed with transparency over the area selected by the user.

Args:

rectangle_geometry (Extent): the extent of the selection. This argument is passed directly by the ArcMAP environmnent upon execution of the add-in.

3.2 common package

The *common* package includes the actual implementation of the analysis algorithms separated in different submodules.

3.2.1 Submodules

common.avevel module

This module implments the code necessary to evauate the average displacement velocity of a group of SqueeSAR scatterers selected by the user.

`common.avevel.evaluate(layer)`

This function evaluates the actual average displacement velocity.

Args: layer (Layer): a reference to the layer containing the SqueeSAR data.

Returns: ave_vel (float): the average displacement velocity of the selected scatterers.

common.subres module

This module implements the subsidence analysis algorithm developed by VIVA.

The technique is fully described in the following paper (available for download here):

Vaccari, A.; Stuecheli, M.; Bruckno, B.; Hoppe, E.; Acton, S.T.; **"Detection of geophysical features in InSAR point cloud data sets using spatiotemporal models,"** *International Journal of Remote Sensing,* vol.34, no.22, pp.8215-8234. doi: 10.1080/01431161.2013.833357.

Note: The current implementation is not optimized for execution speed and is made available for demonstration purpose only. The parameters are automatically evaluated and the user should be careful not to select more than a few hundred scatterers since computational times can be quite long.

`common.subres.evaluate(extent, layer)`

This function creates a raster where each cell represents the minimum value of the residual (difference) between various models of subsidence centered at the cell location and the SqueeSAR dataset. For each location, several spatio-temporal subsidence models are created and for each of the model the average difference between predicted and observed displacements is evaluated. The raster is generated by taking the minimum residual value of every model.

In the current version, the parameters limits are automatically selected (see the source for more information). In future versions, we are planning to give the user the option to select the ranges and steps for each of the parameters. This requires to move the implementation within the toolbox framework.

Note: TODO:

- modify the code to take advantage of the "band" structure in the raster. Each band should incorporate a "slice" of the multi-dimensional residual array: minimum (current returned value), propagated residual, sigma, and alpha. (See the paper for more details)

Args: extent (Extent): the extent object identifying the user-selected area.

layer (Layer): a reference to the layer containing the SqueeSAR data.

Returns: propres (float array): the minimum projection of the residual array.

common.utils module

The `common.utils` module contains function that are required by several other modules within the `common` package.

`common.utils.`**`selectSqueeSARData`**(*extent*, *layer*)

This function translates the extent selected by the user into the spatial reference of the SqueeSAR layer and identifies the features within the selected area.

Args: extent (Extent): the extent object identifying the user-selected area.

layer (Layer): a reference to the layer containing the SqueeSAR data.

Returns: nfeat (int): the number of features (scatterers) within the selected area.

spatref (SpatialReference): the spatial reference of the SqueeSAR layer.

Raises: UserWarning: if there is no data within the selection.

`common.utils.`**`verifySqueeSAR`**()

This function verifies if the selected layer is a SqueeSAR layer, and if the data is available.

Returns: layer (Layer): selected layer or data frame from the table of contents.

md (MapDocument): reference to current map document.

Raises: UserWarning: if an invalid layer is selected.

CHAPTER FOUR

REVISION HISTORY

[0.0.2alpha], 2014-10-10

- Removed requirement of for scipy package.
- Added HISTORY.rst to trace development.
- Modified `config.xml` to target ArcMAP 10.2

[0.0.1alpha], 2014-10-18

- Initial alpha release.

CHAPTER FIVE

INDICES AND TABLES

- *genindex*
- *modindex*
- *search*

c

i

INDEX

Appendix G – University of Alaska Fairbanks – Final Report

F. Mayer, W. Gong, O. Ajadi, and A. Worden – **Contribution of the University of Alaska Fairbanks – Final Report** – August 2016 [download][11]

[11] http://viva-lab.ece.virginia.edu/elecdocs/ritars14/UAF.pdf

InSAR Remote Sensing for Performance Monitoring of Transportation Infrastructure at the Network Level

Contribution of the University of Alaska Fairbanks

Final Report

August 15, 2016

Contributors:

Dr. Franz J. Meyer*, PI, Associate Professor, Geophysical Institute, University of Alaska Fairbanks
Dr. Wenyu Gong, Post-Doctoral Researcher, Geophysical Institute, University of Alaska Fairbanks
Mr. Olaniyi Ajadi, Research Assistant, Geophysical Institute, University of Alaska Fairbanks
Ms. Anna Worden, Research Assistant, Geophysical Institute, University of Alaska Fairbanks

*Corresponding author; email: fjmeyer@alaska.edu

Submitted to the Virginia Transportation Research Council (VTRC)

Table of Contents

1 Introduction

The main activity to be addressed by the UAF team was defined in the originally developed Statement of Work and included the following four subtasks:

"The UAF team will work in collaboration with the Virginia Department of Transportation (VDOT) and the InSAR processing company TRE to analyze the role of Temporary Scatterers (TS) in a transportation infrastructure setting. The team will: (1.1) perform a geophysical analysis of the TS products provided by TRE to understand their information content and applicability to infrastructure performance assessment; (1.2) they will work on understanding the limitations of current TS technology when applied to infrastructure monitoring, and (1.3) develop post processing strategies to maximize the impact of TS. The team will (1.4) communicate findings back to VDOT and TRE. UAF will also interact with TRE to further analyze the full covariance properties of TS and further develop TS technology if deemed necessary and desirable by all parties."

This initial work plan has since been slightly modified to further include (2) an assessment of the benefit of SAR amplitude information for transportation infrastructure monitoring and (3) the development of a first draft of an outreach plan for communicating the benefit of InSAR to the DOT community.

This report summarizes the work that was done within this grant. After providing information about the establishment and start date of the UAF-component of this research project (Section 0), we will describe the research work conducted during the period of performance of this grant. These activities include: (1) Discussions on the nature and limitations of TS products provided by TRE; (2) the development of optimized methods for integrating SAR amplitude information into transportation infrastructure monitoring; and (3) the preparation of outreach material for communicating the benefit of InSAR to the DOT community. Several amplitude analysis methods are presented in Sections 4.2 and 4.3, including methods for the use of SAR amplitude information for identifying *changes* on and around the road networks (e.g., related to road surface degradation, repaving, slope motion or similar activities) as well as methods that support the directly estimation road surface condition status (as quantified by the IRI parameter) from SAR data.

2 Summary of Findings

While most work on SAR-based transportation infrastructure monitoring has focused on using the *phase* component of the SAR signal, our research was dedicated to the use of SAR *amplitude* data for transportation infrastructure analysis. This choice was motivated by our strong belief that SAR amplitude information carries relevant yet typically untapped potential in transportation infrastructure monitoring. Additionally, amplitude analysis requires less specialty knowledge about the SAR image formation process and is, hence, easer to conduct by an end-user such as the DOT.

Our research has shown that SAR amplitude information from high resolution X-band SAR sensors (such as TerraSAR-X, TanDEM-X, or CosmoSkymed) has a range of previously unutilized applications in the analysis of road pavement conditions: (1) We found that time-series analysis of SAR amplitude data can be used to detect *changes in surface conditions on roads* and the environment around roads; (2) we also found that SAR amplitude information can be used to measure *absolute road surface conditions* as quantified by the International Roughness Index (IRI). Here, best performance was achieved for measuring the IRI of secondary roads. As SAR systems can measure these parameters over large areas and at dense repeat frequency, high-resolution SAR sensors should be included into the set of measurement tools used by DOTs for pavement condition analysis.

While we didn't specifically study the influence of spatial resolution on the performance of SAR for road surface analysis, it is likely that high-resolution data of the 1m resolution type are needed for monitoring road surface conditions. This conclusions is related to our finding that SAR data is most useful for measuring the conditions of secondary roads (see Section 4.3), whose typically narrow width are likely requiring high-resolution information.

For more details on our work and its conclusions, please refer to the following paragraphs.

3 Administrative Details

After delays with both the installation of the grant and the transfer of money to UAF, the grant finally was established at UAF at the end of February 2014. Hence, the UAF portion of the project started about 6 months later than related components of this effort.

Much of the project work was planned to be conducted by a Ph.D. student that was to be hired for this grant. Unfortunately, no qualified student could be found for the fall semester 2014. To move this research work forward despite of the lack of a student, a UAF staff member could temporarily be recruited to work part time on this research project. We have since filled the open student position with full-time Master's student Anna Warden (Spring 2015 – Summer 2015) and full-time Ph.D. student Olaniyi Ajadi (Fall 2015 until the end of the project). Both students had sufficient background in GIS and data analysis to effective contributors to this project. Student Ajadi additionally had strong credentials in remote sensing image analysis and processing.

4 Research Achievements

4.1 Research Goals

This research project is focusing on the use of InSAR techniques for monitoring of transportation infrastructure on a network scale. In most applications of InSAR, the investigators utilize time-series information of the *phase* of the acquired SAR data in order to track surface deformation and detect surface changes over time. While the benefit of phase information for monitoring tasks is well established and has been proven in a wealth of test studies, the added value of the *SAR amplitude information* has not yet been rigorously researched.

Hence, the goal of UAF's part of this research project was to establish an optimized processing flow that allows extracting relevant information about pavement conditions and other parameters related to the transportation network from time series of SAR amplitude data. Such information may include (1) the detection of certain types of unstable slopes from an analysis of changes of surface scattering characteristics; (2) the detection of changes of road surface conditions through the detection of image brightness chances with time; and (3) the automatic classification of road surface types through the correlation of backscatter amplitudes to pavement types (extracted from a data base).

In the following we will report on research progress related to topics. As many environmental parameters affecting SAR data are mitigated in a differencing process, detecting changes of a system is often more straightforward than measuring the absolute state of a variable directly. Hence, in Section 4.2 we will first present research on the use of time-series of SAR amplitude data to estimate *changes of road conditions* (Section 3.2). Subsequently, in Section 4.3, we will present our results on estimating *absolute* road surface quality from SAR.

4.2 Assessment of the Benefit of SAR Amplitude Information for Analyzing *Changes in* Road Surface Conditions

4.2.1 Image Pre-Processing Recommendations

Automatic classification and change detection of SAR amplitude images is hampered by two main issues inherent to SAR data. The first one of these is the presence of Speckle in SAR amplitude data, a dominant noise-like image feature that is due to the narrow-band coherent nature of the SAR signal. The salt-and-pepper-type characteristics of speckle noise can be seen in the image example in Figure 1(a). This example highlights the negative implications of Speckle for automatic image classification: The graininess of the image brightness makes it difficult to cleanly identify features of interest from SAR images.

The second problem inherent to SAR data is a strong topographic shading that is caused by the oblique observation geometry of SAR sensors and is leading to local biases of the true surface reflectivity. An example of topographic shading can be seen in the top right quarter of Figure 1(b), where rolling hills cause a brightness difference between the sensor-facing side of the slope (top half) and the opposite-side facing slope (bottom half of feature). The shading effects cause otherwise homogenous surfaces to vary in brightness, hence, significantly complicating image classification procedures.

During the initial stages of this project we addressed the issue of Speckle suppression. A short summary of methods for correcting topographic shading are also mentioned below.

4.2.1.1 Traditional Speckle Filters and their Problems

Two general types of filtering methods have been developed in the past that attempt to suppress speckle in SAR data, namely spatial and temporal filters. Both filter methods lead to the loss of signal resolution

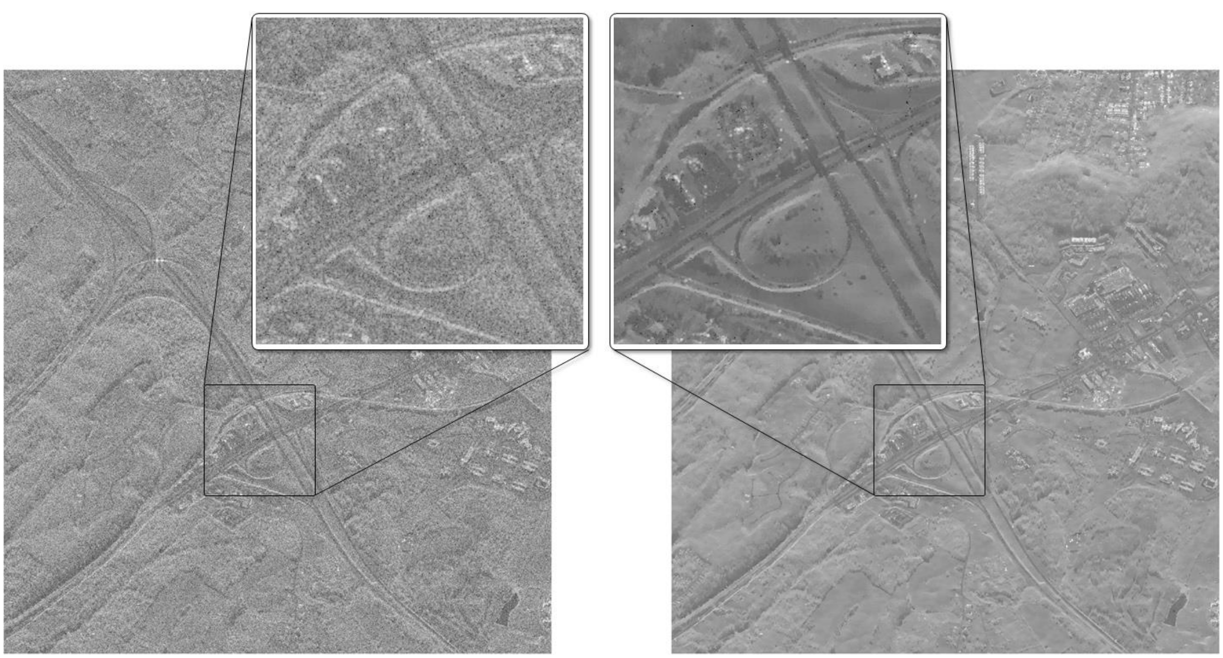

Figure 1: Example of an original (a) and a SqueeSAR-pre-filtered (b) SAR amplitude image. The benefit of pre-filtering is evident on the significant reduction of Speckle noise in (b)

in either space or time. Spatial filters, in their core, perform spatial averaging of nearby pixels to reduce speckle noise. Even though sophisticated versions of such filters exist (Bruniquel and Lopes, 1997; Dekker, 1998; Huang et al., 2009; Lee et al., 1991; Lee et al., 1994; Lopez-Martinez and Pottier, 2007; Novak and Burl, 1990; Sveinsson and Benediktsson, 2003), all versions inevitably result in some loss of image resolution especially in heterogeneous regions. Temporal filters (Adam et al., 2004; Kampes, 2005) analyze the temporal signature of the SAR response whilst ignoring spatial information. Inversely to spatial filters, they preserve spatial resolution but smooth out changes in time.

4.2.1.2 Non-Local Means Filers

Non-local means (Buades et al., 2005) is a relatively recently developed algorithm in image processing for image denoising. Unlike the filters mentioned in Section 4.2.1.1, which take the mean value of a group of pixels surrounding a target pixel to smooth the image, non-local means filtering takes a mean of all pixels in the image, weighted by how similar these pixels are to the target pixel. This results in much greater post-filtering clarity, and less loss of detail in the image compared with local mean algorithms.

If compared with other well-known denoising techniques, such as the Gaussian smoothing model, the anisotropic diffusion model, the total variation denoising, the neighborhood filters and an elegant variant, the Wiener local empirical filter, the translation invariant wavelet thresholding, the non-local means method noise looks more like white noise. Non-local means approaches were first used on SAR data in (Jin et al., 2006) and have since been recognized as a powerful method for removing noise from SAR data (Chen et al., 2014; Deledalle et al., 2010; Liu et al., 2008; Martino et al., 2015).

Our research shows that non-local means filtering leads to a significant improvement of SAR image classification and to a performance improvement in change detection from SAR (Ajadi et al., 2016). We recommend them as an appropriate pre-processing technique for road surface analysis from SAR.

4.2.1.3 The SqueeSAR Solution to Speckle Filtering

One of the most underutilized characteristics of the SqueeSAR algorithm (Ferretti et al., 2011) is its highly sophisticated speckle filtering capability and the related implications on quality improvement of SAR amplitude data. The goal of SqueeSAR is to provide an optimized estimate of the true (noise-free) signal phase at every pixel of a SAR image. To do so, the SqueeSAR algorithm is calculating a full (spatio-temporal) covariance matrix of all SAR observables in a SAR data stack and jointly uses the temporal and spatial information contained therein to adaptively filter the SAR data. In that sense, SqueeSAR has an advantage over the previously mentioned traditional speckle filtering methods as it leads to optimized noise suppression, whilst preserving the original signal resolution in both time and space.

Hence, SqueeSAR is an excellent data pre-processing step for denoising not only the phase but also the amplitude information in a SAR data stack. Figure 1(b) shows the results of the SqueeSAR denoising procedure for one image of a SAR data stack over Staunton, VA. When compared to Figure 1(a), the improvement of image quality and the decrease of the noise level are clearly visible.

In the following we will use SqueeSAR-pre-processed SAR imagery as a basis for all higher-level information retrieval algorithms that were developed to detect changes in time series of SAR amplitude images.

4.2.2 Applying Multi-Scale Change Detection on Pairs of SAR Images

4.2.2.1 Applied Approach

To demonstrate the kind of information that can be extracted from time series of SqueeSAR pre-processed SAR images, we modified a fully automatic multi-scale change detection algorithm that we have developed specifically for autonomous information extraction from time series of SAR data (Ajadi et al., 2016; Meyer et al., 2014). The approach combines advanced multi-scale image processing algorithms with unsupervised automatic thresholding procedures based on Bayesian inferencing. The workflow of our amplitude change detection procedure is depicted in Figure 2 (taken from Meyer et al., 2014). In essence, the approach includes the following steps:

- **Log-scaled ratio image formation and additional pre-filtering:** To identify potential surface changes from SAR data, a ratio image is formed between every image X_i in the SqueeSAR stack and a reference data set X_R, which in the current solution is the pixel-by-pixel median of all images in the data stack. Using ratio images in change detection was first suggested by Dekker (1998) and has since been the basis of many change detection methods (Bazi et al., 2005; Celik, 2010; Coppin et al., 2004). Ratio formation has the advantage that stationary background information can be optimally suppressed while the signal of interest is enhanced. Furthermore, the log-scaling turns the originally multiplicative residual Speckle noise into additive noise, which is easier to treat. A fast non-local mean filter (Liu et al., 2008) is applied to the data to reduce residual Speckle noise whilst preserving the resolution of the data.
- **2D-SWT Decomposition:** A 2D stationary wavelet transform (2D-SWT) is applied to the log-scaled ratio images to further mitigate the effects of speckle noise on the change detection result, whilst preserving details in the resulting change map. Recursively applying the 2D-SWT to the log-ratio image X_{LR} is an efficient way of building a multi-scale representation of the change information captured in the image. At the k^{th} decomposition step, the 2D-SWT is producing (1) a lower resolution version $X_{LR}^{LL_k}$ of X_{LR} as well as (2) three high-frequency representations, capturing the image details in horizontal, vertical, and diagonal direction, respectively. We implemented a decomposition into $K = 6$ resolution levels and use the lower resolution images $X_{LR}^{LL_k}$ at each resolution level to create a final multi-resolution image set X_{MS} according to: $X_{MS} =$

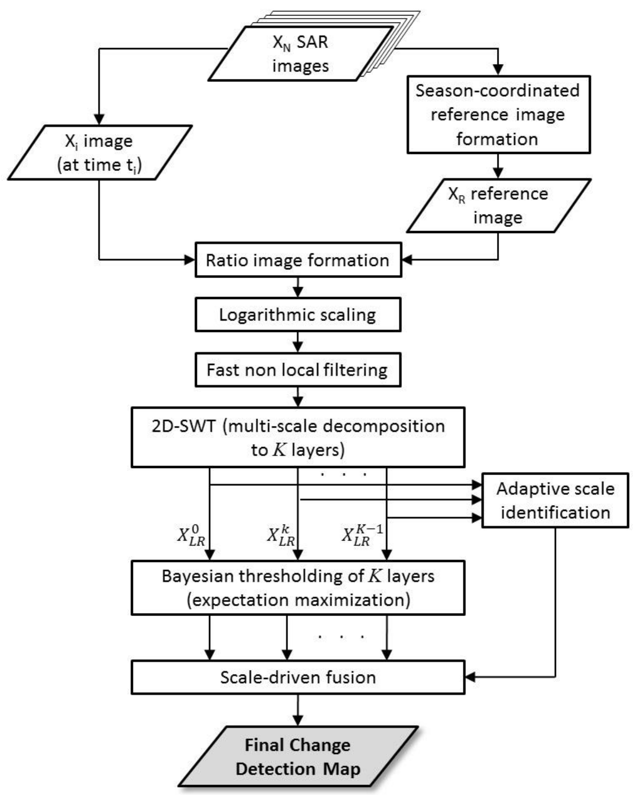

Figure 2: Flow chart of the automatic change detection procedure implemented on time series of SAR amplitude images.

$\{X_{LR}^{LL_0}, \ldots, X_{LR}^{LL_k}, \ldots, X_{LR}^{LL_{K-1}}\}$. At higher decomposition levels, the signal-to-noise ratio of the data is improving yet the spatial detail is decreasing.

- **Automatic change detection using Bayesian Inference:** For all layers of the multi-resolution image set X_{MS} a set of (scale-dependent) detection thresholds is defined that classifies all pixels of X_{MS} into the classes "changed (w_c)" or "unchanged (w_u)", resulting in a sequence of K change detection maps C_{MS}. To automate the determination of the threshold sequence T, a Bayesian inferencing method is employed on the magnitude of X_{MS}. Here, we assume that the probability density function $p(X_{MS}^k)$ of the k^{th} layer of X_{MS} can be modeled as a mixture of the probability density functions associated with the classes w_c and w_u. To estimate the parameters of these probability density functions, an expectation maximization (EM) (Redner and Walker, 1984) algorithm is used, which finds the maximum a-posteriori (MAP) estimates of the densities $p(X_{MS}^k|w_c)$, $p(X_{MS}^k|w_u)$, $p(w_c)$, and $p(w_u)$, in an iterative search conditioned by observations.
- **Scale-Driven Fusion of Multi-Scale Classification Results:** To create the final change detection map, C, the information in the multi-scale change detection series C_{MS} is fused using data across all so-called reliable scales (please see (Meyer et al., 2014) for information on reliable scales). For each pixel, the classification decisions at the reliable scales are combined and the pixel is assigned to the class that obtains the highest number of votes in the set C_{MS}^R.

4.2.2.2 Results of Automatic Change Detection from Image Pairs

To test the validity of this approach for detecting changes related to the transportation network, we analyzed an image segment of a stack of 57 multi-temporal Cosmo SkyMed images over the area of Staunton, VA. One of these 57 image segments is shown in Figure 1(a). The image stack was pre-processed using the SqueeSAR algorithm, resulting in Speckle-filtered data (see Figure 1(b) for a sample of the pre-filtered data). A further 300x300 pixel segment was extracted from the image stack to demonstrate the change detection approach (see Figures 3(a) – (c)).

The previously described multi-scale filtering approach was applied to several time slices of this 57 image deep data stack. To this end, a reference image (X_R) was computed, corresponding to the median of all images in the 57 image stack (see Figure 3(a)). Subsequently, log-ratio images were formed between individual time slices of the image stack and this reference image. Two of these ratio images are shown in Figure 3(d) and (e), corresponding to the log-scaled ratio between X_R and the SAR images acquired on 11/15/11 (Figure 3(b)) and 12/23/13 (Figure 3(c)). The ratio images are scaled such that dark black corresponds to a decrease in signal amplitude by -1dB (related to X_R) while bright white corresponds to a brightness increase by +1dB.

The multi-scale change detection approach was applied to the log-ratio images and change detection images C were calculated for both images instances (see Figure 3(f) and (g)). In a final step, the outlines of the identified change regions are traced and overlain onto the SqueeSAR pre-filtered amplitude images (Figure 3(h) and (i)).

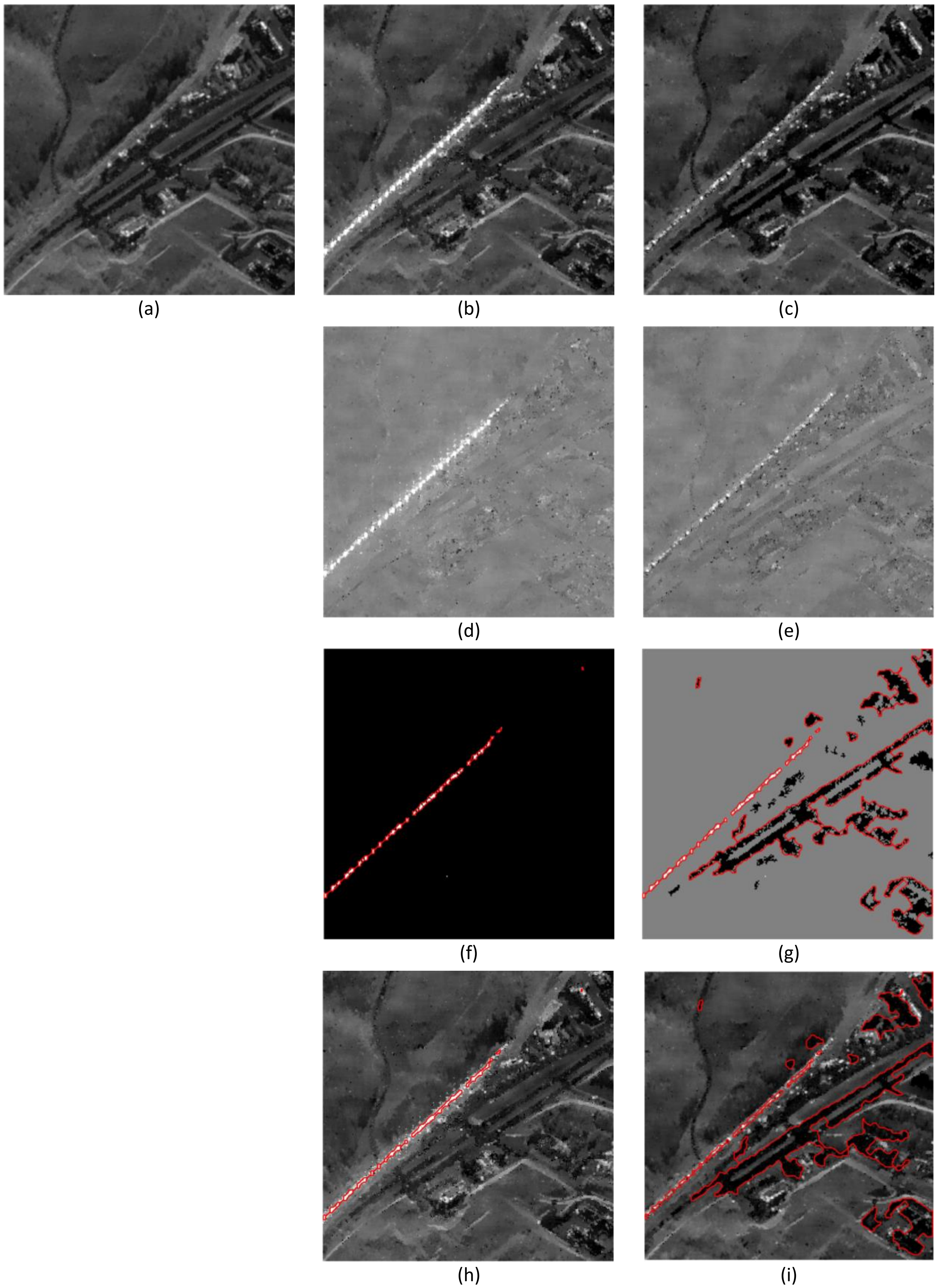

Figure 3: Results of automatic change detection on SqueeSAR pre-filtered amplitude time series data: (a) – (c): Reference image and two filtered image instances; (d) & (e): log-ratio images; (f) & (g): Change detected using multi-scale algorithm; (h) & (i): Outlines of changed areas on amplitude images.

The two examples shown in Figure 3 indicate that SqueeSAR-pre-filtered amplitude time series data has some benefits for the analysis of changes within the imaged area. The change signature identified in Figure 3(b), (d), (f), and (h) is likely due to a non-moving or slow moving train was present on the railroad tracks along Jefferson Hwy during the image acquisition time on Oct 15, 2011. Double-bounce and multi-bounce effects on the train cars contributed to the bright radar cross section that is observed on this day. The observed signature could nicely be delineated.

The changes that were identified on Dec 23, 2013 include similar train-related signatures along the railroad tracks, but also some brightness changes associated with a range of paved surfaces. A decrease in brightness was identified along Jefferson Highway as well as for many of the paved parking lots within the image segment. The reasons behind this change are currently unknown but are most likely related to local weather conditions on the day of image acquisition (e.g., heavy rain or wet snow).

These results indicate the general suitability of SqueeSAR-pre-filtered SAR amplitude time series for surface change detection and that an analysis of pairs of images is useful to detect sudden changes on the road network. In the next sections we expand this research to also consider time-series data.

4.2.3 Detecting Trends in Amplitude Time-Series Data

4.2.3.1 Initial Algorithm Development

In addition to looking for changes between pairs of images, we started investigating the applicability of the pre-filtered SAR data for the detection of brightness trends throughout the three years long image time series.

To gain experience with the information content of the data we developed a first demonstration approach that, while not fully developed, is still sophisticated enough to allow for some conclusions about the applicability of SAR data for this task. The initial processing flow was as follows:

- Import SqueeSAR-pre-filtered and amplitude-calibrated SAR data together with their acquisition dates and stack the data (resulting in a 57 layer deep image stack)
- Perform the following calculations on a pixel-by-pixel basis:
    - Data preparation: Extract the (irregularly sampled) 57 step long amplitude time series
    - Smoothing of the time series: To accommodate irregularly sampled data, a local regression method based on weighted linear least squares is used.
    - Least-squares linear regression: A line is fitted to the smoothed time series using a least-squares approach. Both the line slope and the variance of this line slope are estimated.
    - Identify significant change: Significantly changing pixels are identified using a statistical significance test based on the Student's t-test.

Some results of this analysis are shown in Figure 4. This figure highlights individual image areas for which significant image amplitude trends were identified by our data analysis approach. The first row in Figure 4 shows two areas that are affected by step-like brightness changes. Area 1 in Figure 4(a) shows a sudden increase of the radar cross section by about 0.6 dB in late summer 2013. Conversely, Area 2 in Figure 4(a) shows the opposite behavior, with a drop of image brightness by about 1dB in early summer of 2012. The

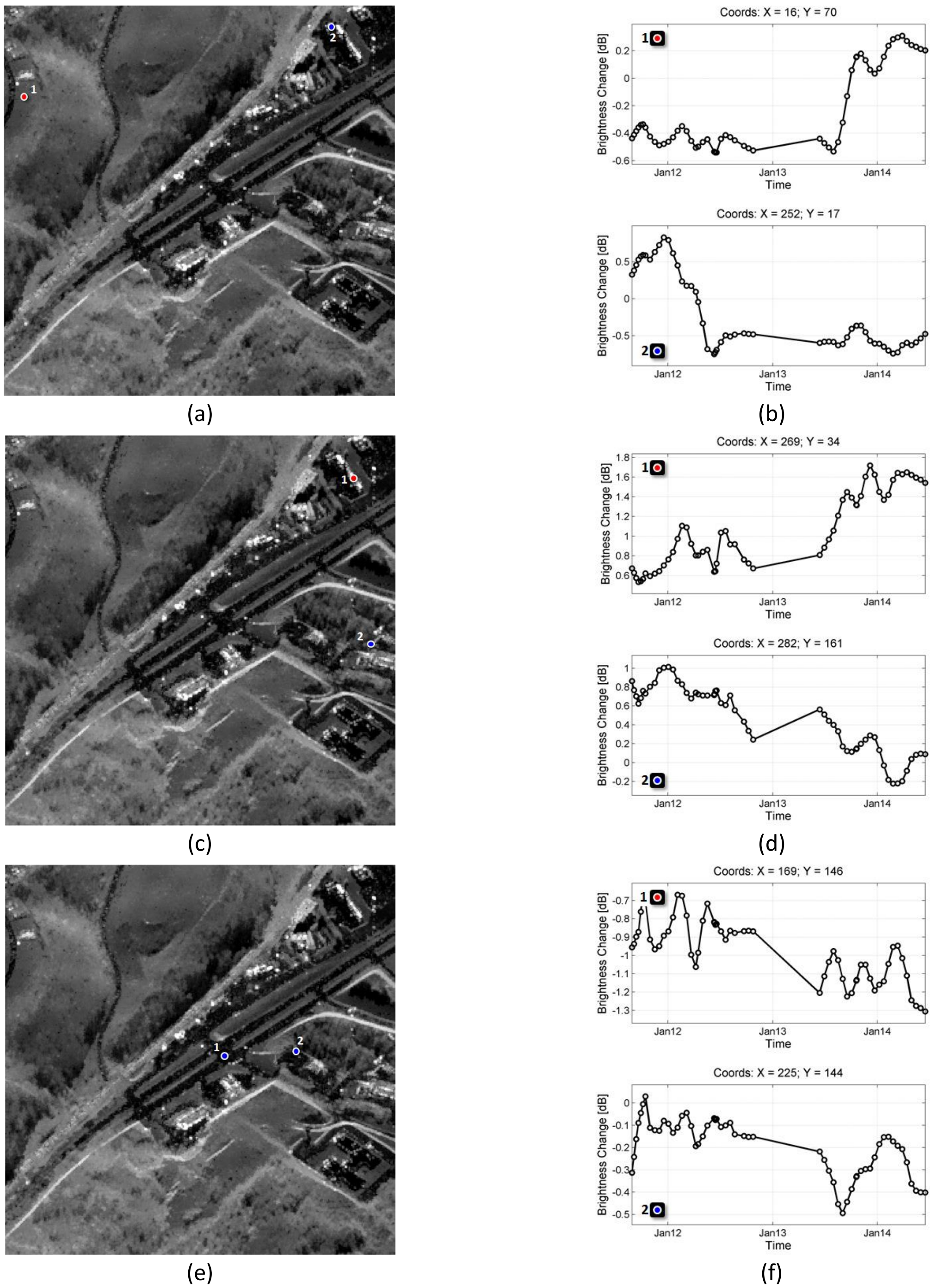

Figure 4: Images areas subject to linear trends in their amplitude time series. First row data shows stepwise trends; second row data shows linear trends in areas outside of the road network; third row shows parts of the road network whose radar amplitude changes with time. All calculations are done in the dB domain.

corresponding amplitude time series information is shown in Figure 4(b). The reasons behind the observed step-like changes are currently unknown.

The second row of Figure 4 focuses on linear changes of image brightness. The two areas highlighted here show linear brightness changes of abou 1dB across the three years of obervation. Both areas seem to correspond to bulid-up areas along Jefferson Highway.

The third row of Figure 4 focuses on trends observed for paved surfaces. Note that for most paved surfaces, no significant change of image brightness could be identified and only few selected areas showed interesting signals. The two examples presented in Figure 4(e) and (f) are affected by very slight darkening of the image amplitude over time.

An analysis of the examples shown in Figure 4 also indicates that, in addition to signatures related to physical surface changes, the time series data are affected by significant short term brightness variations, which limit the ability of SAR amplitude data to detect change. We suspect that these short-term fluctuations are related to changing weather conditions (mostly surface moisture) in the area. Despite these limitations, some potential for SAR-based analysis of transportation networks could be shown.

4.2.3.2 Further Development of the Time-Series Technology

The approach presented in Section 4.2.3.1 was further refined in the second project year to make the detection of true change more robust and to better visualize the results of the change analysis.

The refined version of the approach is analyzing all pixels of a SAR data stack in a manner that is similar to the time-series InSAR method PS-InSAR or SqueeSAR:

- Formation of Data Stack: A 3-d data stack is formed from all available multi-temporal SAR images resulting in a $T \times N \times M$-sized data cube, where T is the number of time steps, and $N \times M$ is the size of each SAR image in pixels. While not necessary, DespecKS-type data are preferred for amplitude analysis.
- Normalization of amplitude data: To achieve data of similar statistical properties, all T image slices are normalized by forming the log-ratio of each image with a temporal average of all images in the stack.
- Interpolation to regular temporal samples: As the data cube is likely irregularly sampled in the time direction T, we interpolate the time-series data to a regular time-grid using a piecewise spline interpolation. The interpolation is necessary to make further processing steps such as filtering or Fourier-type analyses more effective.
- Smoothing of the time series: To filter the time series data, a local regression method based on weighted linear least squares is used. Various filter kernels can be picked.
- Least-squares linear regression: A line is fitted to the smoothed time series using a least-squares approach. Both the line slope and the variance of this line slope are estimated.
- Significance testing of estimated regression slopes: A Student's t-test is applied on the estimated regression slopes to determine whether or not the estimated slopes are significantly different from zero. Slope estimates for which the t-test cannot be rejected at the 95% confidence level are set to zero, such that only significant slopes are reported.
- Significance testing of estimated regression slopes: A Student's t-test is applied on the estimated regression slopes to determine whether or not the estimated slopes are significantly different.

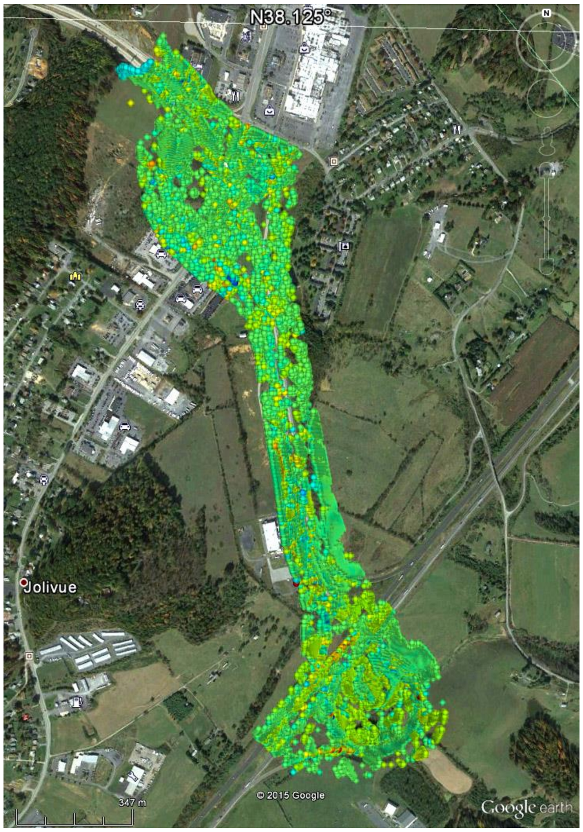

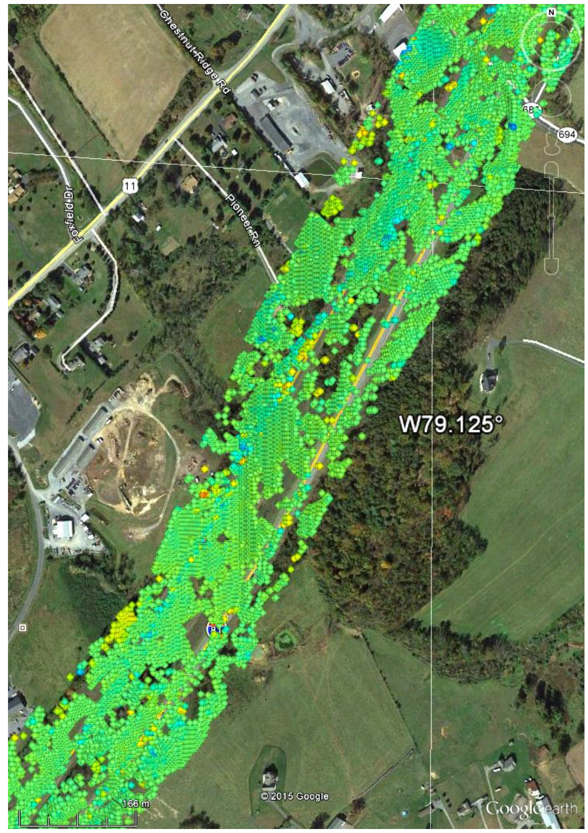

(a) (b)

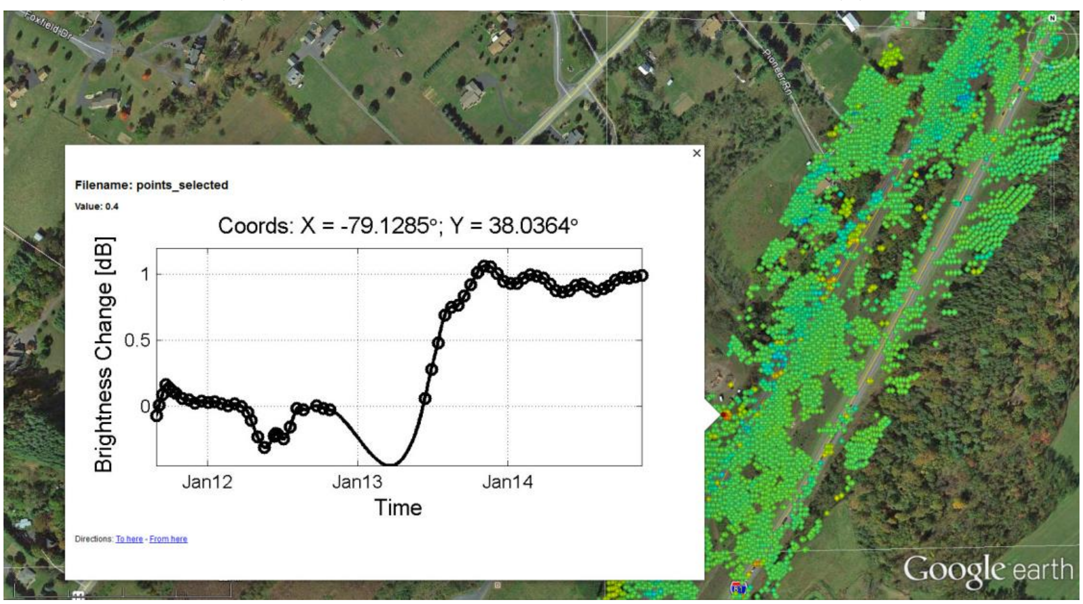

(c)

Figure 5: Examples of SAR Amplitude Time-Series results: (a) area near the intersection of Highway 81 and the Woodrow Wilson Pkwy; (2) segment of Highway 81 between Mint Spring and Greenville; (3) Visualization of full amplitude time series for a point on Highway 81 with significant amplitude change.

- <u>Export of all points with significant slopes to a kmz Google Earth product</u>: All pixels for which a significant change of image brightness was determined are exported to a kmz file for visualization in Google Earth (see Figure 2(a) and (b)). Each location is color-coded according to its estimated amplitude change rate (in dB/year). To support the analysis of the amplitude change data, each color-coded kmz point is associated with a plot of the full amplitude time series (see Figure 3(c)). This way, the type of change (gradual vs. sudden) can be analyzed visually by the user.

Some results of the modified version of the amplitude time-series analysis approach are shown in Figure 5. Figure 5(a) shows the results of amplitude change analysis for an area along Woodrow Wilson Pkwy, near the intersection with Highway 81. Accepted point are color-coded according to their linear amplitude change between -1dB/year (blue) and +1dB/year (red). The density of derived information can be easily seen. Figure 5(b) shows a segment of an analysis that was done for an area along Highway 81 between Mint Springs and Greenville. For this area, the benefit of the availability of the full amplitude time series information is demonstrated (Figure 5(c)). Via mouse click on a point along Highway 81 that was found to have significant linear brightness increase, the full amplitude time-series was visualized. This time-series information shows that this point was affected by a sudden backscatter increase during the second half of 2014, potentially indicating surface breakup around that time.

4.3 Using SAR Amplitude Information to Directly Estimate *Absolute* Road Quality as Quantified by the IRI Parameter

4.3.1 Goals

While the work in Section 4.2 focused on the analysis of changes of road surface conditions, this section will provide a summary of research that was dedicated for absolute road quality assessment.

Approaches were analyzed in years 2 and 3 of this project to assess the feasibility of SAR amplitude information to determine absolute road surface quality. To this end, SAR amplitude data (as well as derived parameters) were correlated to road condition data that were available in the form of International Roughness Index (IRI) measurements.

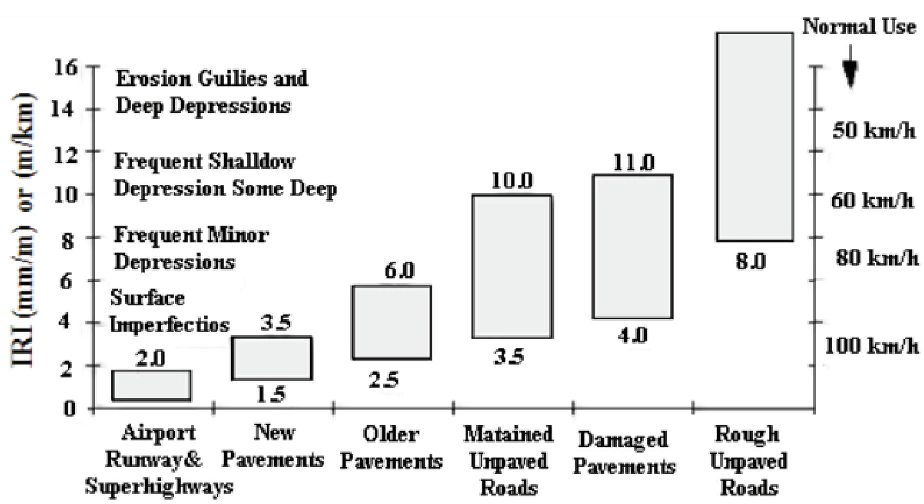

Figure 6: IRI roughness scale and road surface conditions around the world (Sayers and Gillespie, 1986)

In the following, we will first introduce the IRI parameter and its expected relationship to SAR amplitude information (Section 4.3.2). Subsequently, we will summarize our analysis approach (Section 4.3.3), and show first results of IRI estimation from SAR (Section 4.3.4). Finally, we will describe future research ideas that should be pursued to confirm and validate our findings (Section 4.3.5).

4.3.2 The IRI Index and its Expected Relationship to SAR Amplitude Data

The IRI, which was developed by the World Bank in the 1980s, is a profile-based roughness statistic and has become a standard measure for road roughness in the United States. The IRI is designed to estimate the level of vehicle vibration due to the unevenness of the road. The level of vehicle vibration is used as an indicator for the road surface roughness. There are various devices that can be used to measure the IRI, but these devices have to be mounted on an automobile. Technically, the IRI is a mathematical representation of the average rectified slope (which is a filtered ratio of a standard vehicle's accumulated suspension motion (Sayers and Gillespie, 1986)), divided by the distance traveled by the vehicle during a

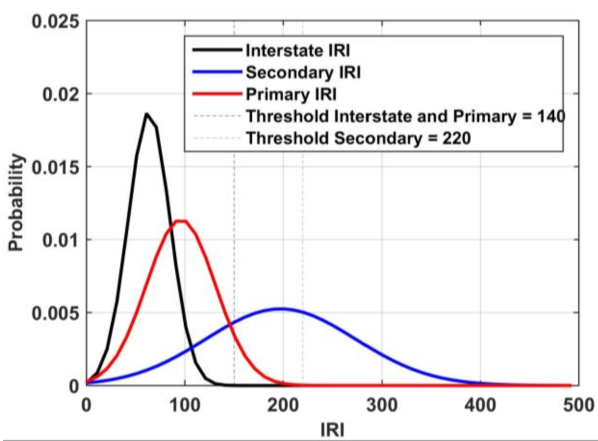

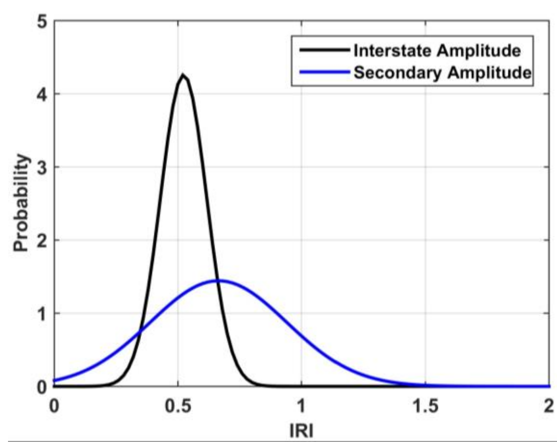

Figure 7: a) Statistical distribution of IRI values for interstates (black), primary roads (red) and secondary roads (blue) for Augusta County, VA. Data was taken in 2012 and 1014. It can be seen that IRI values increase from interstates through to secondary roads; b) Statistical distribution of X-band SAR amplitude data for the interstates and secondary roads shown in Figure 2a). It can be seen that higher IRI values lead to higher SAR amplitudes.

test (km, mi, etc.). Thus, the IRI is estimated based on a simulation of a "Golden Car" which is assumed to be travelling at 80km/hr along the road. Figure 6 shows the IRI roughness scale range as replotted by (Sayers and Gillespie, 1986). The lowest value is 0 for a perfectly smooth road and as the value increases, the roughness increases. The unit of the IRI used in this project is in inches/mile. Also plotted in Figure 6 are typical IRI ranges for various road types and road qualities.

Based on the fact that IRI is an indicator for surface roughness, we expect a positive correlation with SAR amplitude values, which tends to also generally increase with the roughness of a surface. On the one hand, very smooth surface at the scale of the radar wavelength (λ) scatter the incident radiation in the specular direction and result in low backscatter intensity. On the other hand, rougher surfaces cause more of the radar energy to be scattered randomly and resulting in high backscattered intensity. The unit of the SAR amplitude image used in this project is in dB.

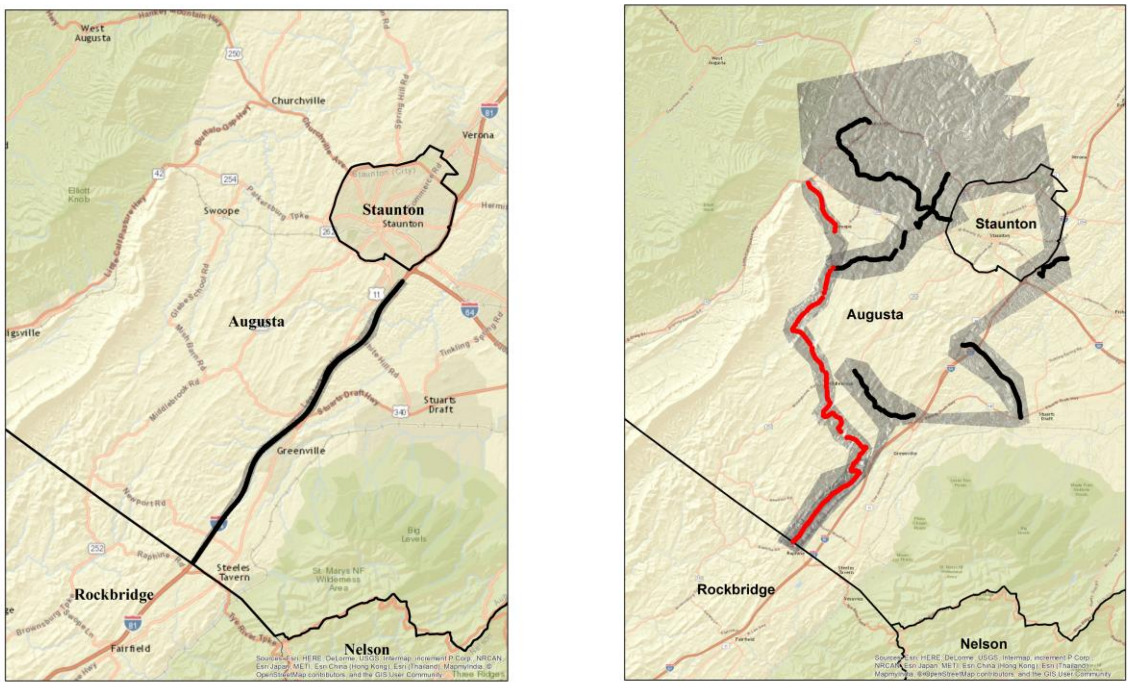

a) b)

Figure 8: Calibration roads used in the cross-correlation analysis of IRI vs SAR amplitude. a) interstate roads used (data acquired in 2012 and 2014 were averaged); b) secondary roads used (red: 2012 data; black: 2014 data).

Figure 7a shows the distribution of IRI values for interstates, primary roads, and secondary roads in Augusta County, VA. The information in Figure 7a was calculated from all IRI measurements of Augusta County acquired in year 2012 (150 miles of interestate roads; 81 miles of secondary roads) and 2014 (180 miles of interstates; 81 miles of secondary roads). It can be seen that, as expected, interstates are most well maintained and show the lowest IRI values, followed by primary and secondary roads. In comparison, Figure 7b shows the statistical distribution SAR amplitude information for interstates (black lines; SAR-based data covers 42% of all IRI data shown in Figure 7a) and secondary roads (blue lines; 100% of IRI values shown in Figure 7a) for the same area. It can be seen that the higher IRI values of secondary roads seem to cause higher brightness values in SAR images. In the following we analyze this relationship further with the goal to use SAR brightnesses for IRI estmation.

4.3.3 Data Analysis Approach

4.3.3.1 Data Pre-Processing

An assessment of the benefits of image pre-filtering for road condition analysis has found that DespecKS^{TM}-preprocessed data (or data that was similarly noise filtered data) was better suited for road surface analysis than the original SAR imagery. This is due to the high-quality Speckle suppression that is done within the DespecKS algorithm (Ferretti et al., 2011). Hence, all of the classification results shown in this report are based on DespecKS-filtered data. For more information, please refer to Section 4.2.1.

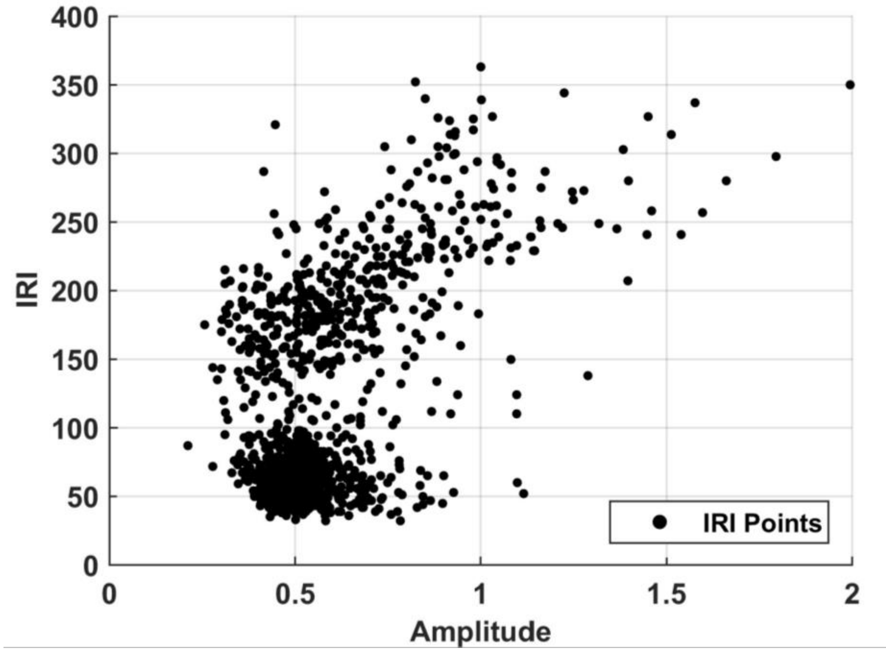

Figure 9: IRI vs SAR amplitude scatter plot for the calibration roads shown in Figure 8.

4.3.3.2 Cross-Correlation Concept

Our analysis was done using a combination of ArcGIS analysis and image and data processing using Matlab. For a set of "calibration" roads in Augusta Country (Figure 8) we overlaid IRI point with their corresponding SAR amplitude information in ArcGIS. Along 55 miles of secondary roads and 62 miles of interstates, we extracted the SAR amplitude information corresponding to each .1mile IRI point and averaged SAR values along the corresponding road segment to create "amplitude vs IRI" scatter plots for an area of interest. We perform a geospatial comparison of road center lines and IRI coordinates to identify and remove IRI points that were misplaced from the road (due to bad coordinate information). We take the remaining points to create the "amplitude vs. IRI" scatter plot shown in Figure 9. A clear correlation between IRI and X-band SAR amplitude information can be identified in this plot. It can be seen that SAR amplitude values are reasonably constant for IRI values between 0 and 130 and start to increase for IRI>130. Comparing this information with Figure 7a) indicates that X-band SAR will be more valuable for estimating IRI on secondary roads than for primary roads and interstates.

4.3.3.3 Model Inversion for IRI Estimation

The obvious correlation between IRI and SAR amplitude data can be utilized to estimate IRI from SAR images. To do so, we developed a forward model to describe the correlation shown in Figure 9. Once a suitable mode was developed, it can be inverted for IRI estimation.

At the current state, we are utilizing an exponential model of the form

$$IRI = \alpha_1 \cdot \left[1 - \exp\left(-\alpha_2 \cdot (A - 0.4)\right)\right] \quad (1)$$

as our forward model, in which the observed IRI (ground truth) is a function of the SAR amplitude data. We estimate the initially unknown model parameters α_1 and α_2 using a least squares fitting approach

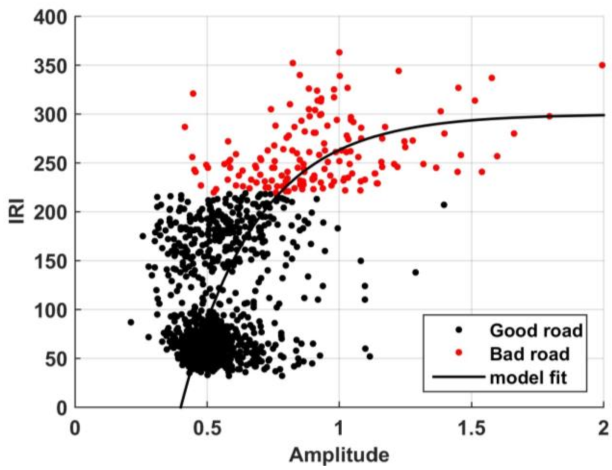

Figure 10: Classification of data samples based on observed IRI ground truth data.

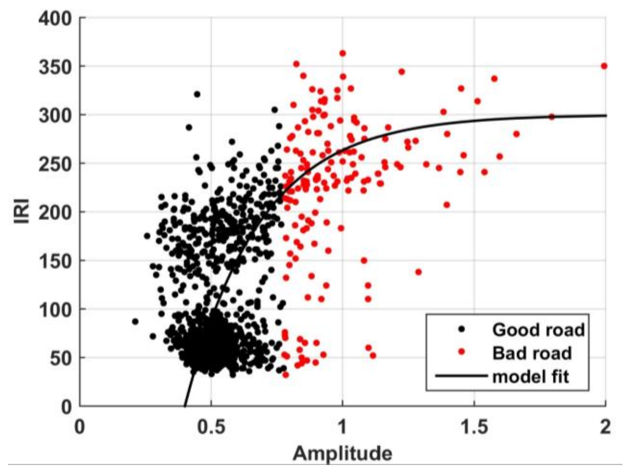

Figure 11: Classification results based on SAR amplitude data

relative to the data in Figure 9. The best fitting model parameters were found to be $\hat{\alpha}_1 = 300$ and $\hat{\alpha}_2 = 3.5$. The quality of the fit can be examined in Figure 10 where the best fitting model is plotted on top of the data samples. With the estimated model parameters, we are now able to predict IRI from SAR amplitude data by using Eq. (1). The model in (1) can be seen as a prediction model that predicts a road segment's IRI value based on the observed SAR amplitude data. Hence, through the prediction of IRI values, a decision can be made about the quality or health of a road can be made based on SAR amplitude observations.

In this experiment we used a threshold of $IRI = 220\ inches/mile$ for discriminating high quality from low quality roads (Eq. (2)).

$$IRI_{thresh} = \begin{cases} Good\ road & = (IRI \leq 220\ inches/mile) \\ Bad\ road & = (IRI > 220\ inches/mile) \end{cases} \tag{2}$$

4.3.4 Summary of Results

Figure 10 shows how the IRI ground-truth samples split into the "good" and "bad" road classes according to the threshold of $IRI_{thresh} = 220\ inches/mile$. It can be seen that "bad" road segments are typically associated with higher backscatter amplitudes than "good" roads, providing some basis for their discrimination using SAR data.

The result of a classification of our data samples based on observed radar amplitude data and the model in (1) is shown in Figure 11 for all the data points shown in Figure 9. It can be seen that, while many of the data samples were classified correctly, there are some mis-classifications near the decision thresholds. To provide quantitative information about the classification performance, we calculated a confusion matrix using both ground truth and classification results. The confusion matrix report, which includes information on the errors of commission and omission, producer and user accuracies, kappa coefficient, and overall accuracy, is displayed in Table 1.

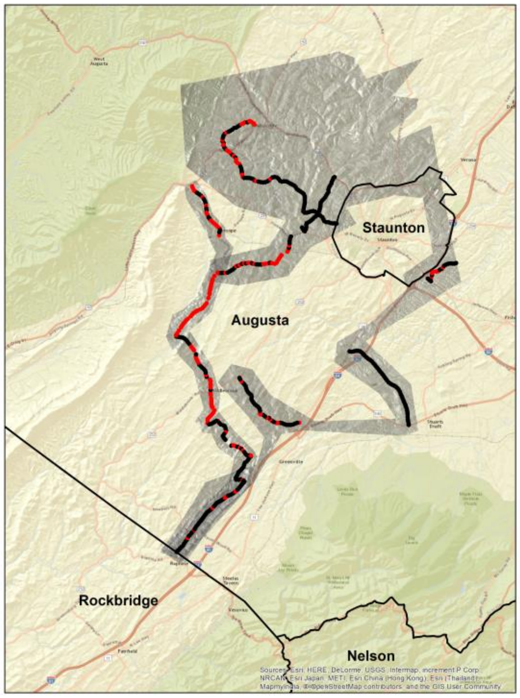

Figure 12: Distribution of good and bad road segments according to ground-truth IRI samples.

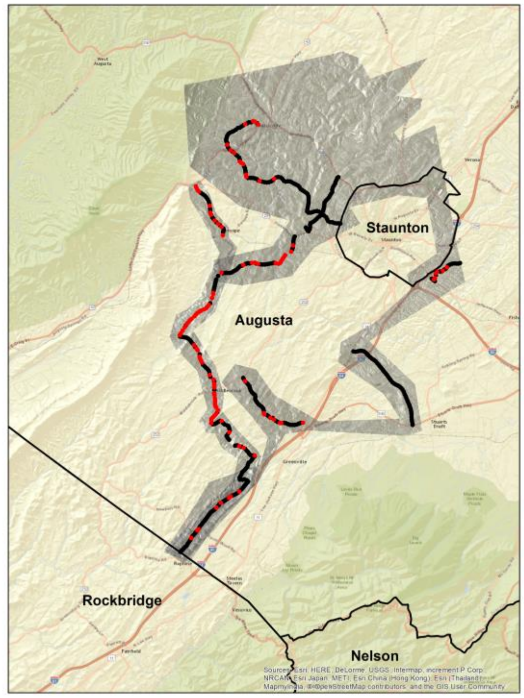

Figure 13: Distribution of good and bad road segments as classified using SAR amplitude data.

The confusion matrix (%) table shows the predicted IRI distribution in % for each ground truth type. About 95.0% of good roads, and 73.5% of bad roads were correctly classified. However, a false positive of 26.5% of good roads were classified as bad roads while a false negative of 5.0% of bad roads were classified as good roads.

Errors of commission represent pixels that belong to another class that were labeled as belonging to the class of interest. The errors of commission can be extracted from the rows (rather than the columns) of

Ground Truth

		Good	Bad	Total
Classification	**Good**	967	42	1009
	Bad	51	116	167
	Total	1018	158	1176

	Good (%)	Bad (%)
Good (%)	95.0%	26.5%
Bad (%)	5.0%	73.5%

		Commission (%)	Omission (%)
Classification	**Good**	4.2%	5.0%
	Bad	30.0%	26.5%

Producer (%)	User (%)
95.0%	95.8%
73.5%	70.0%

Kappa coefficient: **0.67**
Overall Accuracy: **92.1%**

Table 1: Confusion Matrix Report for the data in Figure 9.

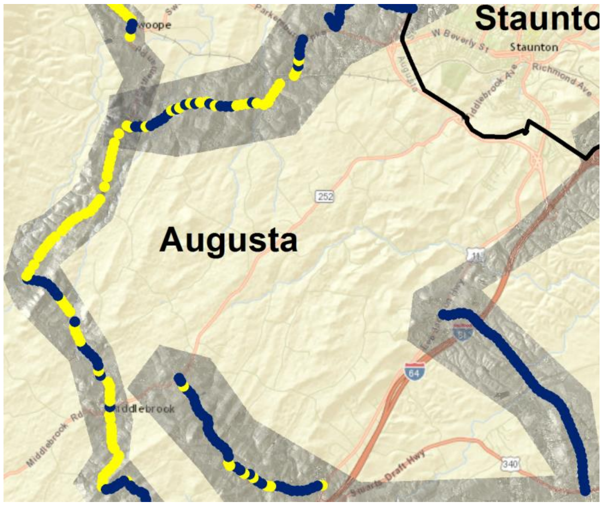

Figure 14: Zoomed-in view of the distribution of good and bad road segments according to ground-truth IRI samples.

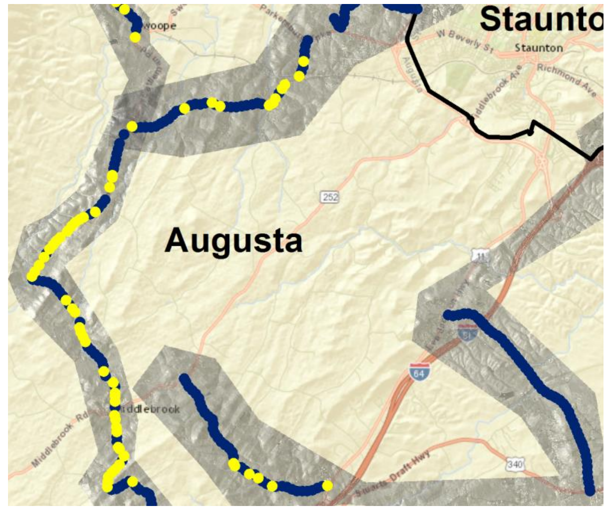

Figure 15: Zoomed-in view of the distribution of good and bad road segments as classified using SAR amplitude data.

the confusion matrix. In our confusion matrix, the bad road class has a total of 167 elements where 116 were classified correctly and 51 were classified incorrectly as good roads. The ratio of the number of pixels classified incorrectly by the total number of pixels in the ground truth class forms an error of commission. For bad roads, the error of commission is 51/167 which equals 30.0%.

Errors of omission represent pixels that belong to the ground truth class but the classification technique has failed to classify them into the proper class. The errors of omission are shown in the columns of the confusion matrix. In our confusion matrix, bad roads had a total of 158 ground truth elements where 116 were classified correctly and 42 bad roads ground truth pixels are classified incorrectly. The ratio of the number of elements classified incorrectly by the total number of elements in the ground truth class forms an error of omission. For bad roads, the error of omission is 42/158 which equals 26.5%.

Figures 12 and 13 provide an example of the classification performance by showing a map representation of both the ground-truth data and classification results. Red and black regions in Figure 12 show the distribution of bad and good road segments according to the IRI ground-truth information. Most of the low quality road segments are concentrated on secondary roads in the vicinity and north of Middlebrook, VA. Figure 13 shows the distribution of good and bad road segments as derived from the SAR amplitude data using Eq. (1). An excellent match between ground-truth data and remote-sensing-based classification results can be seen. This good match is further confirmed by the zoom-in comparison shown in Figures 14 and 15.

4.3.5 Future Work

We are currently in the process of writing this work up in a paper. We are also planning to consolidate and streamline our classification algorithms in Python computer code so that it can be shared with our project partners at VDOT and UVA.

Other future work directions include:

- Testing the stability of the derived forward model (Eq. (1)) for other areas (e.g., we could apply the same model to our data stack near Washington D.C.)
- Comparing our SAR amplitude-based classification approach with another approach developed by UVA that is utilizing phase information for identifying good and bad road segments. A combination of the two algorithms may improve overall classification performance.

5 Development of Outreach Material for Promoting InSAR to the DOT Community

An important secondary goal of this research project is to develop outreach material that can be used to promote the use of InSAR to the DOT community. UAF has been supporting this research component in a number of discussions with VDOT personnel and with members of the InSAR processing company TRE. UAF personnel also conducted a webinar, a 4-day SAR Training Course at UAF as well as a half-day SAR training at the TRB conference in January 2016. More details are as follows.

5.1 Webinar on "Discover Simplified SAR Solutions"

UAF's institutional PI Meyer together with colleague at UAF conducted a 90 minute Webinar on "Discover Simplified SAR Solutions" on September 23, 2015 from 2pm – 3pm ET. The event was hosted by NASA Earthdata and was advertised broadly through their website (https://earthdata.nasa.gov/user-resources/webinars-and-tutorials/webinar-asf-daac-23-sept-2015-news). The event was attended by more than 120 participants from governmental organizations, academia, and industry. The event was recorded and is available at: https://www.youtube.com/watch?v=YC6gDdgZrOw.

5.2 Four-Day Training on the Principles and Applications of SAR at UAF

UAF PI Meyer led a four-day SAR Training course on SAR Principles and Applications on the campus of UAF from August 10 – 13, 2015. This in-person class was limited to 25 seats and was completely booked. The course introduced the students to the principles and applications of microwave remote sensing. It included the sensor technology, platforms, and data portals to retrieve data. Principle processing techniques and applications of active microwave remote sensing data were covered. The laboratory part of the course provided hands-on experience with special processing techniques and the possibility of using these techniques for a student-defined term project in areas of geology, seismology, volcanology, cryosphere, hydrology, environmental sciences, etc. Advanced processing techniques such as InSAR, differential InSAR, or polarimetric SAR were also included.

A review of the class provided excellent feedback on both the content and the teaching methods employed.

5.3 Presentation of Project Results at the 2015 NISAR Applications Workshop

Together with project partner TRE, PI Meyer presented the benefits of InSAR for transportation infrastructure monitoring to the attendees of the NISAR workshop. The presentation was in form of a poster (Figure 16) and attracted significant attention.

5.4 SAR Workshop at TRB'16

On January 14, 2016, UAF PI Meyer led and participated in a half day workshop on "InSAR: A Promising New Tool for Network Wide Transportation Infrastructure Monitoring" at the Transportation Research Board 94th Annual Meeting in Washington, D.C. The workshop provided an overview of InSAR remote sensing technology with a particular focus on transportation applications. It explained the underlying theoretical concepts of satellite-based radar imaging and introduced the basic aspects of InSAR data processing, including the interpretation of InSAR results. Data collected from ongoing and recently completed studies were used to demonstrate the benefits of InSAR technology. Practical examples of monitoring roads, bridges, slopes, and sinkholes were also provided. The workshop ended with a summary of currently available radar systems suitable for infrastructure monitoring and with a listing of InSAR service providers and software packages for data processing.

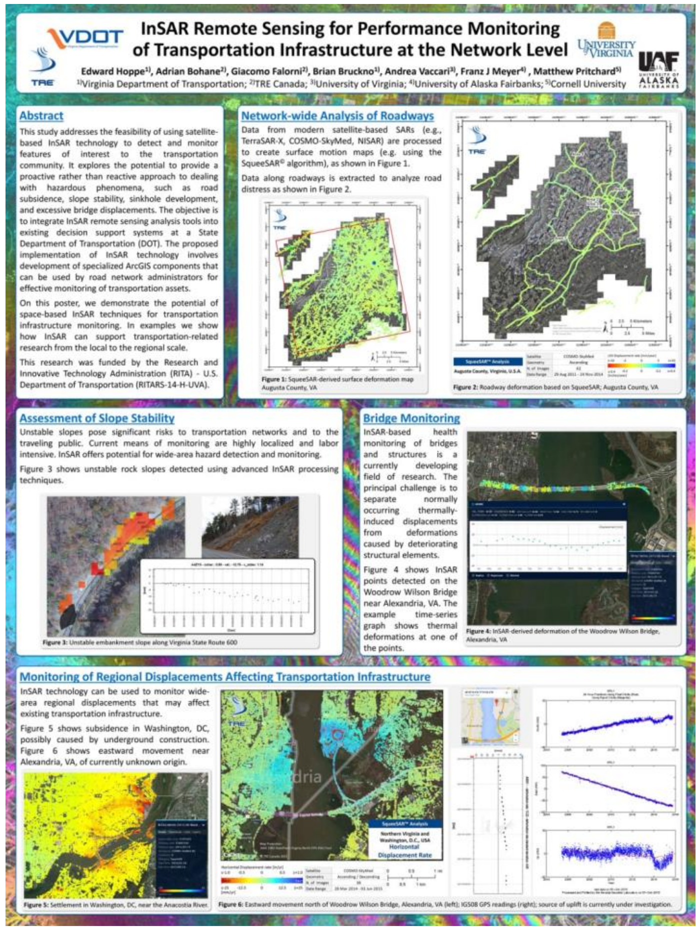

Figure 16: Poster presented at the 2015 NISAR Applications Workshop.

The workshop featured the following presentations:

- FJ Meyer, UAF/ASF: Introduction to InSAR and its Application to Infrastructure Monitoring
- A Bohane, TRE: Practical Examples of InSAR for Transportation and Infrastructure Monitoring
- T. Oommen, Michigan Tech: Application of InSAR for Geotechnical Asset Management
- FJ Meyer, UAF/ASF: Summary of Available Sensors, Service Providers, and Software Packages
- A Moruza, V-DOT: Application of Net Present Benefit Analysis to InSAR Monitoring
- FJ Meyer: UAF/ASF: Workshop Summary, Links to Data and Further Reading Material

More information on the training including PDF versions of the training material can be found at http://viva-lab.ece.virginia.edu/foswiki/bin/view/InSAR/WorkshopTRB2016.

6 Summary

From our work we can draw a few conclusions about the use of SAR amplitude information in transportation infrastructure monitoring as well as the need for SAR and InSAR training to improve the acceptance of InSAR technology by the transportation community:

- We do believe that the addition of amplitude information to the already heavily utilized phase data can improve our ability to detection and describe changes on and around the transportation network.
- We determined that the calculation of log-scaled ratio images is a powerful approach to suppress background, enhance change signatures, and modify the characteristics of noise in SAR data. Hence, log-scaled ratio data are very useful in automatic change detection.
- First results show that both image-to-image changes as well as long term trends can be identified in SqueeSAR pre-processed SAR data.
- We found that SAR amplitude is indeed sensitive to the condition of the road surface as quantified by the IRI parameter. First assessments furthermore show that this sensitivity can be used to retrieve at least rudimentary information about road surface quality from SAR amplitude observations.
- We believe that well designed training workshops can significantly enhance the uptake of InSAR technology by the DOT community. In addition to the basics of InSAR, these workshops should provide concrete processing solutions that are tailored to specific infrastructure monitoring questions. The courses should also include a summary of available data and software packages as well as information on expected cost-benefit enhancements.
- A combination of Webinars with in person workshops is currently seen as a viable approach for communicating and disseminating this information.

A peer-reviewed publication on our main research findings is currently in preparation.

7 Bibliography

Adam, N., Kampes, B., and Eineder, M., 2004, Development of a Scientific Permanent Scatterer System: Modifications for Mixed ERS/ENVISAT Time Series.

Ajadi, O. A., Meyer, F. J., and Webley, P. W., 2016, Change Detection in Synthetic Aperture Radar Images Using a Multiscale-Driven Approach: Remote Sensing, v. 8, no. 6, p. 482.

Bazi, Y., Bruzzone, L., and Melgani, F., 2005, An unsupervised approach based on the generalized Gaussian model to automatic change detection in multitemporal SAR images: IEEE Transactions on Geoscience and Remote Sensing, v. 43, no. 4, p. 874-887.

Bruniquel, J., and Lopes, A., 1997, Multi-variate optimal speckle reduction in SAR imagery: International Journal of Remote Sensing, v. 18, no. 3, p. 603-627.

Buades, A., Coll, B., and Morel, J. M., A non-local algorithm for image denoising, *in* Proceedings 2005 IEEE Computer Society Conference on Computer Vision and Pattern Recognition (CVPR'05)20-25 June 2005 2005, Volume 2, p. 60-65 vol. 62.

Celik, T., 2010, A Bayesian approach to unsupervised multiscale change detection in synthetic aperture radar images: Signal Processing, v. 90, no. 5, p. 1471-1485.

Chen, S., Hou, J., Zhang, H., and Da, B., 2014, De-speckling method based on non-local means and coefficient variation of SAR image: Electronics Letters, v. 50, no. 18, p. 1314-1316.

Coppin, P., Jonckheere, I., Nackaerts, K., Muys, B., and Lambin, E., 2004, Review ArticleDigital change detection methods in ecosystem monitoring: a review: International Journal of Remote Sensing, v. 25, no. 9, p. 1565-1596.

Dekker, R. J., 1998, Speckle filtering in satellite SAR change detection imagery: International Journal of Remote Sensing, v. 19, no. 6, p. 1133-1146.

Deledalle, C. A., Tupin, F., and Denis, L., A non-local approach for SAR and interferometric SAR denoising, *in* Proceedings Geoscience and Remote Sensing Symposium (IGARSS), 2010 IEEE International25-30 July 2010 2010, p. 714-717.

Ferretti, A., Fumagalli, A., Novali, F., Prati, C., Rocca, F., and Rucci, A., 2011, A New Algorithm for Processing Interferometric Data-Stacks: SqueeSAR: IEEE Transactions on Geoscience and Remote Sensing, v. 49, no. 9, p. 3460-3470.

Huang, S.-q., Liu, D.-z., Gao, G.-q., and Guo, X.-j., 2009, A novel method for speckle noise reduction and ship target detection in SAR images: Pattern Recognition, v. 42, no. 7, p. 1533-1542.

Jin, W., Yanwen, G., Yiting, Y., Yanli, L., and Qunsheng, P., Fast Non-Local Algorithm for Image Denoising, *in* Proceedings IEEE International Conference on Image Processing, 20068-11 Oct. 2006 2006, p. 1429-1432.

Kampes, B. M., 2005, Displacement Parameter Estimation using Permanent Scatterer Interferometry.

Lee, J.-S., Grunes, M., and Mango, S. A., 1991, Speckle reduction in multipolarization, multifrequency SAR imagery: Geoscience and Remote Sensing, IEEE Transactions on, v. 29, no. 4, p. 535-544.

Lee, J.-S., Jurkevich, L., Dewaele, P., Wambacq, P., and Oosterlinck, A., 1994, Speckle filtering of synthetic aperture radar images: A review: Remote Sensing Reviews, v. 8, no. 4, p. 313-340.

Liu, Y.-L., Wang, J., Chen, X., Guo, Y.-W., and Peng, Q.-S., 2008, A Robust and Fast Non-Local Means Algorithm for Image Denoising: Journal of Computer Science and Technology, v. 23, no. 2, p. 270-279.

Lopez-Martinez, C., and Pottier, E., 2007, On the Extension of Multidimensional Speckle Noise Model from Single-look to Multilook SAR Imagery: IEEE Transactions on Geoscience and Remote Sensing, v. 45, no. 2, p. 305-320.

Martino, G. D., Simone, A. D., Iodice, A., Riccio, D., and Ruello, G., Non-local means SAR despeckling based on scattering, *in* Proceedings 2015 IEEE International Geoscience and Remote Sensing Symposium (IGARSS)26-31 July 2015 2015, p. 3172-3174.

Meyer, F. J., McAlpin, D. B., Gong, W., Ajadi, O., Arko, S., Webley, P. W., and Dehn, J., 2014, Integrating SAR and derived products into operational volcano monitoring and decision support systems: Isprs Journal of Photogrammetry and Remote Sensing, no. 0.

Novak, L. M., and Burl, M. C., 1990, Optimal speckle reduction in polarimetric SAR imagery: Aerospace and Electronic Systems, IEEE Transactions on, v. 26, no. 2, p. 293-305.

Redner, R., and Walker, H., 1984, Mixture Densities, Maximum Likelihood and the EM Algorithm: SIAM Review, v. 26, no. 2, p. 195-239.

Sayers, M. W., and Gillespie, T. D., 1986, The Ann Arbor road profilometer meeting.

Sveinsson, J. R., and Benediktsson, J. A., 2003, Almost translation invariant wavelet transformations for speckle reduction of SAR images: Geoscience and Remote Sensing, IEEE Transactions on, v. 41, no. 10, p. 2404-2408.

Appendix H – Getting started with ArcGIS Online

Elizabeth V. M. Campbell – **ArcGIS Online – Getting Started** – November 2014 [download][12]

[12] http://viva-lab.ece.virginia.edu/elecdocs/ritars14/ArcGISOnline.pdf

ArcGIS Online – Getting started

Elizabeth V.M. Campbell – 2014-10-18

"ArcGIS Online is a collaborative, cloud-based platform that allows members of an organization to use, create, and share maps, apps, and data, and access authoritative base maps and ArcGIS apps. Through ArcGIS Online, you get access to ESRI's secure cloud, where you can manage, create, and store data as published web layers."

ESRI – http://doc.arcgis.com/en/arcgis-online/reference/what-is-agol.htm

The appeal of ArcGIS Online to a state agency like the Virginia Department of Transportation (VDOT) is multi-fold. One advantage is that the end user is not required to purchase any software. The maps and applications on ArcGIS Online can be viewed through web browsers on multiple platforms. Additionally, the map and feature services hosted and registered on ArcGIS Online can be readily included in analysis performed using ArcGIS for Desktop.

By registering map and feature services on ArcGIS Online and sharing them with either the organization or the public, the services are searchable. This resolves one of the common complaints by members of the organization that they do not know what data layers and services are available and how to access them. If the services are hosted locally on agency servers and just registered on ArcGIS Online then the data seen is "live" and up-to-date.

VDOT has found ArcGIS Online to be a very effective way to make data available to the public to download (Figure 1). We still have an FTP site but we find ArcGIS Online to be very popular. Our current procedure to make a large data set available for download is to create and upload/share a map package which, together with the complete map file itself (MXD), includes also the layer's data and metadata (XML). A release notes document file is uploaded separately so it can be read prior to downloading the dataset.

Scalability is another advantage of using ArcGIS Online for a state agency. Applications that are rarely used except during a crisis, such as a snowstorm or hurricane, can easily accommodate an increase in user traffic with no extra staff support required if the application is hosted on ArcGIS Online. If the necessary data is also hosted on the ArcGIS Online cloud, the application can still function despite local conditions.

Figure 1 - VDOT ArcGIS Online portal.

ArcGIS Online is also useful in situations where we need to share maps and data with people who are not VDOT employees and are external to the organization but should not be considered to be the general public – such as when working with local planning department on proposed road changes. In these situations, we are not ready to make the data public but because the local planners are not VDOT employees, they are not able to access map and feature services hosted on the internal servers. We resolve this problem by creating ArcGIS Online groups for each project area and invite the involved external people and VDOT employees to the group. Since the data sets involved tend to be relatively small due to the limited project area, the map and data is loaded to the ArcGIS Online cloud and the feature services are hosted in the ESRI cloud and shared with the appropriate group. The data and map is available to everyone in the group but only the people in the group. The data and maps cannot be viewed by anyone outside the group even if they are VDOT employees unless they are invited to become members of the group.

This model is expanded when VDOT is involved in collaborative research that includes scientists and engineers in other agencies, universities, and the private sector (Figure 2). Some of the participants may be in other states and counties. Anyone in the group can load data, maps, documents, and scripts to ArcGIS Online and shared them with the group. Anyone in the group can then download them and work on solutions locally. Large frequently changing files and base layers can be hosted as a feature service by participants on their local external-facing server and shared with the ArcGIS Online group eliminating the need for individuals to frequently download the large data sets in order to use the latest data. Applications developed can be shared to another group with limited membership, all of VDOT, or to the Public.

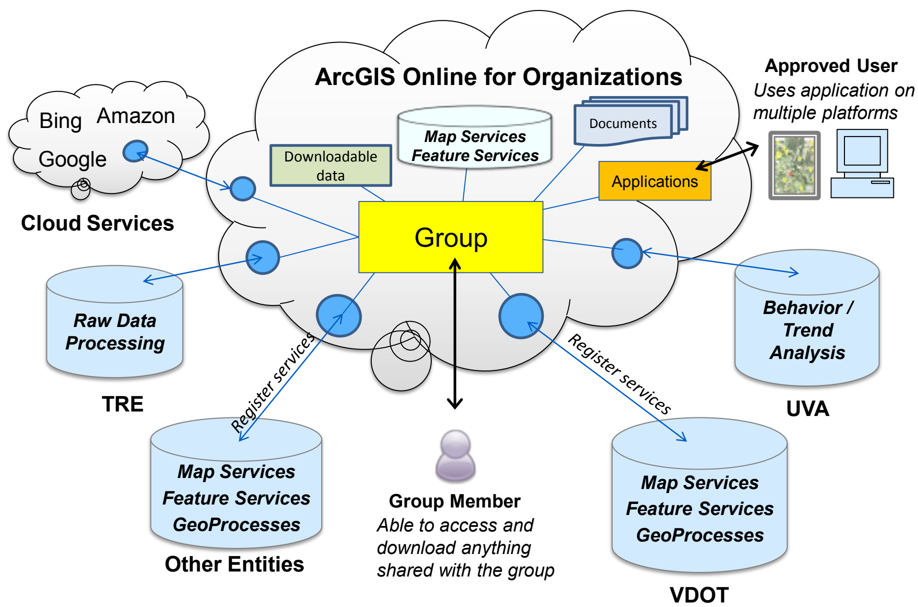

Figure 2 - ArcGIS Online collaborative structure for RITARS-14-H-UVA.

Training

A major advantage of using an off-the-shelf solution such as ArcGIS Online is the existence of professionally developed and maintained documentation and training. In the case of ArcGIS Online ESRI training, documentation, and support is particularly comprehensive.

Training is available both online and in instructor-led classroom settings. The cost ranges from free to several thousand dollars for instructor-led or customized training (Appendix A). The documentation and training are updated to keep in-sync with the constantly changing capabilities of ESRI ArcGIS Online.

A good place to start is the ArcGIS Online Help page for "Get Started" (http://doc.arcgis.com/en/arcgis-online/reference/get-started.htm). The documentation found there gives detailed instructions regarding how to activate your organization's subscription to ArcGIS Online. It is important to remember that the person who will act as the administrator for the organization must activate the subscription. The administrator will set up the general look of the organization's site, configure security settings, roles, and Open Data, invite members to join, and monitor service credits.

Considerations

Some advance planning makes getting started much easier.

The ESRI documentation on the ArcGIS Online Help page for "Get Started" and the online training courses do a good job of explaining the options. The following is a list of some of the most important questions to consider early.

- Number of service credits
- Will you use Secure Sockets Layer (SSL)
- What do you want for your organization's URL?
    - You will need to enter a short name for your organization (1 to 16 alphanumeric characters including hyphens. Other special characters and spaces are not allowed). This short name is used to create the organization's URL. It cannot be once you create it. So give it some thought.
- Do you want to set up enterprise logins? What will be the login standard?
    - If you have hundreds of people who will need to join, you may want to consider an enterprise login.
- What services will be hosted on your agency's servers and what will be hosted on the ESRI cloud
    - You do not have to use agency servers. You can host everything on ESRI's cloud. However you will need to buy more service credits.
- What should be visible only in a group, by the organization, or by the general public
- Is there data that should not be seen outside of the organization?
- What protocols should be followed to elevate data, map, or application to the next level of visibility. Should it be reviewed? A checklist? Who should be able to publish it up?
- Do you want to have naming standards for groups?
- Do you want to have a list of required tags? Or standardized list of tags?
- Will all of the users be internal to the organization? Or will some users be external to the organization but should not be considered to be the general public?
- Role privileges
    - How many publishers? One per group? Do you need to create some custom roles?

Table 1 - Role privileges (from http://doc.arcgis.com/en/arcgis-online/reference/roles.htm).

Privilege	User	Publisher	Administrator	Custom
Use maps and apps	✓	✓	✓	✓
Create content	✓	✓	✓	Optional
Share maps and apps	✓	✓	✓	Optional
Join and create groups	✓	✓	✓	Optional
Edit features	✓	✓	✓	Optional
Publish hosted features and tiles		✓	✓	Optional
Perform analysis		✓	✓	Optional
Manage Open Data sites			✓	Optional
Invite users to organization			✓	Optional
Manage organization resources			✓	Optional
Configure website			✓	
Create custom roles			✓	
View subscription stats			✓	
ArcGIS Marketplace provider (requires organization authorization)			✓	

Virginia Department of Transportation Experience

Virginia Department of Transportation (VDOT) has an Enterprise License Agreements (ELA) with ESRI, which provides maintenance and unlimited use of ArcGIS for Server and Desktop and all extensions. The contract between VDOT and ESRI includes a large number of service credits that, in addition to paying for resource usage and storage on ArcGIS Online, are also used to pay for consulting and training.

VDOT has two sets of servers – one internal-facing only and one external-facing. These servers handle the AGS, the IIS/WebAdaptor, and the Oracle/SDE database. Services published on the internal servers are not viewable by non-VDOT employees. The general policy is to locally host map and feature services for large datasets and for data sets that change frequently. Geoprocessing services are also hosted locally. Calculations that require a lot of computation resources such as tiling and address location of a very large data set are done on agency servers or on desktops.

VDOT has three ArcGIS Online administrators and one custom role for the purpose of inviting users. This custom role allows the administrator to delegate what can be a frequent and time-consuming function. Each group has one publisher who can share the group's items with other groups and with the VDOT-only group. VDOT has two public groups – one for public GIS data and one for the items that will be displayed in the Site's Gallery.

If the author wishes to publish an item to the public, the item is shared to the VDOT-only group and short form explaining the purpose of the item is emailed to the administrator. The item is then reviewed by several people using a check list to insure quality and consistency. When it passes the review the administrator makes the item public.

VDOT ArcGIS Online Review Checklist

- Metadata Completeness Review
    a. Description
    b. Purpose
    c. Access and Use Constraints
    d. Tags
    e. Thumbnail
- Data Confidentiality Review
    a. Is any of the data restricted?
    b. Is any of the data not VDOT's
    c. Have the data owners given permission for the data to be available to the public?
    d. Have the data owners reviewed the map/application?
- Resources Review
    a. Who is the map owner? Does it need to be VDOT?
    b. Where are the data stored? On VDOT servers or in the cloud?
    c. What is the size/expected size of the data layer?
    d. Does the data need to be moved to an external VDOT server?
    e. Does VDOT need to create a map, feature, or geoprocessing services? Internal or external server?
    f. Is there processing functionality? If so –where is the processing done?
    g. What is the expected user demand level? Will it be constant or will it fluctuate?
- Look and Feel, functionality, Logo and Credit Review
    a. Does it have a VDOT logo?
    b. Are the appropriate organizations credited?

c. If print enable – is there a scale, north arrow, VDOT logo, date?
d. Are the appropriate functions enable/disabled – delete, etc
e. Will the public be able to edit or add data?

Conclusion

VDOT's use of ArcGIS Online is expanding. As more people within VDOT learn about ArcGIS Online and see existing applications, more uses for it are found. VDOT IT staff is actively encouraging the staff to take some of the online training classes and are working with groups with VDOT to develop their ideas for use of ArcGIS Online.

Appendix A - A sample listing of the training available.

Source: http://www.esri.com/training/main/arcgis-online-training

Administer an ArcGIS Online Organization

Learn how to manage users, groups, and content; monitor service credit usage; and customize your site's look and feel.

Preparing to Implement ArcGIS Online An ArcGIS Online organizational site facilitates collaboration and easy access to GIS data, maps, and apps across your organization and beyond. This course presents a three-step planning process to align your ArcGIS Online organizational site with your business needs and key workflows.	**Format:**Web Course **Duration:** 1 module (2 hours) **Price:** Free **ArcGIS Version:** 10.1, 10.2
Configuring and Administering an ArcGIS Online Organization ArcGIS Online helps organizations increase the value of their GIS content by making it more broadly available, enabling individuals and teams to do their work better and faster. This course introduces organizational site administrators to workflows for configuring ArcGIS Online general settings, branding the organization's home page; managing site members, groups, and content; and choosing security options that meet the organization's needs.	**Format:**Web Course **Duration:** 1 module (2 hours) **Price:** $32 USD **ArcGIS Version:** 10.2
Performing ArcGIS Online Administrator Tasks An ArcGIS Online organizational site is a living organism. Content is added, updated, and eventually removed. As staff come on board or leave, their member roles must be assigned and retired. Groups need to be managed. Security must be maintained at all times. The administrator's task is to keep the site humming smoothly along as changes occur so that ongoing business needs are met. This course offers ideas and techniques to efficiently manage site members,	**Format:**Web Course **Duration:** 1 module (3 hours) **Price:** $32 USD **ArcGIS Version:** 10.1, 10.2

content, credit consumption, and security over time.	
Best Practices for Your ArcGIS Online Organization ArcGIS Online provides tools and cloud services needed to manage, share, and publish geographic information on interactive maps and apps. In this seminar, you will learn how to configure your ArcGIS Online organizational site's home page, organize content, invite participants, and create a brand identity for the content you publish.	**Format:**Training Seminar **Duration:** 60 minutes **Price:** Free **ArcGIS Version:** 10.2
Power your Enterprise with ArcGIS Apps ArcGIS Online organizational subscriptions include a core set of mapping apps: Collector for ArcGIS, Operations Dashboard for ArcGIS, and Explorer for ArcGIS. This trio of apps allows organization members to quickly and easily find, use, make, and share maps. In this seminar, you will learn what each app does, what differentiates each from the others, and how, together, the apps can help you collect data, manage operations, and boost the overall efficiency of your organization's key ArcGIS-enabled business workflows.	**Format:**Training Seminar **Duration:** 60 minutes **Price:** Free **ArcGIS Version:** 10.2
Get Started with ArcGIS Open Data By using ArcGIS Open Data, a hosted app included with ArcGIS Online subscriptions, you can easily share authoritative content with stakeholders, constituents, and the general public. In this seminar, the presenters show you how to enable the Open Data capabilities in your ArcGIS Online organization, create and configure an Open Data site, share data, and make the data easy to discover and explore. The presenters also demonstrate how to easily search for, filter, and explore data and download it in open formats.	**Format:**Training Seminar **Duration:** 60 minutes **Price:** Free
Offline Data Collection Using Collector for ArcGIS You can use the Collector for ArcGIS app on an Android or iOS	**Format:**Training Seminar **Duration:** 60 minutes

device to take your maps into the field. You can also collect data while offline, and later synchronize your updates when a connection becomes available. In this seminar, the presenters show you how to use Collector for ArcGIS to download maps to your smartphone or tablet and make updates to your geographic information systems (GIS) data without an Internet connection. The presenters also demonstrate how to create new GIS features, as well as update existing ones, while in a disconnected environment.	**Price:** Free

Discover, Create, and Share Content

Learn how to complete your projects using resources available from the ArcGIS Online website and your organization's site. Gain the skills you need to author and share web maps, apps, and other GIS resources.

Creating and Sharing GIS Content Using ArcGIS Online Organizations use ArcGIS Online to facilitate collaboration and efficient access to maps and other GIS resources. This course shows how to publish data and map layers directly to ArcGIS Online as services, then use those services to quickly build a web map. You will also learn how to turn a web map into a web app to provide a focused experience for your audience. Access to an ArcGIS Online organizational account is needed to complete course exercises.	Format: Web Course GIS training accessible 24/7, for self-paced, independent study. Learn more. Duration: 1 module (3 hours) Price: $32 USD ArcGIS Version: 10.2
ArcGIS 4: Sharing Content on the Web ArcGIS supports sharing geographic content across multiple platforms so it is accessible to everyone who needs it, when they need it, however they want to access it. This course teaches how to turn your authoritative GIS data, workflows, and maps into ArcGIS services that can be published to ArcGIS Online, ArcGIS for Server, or Portal for ArcGIS; easily embedded in web maps and websites; accessed by desktop, web, and mobile applications; and deployed to servers on secure internal networks. You will learn how to determine which sharing option is appropriate for your needs.	Format: Instructor-Led Hands-on practice with the latest Esri software in an interactive class led by an expert Esri instructor. Learn more. Duration: 2 days (16 hours) Price: $1,070 USD ArcGIS Version: 10.2 View Class Schedule
Creating Hosted Map Services with ArcGIS Online In this seminar, the presenters show how and why you can use ArcGIS Online to host your services. Hosted services scale to meet demand and can be used to extend your GIS capabilities. You can take advantage of your ArcGIS Online organizational site to make your services available to specific groups or to the general public. The presenters also demonstrate best practices for authoring maps using ArcGIS for Desktop, then publishing your maps to ArcGIS Online as a hosted service. You will learn how to enable a web map with editing capabilities that support both browser and desktop editors.	Format: Training Seminar Free Web-based, hour-long presentations and demonstrations on focused technical topics. Learn more. Duration: 60 minutes Price: Free ArcGIS Version: 10.1

ArcGIS Online Subscriptions for Organizations: Publisher Workflows Have you been tasked to share GIS resources to your organization's ArcGIS Online site? In this workshop, the instructor discusses the types of content you can publish to ArcGIS Online and shows how to author GIS resources to support their planned use. You will also see how including GIS resources in published web maps and web applications extends their value throughout the organization and even to the general public. Tips to help you plan your publishing strategy are given throughout. What can I expect if I attend this workshop? This workshop is intended to quickly give you key information you need to publish content that helps your organization get the most value out of its ArcGIS Online site. During the workshop's open question and answer sessions, you are encouraged to ask the instructor about the topics covered and related questions. A downloadable resource document (PDF) and certificate of completion are included.	Format: Instructor-Led Hands-on practice with the latest Esri software in an interactive class led by an expert Esri instructor. Learn more. Duration: 4 hours Price: $175 USD View Class Schedule
ArcGIS Online Subscriptions for Organizations: User Workflows Your organization's ArcGIS Online site is a source for GIS data, web maps, and other geographic content that can inform and add value to your projects. In this workshop, the instructor shows how to discover content available on an ArcGIS Online organizational site, determine if the content is suitable for your needs, and interact with the content using web maps and Esri Maps for Office. What can I expect if I attend this workshop? This workshop is intended to introduce you to the types of content your organization may distribute through its ArcGIS Online site. You will see how this content helps you infuse your projects with rich geographic context, data-backed intelligence, and visual impact. During the workshop's open question and answer sessions, you are encouraged to ask the instructor about the topics covered and related questions. A downloadable reference document (PDF) and certificate of completion are included.	Format: Instructor-Led Hands-on practice with the latest Esri software in an interactive class led by an expert Esri instructor. Learn more. Duration: 4 hours Price: $175 USD View Class Schedule

Gain Geographic Insight with ArcGIS Online Analysis Tools This seminar introduces the new spatial analysis capabilities included with ArcGIS Online. These ready-to-use spatial analysis tools are hosted in the cloud by Esri, and are designed to provide an intuitive, user-friendly experience. You will learn about the available tools and a recommended approach to performing spatial analysis online. The presenter demonstrates methods to gain insight by analyzing and quantifying patterns and relationships in your data.	Format: Training Seminar Free Web-based, hour-long presentations and demonstrations on focused technical topics. Learn more. Duration: 60 minutes Price: Free ArcGIS Version: 10.2
Increase the Value of ArcGIS Services with ArcGIS Online Sharing GIS resources over the web enables an organization to make better decisions—staff members can collaborate and work with the same geographic knowledge. This seminar describes how to use ArcGIS Online to maximize your ArcGIS for Server web services. The presenters demonstrate how to use ArcGIS Online to transform your ArcGIS Server services into information products that people can easily discover and use from web, mobile, and desktop clients.	Format: Training Seminar Free Web-based, hour-long presentations and demonstrations on focused technical topics. Learn more. Duration: 60 minutes Price: Free ArcGIS Version: 10.1
Spatial Analysis with ArcGIS Online ArcGIS Online is a powerful platform for analyzing data. New spatial analysis tools are continually being added to help you solve common spatial problems. Tools in the map viewer can help you do things such as find locations and hot spots, create drive-time areas, and summarize your data. You can analyze your organization's data, publicly available data from ArcGIS Online, or a combination. The presenters provide you with an overview of the spatial analysis capabilities of ArcGIS Online. You also learn about the benefits of using these analysis tools, how to get started using them, and how to choose the right approach to solve a specific spatial problem.	Format: Training Seminar Free Web-based, hour-long presentations and demonstrations on focused technical topics. Learn more. Duration: 60 minutes Price: Free ArcGIS Version: 10.2
Getting Started with GIS If you are curious about what the acronym "GIS" stands for and what a GIS actually is, this course provides the answers. You will be	Format: Web Course GIS training accessible 24/7, for self-paced,

introduced to the basic components of a GIS and some fundamental concepts that underlie the use of a GIS. As you practice working with GIS maps and geographic data, you will learn how a GIS helps people visualize and create information that can be used to make decisions and solve problems.	independent study. Learn more. Duration: 1 module (4 hours) Price: Free ArcGIS Version: 10.1, 10.2
ArcGIS 1: Introduction to GIS This course teaches what a GIS is and what you can do with it. Working with various components of the ArcGIS platform, you will create GIS maps, explore and analyze the data behind the maps, and learn easy methods to share your maps and analysis results. By the end of the course, you will have a solid understanding of how GIS maps and ArcGIS tools are used to visualize real-world features, discover patterns, obtain information, and communicate that information to others.	Format: Instructor-Led Hands-on practice with the latest Esri software in an interactive class led by an expert Esri instructor. Learn more. Duration: 2 days (16 hours) Price: $1,070 USD ArcGIS Version: 10.2 View Class Schedule

Appendix I – Advisory committee meeting minutes

Minutes of Advisory Committee meeting – May 13, 2014 [download][13]

[13] http://viva-lab.ece.virginia.edu/elecdocs/ritars14/Minutes_051314.pdf

MINUTES

ADVISORY BOARD TELECONFERENCE

INSAR REMOTE SENSING FOR PERFORMANCE MONITORING OF TRANSPORTATION INFRASTRUCTURE AT THE NETWORK LEVEL

May 13, 2014

Attendance: Scott Acton, Andrea Vaccari, Adrian Bohane, Giacomo Falorni, Brian Bruckno, Elizabeth Campbell, Audrey Moruza, Edward Hoppe, Melba Crawford, Scott Anderson, Emmett Heltzel, Chad Allen, Ty Ortiz, Vasanth Ganesan.

I. Welcome and Introduction

Scott Acton welcomed all teleconference participants and called the meeting to order. Members of the research team were introduced, as follows:

- Scott Acton – Professor, Department of Electrical Engineering, University of Virginia
- Andrea Vaccari – Research Associate, University of Virginia
- Adrian Bohane – CEO, TRE Canada Inc.
- Giacomo Falorni, Operations Manager, TRE Canada Inc.
- Brian Bruckno – Engineering Geologist, Virginia DOT
- Elizabeth Campbell – GIS Enterprise Data Manager, Virginia DOT
- Audrey Moruza – Research Economist, VCTIR
- Edward Hoppe – Research Scientist, VCTIR

Members of the advisory board were introduced as follows:

- Melba Crawford – Associate Dean of Engineering, Purdue University
- Scott Anderson – Geotechnical Team Manager, FHWA Resource Center, Lakewood, Colorado
- Emmett Heltzel – State Maintenance Engineer, Virginia DOT
- Chad Allen – Asset Management Manager, Vermont Agency of Transportation
- Ty Ortiz – Geotechnical Program Manager, Colorado Department of Transportation

The meeting was also attended by Mr. Vasanth Ganesan, Assistant to Program Manager, US Department of Transportation.

II. Remote Sensing Study

Scott Acton outlined the remote sensing study, initiated on January 15, 2014. The University of Virginia is leading the effort. TRE Canada provides acquisition and processing of satellite radar data. VDOT/VCTIR team members are contributing to ground validation and data analysis. The primary applications focus on sinkhole detection, slope stability, and bridge displacement monitoring. The objective is to further develop analytical techniques prototyped in the preceding study and implement them into routine operations at the state DOT level. The key is to produce implementable product that will assist in decision making. The role of the advisory board is to help the research team guide the study and provide practical feedback.

III. Open Discussion

Melba Crawford: What are the sensors used for this study?

Adrian Bohane: We are using COSMO-SkyMed radar satellite (X-band) for most of the applications. Also, RADARSAT-2 satellite (C-band) will be used for slope monitoring. We are trying to develop techniques that are independent of the satellite system.

Melba Crawford: Some of the methodology may have to be different, depending on the source, for example L-band processing.

Adrian Bohane: Yes, L-band will require a different approach, but we do not have access to any L-band data on this project.

Melba Crawford: What techniques are used for ground verification?

Elizabeth Campbell: We (VDOT) use a private company for pavement evaluation. Bridges are also inspected periodically (by VDOT crews and consultants).

Chad Allen: Pavement condition application is very interesting from the asset management point of view.

Scott Anderson: This is a good research plan, but we need to know when and how to engage the advisory board in the process. This is important.

Scott Acton: Yes, we will provide appropriate guidelines to the advisory board.

Scott Acton: If you were the recipient, how would you like to have the products of this research delivered? What type of output would be most useful to users?

Scott Anderson: State DOTs will be using consultants for InSAR data processing and then points will be flagged on state GIS maps. DOTs will have to decide on how to act on this information.

Andrea Vaccari: We are using ArcGIS to analyze data. Perhaps there are other tools to consider.

Elizabeth Campbell: We can use ESRI ArcGIS Online framework and create a web based implementation. For example, there could one application developed for some detailed analysis and a simpler one for maintenance personnel to facilitate verifying points of interest in the field. This kind of setup allows for implementation in other state DOTs. There is no need for everyone to use ArcGIS desktop software.

Adrian Bohane: We should elaborate on the network aspect of this study. We will be able to provide data on the network-wide level. Can the advisory board provide some guidance on what kind of network level information would be valuable to a state DOT? Where does remote sensing fit for a DOT at the network level?

Elizabeth Campbell: … and what information would be of most value (bridges, cut slopes, pavement condition, or coastal erosion)?

Melba Crawford: Aging infrastructure. For example, there are a lot of problems with inspecting old steel bridges. This is a national problem.

Scott Anderson: Bridges are critical, money is in pavements. Performance monitoring of bridges and pavements is already required by federal laws. My task is to promote this approach to geotechnical assets - slopes, embankments, retaining walls.

Emmett Heltzel: I agree, more resources are allocated to pavements. The product of your research should be easy to implement. If you can demonstrate that I can capture more of the pavement information then this would be valuable. For other assets, develop strategies for dealing with those assets.

Scott Anderson: The first use of this technology will be as an important learning tool. We need to learn how much things are moving, at what rate, and establish thresholds. As we get more information, we'll learn how to use these new data effectively.

Melba Crawford: You need to engage practitioners.

Brian Bruckno: I was able to use InSAR data on a stormwater management project by identifying locations of active and inactive sinkholes. As a result, the location of the stormwater pond was optimized.

Scott Acton: What is the best way of engaging state DOTs?

Scott Anderson: Web-based training, web deployment, and TRB activities.

Audrey Moruza: Should we consider the output as an asset management tool or as emergency response?

Scott Anderson: This is all about performance, mobility, reliability, and asset management.

Ty Ortiz: It is important to identify the limitations of this technology, what can and cannot be monitored.

Adrian Bohane: We are going to monitor 40 by 40 km areas of interest. We'll process all points within the AOI. Yes, if some slopes are too steep, there will be limitations, but we'll find that out when we process the data. We can determine the percentage of slopes that we can 'see.'

Melba Crawford: This is one type of remote sensing and part of a bigger picture. These things will evolve over time.

Scott Acton: I would like to thank everyone for participating in this meeting. The research team will provide a follow-up document to the advisory board regarding the expectations, points of engagement, and how it all ties into various tasks.

There being no further business, the meeting was adjourned.

Appendix J – Cost/benefit analysis

Audrey K. Moruza – **Economic Analysis of InSAR Technology at VDOT** – July 2016 [download][14]

Audrey K. Moruza – **Application of Net Present Benefit Analysis to InSAR Monitoring: Outline of an Economic Analysis for a Network** – January 2016 [download][15]

Audrey K. Moruza - **Guide to Excel Tool for Estimation of Net Present Benefit of Network-Wide InSAR Monitoring** – November 2016 [download][16]

Link to tool:
http://viva-lab.ece.virginia.edu/elecdocs/ritars14/CBA_Tool.xlsx

[14] http://viva-lab.ece.virginia.edu/elecdocs/ritars14/CBA_InSAR.pdf
[15] http://viva-lab.ece.virginia.edu/elecdocs/ritars14/CBA_TRB.pdf
[16] http://viva-lab.ece.virginia.edu/elecdocs/ritars14/CBA_Tool_Guide.pdf

Economic Analysis of InSAR Technology for VDOT

Audrey K. Moruza, Research Scientist
Virginia Transportation Research Council (VDOT)
July 19, 2016

INTRODUCTION

The economic analysis described here was performed to evaluate Interferometric Synthetic Aperture Radar (InSAR) technology for remote detection and monitoring of surface deformations that impact VDOT roadways and other assets. The analytical framework, i.e., a five-year period over which processed InSAR data are "leased" by VDOT, accommodates the challenge of estimating the technical performance of InSAR in innovative applications, and the analysis purposefully avoids the presumption of a long-term commitment of VDOT resources to InSAR, in particular the development of in-house data processing resources. The analysis guides a short-term decision rather than a long-term decision on the principle that the full capabilities of a new application of even proven technology can appear gradually as field implementation progresses. Consequently, the question addressed by this analysis is how the short-term costs of InSAR to VDOT compare to potential short-term savings to VDOT.

InSAR was originally proposed to VDOT as a technology that could provide advance detection of geohazards such as sinkholes and unstable slopes, and these events were regarded as ready and potentially urgent applications. This analysis, however, examines geohazard and culvert monitoring, assuming network-level InSAR coverage. Monitoring of culverts, particularly metal culverts, was added because (1) ground deformation caused by metal culvert deterioration could be similar to that caused by sinkhole formation, potentially allowing more intense utilization of InSAR data evidence of local subsidence of the type that characterizes sinkholes and some culvert failures; (2) culverts are indispensable to VDOT highway network serviceability; (3) culvert maintenance and replacement expenditures are sizable annual components of VDOT maintenance expenditures; and (4) if combined savings from routine culvert and geohazard monitoring by InSAR were sufficient to make InSAR network coverage cost-effective, other more critical applications such as bridge monitoring or more network-oriented applications such as secondary road pavement monitoring could be tested under live conditions of active InSAR network coverage.

In the sketch-level economic analysis performed for the initial research into InSAR technology for VDOT applications, benefits were defined as savings resulting from a reduction in the number of geohazard repairs occurring as emergencies. Avoidance of emergency events translated in this analysis into benefits for both the public and for VDOT in the form of savings in (1) user costs from emergency work zones, (2) VDOT's liability exposure to claims (fatalities or otherwise), and (3) materials supply costs, all of which were expected to be reduced from present levels by means of advance event detection and proactive intervention.

Although the salient conditions mentioned in the initial analysis do occur on occasion, it was not feasible to develop a general economic analysis based on the excess cost to VDOT of two-phase disposal of waste material caused by emergency operations, or to develop general cases for the social cost of major traffic disruption or the agency cost of VDOT's liability exposure. This is because not all geohazards cause a redundant (two-phase) workflow, cause significant traffic disruption, or claim a life. For geohazards, then, the general case developed for the final economic analysis of InSAR monitoring turns on estimated savings derived from proactively stabilizing a slope (the presumed result of advance slope movement detection) versus repairing the full damage of a failed slope. (Total annual expenditures by VDOT on slope repairs far exceed expenditures on sinkhole repairs.)

The addition of culvert monitoring by InSAR technology further supported a general framework rather than an "extreme case" framework for the final economic analysis. For culverts, monitoring by InSAR offers a choice between timely maintenance (given advance surface deformation detection) and total culvert replacement after maintenance becomes impractical. Moreover, introducing InSAR technology to monitor culvert deterioration displaces no current provider(s) of such services and thus avoids structural resistance to the innovation.

This analysis presumes that InSAR technology can reliably detect at least some early signs of ground deformation associated with geohazards and culvert deterioration, and it estimates fiscal benefits to VDOT from advance warning of these events.

PURPOSE AND SCOPE

The purpose of the final analysis is to determine at an estimate level the cost-effectiveness of InSAR technology to VDOT by comparing potential changes in expenditures in two categories of routine events (with and without the technology) to the cost to VDOT of that technology, i.e., processed InSAR data. VDOT expenditures and technology costs are combined in a simple tool that calculates the net present benefit to VDOT over a period of 5 years. The results serve to guide a short-term procurement decision.

This final economic analysis of InSAR technology assumes that timely maintenance actions (made possible by advance detection of deformation) can and will be taken that avert or delay higher cost replacement or rebuild actions to mitigate the consequences of unanticipated deformation, adding service life to existing assets. The scope of the analysis includes VDOT and district-maintained culverts and all VDOT assets impacted by geohazards.

A corollary of this approach is that if InSAR technology can cause net agency savings by means of proactive but otherwise ordinary maintenance actions, extreme events might be precluded by maintenance performed out of fiscal self-interest. Under this reasoning, extreme events such as loss of life from slope failures into roadways need not play a disproportionate role in the economic analysis relative to actual occurrence since timely maintenance may forfend against some extreme events occurring at all.

METHODS

Data Collection

VDOT expenditures on geohazard mitigation and potential savings on those expenditures derived from InSAR technology are determined by routinely collected data and by practical information from an expert holding a statewide contract with VDOT for geohazard mitigation. VDOT expenditures on culvert replacements and potential savings derived from InSAR technology are determined from routinely collected data and VDOT's electronic construction management database. Both categories required extensive contact with VDOT district and Central Office staff in order to locate and include as much relevant data as possible.

Costs

The collection of costs on culvert replacement and geohazard expenditures was a labor-intensive and time-consuming task in the case study of VDOT. VDOT has inaugurated several electronic data management systems in the last decade that are increasingly interfacing and cross-documenting VDOT activities and expenditures. While these systems have been in transition, however, the collection and verification of data were challenging and tedious tasks. Two salient general problems arose: (1) VDOT districts are permitted a variety of descriptors for the logging of geohazard activities in VDOT's maintenance records; (2) the federal identification numbers for some culverts had been changed after the current fiscal system was implemented by VDOT, effectively causing one culvert to have two federal numbers in VDOT's fiscal system. It required time to fully reveal these problems and yet more time to resolve them for the purposes of this analysis. Other DOTs may find similar problems in data collection.

Geohazards

District and Central Office personnel were interviewed to determine whether geohazard cost datasets already exist locally, and if not, how to access these costs directly (i.e., method of tracking in district). No district offered complete datasets of geohazard expenditures, and all districts reported different local tracking methods for such costs. Since all districts must log geohazard event costs into VDOT's fiscal system when work is performed by state forces and into VDOT's electronic construction management database when work is performed under contract, an original dataset was created from these sources.

Geohazard cost data over the three fiscal year (FY) period of 2013-2015 were collected by searching VDOT's fiscal records of state-force and contract repairs in both the maintenance and the construction databases. All contracts let during the FY 2013-2015 period were included.

The average annual cost of the three-year period was used as a "typical" annual cost in the analysis.

Culvert Replacements

Culvert replacement costs by state forces are available in VDOT's fiscal system under specific Task numbers for numbered assets (large culverts that are VDOT's responsibility) and unnumbered assets (other culverts that are district responsibilities). Costs of culvert replacements (and also rehabilitation) performed under contract are available in VDOT's construction database. Some districts were queried for method of expenditure tracking; any guidance offered was followed on a case-by-case basis.

Culvert replacement costs over the FY 2013-2015 period were collected by searching VDOT's fiscal records of state-force work and contracts in both the maintenance and the construction databases. All pertinent contracts let during the period were included. The average annual cost of the three-year period was used as a "typical" annual cost in the analysis.

Processed InSAR Data

TRE Canada supplied their costs of network coverage for two resolution levels of InSAR data which they process: X-band or *commercial* data and C-band or *free-of-charge* data. Nothing ensures that these costs will be stable into the future or even across vendors in the present.

X-band data, provided by the COSMO-SkyMed (CSK) satellite at 3x3 meter resolution and requiring 80 frames for VDOT network coverage, was recommended with a 16-day repeat cycle and 22 frames per annual "stack." Eighty frames, each captured 22 times per year, are estimated to cost $9.52 million including processing costs. These *commercial* data are higher resolution than the alternative analyzed here.

C-band data, provided by the Sentinel-1 satellite at 5x20 meter resolution and requiring 12 frames for VDOT network coverage, was recommended with a 12-day repeat cycle and 30 frames per annual "stack." Twelve frames, each captured 30 times per year, are estimated to cost $648,000 for network coverage, all of which is processing cost since Sentinel-1 data are otherwise free. C-band data may require follow-up frames of either resolution at additional cost to confirm surface deformation indicated in C-band imagery. These *free-of-charge* data offer medium resolution (i.e., pixel size) compared to the high resolution of the commercial alternative analyzed here.

Analytical Framework

Assumptions

The final economic analysis evaluates InSAR technology under these assumptions:

- VDOT “leases” a package of InSAR data and processing services from a vendor for 5 years;
- Geohazard and culvert expenditures over the FY 2013-2015 period may be averaged to represent a typical year of costs in each category;
- VDOT will not possess or develop in-house capabilities for processing InSAR data within the 5-year lease period;
- 12 months of baseline InSAR data must be collected before benefits are realized;
- Vendor processing costs are stable over the lease period in real terms;
- Sentinel-1 coverage of the eastern U.S. will be adequate to provide the required coverage to VDOT beginning in 2017;
- Sentinel-1 satellite data will continue to be free of charge while processing is priced at market rates.

Potential VDOT Savings Due to InSAR Services

Geohazards

The modeling of potential savings from geohazard monitoring is based on the extensive experience of VDOT’s on-call vendor for slope stabilization projects. The vendor’s expertise was conveyed by phone interview early in the study. After numerous years of holding the statewide contract for slope stabilization and soil nailing, this expert reported that a project which includes road rebuild will cost twice as much on average as a project lacking road rebuild after a slope failure or slide. In this analysis, savings of 50 percent in detected geohazards are assumed to result from the substitution of lower-cost interventions for major reconstruction work which is possible because of advance detection of ground surface deformation and proactive stabilization.

Culvert Replacements

The modeling of potential savings in VDOT expenditures on culvert replacements is based on contracts contained in VDOT’s electronic construction management database. Two contracts let in different districts during the data collection period (FY 2013-2015) provided the dollar costs (by culvert diameter and length) of the various methods of culvert rehabilitation (cured-in-place pipe liner, HDPE/PVC/Polypropylene liner, smooth wall steel pipe liner, corrugated steel pipe liner, and spray-on liner) versus the cost of jack-and-bore replacement. Calculated per square inch of culvert surface area and averaged across all methods over both contracts, rehabilitation methods were estimated to cost about 60 percent of culvert replacement by the jack and bore method, implying average savings of about 40 percent when rehabilitating rather than replacing a culvert. Savings rates vary by specific methods.

Performance Measure

The analysis framework is designed to produce order-of-magnitude estimates of time-discounted net benefits to VDOT gained from X-band and C-band InSAR imagery over a 5-year lease period. The Net Present Benefit in each category is defined in Equation 1:

$$Net\ Present\ Benefit = \sum_i (B_i - C_i)\,/(1+\rho)^i \qquad \text{(Eq. 1)}$$

Where

$i = 1, \ldots 5$ (years)
$\rho =$ discount rate
$B_i =$ benefits to VDOT in year i
$C_i =$ costs to VDOT in year i

The benefits of InSAR technology, B_i, are defined as reductions in annual VDOT expenditures in each event category (culverts and geohazards) that result from InSAR data. Costs, C_i, are defined as annual VDOT expenditures to procure processed InSAR data. Net Present Benefit is the sum of discretely discounted annual net benefits in both categories over the 5-year period.

Equation 2 defines annual benefits to VDOT as reductions in annual event costs for the categories of culverts and geohazards. Further, annual benefits are determined by the model parameters of detection rate (DR) and savings rate (SR):

$$Annual\ VDOT\ benefit\ in\ year\ i = B_i = \qquad \text{(Eq. 2)}$$

$$\sum_{\substack{Culverts,\\ geohazards\ in\ year\ i}} DR_{category,i} \cdot SR_{category,i} \cdot Average\ annual\ total\ cost\ of\ category$$

Where

$i = 1, \ldots 5$ (years)
$DR =$ detection rate of events in category resulting from InSAR services;
$SR =$ savings rate from lower-cost intervention enabled by early detection;
$DR\ and\ SR$ grow annually according to explicitly assumed rates as shown in tool.

Benefits cannot be calculated in the tool without the use of the parameters SR and DR to bridge the gap between available data and model requirements. Although plausible assumptions for SR, which is a function of business practices under the control of VDOT, were made on the basis of research as discussed above, the DR for each event category is a function of the efficacy of InSAR techniques. Thus the DR of both events remains elective and variable in the tool because it is unknown at this point. In a general rather than VDOT application, the tool incorporates both the DR and the SR as elective variables specific to event category.

To summarize, DR is independently variable for each event category, and SR is set at 0.40 for culverts and at 0.50 for geohazards for VDOT's particular analysis. In other words, the tool computation of B_i specific to VDOT's case study allows 40 percent savings for any culvert rehabilitation that pre-empts replacement because of advance detection due to InSAR data and 50 percent savings when VDOT intervenes in geohazard events after early detection by InSAR techniques. It should be noted here that the final actual dollar savings which enter the tool calculations are the product of SR and DR assumptions.

Additionally, the tool can incorporate a "learning curve" as experience is gained by VDOT from matching InSAR data to ground observation over the 5 year lease period. In this model, a learning curve is incorporated by allowing growth in the detection and savings rates over the analysis period. Since SR and DR are independent of each other, being influenced by agency and technology factors respectively, their potential growth rates are similarly independent.

RESULTS AND DISCUSSION

Total estimated costs to VDOT of geohazard repairs and culvert replacements over the period FY 2013-2015 are presented in Table 1. It should be noted that the categorical totals may be incomplete rather than overstated due to the freedom provided at the VDOT district level to track relatively randomly-occurring geohazard costs as is convenient in that district.

Table 1. VDOT (Statewide) Expenditures

	FY 2013	FY 2014	FY 2015
CULVERT REPLACEMENTS	$ 10,976,877	$ 13,457,522	$ 12,433,162
GEOHAZARD REPAIRS	$ 9,002,823	$ 8,114,545	$ 10,338,102
TOTAL	$ 19,979,700	$ 21,572,066	$ 22,771,264

Figure 1 shows the tool containing VDOT expenditure data, assumptions pursuant to the cost to VDOT of X-band data, and the Net Present Benefit results for the X-band package. The Net Present Benefit to VDOT shown in the indicated box is a negative number of large magnitude, and it can be noted that the InSAR package costs about 44 percent of the summed annual cost of the events. To summarize Figure 1, the X-band option is not justifiable in terms of estimated benefits to VDOT relative to the cost of the events to VDOT. On the other hand, with assumed improvements in the detection and savings rates as experience is accumulated with InSAR data (i.e., progress on the learning curve), the annual net loss to VDOT declines over time.

As shown in Figure 1, the culvert DR of 33 percent implies that one of three potential culvert replacement dollars is detected by means of InSAR evidence of ground deformation, and the culvert SR implies that 40 percent of the cost of replacement *for each intervention* is saved by culvert rehabilitation. The geohazard DR of 10 percent implies that one of ten potential geohazard dollars is detected by means of InSAR evidence of ground deformation, and the SR implies that this action saves 50 percent of the costs that would have been incurred *on those interventions* without InSAR services.

The parameter assumptions for culverts imply that 33 percent of culvert replacement dollars pertain to culverts with shallow enough ground cover to display ground deformation in response to InSAR techniques, and that 40 percent of replacement costs can be saved on such culverts that are detected. On the other hand, the parameter assumptions for geohazards rather unsatisfactorily reflect the expert opinion that if the 10 percent of events that are major (i.e., involve road rebuild) can be detected, 50 percent of their costs can be saved. This is because the worst 10 percent of geohazard events probably cost far more than 10 percent of the total geohazard expense over the analysis period. Yet because the parameters are fully variable, this scenario can be harmlessly examined before new parameter assumptions are applied.

The tool result shows that high-resolution InSAR data produces a large negative Net Present Benefit for VDOT over the analysis period. In other words, VDOT's costs for culverts and geohazards do not justify trial of high-resolution InSAR data services under the assumed SR and DR as shown, even with growth in these parameters (and therefore in VDOT's annual benefits).

NETWORK-WIDE						
EVENT COST DATA	2013	2014	2015	ANNUAL AVERAGE		
CULVERT REPLACEMENTS	$ 10,976,877	$ 13,457,522	$ 12,433,162	**$ 12,289,187**		
GEOHAZARD REPAIRS	$ 9,002,823	$ 8,114,545	$ 10,338,102	**$ 9,151,823**		
	$ 19,979,700	*$ 21,572,066*	*$ 22,771,264*	*$ 21,441,010*	COSMO-SkyMed (X-Band) data	
ANNUAL COST OF INSAR DATA						
CSK NETWORK COVERAGE	**$ 9,520,000**	HIGH RESOLUTION				
SENTINEL-1 NETWORK COVERAGE	**$ 648,000**	MED RESOLUTION				
CSK (1 SQ MI COVERAGE)	*$ 62,000*	*CONFIRMATION FRAME COST, SCENARIO 2*				
SENTINEL (1 SQ MI COVERAGE)	*$ 26,000*					
YEAR	0	1	2	3	4	5
DISCOUNT RATE (ρ)	3.0%					
ANNUAL INSAR COST TO VDOT	**$ 9,520,000**	$ 9,520,000	$ 9,520,000	$ 9,520,000	$ 9,520,000	$ 9,520,000
ANNUAL VDOT BENEFITS (B_i)		$ -	$ 2,079,764	$ 2,292,940	$ 2,527,966	$ 2,787,082
INITIAL DETECTION RATE: CULV	33%		33%	35%	36%	38%
INITIAL SAVINGS RATE: CULV	40%		40%	42%	44%	46%
INITIAL DETECTION RATE: GEOHZ	10%		10%	11%	11%	12%
INITIAL SAVINGS RATE: GEOHZ	50%		50%	53%	55%	58%
ANNUAL GROWTH IN DETECTION RATE	5%					
ANNUAL GROWTH IN SAVINGS RATE	5%					
NET ANNUAL VDOT BENEFIT		(9,520,000)	(7,440,236)	(7,227,060)	(6,992,034)	(6,732,918)
NET PRESENT BENEFIT	($34,889,844)					

Figure 1. Cosmo-Skymed InSAR: Baseline Scenario

For the purpose of exploring the threshold parameters at which the X-band option would provide a positive Net Present Benefit given VDOT's costs for culverts and geohazards, perfect detection rates of 100 percent are assumed for each event category while the SR parameters remain unchanged. No growth in DR can exist under this scenario since detection is already perfect, and the SR (or agency response) parameters have no prima facie reason to change if detection is perfect. Figure 2 shows that the net present benefit to VDOT of X-band InSAR data remains highly negative for the 5-year analysis period.

To summarize the promise of X-band InSAR data for VDOT, it is clear that the costs of VDOT events that are currently in the tool are insufficient to justify a 5-year lease period of high-resolution InSAR data. Even with perfect detection, VDOT requires higher event costs—or more event categories—to break even in a 5-year trial of X-band Insar Data.

NETWORK-WIDE						
EVENT COST DATA	2013	2014	2015	ANNUAL AVERAGE		
CULVERT REPLACEMENTS	$ 10,976,877	$ 13,457,522	$ 12,433,162	**$ 12,289,187**		
GEOHAZARD REPAIRS	$ 9,002,823	$ 8,114,545	$ 10,338,102	**$ 9,151,823**		
	$ 19,979,700	*$ 21,572,066*	*$ 22,771,264*	*$ 21,441,010*	COSMO-SkyMed (X-Band) data	
ANNUAL COST OF INSAR DATA						
CSK NETWORK COVERAGE	**$ 9,520,000**	HIGH RESOLUTION				
SENTINEL-1 NETWORK COVERAGE	**$ 648,000**	MED RESOLUTION				
CSK (1 SQ MI COVERAGE)	*$ 62,000*	*CONFIRMATION FRAME COST, SCENARIO 2*				
SENTINEL (1 SQ MI COVERAGE)	*$ 26,000*					
YEAR	0	1	2	3	4	5
DISCOUNT RATE (ρ)	3.0%					
ANNUAL INSAR COST TO VDOT	**$ 9,520,000**	$ 9,520,000	$ 9,520,000	$ 9,520,000	$ 9,520,000	$ 9,520,000
ANNUAL VDOT BENEFITS (B_j)		$ -	$ 9,491,586	$ 9,491,586	$ 9,491,586	$ 9,491,586
INITIAL DETECTION RATE: CULV	100%		100%	100%	100%	100%
INITIAL SAVINGS RATE: CULV	40%		40%	40%	40%	40%
INITIAL DETECTION RATE: GEOHZ	100%		100%	100%	100%	100%
INITIAL SAVINGS RATE: GEOHZ	50%		50%	50%	50%	50%
ANNUAL GROWTH IN DETECTION RATE	0%					
ANNUAL GROWTH IN SAVINGS RATE	0%					
NET ANNUAL VDOT BENEFIT		(9,520,000)	(28,414)	(28,414)	(28,414)	(28,414)
NET PRESENT BENEFIT	**($9,345,258)**					

Figure 2. Cosmo-Skymed InSAR: High Initial Detection Rate Scenario

Figure 3 shows VDOT's net present benefit from lease of the C-band InSAR package, assuming lower detection rates as a consequence of C-band data. Detection rates are set at one in about eight culvert dollars and one in 25 geohazard dollars initially and are assumed to grow as experience increasingly matches InSAR "hot spots" with ground observations.

NETWORK-WIDE						
EVENT COST DATA	2013	2014	2015	ANNUAL AVERAGE		
CULVERT REPLACEMENTS	$ 10,976,877	$ 13,457,522	$ 12,433,162	$ 12,289,187		
GEOHAZARD REPAIRS	$ 9,002,823	$ 8,114,545	$ 10,338,102	$ 9,151,823		
	$ 19,979,700	$ 21,572,066	$ 22,771,264	$ 21,441,010	Sentinel-1 (C-Band) data	
ANNUAL COST OF INSAR DATA						
CSK NETWORK COVERAGE	$ 9,520,000	HIGH RESOLUTION				
SENTINEL-1 NETWORK COVERAGE	$ 648,000	MED RESOLUTION				
CSK (1 SQ MI COVERAGE)	$ 62,000	CONFIRMATION FRAME COST, SCENARIO 2				
SENTINEL (1 SQ MI COVERAGE)	$ 26,000					
YEAR	0	1	2	3	4	5
DISCOUNT RATE (ρ)	3.0%					
ANNUAL INSAR COST TO VDOT	$ 648,000	$ 648,000	$ 648,000	$ 648,000	$ 648,000	$ 648,000
ANNUAL VDOT BENEFITS (B_i)		$ -	$ 1,440,726	$ 1,440,726	$ 1,440,726	$ 1,440,726
INITIAL DETECTION RATE: CULV	20%	$ 2,457,837	20%	20%	20%	20%
INITIAL SAVINGS RATE: CULV	40%	$ 983,135	40%	40%	40%	40%
INITIAL DETECTION RATE: GEOHZ	10%	$ 915,182	10%	10%	10%	10%
INITIAL SAVINGS RATE: GEOHZ	50%	$ 457,591	50%	50%	50%	50%
ANNUAL GROWTH IN DETECTION RATE	0%					
ANNUAL GROWTH IN SAVINGS RATE	0%					
NET ANNUAL VDOT BENEFIT		(648,000)	792,726	792,726	792,726	792,726
NET PRESENT BENEFIT	$2,231,690					

Figure 3. Sentinel-1 InSAR: Baseline Scenario

Figure 3 shows a positive Net Present Benefit over 5 years even with arbitrarily conservative estimates of event detection (which seem to be initially appropriate assumptions for medium-resolution InSAR data). Given a positive Net Present Benefit result, confirmation frames of one square mile of X-band or C-band data could be procured for $62,000 or $26,000, respectively, causing the 5-year Net Present Benefit to approach zero and VDOT to break even. Note that if X-band (high-resolution) follow-up frames were procured and preventive action taken in a given year, calculation of the net present benefit over the analysis period would be iteratively altered by those additional costs and benefits.

CONCLUSIONS AND RECOMMENDATIONS

The analysis performed here seeks to evaluate a novel use of established technology with limited or no field data support of the specific type required for detailed calculation of Net Present Benefit to VDOT. Savings rates (SR) are based on anecdotal evidence and detection rates (DR) are based on plausible conjecture. The tool lacks the rigor that would be possible with event DR determined by a comparison of InSAR surface maps with accurate field data, yet it seeks to guide a short-term decision without that valuable information.

The tool can, however, reasonably eliminate the option of 5-year lease of an X-band (high-resolution) InSAR data package for the monitoring of culverts and geohazards because of an unfavorable Net Present Benefit result for VDOT, even assuming initial DR at 100 percent for both event categories. This outcome may follow simply from the fact that annual cost of the X-band package is about 44 percent of the cost of average annual expenditures by VDOT on the two events considered in this analysis. By this reasoning, however, the outcome could conceivably be reversed if a trial period proved that InSAR technology could provide savings in another costly maintenance activity, such as bridge monitoring or secondary road pavement condition monitoring.

For cost-effectiveness, the C-band (medium-resolution) InSAR data package results contrast sharply with the X-band InSAR package for culvert and geohazard monitoring. The C-band package can be supplemented with a number of follow-up confirmation frames providing closer looks (by X-band or by C-band) at local deformations of interest (i.e., hot spots) while still breaking even for VDOT. Finally, during live network coverage made possible by explicit savings in culverts, field testing for other applications can proceed.

Of the two applications evaluated in this analysis, only a geohazard – specifically a slope failure – has involved loss of life on a VDOT highway. The possibility of events with high potential consequences of failure in spite of low probability of occurrence, and that have no monitoring in use that is comparable to regular InSAR surveillance, would seem to urge the proving of potentially cost-effective network applications of any helpful technology – i.e., a bread-and-butter application such as culvert monitoring that can potentially self-fund, through intentionally captured savings, a period for testing other applications in monitoring more valuable DOT assets.

VDOT's culvert "problem" is sourced in older steel culverts. VDOT has 1,873 steel culverts at present, of which 139 are in "Poor" condition. Steel culverts are noted within the agency for deterioration and VDOT is pursuing new culvert rehabilitation technologies, meanwhile recommending replacement with concrete culverts. These facts suggest that although savings seem available if intentionally captured from careful culvert monitoring and selective rehabilitation, culvert monitoring by InSAR data may ultimately be a short-term, opportunity-driven application rather than a maintenance technology of enduring value to VDOT.

Alternatively, C-band InSAR data could be evaluated as a monitoring system for secondary pavements, of which VDOT maintains more than 49,000 miles (and more than 99,000 lane-miles). VDOT currently spends roughly $100 per mile on secondary system data collection which includes the costs of images, collection of roughness and distress data, data processing, and quality assurance, among other activities, but in some cases for good reason: some secondary routes in parts of the state carry more traffic than interstates in other parts of the state. At a current baseline cost of network coverage C-Band InSAR data of $13 per secondary system mile maintained by VDOT, there would seem to be ample fiscal incentive for exploration of InSAR capabilities in secondary pavement condition assessment before it rivals the cost of current practice at $100 per mile.

For secondary pavement monitoring, the "next step" raises the question of which option provides VDOT with the best long-term value for its dollar of expenditure: (1) annual InSAR monitoring of 100 percent of the secondary system at lower resolution and probably lower cost even after more research and development in the use of processed C-band data for pavement monitoring, with the option of high-resolution individual frames for follow-up or (2) annual ground-based monitoring in higher immediate detail of 20 percent of the secondary system at a higher cost. In other words, VDOT must determine what standard of pavement condition assessment is satisfactory for the secondary roads it maintains as new technology continues to offer options to explore.

The tool results for Sentinel-1 data suggest a trial of medium-resolution InSAR data has the potential to yield good fiscal results for VDOT. Yet a final caveat is in order. The parameter SR implies that savings will be captured by means of agency business practices, and this value-capture may or may not actually occur. At a minimum, intentionality toward capturing savings offered by advance detection of culvert deterioration and geohazard events is a requirement of a trial of InSAR technology.

January 14, 2016

TRB 95TH ANNUAL MEETING
WORKSHOP 879

INTERFEROMETRIC SYNTHETIC APERTURE RADAR:

A Promising New Tool for Network-Wide Transportation Infrastructure Monitoring

Lecture 5: Application of Net Present Benefit Analysis to InSAR Monitoring: Outline of an Economic Analysis for a Network

Audrey Moruza, Virginia Transportation Research Council (VDOT)

Funded by USDOT Commercial Remote Sensing and Spatial Information Program. Disclaimer: The views, opinions, findings and conclusions reflected in this presentation are the responsibility of the author only and do not represent the official policy or position of the USDOT/OST-R, or any State or other entity.

VDOT Virginia Department of Transportation
Michigan Tech
University of Virginia
TRE
UAF University of Alaska Fairbanks

Contact:
Audrey.Moruza@vdot.virginia.gov

Outline of an Economic Analysis for Network Monitoring

VDOT-maintained lane-miles ≈ 127,245
VDOT-maintained structures ≈ 19,500
(≈ 7,550 inventory culverts)

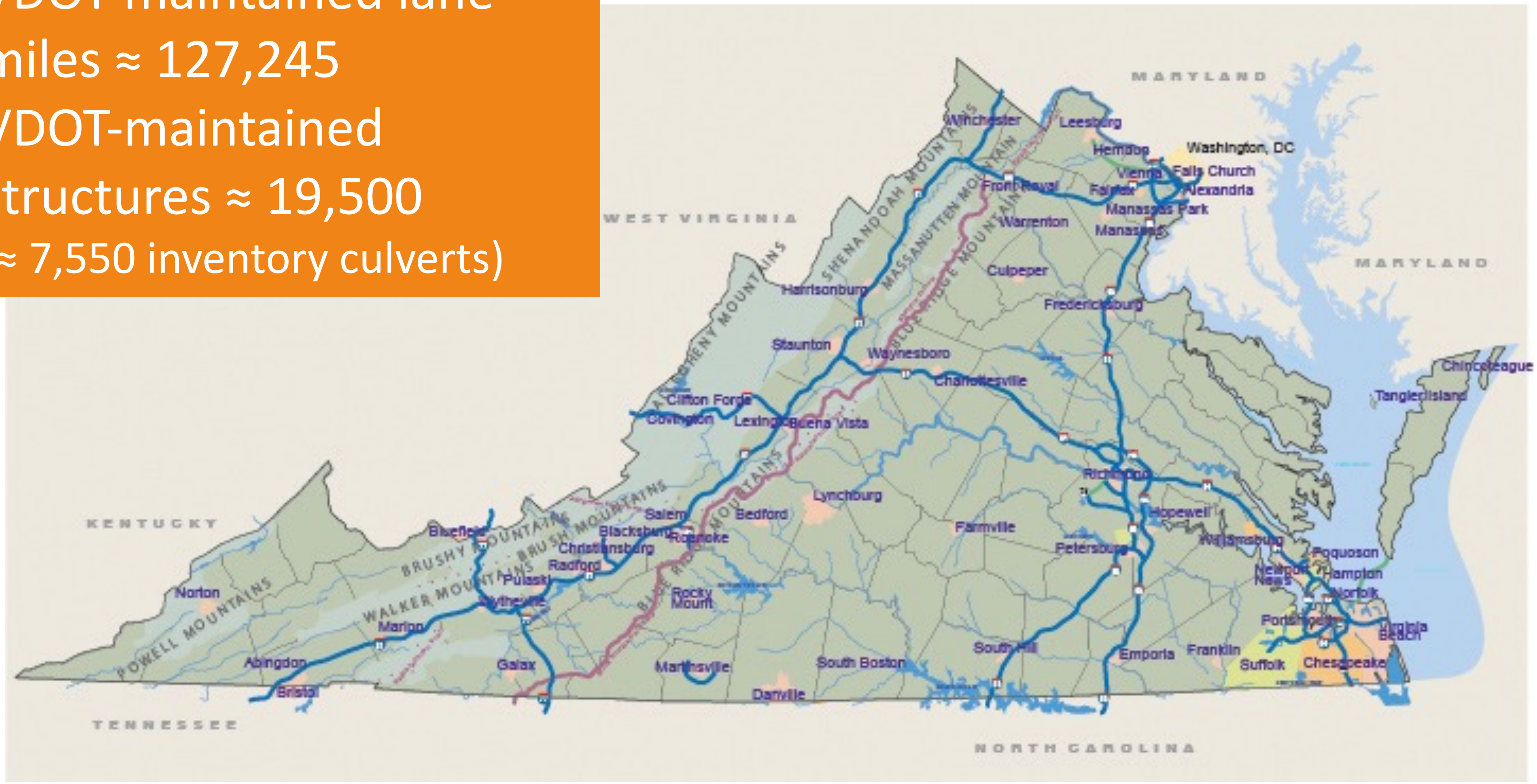

Outline of an Economic Analysis for Network Monitoring

VTRC Virginia Transportation Research Council

Premise

- VDOT has routine events that feature surface deformation, sometimes signaling an emergency event;
- Savings in VDOT expenditures on these events could be significant if timely intervention *prevents* emergencies or costly maintenance;
- How do potential VDOT cost savings compare to the costs of InSAR monitoring?

VTRC
Virginia Transportation Research Council

General Assumptions

- FY 2013-15 event total costs are "typical" of near future;
- No VDOT InSAR data processing capability for the next five years;
- 12-month data collection period to establish a baseline surface map for VDOT assets;
- Stable vendor processing costs for 5 years;
- Adequate Sentinel coverage of the eastern U.S. beginning in 2017;
- Free Sentinel data, but processing at market price.

VDOT Network Applications of InSAR

- Culvert and pipe maintenance (assuming surface expression of deterioration)
- Geohazards: slope failures, slides, sinkholes

VDOT EXPENDITURES STATEWIDE			
	FY 2013	FY 2014	FY 2015
CULVERT REPLACEMENTS	$ 10,976,877	$ 13,457,522	$ 12,433,162
GEOHAZARD REPAIRS	$ 9,191,485	$ 9,446,179	$ 14,454,023
TOTAL	$ 20,168,362	$ 22,903,701	$ 26,887,185

Outline of an Economic Analysis for Network Monitoring

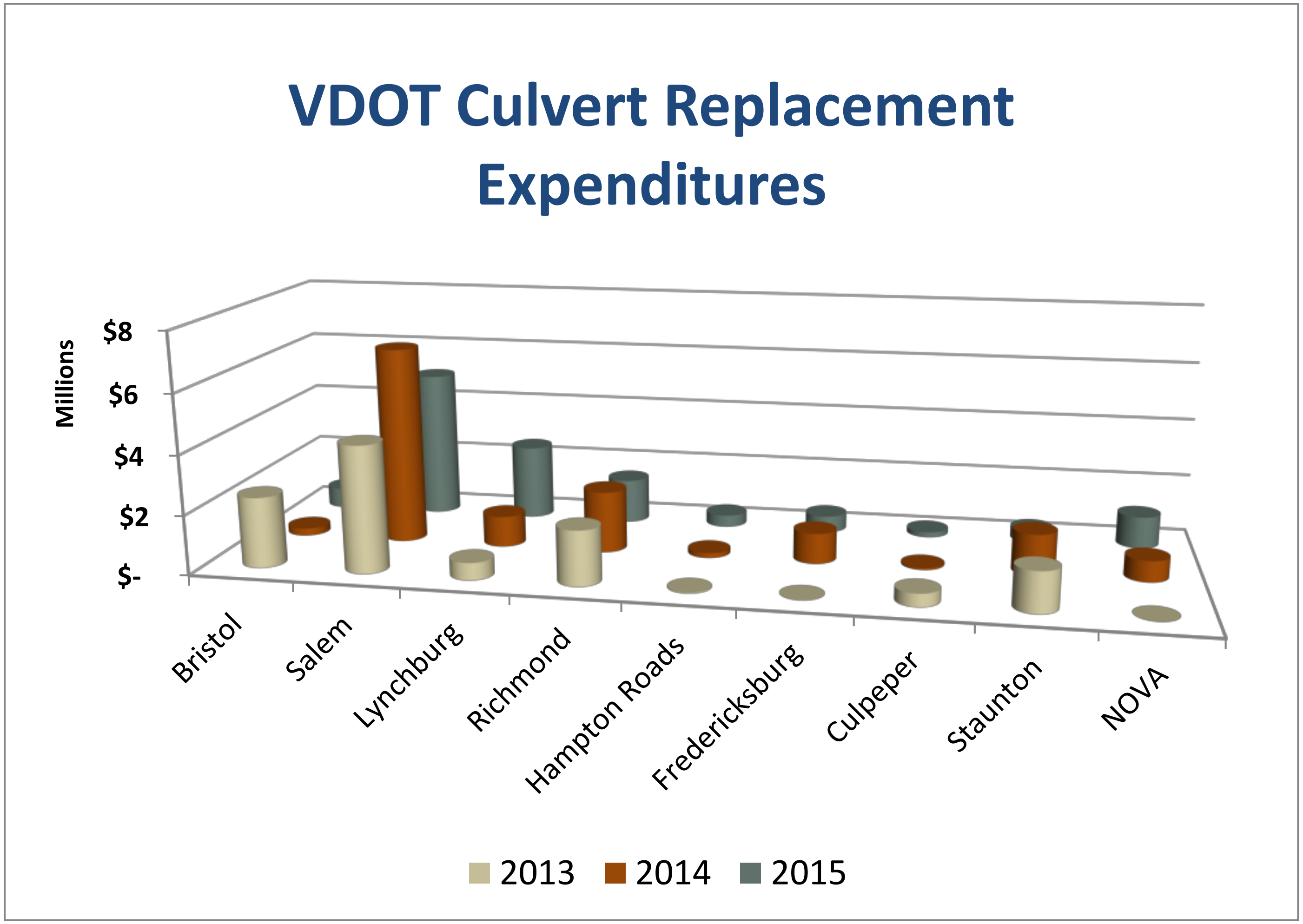

Outline of an Economic Analysis for Network Monitoring

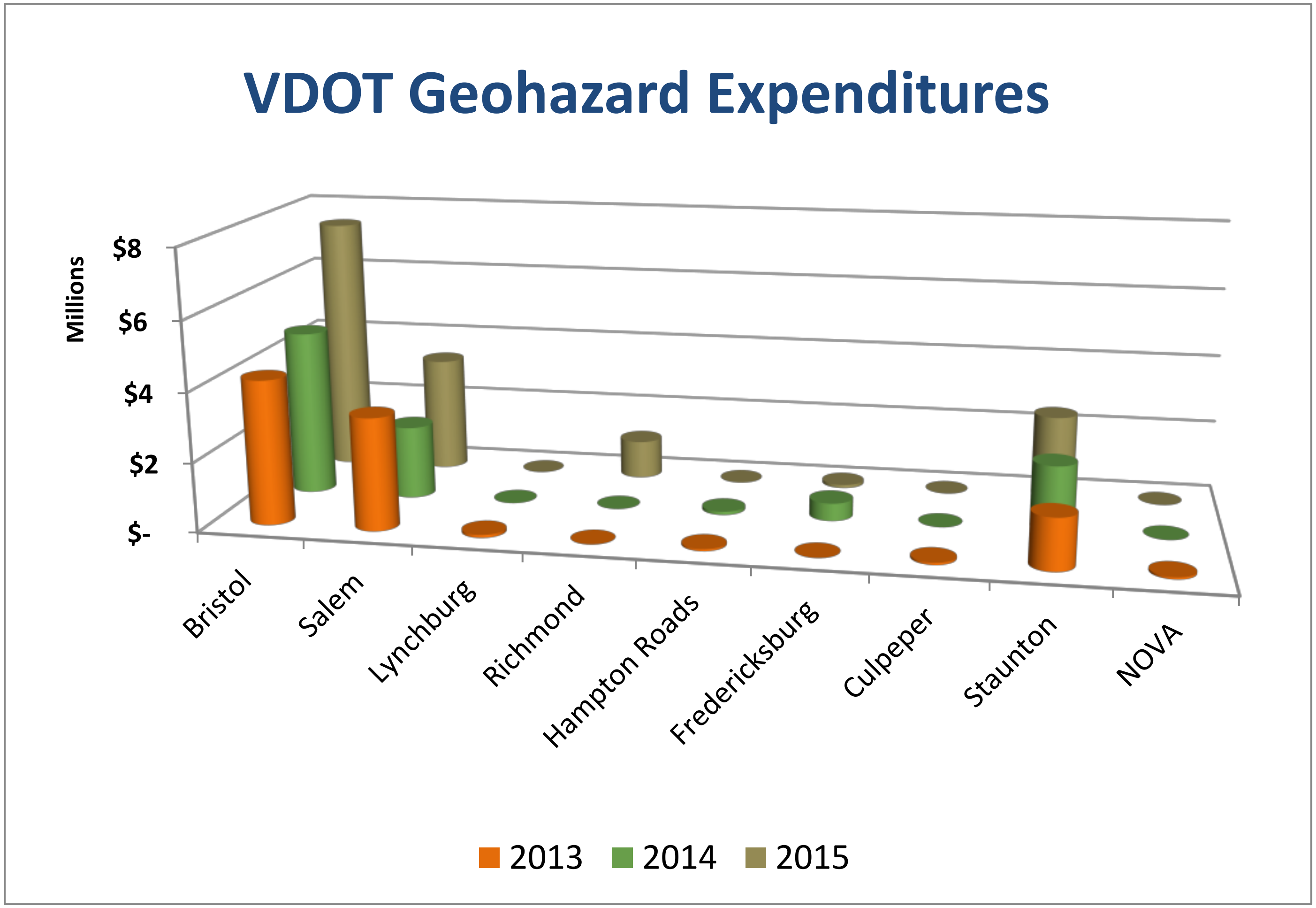

Outline of an Economic Analysis for Network Monitoring

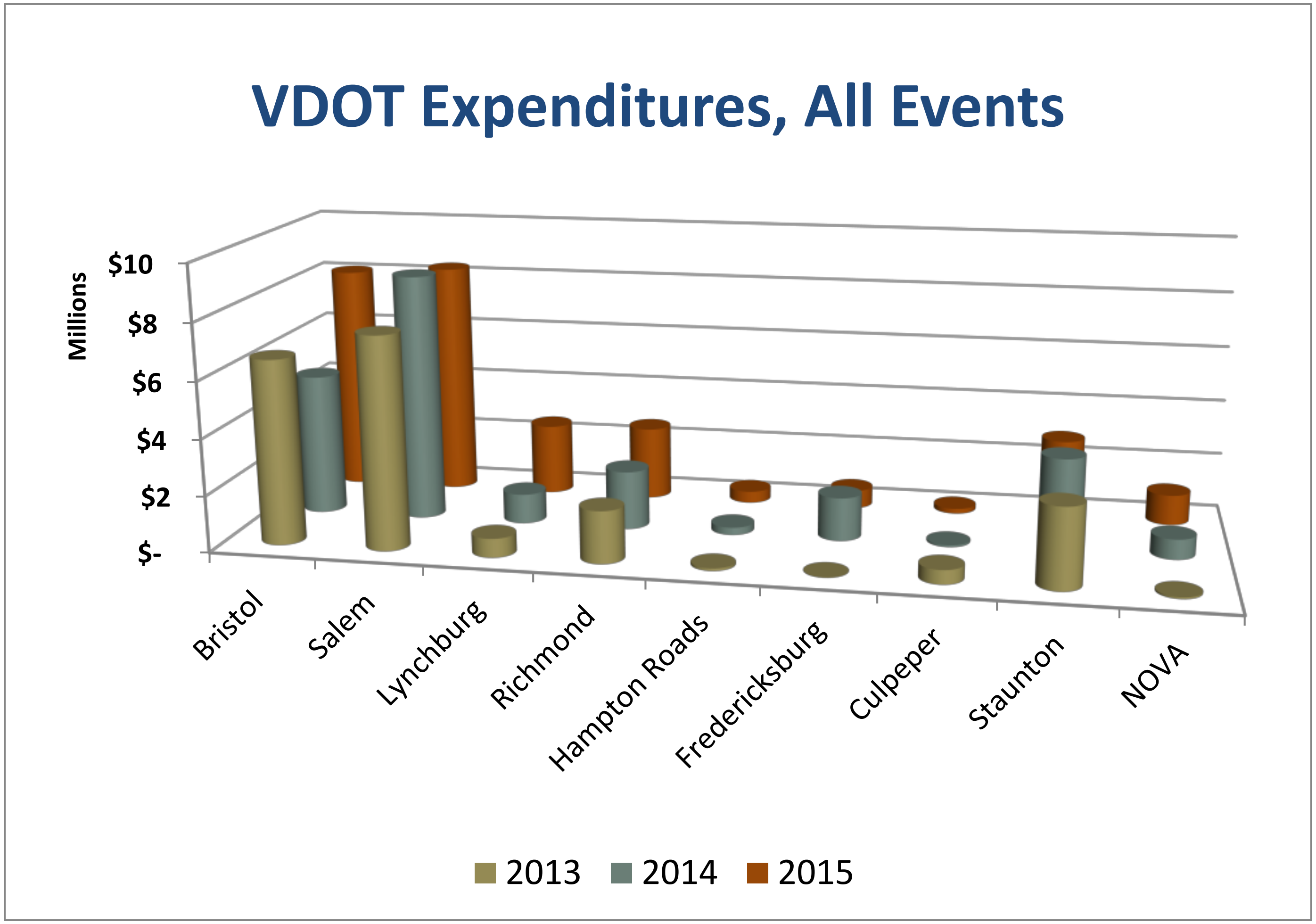

Outline of an Economic Analysis for Network Monitoring

FY13-15 event expenditures fell mainly in 5 of 9 VDOT Districts (containing 64% of VDOT-maintained lane-mi)

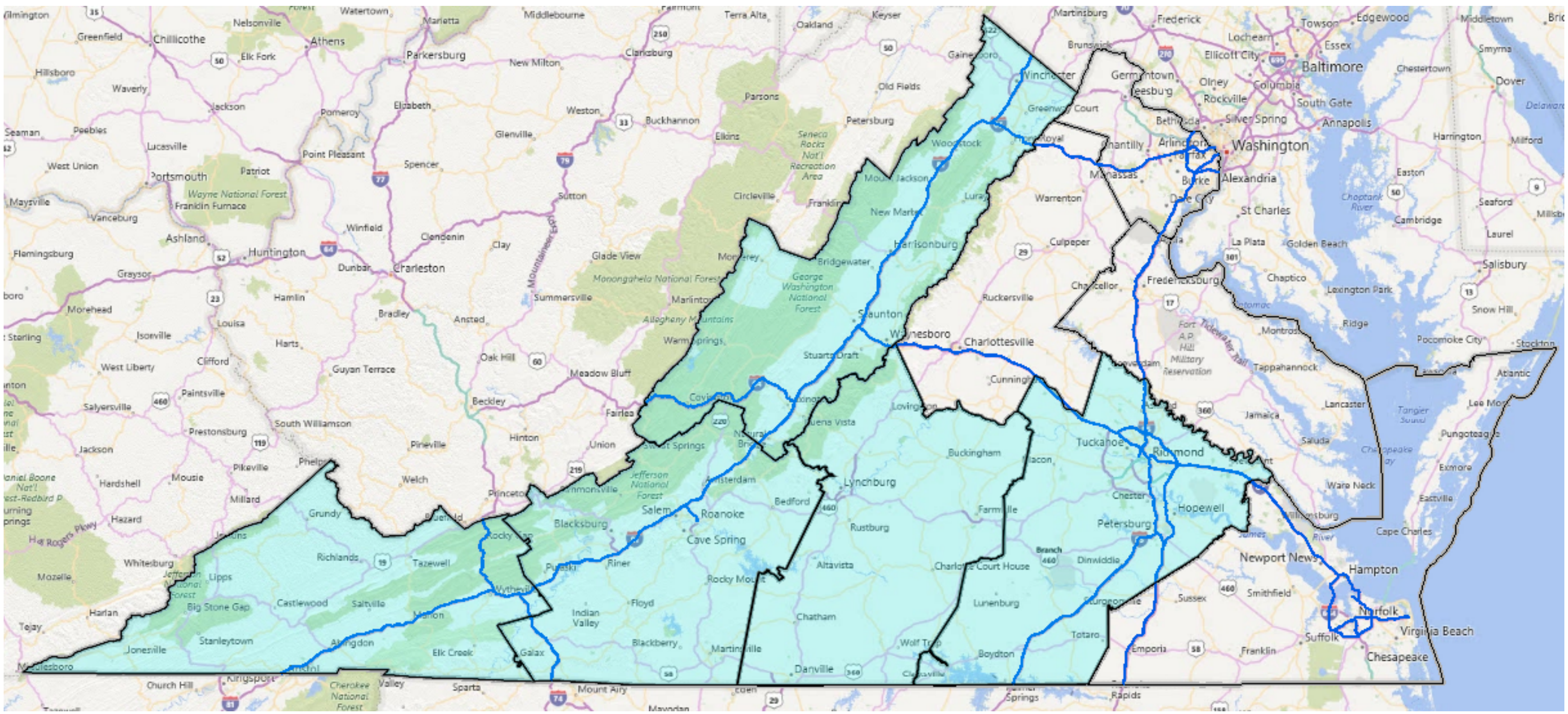

VTRC Virginia Transportation Research Council

Analysis model

VDOT "rents" a package of InSAR data and processing services from a vendor for 5 years:

Scenario 1: High-resolution data

Scenario 2: Low-resolution data supplemented with high-resolution confirmation frames as needed

VTRC Virginia Transportation Research Council

Performance Measure

Discounted net benefit over 5 years, or

Net Present Benefit = $\Sigma\ (B_i - C_i)/(1+\rho)^i$

where i = 1,...5 (year)

ρ = discount rate

B_i = benefits to VDOT in year i

C_i = costs to VDOT in year i

VTRC Virginia Transportation Research Council

Definitions of terms

- "Benefits" = reductions in annual VDOT expenditures on geohazards and culverts
- "Costs" = costs of InSAR data + vendor processing
- Net Present Benefit = sum of discretely discounted annual net benefits over 5 years

Outline of an Economic Analysis for Network Monitoring

Model details

- Net benefits reflect assumptions about event detection rates and potential VDOT savings from early detection;
- Learning curves can be incorporated;
- Can back-calculate feasible InSAR package cost for VDOT, given annual event costs and general assumptions.

VTRC
Virginia Transportation Research Council

Detection Rates

Geohazards

On-call vendor stated that 10% of slope repair work is so extensive that it involves road-rebuild. Assume 10% geohazard detection for baseline.

Culvert deterioration

Assume 33% culvert detection for baseline.

Potential VDOT Savings from Early Detection of Surface Deformation

Geohazards

On-call vendor: 50% of cost could be saved on slopes if road rebuild is avoided by early slope stabilization.

Culverts

Contract analysis suggests 30-50% savings if VDOT can rehab culverts instead of replace.

VTRC Virginia Transportation Research Council

Rehabilitation vs. Replacement Cost

FY15 On-Call Culpeper Contract

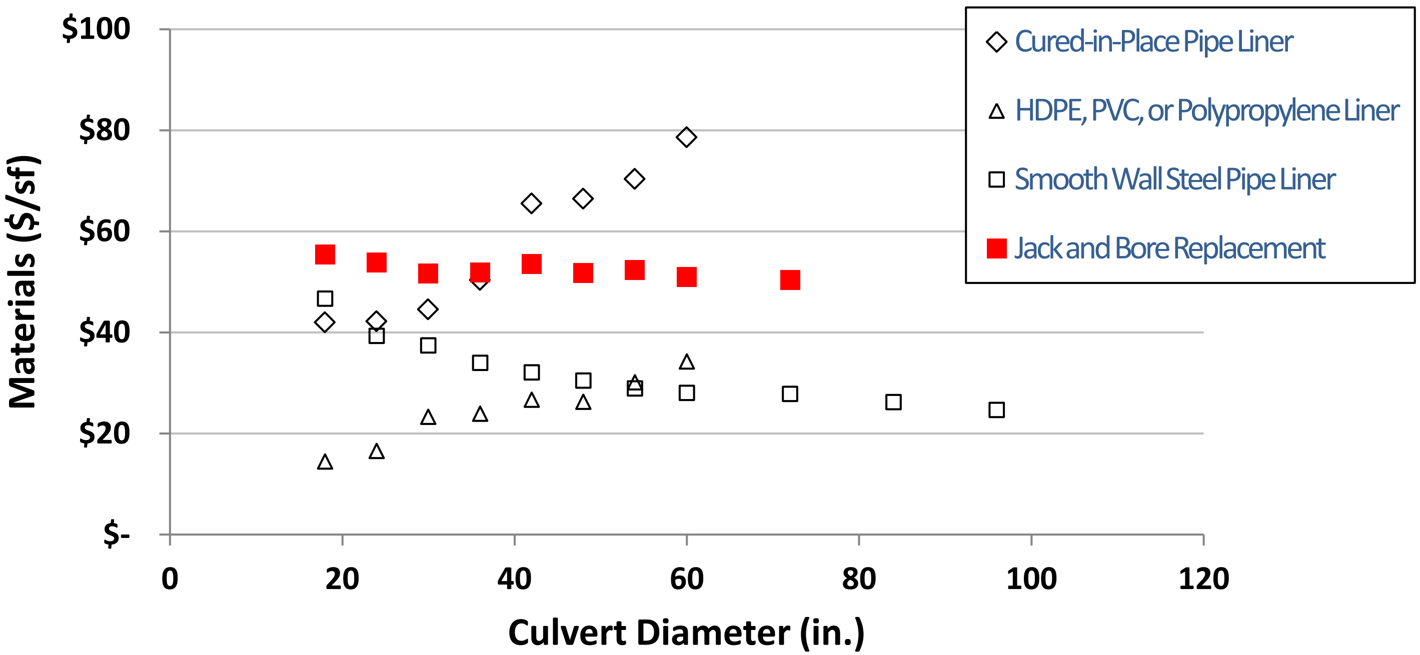

Rehabilitation vs. Replacement Cost

FY15 On-Call Culpeper Contract

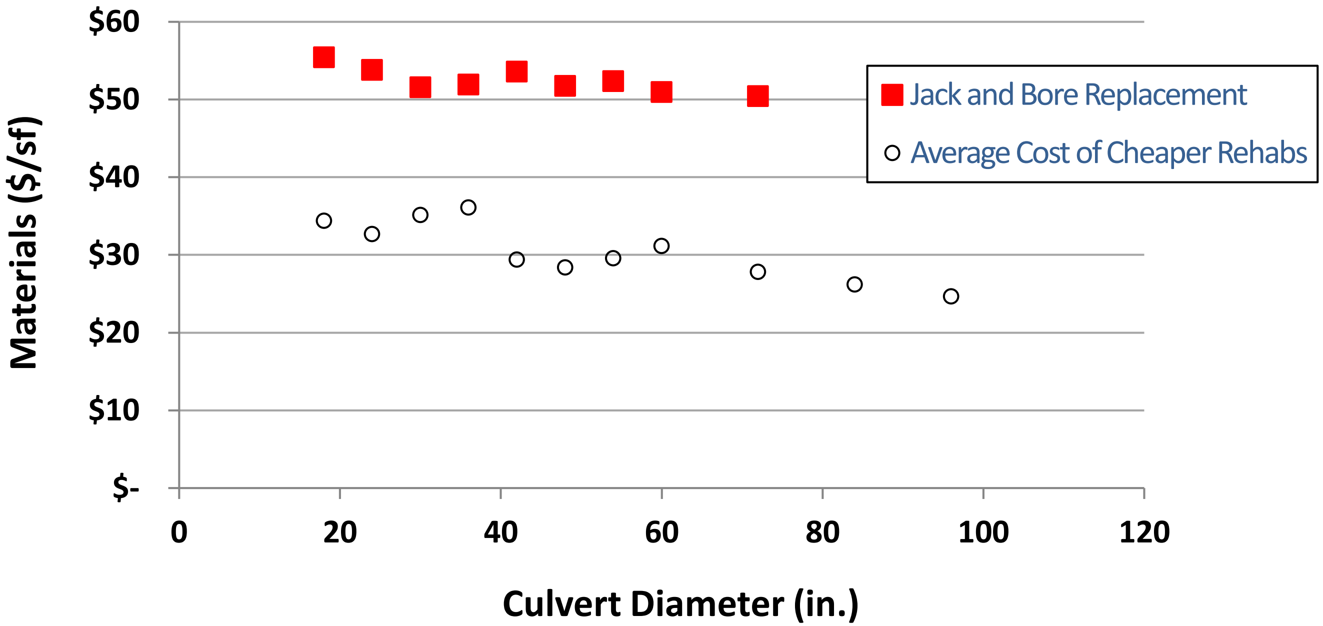

Rehabilitation vs. Replacement Cost

FY15 On-Call Richmond Contract

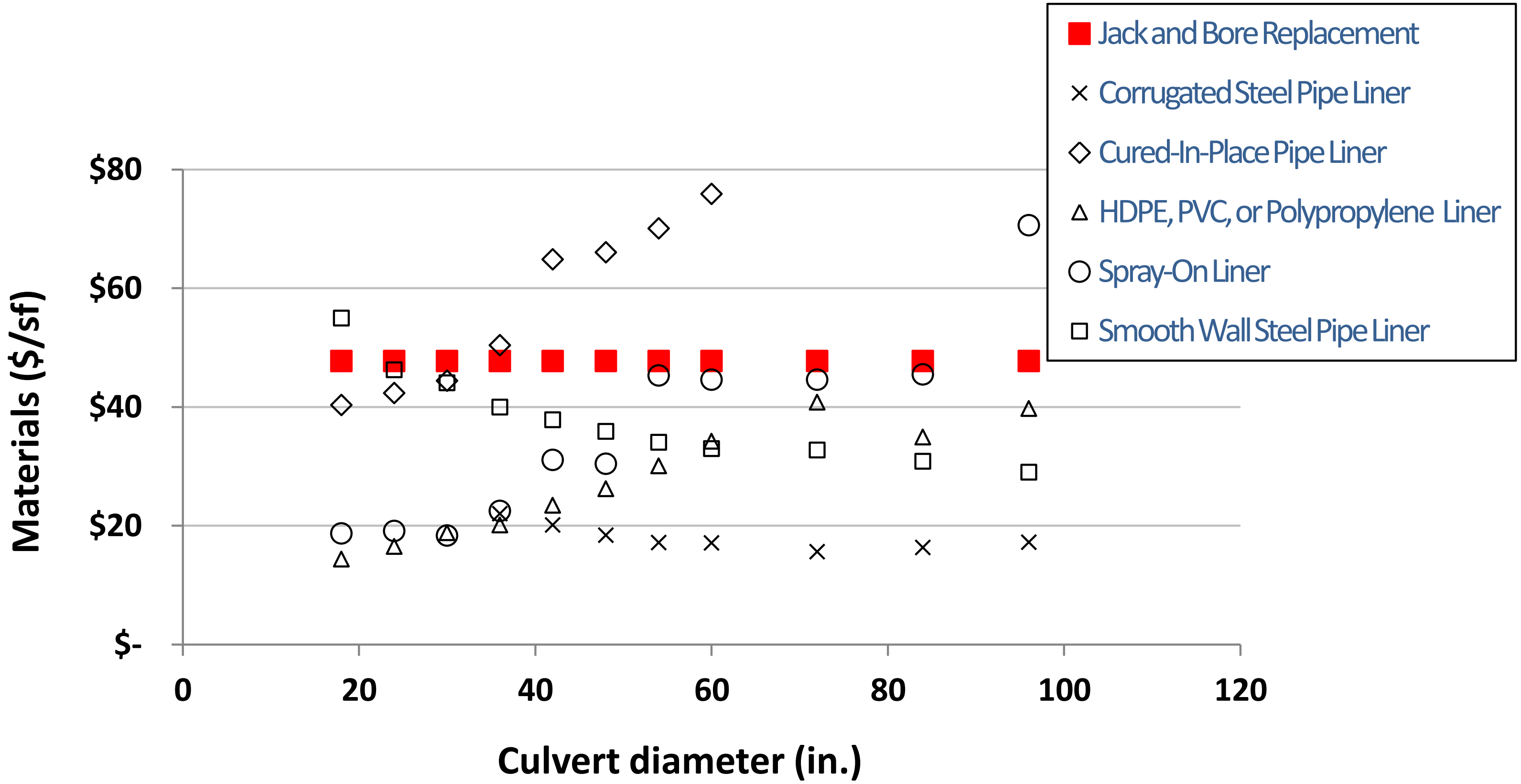

Rehabilitation vs. Replacement Cost

FY15 On-Call Richmond Contract

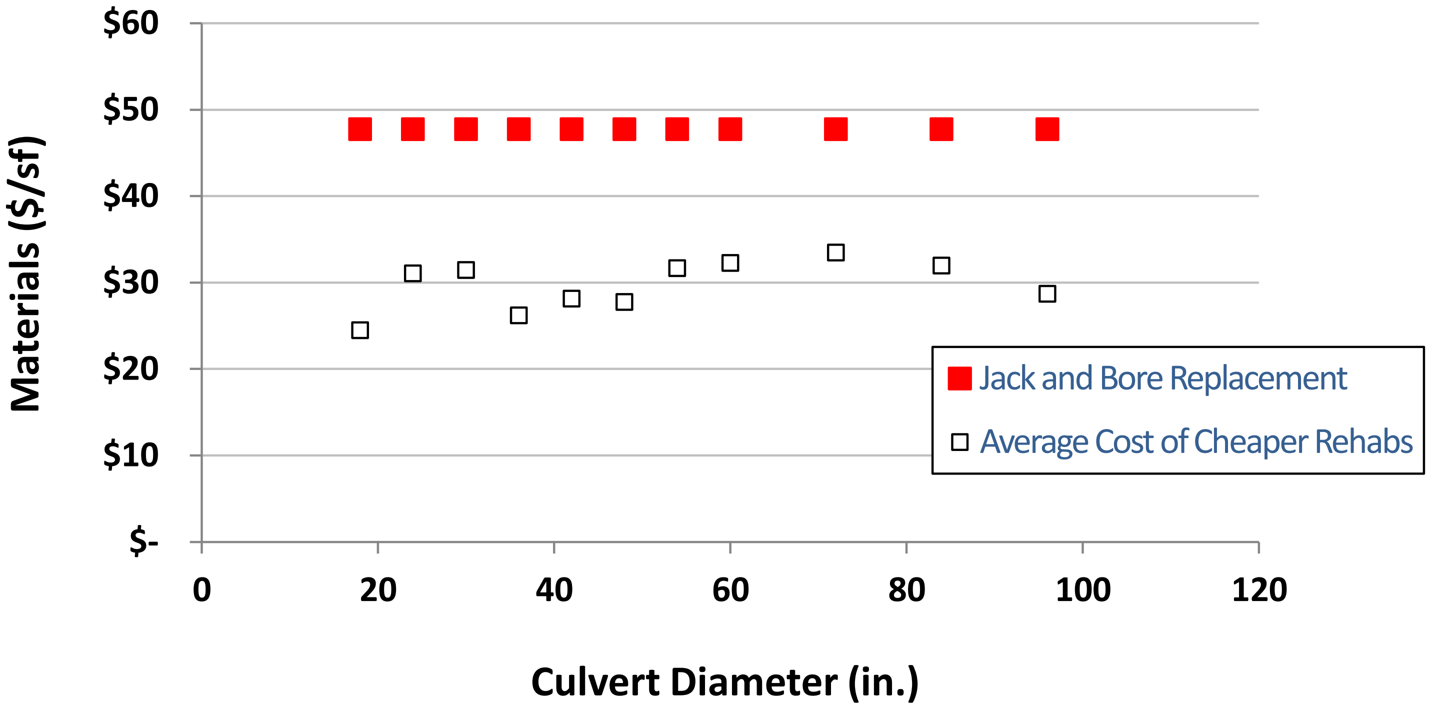

VTRC Virginia Transportation Research Council

Rehabilitation as Percent of Replacement Cost

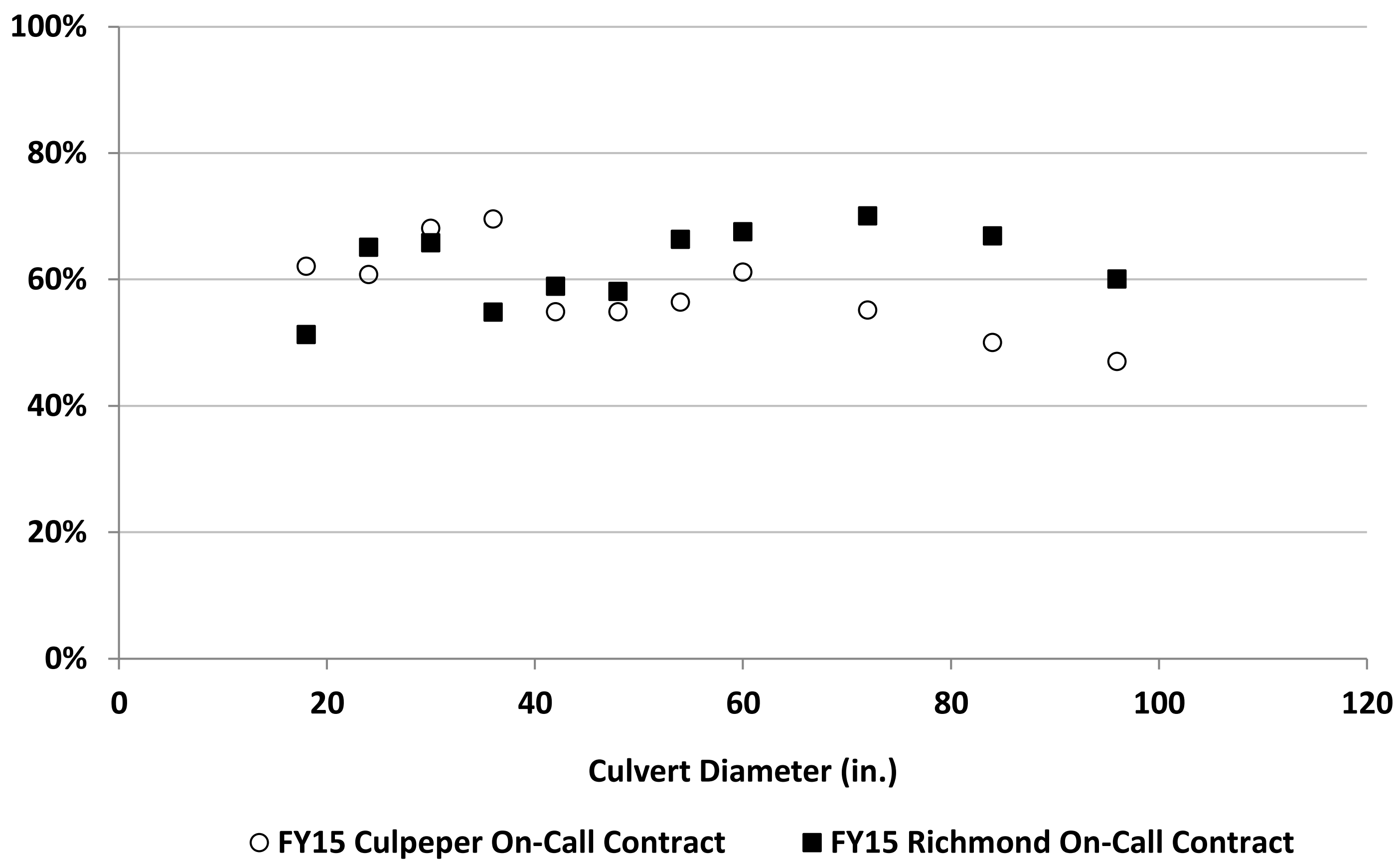

Outline of an Economic Analysis for Network Monitoring

Cost

Scenario 1: High-resolution network data

- COSMO-SkyMed (CSK)
- 3x3 meter resolution
- 16-day repeat → 22 frames in an (annual) stack
- 80 frames for VDOT network coverage
- Estimated annual cost = $9.52 million for network coverage (data + processing costs)

VTRC Virginia Transportation Research Council

Cost (cont'd)

Scenario 2: Lower resolution network data

- SENTINEL (free data)
- 5x20 meter resolution
- 12-day repeat → 30 frames in (annual) stack
- 12 frames for VDOT network coverage
- Estimated annual cost = $648,000 for network coverage (processing cost only)

(Excludes cost(s) of high-resolution confirmation frames)

Outline of an Economic Analysis for Network Monitoring

VTRC Virginia Transportation Research Council

SCENARIO 1: CSK

NETWORK-WIDE						
EVENT COST DATA	2013	2014	2015	ANNUAL AVE		
CULVERT REPLACEMENTS	$ 10,976,877	$ 13,457,522	$ 12,433,162	**$ 12,289,187**		
GEOHAZARD REPAIRS	$ 9,191,485	$ 9,446,179	$ 14,454,023	**$ 11,030,563**		
	$ 20,168,362	$ 22,903,701	$ 26,887,185			
TOOL						
$ 9,520,000	**CSK NETWORK COVERAGE**		**SCENARIO 1**			
$ 648,000	**SENTINEL NETWORK COVERAGE**		**SCENARIO 2**			
$ 62,000	*CSK 1 SQ MI COVERAGE*		*CONFIRMATION FRAME COST, SCENARIO 2*			
$ 26,000	*SENTINEL 1 SQ MI COVERAGE*					
YEAR	0	1	2	3	4	5
DISCOUNT RATE (ρ)	**3.0%**					
GENERAL PRICE INFLATION	**1.5%**					
ANNUAL INSAR COST TO VDOT	**$ 9,520,000**	$ 9,662,800	$ 9,807,742	$ 9,954,858	$ 10,104,181	$ 10,255,744
ANNUAL VDOT BENEFIT		$ -	$ 2,173,701	$ 2,396,505	$ 2,642,147	$ 2,912,967
INITIALANNUAL DR: CULV	**33%**		33%	35%	36%	38%
INITIAL ANNUAL SR: CULV	**40%**		40%	42%	44%	46%
INITIAL ANNUAL DR: GEOHZ	**10%**		10%	11%	11%	12%
INITIAL ANNUAL SR: GEOHZ	**50%**		50%	53%	55%	58%
ANNUAL GROWTH IN DR	**5%**					
ANNUAL GROWTH IN SR	**5%**					
NET ANNUAL VDOT BENEFIT		(9,662,800)	(7,634,041)	(7,558,353)	(7,462,034)	(7,342,777)
NET PRESENT BENEFIT	**($36,458,003)**					

Outline of an Economic Analysis for Network Monitoring

SCENARIO 1: CSK

NETWORK-WIDE						
EVENT COST DATA	2013	2014	2015	ANNUAL AVE		
CULVERT REPLACEMENTS	$ 10,976,877	$ 13,457,522	$ 12,433,162	**$ 12,289,187**		
GEOHAZARD REPAIRS	$ 9,191,485	$ 9,446,179	$ 14,454,023	**$ 11,030,563**		
	$ 20,168,362	$ 22,903,701	$ 26,887,185			
TOOL						
$ 9,520,000	**CSK NETWORK COVERAGE**		**SCENARIO 1**			
$ 648,000	**SENTINEL NETWORK COVERAGE**		**SCENARIO 2**			
$ 62,000	*CSK 1 SQ MI COVERAGE*		*CONFIRMATION FRAME COST, SCENARIO 2*			
$ 26,000	*SENTINEL 1 SQ MI COVERAGE*					
YEAR	0	1	2	3	4	5
DISCOUNT RATE (ρ)	**3.0%**					
GENERAL PRICE INFLATION	**1.5%**					
ANNUAL INSAR COST TO VDOT	**$ 9,520,000**	$ 9,662,800	$ 9,807,742	$ 9,954,858	$ 10,104,181	$ 10,255,744
ANNUAL VDOT BENEFIT		$ -	$ 2,173,701	$ 2,396,505	$ 2,642,147	$ 2,912,967
INITIALANNUAL DR: CULV	**33%**		33%	35%	36%	38%
INITIAL ANNUAL SR: CULV	**40%**		40%	42%	44%	46%
INITIAL ANNUAL DR: GEOHZ	**10%**		10%	11%	11%	12%
INITIAL ANNUAL SR: GEOHZ	**50%**		50%	53%	55%	58%
ANNUAL GROWTH IN DR	**5%**					
ANNUAL GROWTH IN SR	**5%**					
NET ANNUAL VDOT BENEFIT		(9,662,800)	(7,634,041)	(7,558,353)	(7,462,034)	(7,342,777)
NET PRESENT BENEFIT	**($36,458,003)**					

Outline of an Economic Analysis for Network Monitoring

VTRC Virginia Transportation Research Council

NETWORK-WIDE						
EVENT COST DATA	2013	2014	2015	ANNUAL AVE		
CULVERT REPLACEMENTS	$ 10,976,877	$ 13,457,522	$ 12,433,162	**$ 12,289,187**		
GEOHAZARD REPAIRS	$ 9,191,485	$ 9,446,179	$ 14,454,023	**$ 11,030,563**		
	$ 20,168,362	$ 22,903,701	$ 26,887,185			
TOOL						
$ 9,520,000	**CSK NETWORK COVERAGE**		**SCENARIO 1**			
$ 648,000	**SENTINEL NETWORK COVERAGE**		**SCENARIO 2**			
$ 62,000	*CSK 1 SQ MI COVERAGE*		*CONFIRMATION FRAME COST, SCENARIO 2*			
$ 26,000	*SENTINEL 1 SQ MI COVERAGE*					
YEAR	0	1	2	3	4	5
DISCOUNT RATE (ρ)	**3.0%**					
GENERAL PRICE INFLATION	**1.5%**					
ANNUAL INSAR COST TO VDOT	**$ 648,000**	$ 657,720	$ 667,586	$ 677,600	$ 687,764	$ 698,080
ANNUAL VDOT BENEFIT		$ -	$ 2,173,701	$ 2,396,505	$ 2,642,147	$ 2,912,967
INITIALANNUAL DR: CULV	**33%**		33%	35%	36%	38%
INITIAL ANNUAL SR: CULV	**40%**		40%	42%	44%	46%
INITIAL ANNUAL DR: GEOHZ	**10%**		10%	11%	11%	12%
INITIAL ANNUAL SR: GEOHZ	**50%**		50%	53%	55%	58%
ANNUAL GROWTH IN DR	**5%**					
ANNUAL GROWTH IN SR	**5%**					
NET ANNUAL VDOT BENEFIT		(657,720)	1,506,115	1,718,906	1,954,383	2,214,887
NET PRESENT BENEFIT	**$6,001,162**					

SCENARIO 2: SENTINEL

Outline of an Economic Analysis for Network Monitoring

NETWORK-WIDE						
EVENT COST DATA	2013	2014	2015	ANNUAL AVE		
CULVERT REPLACEMENTS	$ 10,976,877	$ 13,457,522	$ 12,433,162	**$ 12,289,187**		
GEOHAZARD REPAIRS	$ 9,191,485	$ 9,446,179	$ 14,454,023	**$ 11,030,563**		
	$ 20,168,362	$ 22,903,701	$ 26,887,185			
TOOL				**SCENARIO 2: SENTINEL**		
$ 9,520,000	**CSK NETWORK COVERAGE**		**SCENARIO 1**			
$ 648,000	**SENTINEL NETWORK COVERAGE**		**SCENARIO 2**			
$ 62,000	*CSK 1 SQ MI COVERAGE*		*CONFIRMATION FRAME COST, SCENARIO 2*			
$ 26,000	*SENTINEL 1 SQ MI COVERAGE*					
YEAR	0	1	2	3	4	5
DISCOUNT RATE (ρ)	**3.0%**					
GENERAL PRICE INFLATION	**1.5%**					
ANNUAL INSAR COST TO VDOT	**$ 648,000**	$ 657,720	$ 667,586	$ 677,600	$ 687,764	$ 698,080
ANNUAL VDOT BENEFIT		$ -	$ 2,173,701	$ 2,396,505	$ 2,642,147	$ 2,912,967
INITIALANNUAL DR: CULV	**33%**		33%	35%	36%	38%
INITIAL ANNUAL SR: CULV	**40%**		40%	42%	44%	46%
INITIAL ANNUAL DR: GEOHZ	**10%**		10%	11%	11%	12%
INITIAL ANNUAL SR: GEOHZ	**50%**		50%	53%	55%	58%
ANNUAL GROWTH IN DR	**5%**					
ANNUAL GROWTH IN SR	**5%**					
NET ANNUAL VDOT BENEFIT		(657,720)	1,506,115	1,718,906	1,954,383	2,214,887
NET PRESENT BENEFIT	**$6,001,162**					

VTRC Virginia Transportation Research Council

Conclusions

- Accuracy of external data is critical to results.
- InSAR monitoring still has to be proven to detect relevant events in advance.
- A large positive Net Present Benefit implies that InSAR monitoring could be beneficial for VDOT geohazard management and culvert maintenance over the next 5 years.

Outline of an Economic Analysis for Network Monitoring

DAVID CRIGGER/BHC

Worker continue to fill and repair a sinkhole on southbound Interstate 81 near exit 13 Thursday morning.

Thanks to
Jean Ann Alexander, Joe Bouchey, Donna Cognata, Phil East, Mike Hall, Ed Hoppe, Winston Lucombe, George McCloud, and Felecia Wade of VDOT for expert assistance in VDOT data access and collection.

Guide to Excel Tool for Estimation of Net Present Benefit of Network-Wide InSAR Monitoring

Audrey K. Moruza, Research Scientist
Virginia Transportation Research Council (VDOT)
November 4, 2016

INTRODUCTION

The Excel spreadsheet tool was created to inform a decision about trial of InSAR technology when the benefits of the technology in specific transportation applications are not precisely known. Uncertainty of the benefits and unavailability of desirable types of data for such an analysis require that parameters, or quantities whose values are selected for the particular circumstances, be introduced to the analysis calculations. When parameters are required, analysis results will feature a level of accuracy in proportion to the order of the least accurate data *or* parameter assumption. Error will be minimized by gathering accurate data where available, by using an appropriate performance measure for the selected analysis period, and by identifying and defining parameters that are of core relevance to the analysis.

There are common features which should be present in any economic analysis of a technology trial. At a minimum these include:

1. Accurate and current costs of activities potentially relieved by the technology;
2. Accurate and current costs of the technology over the analysis period;
3. A relevant analysis period;
4. An explicit performance measure;
5. Variable parameters to bridge the gap between data and model needs.

The Excel spreadsheet tool includes one simple enhancement consisting of an allowance for a “learning curve” during the trial period. In Figure 6, the effect of growth in the effectiveness of the technology and/or growth in agency savings from advance detection of events are shown as a feature of the basic tool.

EXCEL SPREADSHEET TOOL

Data and Parameter Inputs

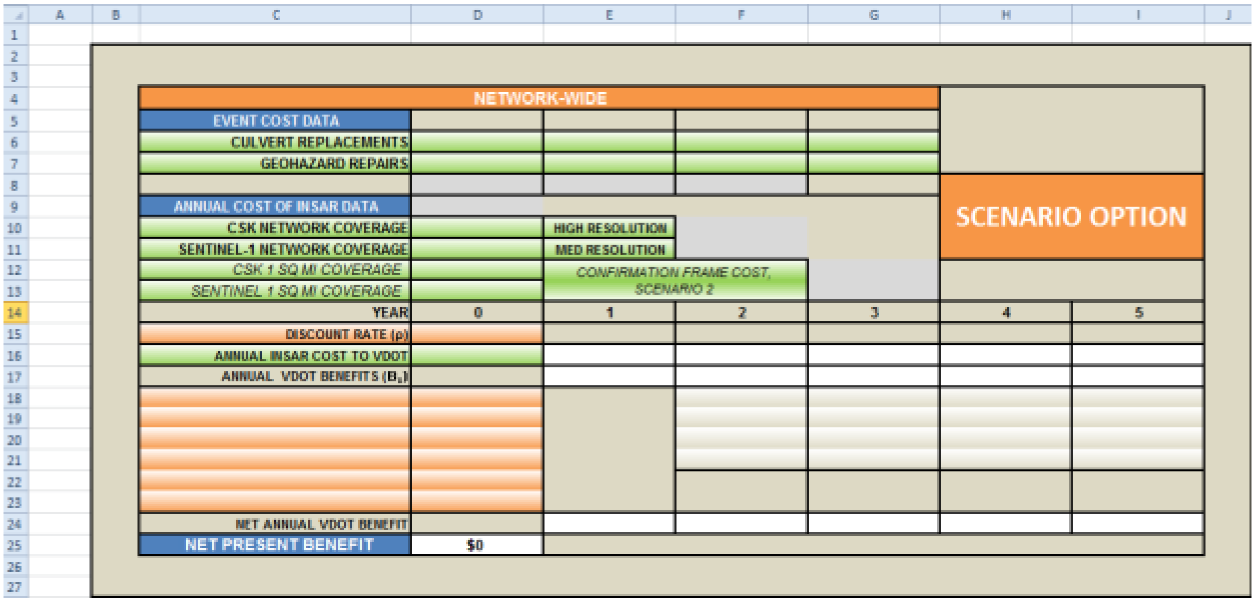

Figure 1. Tool Framework

1. Accurate, current costs for three fiscal years of two VDOT maintenance activities potentially relieved by the technology under evaluation are placed in cells D6 through F7; annual average costs in cells G6 and G7 are used in the calculation of the performance measure.

2. Accurate, current costs of the technology are placed in cells D10 and D11; the cells represent the 2 alternative data scenarios under evaluation. Supplementary technology cost data are placed in cells D12 and D13 but are not linked to performance measure calculation.

3. The analysis period is explicitly represented in row 14.

4. The performance measure employed in this spreadsheet tool is (the Excel formula version of) "Net Present Value" (NPV) of a quantity; the quantities discounted to the present are the separate annual net benefits from the technology under evaluation. Values are placed in cells E24 through I24. Note that there are no benefits from the technology in year 1 during which baseline surface maps are established. The performance measure, NPV of annual net benefits, is located in cell D25.

5. Annual VDOT benefits from the technology, located in Row 17, cannot be calculated without the introduction of parameters to stand in for data or, more precisely, accurate *information* about how well the technology will perform and how ably the transportation agency will capture potential savings resulting from the technology.

Parameters are identified in this spreadsheet tool to separately describe technology performance and agency response. Technology performance is represented by the parameter of "detection rate" (DR); agency response is represented by the parameter of "savings rate"

(SR). DR and SR are independent of each other within and between each event category (i.e., culverts and geohazards for VDOT) and variable in the tool, and they may be assigned values based on expert judgment or for the goal of sensitivity testing. The DRs and SRs are located in cells C18-C21. Their (assumed) values are located in cells D18-D21.

In addition to the enhancement of supplementary technology costs, one additional enhancement is provided in this basic tool: variable growth rates for DR and SR which are located in cells D22 and D23.

Excel Tool Formulas

After input data and parameters are in place, annual VDOT benefits in row 17 and net annual VDOT benefits in row 24 are calculated automatically by means of Excel formulas in the spreadsheet tool.

In row 17, VDOT benefits in year *i* are calculated in cells F17 through I17 according to the following formula:

$$B_i = \sum_{\substack{Culverts,\\ geohazards}} DR_{event,i} \cdot SR_{event,i} \cdot Average\ annual\ cost\ of\ event$$

To summarize, benefits are modeled as an interactive function of the technology performance in detecting subsidence (DR) and the agency response in taking proactive measures (SR), measured as a proportion of average annual expenditures in a given event category, as shown in cells E17 through I17 of Figure 2. Event categories are treated independently and summed.

In row 24 of Figure 2, net annual VDOT benefits from the technology are a simple difference between VDOT's costs for the technology and its benefits from the technology.

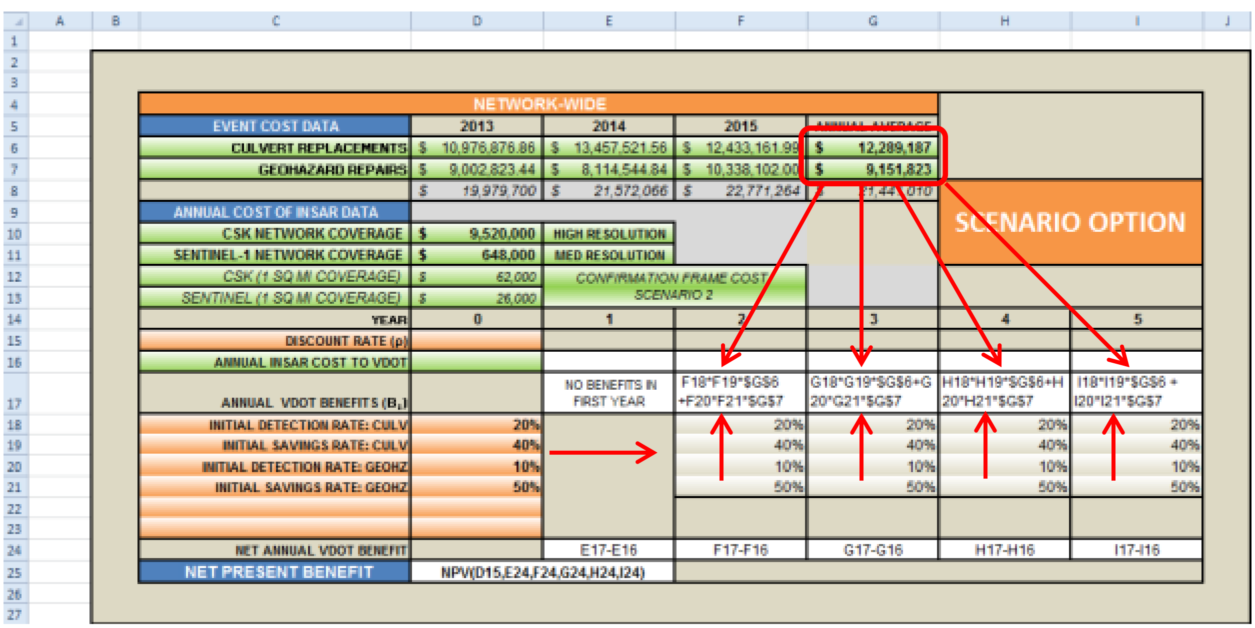

Figure 2. Excel Tool Formulas

Discount Rate and Performance Measure

A discount rate is required for calculation of the “present value” of a future quantity (Fig. 3). Although the discount rate can be varied in this tool, it is not a “parameter” like DR and SR. The NPV of net annual benefits to VDOT is calculated in cell D25 by Excel formula as a function of the discount rate entered into cell D15, after a data scenario (i.e., InSAR data source) is selected. This tool employs a “real” (rather than nominal) discount rate.

NETWORK-WIDE						
EVENT COST DATA	2013	2014	2015	ANNUAL AVERAGE		
CULVERT REPLACEMENTS	$ 10,976,877	$ 13,457,522	$ 12,433,162	$ 12,289,187		
GEOHAZARD REPAIRS	$ 9,002,823	$ 8,114,545	$ 10,338,102	$ 9,151,823		
	$ 19,979,700	$ 21,572,066	$ 22,771,264	$ 21,441,010	SCENARIO OPTION	
ANNUAL COST OF INSAR DATA						
CSK NETWORK COVERAGE	$ 9,520,000	HIGH RESOLUTION				
SENTINEL-1 NETWORK COVERAGE	$ 648,000	MED RESOLUTION				
CSK (1 SQ MI COVERAGE)	$ 62,000	CONFIRMATION FRAME COST, SCENARIO 2				
SENTINEL (1 SQ MI COVERAGE)	$ 26,000					
YEAR	0	1	2	3	4	5
DISCOUNT RATE (p)	3.0%					
ANNUAL INSAR COST TO VDOT		$ -	$ -	$ -	$ -	$ -
ANNUAL VDOT BENEFITS (B,)		$ -	$ 9,491,586	$ 9,491,586	$ 9,491,586	$ 9,491,586
INITIAL DETECTION RATE: CULV	100%		100%	100%	100%	100%
INITIAL SAVINGS RATE: CULV	40%		40%	40%	40%	40%
INITIAL DETECTION RATE: GEOHZ	100%		100%	100%	100%	100%
INITIAL SAVINGS RATE: GEOHZ	50%		50%	50%	50%	50%
ANNUAL GROWTH IN DETECTION RATE	0%					
ANNUAL GROWTH IN SAVINGS RATE	0%					
NET ANNUAL VDOT BENEFIT						
NET PRESENT BENEFIT						

Figure 3. Excel Tool Prior to Specific Option Analysis

The selection of a scenario option (COSMO-SkyMed or Sentinel-1) causes the Excel tool to perform the calculations necessary for generation of the Net Present Benefit performance measure (Fig. 4). The annual InSAR costs for years 1 through 5 (cells E16 through I16) populate automatically upon entry of “=D10” or “=D11” into cell D16.

Moderate values for DRs and SRs are assumed in the parameter cells, and they may be varied according to expert opinion or for purposes of sensitivity testing.

NETWORK-WIDE					COSMO-SkyMed (X-Band) data	
EVENT COST DATA	2013	2014	2015	ANNUAL AVERAGE		
CULVERT REPLACEMENTS	$ 10,976,877	$ 13,457,522	$ 12,433,162	$ **12,289,187**		
GEOHAZARD REPAIRS	$ 9,002,823	$ 8,114,545	$ 10,338,102	$ **9,151,823**		
	$ 19,979,700	*$ 21,572,066*	*$ 22,771,264*	*$ 21,441,010*		
ANNUAL COST OF INSAR DATA						
CSK NETWORK COVERAGE	$ **9,520,000**	HIGH RESOLUTION				
SENTINEL-1 NETWORK COVERAGE	$ **648,000**	MED RESOLUTION				
CSK (1 SQ MI COVERAGE)	*$ 62,000*	*CONFIRMATION FRAME COST, SCENARIO 2*				
SENTINEL (1 SQ MI COVERAGE)	*$ 26,000*					
YEAR	0	1	2	3	4	5
DISCOUNT RATE (ρ)	3.0%					
ANNUAL INSAR COST TO VDOT	$ **9,520,000**	$ 9,520,000	$ 9,520,000	$ 9,520,000	$ 9,520,000	$ 9,520,000
ANNUAL VDOT BENEFITS (B_i)		$ -	$ 4,745,793	$ 4,745,793	$ 4,745,793	$ 4,745,793
INITIAL DETECTION RATE: CULV	50%		50%	50%	50%	50%
INITIAL SAVINGS RATE: CULV	40%		40%	40%	40%	40%
INITIAL DETECTION RATE: GEOHZ	50%		50%	50%	50%	50%
INITIAL SAVINGS RATE: GEOHZ	50%		50%	50%	50%	50%
ANNUAL GROWTH IN DETECTION RATE	0%					
ANNUAL GROWTH IN SAVINGS RATE	0%					
NET ANNUAL VDOT BENEFIT		(9,520,000)	(4,774,207)	(4,774,207)	(4,774,207)	(4,774,207)
NET PRESENT BENEFIT	**($26,472,035)**					

Figure 4. Net Present Benefit Calculation for COSMO-SkyMed Data

The second scenario option is evaluated in Figure 5. Cell D16 is directed to cell D11 ("=D11") to generate the performance measure in cell D25 for Sentinel-1. DRs for both event categories are electively lower in cells D18 and D20 to reflect the medium resolution data of Sentinel-1, in contrast to the high-resolution data produced by COSMO-SkyMed.

NETWORK-WIDE					Sentinel-1 (C-Band) data	
EVENT COST DATA	2013	2014	2015	ANNUAL AVERAGE		
CULVERT REPLACEMENTS	$ 10,976,877	$ 13,457,522	$ 12,433,162	$ **12,289,187**		
GEOHAZARD REPAIRS	$ 9,002,823	$ 8,114,545	$ 10,338,102	$ **9,151,823**		
	$ 19,979,700	*$ 21,572,066*	*$ 22,771,264*	*$ 21,441,010*		
ANNUAL COST OF INSAR DATA						
CSK NETWORK COVERAGE	$ **9,520,000**	HIGH RESOLUTION				
SENTINEL-1 NETWORK COVERAGE	$ **648,000**	MED RESOLUTION				
CSK (1 SQ MI COVERAGE)	*$ 62,000*	*CONFIRMATION FRAME COST, SCENARIO 2*				
SENTINEL (1 SQ MI COVERAGE)	*$ 26,000*					
YEAR	0	1	2	3	4	5
DISCOUNT RATE (ρ)	3.0%					
ANNUAL INSAR COST TO VDOT	$ **648,000**	$ 648,000	$ 648,000	$ 648,000	$ 648,000	$ 648,000
ANNUAL VDOT BENEFITS (B_i)		$ -	$ 1,440,726	$ 1,440,726	$ 1,440,726	$ 1,440,726
INITIAL DETECTION RATE: CULV	20%	*$ 2,457,837*	20%	20%	20%	20%
INITIAL SAVINGS RATE: CULV	40%	***$ 983,135***	40%	40%	40%	40%
INITIAL DETECTION RATE: GEOHZ	10%	*$ 915,182*	10%	10%	10%	10%
INITIAL SAVINGS RATE: GEOHZ	50%	***$ 457,591***	50%	50%	50%	50%
ANNUAL GROWTH IN DETECTION RATE	0%					
ANNUAL GROWTH IN SAVINGS RATE	0%					
NET ANNUAL VDOT BENEFIT		(648,000)	792,726	792,726	792,726	792,726
NET PRESENT BENEFIT	**$2,231,690**					

Figure 5. Net Present Benefit Calculation for Sentinel-1 Data

The tool has a single enhancement that can alter the performance measure for a scenario option: allowance for growth in detection rates and/or in savings rates resulting from advance detection. Figure 6 shows the result of adding such growth to the COSMO-SkyMed results shown in Figure 4. Allowing growth in DR and SR allows VDOT benefits to rise each year of the analysis period. Consequently, the Net Present Benefit of COSMO-SkyMed data is slightly less negative over the period.

NETWORK-WIDE						
EVENT COST DATA	2013	2014	2015	ANNUAL AVERAGE		
CULVERT REPLACEMENTS	$ 10,976,877	$ 13,457,522	$ 12,433,162	**$ 12,289,187**		
GEOHAZARD REPAIRS	$ 9,002,823	$ 8,114,545	$ 10,338,102	**$ 9,151,823**		
	$ 19,979,700	*$ 21,572,066*	*$ 22,771,264*	*$ 21,441,010*	COSMO-SkyMed (X-Band) data	
ANNUAL COST OF INSAR DATA						
CSK NETWORK COVERAGE	$ 9,520,000	HIGH RESOLUTION				
SENTINEL-1 NETWORK COVERAGE	$ 648,000	MED RESOLUTION				
CSK (1 SQ MI COVERAGE)	*$ 62,000*	*CONFIRMATION FRAME COST, SCENARIO 2*				
SENTINEL (1 SQ MI COVERAGE)	*$ 26,000*					
YEAR	0	1	2	3	4	5
DISCOUNT RATE (ρ)	3.0%					
ANNUAL INSAR COST TO VDOT	**$ 9,520,000**	$ 9,520,000	$ 9,520,000	$ 9,520,000	$ 9,520,000	$ 9,520,000
ANNUAL VDOT BENEFITS (B_i)		$ -	$ 4,745,793	$ 5,232,237	$ 5,768,541	$ 6,359,817
INITIAL DETECTION RATE: CULV	50%		50%	53%	55%	58%
INITIAL SAVINGS RATE: CULV	40%		40%	42%	44%	46%
INITIAL DETECTION RATE: GEOHZ	50%		50%	53%	55%	58%
INITIAL SAVINGS RATE: GEOHZ	50%		50%	53%	55%	58%
ANNUAL GROWTH IN DETECTION RATE	5%					
ANNUAL GROWTH IN SAVINGS RATE	5%					
NET ANNUAL VDOT BENEFIT		(9,520,000)	(4,774,207)	(4,287,763)	(3,751,459)	(3,160,183)
NET PRESENT BENEFIT	($23,725,901)					

Figure 6. Net Present Benefit Calculation for COSMO-SkyMed with Growth in DR and SR